Quantum Dots

Fundamentals, Synthesis and Applications

Edited by
Rakshit Ameta
Jayesh P. Bhatt
Suresh C. Ameta

ELSEVIER

Quantum Dots

Fundamentals, Synthesis and Applications

This page intentionally left blank

Quantum Dots

Fundamentals, Synthesis and Applications

Edited by

Rakshit Ameta

Jayesh P. Bhatt

Suresh C. Ameta

ELSEVIER

Elsevier
Radarweg 29, PO Box 211, 1000 AE Amsterdam, Netherlands
The Boulevard, Langford Lane, Kidlington, Oxford OX5 1GB, United Kingdom
50 Hampshire Street, 5th Floor, Cambridge, MA 02139, United States

Notices

Knowledge and best practice in this field are constantly changing. As new research and experience broaden our understanding, changes in research methods, professional practices, or medical treatment may become necessary.

Practitioners and researchers must always rely on their own experience and knowledge in evaluating and using any information, methods, compounds, or experiments described herein. In using such information or methods they should be mindful of their own safety and the safety of others, including parties for whom they have a professional responsibility.

To the fullest extent of the law, neither the Publisher nor the authors, contributors, or editors, assume any liability for any injury and/or damage to persons or property as a matter of products liability, negligence or otherwise, or from any use or operation of any methods, products, instructions, or ideas contained in the material herein.

ISBN: 978-0-12-824153-0

Publisher: Susan Dennis
Acquisitions Editor: Charles Bath
Editorial Project Manager: Ali Afzal-Khan
Production Project Manager: Bharatwaj Varatharajan
Cover Designer: Mark Rogers

Typeset by MPS Limited, Chennai, India

Dedication

Dedicated to Mrs. Anita Ameta
who had been a vital force behind us to complete
this project

This page intentionally left blank

Contents

List of contributors

Luma M. Ahmed Department of Chemistry, College of Science, University of Kerbala, Karbala, Iraq

Chetna Ameta Department of Chemistry, M. L. S. University Udaipur, Rajasthan, India

Garima Ameta Department of Chemistry, M. L. S. University, Udaipur, Rajasthan, India

Rakshit Ameta Department of Chemistry, J. R. N. Rajasthan Vidhyapeeth (Deemed to be University), Udaipur, Rajasthan, India

Rameshwar Ameta Department of Chemistry, PAHER University, Udaipur, Rajasthan, India

Suresh C. Ameta Department of Chemistry, PAHER University, Udaipur, Rajasthan, India

Anca Armăşelu Department of Electrical Engineering and Applied Physics, Faculty of Electrical Engineering and Computer Science, Transilvania University of Brasov, Brasov, Romania

R. Geetha Balakrishna Centre for Nano and Material Sciences, Jain University, Bengaluru, Karnataka, India

Indu Bhati Maribyrnong, VIC, Australia

Jayesh P. Bhatt Department of Chemistry, PAHER University, Udaipur, Rajasthan, India

Priyanka Chundawat Department of Chemistry, M. L. S. University Udaipur, Rajasthan, India

Dharmendra Department of Chemistry, M. L. S. University Udaipur, Rajasthan, India

Neha Godha Department of Chemistry, PAHER University, Udaipur, Rajasthan, India

Meghavi Gupta Department of Chemistry, PAHER University, Udaipur, Rajasthan, India

Chandan Hunsur Ravikumar Centre for Nano and Material Sciences, Jain University, Bengaluru, Karnataka, India; Pilot Plant Development and Training Institute, King Mongkut's University of Technology Thonburi, Thakam, Bangkok, Thailand

Abhilasha Jain Department of Chemistry, St. Xavier's College, Mumbai, Maharashtra, India

Monika Jangid Department of Chemistry, PAHER University, Udaipur, Rajasthan, India

Kanchan K. Jat Department of Chemistry, M. L. S. University Udaipur, Rajasthan, India

Thaqeef M. Jawad Department of Chemistry, College of Science, University of Kerbala, Karbala, Iraq

Priyanka Jhalora Department of Chemistry, PAHER University, Udaipur, Rajasthan, India

M.S. Jyothi Department of Chemistry, AMC Engineering College, Bengaluru, Karnataka, India

Hamad H. Kadium Department of Chemistry, College of Science, University of Kerbala, Karbala, Iraq

Seema Kothari Department of Chemistry, PAHER University, Udaipur, Rajasthan, India

Neelam Kunwar Department of Chemistry, PAHER University, Udaipur, Rajasthan, India

Kushnuma Parveen Khamis Mushayt, Ahad Rafaidah, Kingdom of Saudi Arabia

Shwetharani R Centre for Nano and Material Sciences, Jain University, Bengaluru, Karnataka, India

Avinash K. Rai Department of Chemistry, PAHER University Udaipur, Rajasthan, India

Neetu Shorgar Department of Chemistry, PAHER University, Udaipur, Rajasthan, India

Shubang Vyas Department of Chemistry, PAHER University, Udaipur, Rajasthan, India

Yogeshwari Vyas Department of Chemistry, M. L. S. University Udaipur, Rajasthan, India

Inderjeet Yadav Department of Applied Sciences, University of Technology and Applied Sciences, Alkhuwair, Muscat, Sultanate of Oman

Hetal Zala 1197-1, Uchigashimacho, A-101, Gunma, Ota-Shi, Japan

About the editors

Dr. Rakshit Ameta has a thoroughly first class career, securing first position in his MSc. and was awarded a Gold Medal. He was also given the Fateh Singh Award from Maharana Mewar Foundation, Udaipur for his meritorious performance. After completion of his PhD, he served in Hindustan Zinc Limited, Vedanta Group for 1 year. He has served in M.L. Sukhadia University, Udaipur; University of Kota, Kota, PAHER University, Udaipur, and presently is at J.R.N. Rajasthan Vidyapeeth (Deemed to be University) Udaipur. Under his supervision 12 PhD students have been awarded PhDs on various aspects of Green Chemistry. He has around 140 research publications to his credit in journals of national and international repute. He has a patent to his credit as well. He is a reviewer of around 50 international journals. Dr. Rakshit has successfully organized many National Conferences at University of Kota, Kora; PAHER University, Udaipur; and J.R.N. Rajasthan Vidyapeeth, Udaipur. He has delivered Invited lectures and chaired sessions in 20 national conferences in different parts of the country. Dr. Rakshit has served as a council member (2011−13 and 2020−22) and associate editor, Physical Chemistry Section (2014−16), scientist-in-charge in the Industrial and Applied Chemistry Section (2014−2016) of the Indian Chemical Society, Kolkata, and executive council member (2012−14) and Zonal Secretary (2016−18) of Indian Council of Chemists, Agra. He had been a recipient of the Dr. U.C. Pant Memorial Award, Indian Chemical Society, Kolkata. He has written six books published by Taylor & Francis, UK; Academic Press, Elsevier; Apple Academic Press, and a number of chapters in books by these publishers and also Nova Publishers; Trans-Tech Publications, Springer, etc. His main research focus is on photochemistry, green chemistry, microwave-assisted reactions, environmental chemistry, wastewater treatment, nanochemistry, solar cells, bioactive & conducting polymers.

Dr. Jayesh P. Bhatt received his MSc. from RSTM Nagpur University in 2011. He was awarded his PhD in the year 2019 from PAHER University, Udaipur. Since 2019 he has been working as an assistant professor in the Department of Chemistry, PAHER University, Udaipur. He has done research in the field of nanomaterials, particularly quantum dots, wastewater treatment, etc. Dr. Jayesh has published 11 research articles in journals of

national and international repute and contributed 12 chapters. Currently four PhD students are working under his supervision. He has been honored with the Young Scientist Award at an international conference in 2018, Best Poster Presentation in 2019, Best Oral Presentation in 2020, and Senior Scientist Award for Best Oral Presentation in an international conference (2021).

Prof. Suresh C. Ameta obtained his master's degree from the University of Udaipur and was awarded a gold medal in 1970. He obtained his PhD degree from Vikram University in 1980. He has served as professor and head, Department of Chemistry, North Gujarat University Patan (1994) and M.L. Sukhadia University, Udaipur (2002−05) and head, Department of Polymer Science (2005−08). He also served as dean, P.G. Studies for a period of 4 years (2004−08) in M.L. Sukhadia University, Udaipur and dean, Faculty of Science, PAHER University (2011−18). Now, he is serving as professor of eminence (distinguished professor), Faculty of Science, PAHER University, Udaipur. Prof. Ameta has around 50 years of experience of teaching and research. He has successfully guided 108 students through their PhDs. Prof. Ameta has occupied the prestigious position of President, Indian Chemical Society, Kolkata (2000−01) and is now a lifelong advisor. He was awarded a number of prizes during his career, including the National prize twice for writing chemistry books in Hindi, Prof. M.N. Desai Award, Prof. W.U. Malik Award, Scientist of the Year Award, National Teacher Award, Prof. G.V. Bakore Award, and above all, Life Time Achievement Awards from the Indian Chemical Society (2011), Kolkata, Indian Council of Chemists, Agra (2015) and Association of Chemistry Teachers, Mumbai (2018). Dr. Ameta has more than 400 research papers and 36 books to his credit. He has contributed chapters in books published by Trans-Tech, Switzerland; Nova Science; Taylor & Francis; Elsevier; Springer; and Apple Academic Press. He has 12 books to his credit, including Green Chemistry, Microwave Assisted Organic Synthesis, Solar Energy Conversion and Storage, Group Theory, Photocatalysis, Storage, Advanced Oxidation Processes for Waste Water Treatment, Sonochemistry, etc. The Indian Chemical Society, Kolkata published a special issue of the Journal of Indian Chemical Society on his 60th birthday in 2008 and also instituted a National Prize in his honor as the Prof. Suresh C. Ameta Award to be given to a Senior Scientist of the country from 2003 onwards.

Preface

Nanomaterials have revolutionized many research areas due to their unique optical, electronic, and other properties. Quantum dots have lower dimensions (2−10 nm) in the nanometric range. These quantum dots have a high surface area-to-volume ratio, a quantum confinement effect, and surface Plasmon resonance. As such they have great potential for applications in different fields. The present book is divided into three parts. First, it deals with the basics or fundamentals of quantum dots, while the second part is devoted to various methods of synthesizing quantum dots, including hydrothermal, sol−gel, laser ablation, coprecipitation, biogenic, microwave-assisted, and sonochemical. The third part of the present book is devoted to the possible applications of quantum dots in these areas, such as photocatalysis, solar cells, light-emitting diodes, sensors, photosplitting of water, targeted drug delivery, cancer therapy, etc. The time is not far off when quantum dots will find a firm footing, and they will be considered a miracle particle in the years to come.

Rakshit Ameta
Jayesh P. Bhatt
Suresh C. Ameta

This page intentionally left blank

Chapter 1

Introduction

Suresh C. Ameta
Department of Chemistry, PAHER University, Udaipur, Rajasthan, India

1.1 Introduction

The materials in the nanorange (1−100 nm) are termed as nanomaterials. There are some nanostructured materials with size in the 2−10 nm range, such nanomaterials are called quantum dots. The name quantum dot was given because it is a tiny speck of matter (2−10 nm), which is very small, just like a single point or dot. In other words, it is considered zero-dimensional. The particles inside the quantum dot that carry electricity (electrons and holes) are trapped (constrained) and have well-defined energy levels, following the laws of quantum theory just like individual atoms. There are a few dozen to hundreds or a few thousand atoms. Although these quantum dots are nanocrystals, they behave more like individual atoms; therefore, they have been nicknamed artificial atoms also.

Quantum dots have quantized energy levels. On excitation an electron in the quantum dot jumps to a higher energy level. When this excited electron returns to a lower level, the quantum dot emits a photon of light with the same energy as was originally absorbed. The color of the emitted light depends on the energy levels and it varies from one quantum dot to another. The energy levels of quantum dots are governed by their size and not the substance from which it was made. The quantum dots and their application have been excellently reviewed by different researchers (e.g., Jamieson et al., 2007; Jacak et al., 2013; Michler, 2003; Wu et al., 2019; Molaei, 2019; Divsar, 2020; Nair et al., 2020; Abd Rani et al., 2020; Vyas et al., 2021).

A small quantum dot has a longer bandgap, and hence it requires more energy to excite its electron. As the frequency of emitted light is proportional to the energy, smaller quantum dots emit radiation of higher energy or frequency, that is, shorter wavelengths, while larger quantum dots have closely spaced energy levels and emit photons of lower energy or frequency, that is, longer wavelengths. It means that as the size of quantum dots increases, the quantum dot will emit photons with lower energy or frequency and higher wavelength and vice versa. This is presented in Fig. 1.1.

Quantum Dots. DOI: https://doi.org/10.1016/B978-0-12-824153-0.00001-X

When the size of the quantum dot is greater (diameter 5−6 nm), then it will emit radiation of larger wavelengths with orange or red colors. On the other hand, if the size of quantum dot is smaller (diameter 2−3 nm), then it will emit radiation of shorter wavelengths with blue and green colors. But the actual color depends on the exact size and composition of the quantum dots. Accordingly, a change in color can be observed as the particle size of quantum dots varies. This is clearly visible in Fig. 1.2.

1.1.1 Advantages

These are some advantages of quantum dots and these are:

- High quantum yield
- High photostability
- Symmetric and narrow peak of emission

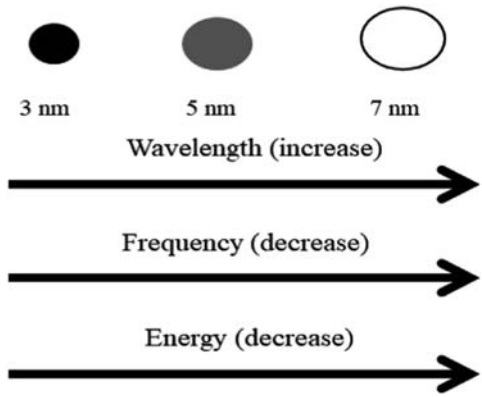

FIGURE 1.1 Relationship between size of quantum dots, energy or frequency of emitted light, and wavelength of radiation.

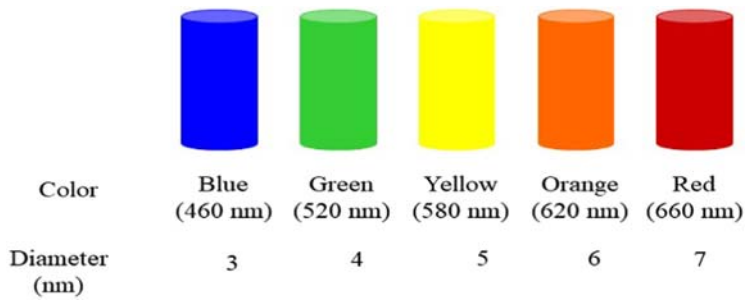

FIGURE 1.2 Change in color with size of quantum dots.

- Longer lifetime
- Possibility to control emission by changing the size and structure of quantum dots
- Brightness
- Resistance to photobleaching as compared to organic fluorophores
- Required small amount of energy for excitation (blue or UV radiation)

1.1.2 Disadvantages

Apart from the advantages, there are some disadvantages of quantum dots such as:

- High toxicity, when used in vivo
- Decline of fluorescence exponentially
- Blinking of quantum dots makes them invisible sometimes
- Quantum yield deterioration
- Extended lifetime may create a problem when rapid degradation is required

1.2 Unique features of quantum dots

Various properties of nanomaterials or quantum dots change as their size is changed. At this stage, the percentage of atoms available at the surface of a semiconducting material becomes quite significant. There are three main factors that are considered responsible for some unique properties in nanomaterials as well as quantum dots, which are significantly or totally different from their counterpart micro-, macro-, or bulk materials. These are:

1.2.1 High surface-to-volume ratio

As the size of the particle approaches a few nm, the surface area-to-volume ratio and surface-to-bulk atom ratio both increase dramatically. Depending on the composition and structure of the material used to produce nanoparticles or quantum dots, properties like absorption or emission wavelength, solubility, transparency, color, catalytic behavior, conductivity, melting point, etc. are changed only by variation in the size of the particle. It leads to some interesting behaviors of quantum dots.

1.2.2 Surface plasmon resonance

Surface plasmon resonance (SPR) is the collective oscillation of valence electrons in a solid stimulated by incident light. Such a resonance condition is established whenever the frequency of light photons matches the natural frequency of oscillating surface electrons against the restoring force of the positive nuclei. This SPR in nanometric structures is termed as localized

SPR (LSPR). LSPRs are collective oscillations of electron charge in metallic nanoparticles or quantum dots that are excited by light. Solutions containing nanoparticles or quantum dots of metals (gold, silver, etc.) are colored due to the SPR of the particles. Some properties like conductivity, dispersible nature, catalytic behavior, optical properties, etc. change with different surface properties of the particle.

1.2.3 Quantum confinement effect

The quantum confinement effect can be observed once the diameter of any material reaches the same magnitude as the de Broglie wavelength of an electron wave function. When materials are so small, their electronic and optical properties deviate substantially from those of bulk materials. Here, energy levels are not continuous but are quantized, that is, discrete, and therefore these materials in the range of nanosize or the size of quantum dots exhibit the quantum confinement effect.

1.3 Classification of quantum dots

Quantum dots are classified mainly into three types and these are:

- core-type quantum dots,
- core−shell quantum dots (CSQDs), and
- alloyed quantum dots.

1.3.1 Core-type quantum dots

These quantum dots can be single component materials, which have uniform internal compositions. The properties of these core-type nanocrystals such as photo- and electroluminescence can be fine-tuned just by simply changing the crystallite size. The examples of core-type quantum dots are chalcogenides (sulfides, selenides, or tellurides) of metals like cadmium, zinc, or lead (Fig. 1.3).

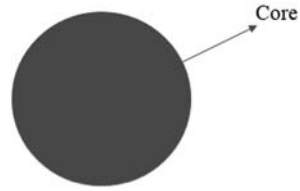

FIGURE 1.3 Core-type quantum dots.

1.3.2 Core–shell quantum dots

The luminescent properties of quantum dots are due to recombination of electron–hole pairs (excitons) through radiative pathways. The decay of an exciton can also occur via nonradiative methods, which reduces the fluorescence quantum yield. One of the possible methods to improve efficiency and brightness of these nanocrystals is to grow a shell of a semiconducting material with higher bandgap around it. Such particles, where small regions of one material are embedded in another with a wider bandgap, are termed CSQDs or core–shell semiconducting nanocrystals (Fig. 1.4). If the order is reversed, then they are called reverse type quantum dots, where a shell is inside the core structure (Fig. 1.5). Coating of quantum dots with some shells improves the quantum yield just by passivizing nonradiative recombination sites. This also makes them more robust to processing conditions, so that they can find use in various applications. CSQDs are classified into two types:

- Core–shell type-I quantum dots (Figs. 1.6 and 1.7)
- Core–shell type-II quantum dots (Figs. 1.8 and 1.9)

1.3.3 Alloyed quantum dots

Although electronic and optical properties of a quantum dot can be tuned by just changing its crystallite size, even then some problems are faced in many applications wherever there are some restrictions on size. Properties of

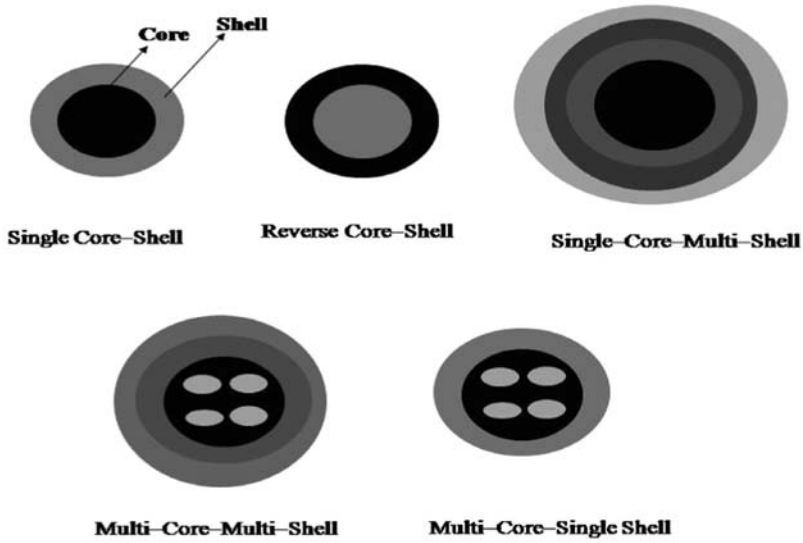

FIGURE 1.4 Core–shell type quantum dots with various arrangements of core–shell.

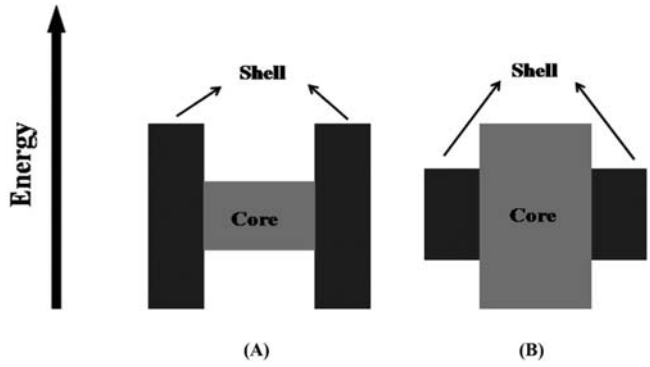

FIGURE 1.5 Core−shell type−I: (A) normal, and (B) reversed quantum dots.

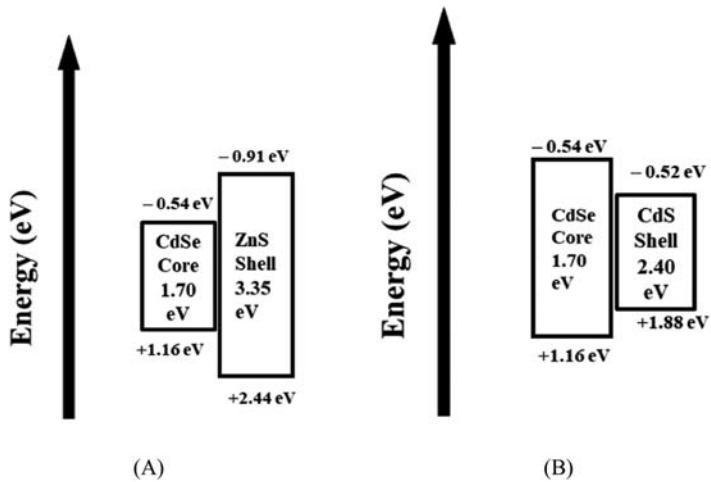

FIGURE 1.6 Energy diagram of core−shell type−I: (A) normal and (B) reversed quantum dots.

quantum dots having multicomponents can be tuned without any change in crystallite size. Such multicomponent systems are called alloyed quantum dots (homogeneous and gradient internal structures) and it is possible to tune their electronic and optical properties by changing their internal structure and composition. These alloyed quantum dots are fabricated by alloying any two semiconductors with different bandgaps (Fig. 1.9). These quantum dots show some interesting properties, which are sometimes very different from the properties of their original bulk counterparts or parent semiconductors. They can be homogeneous in nature or with a particular zone rich in a specific element.

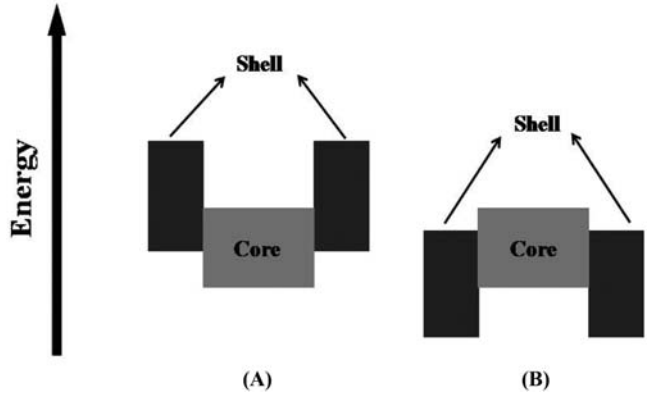

FIGURE 1.7 Core–shell type–II quantum dots. (A) Both the bands (conduction and valence) of shell are higher than core and (B) Both the bands of shell are lower than the core.

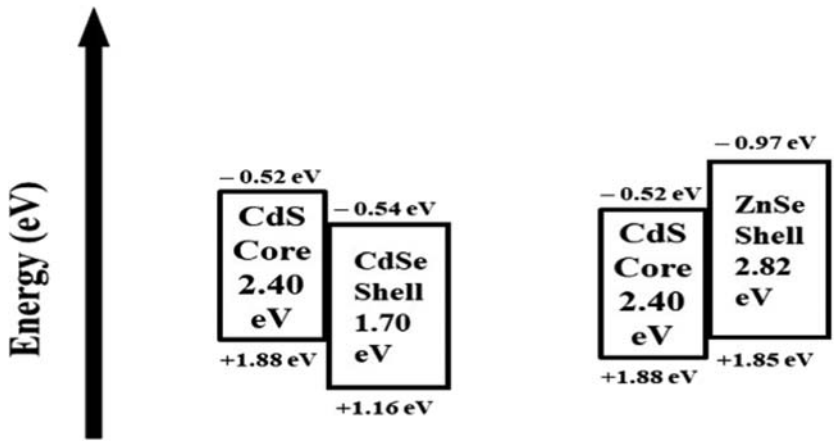

FIGURE 1.8 Energy diagram of core–shell type–II quantum dots.

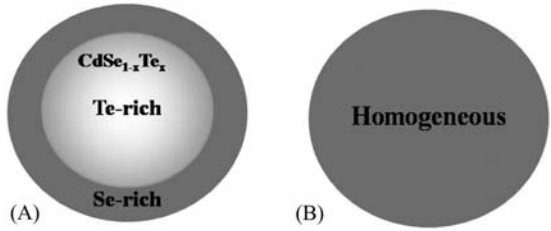

FIGURE 1.9 (A) Specific element (Te- or Se-) rich alloyed quantum dots, and (B) homogeneous alloyed quantum dots.

1.4 Synthesis of quantum dots

A number of routes have been developed for the synthesis of QDs with controlled size, shape, structure, and dimensionality, but generally used techniques are categorized into two approaches:

- top-down approach; and
- bottom-up approach.

New physical properties and applications of nanomaterials are only possible when nanostructured materials are made available with the desired size, shape, morphology, crystal structure, and chemical composition.

1.4.1 Top-down approach

The top-down approach involves breaking the bulk material into nanosized structures or particles. This approach is based on physical methods (Fig. 1.10). These are nothing but an extension of those methods, which are used for producing micro-sized particles. Top-down approaches are relatively simpler as they depend either on the removal/division of the bulk material or on miniaturization of any bulk process of fabrication to produce the nano-desired structures. But there is a problem with this approach, that is, the surface structure prepared is imperfect in nature. Nanostructured materials prepared by this approach are not smooth and have structural defects on the surface and also contain a number of impurities. Examples of such top-down techniques are high-energy wet ball milling, laser ablation, electron beam lithography, liquid phase exfoliation, atomic force manipulation, gas-phase condensation, and aerosol spray.

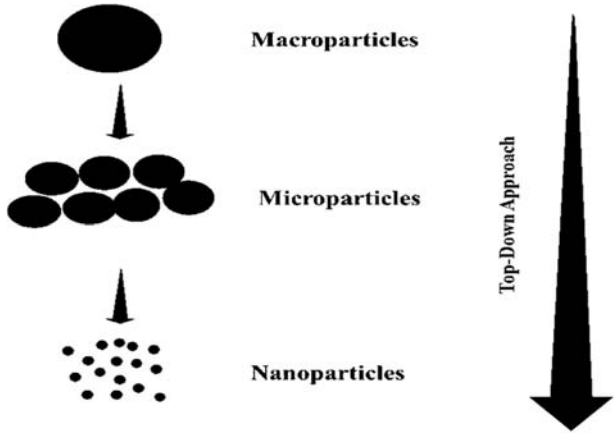

FIGURE 1.10 Top-down approach.

1.4.2 Bottom-up approach

Another approach for this purpose is the bottom-up approach (Fig. 1.11). These are mostly chemical-based methods. These are economical also. This approach builds up a material starting from the bottom, that is, atom-by-atom, molecule-by-molecule, cluster-by cluster, etc. Some of the examples are sol−gel synthesis, hydrothermal synthesis, electrodeposition, organometallic chemical route, reverse-micelle route, colloidal precipitation, and template-assisted sol−gel.

1.4.3 Methods of synthesis

Different methods are available for the synthesis of quantum dots. These are:

- Hydrothermal method
- Sol−gel method
- Laser ablation method
- Coprecipitation method
- Biogenic method
- Microwave-assisted method
- Sonochemical method

1.5 Applications of quantum dots

Although there are numerous applications of quantum dots covering a wide range, the main applications include:

- Solar cells
- Biolabeling
- Bioimaging

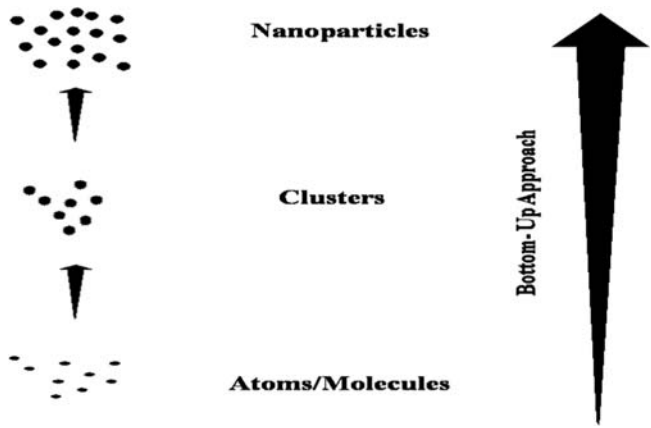

FIGURE 1.11 Bottom-up approach.

- Cancer therapy
- Chemical and biosensors
- Microscopy
- Lasers
- Inkjet printing
- Spin coating
- Photosplitting of water to generate hydrogen
- Light-emitting diodes
- Wastewater treatment using photocatalysts
- Photothermal and photodynamic therapy
- Targeted drug delivery,

This list is not complete and many more new applications will emerge in years to come. Some major applications of quantum dots are depicted in Fig. 1.12.

1.5.1 Solar cells

The world is facing a scarcity of energy resources, as the conventional fuels are either exhausted or reaching an end within the coming few decades. Therefore, there is an urgent demand to search for or to develop some new alternate resources, which are likely to fulfill the demand of the society in forthcoming years. Many attempts have been made in this direction, where sunlight has been used as the source of energy to generate electrical energy.

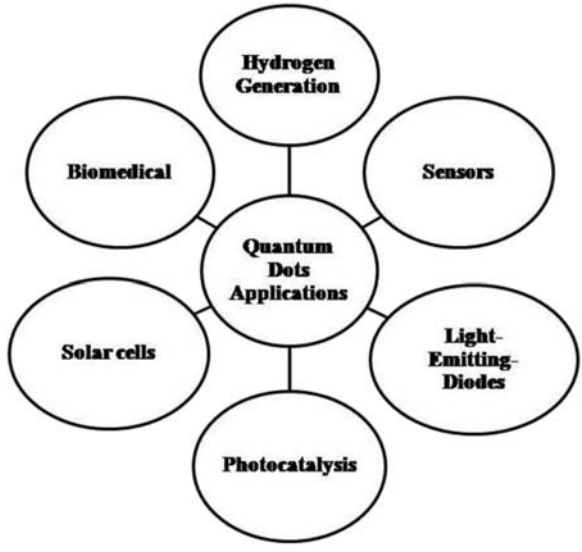

FIGURE 1.12 Different major applications of quantum dots.

It is very important to find some low-cost materials for the conversion and storage of solar energy with good conservation efficiency and long-term storage. Various solar cells are available, such as photovoltaic cells, photogalvanic cells, dye-sensitized solar cells, etc. Nanomaterials are already in use in solar cells, but now quantum dots are also being utilized in some solar cells to increase the efficiency of these cells and prolong their lifetime. Quantum dots sensitized solar cells have become a topic of interest these days, because of some unique properties of quantum dots. The use of pervoskites has also added a new dimension to the field of solar cells.

1.5.2 Sensors

Sensing a particular material or conditions has become a field of general interest in society. There is a long history for developing different and active sensors that can sense the presence of harmful chemicals; but now the presence of nanomaterials or quantum dots has added newer dimensions to the field of sensors. Sensing a specific chemical at ppm or sometimes even at ppb level has become possible by the use of quantum dots, for example, alcohol, ammonia, pesticides, carbon dioxide, nitrogen peroxide, hydrogen sulfide, liquefied petroleum gas (LPG) commonly used drugs (antibiotics, antiseptic, antiinflammatories, antipyretics, etc.), etc. Apart from this, these quantum dots also sense any small variation in the surroundings or environment (chemical and biological) and these can be used for measuring the temperature and humidity of a particular room or area.

1.5.3 Light emitting diodes

Whenever current flows in a semiconductor, electrons and holes recombine. As a result, energy is released in the form of photons. Thus the semiconductor becomes a light source and it is called a light-emitting diode light. Quantum dots are used in fabricating such light-emitting diodes. They can give a variety of colors: green, blue, red, orange, yellow, etc. apart from white. This color depends on the bandgap of that semiconductor, that is, corresponding to the energy of photons. Normally, electrical energy is first converted into heat then into light, but light-emitting diodes convert electrical energy directly into light so that no or negligible electricity is wasted in the form of heat. LEDs find application in a number of areas such as display and lighting (different colors), night vision (security cameras), data communication, agriculture and horticulture (plant growth and improved crop production), antimicrobial properties, etc.

1.5.4 Photocatalysis

Photocatalysis has a beauty in that it can provide the oxidizing as well reducing environment simultaneously in the same vessel, which is not otherwise

possible with any oxidant or a reductant, which gives only one kind of environment. Instead, the oxidant and reductant will react (if both are present there) with each other rather than attacking a particular molecule or entity. It can generate a very strong oxidizing species, hydroxyl radicals in the majority of cases, which are quite effective in degrading the organic pollutants to less harmful or almost harmless end products. Thus the use of quantum dots in photocatalytic degradation can be useful in the complete mineralization of water and air contaminants like dyes, pharmaceuticals, pesticides, nitro and chloro compounds, endocrine-disrupting chemicals, phenols, carbon dioxide, carbon monoxide, nitrogen dioxide, etc. Not only this, quantum dots are now utilized in the photoreduction of carbon dioxide to some useful chemicals, which can be used as synthetic fuels such as methanol or methane. This will solve the problem of the energy crisis on one hand and decrease the amount of carbon dioxide in the atmosphere; thus placing a control on the ever increasing global warming.

1.5.5 Hydrogen generation

The shortage of natural energy resources is becoming a burning problem in the world these days and it is likely to increase exponentially in the coming future. The requirement for energy is regularly increasing and it will be very difficult to depend for a long time on the natural fuels such as wood, coal, kerosene, diesel, petrol, natural gas, or LPG, and therefore there is a pressing demand that some alternative should be developed that can fulfill the demand for energy from society in coming decades. Here, hydrogen enters the scene, It has a high energy storage capacity and can be used as an alternative fuel. It has been predicted to be the fuel of the future. It is presently produced by the consumption of electricity, which is a costly affair. It has been advocated that hydrogen should be generated by the splitting of water photocatalytically in the presence of a light source, and the most preferred one is sunlight, as it freely available at present and it is inexhaustible also. It can be utilized as a source of energy for the future at relatively low cost. The source of hydrogen is water, which is abundantly available, covering almost three-fourths of the Earth, and the final product of its combustion is water again, which is harmless Now, quantum dots are being used in photocatalytic splitting of water to produce hydrogen with relatively high efficiency.

1.5.6 Biomedicals

Quantum dots have great potential for application in the biomedical and biotechnology fields because of their smaller size and other unique properties. They can pass the blood−brain barrier and also can cross the cell boundaries in some cases. These can be used for the diagnosis of a particular disease at earlier stages and hence help in timely treatment. Quantum dots are also

used in targeted drug delivery so that a drug can be supplied to a specific organ or location and as a result, the healthy cells or other parts are not affected adversely. This will increase the efficacy of that drug. They have a bright future in combating dreadful diseases like cancer. They are also effectively utilized in biolabeling and bioimaging processes.

1.6 Conclusion

Quantum dots have certain unique features, such as large surface area-to-volume ratio, quantum confinement effect, and SPR. These make quantum dots quite interesting for possible application in a variety of fields. They are used as photocatalysts for degradation or the removal of a variety of environmental pollutants to smaller fragments, which are almost harmless, reduction of carbon dioxide curbing the ever increasing global warming, photosplitting of water generating hydrogen (the fuel of future), light emitting diodes (display, lighting, plant growth, improved crop production, night vision, antimicrobial activities), biolabeling, bioimaging, targeted drug delivery, solar cells, cancer therapy, sensing a particular compound in very low concentrations (ppm or even sometimes ppb also), etc. Quantum dots will find many more useful applications in the years to come.

References

Abd Rani, U., Ng, L.Y., Ng, C.Y., Mahmoudi, E., 2020. A review of carbon quantum dots and their applications in wastewater treatment. Adv. Colloid Interface Sci. 278. Available from: https://doi.org/10.1016/j.cis.2020.102124.

Divsar, F. (Ed.), 2020. Quantum Dots: Fundamental and Applications. IntechOpen, London.

Jacak, L., Hawrylak, P., Wojs, A., 2013. Quantum Dots. Springer Science & Business Media, Berlin/Heidelberg.

Jamieson, T., Bakhshi, R., Petrova, D., Pocock, R., Imani, M., Seifalian, A.M., 2007. Biological applications of quantum dots. Biomaterials 28 (31), 4717–4732.

Michler, P., 2003. Single Quantum Dots: Fundamentals, Applications and New Concepts. Springer Science & Business Media, Berlin/Heidelberg.

Molaei, M.J., 2019. A review on nanostructured carbon quantum dots and their applications in biotechnology, sensors, and chemiluminescence. Talanta 196, 456–478.

Nair, A., Haponiuk, J.T., Thomas, S., Gopi, S., 2020. Natural carbon-based quantum dots and their applications in drug delivery: a review. Biomed. Pharmacother. 132. Available from: https://doi.org/10.1016/j.biopha.2020.110834.

Vyas, Y., Chundawat, P., Dharmendra, D., Punjabi, P.B., Ameta, C., 2021. Review on hydrogen production photocatalytically using carbon quantum dots: future fuel. Int. J. Hydrog. Energy 46 (75), 37208–37241.

Wu, H.L., Li, X.B., Tung, C.H., Wu, L.Z., 2019. Semiconductor quantum dots: an emerging candidate for CO_2 photoreduction. Adv. Mater. 31 (36). Available from: https://doi.org/10.1002/adma.201900709.

This page intentionally left blank

Chapter 2

Hydrothermal synthesis of quantum dots

Jayesh P. Bhatt and Neha Godha
Department of Chemistry, PAHER University, Udaipur, Rajasthan, India

2.1 Introduction

The term "hydro" means water and "thermal" means heat. This word was first used by the British geologist Sir Roderick Murchison (1841). The action of water at high temperature and pressure has been considered responsible for changes in the Earth's crust, and it leads to the formation of various minerals and rocks. The first report on hydrothermal synthesis was of tiny quartz crystals by freshly precipitated silicic acid (Schafthaul, 1845). Now this term refers to any heterogeneous reaction that is carried out in the presence of aqueous solvents under high temperature and pressure conditions. Artificial diamond was also synthesized by Hannay (1880) using the hydrothermal method and Moissan (1893) also claimed to synthesize artificial diamond.

It is interesting to note that the hydrothermal method keeps a good control on composition and porosity. It is known that materials having high vapor pressure near this melting point normally form nanoparticles (NPs) by this method only. The solvothermal method is almost similar to the hydrothermal method but the only difference is in the wetting liquid, which is usually an organic solvent in place of water. The hydrothermal technique is used in a variety of fields, like chemistry, material science, biology, etc.

The hydrothermal conditions (high pressure and temperature) require a reaction vessel for crystal growth, which is called an autoclave. As some highly corrosive salts are used in the hydrothermal method to synthesize inorganic materials for a longer period reaction time, an autoclave must be able to sustain these highly corrosive materials at high pressure and temperature. The corrosion resistance is the most important property required in the material of the autoclave. Such corrosion-resistant

Quantum Dots. DOI: https://doi.org/10.1016/B978-0-12-824153-0.00002-1

materials include the following materials such as high-strength alloys, stainless steel, iron, titanium, nickel, and cobalt-based alloys. An autoclave is also coated inside with a non-reactive material to avoid corrosion; the most suitable material is Teflon (tetrafluoroethylene). As the Teflon has a larger coefficient of thermal expansion compared with the material enclosed within the liner, the coating of Teflon will expand and contract much more on heating and cooling than the reacting materials present inside the autoclave.

A good hydrothermal autoclave should have the following properties:

- It is inert to acids, bases, and oxidizing agents.
- It should be easy to assemble and dissemble.
- It should have a sufficient length to obtain a desired temperature gradient.
- It should be leakproof at desired temperature and pressure.
- It should bear high pressure and temperature for a longer duration of time.
- Reaction can be carried out under mild hydrothermal conditions of temperature less than 300°C and pressure 250 bars.

Parts of the Teflon-coated autoclave are presented in Fig. 2.1.

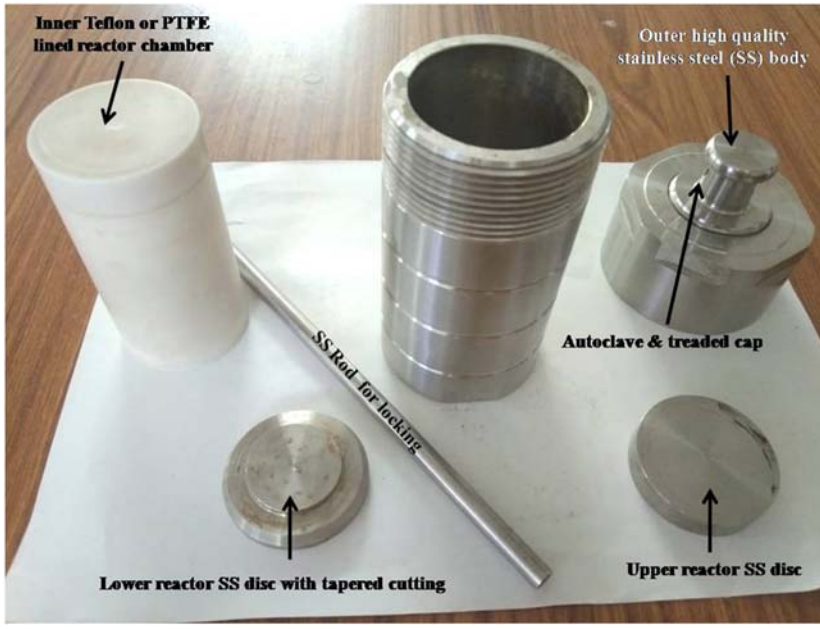

FIGURE 2.1 Teflon-lined autoclave reactor.

2.1.1 Advantages

The following are the advantages of hydrothermal synthesis:

- This method has the ability to create crystallize phases, particularly those that are not stable at the melting point.
- The material having high vapor pressure near its melting point can also be grown by this method.
- This method is suitable for the growth of large and good-quality crystals with a control on their composition.
- Relative cost is lower for this method compared with others.
- The hydrothermal method is more eco-friendly (green) than other methods of synthesis.
- It requires low temperatures, which avoids the problems encountered with high-temperature processes.
- It regulates the uniformity of nucleation, rate growth, aging, etc., which affect morphology, size, and aggregation. Various particle sizes and morphologies can be obtained with the hydrothermal method.
- Materials prepared by this method exhibit differences in point defects as compared with high-temperature synthesis. There are no Schottky defects in tungstates of Ca, Ba, and Sr prepared by this method, which are normally present in these compounds prepared at high temperatures.
- This method can be used in combination with other methods such as microwave, ultrasound, mechanochemistry, electrochemical, etc.

2.1.2 Disadvantages

- One of the major disadvantages of this method is that it needs expensive autoclaves.
- It is not possible to observe the crystal growing inside a steel tube.
- Now autoclaves made of thick-walled glass are used up to 300°C and 10 bar.
- The greatest disadvantages of Teflon lining is that beyond 300°C, it cannot be used because Teflon dissociates, which affects the pH of neutral solutions. This coating tends to get torn and generally must be replaced after experiments.

2.2 Metal-based quantum dots

2.2.1 Metal oxide quantum dots

A simple hydrothermal approach was used by Zhu et al. (2006) for synthesis of SnO_2 quantum dots. Here, hydrazine hydrate was used as the mineralizer and not the commonly used NaOH. The diameters of the SnO_2 NPs were determined to be in the range of 2.3−3.1 nm. A blueshift was observed of

0.28 eV and the bandgap of as-prepared SnO_2 QDs was found to be 3.88 eV. A biomolecule-assisted hydrothermal route was used by Wu et al. (2009) for generating SnO_2 QDs (diameters 10 nm). These were used for photocatalytic degradation of rhodamine B in a basic medium, where its degradation reached almost 100% within 150 min.

Wei et al. (2010) made use of WO_{3-x} QDs (nonstoichiometric) in combination with silver nanowires (Ag NWs) and reported that the incident photon-to-electron conversion efficiency (IPCE) can be increased by 8.5% and dye degradation improved by 40% with the sample $WO_{2.72}$ QD@Ag NW composite.

Perera et al. (2012) prepared TiO_2 nanotube (TNT)/reduced graphene oxide (rGO) composites using an alkaline hydrothermal process. They could achieve this by decorating graphene oxide (GO) layers on TiO_2 NPs. The TiO_2 NPs were found to be small in diameter ($\sim$9 nm). As-prepared composites were used for the photodegradation of malachite green. It was observed that composite with 10% rGO showed the highest photocatalytic activity, which was almost three times higher than pure TNTs.

The Mg-doped VO_2 NPs were synthesized by Zhou et al. (2013) via a hydrothermal method. It was reported that optical bandgap changed from 2.0 eV for pure VO_2 to 2.4 eV on 3.8% Mg doping. Yao et al. (2017) fabricated $CoFe_2O_4$ quantum dots/N-doped graphene ($CoFe_2O_4$ QDs/N-G) composites using the hydrothermal process followed by calcination at high temperatures. It was observed that NPs were homogeneously anchored on the surfaces of graphene sheets and the size of $CoFe_2O_4$ QDs was within 4−12 nm. It was reported that as-obtained $CoFe_2O_4$ QDs/N-G can be used as anode material for lithium-ion batteries (LIBs) with an initial discharge capacity of 1616 mAh g^{-1} maintaining a reversible capacity of 1223 mAh g^{-1} even after 90 cycles at a current of 100 mA g^{-1}.

Ma et al. (2017) observed the effects of N doping on the deposition of $ZnCo_2O_4$ QDs on rGO nanosheets. It was reported that as-prepared $ZnCo_2O_4$ QDs decorated on nitrogen-doped graphene (NG) were 4.3 ± 0.9 nm in diameter and were well-dispersed on the surface. It was indicated that as-obtained $ZnCo_2O_4$/NG hybrids can be used as a battery-type electrode for a hybrid supercapacitor and can deliver high specific capacity, outstanding rate capability, and excellent cycle performance of 301.8 C g^{-1} at 1 A g^{-1}, 84.5% remaining at 30 A g^{-1} and 89.1% after 5000 cycles, respectively.

Min et al. (2017) used a one-step hydrothermal route for preparing GQDs coupled with TiO_2 in the form of composite (TiO_2/GQDs) photocatalysts. They used 1,3,6-trinitropyrene (TNP) as the precursor of GQDs. Here, GQDs act as a photosensitizer as well as an excellent electron acceptor and this composite exhibited a seven times higher evolution rate of H_2. A highly efficient ternary photocatalytic nanocomposite, $ZnFe_2O_4/TiO_2$/CDs, was synthesized by Lu et al. (2018) through a hydrothermal method. This composite was used in the decomposition of rhodamine B. It was also revealed that it

retained its photocatalytic efficiency even after four cycles. A wide range of transition metal-doped TiO_2 (metal/TiO_2) (where M = Co, Ag, Cu, Au, Cr, Ni, Fe, Pt, Pd, and Zn) was prepared by Wu et al. (2018) combining the hydrothermal synthesis with air-thermal treatment. It was observed that 0.5 mol.%-Cu/TiO_2 NFs exhibited the highest photocatalytic activity in the production of hydrogen (208 $\mu mol^{-1}\ h^{-1}$).

SnO_2 QDs/TiO_2 NPs composite was prepared by Jat et al. (2019) via a hydrothermal method. They used stannic chloride (hydrate) as a precursor for SnO_2 quantum dots. It was observed that the photocatalytic activity of the composite was more than titania nanopowder for the degradation of fast green. The effects of various parameters like pH, the concentration of dye, amount of catalyst, and light intensity on the rate of degradation was also studied. It can be a promising method for wastewater treatment. A simple hydrothermal route was reported by Liu et al. (2019a,b) for the synthesis of tungsten oxide quantum dots (WO_{3-x} QDs). They used ammonium tungstate hydrate as a precursor and polyvinyl pyrrolidone. It was reported that this material is photochromic in nature and changes color in the presence of UV or sunlight.

2.2.2 Metal sulfide quantum dots

Zhao et al. (2009) selected thiol ligand, N-acetyl-l-cysteine as a stabilizer for the synthesis of high-quality NIR-emitting CdTe/CdS QDs by an hydrothermal route. It was reported that as-prepared NIR-emitting CdTe/CdS QDs exhibited high photoluminescence quantum yields (45% − 62%) and good photostability. It was also suggested that as-prepared QDs can be used for bioimaging as they have biological compatibility and excellent water solubility. Liu et al. (2012) synthesized water-soluble high-quality ternary $CuInS_2$ quantum dots via hydrothermal synthesis. They used mercaptopropionic acid (MPA) as the stabilizer. It was observed that it can be used to label liver cancer cells. It was also revealed that as-synthesized near-infrared (NIR) $CuInS_2$ QDs have excellent photostability.

The CdSeS quantum dots with diameter of 4.5 nm were prepared by Santra and Kamat (2013), which were highly luminescent. They observed maximum power conversion efficiencies of 3.2% and 3.0% in two- and three-layered tandem quantum dots solar cells, respectively. Liu et al. (2013) synthesized water-soluble $CuInS_2$ ternary quantum dots in aqueous solution, which was capped by MPA. The $CuInS_2$ QDs were covalently linked to 3-aminophenylboronic acid molecules to get functionalized $CuInS_2$ QDs (F-$CuInS_2$ QDs). These QDs were found to be reactive toward vicinal diols in alkaline solution to form five- or six- member cyclic esters.

Water-soluble Mn^{2+}-doped ZnS nanocrystals were synthesized by Zhang et al. (2014). These were surface capped with polyethylene glycol (PEG-ZnS:Mn^{2+}) in aqueous solution. It was reported that the size of particles had

an average diameter of 3 nm with a zinc blende structure. It was also revealed that as-obtained nanocrystals were water soluble and biocompatible. Han et al. (2014) prepared a ternary CdS/ZnO/graphene composite by loading ZnO and CdS NPs in graphene nanosheets using a one-step hydrothermal method. It was reported that as-prepared CdS/ZnO/graphene composite exhibited enhanced photocatalytic activity as compared to pure ZnO and CdS. It was attributed to the light absorption, efficient charge separation, and durability of the composite.

Uniform MoS_2 quantum dots were synthesized by Ren et al. (2015) via a hydrothermal route. It was reported that the as-prepared material has a monolayer thickness with an average size of 3.6 nm. A facile hydrothermal route has been also used by Wang and Ni (2014) for the synthesis of photoluminescent MoS_2 quantum dots. They used sodium molybdate and cysteine as precursors. As-prepared MoS_2 QDs were used to construct a sensor for the detection of 2,4,6-trinitrophenol (TNP) in a wide range of concentration from 0.099 to 36.5 μM with a high detection limit (95 nM). It was reported that this sensor can be applied for the detection of TNP in real samples.

Monolayer MoS_2 quantum dots with lateral size (3 nm) were prepared by Qiao et al. (2015). It was observed that the lateral size of the nanosheets decreases on increasing the number of exfoliations. It was reported that monolayer MoS_2 QDs exhibited higher hydrogen evolution reaction (HER) catalytic activities. Uniformly dispersed ZnS quantum dots (<10 nm) on graphene nanosheets were synthesized by Zhang et al. (2018) via a hydrothermal method. It was reported that as-prepared ZnS/graphene composites can be used as a dual anode for both LIB and sodium-ion batteries with excellent performance.

The Ag_2S/ Bi_4/Ti_3O_{12} heterojunction composite was prepared by Zhao et al. (2019). The Ag_2S quantum dots were assembled onto the surface of $Bi_4Ti_3O_{12}$ nanosheets. Its photocatalytic performance was evaluated for photocatalytic degradation of rhodamine B in aqueous solution under simulated sunlight. It was found that 15 wt.% Ag_2S $Bi_4Ti_3O_{12}$ composite exhibited the highest photocatalytic activity, which was about 2.8 and 4.0 times higher than that of pure $Bi_4Ti_3O_{12}$ and Ag_2S, respectively. This enhanced activity was explained on the basis of Z-scheme electron transfer from $Bi_4Ti_3O_{12}$ (conduction band) to Ag_2S (valence band).

Zeng et al. (2019) synthesized flower-like $MoS_2/Ag_2S/Ag$ nanocomposites. It was reported that as-prepared $MoS_2/Ag_2S/Ag$ nanocomposites can be used as photocatalysts for the photodegradation of tetracycline hydrochloride and Congo red and also for the disinfection of *P. aeruginosa*. It was verified that the electron transport path is a Z-scheme system. A one-step hydrothermal approach was reported by Li et al. (2019) to synthesize water-dispersed MoS_2 quantum dots. These QDs have an ultrasmall size of ~ 3.3 nm. These were loaded on CdS nanorods and then they exhibited an enhanced HER under visible light ($\lambda > 420$ nm) (131.7 mmol h^{-1} g^{-1}), which is about 65-fold the rate of pure CdS (2.0 mmol h^{-1} g^{-1}).

2.2.3 Others

A simple hydrothermal method was developed by Wang and Han (2010) for the synthesis of water-soluble, and NIR-emitting type core−shell CdTe/CdSe quantum dots. They used $CdCl_2$ and Na_2SeO_3 and thiol-capped CdTe QDs as core templates for this purpose. It was revealed that as-prepared CdTe/CdSe QDs showed excellent photostability, good monodispersity, and hardened lattice structure which has a great potential for different biological applications.

A high-performance supercapacitor cathode electrode was developed by Xia et al. (2015). It was composed of well-dispersed $MnCO_3$ quantum dots ($\sim$1.2 nm) decorated on nickel hydrogen carbonate−manganese carbonate ($Ni(HCO_3)_2$−$MnCO_3$). It was reported that as-prepared $MnCO_3$ QDs/NiH−Mn−CO_3 composites exhibited superior supercapacitive performance, which makes them potential cathode materials to be used in high energy density asymmetric supercapacitors.

2.3 Nonmetal-based quantum dots

2.3.1 Carbon-based quantum dots

Yu et al. (2012) prepared ZnO/carbon quantum dots (ZnO/CQDs) nanocomposites by hydrothermal reaction. It was reported that as-obtained photocatalyst can be used for the degradation of toxic gas (methanol and benzene) under visible light exhibiting higher photocatalytic activity (80%, 24 h) as compared to N-doped TiO_2 and ZnO NPs. A simple one-step hydrothermal method was developed by Guo et al. (2013) for the synthesis of highly fluorescent carbon NPs (F-CNPs). It was reported that these F-CNPs exhibited excellent probe ability for the detection of mercury ions in aqueous solution with good sensitivity and selectivity.

Yu et al. (2014a,b) prepared CQDs/TiO_2 nanosheet composites by a simple low-temperature process. The photocatalytic activity of this composite was observed for the degradation of rhodamine B in the presence of visible light irradiation. CQDs modified TiO_2P25 composites (CQDs/P25) were prepared by Yu et al. (2014a,b) via hydrothermal reaction. This composite exhibited enhanced photocatalytic H_2 evolution in the presence of visible light and UV without using any noble metal cocatalyst. Here, CQDs played dual roles for improving photocatalytic activity as they act as an electron reservoir as well as for efficient separation of the electron−hole pairs.

Zhang and Chen (2014) used a hydrothermal route to prepare highly luminescent nitrogen-doped CQDs (NCQDs). They used folic acid as the source of both carbon and nitrogen. It was reported that as-prepared NCQDs have an average size of 4.5 ± 1.0 nm. It was reported that an effective quenching effect of Hg^{2+} ions was achieved, and NCQDs can detect Hg^{2+} ions with a detection limit of 0.23 μM. This type of ions sensor was

successfully applied for the determination of Hg^{2+} in real samples such as tapwater and lake water. A facile method to synthesize stable CDs was reported by Wang et al. (2015) via hydrothermal treatment using glucose in the presence of glutathione. It was reported that as-prepared CDs can be used as pH sensors. Wei et al. (2016) prepared a series of carbon dots (CDs)/$NiCo_2O_4$ composites, It was observed that these samples have good electrical conductivities and exhibited high specific capacitances, cycling stabilities, and superior rate performance. It was revealed that this hybrid supercapacitor exhibited a high energy density up to 62.0 Wh kg^{-1}.

Martins et al. (2016) prepared a new composite of TiO_2 (P25) and N-doped CQDs (P25/NCQD) via a hydrothermal method. It was then used as a catalyst for the photooxidation of NO in the presence of UV and visible light. It was reported that as-prepared P25/NCQD composite exhibited NO conversion (27.0%), which was almost 2.7 times that of P25 (10%). It was also revealed that photodegradation of methylene blue was increased from 68% to 91% on UV irradiation.

Qian et al. (2016) incorporated CQDs with Bi_2WO_6. Then these were used for photocatalytic removal of gaseous volatile organic compounds in the presence of sunlight. It was revealed that CQDs/ Bi_2WO_6 exhibited higher photocatalytic oxidation in degrading toluene and acetone under both UV and visible light.

Wu et al. (2017) synthesized NCQDs by a hydrothermal method. They used microcrystalline cellulose as a source of carbon and ethylenediamine as a nitrogen dopant. It was reported that as-obtained NCQDs particles were spherical with an average diameter of 3.2 nm. When these NCQDs were used as a fluorescent probe for the detection of Fe^{3+} via fluorescent quenching, then they could achieve high sensitivity and selectivity with a limit of detection of 0.21 nM.

A ternary composite of GO/CD/polypyrrole (GO/CDs/PPy) was prepared by Zhang et al. (2017) and then used as an electrode active material for supercapacitors. It was reported that CDs sandwiched between PPy and GO film layer can promote electron transportation in such composites and as a result, charge transfer resistance of the electrode and internal resistance are reduced. It was interesting to note that it retained excellent cycle stability even after 5000 cycles. Liu et al. (2017) monitored the effect of arginine (Arg) on the growth of gold NPs/CQDs (Au/CQDs) composite. Ethylene glycol was used as the reducing as well as stabilizing agent for the preparation of CQDs. The arginine can be detected with a low detection limit of 37 nM using this nanocomposite based on the color change.

A three-dimensional (3D) ternary graphene-CQDs/g-C_3N_4 nanosheet (GA-CQDs/CNN) aerogel was synthesized by He et al. (2018) via a hydrothermal method. It was reported that this ternary photocatalyst could improve the absorption of visible light as well as promote separation of charges. It was observed that methyl orange can be removed up to 91.1% using

GA-CQDs/CNN-24%, which was about 7.6 times more than that with bulk g-C_3N_4 (BCN).

Zhao et al. (2018) synthesized nitrogen-doped CQDs via a hydrothermal method. They used polyacrylamide as both the carbon and nitrogen source. It was reported that as-prepared NCQDs could be used as effective probes for selective and sensitive detection of dopamine with a detection limit of 0.05 μM in the concentration range of 0.1−200 μM. The proposed method was also applied for determination of dopamine in urine samples. Wang et al. (2018) reported a novel ternary photocatalyst, which comprised single atom-dispersed silver and CQDs coloaded with ultrathin g-C_3N_4 (SDAg-CQDs/UCN). It was then used for photocatalytic degradation of naproxen, which involved hydroxylation, decarboxylation, and opening of the naphthalene ring.

Liu et al. (2019a,b) prepared nitrogen and boron codoped CQDs (NB-CQDS) via a one-pot hydrothermal treatment. They used citric acid, borax, and *p*-phenylenediamine for this purpose as the source of carbon, boron, and nitrogen, respectively. It was revealed that NB-CQDs were almost monodispersed with an average particle diameter of 3.53 nm. A sensor was designed using NB-CQDs for the determination of acetone and dopamine with a limit of detection of 0.54 μM and 11 nM, respectively. Aziz et al. (2019) prepared CQDs using branched polyethyleneimine to modify these dots. It was observed that fluorescence of CDs could be efficiently quenched by mercuric ions in aqueous solution. It was revealed that this probe can be used for the detection of Hg^{2+} ions in the concentration range from 20 to 800 nM with a detection limit of 10.0 nM. It provides a simple, selective, and sensitive fluorescence probe for Hg^{2+}.

Wang et al. (2019) used biomass of cyanobacteria as a carbon source for synthesizing fluorescent and water-soluble CQDs via a hydrothermal method. It was reported that as-synthesized CQDs were found to be monodispersed with an average diameter of 2.48 nm. It was observed that as-prepared CQDs exhibited high photostability with no photobleaching, even if kept for a longer time under UV irradiation. One advantage of such CQDs is that they could illuminate the complete cell and differentiate the cytoplasm from nucleus. It was also proposed that biomass of cyanobacteria can be used to fabricate CQDs on a large scale.

Water-soluble highly green fluorescent CQDs were prepared by Dhandapani et al. (2020) via hydrothermal carbonization of cost-effective wastes of fish. It was reported that the as-synthesized sample exhibited photoluminescence with high green emission 406 at the excitation of 330 nm. The UV−Vis spectra showed the presence of two major peaks at 266 and 371, due to $\pi \rightarrow \pi^*$ and $n \rightarrow \pi^*$ transition, respectively. It was revealed that as-prepared CQDs are spherical in shape with size $\sim 6 \pm 1$ nm. It was suggested that as-synthesized CQDs may be used for water treatment and energy application.

Guo and Zhao (2020) synthesized blue emissive NCQDs via the hydrothermal treatment with a high quantum yield as high as 84.79%. They used diethylenetriamine and citric acid as a source of nitrogen and carbon, respectively. It was reported that as-prepared NCQDs exhibited good photostability, and excellent stability in high-salt conditions. It was revealed that as-prepared NCQDs can be used as potential probes for detecting ellagic acid selectively in a concentration range of 0.01−50 μM on the basis of the inner filter effect. It was suggested that there is good biocompatibility of the NCQDs, which indicates that it has a great potential for application in biomedical fields.

Khan et al. (2020) synthesized nitrogen and sulfur codoped water-soluble CQDs (NS-CQDs) via a hydrothermal route. They used L-lysine and thiourea for this purpose. It was reported that as-obtained NS-CQDs have a high quantum yield of 53.19 % with a blue fluorescence on excitation UV light (365 nm). It was revealed that NS-CQDs were spherical in shape with sizes in the range 5−8 nm (average diameter 6.86 nm). It was observed that NS-CQDs can act as a fluorescent probe for the sensitive and selective detection of picric acid in aqueous solution in the concentration range of 1−10 μM with a limit of detection as 0.24 μM. It was reported that these NS-CQDs fluorescent probes can be used to measure the concentration of picric acid in a real water sample of tapwater.

Wei et al. (2020) synthesized boron and nitrogen codoped CQDs (BNCQDs) via a microwave-assisted hydrothermal method. They used boric acid and o-phenylenediamine as the sources of boron, carbon, and nitrogen. It was reported that as-prepared BNCQDs exhibited high QY (13.79%), good biocompatibility, fluorescent stability, and low toxicity, which are necessary requirements for a cell imaging agent. It was revealed that accumulation was increased with an extension of incubation time with HeLa cells, and it was observed that BNCQDs imaging is suitable for cell morphology (Fig. 2.2).

Li et al. (2020) obtained two types of CQDs via a hydrothermal method. These CQDs had luminous peaks at 480 (blue CDs) and 525 nm (green quantum dots). These two QDs were used for the detection of Hg^{2+} ions. It was

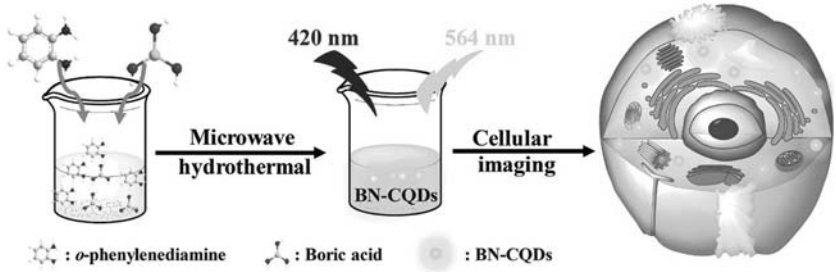

FIGURE 2.2 Synthesis of B, N-doped carbon quantum dots and their use in cellular imaging. *Adapted from Wei, Y., Chen, L., Wang, J., Liu, X., Yang, Y., Yu, S., 2020. Rapid synthesis of BN co-doped yellow emissive carbon quantum dots for cellular imaging. Optical Mater. 100. https://doi.org/10.1016/j.optmat.2019.109647. With Permission.*

observed that mixed CDs could detect Hg^{2+} ions in the range of 0−1.0 μM with a low detection limit of 0.05 μM.

Shahba and Sabet (2020) synthesized highly photoluminescence carbon nanofibers/CQDs using pine fruit via a ball milling-assisted hydrothermal method. It was revealed that the as-obtained product was composed of carbon nanofibers and very tiny nitrogen-doped CDs with a high photoluminescence intensity. The photocatalytic activity of as-prepared material was investigated by degradation of six different dyes (methyl orange, erichrome black T, acid blue, eosin Y, methylene blue, and methyl). It was also reported that it can adsorb Cd^{2+} and Pb^{2+} ions from the water with almost 100% efficiency.

Wang et al. (2020) prepared biomass CQDs via a hydrothermal process. They used four biomass wastes as a source of carbon (magnolia flower, orange peel, paulownia leaves and ginkgo biloba leaves). The as-prepared biomass CQDs exhibited homogeneous particle size, optical properties, stability, and superior water solubility. A quenching effect on fluorescence was observed on the addition of Fe^{3+} ions into CQDs solution. It was reported that as-prepared CQDs have a sensitive response to Fe^{3+} ions and these ions can be measured in the concentration range of 0.2 − 100 μM with the limit of detection of 0.073 μM (Fig. 2.3).

Sharma et al. (2020) synthesized fluorescent CQDs via a hydrothermal approach using red cabbage (rc). It was reported that as-synthesized rcCQDs were having an average size of 3 nm with blue fluorescence and quantum yield of 8.3%. It was interesting to note that rcCQDs exhibited strong antioxidant activities of 56%, 61%, and 91% against hydroxyl,2,2-diphenyl-1-picrylhydrazyl, and potassium permanganate radicals, respectively, which was almost comparable with that of L-ascorbic acid (standard antioxidant). A superior biocompatibility and negligible cytotoxicity of as-synthesized rcCQDs on SH-SY5Y neuroblastoma cells was there as evident from Cell Counting Kit−8 assay. These rcCQDs were also used as a fluorescent probe for biolabeling of *Staphylococcus aureus* and *Escherichia coli*. These rcCQDs can also be utilized as a fluorescent ink, and may found to be suitable for varnish and paints.

Chaudhary et al. (2020) synthesized highly fluorescent NS-CQDs via hydrothermal process. They used banana (*Musa acuminata*) juice as the source of carbon. It was revealed that NS-CQDs were spherical shaped with an average size of 1.27 nm, but with poor crystallinity. The proposed method

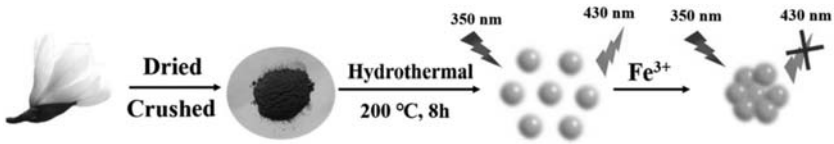

FIGURE 2.3 Preparation of quantum dots from biomass waste and detection of ferric ions. *Adapted from Wang, C., Shi, H., Yang, M., Yan, Y., Liu, E., Ji, Z., et al., 2020. Facile synthesis of novel carbon quantum dots from biomass waste for highly sensitive detection of iron ions. Mater. Res. Bull. 124, https://doi.org/10.1016/j.materresbull.2019.110730. With Permission.*

offers higher quantum yield (32%) compared to samples prepared from other natural sources. It was reported that as-synthesized NS-CQDs can be utilized as a fluorescent probe for the detection of Cu(II) in the concentration range of 1−800 μg mL^{-1} with the LOD of 0.3 μg mL^{-1} in the water sample.

2.3.2 Graphene-based quantum dots

Shen et al. (2012) prepared graphene quantum dots (GQDs) by a one-pot hydrothermal reaction. They used polyethylene glycol (PEG) and small GO sheet as the starting materials. It was reported that as-prepared GQDs-PEG exhibited luminescence properties. Tang et al. (2012) prepared crystalline GQDs that were water soluble. Glucose was used as the source of carbon. As-prepared QDs have an average diameter as small as 1.65 nm. A microwave-assisted hydrothermal method was used for this purpose. It was revealed that as-prepared GQDs can convert blue light into white light, when these GQDs were coated onto a blue light-emitting diode.

Wang et al. (2014) synthesized stable blue fluorescent GQDs via a hydrothermal method. The fluorescence of reoxidized grapheme oxide was quenched by Cu(II) in water. It can be used as a fluorescence sensor for the detection of cupric ions with high selectivity and sensitivity as compared to other metal ions in concentration range of 0−15 μM with a detection limit of 0.226 μM.

Qu et al. (2014) synthesized a series of GQDs via a hydrothermal process. They used citric acid as a carbon precursor and formed an N-free GQD graphite framework. It was reported that N-doped GQDs were prepared using urea. It was reported that the pyrrolic N was transformed to graphite N under these conditions. It was reported that the highest photoluminescence quantum yield PL QY (94%) of N-doped GQDs could be achieved using ethylenediamine as an N source.

Wu et al. (2014) reported the preparation of dicyandiamide (DCD) N-doped high quantum yield GQDs via a hydrothermal method. They used citric acid as the source of carbon. It was observed that N-doping of GQDs can promote a photoluminescence quantum yield (36.5%). It was also revealed that as-obtained N-doped GQDs were pH-sensitive, photostable, and had low toxicity, and therefore can be used as a pH sensor in a wide range from real water to intracellular contents. Ju and Chen (2014) prepared nitrogen-doped GQDs via hydrothermal treatment, a simple and low-cost approach. They used hydrazine as the source of nitrogen. Due to the selective coordination to Fe^{3+}, as-prepared N-GQDs can be used for selective detection of Fe(III) ions in aqueous solution as well as real water samples with a detection limit of 90 nM.

Fei et al. (2014) synthesized GQDs from anthracite coal, and then self-assembly on graphene by hydrothermal treatment. They observed the formation of hybrid nanoplatelets which were then codoped with nitrogen and boron. It was reported that as-prepared composite exhibited excellent oxygen

reduction reaction (ORR) electrocatalysis with higher activity as compared to commercial Pt/C in alkaline media. Lee et al. (2015) synthesized graphene-decorated V_2O_5 nanobelts (GVNBs) via a hydrothermal method. The GVNBs composite with (VO/GO = 3:1) exhibited excellent specific capacitance as compared to other composites and pure materials. This composite also showed excellent cyclic stability and retention of capacitance (82%) even after 5000 cycles.

Permatasari et al. (2016) synthesized GQDs containing N atoms via a hydrothermal method. They used urea and citric acid as the starting materials. It was revealed that as-prepared GQDs were spherical in shape with an average diameter of 2.17 nm. Fan et al. (2017) functionalized covalently arylamine-based polyazomethine with functionalized GO quantum dots (TPAPAM-GOQDs). It was prepared by an amidation reaction to design a ternary memory device with a configuration of gold/TPAPAM-GOQDs/indium tin oxide. It was claimed that this memory device could enhance the memory capacity of a device from the conventional 2^n to 3^n as compared to binary memory devices.

The composites of N, S codoped GQDs (N, S-GQDs)-rGO-TiO_2 nanotubes (TiO_2NT) were prepared by Tian et al. (2017) via alkaline hydrothermal reaction. It was reported that as-prepared N, S-GQDs/10%rGO/TNT composite exhibited the highest photodegradation efficiency for the degradation of methyl orange, which was 1.8 times and 16.3 times more than 10% rGO + TNT and pure TNT, respectively.

Yao et al. (2018) prepared in situ sulfur-doped GQDs via a hydrothermal method, which were decorated with CNPs to give (S-GQDs/CNPs) hybrid. It was reported that S-GQDs were decorated on CNPs by $\pi-\pi$ stacking. In this case, the advantages of both GQDs as well as CNPs are combined, which will facilitate the electron transfer between S-GQDs and CNPs. It was indicated that the layer by layer modified method in the S-GQDs/CNPs hybrid can inhibit the two-electron pathway and cause a four-electron pathway for ORR rate. It was revealed that the as-prepared S-GQDs/CNPs hybrid exhibited a better methanol tolerance along with long-term durability as compared to commercial 20% Pt/C.

A ternary nanocomposite of high fluorescent polyaniline (PANI)/2-acrylamido-2-methylpropanesulfonic acid (AMPSA) capped silver NPs/GO quantum dots (PANI/Ag (AMPSA)/GO QDs) was synthesized by Shokry et al. (2019) via in situ oxidative polymerization of aniline in the presence of Ag (AMPSA) NPs and GO QDs. The Ag(AMPSA) NPs and GO QDs were prepared by reduction by silver nitrate and carbonization of glucose methods, respectively.

GQDs were synthesized by Hoang et al. (2020) from GO via a microwave-assisted hydrothermal method. This proposed method requires a relatively shorter time (10 min.) as compared to conventional hydrothermal routes. It was reported that as-prepared NPs have a diameter of about

2–8 nm. There was a blue emission on exposure to UV irradiation. It was observed that as-synthesized GQDs can be utilized as a hole transport layer in organic solar cells and quantum efficiency of the cell was increased. It was revealed that on mixing P3HT:PCBM polymer and GQDs, potential difference was reduced at the interfaces of the two materials. It was observed that the overall efficiency of the cell was enhanced by 1.43%, which was about a 44% increase compared to pristine cells (0.99%).

2.4 Recent developments

Although hydrothermal synthesis has been used for a long time with good results, there are some recent developments in this direction. Some of these advancements are summarized in Table 2.1.

TABLE 2.1 Synthesis of quantum dots by hydrothermal route.

Source	Application	References
Carbon quantum dots	Fluorescent (emission range 280–420 nm), a highly sensitive and selective probes for detection of Fe^{3+} ions	Latief et al. (2021)
Fingernails carbon quantum dots (FNCQDs/g-C_3N_4)	Cu^{2+} sensing and photodegradation of 2,4-dichlorophenol	Tai et al. (2021)
Carbon quantum dots	Detection of formaldehyde	Amer et al. (2021)
Carbon quantum dots	Detection of Fe^{3+} ions	Raja and Sundaramurthy (2021)
Carbon quantum dots	Bioimaging	Li et al. (2021)
Carbon quantum dots	In vivo bioimaging	Atchudan et al. (2021)
Carbon quantum dots	Sensitivity and detection of highly toxic chromium(VI) ions	Baragau et al. (2021a,b)
N-doped carbon quantum dots	Ion detection and cell imaging	Shen et al. (2021)
Carbon quantum dots	Oil recovery	Baragau et al. (2021a,b)
Carbon quantum dots/ silver nanoparticles	Determination of losartan potassium (pure form and pharmaceutical formulations)	Abdoon and Atawy (2021)

2.5 Conclusion

Various nanomaterials or quantum dots can be easily prepared by the hydrothermal approach. This method has the advantages of a good control on the size of the particle and their morphology. It requires relatively low temperatures, thus avoiding the problems encountered with high-temperature processes. The materials having high vapor pressure near their melting points can also be synthesized using this technique. Apart from this, the hydrothermal method can also be used in combination with some other approaches, such as microwave-assisted, ultrasound-assisted, etc., to give good yields of the desired products with high purity.

References

Abdoon, F.M., Atawy, H.M., 2021. Prospective of microwave-assisted and hydrothermal synthesis of carbon quantum dots/silver nanoparticles for spectrophotometric determination of losartan potassium in pure form and pharmaceutical formulations. Mater. Today: Proc. 42, 2141–2149.

Amer, W.A., Rehab, A.F., Abdelghafar, M.E., Torad, N.L., Atlam, A.S., Ayad, M.M., 2021. Green synthesis of carbon quantum dots from purslane leaves for the detection of formaldehyde using quartz crystal microbalance. Carbon 179, 159–171.

Atchudan, R., Edison, T.N.J.I., Shanmugam, M., Perumal, S., Somanathan, T., Lee, Y.R., 2021. Sustainable synthesis of carbon quantum dots from banana peel waste using hydrothermal process for in vivo bioimaging. Phys. E Low. Dimens. Syst. Nanostruct. 126. Available from: https://doi.org/10.1016/j.physe.2020.114417.

Aziz, K.H.H., Omer, K.M., Hamarawf, R.F., 2019. Lowering the detection limit towards nanomolar mercury ion detection via surface modification of N-doped carbon quantum dots. N. J. Chem. 43 (22), 8677–8683.

Baragau, I.A., Lu, Z., Power, N.P., Morgan, D.J., Bowen, J., Diaz, P., et al., 2021a. Continuous hydrothermal flow synthesis of S-functionalised carbon quantum dots for enhanced oil recovery. Chem. Eng. J. 405. Available from: https://doi.org/10.1016/j.cej.2020.126631.

Baragau, I.A., Power, N.P., Morgan, D.J., Lobo, R.A., Roberts, C.S., Titirici, M.M., et al., 2021b. Efficient continuous hydrothermal flow synthesis of carbon quantum dots from a targeted biomass precursor for on–off metal ions nanosensing. ACS Sustain. Chem. Eng. 9 (6), 2559–2569.

Chaudhary, N., Gupta, P.K., Eremin, S., Solanki, P.R., 2020. One-step green approach to synthesize highly fluorescent carbon quantum dots from banana juice for selective detection of copper ions. J. Environ. Chem. Eng. 8 (3). Available from: https://doi.org/10.1016/j.jece.2020.103720.

Dhandapani, E., Duraisamy, N., Periasamy, P., 2020. Highly green fluorescent carbon quantum dots synthesis via hydrothermal method from fish scale. Mater. Today: Proc. 26. Available from: https://doi.org/10.1016/j.matpr.2021.04.396.

Fan, F., Zhang, B., Cao, Y., Yang, X., Gu, J., Chen, Y., 2017. Conjugated polymer covalently modified graphene oxide quantum dots for ternary electronic memory devices. Nanoscale 9 (30), 10610–10618.

Fei, H., Ye, R., Ye, G., Gong, Y., Peng, Z., Fan, X., 2014. Boron-and nitrogen-doped graphene quantum dots/graphene hybrid nanoplatelets as efficient electrocatalysts for oxygen reduction. ACS Nano 8 (10), 10837–10843.

Guo, Y., Zhao, W., 2020. Hydrothermal synthesis of highly fluorescent nitrogen-doped carbon quantum dots with good biocompatibility and the application for sensing ellagic acid. Spectrochim. Acta Part. A: Mol. Biomol. Spectrosc. 240. Available from: https://doi.org/10.1016/j.saa.2020.118580.

Guo, Y., Wang, Z., Shao, H., Jiang, X., 2013. Hydrothermal synthesis of highly fluorescent carbon nanoparticles from sodium citrate and their use for the detection of mercury ions in an aqueous solution. Carbon 52, 583–589.

Han, W., Ren, L., Qi, X., Liu, Y., Wei, X., Huang, Z., et al., 2014. Synthesis of CdS/ZnO/graphene composite with high-efficiency photoelectrochemical activities under solar radiation. Appl. Surf. Sci. 299, 12–18.

Hannay, J.B., 1880. On the artificial formation of the diamond. Proc. R. Soc. Lond. 30 (200–205), 188–189.

He, H., Huang, L., Zhong, Z., Tan, S., 2018. Constructing three-dimensional porous graphene-carbon quantum dots/g-C_3N_4 nanosheet aerogel metal-free photocatalyst with enhanced photocatalytic activity. Appl. Surf. Sci. 441, 285–294.

Hoang, T.T., Pham, H.P., Tran, Q.T., 2020. A facile microwave-assisted hydrothermal synthesis of graphene quantum dots for organic solar cell efficiency improvement. J. Nanomater. 2020. Available from: https://doi.org/10.1155/2020/3207909.

Jat, K.K., Bhatt, J., Ameta, S.C., 2019. Photodegradation of fast green by using SnO_2 quantum dots/TiO_2 nanoparticles composite. J. Appl. Chem. 8 (1), 139–145.

Ju, J., Chen, W., 2014. Synthesis of highly fluorescent nitrogen-doped graphene quantum dots for sensitive, label-free detection of Fe(III) in aqueous media. Biosens. Bioelectron. 58, 219–225.

Khan, Z.M., Saifi, S., Aslam, Z., Khan, S.A., Zulfequar, M., 2020. A facile one step hydrothermal synthesis of carbon quantum dots for label-free fluorescence sensing approach to detect picric acid in aqueous solution. J. Photochem. Photobiol. A: Chem. 388. Available from: https://doi.org/10.1016/j.jphotochem.2019.112201.

Latief, U., ul Islam, S., Khan, Z.M., Khan, M.S., 2021. A facile green synthesis of functionalized carbon quantum dots as fluorescent probes for a highly selective and sensitive detection of Fe^{3+} ions. Spectrochim. Acta Part. A: Mol. Biomol. Spectrosc. 262. Available from: https://doi.org/10.1016/j.saa.2021.120132.

Lee, M., Balasingam, S.K., Jeong, H.Y., Hong, W.G., Kim, B.H., Jun, Y., 2015. One-step hydrothermal synthesis of graphene decorated V_2O_5 nanobelts for enhanced electrochemical energy storage. Sci. Rep. 5. Available from: https://doi.org/10.1038/srep08151.

Li, X., Lv, X., Li, N., Wu, J., Zheng, Y.Z., Tao, X., 2019. One-step hydrothermal synthesis of high-percentage 1T-phase MoS_2 quantum dots for remarkably enhanced visible-light-driven photocatalytic H_2 evolution. Appl. Catal. B., Environ. 243, 76–85.

Li, D.Y., Wang, S.P., Azad, F., Su, S.C., 2020. Single-step synthesis of polychromatic carbon quantum dots for macroscopic detection of Hg^{2+}. Ecotoxicol. Environ. Safe. 190. Available from: https://doi.org/10.1016/j.ecoenv.2019.110141.

Li, Z., Wang, Q., Zhou, Z., Zhao, S., Zhong, S., Xu, L., et al., 2021. Green synthesis of carbon quantum dots from corn stalk shell by hydrothermal approach in near-critical water and applications in detecting and bioimaging. Microchem. J. 166. Available from: https://doi.org/10.1016/j.microc.2021.106250.

Liu, S., Zhang, H., Qiao, Y., Su, X., 2012. One-pot synthesis of ternary $CuInS_2$ quantum dots with near-infrared fluorescence in aqueous solution. RSC Adv. 2 (3), 819–825.

Liu, S., Shi, F., Zhao, X., Chen, L., Su, X., 2013. 3-Aminophenyl boronic acid-functionalized $CuInS_2$ quantum dots as a near-infrared fluorescence probe for the determination of dopamine. Biosens. Bioelectron. 47, 379–384.

Liu, T., Li, N., Dong, J.X., Zhang, Y., Fan, Y.Z., Lin, S.M., et al., 2017. A colorimetric and fluorometric dual-signal sensor for arginine detection by inhibiting the growth of gold nanoparticles/carbon quantum dots composite. Biosens. Bioelectron. 87, 772–778.

Liu, Q., Hu, C., Wang, X., 2019a. Hydrothermal synthesis of oxygen-deficiency tungsten oxide quantum dots with excellent photochromic reversibility. Appl. Surf. Sci. 480, 404–409.

Liu, Y., Li, W., Wu, P., Ma, C., Wu, X., Xu, M., 2019b. Hydrothermal synthesis of nitrogen and boron co-doped carbon quantum dots for application in acetone and dopamine sensors and multicolor cellular imaging. Sens. Actuators B Chem. 281, 34–43.

Lu, Y., Feng, Y., Wang, F., Zou, X., Chen, Z.F., Chen, P., et al., 2018. Facile hydrothermal synthesis of carbon dots (CDs) doped $ZnFe_2O_4/TiO_2$ hybrid materials with high photocatalytic activity. J. Photochem. Photobiol. A: Chem. 353, 10–18.

Ma, X., Zhang, P., Zhao, Y., Liu, Y., Li, J., Zhou, J.Y., et al., 2017. Role of N doping on the electrochemical performances of $ZnCo_2O_4$ quantum dots/reduced graphene oxide composite nanosheets. Chem. Eng. J. 327, 1000–1010.

Martins, N.C., Angelo, J., Girão, A.V., Trindade, T., Andrade, L., Mendes, A., 2016. N-doped carbon quantum dots/TiO_2 composite with improved photocatalytic activity. Appl. Catal. Environ. 193, 67–74.

Min, S., Hou, J., Lei, Y., Ma, X., Lu, G., 2017. Facile one-step hydrothermal synthesis toward strongly coupled TiO_2/graphene quantum dots photocatalysts for efficient hydrogen evolution. Appl. Surf. Sci. 396, 1375–1382.

Moissan, H. 1893. Le diamant: Conférence faite à la Société des amis de la science le 17 mai [The diamond: Lecture to the Society of Friends of Science 17 May 1893] (in French). Europeana (accessed 27.06.12).

Murchison, R.I., 1841. First sketch of some of the principal results of a second geological survey of Russia. Phil. Mag. J. Sci. 3 (19), 417–422.

Perera, S.D., Mariano, R.G., Vu, K., Nour, N., Seitz, O., Chabal, Y., et al., 2012. Hydrothermal synthesis of graphene-TiO_2 nanotube composites with enhanced photocatalytic activity. ACS Catal. 2 (6), 949–956.

Permatasari, F.A., Aimon, A.H., Iskandar, F., Ogi, T., Okuyama, K., 2016. Role of C-N configurations in the photoluminescence of graphene quantum dots synthesized by a hydrothermal route. Sci. Rep. 6. Available from: https://doi.org/10.1038/srep21042.

Qian, X., Yue, D., Tian, Z., Reng, M., Zhu, Y., Kan, M., et al., 2016. Carbon quantum dots decorated Bi_2WO_6 nanocomposite with enhanced photocatalytic oxidation activity for VOCs. Appl. Catal. B: Environ. 193, 16–21.

Qiao, W., Yan, S., Song, X., Zhang, X., Sun, Y., Chen, X., 2015. Monolayer MoS_2 quantum dots as catalysts for efficient hydrogen evolution. RSC Adv. 5 (118), 97696–97701.

Qu, D., Zheng, M., Zhang, L., Zhao, H., Xie, Z., Jing, X., et al., 2014. Formation mechanism and optimization of highly luminescent N-doped graphene quantum dots. Sci. Rep. 4 (1). Available from: https://doi.org/10.1038/srep05294.

Raja, D., Sundaramurthy, D., 2021. Facile synthesis of fluorescent carbon quantum dots from Betel leafs (Piper betle) for Fe^{3+} sensing. Mater. Today: Proc. 34, 488–492.

Ren, X., Pang, L., Zhang, Y., Ren, X., Fan, H., Liu, S.F., 2015. One-step hydrothermal synthesis of monolayer MoS_2 quantum dots for highly efficient electrocatalytic hydrogen evolution. J. Mater. Chem. A 3 (20), 10693–10697.

Santra, P.K., Kamat, P.V., 2013. Tandem-layered quantum dot solar cells: tuning the photovoltaic response with luminescent ternary cadmium chalcogenides. J. Am. Chem. Soc. 135 (2), 877–885.

Schafthaul, K.F.E., 1845. Gelehrte Anzeigen Bayer. Akad. 20, 557–593.

Shahba, H., Sabet, M., 2020. Two-step and green synthesis of highly fluorescent carbon quantum dots and carbon nanofibers from pine fruit. J. Fluoresc. 30 (4), 927–938.

Sharma, N., Das, G.S., Yun, K., 2020. Green synthesis of multipurpose carbon quantum dots from red cabbage and estimation of their antioxidant potential and bio-labeling activity. Appl. Microbiol. Biotechnol. 104 (16), 7187–7200.

Shen, J., Zhu, Y., Yang, X., Zong, J., Zhang, J., Li, C., 2012. One-pot hydrothermal synthesis of graphene quantum dots surface-passivated by polyethylene glycol and their photoelectric conversion under near-infrared light. N. J. Chem. 36 (1), 97–101.

Shen, T.Y., Jia, P.Y., Chen, D.S., Wang, L.N., 2021. Hydrothermal synthesis of N-doped carbon quantum dots and their application in ion-detection and cell-imaging. Spectrochim. Acta Part. A: Mol. Biomol. Spectrosc. 248. Available from: https://doi.org/10.1016/j.saa.2020.119282.

Shokry, A., Khalil, M.M.A., Ibrahim, H., Soliman, M., Ebrahim, S., 2019. Highly luminescent ternary nanocomposite of polyaniline, silver nanoparticles and graphene oxide quantum dots. Sci. Rep. 9 (1). Available from: https://doi.org/10.1038/s41598-019-53584-6.

Tai, J.Y., Leong, K.H., Saravanan, P., Tan, S.T., Chong, W.C., Sim, L.C., 2021. Facile green synthesis of fingernails derived carbon quantum dots for Cu^{2+} sensing and photodegradation of 2, 4-dichlorophenol. J. Environ. Chem. Eng. 9 (1). Available from: https://doi.org/10.1016/j.jece.2020.104622.

Tang, L., Ji, R., Cao, X., Lin, J., Jiang, H., Li, X., et al., 2012. Deep ultraviolet photoluminescence of water-soluble self-passivated graphene quantum dots. ACS Nano 6 (6), 5102–5511.

Tian, H., Shen, K., Hu, X., Qiao, L., Zheng, W.N., 2017. S co-doped graphene quantum dots-graphene-TiO_2 nanotubes composite with enhanced photocatalytic activity. J. Alloy. Compd. 691, 369–377.

Wang, J., Han, H., 2010. Hydrothermal synthesis of high-quality type-II CdTe/CdSe quantum dots with near-infrared fluorescence. J. Colloid Interface Sci. 351 (1), 83–87.

Wang, Y., Ni, Y., 2014. Molybdenum disulfide quantum dots as a photoluminescence sensing platform for 2,4,6-trinitrophenol detection. Anal. Chem. 86 (15), 7463–7470.

Wang, F., Gu, Z., Lei, W., Wang, W., Xia, X., Hao, Q., 2014. Graphene quantum dots as a fluorescent sensing platform for highly efficient detection of copper (II) ions. Sens. Actuators B: Chem. 190, 516–522.

Wang, C., Xu, Z., Cheng, H., Lin, H., Humphrey, M.G., Zhang, C., 2015. A hydrothermal route to water-stable luminescent carbon dots as nanosensors for pH and temperature. Carbon 82, 87–95.

Wang, F., Wang, Y., Feng, Y., Zeng, Y., Xie, Z., Zhang, Q., 2018. Novel ternary photocatalyst of single atom-dispersed silver and carbon quantum dots co-loaded with ultrathin g-C_3N_4 for broad-spectrum photocatalytic degradation of naproxen. Appl. Catal. B: Environ. 221, 510–520.

Wang, X., Yang, P., Feng, Q., Meng, T., Wei, J., Xu, C., et al., 2019. Green preparation of fluorescent carbon quantum dots from cyanobacteria for biological imaging. Polymers 11 (4). Available from: https://doi.org/10.3390/polym11040616t.

Wang, C., Shi, H., Yang, M., Yan, Y., Liu, E., Ji, Z., et al., 2020. Facile synthesis of novel carbon quantum dots from biomass waste for highly sensitive detection of iron ions. Mater. Res. Bull. 124. Available from: https://doi.org/10.1016/j.materresbull.2019.110730.

Wei, W., Yao, Y., Zhao, Q., Xu, Z., Wang, Q., Zhang, Z., et al., 2010. Oxygen defect-induced localized surface plasmon resonance at the WO_{3-x} quantum dot/silver nanowire interface: SERS and photocatalysis. Nanoscale 11 (12), 5535–5547.

Wei, J.S., Ding, H., Zhang, P., Song, Y.F., Chen, J., Wang, Y.G., et al., 2016. Carbon dots/$NiCo_2O_4$ nanocomposites with various morphologies for high performance supercapacitors. Small 12 (43), 5927–5934.

Wei, Y., Chen, L., Wang, J., Liu, X., Yang, Y., Yu, S., 2020. Rapid synthesis of BN co-doped yellow emissive carbon quantum dots for cellular imaging. Opt. Mater. 100. Available from: https://doi.org/10.1016/j.optmat.2019.109647.

Wu, S., Cao, H., Yin, S., Liu, X., Zhang, X., 2009. Amino acid-assisted hydrothermal synthesis and photocatalysis of SnO_2 nanocrystals. J. Phy. Chem. C. 113 (41), 17893–17898.

Wu, Z.L., Gao, M.X., Wang, T.T., Wan, X.Y., Zheng, L.L., Huang, C.Z., 2014. A general quantitative pH sensor developed with dicyandiamide N-doped high quantum yield graphene quantum dots. Nanoscale 6 (7), 3868–3874.

Wu, P., Li, W., Wu, Q., Liu, Y., Liu, S., 2017. Hydrothermal synthesis of nitrogen-doped carbon quantum dots from microcrystalline cellulose for the detection of Fe^{3+} ions in an acidic environment. RSC Adv. 7 (70), 44144–44153.

Wu, M.C., Wu, P.Y., Lin, T.H., Lin, T.F., 2018. Photocatalytic performance of Cu-doped TiO_2 nanofibers treated by the hydrothermal synthesis and air-thermal treatment. Appl. Surf. Sci. 430, 390–398.

Xia, Q.X., Hui, K.S., Hui, K.N., Kim, S.D., Lim, J.H., Choi, S.Y., 2015. Facile synthesis of manganese carbonate quantum dots/Ni $(HCO_3)_2$–$MnCO_3$ composites as advanced cathode materials for high energy density asymmetric supercapacitors. J. Mater. Chem. 3 (44), 22102–22117.

Yao, L., Deng, H., Huang, Q.A., Su, Q., Du, X., Du, G., 2017. Facile synthesis of $CoFe_2O_4$ quantum dots/N-doped graphene composite with enhanced lithium-storage performance. J. Alloy. Compd. 693, 929–935.

Yao, Y., Guo, Y., Du, W., Tong, X., Zhang, X., 2018. In situ synthesis of sulfur-doped graphene quantum dots decorated carbon nanoparticles hybrid as metal-free electrocatalyst for oxygen reduction reaction. J. Mater. Sci.: Mater. Electron. 29 (20), 17695–17705.

Yu, H., Zhang, H., Huang, H., Liu, Y., Li, H., Ming, H., et al., 2012. ZnO/carbon quantum dots nanocomposites: one-step fabrication and superior photocatalytic ability for toxic gas degradation under visible light at room temperature. N. J. Chem. 36 (4), 1031–1035.

Yu, X., Liu, J., Yu, Y., Zuo, S., Li, B., 2014a. Preparation and visible light photocatalytic activity of carbon quantum dots/TiO_2 nanosheet composites. Carbon 68, 718–724.

Yu, H., Zhao, Y., Zhou, C., Shang, L., Peng, Y., Cao, Y., et al., 2014b. Carbon quantum dots/TiO_2 composites for efficient photocatalytic hydrogen evolution. J. Mater. Chem. 2 (10), 3344–3351.

Zeng, Y., Guo, N., Li, H., Wang, Q., Xu, X., Yu, Y., et al., 2019. Construction of flower-like MoS_2/Ag_2S/Ag Z-scheme photocatalysts with enhanced visible-light photocatalytic activity for water purification. Sci. Total. Environ. 659, 20–32.

Zhang, R., Chen, W., 2014. Nitrogen-doped carbon quantum dots: facile synthesis and application as a "turn-off" fluorescent probe for detection of Hg^{2+} ions. Biosens. Bioelectron. 55, 83–90.

Zhang, Y., Jiang, D., He, Z., Yu, Y., Zhang, H., Jiang, Z., 2014. Hydrothermal synthesis of PEG-capped ZnS:Mn^{2+} quantum dots nanocomposites. Chem. Res. Chin. Univ. 30 (1), 176–180.

Zhang, X., Wang, J., Liu, J., Wu, J., Chen, H., Bi, H., 2017. Design and preparation of a ternary composite of graphene oxide/carbon dots/polypyrrole for supercapacitor application: importance and unique role of carbon dots. Carbon 115, 134–146.

Zhang, R., Wang, Y., Jia, M., Xu, J., Pan, E., 2018. One-pot hydrothermal synthesis of ZnS quantum dots/graphene hybrids as a dual anode for sodium ion and lithium ion batteries. Appl. Surf. Sci. 437, 375–383.

Zhao, D., He, Z., Chan, W.H., Choi, M.M., 2009. Synthesis and characterization of high-quality water-soluble near-infrared-emitting CdTe/CdS quantum dots capped by N-acetyl-L-cysteine via hydrothermal method. J. Phys. Chem. C. 113 (4), 1293–1300.

Zhao, C., Jiao, Y., Hua, J., Yang, J., Yang, Y., 2018. Hydrothermal synthesis of nitrogen-doped carbon quantum dots as fluorescent probes for the detection of dopamine. J. Fluoresc. 28 (1), 269–276.

Zhao, X., Yang, H., Li, R., Cui, Z., Liu, X., 2019. Synthesis of heterojunction photocatalysts composed of Ag_2S quantum dots combined with Bi_4Ti_3 O_{12} nanosheets for the degradation of dyes. Environ. Sci. Res. 26 (6), 5524–5538.

Zhou, J., Gao, Y., Liu, X., Chen, Z., Dai, L., Cao, C., 2013. Mg-doped VO_2 nanoparticles: hydrothermal synthesis, enhanced visible transmittance and decreased metal–insulator transition temperature. Phys. Chem. Chem. Phys. 15 (20), 7505–7511.

Zhu, H., Yang, D., Yu, G., Zhang, H., Yao, K., 2006. A simple hydrothermal route for synthesizing SnO_2 quantum dots. Nanotechnology 17 (9). Available from: https://doi.org/10.1088/0957-4484/17/9/052.

Chapter 3

Sol–gel synthesis of quantum dots

Avinash K. Rai[1] **and Kanchan K. Jat**[2]
[1]*Department of Chemistry, PAHER University Udaipur, Rajasthan, India,* [2]*Department of Chemistry, M. L. S. University Udaipur, Rajasthan, India*

3.1 Introduction

The sol–gel process is a new approach to the preparation of nanomaterials. A sol is a stable dispersion of colloidal particles or polymers in a solvent. It allows a better control in the synthesis of solids. It is a wet-chemical technique used for the preparation of both glassy as well as ceramic materials. The sol–gel process is based on hydrolysis and polycondensation reactions. During this process, first the sol (or solution) is evolved, which gradually proceeds to the formation of a gel-like network containing both a liquid phase and a solid phase. The basic structure (morphology) of the solid phase can have a wide range, starting from discrete colloidal particles to chain-like polymer networks. Synthesis using a sol–gel approach is used in the preparation of ceramic materials such as metal oxides, nitrides, and carbides. It results in the formation of a sol, which turns into a gel after a series of chemical reactions and/or mild thermal treatments. It is finally calcined to obtain the desired product.

- The basic idea behind sol–gel synthesis is to first dissolve the compound in a liquid and then bring it back as a solid; of course in a controlled manner.
- This technique provides facile preparation of compounds by mixing sols of different compounds.
- It avoids problems encountered in coprecipitation methods and gives smaller particles.

Sol–gel is a method for preparing metal oxide glasses, ceramics, etc. First, a chemical precursor or their mixtures are hydrolyzed, forming a solution state, which is converted to a gel state and then it is dehydrated to a ceramic or glass (Fig. 3.1).

Quantum Dots. DOI: https://doi.org/10.1016/B978-0-12-824153-0.00003-3

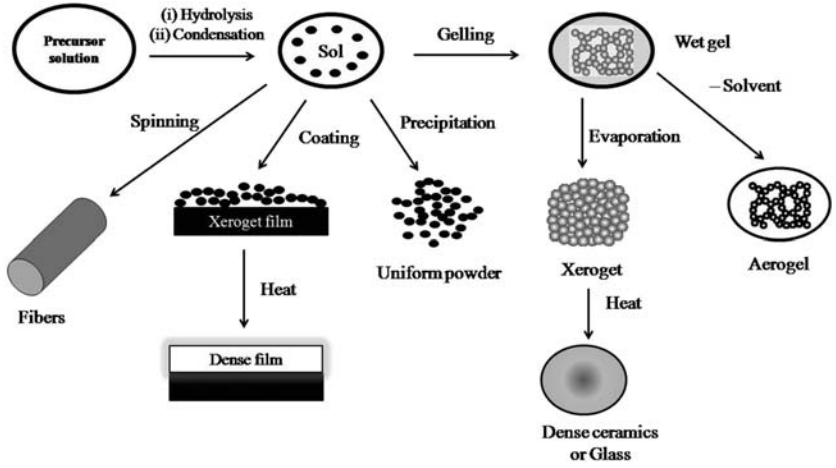

FIGURE 3.1 Different steps involved in sol–gel and related processes.

This technology can be used to prepare thin films, fibers, microspheres, fine powders, etc. It can be used to obtain catalysts, protective coatings, piezoelectric devices, lenses, wave-guides, superconductors, high-strength ceramics, insulating materials, nanoparticles (quantum dots also) etc.

Basically, it involves three steps:

- firstly, partial hydrolysis of metal alkoxides to form reactive monomers;
- condensation of as-prepared monomers to form colloid-like oligomers, known as sol formation; and
- additional hydrolysis leading to polymerization and cross-linking for a gel formation (three-dimensional matrix).

The various steps involved in sol–gel process are:

1. hydrolysis and condensation of compounds (sol formation);
2. gelation (sol–gel transformation);
3. aging; and
4. drying.

In the first step, a sol is formed, which is a stable dispersion of colloidal particles (it may be crystalline or amorphous) or polymers in a solvent. Then gel is formed by a three-dimensional (3D) continuous network, which contains a liquid phase, or by polymer chains. Some agglomerates of colloidal particles are there while the particles have some polymeric aggregates of subcolloidal particles in a polymer gel.

During this process, the solvent is trapped inside the gel as viscosity rapidly increases. Its structure may change considerably with time, depending on temperature, solvent, and pH. The liquid phase still contains agglomerates

and sol particles, which react there and condense on drying of the gel. Originally, the gel is flexible, but on condensation, it becomes more viscous. This will squeeze out the liquid present in the interior of the gel, and shrink it until there is a flexibility in the gel.

3.1.1 Advantages

The following are the advantages of this process:

- It provides a better control of the structure, such as particle size and porosity.
- It provides possibility of incorporating nanosized materials.
- It can ensures an excellent adhesion between top layers and substrate by forming thin coating.
- Relatively high purity is retained.
- It provides a good control on composition.
- It can be carried out at a relatively low temperature.
- There is no need for special or expensive equipment.

3.1.2 Disadvantages

There are some disadvantages of this process also and these are:

- There is long processing time.
- Organic solvents are used, some of which may be toxic.

3.2 Synthesis of quantum dots

3.2.1 Oxides

Lin et al. (2005) synthesized ZnO quantum dots via a simple sol–gel method. It was reported that the average size of these quantum dots can be tailored by variation of the concentration of the precursor of zinc. Size-dependent blueshifts of photoluminescence and absorption spectra revealed the quantum confinement effect. The ZnSe quantum dots were embedded in SiO_2 thin films by Jiang et al. (2004) via a sol–gel process. They used Zn $(Ac)_2 \cdot H_2O$ and H_2SeO_4 as the source of zinc and selenium, respectively. It was indicated that the size of the crystallite was increased with the concentration of selenium.

Li and Qu (2007) prepared CdTe quantum dots-derived composite with silica spheres coated with 5,11,17,23-tetra-*tert*-butyl-25,27-diethoxy-26,28-dihydroxycalix[4]arene (C[4]/SiO_2/CdTe) via a sol − gel approach. It was observed that FL intensity was increased linearly with increasing methomyl (pesticide) concentration (0.1 − 50 μM) with a limit of detection of 0.08 μM. On the other hand, it was negligible as compared to other pesticides, such as

parathion-methyl, fenamithion, acetamiprid, and optunal. Bera et al. (2008) reported synthesis and spectroscopic characterization of sol−gel derived zinc oxide quantum dots of 3−8 nm size. The quantum dots exhibited a broad and strong visible emission peak centered near 520 nm with a quantum efficiency of approximately 5%.

Zhang et al. (2010a) synthesized ZnO quantum dots via a sol − gel route. They used a zinc − oleate complex as a precursor. It was reported that as-obtained ZnO QDs had diameters in the range of 2.2 − 7.8 nm. It was revealed that ionized oxygen vacancies are responsible for the origin and intensity of the visible emission of ZnO QDs, while the visible emission peak position of ZnO QDs is decided by the following two factors:

- size; and
- transition of holes from the valence band to preexisting deep donor energy level.

The ZnO quantum dots were synthesized using the same precursors (Zhang et al., 2010b). It was reported that as-obtained ZnO QDs hexagonal had a wurtzite structure with particle size diameter of 8.9 nm. It was revealed that there is a redshift excitation. It was also observed that visible emission also shifted to the green luminescence band from yellow on increasing the annealing temperature.

Yu et al. (2010) synthesized Eu^{3+}-doped glass ceramics embedded ZnO quantum dots via a sol−gel method. It was revealed that ZnO QDs obtained were in the range of 3−6 nm. It was reported that these glass ceramics had a high transparency in the visible−infrared range, which may be due to the much smaller size of the ZnO QDs as compared to the wavelength of the visible light. CdTe quantum dots-doped TiO_2 photocatalysts were synthesized by Li et al. (2010) via a facile sol−gel method at room temperature. The photocatalytic activities of the as-prepared sample were investigated for the degradation of malachite green. It was found that the sample doped with 0.06 wt.% CdTe QDs exhibited the highest photocatalytic activity.

Chen et al. (2011) also synthesized ZnO quantum dots by a sol−gel method. These QDs exhibited a strong blue emission. It has been reported that ZnO QDs had an average diameter of 16.0−32.2 nm. It was observed that a higher reaction temperature and longer reaction time resulted in larger average size for QDs. It was revealed that a reduction in photoluminescence and increase of the size of ZnO QDs were similar for annealing in nitrogen, vacuum, and air.

Zinc oxide quantum dots with blue emission were synthesized by Han et al. (2012) via a sol−gel method. It was interesting to note that the blue emission was neither due to quantum confinement nor intermediate products. It was achieved only in the presence of Li^+ cations and hydroxide ions. It was revealed that an excess of OH^- ions is responsible for the formation of interstitial oxygen defects, while Li^+ ions can stabilize these defects by

substituting Zn atoms causing a blueshift of the blue emission. The Cd-doped ZnO quantum dots were prepared by Zhang et al. (2012) through a sol−gel method. The effect of Cd concentration and mass ratio of trioctylphosphine oxide (TOPO)/octadecylamine (ODA) on structural and luminescent properties of QDs was also evaluated. It was reported that Cd-doped ZnO QDs are 3−6 nm in diameter. It was observed that QD particle size was found to be reduced on increasing the Cd content. It was revealed that UV and fluorescence spectra both were blueshifted. The best optical performance was achieved when the TOPO/ODA mass ratio was kept 1:2.

The lanthanum-doped ZnO quantum dots were synthesized by Sun et al. (2012) via a modified sol−gel method. It was reported that La-doped quantum dots exhibited enhanced luminescent properties and their quantum yield was 77.9%. Then they prepared anticounterfeiting inks by incorporating these La-doped ZnO QDs into the transparent oil. The sol−gel method was applied by Korala et al. (2013) to fabricate thin films of CdSe and core(shell) CdSe(ZnS) QDs. It was reported that more than twofold enhancement in photocurrent could be achieved with an increase in photovoltage due to passivation of surface defects via overcoating with a thin ZnS shell. As a result as-prepared QD thin films are considered suitable for a wide range of optoelectronic applications.

Ge et al. (2013) fabricated a composite of TiO_2 films with CdTe quantum dots. Different CdTe QDs (green-, yellow-, and red-emitting) were obtained, when thioglycolic acid was used as a capping agent. It was revealed that red-emitting CdTe QDs exhibited a small blueshift of 1 nm, while green-emitting QDs showed a blueshift of 7 nm. A nonhydrolytic sol−gel combustion method was used by Leelavathi et al. (2013) for synthesis of nanocomposites of PbO quantum dots on anatase TiO_2. It was indicated that the photocatalytic activity of quantum dot dispersed TiO_2 was higher than that of TiO_2 and much higher as compared to commercial Degussa P-25.

Zinc oxide quantum dots were synthesized by Kumar et al. (2014) via a simple sol−gel method. They used zinc acetate dehydrate, sodium hydroxide, and methanol as starting materials. A good crystallinity was observed in these QDs with average crystallite sizes $\sim$14 nm. It was suggested that as-synthesized ZnO QDs can be used as the electrode material for dye-sensitized solar cells. Li et al. (2014) synthesized Pr^{3+}-doped semiconductor ZnO quantum dots via a sol−gel method. It was reported that as-obtained ZnO QDs were spherical in shape and the diameter was around 5 nm. It was revealed that emission peaks of aged ZnO QDs exhibited a redshift due to the increasing size of the QDs.

Zhong et al. (2014) synthesized $CuGaS_2$ quantum dots, which were embedded in sodium borosilicate glass matrix by combining two processes: sol−gel and heat treatment in H_2S gas. It was observed that as-obtained $CuGaS_2$ quantum dots had a spherical shape and were uniformly distributed with sizes ranging from 5−25 nm. The formation of stable colloids

containing surface-modified ZnO QDs was reported by Moghaddam et al. (2015) via a sol−gel process in an ultrasonic bath. They used 3-aminopropyltriethoxysilane (APTES) as a capping agent. Alcoholic solutions of zinc acetate and potassium hydroxide were used as the reactants. The formation of nanocrystals of ZnO QDs with average size of ∼3 nm was confirmed. It was suggested that the as-prepared ZnO QDs were found to be suitable for optical and optoelectronic applications.

Liu et al. (2015) synthesized ZnO quantum dots by a sol−gel method. They used (methanol, ethanol, or hexanol) as solvents. It was indicated that as-prepared ZnO QDs were having good dispersion and their size ranged from 3.3−7.7 nm, which could be controlled by variation of the solvents. It was revealed that ZnO QDs exhibited visible emissions ranging from green to orange. Bajaj and Omanwar (2015) synthesized α-Al_2O_3 quantum dots by the stearic acid sol−gel synthesis. The as-prepared sample exhibited good UV absorption and blue emission at 254 and 403 nm, respectively. Gnanasekaran et al. (2015) synthesized TiO_2 quantum dots by the sol−gel method. It was reported that TiO_2 QDs have a pure anatase phase with a tetragonal structure. The photocatalytic activity of TiO_2 QDs have been evaluated for the degradation of methylene blue and methyl orange under UV light irradiation.

The synthesis of TiO_2 quantum dots has been reported by Sood et al. (2015) via a simple sol−gel, template-free method. They also evaluated catalytic behavior of as-synthesized quantum dots by photocatalytic degradation of Indigo carmine dye in the presence of UV light. Chen et al. (2016) synthesized TiO_2 and carbon quantum dots-doped TiO_2 nanocomposite (CQDs/TiO_2 nanocomposite) by a sol−gel approach. They evaluated the photocatalytic activity of TiO_2 and CQDs/TiO_2 composite for the degradation of rhodamine B and cefradine. It was observed that the photocatalytic activity of CQDs/TiO_2 was higher compared to TiO_2.

Miao et al. (2016) prepared visible light responsive carbon quantum dots embedded in mesoporous TiO_2 materials via a sol−gel process. The photocatalytic performance of as-prepared CQDs/meso-Ti-450 was investigated for the degradation of methylene blue. It was revealed that 5% CQDs/meso-Ti-450 can remove almost complete (98%) methylene blue, whereas commercial P25 can remove only 10% of the dye. The TiO_2 (mesoporous) with different concentration of CdS quantum dots was successfully fabricated by Zhou et al. (2017) via a sol−gel method. The photocatalytic activity of the as-prepared CdS/TiO_2 samples was evaluated for the degradation of methyl orange, and it followed the order:

$$2\%\ \mathrm{CdS/TiO_2} > 4\%\ \mathrm{CdS/TiO_2} > 8\%\ \mathrm{CdS/TiO_2} > \text{pure}\ \mathrm{TiO_2} > 1\%\ \mathrm{CdS/TiO_2}.$$

The 2% CdS/TiO_2 has also been used for the degradation of methylthionine chloride, malachite green, rhodamine B, and bisphenol A.

Soumya et al. (2018) synthesized Sn and Ag-doped ZnO quantum dots via a microwave-assisted sol−gel strategy. They used 3-aminopropyl trimethoxy silane as a capping agent. Then these ZQDs were dispersed in methyl methacrylate monomer and polymerized in situ to obtain PMMA/ZQDs. It was indicated that as-prepared doped ZQDs/PMMA hybrid coatings exhibited blue emission under UV light. It was revealed that undoped PMMA/ZQDs hybrid coatings showed only <14% NIR reflectance, which was enhanced by 30% and 23% on doping with Ag and Sn in PMMA/ZQDs hybrids, respectively. It was concluded that these ZQDs doped with Sn and Ag ions on treatment with dye and inorganic coactivators, can find applications in photochromic and UV/NIR shielding solar-control interface coatings.

Ye (2018) used a sol−gel method for the synthesis of stable ZnO QDs. They also observed the effects of reactants concentration, reaction time, and material ratio on particle sizes and defects structures of ZnO. The highest photoluminescence quantum yield (40%) with green emission was observed under UV light excitation (359 nm). Garcia et al. (2019) synthesized TiO_2 quantum dots by sol−gel process. They used ionic liquid (1-*n*-butyl-3-methylimidazolium tetrafluoroborate) as the stabilizing agent. An adhesive resin was formulated by mixing these QDs with methacrylate monomers. As-prepared adhesive resins were evaluated for antibacterial activity, cytotoxicity, polymerization behavior, fracture pattern, degree of conversion, and microtensile bond strength. It was reported that 26 wt.% of $BMI.BF_4$. TiO_2 QDs/$BMI.BF_4$ had a minimum size range of 1.19−7.11 nm, and an average size of 3.54 ± 1.08 nm.

A sol−gel reflux condensation route was developed by Javed et al. (2019) to produce TiO_2 QDs. They used titanium tetraisopropoxide as the precursor, which was first hydrolyzed and followed by reflux condensation for 24 h. It was revealed that as-prepared QDs were spherical in shape with an average crystallite size of 5−7 nm. The energy bandgap of TiO_2 QDs was found to be $\sim$3.76 eV. A series of ZnO quantum dots were prepared by Sowik et al. (2019) modified with rare-earth metals through a sol−gel approach. They selected Eu, Er, Tb, Yb, Ho, and La to modify ZnO QDs. It was observed that as-prepared modified ZnO QDs can degrade phenol in aqueous phase. The order of photocatalytic activity among all these as-obtained nanomaterials followed the order:

$$\mathrm{ZnO/0.09\ mm\_Er} > \mathrm{ZnO/0.18\ mm\_Eu} > \mathrm{ZnO/0.09\ mm\_La} > \mathrm{ZnO/0.27\ mm\_Er} > \mathrm{ZnO/0.18\ mm\_Tb} > \mathrm{pristine\ ZnO\ QDs}.$$

The ZnO and Au textured ZnO-based quantum dot thin film was fabricated by Dey and Sarkar (2020) and used as sensors. The as-fabricated sensor had an operating temperature of 35°C and it could be used for detecting a minute fraction vapors of different alcohols such as methanol, ethanol, propanol, and butanol. An annealing treatment at 350°C temperature was

imposed to improve the response of as-prepared sensors. Mohamed et al. (2020) synthesized three samples of ZnO quantum dots using a modified sol−gel method. It was reported that the average crystallite size, bandgap energy, and active surface area were 7.1 nm, 3.49 eV, and 150.1 $m^2\ g^{-1}$) for a sample prepared at 27°C. The other two samples prepared at 500°C and 900°C had an average particle size of 9.8 and 13.5 nm, respectively. It was observed that the photocatalytic performance decreases as the crystallite size increases in the case of degradation of methyl orange. It was revealed that the as-prepared samples could be recycled eight times.

Zou et al. (2020) prepared water-soluble ZnO quantum dots modified with (3-aminopropyl)triethoxysilane (APTES) by a simple sol−gel method. They displayed strong yellow-green fluorescence. It was observed that the emission from as-prepared NH_2−ZnO QDs was quenched in the presence of Cu^{2+} ions. They designed a fluorescent probe based on an as-prepared sample of NH_2−ZnO QDs for the detection of Cu^{2+} in water with a limit of detection of 1.72 nM. This fluorescent probe had also been applied in drinking water samples. Haghani et al. (2020) also prepared ZnO-QDs using a sol−gel method and then fabricated an optical sensor based on these QDs for the determination of chlorogenic acid (CGA). Tetraethoxysilane and 3-aminopropyltriethoxysilane were used as a cross-linker and functional monomer, respectively, to prepare the molecularly imprinted polymer (MIP). As-prepared ZnO-QDs MIP composite was used to measure CGA in the range of 0.2−5.3 $\mu g\ mL^{-1}$ with a limit of detection of 0.06 $\mu g\ mL^{-1}$. This sensor was also used to measure the concentration of CGA in human plasma samples.

Wang et al. (2020) prepared graphene oxide/WO_3 quantum dots/TiO_2 (GOWT) composite. These GOWT films were prepared by using this GOWT composite powder and $Al(H_2PO_4)_3$ as adhesive and low-cost gauze as substrates. As-prepared GOWT film was used for removal of rhodamine B. It was observed that the degradation rate of rhodamine B was around 2.6 times than GO/TiO_2 films in the presence of UV light. It was proposed that GOWT films can find potential application in sewage treatment without causing any further contamination. Song et al. (2020) used an efficient method to improve the stability of $MAPbBr_3$ QDs by encapsulating them in ZrO_2 sol. It was observed that this three-dimensional network ZrO_2 colloid formed a coating on the surface of $MAPbBr_3$ QDs, which protected these QDs from acid, base, and ultraviolet light. It was revealed that the photoluminescence intensity of as-prepared nanocomposites could retain 95% of its initial value even after 4.5 h in a basic environment and 90% in an acid environment after 10 h.

Schmitz et al. (2020) prepared colloidal ethanolic dispersions of zinc oxide (undoped) and ZnO particles doped with magnesium (II) (ZnO:Mg) via a sol−gel method. The particle sizes of these QDs were found to be 4.26 and 3.65 nm, respectively. As-prepared QDs were then used as nanofillers to obtain zein-based nanocomposite films, which displayed homogeneity, good

visual appearance, and transparency. These thin films have an extended UV-blocking range in the absorbance spectra as compared to those of pure zein. It was observed that ZnO NPs, loaded into zein films exhibited 96.5 ± 4.9% inhibition of growth of *S. aureus*. It was suggested that as-prepared nanocomposites could be used for the development of food packaging and UV protective films.

The ZnS QDs/gelatin nanocomposites were prepared by Guo et al. (2020) using green one-pot method. The method shows advantages such as being an environment friendly strategy, with mild conditions, no need for organic solvents, and simple posttreatment. Here, gelatin acted as the green capping agent apart from being main component in the QDs/gelatin nanocomposites. The presence of gelatin provides the composite with a thermoresponsive sol−gel transition property. As-prepared composite with this property can find potential uses in imaging, fluorescence labeling, and controlled release.

The Fe_3O_4 quantum dots decorated silica (FS) adsorbent were prepared by Rakibuddin and Kim (2020) via a sol−gel method. The formation of Fe_3O_4 quantum dots (organically modified silica surface) with an average size of 3−4 nm was confirmed. One of the samples showed the best arsenic removal efficiency (38.2 mg g^{-1}), which was higher than Fe_3O_4 and silica particles. As-Fe_3O_4 and silica both are environmentally sustainable, therefore this composite could be a potential candidate for the removal of arsenic. Vasiljevic et al. (2020) synthesized iron titanate (Fe_2TiO_5) nanoparticles via a modified sol−gel method followed by calcination. The bandgap of as-prepared iron tantalate was around 2.16 eV. Its photocatalytic activity was evaluated for degradation of methylene blue in the presence of natural sunlight.

Wang and Li (2021) prepared ZnO quantum dots (ZQ) and Ag/ZQ nanocomposites with different percentages of Ag loadings via a sol−gel method. It was observed that the as-fabricated sample of nanocomposite (Ag content of 11 wt.%) exhibited excellent photocatalytic activity for degradation of methylene blue in the presence of Ag11/ZQ, when Ag content was kept at 11%. Xu et al. (2021) prepared CeO_2 QDs through a sol−gel method using a recursor of $Ce(NO_3)_3 \cdot 6H_2O$ as the source of cerium. Then they developed a fluorescence probe based on these CeO_2 quantum dots and used it for highly selective and ultrasensitive direct determination of 4-nitrophenol (4-NP). It was reported that the concentration of 4-NP can be determined in the range of 0.005−75.00 μM with a limit of detection of 1.50 nM. It was also revealed that as-prepared CeO_2 QDs could be applied in the determination of 4-NP in real water samples.

Li et al. (2021) developed ZnO quantum dots using a sol−gel method. They also evaluated the antibacterial activities of ZnO QDs against *Staphylococcus aureus*, *Escherichia coli*, and *Salmonella pullorum*. It was found that the particle size of ZnO QDs was in the range of 3−6 nm. It was reported that as-prepared ZnO QDs inhibited the growth of *S. aureus*,

E. coli, and *S. pullorum* by 94.75 ± 2.28%, 87.06 ± 0.98%, and 85.55 ± 1.15%, respectively. These QDs also reduced the mortality of chicks infected with *S. pullorum* effectively via regulating the balance of the intestinal flora, protecting intestine and liver.

The mesoporous graphene quantum dots-doped TiO_2 (TiO_2-GQD) nanocomposites were prepared by Zhao et al. (2021) through a sol−gel method under ultrasonic radiation. As-prepared TiO_2-GQD nanocomposites exhibited superior performance for sunlight absorption, and photocathodic protection. It was revealed that they can protect the active metal as well as reduce the corrosion rate. It was suggested that TiO_2-GQD nanocomposites could be used in marine engineering for marine corrosion protection in the future.

Zhang et al. (2021) synthesized ZnO QDs using a hydrolysis−condensation reaction. The effect of alkali bases (LiOH, NaOH, and KOH) as well as the ratio of Zn^{2+}:OH^- was investigated on the properties of as-synthesized ZnO QDs and it was observed that the particle size of ZnO QDs prepared in the presence of LiOH and NaOH was smaller as compared to that prepared with KOH. It was reported that ZnO QDs prepared with ratio of Zn^{2+}: LiOH = 1:1 exhibited the best dispersibility and fluorescence performance.

3.2.2 Sulfides

Yamane et al. (1992) prepared CdS dispersed in soda-borosilicate glasses using by the sol−gel process. They used cadmium acetate, tetramethoxysilane, sodium acetate, and triethylborate. The gel formed was exposed to H_2S at 120°C. It was observed that glass containing about 10 wt.% CdS crystallites (4−7 nm in diameter) was obtained by sintering at 590°C. Hayakawa et al. (2000) prepared rare-earth ions and semiconductor nanocrystals using Eu^{3+} doped silica gel with adsorbed cadmium sulfide particles via a sol−gel technique. It was proposed that surface-trapped electrons on CdS particles excited 4 f electrons (nonradiatively) in Eu^{3+} ions via an energy transfer process.

The CdS/ZnO quantum dots were prepared by Wang et al. (2011) via a sol−gel method. They used triethanolamine as a capping agent. The bandgaps for different ratios of CdS/ZnO (1:9, 1:1, and 9:1) were found to be 4.13, 3.93, and 3.11 eV, respectively. The size of as-obtained QDs was found to be in the range of 5−10 nm; of course with some agglomerated particles. Yang et al. (2018) prepared ZnS nanoparticles on nitrogen and sulfur codoped carbon nanosheets (ZnS@NSC) via a sol−gel synthesis. It was reported that nanosheets and ultrafine carbon shells together constituted an N, S codoped carbon framework, providing abundant active sites for sodium storage along with enhanced electrical conductivity. It was revealed that ZnS@NSC could achieve excellent cycling stability (73.6% capacity retention after 380 cycles at 0.5 A g^{-1}) and reversible capacity of 734 mAh g^{-1} at 0.5 A g^{-1}.

The ZnS/CdS/γ-TaON composite was prepared by An et al. (2019) via nitridation of Ta_2O_5 and deposition of CdS and ZnS quantum dots. It was revealed that CdS and ZnS quantum dots (3−8 nm diameter) were uniformly dispersed on the surface of γ-TaON. It was revealed that under optimized condition, H_2 evolution rate of ZnS/CdS/γ-TaON composite was 839.6 $\mu mol\ h^{-1}\ g^{-1}$, which is about 14 times higher than that of CdS/γ-TaON and 47 times higher than Pt loaded γ-TaON sample. Rakibuddin et al. (2020) prepared different MoS_2 morphologies (bulk, flake, and quantum dots) that were then fabricated onto indium tin oxide using the sol−gel method. The MoS_2 bulk, flake, and quantum dots were used as electrochromic anodic layers, and WO_3 as a cathodic layer to fabricate MoS_2/WO_3-based electrochromic devices. It was reported that as-fabricated MoS_2/WO_3 ECDs exhibited high optical contrasts (59%−75%) at 1.5−0 V and 700 nm. It was suggested that solution-processed MoS_2/WO_3-based ECDs can find an application in the processing of flexible and optical devices. Cadmium sulfide nanostructures were prepared by Sonker et al. (2020) using sol−gel method. Then CdS thin films of different thickness were prepared. They used an as-fabricated sample for gas sensing measurements for detecting 20 ppm NO_2 gas.

A phosphorescent probe of type SiO_2-Mn:ZnSQDS-MIP was synthesized by Chen et al. (2020) using MIP as a polymer coating via a sol−gel method. They used thioglycolic acid (TGA)-modified QDs, cephalexin, 3-aminopropyltriethoxysilane and tetraethoxysilane as luminescent materials, template, functional monomer, and cross-linking agent, respectively. It was revealed that cephalexin can be determined in 2.5−50 $\mu g\ L^{-1}$ concentration range with a limit of detection of 0.81 $\mu g\ L^{-1}$. The as-fabricated nanoprobe was applied for determination of cephalexin in (spiked) raw milk and milk powder. Sankar et al. (2020) synthesized Ni-doped CdS nanoparticles with 0.5%, 1.0%, 1.5%, and 2.0% via the sol−gel method. The average crystalline size of the particles was found to range from 8.70 to 9.93 nm. The SEM images indicated combination of metal oxide cubes and rod-like structures with 12−35 nm unequal grain size with excellent crystallinity quality. It was revealed that the bandgap energy decreases from 2.36 to 2.29 eV on increasing the percentage of Ni. Photocatalytic degradation of methylene blue and methyl orange was also carried out and it was found that 94% methyl orange can be degraded in 75 min.

Rempel et al. (2020) synthesized a complex sandwich catalyst, which was based on nanotubular TiO_2 and colloidal cadmium sulfide via a sol−gel method. They investigated the photocatalytic activity of this catalyst for oxidation of acetone in the gas phase under visible light and UV irradiation. Ajibade and Oluwalana (2021) prepared ODA-capped ZnS quantum dots from a bis(morpholinyldithiocarbamato)Zn(II) complex. It was confirmed that an hexagonal wurtzite crystalline phase of ZnS was present in the sample with particle sizes of about 1−3 nm. It was reported that the as-prepared ZnS can be used as photocatalysts for degrading brilliant green, rhodamine B, and their binary mixture. It was revealed that the highest photocatalytic

degradation efficiency of 94% was obtained with a sample with a low photoluminescence intensity. It was also found that ZnS quantum dots can be reused five times without any significant loss in degradation efficiency.

Zaidi and Azam (2021) synthesized zinc sulfide quantum dots using the sol−gel method. They used zinc nitrate and sodium sulfide as the source of zinc and sulfur, respectively. The particle size of as-prepared QDs was found to be 1.74 nm. The antimicrobial activity of these QDs was studied against *Pseudomonas aeruginosa*, where they exhibited good bactericidal activity. Perovskite-sensitized solar cell is an effective hybrid organic−inorganic solar cell device. Sonker et al. (2021) synthesized CdS quantum dots via the sol−gel approach. It was found that the maximum grain diameter was about ~4 nm. It was observed that as-fabricated CdS QD-based dye-sensitized solar cell and PSSC exhibited a maximum power conversion efficiency (η) of 0.5% and 1.8% at 1 Sun condition, which was improved by approximately 72% as compared to the reference cell.

3.2.3 Carbon-based quantum dots

Ke et al. (2017) prepared carbon quantum dots-modified TiO_2 photocatalysts via the sol−gel method. The photocatalytic performance of the as-prepared composite was the degradation of methylene blue in the presence of visible light irradiation and it was observed that the degradation efficiency of methylene blue was high (90%) within 2 h, which is almost 3.6 times higher than compared to TiO_2.

Ensafi et al. (2018) anchored MIP on the surface of GQDss using the sol−gel method. It was used for highly sensitive and selective determination of *p*-nitroaniline (*p*-NA) in the range of 0−15.0 μM. This was also applied to real samples of water and fish with satisfactory results. Molecularly imprinted silica was prepared via the sol−gel method by Yang et al. (2020). They used fipronil as the template, tetraethoxysilane as cross-linker, and 3-aminopropyltriethoxysilane as a functional monomer in the presence of carbon quantum dots. It was reported that blue fluorescence of the CQD@MIS, was quenched in the presence of fipronil, a commonly used insecticide. These QDs can detect fipronil in the range of 0.70 pM to 47 μM with the limit of detection being 19 pM. This method was applied for the determination of fipronil in real samples such as milk, spiked eggs, and tap water.

Yu et al. (2021) developed a composite of carbon nitride quantum dots in situ-doped TiO_2 inverse opal (TiO_2 IO) via the sol−gel method. It was reported that the as-prepared photocatalyst exhibited excellent photocatalytic degradation of toluene and 93% of toluene can be degraded into harmless products such as CO_2 and H_2O under simulated sunlight irradiation. On the other hand, only 37% of toluene was found to degrade in the presence of commercial P25. They also used this composite for the degradation of phenol and rhodamine B. Vyas et al. (2022) synthesized water-soluble, green incandescent CQDs at high yield by carbonization of water hyacinth (*Eichhornia crassipes*) weed. They

fabricated copper sulfide nanoparticles and composite CQDs@CuS. This composite was used for the photocatalytic degradation of brilliant green dye.

3.2.4 Graphene based

A fluorescent sensor was prepared by Zhang et al. (2020) based on water-soluble nitrogen-doped GQDs (N-GQDs), which were coupled with MIPs via a simple sol−gel method. It was then used for detection of tetracycline, an antibiotic. It was revealed that this method can be used in detecting the presence of tetracycline in animal-derived food.

Nickel-cobaltite/GQDs ($NiCo_2O_4$/GQDs) composites were prepared by Kharangarh et al. (2021). It was observed that the as-prepared sample exhibited improved electrical conductivity and can function as electrode materials with higher energy density compared to $NiCo_2O_4$ and GQDs. The observed specific capacitance for the fabricated composite was found to be 481.4 Fg^{-1} at 0.35 Ag^{-1}. It was higher than that of GQDs ($C_{sp} \sim 45.6\ Fg^{-1}$). It was proposed that the as-fabricated composites could be used as superior electrode materials in supercapacitors due to their unique characteristics.

Qiu et al. (2021) prepared cadmium sulfide quantum dots/dodecahedral phosphotungstic acid potassium $K_3PW_{12}O_{40}$ (KPW)/oxygen-doped mesoporous graphite carbon nitride (meso-g-C_3N_4) nanosheets with tandem heterojunctions. It was reported that the photocatalytic production rate of hydrogen formation and photocatalytic removal rate of Cr^{6+} over CdS/KPW/meso-g-C_3N_4 were found to be higher than with KPW and CdS/KPW.

3.3 Others

The CdSe quantum dots sensitized TiO_2 photocatalysts were synthesized by Shi et al. (2014) via the sol−gel method. The photocatalytic performance of as-prepared material was enhanced in the degradation of methylene blue. It was revealed that the catalysts doped with 0.05% CdSe QDs exhibited the highest activity, and the degradation efficiency of methylene blue could reach up to 99.2% within 3 h.

A solvothermal-assisted sol−gel method was reported by Anupama et al. (2021) to synthesize Se quantum dots. It was revealed that Se quantum dots having average size 3−8 nm were obtained with a trigonal crystal structure. It was found that as-prepared selenium quantum dots could work as ideal candidates for inner filter effect-based sensing of curcumin. Liu et al. (2022) synthesized the MIP@CdTe QDs through a simple sol−gel method. They used 3-aminopropyltriethoxysilane and tetraethoxysilane as functional monomer and cross-linker, respectively. These were then used for the determination of ciprofloxacin in the range of 0.5−24 μM with the limit of detection being 0.23 μM. This probe was also applied for the determination of this antibiotic in seawater samples with recoveries ranging between 98% and 110%.

3.4 Conclusion

The sol−gel process can provide nanoparticles of controlled sized and porosity along with purity. It avoids the problems of the coprecipitation method. Quantum dots of metals and metal chalcogenides, carbon, graphene, etc. can be easily prepared using this process. There is a wide scope for preparing quantum dots of different materials using this method.

References

Ajibade, P.A., Oluwalana, A.E., 2021. Photocatalytic degradation of single and binary mixture of brilliant green and rhodamine B dyes by zinc sulfide quantum dots. Molecules 26 (24). Available from: https://doi.org/10.3390/molecules26247686.

An, L., Han, X., Li, Y., Hou, C., Wang, H., Zhang, Q., 2019. ZnS−CdS−TaON nanocomposites with enhanced stability and photocatalytic hydrogen evolution activity. J. Sol−gel Sci. Technol. 91 (1), 82−91.

Anupama, K., Paul, T., Ann Mary, K.A., 2021. Solid-state fluorescent selenium quantum dots by a solvothermal-assisted sol−gel route for curcumin sensing. ACS Omega 6 (33), 21525−21533.

Bajaj, N.S., Omanwar, S.K., 2015. Low-temperature stearic acid sol−gel synthesis of α-Al_2O_3 quantum dots and its optical properties. J. Sol−gel Sci. Technol. 75 (1). Available from: https://doi.org/10.1007/s10971-015-3667-7.

Bera, D., Qian, L., Sabui, S., Santra, S., Holloway, P.H., 2008. Photoluminescence of ZnO quantum dots produced by a sol−gel process. Opt. Mater. 30 (8), 1233−1239.

Chen, J., Shu, J., Anqi, Z., Juyuan, H., Yan, Z., Chen, J., 2016. Synthesis of carbon quantum dots/TiO_2 nanocomposite for photo-degradation of rhodamine B and cefradine. Diam. Relat. Mater. 70, 137−144.

Chen, S., Li, Y., Wu, S., Jiang, X., Yang, H., Su, X., et al., 2020. A phosphorescent probe for cephalexin consisting of mesoporous thioglycolic acid-modified Mn: ZnS quantum dots coated with a molecularly imprinted polymer. Microchim. Acta. 187 (1). Available from: https://doi.org/10.1007/s00604-019-4038-9.

Chen, Z., Li, X.X., Du, G., Chen, N., Suen, A.Y., 2011. A sol−gel method for preparing ZnO quantum dots with strong blue emission. J. Lumin. 131 (10), 2072−2077.

Dey, A., Sarkar, S.K., 2020. Room temperature ZnO and Au-ZnO quantum dots thin film gas sensor fabrication for detecting of volatile organic compound gases. IEEE Sens. J. 20 (21), 12602−12609.

Ensafi, A.A., Nasr-Esfahani, P., Rezaei, B., 2018. Synthesis of molecularly imprinted polymer on carbon quantum dots as an optical sensor for selective fluorescent determination of promethazine hydrochloride. Sens. Actuators B: Chem. 257, 889−896.

Garcia, I.M., Souza, V.S., Hellriegel, C., Scholten, J.D., Collares, F.M., 2019. Ionic liquid−stabilized titania quantum dots applied in adhesive resin. J. Dental Res. 98 (6), 682−688.

Ge, L., Liu, N., Yang, P., Cheng, X., 2013. Composite TiO_2 film with quantum dots fabricated through a sol−gel process. J. Nanosci. Nanotechnol. 13 (4), 2943−2947.

Gnanasekaran, L., Hemamalini, R., Ravichandran, K., 2015. Synthesis and characterization of TiO_2 quantum dots for photocatalytic application. J. Saudi Chem. Soc. 19 (5), 589−594.

Guo, C., Cao, K., Zhang, Z., Xiong, Y., Chen, Y., Wang, Y., 2020. ZnS quantum dots/gelatin nanocomposites with a thermo-responsive sol−gel transition property produced by a facile and green one-pot method. ACS Sustain. Chem. Eng. 8 (11), 4346−4352.

Haghani, S.K., Ensafi, A.A., Kazemifard, N., Rezaei, B., 2020. Development of a selective and sensitive chlorogenic acid fluorimetric sensor using molecularly imprinted polymer ZnO quantum dots. IEEE Sens. J. 20 (11), 5691−5697.

Han, L.L., Cui, L., Wang, W.H., Wang, J.L., Du, X.W., 2012. On the origin of blue emission from ZnO quantum dots synthesized by a sol−gel route. Semicond. Sci. Technol. 27 (6). Available from: https://doi.org/10.1088/0268-1242/27/6/065020.

Hayakawa, T., Selvan, S., Nogami, M., 2000. Energy transfer between Eu^{3+} ions and CdS quantum dots in sol−gel derived CdS/SiO_2: Eu^{3+} gel. J. Sol−gel Sci. Technol. 19 (1), 779−783.

Javed, S., Islam, M., Mujahid, M., 2019. Synthesis and characterization of TiO_2 quantum dots by sol gel reflux condensation method. Ceram. Int. 45 (2), 2676−2679.

Jiang, H., Yao, X., Che, J., Wang, M., Kong, F., 2004. Preparation of ZnSe quantum dots embedded in SiO_2 thin films by sol−gel process. Ceram. Int. 30 (7), 1685−1689.

Ke, J., Li, X., Zhao, Q., Liu, B., Liu, S., Wang, S., 2017. Up conversion carbon quantum dots as visible light responsive component for efficient enhancement of photocatalytic performance. J. Colloid Interface. Sci. 496, 425−433.

Kharangarh, P.R., Ravindra, N.M., Rawal, R., Singh, A., Gupta, V., 2021. Graphene quantum dots decorated on spinel nickel cobaltite nanocomposites for boosting supercapacitor electrode material performance. J. Alloy. Comp. 876. Available from: https://doi.org/10.1016/j.jallcom.2021.159990.

Korala, L., Wang, Z., Liu, Y., Maldonado, S., Brock, S.L., 2013. Uniform thin films of CdSe and CdSe (ZnS) core (shell) quantum dots by sol−gel assembly: enabling photoelectrochemical characterization and electronic applications. ACS Nano 7 (2), 1215−1223.

Kumar, S., Singh, F., Kapoor, A., 2014. Synthesis and characterization of nano-crystalline ZnO quantum dots via sol−gel route for dye-sensitized solar cells. Int. J. Recent. Trends Electr. Electron. Engg 4 (1), 25−29.

Leelavathi, A., Mukherjee, B., Nethravathi, C., Kundu, S., Dhivya, M., Ravishankar, N., et al., 2013. Highly photoactive heterostructures of PbO quantum dots on TiO_2. RSC Adv. 3 (43), 20970−20977.

Li, H., Qu, F., 2007. Synthesis of CdTe quantum dots in sol−gel-derived composite silica spheres coated with calix [4] arene as luminescent probes for pesticides. Chem. Mater. 19 (17), 4148−4154.

Li, Y.S., Jiang, F.L., Xiao, Q., Li, R., Li, K., Zhang, M.F., et al., 2010. Enhanced photocatalytic activities of TiO2 nanocomposites doped with water-soluble mercapto-capped CdTe quantum dots. Appl. Cataly. B: Environ. 101 (1−2), 118−129.

Li, H., Luo, K., Xia, M., Wang, P.W., 2014. Synthesis and optical properties of Pr^{3+}−doped ZnO quantum dots. J. Non-Crystal. Solids 383, 176−180.

Li, Y., Xie, S., Xu, D., Shu, G., Wang, X., 2021. Antibacterial activity of ZnO quantum dots and its protective effects of chicks infected with *Salmonella pullorum*. Nanotechnology 32 (50). Available from: https://doi.org/10.1088/1361-6528/ac2846.

Liu, X., Xing, X., Li, Y., Chen, N., Djerdj, I., Wang, Y., 2015. Controllable synthesis and change of emission color from green to orange of ZnO quantum dots using different solvents. N. J. Chem. 39 (4), 2881−2888.

Lin, K.F., Cheng, H.M., Hsu, H.C., Lin, L.J., Hsieh, W.F., 2005. Band gap variation of size-controlled ZnO quantum dots synthesized by sol−gel method. Chem. Phys. Lett. 409 (4−6), 208−211.

Liu, Y.H., Tan, L.J., Wang, K.P., Wang, J.T., 2022. Rapid detection of ciprofloxacin in seawater based on CdTe quantum dots coated with molecularly imprinted polymers. Int. J. Mod. Phys. B . Available from: https://doi.org/10.1142/S0217979222400124.

Miao, R., Luo, Z., Zhong, W., Chen, S.Y., Jiang, T., Dutta, B., et al., 2016. Mesoporous TiO_2 modified with carbon quantum dots as a high-performance visible light photocatalyst. Appl. Cataly. B: Environ. 189, 26–38.

Moghaddam, E., Youzbashi, A.A., Kazemzadeh, A., Eshraghi, M.J., 2015. Preparation of surface-modified ZnO quantum dots through an ultrasound assisted sol–gel process. Appl. Surf. Sci. 346, 111–114.

Mohamed, W.A., Ibrahem, I.A., El-Sayed, A.M., Galal, H.R., Handal, H., Mousa, H.A., et al., 2020. Zinc oxide quantum dots for textile dyes and real industrial wastewater treatment: solar photocatalytic activity, photoluminescence properties and recycling process. Adv. Powder Technol. 31 (6), 2555–2565.

Qiu, Y., Xing, Z., Guo, M., Zhao, T., Wang, Y., Chen, P., et al., 2021. Cadmium sulfide quantum dots/dodecahedral polyoxometalates/oxygen-doped mesoporous graphite carbon nitride with Z-scheme and type-II as tandem heterojunctions for boosting visible-light-driven photocatalytic performance. J. Colloid Interface Sci. 582, 752–763.

Rakibuddin, M., Kim, H., 2020. Sol–gel derived Fe_3O_4 quantum dot decorated silica composites for effective removal of arsenic (III) from water. Mater. Chem. Phys. 240. Available from: https://doi.org/10.1016/j.matchemphys.2019.122245.

Rakibuddin, M., Shinde, M.A., Kim, H., 2020. Facile sol–gel fabrication of MoS_2 bulk, flake and quantum dot for electrochromic device and their enhanced performance with WO_3. Electrochim. Acta 349. Available from: https://doi.org/10.1016/j.electacta.2020.136403.

Rempel, A.A., Kuznetsova, Y.V., Dorosheva, I.B., Valeeva, A.A., Weinstein, I.A., Kozlova, E. A., et al., 2020. High photocatalytic activity under visible light of sandwich structures based on anodic TiO_2/CdS nanoparticles/Sol–gel TiO_2. Top. Catal. 63 (1), 130–138.

Sankar, M., Jothibas, M., Muthuvel, A., Rajeshwari, A., Jeyakumar, S.J., 2020. Structural, optical and photocatalytic degradation of organic dyes by sol gel prepared Ni doped CdS nanoparticles. Surf. Interfaces 21. Available from: https://doi.org/10.1016/j.surfin.2020.100775.

Schmitz, F., de Albuquerque, M.B.S., Alberton, M.D., Riegel-Vidotti, I.C., Zimmermann, L.M., 2020. Zein films with ZnO and ZnO: Mg quantum dots as functional nanofillers: new nanocomposites for food package with UV-blocker and antimicrobial properties. Poly. Test. 91. Available from: https://doi.org/10.1016/j.polymertesting.2020.106709.

Shi, Y., Ke, J., Zhao, Q.D., Li, X.Y., Zheng, N., Xue, F.H., 2014. Synthesis of CdSe quantum-dots-sensitized TiO_2 nanocomposites with visible-light photocatalytic activity. Adv. Mater. Res. 924. Available from: https://doi.org/10.4028/http://www.scientific.net/AMR.924.3.

Song, T., Feng, X., Ju, H., Fang, T., Zhu, F., Liu, W., et al., 2020. Enhancing acid, base and UV light resistance of halide perovskite $CH_3NH_3PbBr_3$ quantum dots by encapsulation with ZrO_2 sol. J. Alloy. Compd. 816. Available from: https://doi.org/10.1016/j.jallcom.2019.152558.

Sonker, R.K., Yadav, B.C., Gupta, V., Tomar, M., 2020. Synthesis of CdS nanoparticle by sol–gel method as low temperature NO_2 sensor. Mater. Chem. Phys. 239. Available from: https://doi.org/10.1016/j.matchemphys.2019.121975.

Sonker, R.K., Shastri, R., Johari, R., 2021. Superficial synthesis of CdS quantum dots for an efficient perovskite-sensitized solar cell. Energy Fuels 35 (9), 8430–8435.

Sood, S., Kumar, S., Umar, A., Kaur, A., Mehta, S.K., Kansal, S.K., 2015. TiO_2 quantum dots for the photocatalytic degradation of indigo carmine dye. J. Alloy. Comp. 650, 193–198.

Soumya, S., Sheemol, V.N., Amba, P., Mohamed, A.P., Ananthakumar, S., 2018. Sn and Ag doped ZnO quantum dots with PMMA by in situ polymerization for UV/IR protective, photochromic multifunctional hybrid coatings. Sol. Energy Mater. Sol. Cell 174, 554–565.

Sowik, J., Miodyńska, M., Bajorowicz, B., Mikolajczyk, A., Lisowski, W., Klimczuk, T., et al., 2019. Optical and photocatalytic properties of rare earth metal-modified ZnO quantum dots. Appl. Surf. Sci. 464, 651–663.

Sun, L.W., Shi, H.Q., Li, W.N., Xiao, H.M., Fu, S.Y., Cao, X.Z., et al., 2012. Lanthanum-doped ZnO quantum dots with greatly enhanced fluorescent quantum yield. J. Mater. Chem. 22 (17), 8221–8227.

Vasiljevic, Z.Z., Dojcinovic, M.P., Vujancevic, J.D., Jankovic-Castvan, I., Ognjanovic, M., Tadic, N.B., et al., 2020. Photocatalytic degradation of methylene blue under natural sunlight using iron titanate nanoparticles prepared by a modified sol–gel method. R. Soc. Open. Sci. 7 (9). Available from: https://doi.org/10.1098/rsos.200708.

Vyas, Y., Chundawat, P., Dharmendra, D., Jain, A., Punjabi, P.B., Ameta, C., 2022. Biosynthesis and characterization of carbon quantum DOTS@ CuS composite using water hyacinth leaves and its usage in photocatalytic dilapidation of Brilliant Green dye. Mater. Chem. Phys. 281. Available from: https://doi.org/10.1016/j.matchemphys.2022.125921.

Wang, X., Li, J., 2021. Sol–gel fabrication of Ag-Coated ZnO quantum dots nanocomposites with excellent photocatalytic activity. Opt. Mater. 118. Available from: https://doi.org/10.1016/j.optmat.2021.111235.

Wang, Y., Lin, F., Gu, X.L., 2011. Load and resistance factors for progressive collapse resistance design of reinforced concrete building structures. Adv. Mater. Res. 255, 338–344.

Wang, C., Luo, S., Liu, C., Chen, C., 2020. W_{O3} quantum dots enhanced the photocatalytic performances of graphene oxide/Ti_{O2} films under flowing dye solution. Inorg. Chem. Commun. 115. Available from: https://doi.org/10.1016/j.inoche.2020.107875.

Xu, H., Wang, H., Lu, Y., Zeng, Y., Yang, Y., Zhang, Z., et al., 2021. Ce_{O2} quantum dots for highly selective and ultrasensitive fluorescence detection of 4-nitrophenol via the fluorescence resonance energy transfer mechanism. Spectrochim. Acta Part. A: Mol. Biomol. Spectrosc. 262. Available from: https://doi.org/10.1016/j.saa.2021.120115.

Yamane, M., Takada, T., Mackenzie, J.D., Li, C.Y., 1992. Preparation of quantum dots by the sol–gel process. Sol–gel Opt. II 1758, 577–586.

Yang, K., Guo, Q., Li, H., Hao, X., Ma, Y., Yang, M., et al., 2018. Highly efficient sol–gel synthesis for ZnS@ N, S co-doped carbon nanosheets with embedded heterostructure for sodium ion batteries. J. Power Sources 402, 340–344.

Yang, C., Wang, L., Zhang, Z., Chen, Y., Deng, Q., Wang, S., 2020. Fluorometric determination of fipronil by integrating the advantages of molecularly imprinted silica and carbon quantum dots. Microchim. Acta 187 (1). Available from: https://doi.org/10.1007/s00604-019-4005-5.

Ye, Y., 2018. Photoluminescence property adjustment of ZnO quantum dots synthesized via sol–gel method. J. Mater. Sci.: Mater. Electron. 29 (6), 4967–4974.

Yu, Y., Chen, D., Huang, P., Lin, H., Wang, Y., 2010. Structure and luminescence of Eu^{3+} doped glass ceramics embedding ZnO quantum dots. Ceram. Int. 36 (3), 1091–1094.

Yu, J., Caravaca, A., Guillard, C., Vernoux, P., Zhou, L., Wang, L., et al., 2021. Carbon nitride quantum dots modified TiO_2 inverse opal photonic crystal for solving indoor vocs pollution. Catalysts 11 (4). Available from: https://doi.org/10.3390/catal11040464.

Zaidi, R., Azam, A., 2021. Investigation of structural, optical and antibacterial properties of zinc sulphide quantum dots prepared by sol–gel method. In: AIP Conference Proc. 2369, 1, doi: org/10.1063/5.0060815.

Zhang, L., Yin, L., Wang, C., Lun, N., Qi, Y., Xiang, D., 2010a. Origin of visible photoluminescence of ZnO quantum dots: defect-dependent and size-dependent. J. Phys. Chem. C. 114 (21), 9651–9658.

Zhang, X., Hou, S., Mao, H., Wang, J., Zhu, Z., 2010b. Influence of annealing temperature on the photoluminescence properties of ZnO quantum dots. Appl. Surf. Sci. 256 (12), 3862–3865.

Zhang, J., Zhao, S.Q., Zhang, K., Zhou, J.Q., Cai, Y.F., 2012. A study of photoluminescence properties and performance improvement of Cd-doped ZnO quantum dots prepared by the sol–gel method. Nanoscale Res. Lett. 7 (405). Available from: https://doi.org/10.1186/1556-276X-7-405.

Zhang, L., Wang, J., Fang, G., Deng, J., Wang, S., 2020. A molecularly imprinted polymer capped nitrogen-doped graphene quantum dots system for sensitive determination of tetracycline in animal-derived food. ChemistrySelect 5 (2), 839–846.

Zhang, X., Luo, S., Wu, X., Feng, M., Li, Y., Han, H., et al., 2021. Effect of alkali bases on the synthesis of ZnO quantum dots. Open. Chem. 19 (1), 377–384.

Zhao, Z., Li, H., Huang, L., Tan, Y., Liu, F., Li, W., 2021. Preparation of graphene quantum dots-doped TiO_2 nanocomposites via a sol–gel method for photocathodic protection. Mol. Cryst. Liq. Cryst. 2021. Available from: https://doi.org/10.1080/15421406.2021.1966873.

Zhong, J., Zhao, H., Zhang, C., Ma, X., Pei, L., Liang, X., et al., 2014. Sol–gel synthesis and optical properties of $CuGaS_2$ quantum dots embedded in sodium borosilicate glass. J. Alloy. Comp. 610, 392–398.

Zhou, P., Xie, Y., Fang, J., Ling, Y., Yu, C., Liu, X., et al., 2017. CdS quantum dots confined in mesoporous TiO_2 with exceptional photocatalytic performance for degradation of organic pollutants. Chemosphere 178. Available from: https://doi.org/10.1016/j.chemosphere.2017.03.024.

Zou, T., Xing, X., Yang, Y., Wang, Z., Wang, Z., Zhao, R., et al., 2020. Water-soluble ZnO quantum dots modified by (3-aminopropyl) triethoxysilane: the promising fluorescent probe for the selective detection of Cu^{2+} ion in drinking water. J. Alloy. Comp. 825. Available from: https://doi.org/10.1016/j.jallcom.2020.153904.

Chapter 4

Laser ablation synthesis of quantum dots

Neetu Shorgar[1], **Indu Bhati**[2] **and Priyanka Jhalora**[1]
[1]*Department of Chemistry, PAHER University, Udaipur, Rajasthan, India,* [2]*Maribyrnong, VIC, Australia*

4.1 Introduction

LASER or Laser is light amplification by the stimulated emission of radiation. The first laser was built by Maiman (1960) based on theoretical work by Schawlow and Townes (1958). A laser differs from other light sources in the context that it emits coherent light. Its spatial coherence allows it to be focused on a tight spot, which is utilized in laser lithography and cutting. It also allows this laser beam to stay narrow even over great distances (collimation), which finds applications in laser lidar and pointers. Lasers can have temporal coherence also, which can be used to produce a broad spectrum with ultrashort pulses of light but their duration is short enough to be in the order of femtoseconds (10^{-15} s).

Lasers find applications in laser printers, optical disk drives, barcode scanners, fiber-optics, DNA sequencing instruments, lighting displays, laser surgery, photolithography, free-space optical communication, cutting and welding materials, skin treatments, as well as military and law enforcement devices for marking targets and measuring range and speed. The semiconductor lasers (blue to near-UV) have been used in place of light-emitting diodes (LEDs) as a white light source. Such laser devices are used in some car headlights.

4.2 Laser ablation

Laser ablation (LA) is a complex process. The laser will penetrate the surface of the sample and that depends on its wavelength as well as the refractive index of the target material used. A high electric field is generated due to laser irradiation that is enough to remove electrons from the bulk of the sample. These free electrons then collide with the atoms of the sample,

Quantum Dots. DOI: https://doi.org/10.1016/B978-0-12-824153-0.00004-5

transferring their energies. As a result, the target surface is heated, followed by vaporization, plasma formation, nucleation, and agglomeration, resulting in raw patio and/or quantum dots (Fig. 4.1).

The field of LA has been excellently reviewed by various researchers (Kim et al., 2017; Farshbaf et al., 2018; Ravi Kumar et al., 2019).

Mansoureh and Parisa (2018) observed that purity is a very important factor when metal nanoparticles (NPs) are to be applied in biological and medical fields. It is therefore, necessary to prepare metal NPs or quantum dots with the desired shape and size distribution.

4.2.1 Advantages

There are the following advantages in using the LA method:

- It is a simple and versatile method.
- It is relatively low-cost method except the cost of the instrument.
- It is a green approach.
- It does not require toxic chemicals or reagents.
- It provides high production rates.
- It provides good control of particle size.
- It provides particles with good monodispersity.

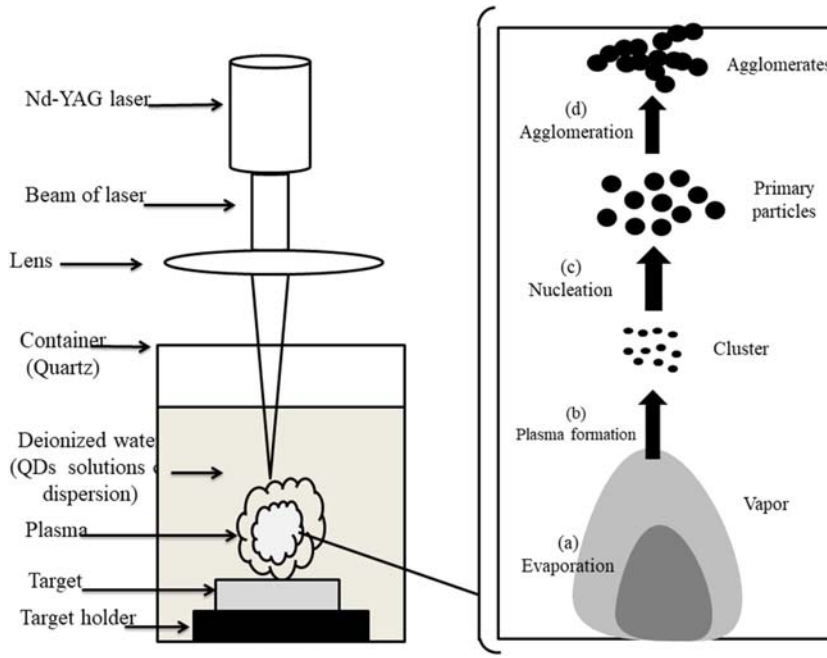

FIGURE 4.1 Laser ablation method for synthesis of quantum dots.

4.2.2 Disadvantages

The LA method has certain disadvantage also and these are:

- It has a slow rate of production of NPs.
- The consumption of energy is high.
- The cost of laser equipment is high.
- Ablation efficiency decreases on using laser for a longer period within a session.

4.3 Metal-based quantum dots

4.3.1 Metals

Silver NPs were produced by Pyatenko et al. (2004) on irradiating Ag target with a laser beam in pure water. They reported that these are very small spherical particles with size in the range of 2−5 nm.

Besner et al. (2005) obtained colloidal gold NPs using femtosecond LA of a gold plate in aqueous solutions. This method makes it possible to functionalize nanomaterial by an appropriate capping ligand. They were able to control the reactivity of as- prepared gold particles and their size by using polymers such as polyethylene glycol and dextran. The size of these NPs was found to be 5 nm, as evident from TEM images. It was also observed that long-term stability of gold particles was improved significantly on adding capping agents. A photoluminescence (PL) signal was also obtained in the violet−blue spectral range. It was revealed that as-functionalized NPs can find potential application in bioimaging and biosensing.

LA synthesis in solution (LASiS) has emerged as a new technique for synthesizing noble metal NPs (NM NPs). It is a "green" method, which does not require additional stabilizing molecules. However, presently LASiS has certain limitations in controlling the size of NM NPs, which can be overcome in the future. Amendola and Meneghetti (2009) reviewed the overview of LASiS.

Monodispersed spherical bismuth (Bi) NPs with diameters of 5−20 nm were synthesized by Verma et al. (2013) using a liquid pulsed LA method. It was reported that ablation time and surfactant ($C_{12}H_{25}NaO_4S$) both played a crucial role in the size of the NPs and their optical properties. It was proposed that such QDs can find potential applications in hypothermia treatment. Malviya and Chattopadhyay (2014) synthesized Ag−Cu alloy NPs through a LA technique under an aqueous medium in four different compositions. The observations were carried out on NPs with core−shell structure of two different sizes: ∼5 and ∼20 nm.

Kőrösi et al. (2016) synthesized ligand-free Ag NPs with particle size of 3 and 20 nm by application of picosecond LA. It was observed that a laser processing system allowed a high control on particle sizes. The effect of size

on the antibacterial activity of these as- synthesized Ag NPs was tested against *Escherichia coli* and *Staphylococcus aureus*. Li and Chen (2016) developed a new strategy for synthesizing stable and monodispersed silver quantum dots by laser fragmentation of bulk Ag in aqueous medium. They used polysorbate 80 as both a dispersing and stabilizing agent. It was revealed that surfactant played an important role in determining the size of these Ag nanostructures. The Ag QDs have excellent photostability of ~500 h and enhanced PL at 510 nm.

Ryabchikov et al. (2016) ablated a gold target using laser radiation (femtosecond) in aqueous solutions of initially prepared Si NPs. It was observed that Au-based spherical colloids were obtained with an average size in the range of 5−10 nm. It was proposed that as-prepared nanostructures can find various applications in the field of catalysis, biomedicine, and photovoltaics. Boltaev et al. (2018) observed that there is a correlation between efficient third harmonic generation in the plasmas and strong nonlinear optical response of silver NPs due to plasmon resonance. It was reported that nonlinear absorption coefficient of Ag NPs (8 nm) was high enough (3×10^{-5} cm W^{-1}) at the wavelength of 1064 nm.

Sadrolhosseini et al. (2019) fabricated gold NPs in the graphene quantum dots (GQDs) solution via LA. The particle size was controlled by changing ablation time from 5 to 25 min. A peak at 319.8 nm was attributed to GQDs. It was observed that particle size was in the range of 11.74−28.29 nm, which was found to decrease with increasing ablation time. Gold NPs in a carbon quantum dots (CQDs) solution were also prepared (Sadrolhosseini et al., 2020) using a LA method. It was observed that the variation in the photoluminescent peak in the presence of the gold NPs was higher compared to pure CQDs. It can be used for the detection of pyrene with a limit of detection of 1 ppm.

4.3.2 Metal oxides

Murali (2001) prepared indium oxide (IO) NPs via a reactive LA method. An average particle size of these particles was found to be 6.6 nm, as evident from XRD and TEM data. These laser ablated samples exhibited a blueshift of 110 meV compared to bulk material. Ajimsha et al. (2007) fabricated luminescent, transparent, and biocompatible ZnO quantum dots in three solvents (water, methanol, and ethanol) using a liquid-phase pulsed LA method. They did not use any surfactant. It was confirmed that crystalline ZnO quantum dots were found to have a uniform size distribution of 7 nm. As-prepared highly luminescent nontoxic ZnO quantum dots could find applications in the field of biomedicine as florescent probes.

A pulsed laser emitting UV radiations was used by Gondal et al. (2009) for the synthesis of nanostructured ZnO and ZnO_2. For the synthesis of NPs of ZnO_2, a highly pure metallic plate of Zn target was kept under repeated

laser irradiation in the presence of H_2O_2 as an oxidizing agent. It was reported that size, optical properties, and morphology of as-synthesized ZnO and ZnO_2 by this method were influenced by postannealing conditions. It was revealed that ZnO_2 was completely converted to ZnO by annealing ZnO_2 for 8 h at 200°C. It was reported that the size of ZnO changes from 5 to 19 nm raising the annealing temperature from 200°C to 600°C. Optical properties as well as bandgap of nano-ZnO were also changed.

Suzuki et al. (2009) used pulsed LA to prepare quantum dots of zinc oxide using differential mobility analyzer (DMA). Initially, irregularly shaped ZnO particles were obtained, but when annealing temperature was increased, then they are transformed into spherical QDs. It was observed that ZnO QDs obtained by this method were crystallized (single crystallites) with a wurtzite structure. The ZnO QDs with average size in the range of 4.8−8.1 nm could be easily prepared by reducing the specified sizes of DMA.

Zheng et al. (2010) prepared ultrafine Y_2O_3:Pr, Yb NPs using femtosecond pulsed LA. It was reported that these spherical particles have a size of about 10 nm (diameter) with a narrow size distribution. As-prepared NPs exhibited significantly improved upconversion intensity as compared to NPs, which were prepared by the sol−gel method.

Zeng et al. (2011) synthesized ZnO quantum dots through laser irradiation of hollow nanospheres of ZnO in liquid medium. It was reported that as-synthesized QDs have diameters ranging between 1 and 8 nm, exhibiting a quantum size effect, which can be tuned by variation of parameters of the laser irradiation process. It was observed that the main PL emission bands evolved are from blue to green, finally reaching ultraviolet peaks. These as-fabricated QDs can show optical and optoelectronic applications.

Eita et al. (2012) fabricated thin UV-blocking films of poly(methyl methacrylate) (PMMA) and ZnO quantum dots via spin-coating. It was revealed that an average thickness of bilayer before heating was 9.5 nm, which reduces to 8.6 nm after heating at 100°C for 1 h. It was also observed that surface roughness was 3.6 and 8.4 nm for one and ten bilayer films, respectively, as evident from atomic force microscopy. The absorption of UV radiation increases with increasing number of bilayers, but transmission was damped at wavelength <375 nm. It was reported that thin films had a high transparency in the visible region. The single layer of PMMA/ZnO QDs thin films was found to be hydrophobic in nature.

Singh and Gopal (2012) used nanosecond (ns) pulsed LA of zinc rod, which was placed on the bottom of a glass vessel containing methanol. As a result, a colloidal solution of drop-shaped zinc oxide quantum dots and their self-assembly into different dendritic nanostructures were obtained. It was observed that average length, width, and aspect ratio of these as-prepared drop-shaped zinc oxide quantum dots were found to be 6 ± 2.4 nm, 3.5 ± 1.4 nm, and 1.69 ± 0.4 nm, respectively. Its PL spectrum exhibited emission peaks in UV, violet, blue, and green spectral regions.

The SnO_2 quantum dots were synthesized by Singh et al. (2012) using LA in liquid. The diameter of the SnO_2 NPs was found in the range of 1−5 nm as evident from HRTEM images. As-prepared SnO_2 QDs exhibited tetragonal crystalline structure. Their PL spectrum showed green and blue emission peaks at 540 nm and 445 nm, respectively. It was proposed that these QDs have great potential for use in biosensors, optoelectronics, etc. Patel et al. (2013) synthesized SnO_2-QDs ($\sim$ 1−5 nm) by LA technique in liquid. Then these QDs were electrophoretically deposited onto the surface of indium tin oxide (ITO)-coated glass electrodes. Then ssDNA/SnO_2-QDs/ITO bioelectrodes were fabricated and these bioelectrodes have been used for DNA hybridization.

Drmosh et al. (2019) fabricated ZnO NPs by decomposing zinc peroxide (ZnO_2) quantum dots, which were synthesized by LA of microstructured Zn powder in 3% H_2O_2. Then rGO/ZnO nanocomposite was prepared from them via pulsed LA in liquid (PLAL). The surface of the rGO/ZnO hybrid was decorated with a Pt thin film so as to get a ternary rGO/ZnO/Pt hybrid nanocomposite. It was observed that this Pt-loaded rGO/ZnO gas sensor (thickness of 2 nm) exhibited selectivity and excellent response for sensing a low concentration of hydrogen. This nanocomposite was found to be 10 and five times better than pure ZnO, and rGO/ZnO nanocomposite, respectively. It was proposed that rGO/ZnO/Pt hybrid nanocomposite is a potential promising candidate for fabricating high-performance gas sensors for H_2.

Mitra et al. (2019) prepared highly crystalline p-type manganese oxide (MnO) wide bandgap semiconductor quantum dots via femtosecond-LA in liquid. This p-type MnO QD material could find applications in the industrial production of high-performance solution-processed deep UV optoelectronics on a large scale. Mostafa et al. (2019) synthesized tungsten oxide QDs with pulsed laser−assisted ablation. They used tungsten (tablet) as a target in liquid media. This method is a green chemical method as it uses only tungsten tablet and water for preparing tungsten oxide without impurities. It was confirmed by morphological analysis that the as-prepared tungsten oxide NPs were quantum dots with average diameter of about 5 nm. They used these as-prepared samples as the catalyst for the degradation of 4-nitrophenol.

Mwafy et al. (2019) prepared zinc oxide NPs using CQD solution through a LA technique. It was observed that ZnO-NPs in the CQD solution were formed with capping of the ZnO NPs (spherical) by a functional group of the CQD. As-prepared ZnO-NPs in the CQD solution had a particle size in the range of 7.5−14.03 nm. These prepared samples were used in the detection of lead and mercury ions in aqueous solution and it was found that a PL peak shift was greater in the presence of mercury ions compared to lead ions.

Kateshiya et al. (2020) developed a facile synthetic route for preparing highly blue fluorescent tyrosine-coated molybdenum oxide quantum dots (Tyr-MoO_3 QDs). They used tyrosine as a surface ligand for the functionalizing MoO_3 QDs.

It was revealed that as-prepared Tyr-MoO_3 QDs could act as a sensor for sensitive as well as rapid identification of imidacloprid via fluorescence quenching mechanism. The as-developed probe was also applied for detection of imidacloprid in real samples.

Wang et al. (2021) synthesized multifunctional ZnO, which was decorated on Fe hierarchical nanostructures using LA technique. They decorated ZnO quantum dots on Fe nanowires, ZnO nanospindles cluster on Fe core and flocky Fe@ZnO core−shell nanospheres (Fe@ZnO CSNSs). As-synthesized Fe@ZnO CSNSs were then used for the photocatalytic degradation of rhodamine B. It was reported that photocatalytic removal of rhodamine B was about 94.1% in the presence of natural light irradiation for 20 min.

4.3.3 Metal sulfides

Formation of quantum dots of ZnSe and CdS was reported under ablation of bulk semiconductors in a liquid environment (ethanol, diethyleneglycol, etc.) by Anikin et al. (2002). It was confirmed that these quantum dots are crystalline in nature with an average size of ∼10−20 nm. Lalayan (2005) prepared colloidal quantum dots of GaAs and CdS semiconductors through LA in the liquid media. The large blueshift of the PL was evaluated, and it was connected to size effects. Luminescence spectra at the wavelength 405 nm (CdS) and 420 nm (GaAs) indicated that sizes of QDs were in the range 2−3 nm.

Zheng et al. (2008) synthesized Cu-doped ZnS (ZnS:Cu) quantum dots in deionized water using femtosecond LA of a bulk (ZnS:Cu) target. It was reported that these quantum dots exhibited good water solubility and colloidal stability. An average size of as-prepared quantum dots varied in the range of 2.1−4.0 nm on changing the laser fluence. It resulted in a redshift of the emission peak.

Ka et al. (2011) synthesized lead sulfide (PbS) NPs layers onto different substrates at room temperature using pulsed laser deposition (PLD). It was reported that average size of these NPs can be controlled by changing the number of LA pulses. A blueshift in PL was observed from 1420 to 880 nm. As-prepared PbS NPs had a diameter of 8.5 nm, which was decreased to 2.5 nm, which confirmed the quantum size effect. Khan and BiBi (2014) synthesized densely packed CdS NPs using ns-pulsed LA. The average size of these NPs was found to be in the range of 5−10 nm. An energy bandgap of around 3.03 eV was attributed to band-to-band transition in CdS.

Ka et al. (2012) used the pulsed LA technique for direct synthesis of single-walled carbon nanotube/PbS-quantum dot (SWCNT/PbS-QD) nanohybrids (NHs). This not only permitted control on the size of the PbS-QDs but also made it possible for integration of these SWCNT/PbS-QD NHs into photoconductive devices with a strong photoresponse. Ka et al. (2014) used a PLD technique for fabricating NH heterojunctions (NH-HJs) solar cells.

They decorated TiO_2 nanorods (TiO_2-NRs) on PbS quantum dots (PbS-QDs). They could achieve NH-HJs-based PV devices with high power conversion efficiency (PCE) (4.85%). It was interesting to note that the PCE of these devices was found to be quite stable for several months in the presence of air. It was also reported that the addition of SWCNTs onto the TiO_2-NRs before decorating them by PbS-QDs further enhanced PCE to 5.3%, which may be due to more light absorption and improved charge collection by SWCNTs.

Darwish et al. (2015) synthesized size-tunable (5−12 nm) cadmium sulfide (nano II−VI semiconductor) with different shapes, such as rod, sphere, rope, etc., using a pulsed laser in liquid environment method. It was confirmed that the NPs are crystalline. These nanomaterials can find application in biosensing and photonics. Gondal et al. (2015) prepared TiO_2/ZnO/CdS QDs using a PLAL technique. Here, ZnO reduces the electron−hole recombination in the TiO_2 while CdS will increase the light harvesting efficiency of TiO_2. The morphology of the composite quantum dots was observed by high-resolution TEM indicating that the size of the composite ranges between 10 and 40 nm. Such a composite can be used for energy harvesting using sunlight.

Baldovi et al. (2016) synthesized MoS_2 quantum dots in colloidal suspensions by LA of commercial MoS_2 in acetonitrile. It was found that there was a lateral size distribution from 5 to 20 nm, as evident from HRTEM images. It was also revealed that these MoS_2 QDs were constituted by 3−6 MoS_2 layers (1.8−4 nm thickness). It was predicted that its photocatalytic activity may be enhanced for H_2 generation in the presence of UV−Vis irradiation using methanol as a sacrificial electron donor. Ka et al. (2016) decorated SWCNTs with PbS quantum dots by the PLD method. As a result, SWCNTs/PbS-QDs NHs were formed. It was found that the number of pulses controlled the average size of PbS-QDs as well as their coverage on the SWCNTs surface. The photoconductive devices were fabricated from these NHs exhibiting an enhanced photoresponse, which was dependent on size of PbS-QDs. The diameter of PbS-QDs was found to be 6.5 nm and bandgap was calculated as 0.86 eV.

The CdS quantum dots with a narrow size distribution were synthesized by Mendonça and de Azevedo (2016) having emission range of 400−700 nm. These were very stable, water-dispersible, and bright. They used a combination of LA technique and thioglycerol, which acted as a catalyst for the hydrolysis of thiosulfate as well as a stabilizing agent. The decomposition of thiosulfate catalyzed by thioglycerol produced S^{2-} ions, which interacted with Cd^{2+} ions to form CdS quantum dots. It was observed that the particle size of monodispersed CDs QDs was about 2.75 nm. As-prepared QDs exhibited bright PL in the yellow-orange region.

Li et al. (2017) fabricated monolayer MoS_2 QDs. They used temporally shaped femtosecond LA of bulk MoS_2 in water. It was revealed that

as-prepared MoS_2 QDs exhibited the highest electrocatalytic activity for the generation of hydrogen evolution reactions (HER) because of the high specific surface area, excellent electrical conductivity, and abundant active edge sites. Caigas et al. (2018) used pulsed LA technology for doping of WS_2 quantum dots with diethylenetriamine (DETA). As-prepared DETA-doped 2H-WS_2 QDs were found to have an average size of $\sim$6 nm. It was interesting to note that PL in WS_2 QDs was enhanced by 74-fold on DETA doping. A dopant-dependent negative photoconductivity was also observed for WS_2 QDs, which may be due to light-induced desorbing of water (oxygen) molecules on the surface.

Ou et al. (2018) reported an ultrafast LA method for the synthesis of MoS_2 quantum dots. It was also revealed that as-prepared QDs exhibited stability and high activity in the electrocatalytic HER. This was attributed to defective structure, very large surface area, high conductivity, and abundance of active sites. As-prepared QDs could be used in sensing, optics, conversion technologies, and energy storage. Sunitha et al. (2018) prepared MoS_2 QDs by pulsed LA from bulk MoS_2 pellets in deionized water. A hexagonal structure of as-prepared MoS_2 pellet was confirmed by XRD and Raman spectra. The mean particle size of these MoS_2 QDs was found to be in the range of 2−30 nm. Kuriakose et al. (2019) synthesized Au-CdS core−shell structure via a laser-assisted method. A gold core was obtained with 8.8 nm average particle size, which was surrounded by a shell coating of CdS (5.8 nm; average diameter). They observed that the rate of photodegradation of methylene blue was more in the presence of Au/CdS core shell as compared to only CdS.

Nguyen et al. (2019a) developed a simple and green route to synthesize highly photoluminescent MoS_2/WS_2 QDs using LA (femtosecond) of raw MoS_2/WS_2 powders. It was reported that as-prepared MoS_2/WS_2 QDs exhibited excellent photostability and intense PL in the blue region with a PLQY of 22.5%. An intense fluorescent emission was attributed to the presence of abundant surface functional groups, such as C−O, CO, and C−N, which can introduce new surface-state emission centers efficiently. Xu et al. (2019) reported a facile method for the synthesis of molybdenum disulfide QDs and tungsten disulfide QDs using LA (femtosecond) and sonication-assisted liquid exfoliation. Average size of these quantum dots was determined to be 3.7 and 2.1 nm, respectively. These MoS_2 and WS_2 QDs exhibited bright blue−green luminescence in the presence of UV irradiation, which may be due to the abundance of functional groups on their surfaces.

An et al. (2020) attempted different methods to produce MoS_2 QDs, such as substrate growth, exfoliation, and colloidal synthesis. MoS_2 QDs with a size of 10 nm were obtained. The resistive switching devices were fabricated using as-prepared MoS_2 QD samples. These devices exhibited a stable unipolar resistive switching behavior without any electroforming process. Soheyli et al. (2020) prepared multicomponent In-based QDs in aqueous phase. They could also tune absorption and PL emission spectra of these

QDs by changing composition of QDs such as Ag-In-S/ZnS, Zn-Ag-In-S/ZnS, and Cu-Ag-In-S/ZnS core/shell QDs. They could produce intense emission by colloidal QDs with amber, green, and red colors. According to them, there is a potential in AgInS-based/ZnS QDs to be used as theranostic agents for treatment and imaging of cancer.

Zhao et al. (2020) designed and fabricated near-infrared fluorescence. When these amorphous Ag_2S QDs were doped by Cu, then a redshift of nontoxic amorphous $Ag_{2-x}Cu_xS$ quantum dots was observed, which improved photothermal conversion efficiency to 44.0%. This may be attributed to the generation of intragap states introduced on Cu doping. It was also revealed that as-prepared amorphous $Ag_{2-x}Cu_xS$ QDs exhibited high long-term biocompatibility also. The MoS_2 quantum dots were synthesized by Pradhan et al. (2021) via pulsed LA assisted photoexfoliation of solid MoS_2 target in distilled water. The average sizes of these MoS_2 quantum dots were $\sim$4, 2.9, and 6.1 nm, when ablation durations were 5, 10, and 20 min, respectively at a fixed laser energy of 40 mJ. The quantum dots resulted in luminescence in the visible region. The as-synthesized MoS_2 quantum dots (colloidal solution) in distilled water exhibited a redshift from excitation wavelength-dependent luminescence, which shifted to longer wavelength by varying excitation wavelength from 290 to 390 nm. It was observed that MoS_2 quantum dots exhibited higher rate of generating hydrogen.

4.3.4 Metal selenides

Singh et al. (2010) could achieve selenium QDs (with 2.74 $\pm$ 2.32 nm diameter) on laser irradiation for 15 min. It was reported that almost 3.75 $\pm$ 0.15 nm size is the quantum confinement limit for QDs of selenium. It was observed that surface defect density of these QDs increases, and defect/electron trap level energy decreases with the time of laser irradiation. CdSe quantum dots were prepared by Horoz et al. (2012) by LA in water. It was reported that as-synthesized CdSe QDs (wurtzite crystal structure) were having average particle size of around 5 nm. These QDs can be attached to ZnO nanowires, so that they can find applications in QD-sensitized nanowire solar cells.

Yang et al. (2017) proposed a femtosecond LA in microfluidics approach, which is free from toxic chemicals. ZnSe quantum dots were found to be in the range of 4−6 nm using hyperbranched polyethyleneimine as functional and structural coated layer; both. An aqueous nanosized micelles consisting of these quantum dots exhibited emission of bright green light. These quantum dots have a great potential for biomedical imaging. Je et al. (2018) synthesized PbSe QDs via PLIL method. It was found that as-prepared sample in PVP solution resulted in the formation of PbSe QDs rock salt crystalline with size of about 6.83 nm. The particle size of PbSe QDs was found to be dependent on wavelength and power of the laser as well as type and concentration of the surfactants.

Balati et al. (2019) synthesized $MoSe_2$ nanosheets, inorganic fullerene-like (IF) $MoSe_2$ and MoO_3 quantum dots using PLAL method. It was then followed by a microwave treatment of bulk-$MoSe_2$ powders. It was interesting to note that two successive microwave steps changed orientation of $MoSe_2$ crystal from horizontal to vertical.

AlGhamdi et al. (2020) reported dye sensitized solar cells, where a TiO_2 photoanode was cosensitized by organic dye N719 and CdSe quantum dots. The photovoltaic performance of this cell (cosensitized with an optimum concentration of CdSe-QDs) was found to be better than that cell, where photoanode was sensitized by N719 dye. It was observed that photovoltaic conversion efficiency of this cell cosensitized by CdSe-QDs (1 mg/15 mL of ethanol) and N719 dye was 7.09%, which was almost 37% rise in photovoltaic efficiency, as compared to the cell, which is sensitized by the N719 dye only.

Omran et al. (2021) prepared cadmium selenide quantum dots using clean-LA in ethanol. It was reported that as-prepared CdSe QDs has a cubic crystal structure with average particle size of 4 nm. These QDs can find application in dye-sensitized solar cells with higher conversion efficiency.

4.4 Nonmetal-based quantum dots

4.4.1 Carbon-based quantum dots

Yu et al. (2014) prepared CQDs/TiO_2 nanosheet (TNS) composites via a simple low-temperature process. It was indicated that TNS were combined well with CQDs via surface carbon−oxygen groups. The photocatalytic activity of this composite was investigated for degradation of rhodamine B in presence of visible light, which was more as compared with CQDs/P25 composites and TNS only.

Nguyen et al. (2016) prepared carbon nanodots (C-dots) using femtosecond LA of graphite powders. Here, they used polyethylene glycol (PEG200N) solution and different concentrations of graphite. The photoluminescent quantum yield of as-prepared C-dots was significantly increased on decreasing the graphite concentration, reaching up to 21%. These C-dots could be used as an efficient fluorescent nanosensor probes for selective and sensitive detection of Fe^{3+} ions because of their high PL.

Synthesis of fluorescent carbon dots-like nanostructures (CNDs) was reported by Reyes et al. (2016) via LA of a carbon solid target in liquid. It was reported that size of close-spherical amorphous CNDs ranged between 5 and 20 nm. An efficient light emission due to excitation at 3.54 eV was observed with the PL intensity, which was centered at 3.23 eV. It was possible to tune the emission wavelength of the CNDs from the near-UV to the green region by adjusting ablation time as well as by modification of ablation and excitation laser wavelength.

Nguyen et al. (2019b) prepared C-dots with broad emissions via femtosecond LA in ethylenediamine solution. The C-dots were found suitable for a broad range of applications, including optical down-conversion devices, bioimaging, and biosensors by selecting different excitation wavelengths without changing their structures. As-prepared C-dots exhibited broad PL from blue to green regions. It was reported that abundant of functional groups created were on the surface of C-dots such as C-N, C-H, and C-O.

Ren et al. (2019) fabricated N-doped micropore CQDs (NM-CQDs) from biomass using a pulsed LA method with a high quantum yield and dual-wavelength PL emission. They observed two coexisting indigo−blue PL emissions in these QODs. The fluorescence lifetime and quantum yield of as-obtained NM-CQDs were as high as 6.56 ns and 32.4%, respectively. It was reported that these NM-CQDs are quite suitable for cellular staining images due to stable and strong PL emission. This high fluorescence of NM-CQDs can find a great potential in engineering and biomedical imaging.

Cui et al. (2020) fabricated CQDs through ultrafast dual beam pulsed LA using low-cost carbon cloth. As-prepared CQDs were homogeneous and the quantum yield of emission was around 35.4%. These QDs exhibited a good stability and excellent performance for anti-jamming, so that these were found suitable for cell bioimaging.

It is difficult to introduce S into the carbon framework of GQDs as its size is much larger than that of C atoms, as-compared to B and N. Kang et al. (2020) reported a one-step and simple method for synthesizing sulfur-doped GQDs (S-GQDs) using PLAL process. It was observed that these S-GQDs exhibited an increased fluorescence quantum yields from 0.8 to 3.89% and excellent photostability. This method of preparing S-GQDs will open up new avenues for their potential applications.

4.4.2 Graphene-based quantum dots

Russo et al. (2014) developed a method for mass production of porous graphene (PG) and GQDs. They used femtosecond LA of highly oriented pyrolytic graphite for this purpose. It was observed that PG layers float at the water−air interface, and on the contrary, GQDs were found dispersed in the solution. It was confirmed that GQDs have dimensions in the range of 2−5 nm. They explained the formation of these materials on the basis of mechanisms, which involved coal gasification and water breakdown.

Habiba et al. (2015) fabricated GQDs (Ag-GQDs) decorated nanocomposites of silver NPs using pulsed laser. Then these nanocomposites were PEGylated, increasing their solubility in aqueous solutions and biocompatibility. The size of GQDs was in the range of 1.6−4 nm. The antibacterial activity of as-synthesized Ag-GQDs was evaluated and compared against Gram-negative (*Pseudomonas aeruginosa*) and Gram-positive bacteria (*S. aureus*) and it was found high as compared to and that of GQDs and

commercial silver NPs (Ag-NPs). It was reported that cell viability was maintained at 100% for normal mammalian cells, which were incubated with Ag-GQDs. As-prepared Ag-GQDs have potential applications in self-sterile textiles, antibacterial coatings, and personal care products.

Narasimhan et al. (2017) synthesized high-quality water-soluble GQDs using a ns pulsed laser and used these GQDs as fluorescent imaging agent. Their emission properties were attributed to the functional groups such as hydroxyl and carboxyl groups on the surface or edges. A deep red fluorescence was observed from the implanted region.

Santiago et al. (2017) synthesized N-doped GQDs using pulsed LA with diethylenetriamine (DETA). As-synthesized N-doped GQDs had an average size of about 3.4 nm and its atomic ratio (N/C) was 26%. It was reported that N-doped GQDs emitted PL with a factor 66 as compared to pristine GQDs. GQDs were synthesized by Calabro et al. (2018) via chemical oxidation of carbon nanoonions (nCNOs) followed by pulsed LA of these nCNOs to give CO-GQDS. Average diameter of these CO-GQDs was found to be 4.1 nm.

Novoa-De León et al. (2019) synthesized nitrogen-doped GQDs (N-GQDs) using PLAL. They ablated graphite target in dimethylformamide (solvent and nitrogen source, both). It was observed that these N-GQDs consists of a graphitic core with particle size of about 3 nm as well as oxygen and nitrogen functionalities. They used as-prepared N-GQDs dispersion for selective detection of ascorbic acid via a signal-on and signal-off system. These N-GQDs could also be used as PL sensor for metal ions.

4.5 Others

Goodwin et al. (1997) synthesized nanocrystalline GaN via reactive LA of gallium metal in nitrogen atmosphere. It was observed that these crystallites were as small as 2 nm (diameter). It was revealed by size-selective PL and PL excitation spectroscopy that there is a continuous range of blueshifted emissions and absorptions as compared to bulk value for gallium nitride.

Wu et al. (2005) synthesized semiconducting nanocrystals using picosecond pulsed LA. The crystalline nanometer-sized Si particles with average sizes ranging between 1−5 nm exhibited strong quantum confinement effects. Raman spectra confirmed the crystalline nature of these NPs, which showed significant shifts due to confinement. It was revealed that these quantum dots are promising candidates for solar cells.

Yoon et al. (2005) fabricated amorphous GaN quantum dots (a-GaN QDs) at room temperature using a LA technique and densified GaN target. An average particle size of as-prepared a-GaN QDs was found to be 7.9 nm. It was revealed that PL and absorption spectra exhibited a strong emission band centered at 3.9 eV, which was slightly shifted (0.5 eV), that is, a blueshift from the bandgap energy of the GaN crystal. This shift confirmed the

quantum confinement effect. Almeida et al. (2009) reported a LA route for synthesis of thiol capped CdTe colloidal quantum dots. They opined that these NPs were compatible for silica capping, which indicated that they could find application as fluorescent markers.

Qin et al. (2011) carried out Cu doping of ZnO quantum dots by LA of Zn/Cu composite targets immersed in PVP aqueous solution. Firstly, Zn/Cu core−shell particles were synthesized by a galvanic replacement reaction, followed by LA. It was reported that a large amount of Cu-doped ZnO QDs could be produced with ultrafine size, high stability, and good dispersibility. They also controlled dopant concentration (1.8%−4.8%) by just changing the atomic content of Cu in Zn/Cu composite targets. Zakharko et al. (2011) reported synthesis of luminescent SiC quantum dots using LA in pure deionized water. A higher colloidal stability was present for these laser-produced NPs. Long-term stability of colloidal solutions (as-prepared SiC quantum dots) is due to surface charges related to carboxylate anions. It was observed that emission from the Se QDs is centered at 2.75 eV and it does not depend on the laser power used for ablation.

Bagga et al. (2013) reported the synthesis of protein-functionalized luminescent silicon NPs using infrared ultrafast LA. They used silicon in an aqueous solution of *S. aureus* protein A for this purpose. Quantum dots of protein A-capped silicon (8 nm) were obtained with blue−green photoemissions. The biological functionality of these QDs was also studied by them. It was revealed that these Si-based bionanostructures bind IgG selectively in the cells, and therefore, these quantum dots may be suitable for biological applications, such as biomarkers for in vivo applications such as cell labeling, cell staining, and controlled drug delivery.

Gongalsky et al. (2016) reported a secondary toxicity problem of solution of brightly luminescent water-dispersible Si-based QDs using laser-assisted synthesis. These QDs do not exhibit any sign of toxicity; rather they show excellent cellular uptake and biodegradability making them an ideal candidate for bioimaging applications. Rodio et al. (2016) prepared amine-terminated, ultrasmall silicon NPs (Si NPs) in one step by introducing organosilane in Si NPs colloidal solution, which was prepared by ultrafast LA. It was confirmed that the successfully functionalized Si NPs was leading to 5 nm Si dots covered by a thick layer aminopropyltriethoxysilane. Such particles can find some biomedical applications such as biolabels, clinical setting, vector delivery, and contrast agents.

Rasouli et al. (2017) reported that the efficiency of photovoltaic solar cells can be increased by luminescent Si NPs. Sub Si NPs (10 nm) were synthesized using a pulsed LA technique. As-prepared ultrasmall Si NPs show PL characteristics at 517 and 425 nm upon excitation by UV light. The polycrystalline commercial solar cells are coated with these luminescent Si NPs giving an efficiency of about 10%.

Ren et al. (2018) synthesized black phosphorus quantum dots (BPQDs) using pulsed LA. They used isopropyl ether as a solvent. It was reported that QDs have average diameter of about 6 nm and also a height of about 1.1 nm. It was revealed that the PL quantum yield of as-prepared sample was about 20.7 %, which was almost three times higher than that of BPQDs prepared by some other means, for example, ultrasonic exfoliation (about 7.2 %). A stable and blue−violet emission was observed with BPQDs. Apart from it, BPQDs are also utilized in bioimaging in HeLa cells, with excellent biocompatibility. It was also revealed that as-obtained BPQDs have promising potential for biomedical applications, such as bioimaging, biolabeling, and drug delivery.

Most of the methods for synthesis of boron nitride quantum dots (BNQDs) are either complex or time-consuming. Xu et al. (2019) synthesized few-layer BNQDs by liquid-phase ultrashort laser pulse ablation and ultrasonic-assisted exfoliation methods. It was revealed that as-prepared BNQDs have an average size of about 2.1 nm. These BNQDs exhibited bright luminescence emission in the presence of UV light due to abundant surface functional groups. Anjana et al. (2020) prepared Er, Yb-codoped fluorapatite NPs using liquid-phase pulsed LA. A transparent colloidal solution had NPs sizes in the range of 2−4 nm. It was claimed that as-synthesized NPs dispersed in water are biocompatible and can find applications for cell imaging.

Morozova et al. (2020) focused on the possible use of silicon quantum dots ranging from 1 to 10 nm for LED. These QDs have a great potential as optoelectronic devices and fluorescent biomarking agents as they can exhibit blue and red fluorescence. Their biocompatibility compared to conventional toxic group II−VI and III−V metal-based quantum dots makes their practical utilization even more attractive to prevent environmental pollution and harm to living organisms. Sergeev et al. (2020) observed that coupling of HgTe QDs with lattice plasmons decreases the influence of nonradiative decay losses and IR absorption bands of dodecanethiol, which was used as a ligand on the QDs. It was reported that the ease of chemical synthesis and processing of HgTe QDs along with scalability of the direct laser fabrication of nanoantennas with tailored plasmonic responses helps in designing IR-range devices for different applications such as detectors, emitters, sensors, and security systems.

It is bit difficult to tune the PL properties of BNQDs and obtain these QDs with intense and desired PL emission. Recently, Nguyen et al. (2021) proposed a method to synthesize and functionalize BN QDs using femtosecond LA in an organic solution with tunable PL from ultraviolet to green region. It is all due to carbene zigzag edges, which are formed on the surface of BNQDs resulting in effective emission. There is a redshift in colors by increasing the content of carboxyl group on the carbene zigzag edges.

Soliman et al. (2021) synthesized stainless steel grade 304 QDs through LA in water. These were then used in the treatment of laryngeal carcinoma in vitro, without using any external laser source or magnet for hyperthermia. It was revealed that valence of chromium is +3 in these QDs and these show a resonance fluorescence property in the NIR band. It was observed that a dilute solution of QDs, on addition to cell culture medium, suppressed VEGF gene expression and cell proliferation; both of which indicated the death of cancer cells. The +3 valence of Cr and lower percentage of QDs exclude any possibility of QDs toxicity. The most plausible mechanism for death of cancer cells is due to heat shock of NIR resonance fluorescence of QDs.

4.6 Recent developments

LA is a fast-growing technique for the preparation of quantum dots. Some recent advances in this direction are shown in Table 4.1.

TABLE 4.1 Preparation of quantum dots by laser ablation.

Quantum dots	Application	References
Graphene	2D Material defect engineering	Li et al. (2021)
Graphene	Fluorescent probe for detection of Fe^{3+} ions	Shen et al. (2021)
Graphene	Detection of Fe^{+3} (500 nM to 50 μM)	Kang et al. (2022)
Carbon quantum dots	Alleviating amyloid-β mediated neurotoxicity	Li et al. (2022)
Antimony materials with perovskite quantum dots	To protect human eyes and optical equipment from high-power laser damage	Liang et al. (2022)
CQD@$LaPO_4$:Eu^{3+}	Bioimaging of plant cells and as ink for security	Raikwar (2022)
CuO NPs-CNPs	Antimicrobial and antiproliferative activities against breast cancer cell lines, MCF-7	Mohammed et al. (2022)
PVA/CMC/MoO_3NPs	Enhanced optical and electrical characterization of polymeric films	Asnag et al. (2022)
Graphitic carbon quantum dot	Catalytic dehydrogenation and carbonization	Chen et al. (2022)

4.7 Conclusion

Various metals and metal chalcogenides quantum dots can be easily prepared by the LA method. It is equally effective in the preparation of carbon and GQDs. These quantum dots have a very high degree of purity as no chemical is added from outside and a target is exposed to the laser. This method of synthesis is welcome because it provides high-purity quantum dots and in a shorter time; however, the high cost of the equipment is still a concern. This method of synthesis will surpass all other methods in the forthcoming decades.

References

Ajimsha, R.S., Anoop, G., Aravind, A., Jayaraj, M.K., 2007. Luminescence from surfactant-free ZnO quantum dots prepared by laser ablation in liquid. Electrochem. Solid. State Lett. 11 (2). Available from: https://doi.org/10.1149/1.2820767.

AlGhamdi, J.M., AlOmar, S., Gondal, M.A., Moqbel, R., Dastageer, M.A., 2020. Enhanced efficiency of dye co-sensitized solar cells based on pulsed-laser-synthesized cadmium-selenide quantum dots. Sol. Energy 209, 108–117.

Almeida, D.B., Rodriguez, E., Moreira, R.S., Agouram, S., Barbosa, L.C., Jimenez, E., et al., 2009. Laser ablation synthesis route of CdTe colloidal quantum dots for biological applications. In: European Conference on Biomedical Optics. Opt. Soc. Am. Available from: https://doi.org/10.1364/ecbo.2009.7371_0f.

Amendola, V., Meneghetti, M., 2009. Laser ablation synthesis in solution and size manipulation of noble metal nanoparticles. Phys. Chem. Chem. Phys. 11 (20), 3805–3821.

An, S.J., Park, D.Y., Lee, C., Bang, S., Nguyen, D.A., Kim, S.H., et al., 2020. Facile preparation of molybdenum disulfide quantum dots using a femtosecond laser. Appl. Surf. Sci. 511. Available from: https://doi.org/10.1016/j.apsusc.2020.145507.

Anikin, K.V., Melnik, N.N., Simakin, A.V., Shafeev, G.A., Voronov, V.V., Vitukhnovsky, A.G., 2002. Formation of ZnSe and CdS quantum dots via laser ablation in liquids. Chem. Phys. Lett. 366 (3-4), 357–360.

Anjana, R., Krishnapriya, T.K., Jayaraj, M.K., 2020. Clean synthesis of Er, Yb doped fluorapatite upconversion luminescent nanoparticles through liquid phase pulsed laser ablation. Opt. Laser Technol. 131. Available from: https://doi.org/10.1016/j.optlastec.2020.106452.

Asnag, G.M., Awwad, N.S., Ibrahium, H.A., Moustapha, M.E., Alqahtani, M.S., Menazea, A.A., 2022. One-Pot pulsed laser ablation route assisted molybdenum trioxide nano-belts doped in PVA/CMC blend for the optical and electrical properties enhancement. J. Inorg. Organometal. Poly. Mater. . Available from: https://doi.org/10.1007/s10904-022-02257-5.

Bagga, K., Barchanski, A., Intartaglia, R., Dante, S., Marotta, R., Diaspro, A., et al., 2013. Laser-assisted synthesis of *Staphylococcus aureus* protein-capped silicon quantum dots as bio-functional nanoprobes. Laser Phys. Lett. 10 (6). Available from: https://doi.org/10.1088/1612-2011/10/6/065603.

Balati, A., Bazilio, A., Shahriar, A., Nash, K., Shipley, H.J., 2019. Simultaneous formation of ultra-thin MoSe2 nanosheets, inorganic fullerene-like $MoSe_2$ and MoO_3 quantum dots using fast and ecofriendly pulsed laser ablation in liquid followed by microwave treatment. Mater. Sci. Semicond. Process. 99, 68–77.

Baldovi, H.G., Latorre-Sánchez, M., Esteve-Adell, I., Khan, A., Asiri, A.M., Kosa, S.A., 2016. Generation of MoS_2 quantum dots by laser ablation of MoS_2 particles in suspension and their photocatalytic activity for H_2 generation. J. Nanopart. Res. 18 (8). Available from: https://doi.org/10.1007/s11051-016-3540-9.

Besner, S., Kabashin, A.V., Meunier, M., Winnik, F.M., 2005. Fabrication of functionalized gold nanoparticles by femtosecond laser ablation in aqueous solutions of biopolymers. Int. Soc. Opt. Photonics 5969. Available from: https://doi.org/10.1117/12.628885.

Boltaev, G.S., Ganeev, R.A., Krishnendu, P.S., Maurya, S.K., Redkin, P.V., Rao, K.S., et al., 2018. Strong third-order optical nonlinearities of Ag nanoparticles synthesized by laser ablation of bulk silver in water and air. Appl. Phys. A. 124 (11). Available from: https://doi.org/10.1007/s00339-018-2195-z.

Caigas, S.P., Cheng, M.C., Lin, T.N., Santiago, S.R.M.S., Yuan, C.T., Yang, C.C., et al., 2018. P-type doping of WS2 quantum dots via pulsed laser ablation. ACS Photonics 5 (12), 4828−4837.

Calabro, R.L., Yang, D.S., Kim, D.Y., 2018. Liquid-phase laser ablation synthesis of graphene quantum dots from carbon nano-onions: comparison with chemical oxidation. J. Coll. Interf. Sci. 527, 132−140.

Chen, H.R., Meng, W.M., Wang, R.Y., Chen, F.L., Li, T., Wang, D.D., et al., 2022. Engineering highly graphitic carbon quantum dots by catalytic dehydrogenation and carbonization of Ti_3C_2Tx-MXene wrapped polystyrene spheres. Carbon 190. Available from: https://doi.org/10.1016/j.carbon.2022.01.028.

Cui, L., Ren, X., Wang, J., Sun, M., 2020. Synthesis of homogeneous carbon quantum dots by ultrafast dual-beam pulsed laser ablation for bioimaging. Mater. Today Nano 12. Available from: https://doi.org/10.1016/j.mtnano.2020.100091.

Darwish, A.M., Eisa, W.H., Shabaka, A.A., Talaat, M.H., 2015. Synthesis of nano-cadmium sulfide by pulsed laser ablation in liquid environment. Spectrosc. Lett. 48 (9), 638−645.

Drmosh, Q.A., Yamani, Z.H., Hendi, A.H., Gondal, M.A., Moqbel, R.A., Saleh, T.A., et al., 2019. A novel approach to fabricating a ternary rGO/ZnO/Pt system for high-performance hydrogen sensor at low operating temperatures. Appl. Surf. Sci. 464, 616−626.

Eita, M., Wagberg, L., Muhammed, M., 2012. Spin-assisted multilayers of poly (methyl methacrylate) and zinc oxide quantum dots for ultraviolet-blocking applications. ACS Appl. Mater. Interf. 4 (6), 2920−2925.

Farshbaf, M., Davaran, S., Rahimi, F., Annabi, N., Salehi, R., Akbarzadeh, A., 2018. Carbon quantum dots: recent progresses on synthesis, surface modification and applications. Artif. Cell Nanomed. Biotechnol. 46 (7), 1331−1348.

Gondal, M.A., Drmosh, Q.A., Yamani, Z.H., Saleh, T.A., 2009. Synthesis of ZnO_2 nanoparticles by laser ablation in liquid and their annealing transformation into ZnO nanoparticles. Appl. Surf. Sci. 256 (1), 298−304.

Gondal, M.A., Ilyas, A.M., Fasasi, T.A., Dastageer, M.A., Seddigi, Z.S., Qahtan, T.F., et al., 2015. Synthesis of green TiO_2/ZnO/CdS hybrid nano-catalyst for efficient light harvesting using an elegant pulsed laser ablation in liquids method. Appl. Surf. Sci. 357, 2217−2222.

Gongalsky, M.B., Osminkina, L.A., Pereira, A., Manankov, A.A., Fedorenko, A.A., Vasiliev, A. N., et al., 2016. Laser-synthesized oxide-passivated bright Si quantum dots for bioimaging. Sci. Rep. 6 (1). Available from: https://doi.org/10.1038/srep24732.

Goodwin, T.J., Leppert, V.J., Risbud, S.H., Kennedy, I.M., Lee, H.W., 1997. Synthesis of gallium nitride quantum dots through reactive laser ablation. Appl. Phys. Lett. 70 (23), 3122−3124.

Habiba, K., Bracho-Rincon, D.P., Gonzalez-Feliciano, J.A., Villalobos-Santos, J.C., Makarov, V. I., Ortiz, D., et al., 2015. Synergistic antibacterial activity of PEGylated silver−graphene quantum dots nanocomposites. Appl. Mater. Today 1 (2), 80−87.

Horoz, S., Lu, L., Dai, Q., Chen, J., Yakami, B., Pikal, J.M., et al., 2012. CdSe quantum dots synthesized by laser ablation in water and their photovoltaic applications. Appl. Phys. Lett. 101 (22). Available from: https://doi.org/10.1063/1.4768706.

Je, M., Jung, H.J., Koutavarapu, R., Lee, S.J., Lee, S.H., Kim, S.K., et al., 2018. Pulsed laser irradiation synthesis of lead selenide quantum dots from lead and selenium salts in various surfactants. Mater. Chem. Phys. 217, 427−436.

Ka, I., Ma, D., El Khakani, M.A., 2011. Tailoring the photoluminescence of PbS-nanoparticles layers deposited by means of the pulsed laser ablation technique. J. Nanopart. Res. 13 (6), 2269−2274.

Ka, I., Le Borgne, V., Ma, D., El Khakani, M.A., 2012. Pulsed laser ablation based direct synthesis of single-wall carbon nanotube/PbS quantum dot nanohybrids exhibiting strong, spectrally wide and fast photoresponse. Adv. Mater. 24 (47), 6289−6294.

Ka, I., Gonfa, B., Le Borgne, V., Ma, D., El Khakani, M.A., 2014. Pulsed laser ablation based synthesis of PbS-quantum dots-decorated one-dimensional nanostructures and their direct integration into highly efficient nanohybrid heterojunction-based solar cells. Adv. Funct. Mater. 24, 4042−4050.

Ka, I., Le Borgne, V., Fujisawa, K., Hayashi, T., Kim, Y.A., Endo, M., et al., 2016. Multiple exciton generation induced enhancement of the photoresponse of pulsed-laser-ablation synthesized single-wall-carbon-nanotube/PbS-quantum-dots nanohybrids. Sci. Rep. 6 (1). Available from: https://doi.org/10.1038/srep20083.

Kang, S., Jeong, Y.K., Jung, K.H., Son, Y., Kim, W.R., Ryu, J.H., et al., 2020. One-step synthesis of sulfur-incorporated graphene quantum dots using pulsed laser ablation for enhancing optical properties. Opt. Exp. 28 (15), 21659−21667.

Kang, S., Han, H., Lee, K., Kim, K.M., 2022. Ultrasensitive detection of Fe^{3+} ions using functionalized graphene quantum dots fabricated by a one-step pulsed laser ablation process. ACS Omega 7, 2074−2081.

Kateshiya, M.R., Malek, N.I., Kailasa, S.K., 2020. Facile synthesis of highly blue fluorescent tyrosine coated molybdenum oxide quantum dots for the detection of imidacloprid pesticide. J. Mol. Liq. 319. Available from: https://doi.org/10.1016/j.molliq.2020.114329.

Khan, T., BiBi, T., 2014. Application of NS pulsed laser ablation for dense CdS nanoparticles deposition in argon atmosphere. Sop. Trans. Appl. Phys. 1 (2), 48−54.

Kim, M., Osone, S., Kim, T., Higashi, H., Seto, T., 2017. Synthesis of nanoparticles by laser ablation: a review. KONA Powder Part. J. 34 (2014), 80−90.

Kőrösi, L., Rodio, M., Dömötör, D., Kovács, T., Papp, S., Diaspro, A., et al., 2016. Ultrasmall, ligand-free Ag nanoparticles with high antibacterial activity prepared by pulsed laser ablation in liquid. J. Chem. 2016. Available from: https://doi.org/10.1155/2016/4143560.

Kuriakose, A.C., Nampoori, V.P.N., Thomas, S., 2019. Facile synthesis of Au/CdS core-shell nanocomposites using laser ablation technique. Mater. Sci. Semicond. Process. 101, 124−130.

Lalayan, A.A., 2005. Formation of colloidal GaAs and CdS quantum dots by laser ablation in liquid media. Appl. Surf. Sci. 248 (1-4), 209−212.

Li, S., Chen, M., 2016. Convenient synthesis of stable silver quantum dots with enhanced photoluminescence emission by laser fragmentation. Chin. Phys. B 25 (4). Available from: https://doi.org/10.1088/1674-1056/25/4/046103.

Li, B., Jiang, L., Li, X., Ran, P., Zuo, P., Wang, A., et al., 2017. Preparation of monolayer MoS_2 quantum dots using temporally shaped femtosecond laser ablation of bulk MoS_2 targets in water. Sci. Rep. 7 (1). Available from: https://doi.org/10.1038/s41598-017-10632-3.

Li, X., Li, X., Jiang, L., Zuo, P., Zhao, Y., Wang, S., et al., 2021. Preparation of twin graphene quantum dots through the electric-field-assisted femtosecond laser ablation of graphene dispersions. Carbon 185, 384–394.

Li, H., Zhang, Y., Ding, J., Wu, T., Cai, S., Zhang, W., et al., 2022. Synthesis of carbon quantum dots for application of alleviating amyloid-β mediated neurotoxicity. Colloids Surf. B: Biointerfaces . Available from: https://doi.org/10.1016/j.colsurfb.2022.112373.

Liang, L., Shen, W., Wang, J., Ma, T., Chen, J., 2022. Nonlinear absorption of $CsPbBr_3$/antimonene blend materials prepared by laser ablation in liquid. Opt. Mater. 123. Available from: https://doi.org/10.1016/j.optmat.2021.111901.

Maiman, T., 1960. Stimulated optical radiation in ruby. Nature 187, 493–494.

Malviya, K.D., Chattopadhyay, K., 2014. Synthesis and mechanism of composition and size dependent morphology selection in nanoparticles of Ag–Cu alloys processed by laser ablation under liquid medium. J. Phys. Chem. C. 118 (24), 13228–13237.

Mansoureh, G., Parisa, V., 2018. Synthesis of metal nanoparticles using laser ablation technique. Emerging Applications of Nanoparticles and Architecture Nanostructures. Elsevier, Amsterdam, pp. 575–596.

Mendonça, L.T., de Azevedo, W.M., 2016. A fast bottom-up route for preparing CdS quantum dots using laser ablation in a liquid environment. J. Luminescen. 171, 79–84.

Mitra, S., Pak, Y., Alaal, N., Hedhili, M.N., Almalawi, D.R., Alwadai, N., et al., 2019. Novel P-Type wide bandgap manganese oxide quantum dots operating at deep uv range for optoelectronic devices. Adv. Opt. Mater. 7 (21). Available from: https://doi.org/10.1002/adom.201900801.

Mohammed, S.A., Khashan, K.S., Jabir, M.S., Abdulameer, F.A., Sulaiman, G.M., Al-Omar, M. S., et al., 2022. Copper oxide nanoparticle-decorated carbon nanoparticle composite colloidal preparation through laser ablation for antimicrobial and antiproliferative actions against breast cancer cell line, MCF-7. BioMed. Res. Int. 2022. Available from: https://doi.org/10.1155/2022/9863616.

Morozova, S., Alikina, M., Vinogradov, A., Pagliaro, M., 2020. Silicon quantum dots: synthesis, encapsulation, and application in light-emitting diodes. Front. Chem. 8. Available from: https://doi.org/10.3389/fchem.2020.00191.

Mostafa, A.M., Yousef, S.A., Eisa, W.H., Ewaida, M.A., Al-Ashkar, E.A., 2019. WO_3 quantum dot: synthesis, characterization and catalytic activity. J. Mol. Struct. 1185, 351–356.

Murali, A.K., 2001. Laser Ablation Synthesis of Indium Oxide Quantum Dots and a Kinetic Study of the Oxide to Nitride Conversion (Ph.D. thesis). University of California, Davis.

Mwafy, E.A., Hasanin, M.S., Mostafa, A.M., 2019. Cadmium oxide/TEMPO-oxidized cellulose nanocomposites produced by pulsed laser ablation in liquid environment: synthesis, characterization, and antimicrobial activity. Opt. Laser Technol. 120. Available from: https://doi.org/10.1016/j.optlastec.2019.105744.

Narasimhan, A.K., Santra, T.S., Rao, M.R., Krishnamurthi, G., 2017. Oxygenated graphene quantum dots (GQDs) synthesized using laser ablation for long-term real-time tracking and imaging. RSC Adv. 7 (85), 53822–53829.

Nguyen, V., Yan, L., Si, J., Hou, X., 2016. Femtosecond laser-assisted synthesis of highly photoluminescent carbon nanodots for Fe^{3+} detection with high sensitivity and selectivity. Opt. Mater. Exp. 6 (2), 312–320.

Nguyen, V., Dong, Q., Yan, L., Zhao, N., Le, P.H., 2019a. Facile synthesis of photoluminescent MoS_2 and WS_2 quantum dots with strong surface-state emission. J. Lumin. 214. Available from: https://doi.org/10.1016/j.jlumin.2019.116554.

Nguyen, V., Yan, L., Si, J., 2019b August. Synthesis of broad photoluminescence carbon nanodots by femtosecond laser ablation in liquid. In: 2016 IEEE 16th International Conference on Nanotechnology (IEEE-NANO). IEEE, pp. 901–903.

Nguyen, V., Yan, L., Zhao, N., Van Canh, N., Hang, N.T.N., Le, P.H., 2021. Tuning photoluminescence of boron nitride quantum dots via surface functionalization by femtosecond laser ablation. J. Mol. Struc. Available from: https://doi.org/10.1016/j.molstruc.2021.130922.

Novoa-De León, I.C., Johny, J., Vázquez-Rodríguez, S., García-Gómez, N., Carranza-Bernal, S., Mendivil, I., et al., 2019. Tuning the luminescence of nitrogen-doped graphene quantum dots synthesized by pulsed laser ablation in liquid and their use as a selective photoluminescence on–off–on probe for ascorbic acid detection. Carbon 150, 455–464.

Omran, Z.H., Salman, O.N., Ali, A.K., 2021. Preparation CdSe quantum dots using laser ablation technique for dye-sensitized solar cell. Int. J. Nanoelectron. Mater. 14 (1), 61–70.

Ou, G., Fan, P., Ke, X., Xu, Y., Huang, K., Wei, H., et al., 2018. Defective molybdenum sulfide quantum dots as highly active hydrogen evolution electrocatalysts. Nano Res. 11 (2), 751–761.

Patel, M.K., Singh, J., Singh, M.K., Agrawal, V.V., Ansari, S.G., Malhotra, B.D., 2013. Tin oxide quantum dot based DNA sensor for pathogen detection. J. Nanosc. Nanotechnol. 13 (3), 1671–1678.

Pradhan, G., Dey, P.P., Khare, A., Sharma, A.K., 2021. Synthesis and size modulation of MoS_2 quantum dots by pulsed laser ablation in liquid for viable hydrogen generation. J. Appl. Phys. 129 (2). Available from: https://doi.org/10.1063/5.0022833.

Pyatenko, A., Shimokawa, K., Yamaguchi, M., Nishimura, O., Suzuki, M., 2004. Synthesis of silver nanoparticles by laser ablation in pure water. Appl. Phys. A. 79 (4-6), 803–806.

Qin, W.J., Sun, J., Yang, J., Du, X.W., 2011. Control of Cu-doping and optical properties of ZnO quantum dots by laser ablation of composite targets. Mater. Chem. Phys. 130 (1-2), 425–430.

Raikwar, V.R., 2022. Synthesis and study of carbon quantum dots (CQDs) for enhancement of luminescence intensity of CQD@$LaPO_4$: Eu^{3+} nanocomposite. Mater. Chem. Phys. 275. Available from: https://doi.org/10.1016/j.matchemphys.2021.125277.

Rasouli, H.R., Ghobadi, A., Ghobadi, T.U., Ates, H., Topalli, K., Okyay, A.K., 2017. Nanosecond pulsed laser ablated sub-10 nm silicon nanoparticles for improving photovoltaic conversion efficiency of commercial solar cells. J. Opt. 19 (10). Available from: https://doi.org/10.1088/2040-8986/aa84dd.

Ravi Kumar, S., Lies, B., Zhang, X., Lyu, H., Qin, H., 2019. Laser ablation of polymers: a review. Polym. Int. 68 (8), 1391–1401.

Ren, X., Zhang, F., Zhang, X., 2018. Synthesis of black phosphorus quantum dots with high quantum yield by pulsed laser ablation for cell bioimaging. Chem. Asian J. 13 (14), 1842–1846.

Ren, X., Zhang, F., Guo, B., Gao, N., Zhang, X., 2019. Synthesis of N-doped micropore carbon quantum dots with high quantum yield and dual-wavelength photoluminescence emission from biomass for cellular imaging. Nanomater 9 (4). Available from: https://doi.org/10.3390/nano9040495.

Reyes, D., Camacho, M., Camacho, M., Mayorga, M., Weathers, D., Salamo, G., et al., 2016. Laser ablated carbon nanodots for light emission. Nanoscale Res. Lett. 11 (1), 1–11.

Rodio, M., Brescia, R., Diaspro, A., Intartaglia, R., 2016. Direct surface modification of ligand-free silicon quantum dots prepared by femtosecond laser ablation in deionized water. J. Coll. Interf. Sci. 465, 242–248.

Russo, P., Hu, A., Compagnini, G., Duley, W.W., Zhou, N.Y., 2014. Femtosecond laser ablation of highly oriented pyrolytic graphite: a green route for large-scale production of porous graphene and graphene quantum dots. Nanoscale 6 (4), 2381–2389.

Ryabchikov, Y.V., Popov, A.A., Sentis, M., Timoshenko, V.Y., Kabashin, A.V., 2016. March. Structural properties of gold-silicon nanohybrids formed by femtosecond laser ablation in water at different fluences. Synth. Photonics Nanoscale Mater. XIII 9737, 54–59.

Sadrolhosseini, A.R., Rashid, S.A., Shafie, S., Nezakati, H., 2019. Laser ablation synthesis of gold nanoparticle to enhance the fluorescence properties of graphene quantum dots. J. Laser Appl. 31 (2). Available from: https://doi.org/10.2351/1.5046062.

Sadrolhosseini, A.R., Krishnan, G., Safie, S., Beygisangchin, M., Rashid, S.A., Harun, S.W., 2020. Enhancement of the fluorescence property of carbon quantum dots based on laser ablated gold nanoparticles to evaluate pyrene. Opt. Mater. Exp. 10 (9), 2227–2241.

Santiago, S.R.M., Lin, T.N., Chang, C.H., Wong, Y.A., Lin, C.A.J., Yuan, C.T., et al., 2017. Synthesis of N-doped graphene quantum dots by pulsed laser ablation with diethylenetriamine (DETA) and their photoluminescence. Phys. Chem. Chem. Phys. 19 (33), 22395–22400.

Schawlow, A.L., Townes, C.H., 1958. Infrared and optical masers. Phys. Rev. 112 (6), 1940–1949.

Sergeev, A.A., Pavlov, D.V., Kuchmizhak, A.A., Lapine, M.V., Yiu, W.K., Dong, Y., et al., 2020. Tailoring spontaneous infrared emission of HgTe quantum dots with laser-printed plasmonic arrays. Light. Sci. Appl. 9 (1). Available from: https://doi.org/10.1038/s41377-020-0247-6.

Shen, L., Zhou, S., Huang, F., Zhou, H., Zhang, H., Wang, S., et al., 2021. Nitrogen-doped graphene quantum dots synthesized by femtosecond laser ablation in liquid from laser induced graphene. Nanotechnol. 33 (11). Available from: https://doi.org/10.1088/1361-6528/ac4069.

Singh, S.C., Gopal, R., 2012. Drop shaped zinc oxide quantum dots and their self-assembly into dendritic nanostructures: liquid assisted pulsed laser ablation and characterizations. Appl. Surf. Sci. 258 (7), 2211–2218.

Singh, S.C., Mishra, S.K., Srivastava, R.K., Gopal, R., 2010. Optical properties of selenium quantum dots produced with laser irradiation of water suspended Se nanoparticles. J. Phys. Chem. C. 114 (41), 17374–17384.

Singh, M.K., Mathpal, M.C., Agarwal, A., 2012. Optical properties of SnO_2 quantum dots synthesized by laser ablation in liquid. Chem. Phys. Lett. 536, 87–91.

Soheyli, E., Ghaemi, B., Sahraei, R., Sabzevari, Z., Kharrazi, S., Amani, A., 2020. Colloidal synthesis of tunably luminescent AgInS-based/ZnS core/shell quantum dots as biocompatible nano-probe for high-contrast fluorescence bioimaging. Mater. Sci. Eng. C. 111. Available from: https://doi.org/10.1016/j.msec.2020.110807.

Soliman, W., Yamani, R.N., Sabry, D., Mostafa, A., 2021. Stainless steel quantum dots and its resonance fluorescence impact as new therapeutic agents for Laryngeal carcinoma treatment: in vitro study. Opt. Laser Technol. 142. Available from: https://doi.org/10.1016/j.optlastec.2021.107263.

Sunitha, A.P., Hajara, P., Shaji, M., Jayaraj, M.K., Saji, K.J., 2018. Luminescent MoS_2 quantum dots with reverse saturable absorption prepared by pulsed laser ablation. J. Lumin. 203, 313–321.

Suzuki, K., Inoguchi, M., Kageyama, K., Takagi, H., Sakabe, Y., 2009. Well-crystallized zinc oxide quantum dots with narrow size distribution. J. Nanopart. Res. 11 (6), 1349–1360.

Verma, R.K., Kumar, K., Rai, S.B., 2013. Near infrared induced optical heating in laser ablated Bi quantum dots. J. Coll. Inter. Sci. 390 (1), 11–16.

Wang, X., Zhu, C., Jin, L., Lin, K., Shao, Y., Yang, J., et al., 2021. Rational synthesis of ZnO decorated Fe hierarchical nanostructures for enhanced photocatalytic performance by long-pulse-width laser ablation of binary alloys target. J. Alloy. Comp. 868. Available from: https://doi.org/10.1016/j.jallcom.2021.159171.

Wu, M.H., Mu, R., Ueda, A., Henderson, D.O., Vlahovic, B., 2005. Production of silicon quantum dots for photovoltaic applications by picosecond pulsed laser ablation. Mater. Sci. Eng. B. 116 (3), 273–277.

Xu, Y., Yan, L., Si, J., Zhao, N., 2019. Femtosecond laser-assisted fabrication of fluorescent boron nitride quantum dots. In: 2019 IEEE International Conference on Manipulation, Manufacturing and Measurement on the Nanoscale (3M-NANO). IEEE, pp. 7–10, Available from: https://doi.org/10.1109/3M-NANO46308.2019.8947381.

Yang, C., Feng, G., Dai, S., Wang, S., Li, G., Zhang, H., et al., 2017. Femtosecond pulsed laser ablation in microfluidics for synthesis of photoluminescent ZnSe quantum dots. Appl. Surf. Sci. 414, 205–211.

Yoon, J.W., Shim, S.H., Shim, K.B., Koshizaki, N., Kwon, Y.S., 2005. Quantum confinement effect of amorphous GaN quantum dots prepared by pulsed-laser ablation. Jpn. J. Appl. Phys. 44 (1S). Available from: https://doi.org/10.1143/JJAP.44.788.

Yu, X., Liu, J., Yu, Y., Zuo, S., Li, B., 2014. Preparation and visible light photocatalytic activity of carbon quantum dots/TiO2 nanosheet composites. Carbon 68, 718–724.

Zakharko, Y., Rioux, D., Patskovsky, S., Lysenko, V., Marty, O., Bluet, J.M., et al., 2011. Direct synthesis of luminescent SiC quantum dots in water by laser ablation. Phys. Status Solidi RRL. 5 (8), 292–294.

Zeng, H., Yang, S., Cai, W., 2011. Reshaping formation and luminescence evolution of ZnO quantum dots by laser-induced fragmentation in liquid. J. Phys. Chem. C. 115 (12), 5038–5043.

Zhao, Y., Song, M., Yang, X., Yang, J., Du, C., Wang, G., et al., 2020. Amorphous Ag_2-xCuxS quantum dots: "all-in-one" theranostic nanomedicines for near-infrared fluorescence/photoacoustics dual-modal-imaging-guided photothermal therapy. Chem. Eng. J. 399. Available from: https://doi.org/10.1016/j.cej.2020.125777.

Zheng, J., Zheng, Z., Gong, W., Hu, X., Gao, W., Ren, X., et al., 2008. Stable, small, and water-soluble Cu-doped ZnS quantum dots prepared via femtosecond laser ablation. Chem. Phys. Lett. 465 (4–6), 275–278.

Zheng, C.B., Xia, Y.Q., Qin, F., Yu, Y., Miao, J.P., Zhang, Z.G., et al., 2010. Femtosecond pulsed laser induced synthesis of ultrafine Y_2O_3: Pr, Yb nanoparticles with improved upconversion efficiency. Chem. Phys. Lett. 496 (4–6), 316–320.

This page intentionally left blank

Chapter 5

Coprecipitation synthesis of quantum dots

Monika Jangid and Seema Kothari
Department of Chemistry, PAHER University, Udaipur, Rajasthan, India

5.1 Introduction

The coprecipitation method is used to prepare uniform compositions in homogeneous solution of two or more ions through precipitation reaction. It is an important method for the synthesis of some materials containing two or more elements. What is the difference between the precipitation and coprecipitation? The process of precipitation is the settling down of some insoluble particles from a homogeneous solution. This insoluble compound forms precipitates. Whereas coprecipitation is a process, where normally soluble compounds are thrown out of solution in the form of a precipitate. The coprecipitation is most commonly used for synthesis of nanoparticles and quantum dots (QDs). Different operational parameters like material, pH, concentration of the initial solutions, reaction temperature and time play important roles in getting nanoparticles or QDs with the desired shapes and sizes.

It is a simple, economical, and industrially viable technique that is normally used for the synthesis of important oxide materials. The various steps involved in this process are shown schematically in the flow chart in Fig. 5.1. It is possible to prepare flowable powders using this process without any additional agglomeration steps. One can tailor such a process to obtain nano- or microsized particles by adjusting the pH, temperature, solvents, and the precipitating agent.

5.1.1 Advantages

1. It is a most useful method for controlling the sizes of nanoparticles.
2. It is commonly used in the biomedical applications, because it is easy to apply and almost harmless.

Quantum Dots. DOI: https://doi.org/10.1016/B978-0-12-824153-0.00005-7

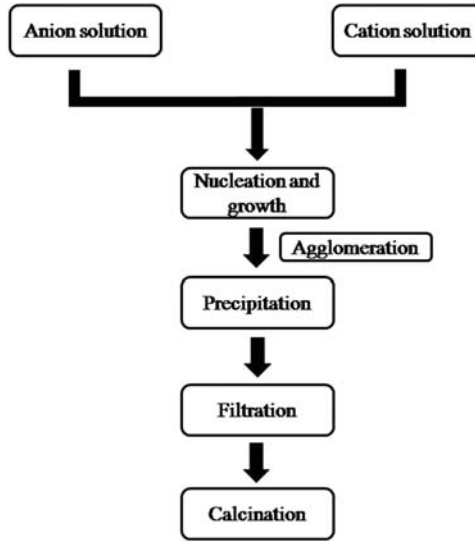

FIGURE 5.1 Flow chart of coprecipitation method.

3. In this method, nanoparticles are prepared from aqueous salt solutions, just by adding a base under an inert atmosphere at room temperature as well as at high temperatures.
4. It can be carried out at lower reaction temperature and with shorter reaction time.

5.1.2 Disadvantages

1. In this process, there in a problem because some undesired impurities may also coprecipitate with the analyte.
2. Distribution of shape of nanoparticles may be uncontrollable and size may be irregular.
3. The products are generally insoluble because of the high supersaturation condition, which is necessary to induce precipitation.
4. Salts may have similar solubilities.
5. It is often difficult to have material of high purity and accurate stoichiometry.
6. It is not cost effective in some cases.
7. One of the troubles with this method of synthesis of nanoparticles is the tendency of particles to agglomerate.

5.2 Classification of coprecipitation

Mainly, there are four types of coprecipitation:

1. surface adsorption;
2. mixed−crystal formation;
3. occulation; and
4. mechanical entrapment.

Out of these four, surface adsorption and mixed-crystal formation are equilibrium processes, while occulation and mechanical entrapment are due to the kinetics of crystal growth.

1. *Surface adsorption*: It is a common method of coprecipitation. Here, a significant contamination of precipitates occurs with large specific surface areas (coagulated colloids). Coagulation of a colloid does not decrease the amount of adsorption significantly. Therefore, the overall effect of surface adsorption is carrying down of an otherwise soluble compound as a surface contaminant.
2. *Mixed−crystal formation*: In this type of coprecipitation, one of the ions in the crystal lattice of a solid is replaced by an ion of another element. The extent of mixed-crystal contamination obeys the law of mass action and increases as the ratio of contaminant to analyte concentration increases.
3. *Occulation entrapment*: When a crystal is growing rapidly during precipitation formation, foreign ions in the counter ion layer may become trapped or occluded within the growing crystal. Occlusion is a type of coprecipitation, in which a compound is trapped within a pocket formed during rapid crystal growth.
4. *Mechanical entrapment*: Mechanical entrapment occurs when crystals lie close together during growth. Occlusion and mechanical entrapment are confined to crystalline precipitate. Both are at a minimum when the rate of precipitation formation is low.

5.3 Synthesis of quantum dots

5.3.1 Metal oxide quantum dots

Jbara et al. (2017) used the coprecipitation technique to synthesize gamma-Al_2O_3 (γ-Al_2O_3) nanopowders. As-prepared alumina nanopowders have particle diameter from 6−24 nm, as evident from XRD. Almost all particles were spherical in shape, but some particles acquired more regular hexagonal shapes on increasing annealing temperature, maybe due to agglomeration of nanoparticles. Zhao et al. (2018) synthesized graphene oxide/Mg-doped ZnO/tungsten oxide QDs composites via the coprecipitation method. It was reported that this composite exhibited photocatalytic activity that was almost 6.58 times higher than that of the composite without tungsten oxide. Transition-metal (Cr, Mn, Fe, Co, and Ni)- doped SnO_2 QDs were synthesized by Sharma et al. (2020) using the coprecipitation method. These QDs were capped by polyvinyl pyrrolidone. The size of as-synthesized particles was found to be 2.5 nm.

Sarkar et al. (2020) synthesized carbon-quantum-dot-embedded iron oxide nanoparticles (CQD@Fe_3O_4 NPs). The Fe_3O_4 NPs and CQD@Fe_3O_4 NPs were synthesized by the wet chemical coprecipitation method. A nearly spherical structure with an average size of about 7 nm was obtained for Fe_3O_4, while CQDs were around 2 nm in size in CQD@Fe_3O_4 NPs as evident from HRTEM. Hernandez et al. (2020) synthesized Fe_3O_4 MNPs modified with three different amino acids (AA): L-tryptophan, l-phenylalanine, and l-tyrosine via the coprecipitation method without using a spacer agent. This nanocomposite has high stability and good dispersibility in water and can be used in various biomedical and environmental applications.

Ragupathi et al. (2021) used the coprecipitation method for the synthesis of ZnO QDs and MPS organosilane modified ZnO@MPS. It was observed that as-prepared ZnO QDs and ZnO@MPS exhibited size reduction, better dispersion, and lower aggregation as compared to ZnO QDs. They also studied the antibacterial activities of these against *Staphylococcus aureus*, *Escherichia coli*, *Klebsiella pneumoniae*, and *Enterococcus faecalis*, and observed that ZnO@MPS QDs exhibited significant zones of inhibition, which may be due to smaller particle size.

Masmali et al. (2022) used ZnO and $ZnFe_2O_4$ as working electrodes in the QDs sensitized solar cells (QDSSCs). It was observed that $ZnFe_2O_4$ can enhance light absorption and its bandgap is 2.12 eV. They synthesized ZnO and $ZnFe_2O_4$ nanoparticles via coprecipitation. As-prepared mesoporous thin films of ZnO and $ZnFe_2O_4$ were sensitized with Ag_2S and CdS and then used as photoanodes in QDSSCs. It was revealed that Ag_2S sensitized photoanodes exhibited higher charge carrier resistance, shorter electron lifetime, and low fill factor as compared to CdS-based photoanodes.

Niu et al. (2022) prepared Cu_2O/SnO_2 QDs/ZnO arrays pn junction via a continuous sputtering−hydrothermal−coprecipitation method. It was reported that the as-prepared transparent photovoltaic device exhibited high transmittance ($\sim$80%) and photovoltaic enhancement ($\sim 1.5 \times 10^{-3}$ folds) (PCE = 1.03%), It was attributed to SnO_2 QDs, which have appropriate Fermi level increasing the charge carrier concentration/mobility, but high transparency was balanced.

5.3.2 Metal sulfides

Cadmium sulfide QDs were synthesized by Mishra et al. (2011) via a coprecipitation method. X-ray diffraction revealed that cubical zinc blend structure was present in CdS nanoparticles. It was found that CdS QDs are of 2−5 nm in size as evident from TEM data. A blue shift of 0.48 eV UV−V is absorption data was observed that compared to bulk CdS. Rahdar et al. (2012) synthesized ZnS:Cr nanoparticles by the coprecipitation method. It was possible to prepare different sized ZnS:Cr nanoparticles using this simple chemical method using different molar concentration of doping agent. They observed

that mean crystallite size of these particles ranged between 1.5 and 2.45 nm, which depended on the molar concentration of the doping agent.

Giribabu et al. (2012) synthesized $Cd_1 - _xMg_xS$ nanoparticles by the coprecipitation method. It was revealed that the structural phase transition is present from cubic to hexagonal and there is an increase in the average size of the nanoparticles (range 1.4−2.8 nm) on increasing content of Mg. The ZnS QDs along with their Be^{2+} and Mg^{2+} derivatives ($Zn_{1-x}Be_xS$ and $Zn_{1-x}Mg_xS$) were prepared by Iqbal and Iqbal (2013) via the coprecipitation route. The synthesized QDs are stable for a period of up to 7 months. It was found that particles were having cubic closed packed structure with an average particle size of 2−3 nm. It was proposed that these QDs may find applications in light-emitting diodes, sensors, coatings, and phosphor.

Zinc sulfide QDs (pure and doped with Fe^{3+}) were prepared by Shamsipur and Rajabi (2014) via a chemical coprecipitation method. The effect of different operational parameters on the decolorization of methyl violet, such as pH, initial dye concentration, dopant content, dosage of nanophotocatalyst, and UV irradiation time, were studied. It was observed that doping of ZnS QDs with Fe^{3+} enhanced its efficiency, as evident from the increased rate of dye removal. Rofouei et al. (2015) synthesized ultrasmall glycine dithiocarbamate (GDTC)-functionalized manganese doped ZnS (GDTC-Mn:ZnS) QDs via the coprecipitation method. It was then used as a sensor for cerous ions in concentration range of 2.0×10^{-6} to 3.2×10^{-5} mol L^{-1}, with a detection limit of 2.29×10^{-7} mol.L^{-1}. Tyagi et al. (2014) synthesized size tunable cadmium sulfide QDs via wet chemical coprecipitation method at pH 9 and 10.5 and different temperatures, that is, 35°C, 50°C, and 65°C. They used cadmium chloride and thiourea as precursors, while ammonium hydroxide was used as a precipitating agent and mercaptoethanol as a surfactant.

Elavarthi et al. (2016) synthesized undoped and Cr-doped CdS nanoparticles via the coprecipitation method. The average particle size was found to be 4−5 nm. Yadav et al. (2016) prepared copper-doped $Cd_1 - _xZn_xS$ QDs using a chemical coprecipitation method. The Cu-doped QDs have an hexagonal structure with average crystallite size in the range 2−12 nm. Sakthivel and Muthukumaran (2016) synthesized $Zn_{0.98} - _xCu_xMn_{0.02}S$ QDs (Cu and Mn codoped) with different copper concentrations (where $x = 0$, 0.02, 0.04) through a coprecipitation technique. The $Zn_{0.98}Mn_{0.02}S$ was in the cubic phase, which gives a mixture of cubic as well as hexagonal phases on Cu-doping. The bandgap was found to range between 3.3 and 3.93 eV on Mn and Cu codoping. These codoped zinc sulfide QDs can find use in optoelectronic devices. Youngjin and Jongsung (2016) prepared silica nanospheres containing magnetic particles. Then CdSe/ZnS QDs were functionalized and incorporated into these silica nanospheres. It was reported that fluorescence from as-prepared QDs was quenched and this magnetic silica−QD−DNA probe can be used to detect a particular DNA.

The $Zn_{0.98-x}Ni_xMn_{0.02}S$ QDs were synthesized by Sakthivel and Muthukumaran (2017) via a coprecipitation method. They reported that the average crystallite size was 1.3−1.8 nm. A red shift was observed in absorption and intensity was increased on increasing concentration of Ni. The bandgap of as-prepared samples ranged between 3.56 and 3.93 eV. As-prepared material can be used in optoelectronic devices and also as a buffer material in solar cells. Zinc sulfide QDs and transition metal-doped ZnS nanocrystals were prepared by Jabeen et al. (2017) by a coprecipitation method.

Zhang et al. (2017) synthesized hybrid rGO/$CoFe_2O_4$/ZnS nanocomposites via a combination of hydrothermal and coprecipitation route. It was reported that ZnS QDs and $CoFe_2O_4$ nanoparticles had an average diameter of 3−8 and 10−20 nm, respectively, and these were anchored on graphene sheets. It was proposed that the as-prepared nanocomposites have a potential for use in stealth camouflage techniques.

Kaur et al. (2017) synthesized ZnS QDs via a coprecipitation technique. They used sodium dodecyl sulfate as a stabilizing agent. They used these ZnS QDs as a photocatalyst for degrading brilliant green under sunlight. They could achieve about 88% degradation of brilliant green.

Desai et al. (2018) synthesized PVP-coated ZnS nanoparticles doped with transition metals by a wet chemical coprecipitation method. The average particle size of these PVP−ZnS nanoparticles was around 2.6 nm. Cobalt-alloyed ZnS QDs were synthesized by Horoz (2018) via a coprecipitation method. It was found that Cobalt-alloyed ZnS QDs had a cubic structure with size 2.71 nm, which is little bit smaller than the size of pure ZnS QDs (2.72 nm). It was revealed that there was a blueshift compared to pure ZnS QDs.

Ashokkumar and Boopathyraja (2018) prepared $Zn_{1-x}Mg_xS$ QDs by a coprecipitation method. It was observed that Mg dopant did not affect the cubic blende structure of ZnS QDs. The average crystallite size increases from ∼1.7−2 nm at initial doping of Mg (20%). It was revealed that the bandgap of the QD was decreased at initial doping of Mg due to the quantum confinement effect but at a higher doping level the bandgap was found to be increased. Sakthivel and Muthukumaran (2018) prepared Cobalt-alloyed (0%−4%) $Zn_{0.98}Mn_{0.02}S$ QDs by a coprecipitation method. It was found that the average crystallite size of the particles was around 3 nm. It was reported that average crystallite size of as-prepared QDs was ∼3 nm. Rafiq et al. (2019) prepared ZnS QDs via the coprecipitation method. They used 2-mercaptoethanol as a capping agent. An average crystallite size of ZnS QDs was found to be 4.2 nm. These uncapped ZnS QD were used for photocatalytic degradation of methylene blue.

Mansur et al. (2019) prepared fluorescent ternary and quaternary QD nanostructures based on $AgInS_2$ core and ZnS shell. These QDs were stabilized with carboxymethyl cellulose polymer ligand. They prepared colloidal $AgInS_2$ QDs by a coprecipitation process. Sizes of $AgInS_2$ and $AgInS_2$/ZnS

QDs range were in the of 8.5 ± 2.4 nm and 3.2 ± 1.1 nm under acidic or alkaline media, respectively. Yu et al. (2019) used chitosan (CS) as a biomacromolecule model and surface ligands to synthesize CuS QDs via the coprecipitation method. These CuS-CS QDs were conjugated with folic acid (FA). It was reported that the size of CuS-CS-FA QDs was around 4 nm. It was revealed that CuS-CS-FA QD can be effectively targeted and accumulated in the tumor reaching the peak dose in 1 h, when CuS-CS-FA QDs dispersion was injected (intravenously) into the tumor-bearing mice.

Devadoss et al. (2019) synthesized Zn, Cr codoped CdS QDs via a coprecipitation method. They carried out this synthesis at room temperature without using any capping agent. It was observed that samples have cubic structures, which remained unaffected by the presence of Cr, but the crystallite size was found to be reduced in the order of ~2 nm. The presence of Cr was considered responsible for a blueshift. The ZnS QD (Mg, Mn codoped) were synthesized by Sakthivel et al. (2019) using a coprecipitation method. The particle size in the range of ~2 nm. A redshift was observed with an increase in Mg doping concentration, which will reduce the bandgap.

Meng et al. (2020) synthesized cadmium sulfide QDs through the coprecipitation method. It was observed that there was a blue shift of 0.48 eV compared to that of bulk CdS. The particles size of CdS QDs was found to be 3.665 nm. Abha et al. (2020) synthesized Mn:ZnS/BSA QDs by a chemical coprecipitation method. It was reported that Mn:ZnS/BSA QDs can serve as an effective sensor platform for dopamine. The luminescence of Mn:ZnS/BSA QDs was found to decrease linearly with increasing concentration of dopamine in the range from 6.6 to 50.6 nM.

Ibraheema et al. (2020) synthesized the ability to tune the paramagnetic effect of Co-doped CdSQDs, which were prepared by a coprecipitation route with varied Co^{2+} concentrations. It was reported that the highest possible paramagnetic effect in the CdS semiconducting matrix exhibited bandgap in the visible range (2.76 eV). Sharma et al. (2021) prepared polyvinlypyrrolidone (PVP) capped CuS QDs ($Cu_1 - _xTM_xS$) via the chemical coprecipitation route. They also doped these QDs with some magnetic transition metals (TM = Fe, Cr and Co).

5.3.3 Metal selenide quantum dots

CdSe QDs were synthesized by Verma et al. (2016) via the chemical coprecipitation method. It was revealed that the cubic phase of the crystalline CdSe transformed to stable hexagonal phase at 317°C and the average particle size of these QDs ranged between (3−5 nm).

Lewis et al. (2016) synthesized semiconducting heterostructures composed of cadmium selenide QDs attached onto the surfaces of Eu-doped and Pr-doped $CaTiO_3$. It was observed that 2.7-nm diameter ligand-functionalized CdSe QDs were attached to $CaTiO_3$-based spherical assemblies. Ag_2Se QDs were prepared

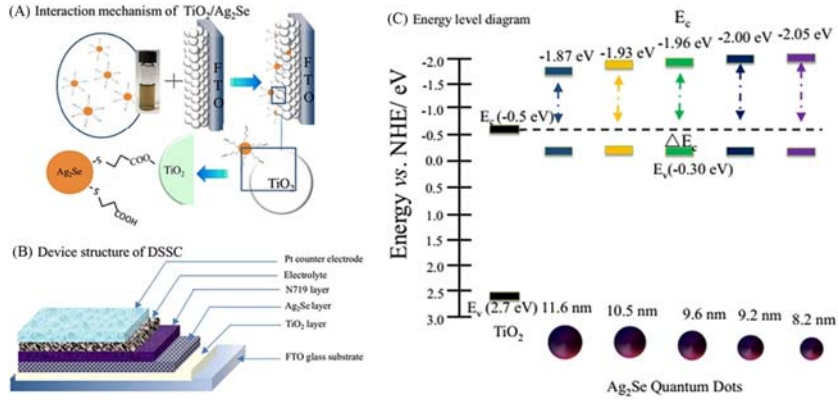

FIGURE 5.2 Dye sensitized solar cells using Ag_2Se quantum dots. *Adapted from Zhang, Z., Yang, Y., Gao, J., Xiao, S., Zhou, C., Pan, D., et al., 2018. Highly efficient Ag_2Se quantum dots blocking layer for solid-state dye-sensitized solar cells: size effects on device performances. Mater. Today Energy 7, 27–36 with permission.*

by Zhang et al. (2018) using a coprecipitation method and then used in solid-state dye-sensitized solar cells (Fig. 5.2). It was revealed that monodispersed Ag_2Se QDs had average sizes ranging between 8.2–11.6 nm. The highest power conversion efficiency of Ag_2Se QDs (9.6 nm)-based solar cells was reported to be 5.89%.

5.3.4 Carbon-based

A graphene QDs and CoNiAl-layered double-hydroxide composite was synthesized by Samuei et al. (2017) through a coprecipitation method. They fabricated a modified carbon paste electrode containing this nanocomposite that was used as a nonenzymatic sensor for determination of glucose. It was reported that the as-prepared sensor offered high reproducibility, fast response time, good electrocatalytic properties, and stability. It was revealed that the as-constructed sensor exhibited sensitivity in a wide range of concentrations of glucose (0.01–14.0 mM) with a limit of detection of 6 μM.

It was revealed that the $NiFe_2O_4$/GQD sample exhibited the highest catalytic activity and completed the reduction in a minute to afford p-aminophenol. The catalysts displayed good stability, can be recovered using a magnetic field, and can be recycled for six experiments with a conversion percentage of >95%.

Sharma et al. (2018) prepared iron nanoparticles, Fe@carbon QDs, and Fe/Ag@carbon QDs nanocomposites by a simple coprecipitation/reduction method. The photocatalytic activity of Fe, Fe@CQDs, and Fe/Ag@CQDs was evaluated for the removal of fast green dye. The catalytic nature of as-synthesized materials was also investigated for the esterification of acetic

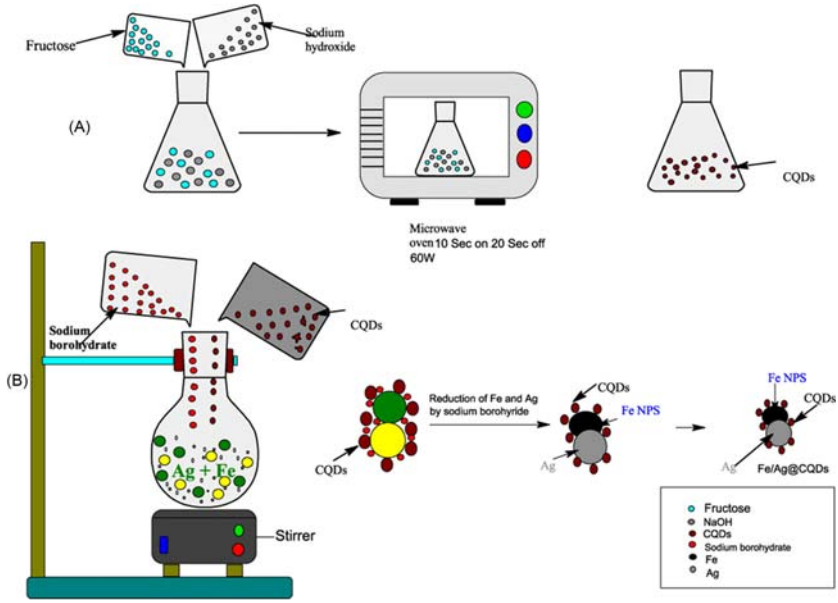

FIGURE 5.3 Use of iron-based quantum dots and nanocomposites for degradation, oxidation, and esterification. *Adapted from Sharma, G., Kumar, A., Naushad, M., Kumar, A., Ala'a, H., Dhiman, P., et al., 2018. Photoremediation of toxic dye from aqueous environment using monometallic and bimetallic quantum dots based nanocomposites. J. Clean. Product. 172, 2919–2930 with permission.*

acid and oxidation of benzyl alcohol (Fig. 5.3). It was reported that oxidation of benzyl alcohol with H_2O_2 with Fe NPs gave the highest yield (87%), while esterification of acetic acid with different alcohols (ethyl, isopropyl and butyl) showed that butyl alcohol gave a maximum yield of 82%, 80%, and 84% with Fe NPs, Fe@CQDs, and Fe/Ag@CQDs, respectively.

Lin et al. (2019) anchored nitrogen-doped carbon QDs (NCDs) and graphitic carbon nitride QDs (CNQDs) on the surface of $BiVO_4$ microspheres to fabricate $BiVO_4$/CNQDs/NCDs composite via the coprecipitation method. It was reported that as-synthesized $BiVO_4$/CNQDs/NCDs exhibited an excellent photocatalytic activity for the degradation of rhodamine B as well as tetracycline under UV illumination as compared to pure $BiVO_4$, $BiVO_4$/CNQDs, and $BiVO_4$/NCDs (Fig. 5.4).

5.3.5 Graphene-based

Wu et al. (2014) prepared composites of GQDs and Fe_3O_4 nanoparticles (GQDs/Fe_3O_4) via a coprecipitation method. It was reported that as-prepared GQDs/Fe_3O_4 composites exhibited a better stability and reusability as compared to natural peroxidases. This GQDs/Fe_3O_4 composite was also used as

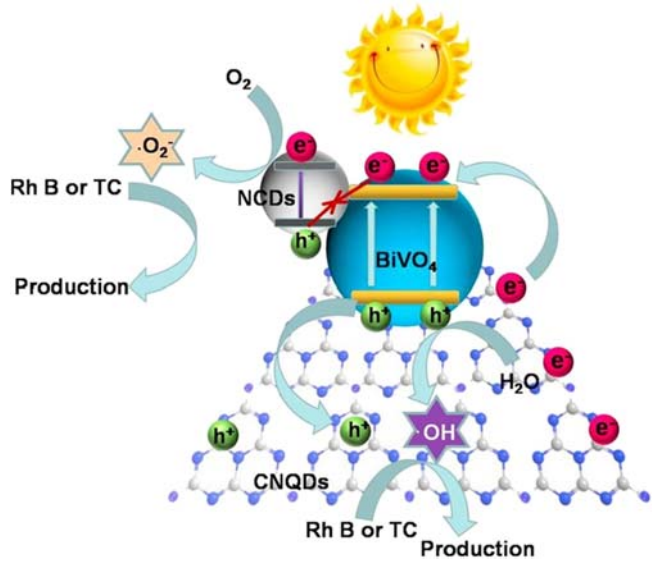

FIGURE 5.4 Use of $BiVO_4$/CNQDs/NCDs composite for degradation of rhodamine B and tetracycline. *Adapted from Lin, X., Liu, C., Wang, J., Yang, S., Shi, J., Hong, Y., 2019. Graphitic carbon nitride quantum dots and nitrogen-doped carbon quantum dots co-decorated with $BiVO_4$ microspheres: a ternary heterostructure photocatalyst for water purification. Sep. Purif. Technol. 226, 117–127, 2019, with permission.*

a catalyst for the removal of phenolic compounds (nine in all). It showed better or sometimes comparable removal efficiencies for phenolic compounds as compared to native horseradish peroxidase.

Ramachandran et al. (2018) developed a method for the synthesis of graphene QDs/cobalt ferrite nanocomposite. They synthesized graphene QDs using citric acid, which was followed by coprecipitation of cobalt ferrite nanoparticles on these graphene QDs. It was reported that as-synthesized nanocomposite exhibited good superparamagnetic properties and fluorescence, which are useful in biomedical applications.

Naghshbandi et al. (2018) synthesized graphene QDs and metal ferrites (MFe_2O_4; where, M = Ni, Co) nanocomposites via a coprecipitation method. They used these nanocomposites as catalysts in the reduction of p-nitrophenol. It was reported that the $NiFe_2O_4$/GQD composite exhibited the optimum catalytic activity and the reduction of p-nitrophenol was completed within 1 min. It was revealed that these catalysts can be separated by a magnetic field using an external magnet. They also show good stability and these can be reused for six cycles retaining activity of around 95%.

The catalytic activity of as-prepared nanocomposites and metal ferities for the reduction of p-nitrophenol was found to follow the order:

$$NiFe_2O_4/GQD > CoFe_2O_4/GQD > NiFe_2O_4 > CoFe_2O_4.$$

Zhao et al. (2021) synthesized graphitic carbon nitride QDs by incorporating the unique organic functional group of barbituric acid into the framework of the carbon nitride structure by supramolecular preorganization. Then three CNQDs were introduced onto basic zinc carbonate (BZC) surface via the coprecipitation method. It was reported that the as-prepared CNQDs/BZC composite exhibited a higher degradation efficiency of tetracycline, which was about 2.4 times higher than that of ZnO. It was revealed that $^{\bullet}O_2^-$ and $^{\bullet}OH$ radicals played major roles in degradation due to the suitable bandgap.

Hsieh et al. (2022) introduced N-GQDs in rGO, which efficiently facilitates the photocatalytic activity of composite. It was reported that an ultrahigh removal ratio ($\sim$100%) and improved rate constant could be achieved with this GQD/ZnO catalyst (1.74 more as compared to pristine ZnO). It was revealed that the presence of N-GQDs increased the absorption in the visible light region and photoinduced charge carrier, and as a result photocatalytic activity was increased. It was observed that as-prepared GQD/ZnO composite can be used as a photocatalyst for degrading metronidazole in the presence of UV−light irradiation.

5.3.6 Others

Lan et al. (2014) prepared hybrid nanocomposites of Zn-Cr layered double hydroxide (ZnCr-LDH) and graphene through a coprecipitation method. It was reported that ZnCr-LDH nanoplatelets had a diameter $\sim$6 nm and these were well dispersed on the graphene surface. These hybrid ZnCr-LDH/graphene nanocomposites were used for the photocatalytic degradation of rhodamine B, which has a higher rate as compared to ZnCr-LDH.

Bahadori et al. (2021) used a coprecipitation-assisted solvothermal method to synthesize covalent organic frameworks (COFs) QDs, which were modified with biochar. It was found that as-synthesized COFs QD nanostructures have an average size of about 3.68 nm. These nanocomposite structures were then utilized for decolorizing methyl blue, methyl orange, and methyl red.

5.4 Conclusion

Various QDs (metals, metal oxides, metal sulfides, carbon, and graphene-based materials) can be synthesized successfully using the coprecipitation approach. It is an eco-friendly and relatively low-cost approach to synthesize nanomaterials. It can also be used to prepare larger amounts of QDs on an industrial scale. As-synthesized QDs have great potential for application in varied fields of interest such as bioimaging, sensors, solar cells, water splitting, and light-emitting diodes.

References

Abha, K., Sumithra, I.S., Suji, S., Anjana, R.R., Anjali Devi, J.S., Nebu, J., et al., 2020. Dopamine-induced photoluminescence quenching of bovine serum albumin−capped manganese-doped zinc sulphide quantum dots. Anal. Bioanal. Chem. 412, 5671−5681.

Ashokkumar, M., Boopathyraja, A., 2018. Structural and optical properties of Mg doped ZnS quantum dots and biological applications. Superlattices Microstruct. 113, 236−243.

Bahadori, A., Ranjbar, M., Asadipour, A., Kalantari-Khandani, S., 2021. Covalent organic frameworks (COFs) quantum dots as supramolecular cages modified with biochar as nanobio photocatalyst for degradation of organic dyes. J. Mater. Sci.: Mater. Electron. 32 (18), 23018−23029.

Desai, N. V., Shaikh, I. A., Rawal, K. G., Shah, D.V. 2018. Synthesis, structural and optical properties of PVP coated transition metal doped ZnS nanoparticles. AIP Conf. Proceed., 1953 (1), 030149.

Devadoss, I., Sakthivel, P., Muthukumaran, S., Sudhakar, N., 2019. Enhanced blue-light emission on $Cd_{0.9-x}Zn_{0.1}Cr_xS$ ($0 \leq x \leq 0.05$) quantum dots. Ceram. Int. 45 (3), 3833−3838.

Elavarthi, P., Kumar, A.A., Murali, G., Reddy, D.A., Gunasekhar, K.R., 2016. Room temperature ferromagnetism and white light emissive CdS: Cr nanoparticles synthesized by chemical coprecipitation method. J. Alloy Compd. 656, 510−517.

Giribabu, G., Murali, G., Reddy, D.A., Vijayalakshmi, R.P., Rao, M., 2012. Effect of Mg doping on the structural and optical properties of CdS nanoparticles synthesized by co-precipitation Method. J. Nano Electron. Phys. 4 (4). Available from: http://essuir.sumdu.edu.ua/handle/123456789/30285.

Hernandez, I.P., Velazquez, E.R., Meda, M.A., Galindo, J.T.E., Delgado, F.P., Guizar, A.T., et al., 2020. Magnetic nanocomposite with fluorescence enhancement effect based on amino acid coated-Fe_3O_4 functionalized with quantum dots. Mater. Chem. Phys. 25 (1). Available from: https://doi.org/10.1016/j.matchemphys.2020.123082.

Horoz, S., 2018. Synthesis of cobalt-alloyed ZnS quantum dots and investigation of their characteristics. Mater. Technol. 52 (5), 555−559.

Hsieh, M.L., Juang, R.S., Gandomi, Y.A., Fu, C.C., Hsieh, C.T., Liu, W.R., 2022. Synthesis and characterization of high-performance ZnO/graphene quantum dot composites for photocatalytic degradation of metronidazole. J. Taiwan. Inst. Chem. Eng. 131. Available from: https://doi.org/10.1016/j.jtice.2021.104180.

Ibraheema, F., Mahdy, M.A., Ortega, J.E., Rogero, C., Mahdy, I.A., El-Sayed, A., 2020. Tuning paramagnetic effect of Co-doped CdS diluted magnetic semiconductor quantum dots. J. Alloy Compd. 835. Available from: https://doi.org/10.1016/j.jallcom.2020.155196.

Iqbal, M.J., Iqbal, S., 2013. Synthesis of stable and highly luminescent beryllium and magnesium doped ZnS quantum dots suitable for design of photonic and sensor material. J. Lumin. 134, 739−746.

Jabeen, U., Adhikari, T., Shah, S.M., Pathak, D., Nunzi, J.M., 2017. Synthesis, characterization and photovoltaic performance of Mn-doped ZnS quantum dots-P3HT hybrid bulk heterojunction solar cells. Opt. Mater. 73, 754−762.

Jbara, A.S., Othaman, Z., Ati, A.A., Saeed, M.A., 2017. Characterization of γ-Al_2O_3 nanopowders synthesized by coprecipitation method. Mater. Chem. Phys. 188, 24−29.

Kaur, S., Sharma, S., Umar, A., Singh, S., Mehta, S.K., Kansal, S.K., 2017. Solar light driven enhanced photocatalytic degradation of brilliant green dye based on ZnS quantum dots. Superlattices Microstruct. 103, 365−375.

Lan, M., Fan, G., Yang, L., Li, F., 2014. Significantly enhanced visible-light-induced photocatalytic performance of hybrid Zn−Cr layered double hydroxide/graphene nanocomposite and the mechanism study. Ind. Eng. Chem. Res. 53 (33), 12943−12952.

Lewis, C.S., Liu, H., Han, J., Wang, L., Yue, S., Brennan, N.A., et al., 2016. Probing charge transfer in a novel class of luminescent perovskite-based heterostructures composed of quantum dots bound to RE-activated $CaTiO_3$ phosphors. Nanoscale 8 (4), 2129−2142.

Lin, X., Liu, C., Wang, J., Yang, S., Shi, J., Hong, Y., 2019. Graphitic carbon nitride quantum dots and nitrogen-doped carbon quantum dots co-decorated with $BiVO_4$ microspheres: a ternary heterostructure photocatalyst for water purification. Sep. Purif. Technol. 226, 117−127.

Mansur, A.A., Mansur, H.S., Tabare, C., Paiva, A., Capanema, N.S., 2019. Eco-friendly $AgInS_2$/ZnS quantum dot nanohybrids with tunable luminescent properties modulated by pH-sensitive biopolymer for potential solar energy harvesting applications. J. Mater. Sci. Mater. Electron. 30 (18), 16702−16717.

Masmali, N.A., Osman, Z., Arof, A.K., 2022. Comparison between silver sulfide and cadmium sulfide quantum dots in ZnO and ZnO/$ZnFe_2O_4$ photoanode of quantum dots sensitized solar cells. Ionics 28, 2007−2020.

Meng, X., Zhang, C., Dong, C., Sun, W., Ji, D., Ding, Y., 2020. Carbon quantum dots assisted strategy to synthesize Co@NC for boosting photocatalytic hydrogen evolution performance of CdS. Chem. Eng. J. 389. Available from: https://doi.org/10.1016/j.cej.2020.124432.

Mishra, S.K., Srivastava, R.K., Prakash, S.G., Yadav, R.S., Panday, A.C., 2011. Structural, photoconductivity and photoluminescence characterization of cadmium sulfide quantum dots prepared by a coprecipitation method. Electron. Mater. Lett. 7 (1), 31−38.

Naghshbandi, Z., Arsalani, N., Zakerhamidi, M.S., Geckeler, K.E., 2018. A novel synthesis of magnetic and photoluminescent graphene quantum dots/MFe_2O_4 (M = Ni, Co) nanocomposites for catalytic application. Appl. Surf. Sci. 443, 484−491.

Niu, J., Pan, J., Fu, W., Xiao, G., Fu, Y., Cao, J., et al., 2022. The photovoltaic enhancement of Cu_2O/SnO_2 quantum dots/ZnO arrays transparent pn junction device via carrier injection and potential transition of SnO_2 QDs. J. Materi. Sci.: Materi. Electron. 33 (9), 7300−7311.

Rafiq, A., Imran, M., Ikram, M., Naz, M., Aqeel, M., Majeed, H., et al., 2019. Photocatalytic and catalytic degradation of organic dye by uncapped and capped ZnS quantum dots. Mater. Res. Express 6 (5). Available from: https://doi.org/10.1088/2053-1591/aaff8e.

Ragupathi, H., Choe, Y., Arockiaraj, A., 2021. Preferential killing of bacterial cells by surface-modified organosilane-treated ZnO quantum dots synthesized through a coprecipitation method. N. J. Chem. 45 (29), 12986−12995.

Rahdar, A., Asnaasahri Eivari1, H., Sarhaddi, R., 2012. Study of structural and optical properties of ZnS:Cr nanoparticles synthesized by coprecipitation method. Indian J. Sci. Technol. 5 (1), 1855−1858.

Ramachandran, S., Sathishkumar, M., Kothurkar, N.K., Senthilkumar, R. 2018. Synthesis and characterization of graphene quantum dots/cobalt ferrite nanocomposite. In IOP Conf. Ser.: Mater. Sci. Eng. 310 (1). Available from: https://doi.org/10.1088/1757-899X/310/1/012139.

Rofouei, M.K., Tajarrod, N., Masteri-Farahani, M., Zadmard, R., 2015. A new fluorescence sensor for Cerium (III) ion using glycine dithiocarbamate capped manganese doped ZnS quantum dots. J. Fluoresc. 25 (6), 1855−1866.

Sakthivel, P., Muthukumaran, S., 2016. Crystallographic, structural and band gap tailoring of $Zn_{0.98}Mn_{0.02}S$ quantum dots Co-doped with Cu by co-precipitation method. J. Inorg. Organometal. Poly. Mater. 26 (3), 563−571.

Sakthivel, P., Muthukumaran, S., 2017. Investigation of Ni influence on structural and band gap tuning of $Zn_{0.98}Mn_{0.02}S$ quantum dots by coprecipitation method. J. Mater. Sci.: Mater. Electron. 28 (11), 8309–8315.

Sakthivel, P., Muthukumaran, S., 2018. Influence of Co^{2+} on electrical and optical behavior of Mn^{2+}–doped ZnS quantum dots. Opt. Laser Technol. 103, 109–117.

Sakthivel, P., Venkatesan, G.P., Subramaniam, K., Muthukrishnan, P., 2019. Structural, optical, photoluminescence and electrochemical behaviors of Mg, Mn dual-doped ZnS quantum dots. J. Mater. Sci.: Mater. Electron. 30 (13), 11984–11993.

Samuei, S., Fakkar, J., Rezvani, Z., Shomali, A., Habibi, B., 2017. Synthesis and characterization of graphene quantum dots/CoNiAl-layered double-hydroxide nanocomposite: application as a glucose sensor. Anal. Biochem. 521, 31–39.

Sarkar, T., Dhiman, T.K., Sajwan, R.K., Sri, S., Solanki, P.R., 2020. Studies on carbon-quantum-dot-embedded iron oxide nanoparticles and their electrochemical response. Nanotechnology 31 (35). Available from: https://doi.org/10.1088/1361-6528/ab925e.

Shamsipur, M., Rajabi, H.R., 2014. Study of photocatalytic activity of ZnS quantum dots as efficient nanoparticles for removal of methyl violet: effect of ferric ion doping. Spectrochim. Acta A Mol. Biomol. Spectrosc. 122, 260–267.

Sharma, G., Kumar, A., Naushad, M., Kumar, A., Ala'a, H., Dhiman, P., et al., 2018. Photoremediation of toxic dye from aqueous environment using monometallic and bimetallic quantum dots based nanocomposites. J. Clean. Product. 172, 2919–2930.

Sharma, L.K., Choubey, R.K., Mukherjee, S., 2020. Spin-flop in transition-metal-doped SnO_2 quantum dots. Mater. Chem. Phys. 254. Available from: https://doi.org/10.1016/j.matchemphys.2020.123537.

Sharma, L.K., Kar, M., Choubey, R.K., Mukherjee, S., 2021. Low field magnetic interactions in the transition metals doped CuS quantum dots. Chem. Phys. Lett. 780. Available from: https://doi.org/10.1016/j.cplett.2021.138902.

Tyagi, C., Sharma, A., Kurchania, R., 2014. Synthesis of CdS quantum dots using wet chemical coprecipitation method. J. Non-Oxide Glasses 6 (2), 23–26.

Verma, M., Patidar, D., Sharma, K.B., Saxena, N.S., 2016. Phase transformations and thermal stability of CdSe quantum dots: cubic to hexagonal. J. Inorg. Organometal. Poly. Mater. 26 (1), 75–80.

Wu, X., Zhang, Y., Han, T., Wu, H., Guo, S., Zhang, J., 2014. Composite of graphene quantum dots and Fe_3O_4 nanoparticles: peroxidase activity and application in phenolic compound removal. RSC Adv. 4, 3299–3305.

Yadav, I., Ahlawat, D.S., Ahlawat, R., 2016. Cu-doped $Cd_{1-x}Zn_xS$ alloy: synthesis and structural investigations. Appl. Phys. A 122 (3). Available from: https://doi.org/10.1007/s00339-016-9745-z.

Youngjin, D., Jongsung, K., 2016. The preparation of magnetic silica nanospheres and incorporation of CdSe/ZnS quantum dots-DNA Probe. J. Nanosci. Nanotechnol. 16 (3), 2488–2491.

Yu, W., Yu, N., Wang, Z., Li, X., Song, C., Jiang, R., et al., 2019. Chitosan-mediated green synthesis and folic-acid modification of CuS quantum dots for photoacoustic imaging guided photothermal therapy of tumor. J. Colloid Interface Sci. 555, 480–488.

Zhang, N., Huang, Y., Zong, M., Ding, X., Li, S., Wang, M., 2017. Synthesis of ZnS quantum dots and $CoFe_2O_4$ nanoparticles co-loaded with graphene nanosheets as an efficient broad band EM wave absorber. Chem. Eng. J. 308, 214–221.

Zhang, Z., Yang, Y., Gao, J., Xiao, S., Zhou, C., Pan, D., et al., 2018. Highly efficient Ag_2Se quantum dots blocking layer for solid-state dye-sensitized solar cells: size effects on device performances. Mater. Today Energy 7, 27–36.

Zhao, H., Fang, Q., Chen, C., Chao, Z., Tsang, Y., Wu, Y., 2018. WO_3 quantum dots decorated GO/Mg-doped ZnO composites for enhanced photocatalytic activity under nature sunlight. Appl. Organomet. Chem. 32 (9). Available from: https://doi.org/10.1002/aoc.4449.

Zhao, P., Jin, B., Zhang, Q., Peng, R., 2021. Fabrication and photocatalytic activity of graphitic-C_3N_4 quantum dots-decorated basic zinc carbonate prepared by a co-precipitation method. Phys. Chem. Chem. Phys. 23 (36), 20329–20339.

This page intentionally left blank

Chapter 6

Biogenic synthesis of quantum dots

Meghavi Gupta[1], **Inderjeet Yadav**[2] **and Abhilasha Jain**[3]
[1]*Department of Chemistry, PAHER University, Udaipur, Rajasthan, India,* [2]*Department of Applied Sciences, University of Technology and Applied Sciences, Alkhuwair, Muscat, Sultanate of Oman,* [3]*Department of Chemistry, St. Xavier's College, Mumbai, Maharashtra, India*

6.1 Introduction

The synthesis of designer solid state materials by living organisms is an emerging field of research. As there is a growing trend in biomedical applications of quantum dots, biosynthesized nanomaterials are attracting the attention of researchers these days due to their biocompatible, low-energy consumption, economic, and tunable characteristics.

Zero-dimensional semiconductor quantum dots (<10 nm) have received great attention because of their potential use in biomedical applications (diagnosis and therapy), where larger nanoparticles (>10 nm) were not found to be suitable.

Biosynthesis of quantum dots is an alternate green method for the production of quantum dots with superior properties, such as tunable size, emission spectra, and a longer fluorescence lifetime. Biosynthesis of quantum dots offers other several advantages over other existing conventional chemical synthesis routes, such as low cost, eco-friendliness, and no need for any further modification of the products. Controlled monodispersity, chemical compositions, desired morphologies, and particle size could be achieved with the biosynthesis method.

However, still manipulation and control of biosynthesis of QDs remain slightly difficult because of the lack of knowledge of the mechanisms necessary for the biosynthesis or the effect of the biosynthesizing organisms is still insufficient.

Synthesis of QDs can be carried out using plants (*Avena sativa*, *Azadirachta indica*, *Alovera*, *Mangifera indica*, etc.) fungi (*Fusarium oxysporum*, *Phanerochaete chrysosporium*, *Pleurotus ostreatus*, etc.), bacteria (*Escherichia coli, Pseudomonas, Staphylococcus aureus, Acidithiobacillus*

Quantum Dots. DOI: https://doi.org/10.1016/B978-0-12-824153-0.00006-9

genus, etc.), and enzymes. There are many more plants, bacteria, enzymes, fungi, etc., which are still unexplored although they have a great potential for preparing quantum dots.

6.1.1 Advantages

1. It is a green chemical route.
2. It is relatively less time consuming.
3. Ambient conditions are required, and not harsh conditions.
4. It is based on natural materials such as plant extracts, enzymes, bacteria, fungi, etc.

6.1.2 Disadvantages

1. It is based on plants, which means a limited source.
2. It may cause additional problems, particularly when bacteria and fungi are used, unless carried out under control.
3. Difficult to control the size of nanocrystal.

6.2 Plants

Wang et al. (2005) prepared ZnS semiconductor nanoparticles in situ in chitosan film. It was revealed that the chitosan template was monodispersed and passivated. The average size was found to be 3.4 nm. Rosano-Ortega et al. (2006) synthesized Mn nanoparticles in the range of 1−4 nm using water hyacinth. It was reported that the as-obtained particles have a well controlled size. It was also revealed that small clusters in the range of 1−2 nm were generated, when the pH was kept at 5. It was also found that smallest aggregates with polyhedron shapes were stable in nature.

Wang et al. (2009) synthesized water-soluble biocompatible and monodispersed CdS, ZnS, and CdSe quantum dots using natural chitosan derivatives as stabilizers. It was revealed that nanoparticles with average size of 3−5 nm were obtained. It was found that the photoluminescence of QDs was enhanced and surface defects were passivated. It was found that the size of particles and photoluminescence intensity can be controlled by varying the concentration of precursor ions and stabilizer, refluxing the time and molar ratio of metal ions with sulfide. The resulting biopolymer/QDs composite can be potentially applied as a biosensor or fluorescence tags in biological systems. An efficient and green method for plant-based biosynthesis of CdS quantum dots has been reported by Borovaya et al. (2014). They used hairy root culture of *Linaria maroccana* L. for this purpose. The *Linaria* root extract was incubated with sodium sulfide and cadmium sulfate to give stable luminescent CdS nanocrystals. It was revealed that as-obtained QDs were spherical in shape with a size ranging from 5 to 7 nm. The wurtzite

crystalline structure of as-synthesized CdSQDs was confirmed by electron diffraction.

Bhattacharjee and Ahmaruzzaman (2015) synthesized SnO_2 QDs by a green biological route using sugar cane juice. It was predicated that biomolecules present in sugar cane juice act as both capping agent and complexing agent. It was observed that spherical SnO_2 quantum dots were obtained with particle size ranging between ~2.5 and 4.5 nm. It was revealed that a blue-shift in the bandgap energy was there with decreasing particle size. As-synthesized SnO_2 QDs were then used for photocatalytic degradation of methylene blue and rose Bengal under direct sunlight. The catalytic activity of these biosynthesized QDs was also evaluated for reduction of p-nitrophenol to p-aminophenol in the presence of sodium borohydride in water. It was revealed that 99.5% of p-nitrophenol was reduced in these conditions within 1 h.

Ouyang and Sun (2016) used wheat endosperm cells in the biosynthesis of Ag_2S QDs. The delivered precursors of QDs into cultured wheat endosperm cells provided Ag_2S QDs in an aging process under the effect of endogenous glutathione in the cells. It was observed that these intracellularly synthesized near-infrared (NIR) fluorescent QDs were highly photostable and can be used for bioimaging. The biosynthesis of HgTe quantum dots has been reported by Green et al. (2016) in a living plant via a mutual antagonistic reaction. It was observed that when *Allium fistulosum* was exposed to mercury and tellurium salts, it afforded crystalline HgTe quantum dots (nonpassivated) under ambient conditions. These QDs exhibited emission in the near-infrared spectral region, which is the suitable range for finding applications in solar energy conversion and telecommunications.

The hairy roots of tomato (*Solanum lycopersicum*) and also fission yeast (*Schizosaccharomyces pombe*) were used by Al-Shalabi and Doran (2016) for biological synthesis of CdS quantum dots. It was observed that the growth rate with hairy roots was much slower compared with yeast, so they can be utilized for large-scale production. It was revealed that CdS crystallites obtained with yeast were smaller in size (2−6 nm diameters) as compared to QDs obtained using the roots (4−10 nm diameters). Borovaya et al. (2016) prepared water-soluble CdS quantum dots. They used bright yellow-2 (BY-2) cell suspension culture for this purpose, which acted as both stabilizing and capping agent. It was indicated that CdS QDs were crystalline and spherical in shape, ranging from 3 to 7 nm (diameter). It was revealed that as-synthesized CdS QDs were almost nontoxic in low concentrations using *Nicotiana tabacum* protoplasts as a model.

A simple and eco-friendly method for biosynthesis of luminescent ZnO quantum dots (well dispersed) was reported by Kaviya et al. (2017) using pomegranate peel extract. The use of this method avoided the use of strong commercial stabilizing agents, higher temperature, pH conditions, and inert atmosphere. It was revealed the as-obtained ZnO QDs had an average size

distribution around 4 nm. These ZnO QDs were water soluble and found to be stable for almost 1 year. As the emission from ZnO QDs was quenched on adding Cr^{3+} ions, the presence of these ions can be detected up to 2 nM in aqueous solution. Silva et al. (2017) biosynthesized Ag quantum particles using *Eichhornia crassipes* biomass. It was reported that the shape, size, structure, and composition of QDs were dependent on the amounts of hydrolyzable tannins in this plant. It was revealed that the amounts of hydrolyzable tannins were highest in the leaves of this plant. These QDs were found to be nearly spherical in shape; however, these were mostly polyhedral. It was observed that leaf biomass could produce quantum dots with sizes <10 nm and these were mostly AgO, and not Ag.

Begum and Ahmaruzzaman (2018) used microwave heating for the biosynthesis of SnO_2 quantum dots using *Parkia speciosa* Hassk pods extract. As-synthesized SnO_2 QDs were then used as a photocatalyst for the degradation of acid yellow 23 (a food dye) in aqueous solution in the presence of UV254 light. It was reported that biosynthesized SnO_2 QDs could degrade acid yellow 23 with photocatalytic efficiency (98%) in 24 min. It was claimed that these SnO_2 QDs can be reused for up to five consecutive cycles without losing efficiency and stability. Shivaji et al. (2018) developed a green biogenic synthesis for preparing CdS QDs using tea leaf extract (*Camellia sinensis*). It was found that the particle size of QDs was in the range of 2−5 nm. They also investigated the biological activity of these CdS QDs and it was observed that they exhibited cytotoxicity toward A549 cancer cells. This activity was also compared with a standard drug, cisplatin, with comparable results.

An efficient and green approach was reported by Alvand et al. (2019) for synthesis of cadmium telluride quantum dots. They used an aqueous extract of fruits of *Ficus johannis* plant. Two extraction methods were used for extraction: (1) microwave-assisted extraction (MWAE) and (2) ultrasonic-assisted extraction (USAE). These plant extracts were used as natural stabilizing precursors for synthesizing CdTe QDs. The average particle size of as-prepared QDs was calculated as 1.2 nm. It was indicated that these CdTe QDs have negligible genotoxicity and toxicity impacts. Fatimah et al. (2020) biosynthesized SnO_2 quantum dots using flower extract of Aparajitha (*Clitoria ternatea*) as a reducing agent. This flower extract contains flavonoids as well as flavanols, which can reduce Sn^{2+} precursors into Sn° NPs, which are then oxidized to SnO_2 QDs (4−10 nm). A blueshift was observed in the wavelength of biosynthesized SnO_2 QDs. These QDs were there used for photocatalytic degradation of rhoadamine blue under UV irradiation.

Biosynthesis of CdS QDs has been reported by Gholami et al. (2020) using aqueous extracts of regenerated hairy roots of *Rhaphanus sativus* L. It was observed that as-obtained particles were spherical in shape with size ranging between 2 and 7 nm. It was also reported that these CdS QDs exhibited more apoptosis effect on MCF-7 breast cancer cells as compared to

AGS gastric cancer cell lines. Kandasamy et al. (2020) reported the synthesis of CdS quantum dots using fruit sap of *Opuntia ficus indica* (as green template). It was revealed that QDs were spherical in shape.

A green chemical route for the synthesis of copper quantum dots has been developed by Rani et al. (2020) using leaf extract of *M. indica* (L.). They used copper sulfate as the source of copper. It was proposed that a polyphenolic compound (mangiferin) in leaf extract of *M. indica* may act as a capping, reducing, and stabilizing agent during the preparation of Cu QDs. As-obtained Cu QDs were stable and spherical in shape with size ranging from 4−7 nm. It was reported that these Cu QDs can degrade methylene blue and possess higher antimicrobial activity and scavenging activity of free radical.

Zaman et al. (2020) reported the biogenic synthesis of cupric oxide nanoparticles using leaf and fruit extracts of *Tamarindus indica* L. These extracts acted as capping and reducing agents. It was observed that CuO quantum dots of size 5−10 nm could be obtained using fruit extract, but larger particles (50−100 nm) were obtained on using leaf extract. The photocatalytic activity of as-synthesized QDs was evaluated for the degradation of rhodamine B under UV−Vis light illumination. It was reported that QDs obtained with leaf extract could degrade 65% of rhodamine B in 2 h, while quantum dots prepared using fruit extract degraded 77% of the dye. These QDs exhibited an excellent photostability and in vitro antimicrobial activity against bacterial strains *S. typhi*, *E. coli*, and *L. acidophilus*.

Das and Dhar (2020) reported a method for the synthesis of tin dioxide quantum dots. They used the shoots of *C. sinensis* as a stabilizer and reducing agent. It was observed that as-prepared tin dioxide quantum dots had a flake-like morphology and were crystalline with an average size of 4.3 nm. As-obtained SnO_2 quantum dots were then used for photocatalytic degradation of thiamethoxam. They could achieve 57% degradation within 45 min.

The extracts of medicinal plants such as *Bryophyllum pinnatum*, *Mentha arvensis*, and *Dalbergia sissoo* were used by Kumar et al. (2021) to prepare Ag NPs by reducing silver nitrate. Then, Ag NP-conjugated L-cysteine-capped ZnS:Mn quantum dots were also fabricated, which exhibited antimicrobial activity against *E. coli* and *S. aureus*. This work may provide new avenues for synthesizing plasmonic NPs using nontoxic material to be used as detectors and biosensors.

The synthesis of CdS quantum dots was carried out by Tudu et al. (2021) using *Ocimum sanctum* (Tulsi) leaf extract. It was reported that the phytochemicals of Tulsi leaf extract played an important role in controlling particle size and morphology. The average crystallite size of these biosynthesized QDs was found to be in the range of 3.6−3.0 nm It is interesting to note that the bandgap of the capped CdS QDs increases with increasing extract concentration, but on the contrary particle size decreases.

Pugazhenthiran et al. (2021) prepared monodispersed silver quantum dots via a green synthesis method. They used sweet lime (*Citrus limetta*) peel

extract for this biosynthesis. It was reported that face-centered-cubic Ag QDs with size (<5 nm) were obtained. The presence of carbohydrate and citrate were considered responsible for the formation of small Ag QDs with good stability. It was also indicated that as-synthesized Ag QDs were able to cause the death of cancer cells (71%) even at a low concentration (100 $\mu g\ mL^{-1}$).

Raja and Sundaramurthy (2021) used betel leaves (piper betle) for green synthesis of fluorescent carbon quantum dots. They reported that as-prepared carbon dots were selective in the detection of Fe^{3+} ions in aqueous medium. They have detected successfully the presence of ferric ions even in the presence of interfering metal ions such as Ca^{2+}, Mg^{2+}, Cu^{2+}, Ag^{+}, Fe^{2+}, Hg^{2+}, Cd^{2+}, Fe^{3+}, and Pb^{2+} at the same concentrations. It was reported that it was possible to detect Fe^{3+} ions in the concentration range of 50−150 nM with high sensitivity.

6.3 Bacteria

A facile route for the synthesis of cadmium sulfide nanoparticles has been reported by Bai et al. (2009) using the photosynthetic bacteria *Rhodopseudomonas palustris*. It was observed that the cadmium sulfate solution incubated with *R. palustris* biomass changed its color to yellow after 2 days. As-obtained CdS nanoparticles had an average size of 8.01 ± 0.25 nm with uniform distribution, as evident from by TEM images. A bacterial synthesis for cadmium telluride quantum dots with tunable fluorescence emission has been reported by Bao et al. (2010a) using *E. coli*. It was observed that these QDs exhibited size-tunable optical properties with fluorescence emission at 488−551 nm. It was revealed that these biosynthesized QDs have great potential in a wide range of biolabeling and bioimaging applications.

Mi et al. (2011) prepared CdS quantum dots using genetically engineered *E. coli* by introducing foreign genes encoding a CdS binding peptide. They prepared CdS QDs through two methods: lysis, and freezing−thawing of cells. It was claimed that biologically synthesized CdS QDs may be more biocompatible probes in bioimaging and biolabeling. Suresh et al. (2011) reported an efficient synthesis of extracellular silver sulfide nanoparticles using the metal-reducing bacterium *Shewanella oneidensis*. It was observed that particles were homogeneously shaped, monodispersed, and produced with high yield (85%). It was also revealed that as-prepared particles were a spherical shape with a mean diameter of 9 ± 3.5 nm. As-fabricated QDs particles are biocompatible and dispersible. They have an excellent potential for application in electronic devices, optical imaging, and solar cells.

Jiang et al. (2012) prepared cadmium sulfide quantum dots via in situ crosslinked chitosan hydrogel films. It was confirmed that crosslinked chitosan hydrogel films provided a confined matrix for CdS QDs growth. As-prepared CdS QDs/chitosan composite films slow photocatalytic activity for

degradation of methyl orange solution in the presence of visible light. Luminescent CdSe quantum dots were synthesized by Fellowes et al. (2013). They used bacterially derived selenide (Se^{2-}) as the precursor. Biogenic Se^{2-} was produced by the reduction of Se(IV) by *Veillonella atypica*. It was reported that biological Se^{2-} formed smaller and narrower size distributed QDs as compared to borohydride-reduced Se(IV) under similar conditions.

Kominkova et al. (2014) evaluated the effect of CdTe quantum dots on *Collembolans*, the earthworm *Eisenia fetida*, and *E. coli*. They also studied the effect of biosynthesis of QDs in *E. fetida* and *E. coli*. It was revealed that biosynthesis in earthworms can be a protective mechanism of its own; while it is probably a by-product of protective mechanisms in *E. coli*. Yan et al. (2014) proposed a green and efficient biosynthesis method for preparing CdSe QDs using *E. coli* cells as biological matrix. These QDs were fluorescence-tunable and biocompatible. It was observed that there was a surface protein capping layer outside QDs, as evident from FT-IR data. It was suggested that as-prepared quantum dots may prove to be an excellent fluorescent marker for broad bioimaging and biolabeling.

Gallardo et al. (2014) isolated oxidative stress-resistant bacteria (*Pseudomonas* spp.) from Antarctica and then used them for biosynthesis of CdS QDs at 15°C. It was reported that there was a change in fluorescence color (green to red), which was found to be time dependent. Yang et al. (2015) engineered a bacterial strain for biosynthesis of CdS quantum dots. It was reported that extracellular and water-soluble CdS quantum dots were obtained on using this strain at ambient pressure and temperatures with low-cost precursors. The biosynthesis of α- and β- forms of ZnS quantum dots was developed by Yue et al. (2016) using *Clostridiaceae* sp. They used different concentrations of hydroxypropyl starch as dispersant in this process. It was indicated that as-obtained α-ZnS quantum dots had a wurtzite structure with a low dose of hydroxypropyl starch, while β-ZnS quantum dots were prepared with a sphalerite structure with a high dose. It was also revealed that β-ZnS quantum dots exhibited a redshift as compared to α-ZnS quantum dots.

Fluorescent *Bacillus subtilis* cells were developed as probes for imaging applications and to explore behaviorial interaction between *B. subtilis* and *S. aureus*. A controlled biosynthesis of CdSe quantum dots was developed by Yan et al. (2016) using living *B. subtilis* cells. It was reported that *B. subtilis* cells inhibit the growth of nearby *S. aureus* cells. Such inhibition was affected by both growth stage as well as amount of surrounding *B. subtilis* cells.

Ulloa et al. (2016) reported the biosynthesis of cadmium sulfide QDs using acidophilic bacteria *Acidithiobacillus genus*. These CdS QDs were obtained when *Acidithiobacillus thiooxidans*, *A. ferrooxidans*, and *A. caldus* cells were exposed to sublethal cadmium concentrations in the presence of glutathione and cysteine. It was revealed that fluorescence of cadmium-exposed cells moves from green to red with time of incubation. It was

reported that an average size of 6 and 10 nm was found to show green and red QDs, respectively.

Yan et al. (2017) reported a green biosynthesis of cadmium sulfide quantum dots. Here, *E. coli* was selected as a biomatrix. It was revealed that these CdS quantum dots emitted a blue−green fluorescence under UV excitation. It was indicated that the antibiotic resistance of *E. coli* had a slight decrease when CdS quantum dots were prepared at mild temperature. Kominkova et al. (2017) obtained CdTe QDs by the extracellular biosynthesis by *E. coli*. These CdTeQDs were also prepared by microwave-assisted synthesis. The toxicity of as-obtained QDs was tested using three cell lines, Human Prostate Cancer cells (PC-3), Human Foreskin Fibroblast (HFF), and Breast Cancer cells (MCF-7), and it was observed that the toxicity of biosynthesized QDs to the PC-3 cell lines was almost 35% lower as compared to QDs prepared by the microwave technique.

Qi et al. (2017) used a low-cost hydroxypropyl starch (HPS) to assist sulfate-reducing bacteria (SRB) in the synthesis of ZnS QDs. It was indicated that HPS enhanced the growth of SRB and reduction of sulfate ions into sulfide, which blocked the interaction between sulfide and zinc ions to control the nucleation as well as growth of ZnS QDs. It was observed that average crystal size of as-prepared ZnS QDs decreases from 5.95 to 3.34 nm on increasing the concentration of HPS. There was a blueshift in the absorption peak, which may be due to the quantum confinement effect. The color of photoluminescence spectrum was found to be changed from red to yellow, which is evidence of tunable PL of ZnS QDs. The production of CdS QDs was reported by Ulloa et al. (2018) by acidophilic bacteria, of the *Acidithiobacillus* genus. It was observed that the addition of inorganic phosphate to *A. thiooxidans* ATCC 19703 cultures favored the biosynthesis of CdS QDs in the acidic range (pH 3.5). It was also indicated that phosphate contributes to the biosynthesis of CdS QDs by influencing uptake and tolerance to cadmium.

Yan et al. (2018) produced high-quality CdSe QDs in *Bacillus amyloliquefaciens*. This process has the benefits of short reaction time, high yield, mild synthetic conditions, and good reproducibility. Then as-obtained CdSe QDs were used as a probe for detecting copper(II) ions in blood plasma. It was observed that the protein envelope on the QD surface does not permit interference by others due to selective permeability of the bacterial cell membrane. It was revealed that copper ions in human blood plasma samples could be accurately determined in the range (15.6−18.5 $\mu mol\ L^{-1}$), which is almost similar to results obtained with atomic absorption spectroscopy. Biosynthesis of CdS quantum dots sensitized nanorod arrays of ZnO was reported by Yang et al. (2018). These ZnO nanorod arrays were prepared on FTO using a simple galvanic-cell-based approach. Therefore, these were introduced silanized by (3-aminopropyl)triethoxysilane (APTES) with amino groups, so that Cd^{2+} can be introduced. As-synthesized CdS/ZnO heterostructure was used as photoelectrochemical (PEC)

sensing platform, which exhibited detection sensitivity of 32 CFV m L^{-1} for sulfate-reducing bacteria (SRB). This work can help in the detection of physiological messenger molecules such as hydrogen sulfide.

The role of volatile sulfur compounds was investigated by Gallardo-Benavente et al. (2019) in the biosynthesis of CdS QDs using Antarctic strain *Pseudomonas fragi* GC01. They used different sulfur sources such as sulfite, sulfide, sulfate, thiosulfate, cysteine, and methionine. Intracellular biosynthesis was therefore all sulfur sources except acetylcysteine (Cys) and methionine (Met), where extracellular biosynthesis was there. It was observed that as-synthesized CdSQDs were in the range of 2−16 nm (size). The importance of methane thiol (MeSH) was also confirmed in the biosynthesis of QD. An extracellular biosynthesis of ZnS QDs has been reported by Qi et al. (2019) via a molecular mediation mechanism, which was due to mixed SRB. It was observed that particle size of biogenic ZnS QDs was found to be 6.5 nm. This molecular mediation mechanism was triggered by the peculiar extracellular proteins (Eps) for the higher yield of biosynthesized ZnS QDs. Some other metal sulfide QDs were also prepared, such as CuS, PbS, and CdS.

Bruna et al. (2019) reported biological synthesis of CdS QDs using by polyextremophile halophilic bacteria *Halobacillus* sp. DS2, which was isolated from Uyuni Salt Flat (Bolivia), Atacama salt Flat (Chile), and the Dead Sea (Israel). As-prepared QDs were hexagonal in shape and monodispersed with size ranging between 2 and 5 nm. Abou-Assy et al. (2019) synthesized CdSe QDs using *Providencia vermicola* BGRW. These bacteria had the ability to resist many metals such as silver, cadmium, copper, zinc, nickel, lead, bismuth, and cobalt. It was revealed that biosynthesized CdSe QDs were cubic in shape with a size range of 2−4 nm.

The formation of CdS_xSe_{1-x} QDs has been reported by Tian et al. (2019). These QDs have quantum yield (5.2%) and size of 2.0 ± 0.4 nm. As-prepared QDs (without extra modification) were then used for bioimaging of cancer cells and tumor tissue of mice.

Qi et al. (2019) reported extracellular biosynthesis of ZnS QDs with high yield. As-prepared biogenic ZnS QDs had an average crystallite size of 6.5 nm with better uniformity and greater PL activity than obtained by a chemical route. They have fabricated other QDs such as PbS, CuS, and CdS through this method.

Anthony et al. (2020) synthesized fluorescent carbon quantum dots by nitric acid treatment. They used rice-biryani (processed white rice waste) as a precursor of carbon. As-prepared CQDs were modified further by a two-step process:

1. preparation of reduced-state CQDs (r-CQDs) using borohydride as reductant; and
2. rigidifying with a tripeptide such as glutathione (r-CQDs-GS).

It was observed that QY was enhanced from 5.46% for bare CQDs to 41% for (r-CQDs-GS). As-prepared r-CQDs-GS had an average particle size in the range of $2-5$ nm. It was reported that about 90% cell viability and normal morphology was retained even after treated with r-CQDs-GS concentrations up to $100\,\mu g\,mL^{-1}$. It was reported that r-CQDs-GS could find applications in in vitro/in vivo bioimaging.

Öcal et al. (2020) achieved intracellular preparation of PbS QDs using *Pseudomonas aeruginosa* ATCC 27853. It was revealed that these intracellular biosynthesized PbS QDs had a particle size in the range of 3.47−11.45 nm. As-synthesized PbS QDs showed antibacterial activity against *E. coli*, *Proteus mirabilis*, *Micrococcus luteus*, and *Bacillus cereus*. Órdenes-Aenishanslins et al. (2020) synthesized CdS, Ag_2S, and CdSAg nanocrystals with size less than 15 nm. As-produced CdSAg ternary QDs exhibited high stability, fluorescence, and good quantum yield (36.13%). They could also produce soluble Ag_2S nanoparticles without any traces of Cd. All these three biosynthesized QDs were used as photosensitizers, where CdSAg QDs exhibited the best photovoltaic performance. It was revealed that these nanoparticles are formed in the extracellular space of bacterial cells exposed to cysteine and cadmium chloride.

Sulfate-reducing bacteria are present in anaerobic granular sludge and convert sulfate into sulfide. Jacob et al. (2020) coupled sulfate reduction with precipitation of zinc in ZnS quantum dots. It was reported that biogenic ZnS QDs had an average particle size of 5−7 nm. They determined the bandgap energy of as-synthesized ZnS QDs to be 3.84 eV. These QDs can be used as an effective photocatalyst for the photo-assisted decolorization of Congo red. Ashengroph et al. (2020) developed a method for the biosynthesis of cadmium sulfide quantum dots using a strain of *Pseudomonas chlororaphis*. It was reported that spherical CdS QDs were produced with an average size of 6.7 ± 2.4 nm.

The biosynthetic ternary ZnCdS QDs were prepared by Qi et al. (2021a) by sulfate-reducing bacteria. It was reported that these ternary ZnCdS QDs were monodispersed, spherical in shape, with an average crystallite size as 6.12 nm. The bandgap energy of these QDs were determined to be 2.35−2.72 eV. ZnCdS QDs exhibited remarkable photocatalytic activity for hydrogen evolution ($3.752\,mmol\,h^{-1}\,g^{-1}$) under visible light without using any noble metal cocatalysts. An extracellular biosynthesis of ternary $Zn_xCd_{1-x}S$ QDs has been reported by Qi et al. (2021b) using sulfate-reducing bacteria. It was revealed that these QDs with size of 3.50−4.64 nm could be achieved within half an hour. It was reported that these biogenic QDs exhibited high stability in gastric acid and excellent biocompatibility and biosafety, so that these can enter growing HeLa cells.

Carrasco et al. (2021) analyzed the ability of Antarctic lithobiontic bacterium *Pedobacter* sp. UYP1 in the synthesis of cadmium sulfide quantum dots. Yellow−green and orange−red fluorescent emissions were observed

after 20 and 80 min of synthesis in the presence of UV light, respectively. It was revealed that QDs were obtained with size of 3.07 nm, which were then used as photosensitizers in solar cells. As-fabricated solar cells displayed $V_{oc} = 162$ mV, $J_{sc} = 0.0110$ mA cm^{-2}, and conversion efficiency up to 0.0016%. An anaerobic approach was developed by Xu et al. (2021a) for the biosynthesis of CdS quantum dots (cubic phase and hexagonal phase) using *S. oneidensis* Mr-1. It was reported that as-synthesized hexagonal CdS QDs exhibited high photocatalytic hydrogen evolution (21 mmol g^{-1}CdS h^{-1}).

6.4 Fungi

It was reported by Ahmad et al. (2005) that the synthesis of gold nanoparticles can be controlled in the presence of the fungus *Trichothecium* sp. It was observed that as-prepared gold nanoparticles were spherical, rod-like, and triangular shaped. The synthesis of highly luminescent CdSe quantum dots were reported by Kumar et al. (2007) at room temperature. They used *F. oxysporum*, a fungus incubated with a mixture of $SeCl_4$ and $CdCl_2$. A controllable synthesis of CdSe quantum dots has been reported by Cui et al. (2009) using living yeast cells as a biosynthesizer. These CdSe QDs can be synthesized at 30°C instead of at 300°C, as required in other methods. Apart from this, a control over photoluminescence could be achieved also.

A simple and efficient biosynthesis was reported by Bao et al. (2010b) to prepare biocompatible cadmium telluride quantum dots using yeast cells. It was revealed that as-prepared CdTe QDs are formed via extracellular growth and then an endocytosis pathway. These CdTe QDs are protein-capped with good crystallinity and uniform size (2−3.6 nm). As-prepared QDs are highly soluble in water and exhibit good biocompatibility. The fluorescent biocompatible CdTe QDs can find use in biolabeling and bioimaging applications.

The live yeast cell were used for biosynthesis of CdSe quantum dots by Wang et al. (2010). They prepared seleniumized yeast cells before loading. It was also reported that the on-chip biosynthesis required only 0.5×10^{-4} M concentration of cadmium chloride and only 4−5 h incubation time to obtain the optimum yield of CdSe quantum dots.

Saa et al. (2010) generated CdS quantum dots by enzymatic products. This provided an analytical assay to detect the enzymatic activity of alkaline phosphatase and acetylcholine esterase. The rate of decomposition of sodium thiosulfate to give hydrogen sulfide increases in the presence of thiocholine, which is produced by acetylthiocholine after hydrolysis by acetylcholine esterase. This H_2S in the presence of cadmium sulfate yields CdS quantum dots. This assay was also applied to detect acetylcholine esterase inhibitors.

The cadmium sulfide quantum dots were biosynthesized by Huang et al. (2012) using *Saccharomyces cerevisiae* yeast. It was reported that as-prepared CdS QDs emit blue−green fluorescence under UV light.

Syed and Ahmad (2013) reported fungal-mediated synthesis of CdTe quantum dots using the fungus *F. oxysporum*. They used cadmium chloride and tellurium chloride as the precursor of Cd and Te, respectively. It was observed that these CdTe QDs are highly fluorescent and exhibited antibacterial activity against Gram-positive as well as Gram-negative bacteria. A mechanism-oriented strategy was reported by Li et al. (2013) for controlling the biosynthesis of CdSe quantum dots (fluorescent) through metabolic engineering in yeast cells. It was reported that the glutathione metabolic pathway controlled the intracellular formation of CdSe QDs. It was revealed that yeast cells were homogeneously transformed into efficient cell-factories at the single-cell level, which provides a way to direct the cellular metabolism toward formation of CdSe QDs.

Chen et al. (2014) developed a method for extracellular microbial synthesis of CdSQDs. They used white rot fungus *P. chrysosporium*. This fungus was incubated with a solution of cadmium nitrate tetrahydrate, which turned yellow after 12 h, which indicated that CdSQDs are formed. These QDs exhibited a blue fluorescence (458 nm). The average particle size was calculated to be 2.56 nm with uniform size and good crystallinity. It was revealed that secretion of proteins and cysteine was found to play a dominant role in the stabilization and formation of CdS QDs. Borovaya et al. (2015) reported a reproducible, efficient, and eco−friendly biosynthesis of CdSQDs using mycelium of basidiomycete fungus *P. ostreatus*. The CdSQDs were synthesized using sodium sulfide and cadmium sulfate by incubating *P. ostreatus* mycelium. It was reported that as-prepared quantum dots were spherical in shape ranging between 4 to 5 nm size.

The cadmium selenium quantum dots were synthesized by Wu et al. (2015) using *S. cerevisiae* (ATCC9763). They used sodium selenide and cadmium chloride as the source of selenium and cadmium, respectively. It was reported that the biosynthesized CdSe QDs exhibited much lower cytotoxicity as compared to that obtained with hydrothermally synthesized thioglycolic acid (TGA)-capped CdSe. An efficient method for biosynthesis of CdTe and CdS has been reported by Mareeswari et al. (2016) using fungus *Rhizopus stolonifer*. It was observed that suspension of as-prepared quantum dots exhibited greenish-blue and purple luminescence. It was indicated that these quantum dots are biocompatible in nature. A good contrast in imaging was observed, when these quantum dots were incorporated in human breast adenocarcinoma Michigan Cancer Foundation-7 cell lines.

Polycrystalline ZnS quantum dots were synthesized by Uddandarao (2016) from an endophytic fungus *Aspergillus flavus*. It was revealed that they formed a spherical shape. *A. flavus* was isolated from a medicinal plant *Nothapodytes foetida*. It was proposed that quantum dots synthesized from this fungus may exhibit a great potential in medical and environmental applications. The CdSe QDs were synthesized by Yamaguchi et al. (2016) using *F. oxysporum*. It was reported that CdSe quantum dots were obtained from

the mycelial cells of *F. oxysporum*. It was also revealed that superoxide is accumulated, which may play an important role in reducing Se^{4+} to Se^{2-}; thus, inhibiting the aggregation of CdSe to form nanoparticles.

Jacob et al. (2017) reported the biosynthesis of PbSe QD using marine *Aspergillus terreus*. It was observed that an increase in the total protein content was present in the reaction mixture after biosynthesis. The involvement of metallothioneins (metal binding peptides) and other antioxidant enzymes was confirmed, and it may play an important role in biosynthesis of PbSe QDs. Brooks and Lefebvre (2017) synthesized CdSe quantum dots in the cytoplasm on treating *S. cerevisiae* sequentially with sodium selenite and cadmium chloride. As-prepared CdSe QDs exhibited a yellow fluorescence (540 nm). The presence of glutathione contributed to this biosynthetic process as it inhibited when it was applied after selenite treatment but before the addition of cadmium. It was revealed that by optimizing each aspect the production of CdSe QDs was increased 70% in this case.

Sandoval-Cárdenas et al. (2017) used a sulfur toxic waste, which was recovered after hydrodesulfurization of Mexican oil's sour acid gases. They synthesized cadmium sulfide quantum dots (hydrophilic) via a green method using a fungus, *F. oxysporum*. The mycelia of *F. oxysporum f.* sp. *lycopersici* were incubated with cadmium nitrate (1 mM) and sulfur waste (1% w/v) for 24 h, and then filtered to provide a yellow solution of cadmium sulfide quantum dots. As-obtained CdS QDs were biocompatible, hydrophilic, and stable in nature. It was also revealed that CdS QDs had a wurtzite crystalline structure with size of 6.116 ± 2.111 nm (diameter).

The cadmium selenide QDs were prepared by Tian et al. (2017) in vivo using *Candida utilis* WSH02−08. It was observed that fluorescence properties of these QDs can be turned using different precursor concentrations. It was found that as-synthesized QDs with longer photostable life time and high fluorescence intensity could be obtained by keeping Cd content higher than Se. It was suggested that such synthesized QDs can find application in live-cell imaging without any further modification. A white rot fungus *Trametes versicolor* was used by Qin et al. (2018) for biosynthesis of cadmium sulfide quantum dots. As-obtained cadmium sulfide quantum dots were found to be biocompatible and stable and therefore could have great potential in biological and biomedical applications.

Biosynthesis of CdSe QDs was reported by Shao et al. (2018) using *S. cerevisiae*. The selenocysteine was considered (SeCys) as the primary precursor of selenium in the intracellular biosynthesis of these QDs. It was revealed that the selenomethionine (SeMet)-to-SeCys pathway regulated biosynthesis of CdSe QD. The biosynthesis of ZnS QDs was reported by Jacob et al. (2019a) using the fungus *Aspergillus* sp. It was observed that as-prepared QDs were spherical and crystalline with a mean diameter of 6.3 nm. These ZnS QDs can find numerous applications in the fields of photocatalysis, medical imaging, and biosensing.

Jacob et al. (2019b) biosynthesized ZnS quantum dots from Zn-tolerant *Penicillium* sp. They also revealed that spherical particles of ZnS QDs were obtained with an average diameter of 11.08 nm. As-prepared biogenic ZnS were used for the photodegradation of methylene blue and this degradation efficiency was increased on increasing ZnS nanocatalyst/dye ratio reaching an equilibrium within six hours. These ZnS nanohybrids can find practical utility in the removal of different pollutants released from paper, textile, and dyeing industries. The carbon quantum dots were doped with nitrogen and sulfur (N,S-CDs) by Shi et al. (2019) using fungus fibers. It was reported that N,S-CDs exhibited excellent stability with high quantum yield as well as being water soluble with activity as quenching-based detection and cellular imaging of cancer cells. These QDs can be used as fluorescent probe for efficient, sensitive, and selective probe determination of tetracyclines the linear range of 0.5 to 47.6 μM, with a limit of detection of 15.6 nM. They also prepared test papers using N,S-CDs, which could detect tetracyclines present in aquiculture wastewater in lesser time.

Cao et al. (2020) biosynthesized CdSe QDs using a yeast *Rhodotorula mucilaginosa* PA-1 under aerobic conditions. It was reported that concentration of cadmium ions decides synthesis of CdSeQDs and not the selenium ions. It was found that bio-synthesized CdSe QDs had a narrow size distribution in the range of 3.2 ± 0.4 nm. These QDs exhibited excellent photocatalytic activity in degradation of malachite green in presence of ultraviolet and visible light. The photocatalytic degradation efficiency of malachite green under ultraviolet light was 86.5% after, while it was 94.28% under visible light. A green system was developed by Xu et al. (2020) for the biosynthesis of CdS_xSe_{1-x} QDs by *Phomopsis* sp. XP-8. The QDs were shown to have a CdS0.75Se0.25@oligopeptide transporter structure. It was observed that these QDs were monodispersed with a uniform spherical shape with diameter as 3.22 ± 0.07 nm. These QDs are water soluble and exhibited excellent fluorescence. It was revealed that they can be used as a sensor for detecting chloramphenicol (CAP) in the range of 3.13 to 500 $\mu g\ L^{-1}$ with a limit of detection of 0.89 $\mu g\ L^{-1}$. The detection method was highly selective for CAP with minimal interference from other antibiotics and it was also used successfully to detect CAP in milk samples.

A biosynthesis method to synthesize Ag_2Se QDs was developed by Liu et al. (2021) using *S. cerevisiae*. It was reported that nanoparticles obtained by extracellular purification had a uniform size of 3.9 ± 0.6 nm. These Ag_2Se QDs had good biocompatibility, maybe due to capping by protein. It was observed that the as-synthesized Ag_2Se QDs had lower toxicity and these could be used for in vivo imaging.

Xu et al. (2021a,b) developed a method to biosynthesize $Cd_{0.5}Zn_{0.5}S$ quantum dots using filamentous fungus *Phomopsis* sp. XP-8. It was reported that heterogeneous catalyst functionalized composite mycelium pellets (CMP) exhibited an enhanced visible light degradation activity. The catalytic

activity was also improved as biosorption capacity of CMP increased the contact rate between organic dyes and catalysts. This CMP has high mechanical strength and is easy to separate and recycle; thus the problems of recovery after use and secondary pollution of the environment were avoided.

6.5 Others

Ascencio et al. (2006) obtained small metallic nanoparticles of neodymium via biosynthesis. They could obtain particles of 1−8 nm depending on pH conditions. It was also revealed that smaller clusters were obtained at pH 5, but nanorods were formed at pH 10. Yu et al. (2006) synthesized water-soluble CdSe-ZnS (core-shell) QDs. The g-aminobutyric acid (GABA), an inhibitory transmitter in the central nervous system of mammals, was then bioconjugated to these QDs in the presence of N-hydroxysuccinimide (NHS) and 1-ethyl-3-(3)-dimethylaminopropyl carbodiimide (EDC) to make a fluorescence probe. They could detect GABA binding sites on protoplast membrane of both pollen as well as somatic cells using.

One-pot synthesis of neoglycoconjugates with a reactive thiol group was reported by Babu et al. (2007). Their functionalization with carbohydrates can provide high solubility and stabilization of CdSe − ZnS quantum dots. They used melibiose, lactose, and maltotriose to obtain three different sizes of quantum dots. These sugar-QDs were found to be very selective in the detection of lictin. Huilan et al. (2008) developed a bioinspired technique to synthesize hybrid nanocomposites. It consisted of well-dispersed CdS quantum dots on silk fibroin fibers (SFF). It was observed that biomaterial SFF acts as both a supporting substrate and functional sites for in situ generation of CdSQD. As-prepared CdSQDs/SFF nanocomposites can be used as novel luminescent, photoelectron transfer devices and in photocatalysis.

Manzoor et al. (2009) reported the synthesis of luminescent quantum dots, which were conjugated with a cancer-targeting ligand, folic acid (FA). Doped QDs were prepared by a simple aqueous method at room temperature. It was observed that these QDs are monodispersed with an average size ∼4 nm. The dopants selected were Al^{3+}, Cu^{2+}, Mn^{2+}, and F^{-} and color tunability could be achieved ranging from blue (480 nm) to red (622 nm). It was claimed that nontoxic, Hg-, Pb-, Cd-, Te-, and Se-free luminescent QDs can be used for targeted cancer imaging.

Dong et al. (2009) used l-glutathione (GSH) as a stabilizer for the preparation of CdTe quantum dots in aqueous solution. It was reported that as-prepared QDs were linked to prostate-specific antigen (PSA) for indirect labeling of fixed prostate cancer cells. It was indicated that as-prepared QD-based probes were fluorescent markers and exhibited excellent photostability and spectral properties. These were found to be much better than organic dyes in target detection. It was also suggested that the l-glutathione capped

CdTe had low cytotoxicity as these QDs did not show a detectable effect on cell growth after culturing for three days.

Stürzenbaum et al. (2013) showed that an earthworm's metal detoxification pathway can be used to produce cadmium telluride (CdTe) quantum dots. It was observed that these QDs are water soluble and luminescent in green region. They exposed standard wild-type *Lumbricus rubellus* earthworms to soil that was spiked with cadmium chloride and Na_2TeO_3 salts for 11 days. They isolated luminescent quantum dots from chloragogenous tissues surrounding the gut of the earthworm and used them in live-cell imaging.

Tan et al. (2013) reported that near-infrared fluorescent silver sulfide quantum dots can be synthesized in hepatoma carcinoma cells (HepG2) cancer cells, which is intracellular synthesis. Silver sulfide quantum dots were synthesized by delivering quantum dot precursors into cultured HepG2 cells and these can be used for cell imaging. Zhang et al. (2020) developed CdSe/CdS QDs and used these as a fluorescence sensor for Hg^{2+} detection with high sensitivity in the range of 0.25−100 nM with a limit of detection of 0.01 nM. The as-fabricated sensor exhibited a high selectivity for Hg^{2+} detection of mercuric ion even in the presence of other metal ions and it gave satisfactory results in the case of some samples such as tap water, river water, and landfill.

6.6 Conclusion

Various chemical and physical methods for the synthesis of quantum dots have their own demerits. The majority of them are not green in nature. Biosynthesis methods have certain advantages, such as they are clean, nontoxic, and eco-friendly in nature. In this technique, no hazardous chemicals or reagents are required and harsh conditions are avoided. It is interesting that several nanoparticles (quantum dots) can be easily biosynthesized, which is sometimes not possible by the conventional chemical synthesis. The field of biogenic synthesis is a fairly new and exciting area of research and it has a great potential for further development.

References

Abou-Assy, R.S., El-Deeb, B.A., Al-Talhi, A.D., Mostafa, N.Y., 2019. Biosynthesis of cadmium selenide quantum dots by *Providencia vermicola*. Afr. J. Microbiol. Res. 13 (6), 106−121.

Ahmad, A., Senapati, S., Khan, M.I., Kumar, R., Sastry, M., 2005. Extra-/intracellular biosynthesis of gold nanoparticles by an alkalotolerant fungus, *Trichothecium* sp. J. Biomed. Nanotechnol. 1 (1), 47−53.

Al-Shalabi, Z., Doran, P.M., 2016. Biosynthesis of fluorescent CdS nanocrystals with semiconductor properties: comparison of microbial and plant production systems. J. Biotechnol. 223, 13−23.

Alvand, Z.M., Rajabi, H.R., Mirzaei, A., Masoumiasl, A., Sadatfaraji, H., 2019. Rapid and green synthesis of cadmium telluride quantum dots with low toxicity based on a plant-mediated approach after microwave and ultrasonic assisted extraction: synthesis, characterization, biological potentials and comparison study. Mater. Sci. Eng.: C 98, 535–544.

Anthony, A.M., Murugan, R., Subramanian, R., Selvarangan, G.K., Pandurangan, P., Dhanasekaran, A., et al., 2020. Ultra-radiant photoluminescence of glutathione rigidified reduced carbon quantum dots (r-CQDs) derived from ice-biryani for in vitro and in vivo bioimaging applications. Colloids Surf. A: Physicochem. Eng. Asp. 586. Available from: https://doi.org/10.1016/j.colsurfa.2019.124266.

Ascencio, J.A., Canizal, G., Medina-Flores, A., Bejar, L., Tavera, L., Matamoros, H., et al., 2006. Neodymium nanoparticles: biosynthesis and structural analysis. J. Nanosci. Nanotechnol. 6 (4), 1044–1049.

Ashengroph, M., Khaledi, A., Bolbanabad, E.M., 2020. Extracellular biosynthesis of cadmium sulphide quantum dot using cell-free extract of *Pseudomonas chlororaphis* CHR05 and its antibacterial activity. Process. Biochem. 89, 63–70.

Babu, P., Sinha, S., Surolia, A., 2007. Sugar–quantum dot conjugates for a selective and sensitive detection of lectins. Bioconjug. Chem. 18 (1), 146–151.

Bai, H.J., Zhang, Z.M., Guo, Y., Yang, G.E., 2009. Biosynthesis of cadmium sulfide nanoparticles by photosynthetic bacteria *Rhodopseudomonas palustris*. Colloids Surf. B: Biointerf. 70 (1), 142–146.

Bao, H., Hao, N., Yang, Y., Zhao, D., 2010a. Biosynthesis of biocompatible cadmium telluride quantum dots using yeast cells. Nano Res. 3 (7), 481–489.

Bao, H., Lu, Z., Cui, X., Qiao, Y., Guo, J., Anderson, J.M., et al., 2010b. Extracellular microbial synthesis of biocompatible CdTe quantum dots. Acta Biomater. 6 (9), 3534–3541.

Begum, S., Ahmaruzzaman, M., 2018. Green synthesis of SnO2 quantum dots using Parkia speciosa Hassk pods extract for the evaluation of anti-oxidant and photocatalytic properties. J. Photochem. Photobiol. B: Biol. 184, 44–53.

Bhattacharjee, A., Ahmaruzzaman, M., 2015. Photocatalytic-degradation and reduction of organic compounds using SnO2 quantum dots (via a green route) under direct sunlight. RSC Adv. 5 (81), 66122–66133.

Borovaya, M.N., Naumenko, A.P., Matvieieva, N.A., Blume, Y.B., Yemets, A.I., 2014. Biosynthesis of luminescent CdS quantum dots using plant hairy root culture. Nanoscale Res. Lett. 9 (1). Available from: https://doi.org/10.1186/1556-276X-9-686.

Borovaya, M., Pirko, Y., Krupodorova, T., Naumenko, A., Blume, Y., Yemets, A., 2015. Biosynthesis of cadmium sulphide quantum dots by using *Pleurotus ostreatus* (Jacq.) P. Kumm. Biotechnol. Biotechnol. Equip. 29 (6), 1156–1163.

Borovaya, M.N., Burlaka, O.M., Naumenko, A.P., Blume, Y.B., Yemets, A.I., 2016. Extracellular synthesis of luminescent CdS quantum dots using plant cell culture. Nanoscale Res. Lett. 11 (1). Available from: https://doi.org/10.1186/s11671-016-1314-z.

Brooks, J., Lefebvre, D.D., 2017. Optimization of conditions for cadmium selenide quantum dot biosynthesis in *Saccharomyces cerevisiae*. Appl. Microbiol. Biotechnol. 101 (7), 2735–2745.

Bruna, N., Collao, B., Tello, A., Caravantes, P., Díaz-Silva, N., Monrás, J.P., et al., 2019. Synthesis of salt-stable fluorescent nanoparticles (quantum dots) by polyextremophile halophilic bacteria. Sci. Rep. 9 (1). Available from: https://doi.org/10.1038/s41598-018-38330-8.

Cao, K., Chen, M.M., Chang, F.Y., Cheng, Y.Y., Tian, L.J., Li, F., et al., 2020. The biosynthesis of cadmium selenide quantum dots by *Rhodotorula mucilaginosa* PA-1 for photocatalysis. Biochem. Eng. J. 156. Available from: https://doi.org/10.1016/j.bej.2020.107497.

Carrasco, V., Amarelle, V., Lagos-Moraga, S., Quezada, C.P., Espinoza-González, R., Faccio, R., et al., 2021. Production of cadmium sulfide quantum dots by the lithobiontic Antarctic strain *Pedobacter* sp. UYP1 and their application as photosensitizer in solar cells. Microb. Cell Factories 20 (1). Available from: https://doi.org/10.1186/s12934-021-01531-4.

Chen, G., Yi, B., Zeng, G., Niu, Q., Yan, M., Chen, A., et al., 2014. Facile green extracellular biosynthesis of CdS quantum dots by white rot fungus *Phanerochaete chrysosporium*. Colloids Surf. B: Biointerfaces 117, 199–205.

Cui, R., Liu, H.H., Xie, H.Y., Zhang, Z.L., Yang, Y.R., Pang, D.W., et al., 2009. Living yeast cells as a controllable biosynthesizer for fluorescent quantum dots. Adv. Funct. Mater. 19 (15), 2359–2364.

Das, J., Dhar, S.S., 2020. Synthesis of SnO2 quantum dots mediated by *Camellia sinensis* shoots for degradation of thiamethoxam. Toxicol. Environ. Chem. 102 (1–4), 186–196.

Dong, W., Guo, L., Wang, M., Xu, S., 2009. CdTe QDs-based prostate-specific antigen probe for human prostate cancer cell imaging. J. Lumin. 129 (9), 926–930.

Fatimah, I., Sahroni, I., Muraza, O., Doong, R.A., 2020. One-pot biosynthesis of SnO2 quantum dots mediated by Clitoriaternatea flower extract for photocatalytic degradation of rhodamine B. J. Environ. Chem. Eng. 8 (4). Available from: https://doi.org/10.1016/j.jece.2020.103879.

Fellowes, J.W., Pattrick, R.A.D., Lloyd, J.R., Charnock, J.M., Coker, V.S., Mosselmans, J.F.W., et al., 2013. Ex situ formation of metal selenide quantum dots using bacterially derived selenide precursors. Nanotechnology 24 (14). Available from: https://doi.org/10.1088/0957-4484/24/14/145603.

Gallardo, C., Monrás, J.P., Plaza, D.O., Collao, B., Saona, L.A., Durán-Toro, V., et al., 2014. Low-temperature biosynthesis of fluorescent semiconductor nanoparticles (CdS) by oxidative stress resistant Antarctic bacteria. J. Biotechnol. 187, 108–115.

Gallardo-Benavente, C., Carrión, O., Todd, J.D., Pieretti, J.C., Seabra, A.B., Durán, N., et al., 2019. Biosynthesis of CdS quantum dots mediated by volatile sulfur compounds released by Antarctic *Pseudomonas fragi*. Front. Microbiol. 10. Available from: https://doi.org/10.3389/fmicb.2019.01866.

Gholami, Z., Dadmehr, M., Jelodar, N.B., Hosseini, M., Parizi, A.P., 2020. One-pot biosynthesis of CdS quantum dots through in vitro regeneration of hairy roots of *Rhaphanus sativus* L. and their apoptosis effect on MCF-7 and AGS cancerous human cell lines. Mater. Res. Express 7 (1). Available from: https://doi.org/10.1088/2053-1591/ab66ea.

Green, M., Haigh, S.J., Lewis, E.A., Sandiford, L., Burkitt-Gray, M., Fleck, R., et al., 2016. The biosynthesis of infrared-emitting quantum dots in allium fistulosum. Sci. Rep. 6 (1). Available from: https://doi.org/10.1038/srep20480.

Huang, H., He, M., Wang, W., Liu, J., Mi, C., Xu, S., 2012. Biosynthesis of CdS quantum dots in *Saccharomyces cerevisiae* and spectroscopic characterization. Spectrosc. Spectr. Anal. 32 (4), 1090–1093.

Huilan, S., Jie, H., Qun, D., Di, Z., Qixin, G., 2008. In situ synthesis and photoluminescence of QD-CdS on silk fibroin fibers at room temperature. Nanotechnology (Print.) 19. Available from: https://doi.org/10.1088/0957-4484/19/02/025601.

Jacob, J.M., Sharma, S., Balakrishnan, R.M., 2017. Exploring the fungal protein cadre in the biosynthesis of PbSe quantum dots. J. Hazard. Mater. 324, 54–61.

Jacob, J.M., Rajan, R., Tom, T.C., Kumar, V.S., Kurup, G.G., Shanmuganathan, R., et al., 2019a. Biogenic design of ZnS quantum dots-insights into their in-vitro cytotoxicity, photocatalysis and biosensing properties. Ceram. Int. 45 (18), 24193–24201.

Jacob, J.M., Rajan, R., Aji, M., Kurup, G.G., Pugazhendhi, A., 2019b. Bio-inspired ZnS quantum dots as efficient photo catalysts for the degradation of methylene blue in aqueous phase. Ceram. Int. 45 (4), 4857–4862.

Jacob, J.M., Sinharoy, A., Lens, P.N., 2020. Photocatalytic degradation of congo red by zinc sulfide quantum dots produced by anaerobic granular sludge. Environ. Technol. 41. Available from: https://doi.org/10.1080/09593330.2020.1856940.

Jiang, R., Zhu, H., Yao, J., Fu, Y., Guan, Y., 2012. Chitosan hydrogel films as a template for mild biosynthesis of CdS quantum dots with highly efficient photocatalytic activity. Appl. Surf. Sci. 258 (8), 3513–3518.

Kandasamy, K., Venkatesh, M., Khadar, Y.S., Rajasingh, P., 2020. One-pot green synthesis of CdS quantum dots using *Opuntia ficus*-indica fruit sap. Mater. Today: Proc. 26, 3503–3506.

Kaviya, S., Kabila, S., Jayasree, K.V., 2017. Room temperature biosynthesis of greatly stable fluorescent ZnO quantum dots for the selective detection of Cr3 + ions. Mater. Res. Bullet. 95, 163–168.

Kominkova, M., Michalek, P., Moulick, A., Nemcova, B., Zitka, O., Kopel, P., et al., 2014. Biosynthesis of quantum dots (CdTe) and its effect on *Eisenia fetida* and *Escherichia coli*. Chromatographia 77 (21), 1441–1449.

Kominkova, M., Milosavljevic, V., Vitek, P., Polanska, H., Cihalova, K., Dostalova, S., et al., 2017. Comparative study on toxicity of extracellularly biosynthesized and laboratory synthesized CdTe quantum dots. J. Biotechnol. 241, 193–200.

Kumar, S.A., Ansary, A.A., Ahmad, A., Khan, M.I., 2007. Extracellular biosynthesis of CdSe quantum dots by the fungus, *Fusarium oxysporum*. J. Biomed. Nanotechnol. 3, 190–194.

Kumar, S., Taneja, S., Banyal, S., Singhal, M., Kumar, V., Sahare, S., et al., 2021. Biosynthesised silver nanoparticle-conjugated l-cysteine ceiled Mn: ZnS quantum dots for eco-friendly biosensor and antimicrobial applications. J. Electron. Mater. 50 (7), 3986–3995.

Li, Y., Cui, R., Zhang, P., Chen, B.B., Tian, Z.Q., Li, L., et al., 2013. Mechanism-oriented controllability of intracellular quantum dots formation: the role of glutathione metabolic pathway. ACS Nano 7 (3), 2240–2248.

Liu, J., Zheng, D., Zhong, L., Gong, A., Wu, S., Xie, Z., 2021. Biosynthesis of biocompatibility Ag_2Se quantum dots in Saccharomyces cerevisiae and its application. Biochem. Biophys. Res. Commun. 544, 60–64.

Manzoor, K., Johny, S., Thomas, D., Setua, S., Menon, D., Nair, S., 2009. Bio-conjugated luminescent quantum dots of doped ZnS: a cyto-friendly system for targeted cancer imaging. Nanotechnology 20 (6). Available from: https://doi.org/10.1088/0957-4484/20/6/065102.

Mareeswari, P., Brijitta, J., Etti, S.H., Meganathan, C., Kaliaraj, G.S., 2016. Rhizopus stolonifer mediated biosynthesis of biocompatible cadmium chalcogenide quantum dots. Enzyme Microb. Technol. 95, 225–229.

Mi, C., Wang, Y., Zhang, J., Huang, H., Xu, L., Wang, S., et al., 2011. Biosynthesis and characterization of CdS quantum dots in genetically engineered *Escherichia coli*. J. Biotechnol. 153 (3–4), 125–132.

Öcal, N., Ceylan, A., Duman, F., 2020. Intracellular biosynthesis of PbS quantum dots using Pseudomonas aeruginosa ATCC 27853: evaluation of antibacterial effects and DNA cleavage activities. World J. Microbiol. Biotechnol. 36 (10). Available from: https://doi.org/10.1007/s11274-020-02917-z.

Órdenes-Aenishanslins, N., Anziani-Ostuni, G., Monrás, J.P., Tello, A., Bravo, D., Toro-Ascuy, D., et al., 2020. Bacterial synthesis of ternary CdSAg quantum dots through cation exchange: tuning the composition and properties of biological nanoparticles for bioimaging

and photovoltaic applications. Microorganisms 8 (5). Available from: https://doi.org/10.3390/microorganisms8050631.

Ouyang, W., Sun, J., 2016. Biosynthesis of silver sulfide quantum dots in wheat endosperm cells. Mater. Lett. 164, 397–400.

Pugazhenthiran, N., Murugesan, S., Muneeswaran, T., Suresh, S., Kandasamy, M., Valdés, H., et al., 2021. Biocidal activity of citrus limetta peel extract mediated green synthesized silver quantum dots against MCF-7 cancer cells and pathogenic bacteria. J. Environ. Chem. Eng. 9 (2). Available from: https://doi.org/10.1016/j.jece.2021.105089.

Qi, S., Zhang, M., Guo, X., Yue, L., Wang, J., Shao, Z., et al., 2017. Controlled extracellular biosynthesis of ZnS quantum dots by sulphate reduction bacteria in the presence of hydroxypropyl starch as a mediator. J. Nanopart. Res. 19 (6), 1–13. Available from: https://doi.org/10.1007/s11051-017-3899-2.

Qi, S., Yang, S., Chen, J., Niu, T., Yang, Y., Xin, B., 2019. High-yield extracellular biosynthesis of ZnS quantum dots through a unique molecular mediation mechanism by the peculiar extracellular proteins secreted by a mixed sulfate reducing bacteria. ACS Appl. Mater. Interfaces 11 (11), 10442–10451.

Qi, S., Miao, Y., Chen, J., Chu, H., Tian, B., Wu, B., et al., 2021a. Controlled biosynthesis of ZnCdS quantum dots with visible-light-driven photocatalytic hydrogen production activity. Nanomaterials 11 (6). Available from: https://doi.org/10.3390/nano11061357.

Qi, S., Chen, J., Bai, X., Miao, Y., Yang, S., Qian, C., et al., 2021b. Quick extracellular biosynthesis of low-cadmium ZnxCd1 − xS quantum dots with full-visible-region tuneable high fluorescence and its application potential assessment in cell imaging. RSC Adv. 11 (35), 21813–21823.

Qin, Z., Yue, Q., Liang, Y., Zhang, J., Zhou, L., Hidalgo, O.B., et al., 2018. Extracellular biosynthesis of biocompatible cadmium sulfide quantum dots using *Trametes versicolor*. J. Biotechnol. 284, 52–56.

Raja, D., Sundaramurthy, D., 2021. Facile synthesis of fluorescent carbon quantum dots from Betel leafs (Piper betle) for Fe3 + sensing. Mater. Today: Proc. 34, 488–492.

Rani, H., Singh, S.P., Yadav, T.P., Khan, M.S., Ansari, M.I., Singh, A.K., 2020. In-vitro catalytic, antimicrobial and antioxidant activities of bioengineered copper quantum dots using *Mangifera indica* (L.) leaf extract. Mater. Chem. Phys. 239. Available from: https://doi.org/10.1016/j.matchemphys.2019.122052.

Rosano-Ortega, G., Schabes-Retchkiman, P., Zorrilla, C., Liu, H.B., Canizal, G., Avila-Pérez, P., et al., 2006. Synthesis and characterization of Mn quantum dots by bioreduction with water hyacinth. J. Nanosci. Nanotechnol. 6 (1), 151–156.

Saa, L., Virel, A., Sanchez-Lopez, J., Pavlov, V., 2010. Analytical applications of enzymatic growth of quantum dots. Chem.–A Eur. J. 16 (21), 6187–6192.

Sandoval-Cárdenas, I., Gómez-Ramírez, M., Rojas-Avelizapa, N.G., 2017. Use of a sulfur waste for biosynthesis of cadmium sulfide quantum dots with *Fusarium oxysporum* f. sp. lycopersici. Mater. Sci. Semicond. Process. 63, 33–39.

Shao, M., Zhang, R., Wang, C., Hu, B., Pang, D., Xie, Z., 2018. Living cell synthesis of CdSe quantum dots: manipulation based on the transformation mechanism of intracellular Se-precursors. Nano Res. 11 (5), 2498–2511.

Shi, C., Qi, H., Ma, R., Sun, Z., Xiao, L., Wei, G., et al., 2019. N, S-self-doped carbon quantum dots from fungus fibers for sensing tetracyclines and for bioimaging cancer cells. Mater. Sci. Eng. C. 105. Available from: https://doi.org/10.1016/j.msec.2019.110132.

Shivaji, K., Mani, S., Ponmurugan, P., De Castro, C.S., Lloyd Davies, M., Balasubramanian, M. G., et al., 2018. Green-synthesis-derived CdS quantum dots using tea leaf extract:

antimicrobial, bioimaging, and therapeutic applications in lung cancer cells. ACS Appl. Nano Mater. 1 (4), 1683–1693.

Silva, A., Martínez-Gallegos, S., Rosano-Ortega, G., Schabes-Retchkiman, P., Vega-Lebrún, C., Albiter, V., 2017. Nanotoxicity for *E. Coli* and characterization of silver quantum dots produced by biosynthesis with *Eichhornia crassipes*. J. Nanostruct. 7 (1). Available from: https://doi.org/10.22052/JNS.2017.01.001.

Stürzenbaum, S.R., Höckner, M., Panneerselvam, A., Levitt, J., Bouillard, J.S., Taniguchi, S., et al., 2013. Biosynthesis of luminescent quantum dots in an earthworm. Nat. Nanotechnol. 8 (1), 57–60.

Suresh, A.K., Doktycz, M.J., Wang, W., Moon, J.W., Gu, B., Meyer III, H.M., et al., 2011. Monodispersed biocompatible silver sulfide nanoparticles: facile extracellular biosynthesis using the γ-proteobacterium, *Shewanellaoneidensis*. Acta Biomater. 7 (12), 4253–4258.

Syed, A., Ahmad, A., 2013. Extracellular biosynthesis of CdTe quantum dots by the fungus *Fusarium oxysporum* and their anti-bacterial activity. Spectrochim. Acta Part. A: Mol. Biomol, Spectrosc. 106, 41–47.

Tan, L., Wan, A., Li, H., 2013. Synthesis of near-infrared quantum dots in cultured cancer cells. ACS Appl. Mater. Interf. 6 (1), 18–23.

Tian, L.J., Zhou, N.Q., Liu, X.W., Liu, J.H., Zhang, X., Huang, H., et al., 2017. A sustainable biogenic route to synthesize quantum dots with tunable fluorescence properties for live cell imaging. Biochem. Eng. J. 124, 130–137.

Tian, L.J., Min, Y., Li, W.W., Chen, J.J., Zhou, N.Q., Zhu, T.T., et al., 2019. Substrate metabolism-driven assembly of high-quality CdSxSe1−x quantum dots in *Escherichia coli*: molecular mechanisms and bioimaging application. ACS Nano 13 (5), 5841–5851.

Tudu, S.C., Zubko, M., Kusz, J., Bhattacharjee, A., 2021. Structural, optical and dielectric studies of wurtzite-type CdS quantum dots green synthesised using *Ocimum sanctum* (Tulsi) leaf extract. Adv. Nat. Sci.: Nanosci. Nanotechnol. 12 (3). Available from: https://doi.org/10.1088/2043-6262/ac2732.

Uddandarao, P., 2016. ZnS semiconductor quantum dots production by an endophytic fungus *Aspergillus flavus*. Mater. Sci. Eng. B 207, 26–32.

Ulloa, G., Collao, B., Araneda, M., Escobar, B., Álvarez, S., Bravo, D., et al., 2016. Use of acidophilic bacteria of the genus Acidithiobacillus to biosynthesize CdS fluorescent nanoparticles (quantum dots) with high tolerance to acidic pH. Enzyme Microb. Technol. 95, 217–224.

Ulloa, G., Quezada, C.P., Araneda, M., Escobar, B., Fuentes, E., Álvarez, S.A., et al., 2018. Phosphate favors the biosynthesis of CdS quantum dots in *Acidithiobacillus thiooxidans* ATCC 19703 by improving metal uptake and tolerance. Front. Microbiol. 9. Available from: https://doi.org/10.3389/fmicb.2018.00234.

Wang, X., Du, Y., Ding, S., Fan, L., Shi, X., Wang, Q., et al., 2005. Large two-photon absorbance of chitosan–ZnS quantum dots nanocomposite film. Phys. E: Low-Dimens. Syst. Nanostruct. 30 (1–2), 96–100.

Wang, X., Li, Y., Du, Y., 2009. Novel water-soluble chitosan derivatives/quantum dots nanocomposite: synthesis, characterization and photoluminescence properties. J. Nanosci. Nanotechnol. 9 (12), 6866–6875.

Wang, L., Zhang, Z. L., Cui, R., Liu, H. H., Li, J., Liu, S. L., et al., 2010. Dynamic tracking of single cell synthesis of cdse quantum dots with a microflufidic device. In: Proceedings of the Fourteenth International Conference on Miniaturized Systems for Chemistry and Life Sciences, pp. 1868–1870.

Wu, S.M., Su, Y., Liang, R.R., Ai, X.X., Qian, J., Wang, C., et al., 2015. Crucial factors in biosynthesis of fluorescent CdSe quantum dots in *Saccharomyces cerevisiae*. RSC Adv. 5 (96), 79184–79191.

Xu, X., Yang, Y., Jin, H., Pang, B., Yang, R., Yan, L., et al., 2020. Fungal in situ assembly gives novel properties to CdSxSe1−x quantum dots for sensitive label-free detection of chloramphenicol. ACS Sustain. Chem. Eng. 8 (17), 6806–6814.

Xu, L.X., Wang, Y.Z., Zhou, D., Chen, M.Y., Yang, X.J., Ye, X.M., et al., 2021a. Bio-metabolism-driven crystalline-engineering of CdS quantum dots for highly active photocatalytic H2 evolution. ChemistrySelect 6 (15), 3702–3706.

Xu, X., Yang, Y., Jin, H., Pang, B., Jiang, C., Shao, D., et al., 2021b. Filamentous fungal in situ biosynthesis of heterogeneous Au/Cd0.5Zn0.5S nano-photocatalyst: a macroscopic assembly strategy for preparing composite mycelial pellets with visible light degradation ability. J. Hazard. Mater. 406. Available from: https://doi.org/10.1016/j.jhazmat.2020.124797.

Yamaguchi, T., Tsuruda, Y., Furukawa, T., Negishi, L., Imura, Y., Sakuda, S., et al., 2016. Synthesis of CdSe quantum dots using *Fusarium oxysporum*. Mater 9 (10). Available from: https://doi.org/10.3390/ma9100855.

Yan, Z., Qian, J., Gu, Y., Su, Y., Ai, X., Wu, S., 2014. Green biosynthesis of biocompatible CdSe quantum dots in living *Escherichia coli* cells. Mater. Res. Express 1 (1). Available from: https://doi.org/10.1088/2053-1591/1/1/015401.

Yan, Z.Y., Ai, X.X., Su, Y.L., Liu, X.Y., Shan, X.H., Wu, S.M., 2016. Intracellular biosynthesis of fluorescent CdSe quantum dots in *Bacillus subtilis*: a strategy to construct signaling bacterial probes for visually detecting interaction between *Bacillus subtilis* and *Staphylococcus aureus*. Microsc. Microanal. 22 (1), 13–21.

Yan, Z.Y., Du, Q.Q., Qian, J., Wan, D.Y., Wu, S.M., 2017. Eco-friendly intracellular biosynthesis of CdS quantum dots without changing *Escherichia coli*'s antibiotic resistance. Enzyme Microb. Technol. 96, 96–102.

Yan, Z.Y., Yao, C.X., Wan, D.Y., Wang, L.L., Du, Q.Q., Li, Z.Q., et al., 2018. A sensitive and simple method for detecting Cu2 + in plasma using fluorescent *Bacillus amyloliquefaciens* containing intracellularly biosynthesized CdSe quantum dots. Enzyme Microb. Technol. 119, 37–44.

Yang, Z., Lu, L., Berard, V.F., He, Q., Kiely, C.J., Berger, B.W., et al., 2015. Biomanufacturing of CdS quantum dots. Green. Chem. 17 (7), 3775–3782.

Yang, Z., Wang, Y., Zhang, D., 2018. A novel signal-on photoelectrochemical sensing platform based on biosynthesis of CdS quantum dots sensitizing ZnO nanorod arrays. Sens. Actuators B: Chem. 261, 515–521.

Yu, G., Liang, J., He, Z., Sun, M., 2006. Quantum dot-mediated detection of γ-aminobutyric acid binding sites on the surface of living pollen protoplasts in tobacco. Chem. Biol. 13 (7), 723–731.

Yue, L., Qi, S., Wang, J., Cai, J., Xin, B., 2016. Controllable biosynthesis and characterization of α-ZnS and β-ZnS quantum dots: comparing their optical properties. Mater. Sci. Semicond. Process. 56, 115–118.

Zaman, M.B., Poolla, R., Singh, P., Gudipati, T., 2020. Biogenic synthesis of CuO nanoparticles using *Tamarindus indica* L. and a study of their photocatalytic and antibacterial activity. Environ. Nanotechnol. Monitor. Manage. 14. Available from: https://doi.org/10.1016/j.enmm.2020.100346.

Zhang, Y., Xiao, J.Y., Zhu, Y., Tian, L.J., Wang, W.K., Zhu, T.T., et al., 2020. Fluorescence sensor based on biosynthetic CdSe/CdS quantum dots and liposome carrier signal amplification for mercury detection. Anal. Chem. 92 (5), 3990–3997.

Chapter 7

Microwave-assisted synthesis of quantum dots

Chetna Ameta, Yogeshwari Vyas, Priyanka Chundawat and Dharmendra
Department of Chemistry, M. L. S. University Udaipur, Rajasthan, India

7.1 Introduction

Quantum dot (QD) materials have huge potential for the expansion of novel analytical approaches because of their tiny nanosizes, typically <10 nm for various specific applications (Kumar et al., 2018). Over the last few decades, QDs of different materials have attracted increasing attention in various research fields, for example, as fluorescent biological labels, solar cells, and optoelectronic transistor components, as they have unique size-tunable electronic and optical properties (Kim and Yoon, 2014). Carbon-based QDs, for example, graphene QDs (GQDs), carbon QDs (CQDs), and several types of semiconducting QDs have potential in planning and tuning fluorescent probes (Lim et al., 2015). The zero-dimensional (0D) GQDs generated using top-down methods like electrochemical synthesis, chemical ablation from graphene, oxygen plasma treatment, etc. display a dynamic area of superior interest (Wang et al., 2015a,b). The semiconducting QDs, particularly cadmium telluride (CdTe), cadmium selenide (CdSe), and cadmium sulfide (CdS), have been investigated extensively due to their fluorescent properties in the near-infrared, infrared, and observable spectra (Rodrigues et al., 2017). Lee et al. (2004) reported the production and analysis of size-sensitive and outstanding selective QD structures. Several methods have been employed for synthesizing QD structures using various chemicals; although other synthesis techniques are time-consuming and require costly equipment. Consequently, there is a necessity for a quick, sensitive, simple, and selective process for large-scale production of all types of QDs.

Research is focused on precise experiments for less time-consuming, facile, and fast synthetic methods without losing any heat into the surroundings. Microwave (MW)-aided synthesis provides a facile and fast approach, since it has an alternate energy source and it is exploited widely due to its power of control on volumetric and inner heating of constituents (Agranovich et al., 2017).

Quantum Dots. DOI: https://doi.org/10.1016/B978-0-12-824153-0.00007-0

Recently, more attraction has been paid to MW-assisted generation of inorganic/organic nanostructured materials in different media (gaseous and liquid) and future studies are significant. MWs are largely employed in the synthesis of QD materials, since the interaction is strong with MW rays generating uniform heating and higher heating rates. Thus MW synthesis of metal oxides supported on graphene sheets (Kumar et al., 2014), metal oxide NPs (nanoparticles), and nanostructured carbon materials (Zhang and Liu, 2012) has been studied. Apart from (3D) carbon hybrid metal such as oxide-held graphene and CNTs, activated carbons and carbon nanocapsules were also synthesized (Hu et al., 2012). The MW-assisted path is a quite promising, clean, economic, and low-temperature synthetic route with huge potential. One of the ultimate and notable advantages is that it yields a specific shape and size of QD that depends on the experimental parameters. These MW-assisted synthesized QDs are useful for current and developing technologies and may play a noteworthy role in numerous research areas.

The basic use of MW technology is in the field of transmission of energy or telecommunication by electromagnetic waves. MWs are electromagnetic radiation, ranging between infrared radiation and radiofrequencies. These have frequencies between 300 GHz (1 mm) and 0.3 GHz (1 m). The irradiation technique for rapid heating is based on the principle that materials absorb electromagnetic energy and convert it into heat. The electromagnetic energy transferred from MWs to the irradiated material is believed to occur either through relaxation or resonance. Only contracted frequency windows located at 0.915 and 2.54 GHz are appropriate for MW heating purposes. The MW entails coordinated perpendicular oscillations of magnetic and electric fields. These MW rays are absorbed by materials causing heating, which is known as dielectric heating. This heating is not the same as in the case of conventional form of heating, since energy is transferred in the form of radiation at the surface in MW heating, whereas thermal energy is transported to the material's bulk through conduction.

MW heating is a quick and simple process which is why it is widely employed nowadays in academia and industries for the synthesis of several kinds of QDs. This process results in speedy and even heating (volumetric). Thus, MW is an essential tool in all branches of green synthesis approaches since the time of its origin (Giguere et al., 1986). A wide range of QDs can be synthesized for industrial uses by putting extra efforts into MW-aided synthesis.

7.1.1 Advantages

The MW-assisted production of QDs has numerous advantages compared to conventional routes. The major benefit is the molecular interaction of reagents with an electromagnetic field without direct contact. This method is safe, eco-friendly, with energy proficiency and selectivity, and provides high

yield in a shorter time. All such advantages of MW-assisted synthesis are shown in Fig. 7.1.

7.1.2 Disadvantages

Apart from the many advantages of MW-assisted synthesis, there are some disadvantages or limitations associated with its use in organic synthesis.

1. There is lesser penetration depth in some cases.
2. Metallic substrates or metallic reagents cannot be used for synthesis.
3. Only polar solvents are used, which can interact with the MW.
4. Heating reactions above boiling point of the solvent can generate high pressure, which may cause an explosion.
5. In some cases, the yields are not reproducible because of uneven heating, particularly while using a domestic MW oven.

7.2 Synthesis of core-type quantum dots

Core-type QDs are made up of a single material, basically a metallic chalcogenide like CdTe, CdS, CdSe, PbS, SnO_2, etc. The existing oil-bath heating techniques transfer heat internally from the source (heat), while radiowaves in MW-mediated heating exactly pierce the wall of the vessel to excite polar units like alcohol, water, and fatty acids. Polar molecules absorb this radiation and transform it directly into nuclear motion to convert it into heat. The complete procedure is different from ordinary oil-bath heating since the heat is generated via a native domain by exciting molecules/atoms rather than

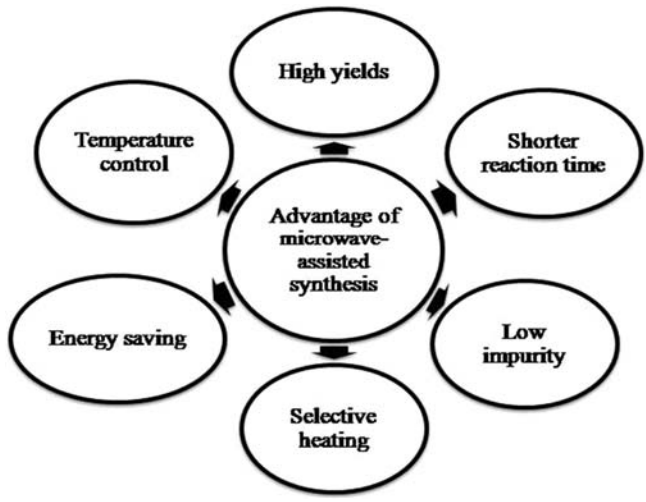

FIGURE 7.1 Advantages of microwave-assisted synthesis.

conduction. Hence, there is no need to drift heat internally by conduction, since all particles are excited simultaneously in the MW field. The use of MW heating in accelerating chemical reactions has fascinated the scientific world extensively in the last few decades. The reducing time of the reaction is not only its merit but it has improved controllability, allowed larger production yields, greener reactions, and reproducibility.

7.2.1 Oxide quantum dots

7.2.1.1 SnO_2 quantum dots

Semiconductor QDs such as tin oxide are attractive materials because of their unique physical and optical properties (Han et al., 2010; Bajorowicz et al., 2018). Tin oxide (SnO_2) has a broad bandgap of 3.6 eV at room temperature. It is a pure n-type semiconductor oxide and it has been widely used in gas sensors, dye-sensitized solar cells (DSSCs), photocatalysts, lithium-ion batteries, and transparent electrodes (Shi and Lin, 2010; Wang et al., 2011a; Wang et al., 2012; Song et al., 2013). Various methods are available for the production of tin oxide such as wet chemical method, laser ablation routes, and MW irradiation technique (Pang et al., 2001; Xiao et al., 2010; Wang et al., 2012, Singh et al., 2012). But most of them require the use of toxic poisonous compounds, critical reaction conditions, and long periods of time. Therefore, there is a challenge for the synthesis of SnO_2 QDs in a fast facile, greener way on an industrial scale. Among several approaches, MW heating has several advantages including better control over the size, lesser reaction time, and even nucleation of precipitates in suspension. Several research teams have utilized MW technique for synthesizing SnO_2 QDs (Xiao et al., 2010; Liu et al., 2013; Bhattacharjee and Ahmaruzzaman, 2015; Begum et al., 2016; Zhu et al., 2016).

Liu et al. (2013) fabricated SnO_2 QDs using MW-irradiation in 10 min. at 150°C with (150 W). These QDs were then used for photocatalytic degradation of methylene blue. The $SnCl_4$ was used as a source of tin. It was revealed that QDs were having particle size of about 3−5 nm. A green synthetic technique was developed for preparation of SnO_2 QDs using MW irradiation. Amino acids (aspartic, glutamic, L-lysine, serine) were used by them. (Bhattacharjee and Ahmaruzzaman, 2015; Begum et al., 2016).

Bhattacharjee and Ahmaruzzaman (2015) obtained globular SnO_2 QDs, when aspartic or glutamic acid (amino acids) and stannous chloride were used as starting materials. It was revealed that diameter of SnO_2 was found to be 1.6 and 2.6 nm for glutamic and aspartic acid, respectively. As-produced QDs were used as an efficient photocatalyst in degradation of two dyes; eosin Y and rose Bengal in presence of solar isolation.

Begum et al. (2016) prepared SnO_2 QDs using L-lysine monohydrate, and sodium dodecyl sulfate (surfactant) under MW exposure. They used these QDs in degradation of humic acid. Then the reaction solution was

given MW treatment. It was revealed that sizes of SnO_2 QDs obtained was 2.3 nm. They used these QDs for degredation of humic acid on solar exposure for 3 h. Begum and Ahmaruzzaman (2018) used *Parkia speciosa* Hassk pods extract in a green economical and less time-consuming process for synthesizing SnO_2 QDs in presence of MW irradiation. As-produced QDs were then used in photodegradation of acid yellow 23. It was reported that QDs also have scavenging activity. It was revealed that average crystallite size of as-obtained SnO_2 QDs was found in the range of 1.5−1.9 nm.

Tin oxide QDs have been prepared by Zhu et al. (2016) using a MW-assisted method. It was reported that SnO_2 QDs (organic component-wrapped) can be synthesized with size 2−4 nm in only 30 s. If these SnO_2 QDs can be obtained by annealing the organic component-wrapped SnO_2 QDs in air at 400°C in 4 h, then QDs with good crystallinity and bigger size (5−10 nm) could be obtained. As-prepared QDs exhibited an excellent sensitivity toward vapors of ethanol as a sensor.

Zhu et al. (2016) reported MW-aided preparation of SnO_2 QDs. They used a mixture of $SnCl_4$, oleic acid (OA), C_2H_5OH, oleylamine (OLA), and H_2O and exposed it to MW (200 W) for different time intervals (0.5−20 min). It was revealed that QDs with diameter of 2−4 nm could be obtained on 0.5 min exposure, but on increasing time to 20 min, QDs are obtained with a larger size of 8−20 nm. Xiao et al. (2010) prepared highly crystalline QDs of SnO_2 under MW irradiation. This involved dissolving $Sn(OtBu)_4$ and 1-butyl-3-methylimidazolium tetrafluoroborate (desiccated) in an inert atmosphere of argon and 1 min exposure to MW irradiation. As-obtained SnO_2 QDs were spherical, monodispersed, and crystalline in nature with size of 4.27 ± 0.67 nm.

A synthetic route was reported by Parthibavarman et al. (2019) for pure and Ag-doped SnO_2 QDs under MW irradiation. It was revealed by TEM images that average particle size of QDs increases on Ag doping. A smaller bandgap (3.54−3.09 eV) was observed on Ag doping. The photocatalytic degradation of rhodamine B and methylene blue was observed in with as-obtained catalyst. A maximum efficiency (97.5%) for degradation of rhodamine B could be achieved in the presence of visible light irradiation. As-obtained Ag−SnO_2 QDs catalyst can be reused and these are stable after even seven cycles.

Mohanta and Ahmaruzzaman (2020) used *Allamanda cathartica* leaf extract for synthesis of SnO_2 QDs. They boiled chopped leaves in water and stannous chloride solution was added dropwise under continuous sonication. On addition of carbon nanoflakes and sonication, a greyish solution was obtained. This solution was exposed to MWs. As-obtained SnO_2 QDs were then used for the removal of bisphenol A.

7.2.1.2 Co_3O_4 quantum dots

Uniform Co_3O_4 octahedrons were obtained by Zhang et al. (2012a,b) via a MW method. Here, various carbon materials were used, which not only acted

as a secondary heater, but also as an agent for directing morphology. A weak ferromagnetic property was found in octahedral Co_3O_4 as-obtained carbon nanotubes using MW.

Zhou et al. (2014) synthesized Co_3O_4 QDs/graphene composites via a MW irradiation method. The crystals of Co_3O_4 were found to be in the size of 3−8 nm. These composites exhibited a high rate capability as well as enhanced cycling performance on use as anode materials for Li-ion batteries. In addition, the well-dispersed Co_3O_4 nanodots and the synergetic effect between graphene nanosheets (conductive and flexible) also gave a better electrochemical performance due to reducing the diffusion pathway of lithium ions and the high surface area.

7.2.1.3 ZnO quantum dots

Lu et al. (2011) synthesized ZnO QDs using zinc sulfate heptahydrate as a precursor. They mixed a Zn precursor with GO. They utilized NaOH for precipitation, where a chocolatey−black suspension was obtained. It was then placed in a MW for half an hour at 150°C. The as-prepared product was filtered and dried at 70°C for a day. This composite was utilized for electrochemical superconductors, and it was proved that ZnO QDs exhibited enhanced activity as compared to GO only.

The Ag and Sn-doped ZnO QDs (ZQDs) were synthesized by Soumya et al. (2018) via a MW-assisted sol−gel method. They used 3-aminopropyl trimethoxy silane as a capping agent. As-obtained ZQDs were then dispersed in methyl methacrylate (MMA) monomer to obtain polymethyl methacrylate (PMMA)/ZQDs. It was observed that doped PMMA/ZQDs hybrid coatings exhibited a blue emission in the presence of UV light. A photochromic dye (spiropyran) was introduced in the doped PMMA/ZQDs hybrids and it displayed photochromic behavior with a red emission. This hybrid can be used in solar radiation control active interface layers.

Rangel-Mendez et al. (2018) reported solvothermal synthesis of C-doped ZnO and TiO_2 hybrid materials under MW irradiation. Titanium isopropoxide, saccharose, and zinc acetate were used as sources of Ti, Zn, and C, respectively. There was a redshift in bandgap of these semiconductors. The TiO_2-C and ZnO-C was obtained (3.02 and 3.13 eV), which was attributed to C-doping effect. It was indicated that these present materials can find application as photoelectrodes for QD-sensitized solar cells (QSSCs).

The nanocomplex was prepared of ZnO QDs by a MW-assisted reaction in the presence of avobenzone (Av) (Asok et al., 2018). It was reported that ZnO QDs can catalyze the formation of highly photostable surface enolate species via an aldol condensation reaction. It was observed that molar absorptivity and photostability was extended beyond the UV-A filtering range, and therefore it can provide a visible emission color matching human skin.

7.2.1.4 WO_3 quantum dots

Le Houx et al. (2009) carried out the synthesis of WO_3 QDs by both MW and conventional heating and compared the results. It was reported that particles obtained with MW-heating were more suitable compared to conventional heating or routine preparation. There have greater specific surfaces and particle size, ranging between 5 and 30 nm.

Wang et al. (2015a,b) fabricated tungsten oxide QDs using a one-pot MW-assisted method. It was reported that as-obtained WO_3 QDs have a size ranging from 2 to 3 nm. These WO_3 QDs exhibited significant photonic/thermal stabilities. It was interesting to note that a colorless aqueous suspension of WO_3 QDs turned blue in the presence of sunlight in 10 s indicating its photochromic behavior. This type of behavior was attributed to surface oxygen vacancies as well as exposed reactive sites of ultrafine WO_3 QDs.

7.2.1.5 SiO_2 quantum dots

Mao et al. (2014) prepared N-acetyl-L-cysteine-stabilized CdTe/CdS@ZnS−SiO_2 QDs red-luminescent under MW irradiation. The Stober method was used for coating silica on CdTe/CdS QDs. The as-compared QDs exhibited high photoluminescence (PL), low biotoxicity, and superoptical stability. They utilized the QDs in a low-power surface-mounted and a high-power device.

7.2.1.6 CeO_2 quantum dots

Lehnen et al. (2014) prepared CeO_2 QDs via MW-solvothermal synthesis of N-methylpyrrolidone. The synthesis procedure involves a MW reactor at 50 W at 150°C and 1.5 bar for 5−15 min. It was observed that crystallinity of CeO_2 QDs was improved, when reaction time was kept at 15 min. The product was collected after centrifugation and purification. The average size of CeO_2 QDs was found to be 4.3 nm. He et al. (2017) synthesized CeO_2 QDs using a MW-assisted method. A mixture of OLA and cerium (III) nitrate hexahydrate was first heated for half an hour at 80°C under vacuum and then placed in a MW oven at 180°C. These QDs were cooled down and washed and were then kept dispersed in tetrahydrofuran and stored at −20°C.

Soren et al. (2015) fabricated CeO_2 QDs via MW-assisted synthesis. In MW-hydrothermal synthesis, autoclave cerric ammonium nitrate and NaOH were used in the ratio (1:6) with water and pH was adjusted to 10 and exposed to MW irradiation, while in MW solvothermal synthesis, cerric ammonium nitrate and 1,4-butanediol were used and pH was maintained at 6. This mixture was then exposed to MW rays for 20 min. It was revealed that MW-mediated solvothermal method could yield less agglomerated and smaller size QDs (5−10 nm), whereas larger NPs size (15−20 nm) was produced on using the MW-mediated hydrothermal technique.

7.2.1.7 TiO_2 quantum dots

Alves et al. (2018) reported the synthesis of graphene-TiO_2 QDs via the MW-oleothermal method. They mixed OLA, graphene oxide (GO), OA, 98% titanium propoxide, and Triton-X under magnetic stirring at ambient conditions, which was followed by the oleothermal method and sonicated for 15 min in the presence of MW radiation. It was observed that the diameter of synthesized QDs was found to be around 3 nm.

7.2.1.8 MoO_2 quantum dots

Cao et al. (2020) fabricated phosphorus and nitrogen codoped MoOx QDs (N,P-MoOx QDs) using MW-assisted method. The $H_3P(Mo_3O_{10})_4.xH_2O$, glutathione (GSH), and ultrapure water were mixed, stirred, and sonicated for 5 min. The mixture was placed under MW radiation in an autoclave for 8 min after adding ammonium solution.

7.2.1.9 CuO quantum dots

The CuO QDs were prepared by Bekru et al. (2021) using the MW-assisted modified method. They used copper acetate as the source of copper extract of leaves of *Cordia africana* Lam. Then, the mixture was irradiated by MWs (1000 W) for 9 min. A brown precipitate of CuO QDs was obtained and thius were utilized in the reduction of 4-nitrophenols. Felix et al. (2015) also synthesized CuO QDs using a MW-assisted method. An average size of CuO QDs was found to be about 4 nm. As-prepared CuO QDs exhibited high sensitivity for electrochemical sensing as compared to their microcounterparts.

7.2.2 Sulfide quantum dots

7.2.2.1 CdS quantum dots

Alehdaghi et al. (2020) obtained CdS QDs and examined the consequence of gamma radiation on their chemical and physical properties. These QDs were prepared in less than 10 min under MW radiation. They studied the PL and transmittance characteristics of CdS QDs. The size of CdS QDs was confirmed as 3−4 nm from TEM analysis. It was revealed that degradation of PL of QDs was found to be inversely dependent on concentration. The redshift was found to be more with a lower size of QDs. It was claimed that as-prepared CdS QDs may be promising material for use as a gamma dosimeter.

Zheng et al. (2010) synthesized mesoporous CdS QDs via a simple and cost-effective method (in situ conditions). They used OA. A soft template for MW treatment was used instead of sintering, because the mesostructure is destructed under this condition. It was observed that on adding Na_2S, the color of the gel changed to yellow. It was revealed that both these samples of CdS QDs (naturally evaporated and MW irradiated) had a size of 3−4 nm.

Fregnaux et al. (2013) made a comparative study of CdS formation via single-source precursor methodology (SSPM) and MW synthetic route (MWSR). The average particle size of QDs ranged between 4.5−5.2 and 2.8−4.5 nm when prepared with MWSR and SSPM techniques, respectively. It was observed that CdS QDs prepared by MWSR had a cubic structure, while SSPM afforded QDs with hexagonal structure. It was also concluded that there is better optical quality in MWSR-grown QDs. It was revealed that a stable behavior of QDs was due to the absence of S vacancies when treated in air.

Alehdaghi et al. (2014) synthesized CdS QDS by dissolving both in S as well as Cd precursor deionized water, followed by the addition of TGA. It turned into a milky solution, which was made transparent by adding ammonia. This solution was then exposed to MWs for various time intervals to afford QDs of different sizes. Liu et al. (2014) synthesized CdS QDs using the MW-assisted chemical bath deposition technique. They utilized thiourea and cadmium nitrate as precursor solutions. Then TiO_2 film was introduced containing a precursor solution, and it was placed under MW exposure for 20 min. The crystal size of as-obtained QDs was found to be 5 nm.

Butova et al. (2017) prepared CdS QDs via a MW hydrothermal method in 5 min. They stabilized these QDs with 4,4'-bipyridine and dioctyl sodium sulfosuccinate. They also investigated the impact of different capping mediators on particle shape, size distribution, and properties. They used cadmium nitrate as precursors. It was revealed that Cds QDs were about 5 nm in size. It was revealed that smaller particle size was obtained when 4, 4'- bipyridine was used as a stabilizer.

The CdS QDs were also prepared by Radzi et al. (2020). They used a mixture of solutions of $C_{10}H_{17}N_3O_6S$ (GSH), and $CdCl_2$, and added Na_2S to these drop wise. This mixture was heated at 150°C in a MW reactor for 1 min only. It was revealed that the average diameter of CdsQDs produced was found to be 5.8 ± 0.3 nm. These QDs were embedded into PVA (polyvinyl alcohol) (matrix film) and were used in an absorber in Q-switches.

7.2.2.2 ZnS quantum dots

ZnS is a significant type of II-VI semiconductor QD because of its luminous properties. ZnS crystals are in two phases: hexagonal phase (wurtzite form) and cubic phase (zinc blende, sphalerite). The bandgap of ZnS falls in the range of 3.68−3.80 eV. It was observed that the cubic phase of ZnS is more stable at lower temperatures, but at higher temperatures it transforms to its wurtzite phase. MW-irradiation is an efficient and eco-friendly method as it provides high-purity particles, a greater yield of QDs, requires a simple reaction medium, has a lesser reaction time, and is an economically visible route. Here, capping agents may play an important role in enhancing the properties of QDs, such as luminescent nature, stability, and morphology, which prevents their agglomeration.

Ayodhya and Veerabhadram (2018) prepared ZnS QDs (undoped and doped) under MW irradiation. They used Rh^{3+}, Pd^{2+}, and Zr^{2+} as dopant materials. The precursor solutions (zinc acetate and sodium sulfide) were prepared in water. The white colored ZnS was obtained on MW irradiation (1000 W) on exposure of a mixture of precursor solutions for 10 min. Undoped and doped ZnS QDs were prepared in the absence and presence of dopant. The structure of ZnS QDs was cubic and the size of these as-prepared QDs ranged between 2 and 10 nm. It was observed that both these ZnS QDs exhibited superior fluorescence quenching with the cysteine molecules and these can be used as an efficient fluorescent material for quenching and binding practices.

Mathew et al. (2010) fabricated folic acid (FA) conjugated carboxymethyl chitosan (CMC), which was coordinated to Mn-doped ZnS QD (FA−CMC−ZnS:Mn) nanoparticles. The zinc acetate, manganese sulfate, and sodium sulfide were used as precursors of zinc, manganese, and sulfur, respectively. A white colloid was obtained, which was treated under MW irradiation for 1 min. These as-obtained QDs were utilized for monitoring, targeting drug delivery, and imaging of breast cancer cells.

Shahid et al. (2012) reported MW-assisted fabrication of ZnS QDs (wurtzite). The size of as-obtained QDs was 3 nm. Saravanan et al. (2012) made a comparison between MW and conventional techniques for preparation of ZnS QDs. They used sodium sulfide and zinc acetate as the source of sulfur and zinc, respectively. It was revealed that the size of QDs prepared using the MW method was very small (diameter $\sim$3 nm). It was revealed that these QDs were almost 30 times smaller than those produced by the conventional method. The bandgap of bulk ZnS was 3.67 eV, which was found to increase to 3.9 eV on MW treatment.

Zhu et al. (2014) synthesized Mn-ZnS QDs via MW-assisted technique. Zinc nitrate and manganese chloride were selected as the source of zinc and manganese, respectively. A solution of sodium sulfide was added to sodium palmitate solution. The mixture was kept under MW irradiation (260 W) for 35 min. It was revealed that the average particle size of Mn−ZnS QDs was found to be 4.2 nm as evident from HRTEM images.

He et al. (2019) reported a facile method of producing copper-doped ZnS QDs (ZnS:Cu QDs) using MW irradiation. They used 3-mercaptopropionic acid as a source of sulfide as well as a stabilizer. The copper sulfate and zinc acetate were used as precursor of copper and zinc, respectively. It was observed that the size of QDs increased very little from 4.1 to 4.7 nm on increasing the time from 10 min to 2 h. As-prepared ZnS:Cu QDs were utilized in the lighting device. It was interesting to note that as the time of exposure was increased, the emission color of ZnS:Cu QDs changed from blue → green → yellow → orange−red.

Shaheen et al. (2020) synthesized zinc sulfide QDs by MW route. They found 1-dodecyl-3-ethylimidazolium bromide, surface active ionic liquid

suitable as a capping agent because of its amphiphilic nature, superior aggregation property, and eco-friendly behavior. As-obtained QDs were found to be thermally stable with a size of 3.03 nm (diameter). They also reported their application as a sensor for ascorbic acid. The fluorescence property of QDs was attributed to high sensitivity, low cost, and ease.

7.2.2.3 PbS quantum dots

He et al. (2012) prepared PbS QDs. They used lead chloride and thioacetamide as the source of lead and sulfur, respectively, and 3-mercaptopropionic acid as a stabilizer. The reaction mixture was exposed to MW irradiation (960 W) only for 40 s. As-obtained PbS QDs solution was light gray-green in color and the particle size of PbS QDs was 5 nm in diameter.

Liu et al. (2019) embedded $Pb(DMDC)_2$ with PbS QDs by reducing dimethyl dithiocarbamate (DMDC) in ethanol. It was further treated by MW and ultrasonic−irradiation (200 W). The color of the solution was finally changed from colorless to black, which indicates the formation of PbS QDs.

Molaei et al. (2020) prepared PbS QDs in water using LG as a stabilizer and for distribution in the blood transmission. They mixed lead acetate and LG before the treatment by MW irradiation for 30 s after addition of sodium sulfide.

7.2.2.4 CuS quantum dots

Nethravathi et al. (2019) utilized MW irradiation in the synthesis of CuS QDs. They used sonication before MW exposure. They used copper hydroxydodecylsulfate and thiourea as a precursor of copper and sulfur, respectively. The resulting mixture was treated with MW (800 W) for 5 min. Black colored CuS QDs were obtained. These QDs were used for photocatalytic degradation of methylene blue, methyl orange, and 4-chlorophenol in sunlight. They were separated via centrifugation and purified by washing and then dried.

CuS QDs were synthesized by Chaudhary et al. (2014) in very high yield in MWs in 2 min. The particle size of as-obtained QDs was in the range of 2−3 nm. These CuS QDs were used as a catalyst in Biginelli reaction under solvent-free conditions affording dihydropyrimidinones in excellent yields. This catalyst can be recovered and reused for a number of cycles. Malankowska et al. (2020) obtained CuS_2 QDs under MW irradiation. The size of CuS_2 QDs was found to be 2−3 nm. The efficiency of CuS_2 QDs and QDs-sensitized TiO_2 composites was evaluated in the degradation of toluene under LED irradiation.

7.2.2.5 AgS quantum dots

Mir et al. (2018a) prepared silver indium sulfide (AIS@ZnS) core−shell QDs via a MW-assisted method. They used a stabilizer GSH. The appearance of a

golden color indicates the formation of silver−indium sulfide QDs. An average diameter of core and core−shell nanocrystals diameter was found to be 2.5−3.25 nm, with corresponding bandgap and yield of 2.3−3.1 and 2.4−3.5 eV and 26% and 49%, respectively. The core−shell QDs display color-tunable production in the noticeable region (500−600 nm) by varying the Ag:In molar ratio.

Mirahmadi et al. (2020) synthesized Ag_2S and Ag_2S@ZnS QDs via a MW method. These as-prepared Ag_2S and Ag_2S@ZnS QDs were used as cosensitizers in the fabrication of QDs solar cells (QDSCs), where an enhancement of cell efficiency (3%) and short current density (12.5 mA cm^{-2}) could be achieved.

7.2.3 Selenide quantum dots

7.2.3.1 CdSe quantum dots

Attempts were made to produce CdSe QDs (Peng and Peng, 2001; Li et al., 2003). Here, organic phosphine and cadmium oxide/organometallic precursors were utilized as ligand and crude material in a temperature range of 250°C−350°C. As-produced CdSe NPs were found to be soluble only in nonpolar solvents unless some surface modification is made. It has been observed that PL of CdSe QD was reduced, if any surface alteration is being made since it is hypersensitive to the surface characteristics (Nazzal et al., 2003). So, it is necessary to develop a directly water-soluble production route. The commercial preparation of CdSe has its own limitations, such as the use of poisonous organic phosphines, elevated temperature, and costs linked with oxygen-free equipment. Therefore, there is a necessity for a pathway that is greener, with harmless chemicals, lower temperatures, and fast reaction method. The CdSe QDs can be utilized in photovoltaic biomedical engineering lasers and solar drive cells (Peng, 2002; Pradhan and Peng, 2007). The MW-assisted heating method is easy as well as there is swift control of the reaction.

Wang et al. (2004) were able to produce fairly stable CdSe NPs utilizing MW heating of 1,1-dimethylselenourea and cadmium perchlorate (in the presence of citrate). They used MW (900 W) for preparation of CdSe QDs. Zhu et al. (2009) reported MW-assisted synthesis of CdSe QDs. They used OA as a nonphosphine ligand. Cadmium oxide and diesel were mixed with OA, followed by the addition of selenium powder in diesel and glycerol. This mixture was exposed to MW (170 W) for 2 min.

A rapid MW-assisted process was developed by Zhang et al. (2012a,b) to produce protein-conjugated CdSe QDs. They used ribonuclease A (RNase A) as a template for the generation of CdSe clusters. These clusters were found to be less toxic and exhibited excellent stability. The MW exposure was required for 5 min. It was revealed that the shape of QDs was regular

spherical with an average size of 5 nm. Moghaddam et al. (2012) reported a one-pot protocol for the synthesis of monodispersed colloidal CdSe QDs with the help of MW radiation. Here, 1-octadecene (ODE) played a dual role of a solvent and reducing agent. They observed that CdSe QDs can be fabricated with different sources of cadmium, where their particle sizes ranged between 0.5 and 4 nm.

Xuan et al. (2013) prepared CdSe QDs via MW-assisted synthesis for use in white light-emitting diodes with outstanding color rendering features. It was reported that size and optical properties of these QDs can be modified by changing the MW power growth temperature as well as reaction interval and molar ratio of Cd^{2+} with Se. It was revealed that as-produced QDs exhibited spherical shapes with a diameter of 4.8 nm.

CdSe QDs were prepared by Mehrjoo et al. (2017) using the MW-assisted method. They used TGA as a capping agent and $CdSO_4$ and Na_2SeO_3 as precursors. The MW (720 W) was used for 90 s for their synthesis. It was reported that as-produced CdSe QDs were found to be 5 nm in size. Then, these QDs were used for the degradation of methyl orange.

Abolghasemi et al. (2019) also used an MW-assisted method for the production of CdSe QDs. They used CdO and Se powder as precursors. It was observed that the particle size of CdSe QDs varied in the range of 5−7 nm. It was indicated that as-prepared QDs can be used in solar cells (as a sensitizer) with an efficiency of 3.57%.

7.2.4 Telluride quantum dots

7.2.4.1 ZnTe quantum dots

Alvand et al. (2019) synthesized zinc telluride QDs (ZnTe QDs) using the aqueous extract of *Ficus johannis*. Ultrasonic as well as MW techniques were applied for the preparation of plant extracts, which can be utilized as stabilizing precursors during the synthesis of ZnTe QDs. The nanoparticles of ZnTe QDs had an average size of 8 nm. It was reported that as-prepared QDs produced antimicrobial, antifungal, and antioxidant properties.

A series of $Zn_{1-x}Pm_xTe$ QDs was synthesized by Al-Harthi et al. (2021) via 4,4-bis-*N*-1-naphyl-*N*-phenylaminobiphenyl through MW-assisted method. These QDs showed remarkable optoelectronic properties. It was observed that the bandgap of ZnTe QDs was reduced from 3.06 to 2.8 eV in the presence of promethium ions and particle size was increased from 1.4 to 4.3 nm. The inclusion of promethium ions in these QDs ions was found to be responsible for tuning the color of QDs in the visible region. It was suggested that as-prepared $Zn_{1-x}Pm_xTe$ QDs can find potential application in photovoltaic devices.

Du et al. (2012) developed a MW-assisted method for synthesis of GSH-capped $Zn_{1-x}Cd_xTe$ alloyed QDs. They used Na_2TeO_3 as a source

of tellurium. The photoluminescent quantum yield of as-synthesized alloyed QDs could reach up to 90%. As-prepared $Zn_{1-x}Cd_xTe$ alloyed QDs have a potential as biological fluorescent labels in different biological applications.

Zhan et al. (2013) prepared CdSe QDs covered by double-shells of CdZnS and CdS using a one-pot MW-assisted route. It was reported that as-prepared CdSe/CdS/CdZnS core−shell−shell (CSS) QDs exhibited high crystallinity and high-fluorescence quantum yield of 90%. As-obtained QDs also displayed stability toward light, acid, and oxidation. These CSS particles have an average size of QDs around 3.2 nm. It was revealed that as-prepared QDs can find a potential for fluorescent QDs-based biological applications.

Kim and Kim (2016) synthesized CdZnTe QDs using MW irradiation in aqueous solution. They used 3-mercaptopropionic acid as a stabilizer. Zinc nitrate, cadmium nitrate, and NaHTe were used as precursors of Zn, Cd, and Te, respectively. It was reported that absorbance spectra and PL of these QDs exhibited a redshift.

7.2.4.2 CdTe quantum dots

CdTe has found varied applications like sensors, photovoltaic devices, bioimaging, and biolabeling because of its higher quantum efficiency. These are synthesized via aqueous and nonaqueous methods such as thermal breakdown, solvothermal, MW, and sonochemical treatment routes. MW irradiation has several advantages over other methods.

He et al. (2006) synthesized CdTe QDs with a MW-assisted method. They used NaHTe and $CdCl_2$ as precursors solutions of Te and Cd respectively. The 3-mercaptopropionic acid was utilized as a stabilizer. Kanwal et al. (2010) also used this method with slight modifications. Here, mercaptosuccinic acid was used as a stabilizer. It was observed that dimensions of CdTe QDs can be changed by simply changing the time intervals of heating. It was also revealed by Wang et al. (2008) that production of CdTe QDs with mercap to succinic acid as a stabilizer consumed less time and as-obtained QDs exhibited durable PL with high quantum yield.

Kominkova et al. (2017) prepared CdTe QDs by MW treatment. They used Na_2TeO_3 as the precursor of tellurium. The reaction mixture was heated under MW (300 W) for 10 min. Molaei et al. (2015) also prepared CdTe QDs. They used $CdSO_4$ and NaHTe as the precursor of Cd and Te, respectively. Here, TGA was used as a capping agent. In the final stage, a yellow-orange solution was obtained, which was placed under MW (720 W) for various time periods. The diameter of as-obtained CdTe QDs was found to be 2.5 nm.

Singh et al. (2017) fabricated CdTe QDs using $CdCl_2$ and TeO_2 as the precursor of Cd and Te, respectively. The MPA was also mixed in this solution in 100 mL milli-Q water. Then this mixture was exposed to MW irradiation

(300 W). It was observed that spherical QDs were obtained in a cubic structure and an average diameter of 2.5 nm was evident from XRD and TEM analysis. A redshift was also found with a change in particle size on increasing the time of exposure. These as-fabricated CdTe QDs were then used in latent fingerprinting and it was claimed that only a few seconds were needed to detect fingermarks under UV treatment.

Singh et al. (2017) used the one-step MW irradiation method for the synthesis of capped CdTe QDs. They used 3-mercaptopropionic acid as capping agent. The TeO_2 was used as the source of tellurium in place of commonly used Te powder, Na_2TeO_3, or Al_2TeO_3. The average particle size of the QDs was found in the range of 2−3 nm. These capped CdTe QDs can be used for latent fingerprinting.

MW irradiation route was developed by Duan et al. (2009) for the synthesis of CdTe QDs. The 3-mercaptopropionic acid was used as stabilizer. It was revealed that as-obtained CdTe QDs could be used as fluorescent probes for detect ion of mercuric ions in aqueous solution with a detection limit of 2.7×10^{-9} mol L^{-1}.

Ribeiro et al. (2017) reported a MW-assisted synthesis of CdTe QDs. They used three different ligands (2-mercaptoethanesulfonate, 3-mercaptopropionic acid, and L-GSH reduced) as capping agents. They could achieve CdTe QDs with quantum yield of ∼60%. A simple synthesis of CdTe QDs has been reported by Chen et al. (2015a) under MW irradiation. They used GSH as a modifier. It was revealed that as-prepared CdTe/CdS QDs were more dispersible and exhibited higher fluorescence intensity.

Dong and Ren (2012) developed a MW-assisted method for synthesis of CdTe QDs. They used long-chain thiols-mercaptoundecanoic acid (MUA) as surface ligand. It was revealed that as-obtained MUA-coated CdTe QDs were having have good stability, small diameter, long lifetime, and high luminescence. It was also revealed that these MUA-coated QDs could be used for HeLa cell imaging.

A MW-assisted synthesis of water-soluble cadmium telluride QDs was reported by Alibolandi et al. (2014). They used sodium tellurite and cadmium chloride as the source of Te and Cd, respectively. The mercaptosuccinic acid was used as a capping agent, CdTe nanocrystals with different colors ranging from blue to orange were obtained in less than one hour. It was revealed that qualified AS1411-aptamer-conjugated QDs exhibited that these can be used as excellent nanoprobes for targeting of cancer and molecular imaging. Bichpuria and Oudhia (2016) prepared GSH capped CdTe QDs (GSH-CdTe QDs) using a MW assisted wet chemical method. It was observed that high loss tangents and high boiling point were effective in controlling the size dispersion of QDs in MW-assisted synthesis.

7.2.5 Other quantum dots

A MW-assisted synthesis of silver indium sulfide (AIS) and AgInS@ZnS (AIS@ZnS) core−shell QDs was reported by Mir et al. (2018b). They used

GSH as a stabilizing agent. An average particle size of 2.5 and 3.25 nm was obtained for core and core−shell nanocrystals with bandgap as 2.3−3.1 and 2.4−3.5 eV, respectively. It was revealed that AIS@ZnS particles can easily penetrate the cells. It was suggested that as-obtained QDs have the potential to be used as antifungal and photodynamic agents as well as in high contrast cell imaging.

Fitzmorris et al. (2015) synthesized $CuInS_2$ QD cores using a MW-assisted reaction. It was indicated that the $CuInS_2$/ZnS (core/shell) QDs were ~98% ZnS, while In and Cu were present in lower concentrations. It was reported that PL stability was improved with ZnS shell and PL down conversion efficiency of ~65% was there on using a blue LED source.

Hong et al. (2015) synthesized $CuInS_2$/ZnS (core/shell) QDs via one-pot MW irradiation. It was observed that as-prepared QDs exhibited emission ranging from the red to NIR. The as-prepared CIS/ZnS QDs not only possess a high PLQY (56%) but also exhibit a large Stokes shift. It was revealed that these QDs can convert near UV and blue light in the Si solar cell with lower sensitivity to red and NIR light, where these solar cell has relatively higher sensitivity. Especially when they were first embedded into a PMMA transparent matrix to form a composite film as a luminescent downshifting layer for Si solar cell, the photoelectric conversion efficiency of the cell shows a marked enhancement by spectral downshifting as compared to the bare glass substrate, and the maximum achieved is 16.21%.

A green MW-assisted synthesis of $CuInS_2$ (CIS) and $CuInS_2$@ZnS core−shell QDs (CIS@ZnS) was reported by Mir et al. (2018b). They also used GSH as a stabilizer. The average particle size of CIS and CIS@ZnS was found to be 2.9 and 3.5 nm, respectively. It was observed that core−shell QDs exhibited better binding with lysozyme as compared to core structures.

Yang et al. (2012) synthesized Cu-doped ternary ZnCdS QDs (ZnCdS:Cu QDs) using a MW-assisted method in aqueous solution. They prepared samples at different Cd concentrations. These ternary QDs were found to be dispersible in water solution. It was observed that their PL peak was red-shifted and quantum yield of these QDs could reach as high as 12% depending on the doping concentration of Cu. It was concluded that as-fabricated ZnCdS:Cu ternary QDs may find application in fields such as bioimaging, sensing, and light-emitting diodes.

7.3 Synthesis of core−shell quantum dots

Core−shell QDs (CSQDs) have a solid core that is encapsulated within a second QDs material with an upper bandgap. Such hybrid particles have an enhanced quantum yield over QDs of single material. The II−VI compounds are useful for many purposes such as sensors, solar cells, probes, LEDs, photocatalysts, etc. QDs have a very high surface-to-volume ratio (around 80%) of atoms. They can provide various interesting properties. The CdSe

QDs have been exclusively investigated, which can be further improved by having a shell of ZnS as its bandgap is high compared to CdSe. The CSQDs can be categorized depending on the position of conduction and valence bands in the semiconductor materials. If the core has a larger bandgap as compared to the shell, then these are known as type I or conversely (inverse type I). On the other hand, if the conduction band or valence band of the core is placed within the bandgap of the shell, then these are classified as type II, CS QDs.

7.3.1 Type I CS quantum dots

Ziegler et al. (2007) used a green method to synthesize a ZnS shell over a CdSe core using MW irradiation. The proximity of core and shell was examined by the thiophenol test. Formation of the shell was started by MW exposure (within 30 s at 800 W). The mixture was then stirred for a minute and exposed to MWs (600 W).

Duran et al. (2014) reported a rapid method for the synthesis of water-soluble CdSe/ZnS QDs using MW technique. They used L-cysteine, cysteamine, and 3-MPA as thiol ligands. It was found that CdSe core was covered by ZnS shell. This method also increased the crystallinity of ZnS (shell).

Molaei et al. (2016) prepared CdSe/CdS CSQDs by an MW-assisted method in a single pot. They used two methods: MW irradiation (720 W) and chemical reaction (between NaHSe, $CdSO_4$, and TGA as capping ligand). It was observed that a CdS shell was developed on the CdSe. The formation of CdSe/CdS core−shell QDs is given as:

$$\mathbf{CdSO_4} + \mathrm{TGA} \xrightarrow[\mathbf{MW}]{\mathbf{NaHSe}} \mathbf{CdSeQDs}$$

$$\mathrm{CdSeQDs} + \mathbf{CdSO_4} \xrightarrow[\mathbf{MW}]{\mathbf{Na_2S_2O_3}} \mathrm{CdSe/CdS}\ \ \mathbf{CS\ \ QDs}$$

7.3.2 Inverse type I CS quantum dots

Shen et al. (2012) reported MW-assisted fabrication of highly luminescent cadmium selenide tellurium@zinc sulfide-silicon dioxide (CdSeTe@ZnS-SiO_2) QDs, which are helpful in detecting Cu(II) ions. These QDs were prepared with ZnS-like clusters, which were incorporated into the shell of SiO_2 in the presence of MW irradiation. The Zn^{2+} and GSH were utilized as precursors for ZnS. An average diameter of CdSeTe QDs was found to be 3.9 nm. It was reported that as-prepared CSS QDs have high luminescence and water solubility.

Ma et al. (2013) utilized a MW irradiation oven for the synthesis of GSH-capped ZnSe/ZnS core−shell QDs. Zinc acetate and KHSe were used as the source of zinc and selenium, respectively. The GSH was utilized as a capping agent. The molar ratio of Zn:GSH:KHSe was kept as 1:1.6:0.1 for better results.

Ebrahimi and Souri (2020) synthesized ZnSe:Cu@ZnS core−shell QDs using a MW-assisted colloidal method. It required 6 min of exposure to MW irradiation. It involves ZnSe and ZnSe:Cu semiconducting NCs in aqueous medium. The thioglycolic acid was used as a capping agent so that no agglomeration occurred. The NaHSe was prepared by reaction of Se with $NaBH_4$.

7.3.3 Type II CS quantum dots

Sai and Kong (2011) synthesized crystalline, water-soluble CS QDs (CdTe/CdSe QDs) via a MW technique. These are type II QDs. The solution of cadmium chloride (N_2-saturated) and NaHTe in the presence of MPA was exposed to MW irradiation for core formation (CdTe) for 2 min. It was reported that as-prepared QDs were monodispersed with a crystalline nature and size of 2 nm.

The MW-assisted technique was used by Chen et al. (2015b) to synthesize GSH conjugated CdTe (core)/CdSe (shell) QDs (CS QDs). The core QDs was prepared using cadmium chloride and MPA solutions. They used NaHTe solution as a source of Te. The resultant solution was exposed to MW irradiation for 2 min. The NaHSe solution was used as a precursor for selenium. Then, a solution of CdTe core QDs was added and exposed to MW for 20 min.

7.3.4 Inverse Type II CS quantum dots

Ren et al. (2013) produced PbS/CdS CS QDs via MW-assisted cation interchange method. A mixture of CdO, 1-ODE, and OA was heated in an oil bath until color disappeared. Then PbS QDs were injected using a syringe and the resultant solution was heated under MW (300 W) irradiation. It was observed that CS QDs were monodispersed with QY of 57%, which was almost 1.4 times more in the case of MW-assisted preparation as compared to the oil bath method.

7.3.5 Core−shell−shell quantum dots

The CSS (CdTe/CdS/ZnS) QDs were synthesized by He et al. (2008) under MW irradiation. As-prepared CSS QDs may be found useful as fluorescent probes in biological applications as these have good spectral properties, good biocompatibility, aqueous dispersibility, and excellent photostability (Fig. 7.2).

Wang et al. (2013) synthesized CdTe/CdS/ZnS QDs under MW irradiation for 10 min. The average particle size of CdTe/CdS/ZnS QDs was found to be >8 nm. It was reported that as-prepared CdTe/CdS/ZnS CSS QDs showed a maximum emission wavelength of 780 nm. Their synthesis is diagrammatically presented in Fig. 7.3.

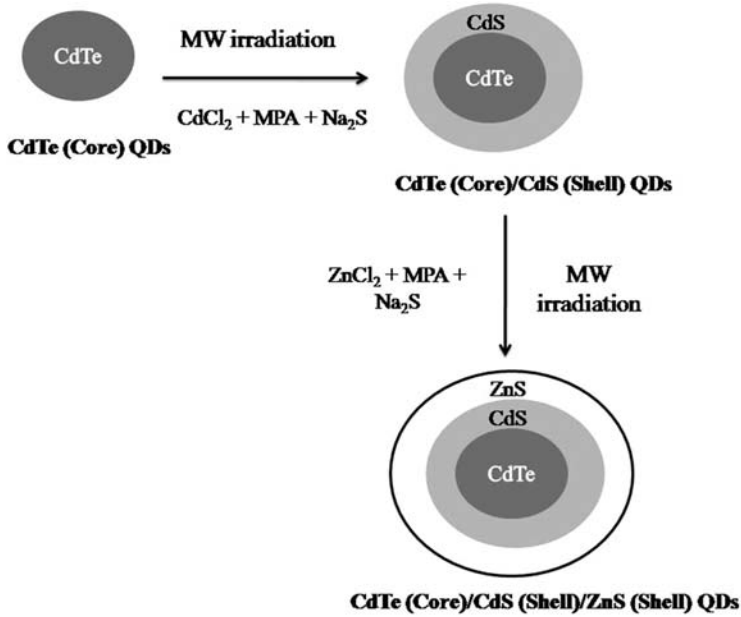

FIGURE 7.2 Microwave-assisted preparation of CdTe (core)/CdS (shell-I)/ZnS (shell-II) QDs.

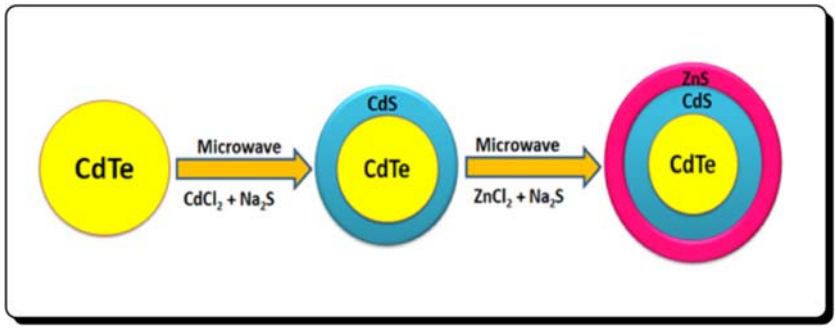

FIGURE 7.3 Microwave-assisted production of water-dispersed CdTe/CdS/ZnS core−shell−shell quantum dots. *Adapted Wang et al., 2013. Biomaterials 34 (37), 9509−9518. With Permission.*

7.4 Synthesis of alloyed quantum dots

These include multiple materials, but in the same combination. Therefore, combinations of two diverse semiconductors with unlike bandgaps may introduce some unique properties to the dots.

ZnSe QDs are interesting as these have the potential to be used in solar cells, diodes, scintillators, etc. (Abd Elhamid et al., 2018). Huang and Han (2010) have developed a simple plan for preparing GSH-capped ZnSe QDs

under MW irradiation. The Na_2SeO_3 was used as a source of Se. The GSH, zinc nitrate, Na_2SeO_3, and surplus $NaBH_4$ were mixed and exposed to MWs treatment (300 W) for 1 h. It was revealed that as-prepared ZnSe QDs had cubic shapes and ZnS spherical shapes with diameters in the range of 2−3 nm.

Qian et al. (2005) developed a seed-mediated technique for the synthesis of alloyed QDs (CdSe−CdS) under MW irradiation in aqueous phase. They prepared CdSe seeds by a reaction between Cd^{2+} and NaHSe. The MPA was used as a source of sulfide ions followed by MW exposure (1000 W). It was observed that the black-colored solution turned to white after 3 h. The NaHSe was prepared by $NaBH_4$ and Se powder. Again, the resultant solution was irradiated with MWs at for 5 min^{-1} h. It was reported that the size of alloyed QDs was 28 nm with QY of 25%.

Yang et al. (2013) synthesized CdSe-TeS alloyed QDs in aqueous solution using MW radiation. They used $CdCl_2$, NaHTe, and NaHSe as sources of Cd, Te, and Se, respectively. The MPA served as a source of sulfur and acted as a stabilizer also. These alloyed QDs could achieve 57.7% QY and are used in cancer imaging.

A simple MW treatment procedure for the preparation of $CdSe_xTe_{1-x}$−CdS QDs was reported by Luo et al. (2014). They carried out this MW-assisted method in two steps:

1. CdS shell ($CdSe_xTe_{1-x}$-CdS-I) was prepared by 3-mercaptopropionic acid capped $CdSe_xTe_{1-x}$ QDs.
2. CdS layer formation on the $CdSe_xTe_{1-x}$ core.

It was revealed that the XRD data supported the formation of alloyed QDs and the size of QDs was found to be 3.2 nm. These QDs were used in QSSCs.

Al-Hazmi et al. (2020) prepared nanocrystalline $Zn_{1-x}Pa_xTe$ ($0 \leq x \leq 0.09$) QDs using poly[(9,9-bis(3′-(N,Ndimethylamino)propyl)-2,7-fluorene)-alt-2,7-(9,9-dioctylfluorene)] via a MW-assisted method. They used a solution of poly[(9,9-bis(3′-(N,N-dimethylamino)propyl)-2,7-fluorene)-alt-2,7-(9,9-dioctylfluorene)], OLA, and 1-ODE, zinc acetate, trioctylphosphine telluride, and a sufficient amount of protactinium chloride. The resultant solution was irradiated with MWs (1200 W) for 2 h. They could obtain crystalline and monodispersed $Zn_{1-x}Pa_xTe$ QDs with a size ranging between 3 and 8 nm and very good QY up to 95%.

Mubiayi et al. (2020) synthesized $CuInGaSe_2$ QDs using MW exposure. Equal quantities and concentration of tri-n-octylphosphine (TOP) capped copper, gallium, and indium chloride in solvent OLA were mixed and MW (500 W) exposure was given for 10 min. Then TOPSe was injected and it was irradiated again with MW (600 W) for 10 min. It was observed that as-obtained QDs were pyramidal in shape with a crystalline nature and had

an average diameter of 10 nm. It was reported that films of as-prepared QDs can be applied as a counter electrode in DSSCs.

7.5 Carbon and graphene quantum dots

Graphite and GO are normally used for the preparation of GQDs. Several workers have used these precursors with different methods, but the MW technique was found to be better for this purpose. Li et al. (2012) synthesized greenish-yellow and blue GQDs (g-GQDs and b-GQDs). They did not utilize a stabilizer in this method. It was reported that PL QY of b-GQDs and gGQDs was found to be 22.9% and 11.7%, respectively. Their average diameter of QDs was found to be in the range of 2−7 nm.

The GQDs were also synthesized by Chen et al. (2012) using a MW-hydrothermal method. They used GO as the precursor of GQDs in the presence of nitric and sulfuric acids and exposed them to MWs (200°C) for 5 min. The size of as-prepared QDs was in the range of 2−5 nm. The MW-assisted hydrothermal method was also used by Chen et al. (2013) for the synthesis of pyrrole-ring functionalized GQDs (p-GQDs). They used the similar MW conditions here. It was reported that the final solution was pink and particle size ranged between 2 and 6 nm.

Shin et al. (2014) prepared GQDs directly from graphite powder in large amounts under MW irradiation (600 W) for 1 h. An average particle size of GQDs was found to be below 8 nm only. Carbon black, lamp black, and candle soot were used by Wang et al. (2011b) for the generation of CQDs.

Alves et al. (2018) synthesized grapheme TiO_2-QDs via nanoemulsification. They used different precursors of carbon (GO, Triton-X, n-heptane, OLA, OA) and titanium propoxide as precursors of TiO_2. The MW exposure (300 W) was given to get QDs of globular shape with 3.3 nm.

Li et al. (2018) prepared S, N-carbon QDs under MW irradiation for 7 min. They used thiourea as the source of dopant (S, N). Later, they used as-prepared QDs for the reduction of carbon dioxide. Jusuf et al. (2018) made use of eggshell for preparing CQDs under MW irradiation (560 W) for 2 min CQDs and used these QDs in the degradation of pollutants. It was reported that as-prepared CQDs were 3.88 nm in diameter. Yang et al. (2018) used xylan and ammonium hydroxide as a carbon-precursor and source of dopant (N) to prepare fabricate nitrogen-doped CQDs under an MW approach (200 W) for 10 min. A change in color of the solution was observed from dull yellow to brown.

7.6 Recent developments

There has been rapid progress in the field of MW-assisted synthesis of different QDs and their varied applications in last few decades. Some recent advances are summarized in Table 7.1.

TABLE 7.1 Synthesis of quantum dots under microwave irradiation.

Quantum dots	Size (nm)	Applications	References
CdTe	2.6–3.5	Ratiometric fluorescence sensor	Amiri and Hosseini (2020)
$CuInGaSe_2$	10	Ultrasonic spray system	Mubiayi et al. (2020)
SnO_2	1–1.5	Planar perovskite solar cells	Xu et al. (2021)
Graphene	3.78	Photocatalytic degradation of dyes	Van Tam et al. (2019)
Boron and nitrogen-rich graphitic	2	Fluorescence of photosynthetic pigments	Budak et al. (2020)
Graphitic carbon nitride	<10	Photocatalytic removal of heavy metals	Shorie et al. (2019)
Sulfur dots	3.58–4.00	Photoluminescence	Hu et al. (2020)
Niobium pentoxide	4	Photocatalytical processes	Nakagomi et al. (2019)
Carbon quantum dots	2	Photocatalytic degradation of synthetic dyes.	Zhang et al. (2020)
Nitrogen doped carbon	4.5	Fluorescence detection	Du et al. (2019)
Fe–BiOBr–N	12.93–8.43	Photocatalytic properties	Lopez-Velazquez et al. (2021)

7.7 Conclusion

This chapter highlights the generation of QDs by MW-assisted synthesis. These QDs have found various applications in varied fields such as sensors, LED, photocatalyst, solar cells, biomedicals (drug target delivery, cancer therapy, biolabeling, bioimaging, etc.). One can control/modify the parameter of QDs. This technique has many other advantages over conventional methods. The MW process has also been used in combination with solvothermal, ultrasound, and hydrothermal methods for a better yield and within a limited time, that is, within minutes or sometimes even in seconds. The use of MW technique has great potential in providing uniform and homogeneous QDs and it will prove to be an asset in the years to come.

References

Abd Elhamid, A.M., Aboulfotouh, A.M., Hafez, M.A., Azzouz, I.M., 2018. Structural effect of Ni-Cu catalysts for graphene growth by pulsed laser deposition. Thin Solid. Films 653, 93–100.

Abolghasemi, R., Rasuli, R., Alizadeh, M., 2019. Microwave-assisted growth of high-quality CdSe quantum dots and its application as a sensitizer in photovoltaic cells. Mater. Today Commun. 22. Available from: https://doi.org/10.1016/j.mtcomm.2019.100827.

Agranovich, I.P.B., Katz, G., Bezman, D., Feldman, Y., 2017. Microwave dielectric spectroscopy study of water dynamics in normal and contaminated raw bovine milk. Colloids Surf. B 154, 391–396.

Alehdaghi, H., Marandi, M., Molaei, M., Irajizad, A., Taghavinia, N., 2014. Facile synthesis of gradient alloyed $Zn_xCd_{1-x}S$ nanocrystals using a microwave-assisted method. J. Alloy Comp. 586, 380–384.

Alehdaghi, H., Assar, E., Azadegan, B., Baedi, J., Mowlavi, A.A., 2020. Investigation of optical and structural properties of aqueous CdS quantum dots under gamma irradiation. Radiat. Phys. Chem. 166. Available from: https://doi.org/10.1016/j.radphyschem.2019.108476.

Al-Harthi, A.M., Al-Marzouki, F., Elsayed, W., 2021. Development of highly luminescent and color-tunable $Zn_{1-x}Pm_xTe$ QDs synthesized using 4, 4-bis-N-1-naphyl-N-phenylaminobiphenyl assisted microwave technique for solar cell applications. Optik 227. Available from: https://doi.org/10.1016/j.ijleo.2020.166031.

Al-Hazmi, F., Al-Ghamdi, A.A., Alshehrei, A., Alsayed, W., 2020. Synthesis, optical and luminescence behavior of $Zn_{1-x}Pa_xTe$ ($0 \leq x \leq 0.09$) ceramics prepared via poly[(9,9-bis(3′-(N, N-dimethylamino)propyl)-2,7-fluorene)-alt-2,7-(9,9-dioctylfluorene)] assisted microwave approach. Optik 202. Available from: https://doi.org/10.1016/j.ijleo.2019.163703.

Alibolandi, M., Abnous, K., Ramezani, M., Hosseinkhani, H., Hadizadeh, F., 2014. Synthesis of AS1411-aptamer-conjugated CdTe quantum dots with high fluorescence strength for probe labelingtumor cells. J. Fluoresc. 24 (5), 1519–1529.

Alvand, Z.M., Rajabi, H.R., Mirzaei, A., Masoumiasl, A., Sadatfaraji, H., 2019. Rapid and green synthesis of cadmium telluride quantum dots with low toxicity based on a plant-mediated approach after microwave and ultrasonic assisted extraction: synthesis, characterization, biological potentials and comparison study. Mater. Sci. Eng. C. 98, 535–544.

Alves, A.K., Frantz, A.C.S., Berutti, F.A., 2018. Microwave-assisted oleothermal synthesis of graphene-TiO_2 quantum dots for photoelectrochemical oxygen evolution reaction. FlatChem. 12, 26–34. Available from: https://doi.org/10.1016/j.flatc.2018.12.001.

Amiri, N.S., Hosseini, M.R.M., 2020. Application of ratiometric fluorescence sensor-based microwave-assisted synthesized CdTe quantum dots and mesoporous structured epitope-imprinted polymers for highly efficient determination of tyrosine phosphopeptide. Ana. Methods 12 (1), 63–72.

Asok, A., Deshlahra, P., Ramachandran, A.M., Kulkarni, A.R., 2018. Multifunctional photostable nanocomplex of ZnO quantum dots and avobenzone via the promotion of enolate tautomer. Glob. Chall. 2 (11). Available from: https://doi.org/10.1002/gch2.201800025.

Ayodhya, D., Veerabhadram, G., 2018. Microwave-assisted synthesis, characterization and photoluminescence interaction studies of undoped, Zr^{2+}, Rh^{3+} and Pd^{2+} doped ZnS quantum dots. Mater. Discov. 12. Available from: https://doi.org/10.1016/j.md.2018.08.001.

Bajorowicz, B., Kobylanski, M.P., Go ła˛biewska, A., Nadolna, J., ZaleskaMedynska, A., Malankowska, A., 2018. Quantum dot-decorated semiconductor micro- and nanoparticles: a review of their synthesis, characterization and application in photocatalysis. Adv. Colloid Interface Sci. 256, 352–372.

Begum, S., Ahmaruzzaman, M., 2018. Green synthesis of SnO_2 quantum dots using Parkia speciosa Hassk pods extract for the evaluation of anti-oxidant and photocatalytic properties. J. Photochem. Photobiol. B: Biol. 184, 44–53.

Begum, S., Devi, T.B., Ahmaruzzaman, M., 2016. Surfactant mediated facile fabrication of SnO_2 quantum dots and their degradation behavior of humic acid. Mater. Lett. 185, 123–126.

Bekru, A.G., Zelekew, O.A., Andoshe, D.M., Sabir, F.K., Eswaramoorthy, R., 2021. Microwave-assisted synthesis of CuO Nanoparticles using cordiaafricana lam. leaf extract for 4-nitrophenol reduction. J. Nanotechnol. 2021. Available from: https://doi.org/10.1155/2021/5581621.

Bhattacharjee, A., Ahmaruzzaman, M., 2015. A novel and green process for the production of tin oxide quantum dots and its application as a photocatalyst for the degradation of dyes from aqueous phase. J. Colloid Interface Sci. 448, 130–139.

Bichpuria, P., Oudhia, A., 2016. Effective size control through solvents in microwave aided synthesis of GSH-CdTe quantum dots. IOSR J. Appl. Phy. 8 (4). Available from: https://doi.org/10.9790/4861-0804010105.

Budak, E., Aykut, S., Paşaoğlu, M.E., Ünlü, C., 2020. Microwave assisted synthesis of boron and nitrogen rich graphitic quantum dots to enhance fluorescence of photosynthetic pigments. Mater. Today Communi. 24. Available from: https://doi.org/10.1016/j.mtcomm.2020.100975.

Butova, V.V., Budnyk, A.P., Lastovina, T.A., Kravtsova, A.N., Soldatov, A.V., 2017. Rapid microwave synthesis of CdS quantum dots stabilized with 4,4' -bipyridine and dioctyl sodium sulfosuccinate. Mendeleev Commun. 27 (3), 313–314.

Cao, H., Tang, M., Wang, X., Shi, W., 2020. Facile and rapid synthesis of color-tunable molybdenum oxide quantum dots as a versatile probe for fluorescence imaging and environmental monitoring. Analyst 145. Available from: https://doi.org/10.1039/d0an01510e.

Chaudhary, G.R., Bansal, P., Mehta, S.K., 2014. Recyclable CuS quantum dots as heterogeneous catalyst for Biginelli reaction under solvent free conditions. Chem. Eng. J. 243, 217–224.

Chen, S., Liu, J.W., Chen, M.L., Chen, X.W., Wang, J.H., 2012. Unusual emission transformation of graphene quantum dots induced by self-assembled aggregation. Chem. Commun. 48, 7637–7639.

Chen, S., Hai, X., Xia, C., Chen, X.W., Wang, J.H., 2013. Preparation of excitationindependent photoluminescent graphene quantum dots with visible-light excitation/emission for cell imaging. Chem. Eur. J. 19, 15918–15923.

Chen, X., Li, L., Lai, Y., Yan, J., Tang, Y., Wang, X., 2015a. Microwave-assisted synthesis of glutathione-capped CdTe/CdSe near-infrared quantum dots for cell imaging. Int. J. Mol. Sci. 16, 11500–11508.

Chen, J., Xiao, A., Zhang, Z., Yu, Y., Yan, Z., 2015b. The synthesis and modification of CdTe/CdS core shell quantum dots. Spectrochim. Acta Part. A: Mole. Biomole. Spectrosc. 151, 506–509.

Dong, C., Ren, J., 2012. Water-soluble mercaptoundecanoic acid (MUA)-coated CdTe quantum dots: one-step microwave synthesis, characterization and cancer cell imaging. Luminescence 27 (3), 199–203.

Du, J., Li, X., Wang, S., Wu, Y., Hao, X., Xu, C., et al., 2012. Microwave-assisted synthesis of highly luminescent glutathione-capped Zn 1 − x Cd x Te alloyed quantum dots with excellent biocompatibility. J. Mater. Chem. 22 (22), 11390–11395.

Du, F., Cheng, Z., Lai, Z., Ruan, G., Zhao, C., 2019. Red-emissive nitrogen doped carbon quantum dots for highly selective and sensitive fluorescence detection of the alachlor herbicide in soil samples. N. J. Chem. 43 (47), 18695–18701.

Duan, J., Song, L., Zhan, J., 2009. One-pot synthesis of highly luminescent CdTe quantum dots by microwave irradiation reduction and their Hg^{2+}-sensitive properties. Nano Res. 2 (1), 61–68.

Duran, G.M., Plata, M.R., Zougagh, M., Contento, A.M., Ríos, A., 2014. Microwave-assisted synthesis of water soluble thiol capped CdSe/ZnS quantum dots and its interaction with sulfonylurea herbicides. J. Colloid Interface Sci. 428, 235–241.

Ebrahimi, S., Souri, D., 2020. Green synthesis and optical properties of ZnSe:Cu@ZnS core/shell nanocrystals fabricated by new photochemical microwave-assisted colloidal method. J. Alloy. Comp. 840. Available from: https://doi.org/10.1016/j.jallcom.2020.155712.

Felix, S., Chakkravarthy, R.B.P., Grace, A.N. 2015. Microwave assisted synthesis of copper oxide and its application in electrochemical sensing. IOP Conf. Ser.: Mater. Sci. Eng., 73, doi: 10.1088/1757-899x/73/1/012115.

Fitzmorris, R.C., Oleksak, R.P., Zhou, Z., Mangum, B.D., Kurtin, J.N., Herman, G.S., 2015. Structural and optical characterization of $CuInS_2$ quantum dots synthesized by microwave-assisted continuous flow methods. J. Nanopart. Res. 17 (7). Available from: https://doi.org/10.1007/s11051-015-3123-1.

Fregnaux, M., Dalmasso, S., Durand, P., Zhang, Y., Gaumet, J.-J., Laurenti, J.-P., 2013. Fast-grown CdS quantum dots: single-source precursor approach vs microwave route. Mater. Chem. Phys. 142 (1), 52–60.

Giguere, R.J., Bray, T.L., Duncan, S.M., Majetich, G., 1986. Application of commercial microwave ovens to organic synthesis. Tetrahedron Lett. 27, 4945–4948.

Han, H., Francesco, G.D., Maye, M.M., 2010. Size control and photophysical properties of quantum dots prepared via a novel tunable hydrothermal route. J. Phys. Chem. C. 114 (45), 19270–19277.

He, Y., Lu, H.-T., Sai, L.-M., Lai, W.-Y., Fan, Q.-L., Wang, L.-H., et al., 2006. Synthesis of CdTe nanocrystals through program process of microwave irradiation. J. Phys. Chem. B. 110 (27), 13352–13356.

He, Y., Lu, H.T., Sai, L.M., Su, Y.Y., Hu, M., Fan, C.H., et al., 2008. Microwave synthesis of water-dispersed CdTe/CdS/ZnS core-shell-shell quantum dots with excellent photostability and biocompatibility. Adv. Mater. 20 (18), 3416–3421.

He, X., Demchenko, I.N., Stolte, W.C., van Buuren, A., Liang, H., 2012. Synthesis and transformation of Zn-doped PbS quantum dots. J. Phys. Chem. C. 116 (41), 22001–22008.

He, J., Zhou, L., Liu, J., Yang, L., Zou, L., Xiang, J., et al., 2017. Modulation of surface structure and catalytic properties of cerium oxide nanoparticles by thermal and microwave synthesis techniques. App. Surf. Sci. 402, 469–477.

He, L., Yang, L., Liu, B., Zhang, J., Zhang, C., Liu, S., et al., 2019. One-pot synthesis of color-tunable copper doped zinc sulfide quantum dots for solid-state lighting devices. J. Alloy. Comp. 787, 537–542.

Hong, M., Xuan, T., Liu, J., Jiang, Z., Chen, Y., Chen, X., et al., 2015. Air-exposing microwave-assisted synthesis of $CuInS_2$/ZnS quantum dots for silicon solar cells with enhanced photovoltaic performance. RSC Adv. 5 (124), 102682–102688.

Hu, H., Zhao, Z., Zhou, Q., Gogotsi, Y., Qiu, J., 2012. The role of microwave absorption on formation of graphene from graphite oxide. Carbon 50, 3267–3273.

Hu, Z., Dai, H., Wei, X., Su, D., Wei, C., Chen, Y., et al., 2020. 49.25% efficient cyan emissive sulfur dots via a microwave-assisted route. RSC Adv. 10 (29), 17266–17269.

Huang, L., Han, H., 2010. One-step synthesis of water-soluble ZnSe quantum dots via microwave irradiation. Mater. Lett. 64, 1099–1101.

Jusuf, B.N., Sambudi, N.S., Isnaeni, Samsuri, S., 2018. Microwave-assisted synthesis of carbon dots from eggshell membrane ashes by using sodium hydroxide and their usage for degradation of methylene blue. J. Environ. Chem. Eng. 6, 7426–7433.

Kanwal, S., Traore, Z., Zhao, C., Su, X., 2010. Enhancement effect of CdTe quantum dots–IgG bioconjugates on chemiluminescence of luminol–H_2O_2 system. J. Luminescence. 130 (10), 1901–1906.

Kim, D., Kim, J., 2016. Synthesis of CdZnTe quantum dots in the aqueous phase by microwave irradiation. J. Nanosci. Nanotechnol. 16 (8), 8411−8414.

Kim, H.S., Yoon, K.B., 2014. Preparation and characterization of CdS and PbS quantum dots in zeolite Y and their applications for nonlinear optical materials and solar cell. Coord. Chem. Rev. 263, 239−256.

Kominkova, M., Milosavljevic, V., Vitek, P., Polanska, H., Cihalova, K., Dostalova, S., et al., 2017. Comparative study on toxicity of extracellularly biosynthesized and laboratory synthesized CdTe quantum dots. J. Biotech. 241, 193−200.

Kumar, R., Kim, H.-J., Park, S., Srivastava, A., Oh, I.-K., 2014. Graphene-wrapped and cobalt oxide-intercalated hybrid for extremely durable super-capacitor with ultrahigh energy and power densities. Carbon 79, 192−202.

Kumar, R., Joanni, E., Singh, R.K., Singh, D.P., Moshkalev, S.A., 2018. Recent advances in the synthesis and modification of carbon-based 2D materials for application in energy conversion and storage. Prog. Energy Combust. Sci. 67, 115−157.

Le Houx, N., Pourroy, G., Camerel, F., Comet, M., Spitzer, D., 2009. WO_3 nanoparticles in the 5 − 30 nm range by solvothermal synthesis under microwave or resistive heating. J. Phys. Chem. C. 114 (1), 155−161.

Lee, J., Yang, C.S., Chang, C.T., Liu, J., Chou, W.C., Lai, C.M., et al., 2004. Analysis of size distributions of type II ZnTe/ZnSe quantum dots. Phys. Status Solidi. 241, 3532−3543.

Lehnen, T., Schläfer, J., Mathur, S., 2014. Rapid microwave synthesis of CeO_2 quantum dots. Z. Anorg. Allg. Chem. 640 (5), 819−825.

Li, J.J., Wang, Y.A., Guo, W., Keay, J.C., Mishima, T.D., Johnson, M.B., et al., 2003. Large-scale synthesis of nearly monodisperse CdSe/CdS core/shell nanocrystals using air-stable reagents via successive ion layer adsorption and reaction. J. Am. Chem. Soc. 125 (41), 12567−12575.

Li, L.L., Ji, J., Fei, R., Wang, C.Z., Lu, Q., Zhang, J.R., et al., 2012. A facile microwave avenue to electrochemiluminescenttwo-color graphene quantum dots. Adv. Funct. Mater. 22, 2971−2979.

Li, M., Wang, M., Zhu, L., Li, Y., Yan, Z., Shen, Z., et al., 2018. Facile microwave assisted synthesis of N-rich carbon quantum dots/dual-phase TiO_2heterostructured nanocomposites with high activity in CO_2 photoreduction. Appl.Catal. B: Environ. 231, 269−276.

Lim, S.Y., Shen, W., Gao, Z., 2015. Carbon quantum dots and their applications. Chem. Soc. Rev. 44, 362−381.

Liu, X., Pan, L., Chen, T., Li, J., Yu, K., Sun, Z., et al., 2013. Visible light photocatalytic degradation of methylene blue by SnO_2 quantum dots prepared via microwave-assisted method. Catal. Sci. Technol. 3, 1805−1809.

Liu, X., Pan, L., Lv, T., Sun, Z., 2014. CdS sensitized TiO_2 film for photocatalytic reduction of Cr (VI) by microwave-assisted chemical bath deposition method. J. Alloy. Comp. 583, 390−395.

Liu, A., Jin, H., Li, J., Chen, L., Zheng, H., Mao, X., et al., 2019. One-step facile synthesis of PbS quantum dots/Pb $(DMDC)_2$ hybrids and their application as a low-cost SERS substrate. J. Raman Spectrosc. 50, 1445−1451.

Lopez-Velazquez, K., Guzman-Mar, J.L., Hernández-Ramírez, A., Gonzalez-Juarez, E., Villanueva-Rodriguez, M., 2021. Synthesis of Fe−BiOBr−N by microwave-assisted solvothermal method: characterization and evaluation of its photocatalytic properties. Mater. Sci. Semiconduc. Process. 123, 105499.

Lu, T., Pan, L., Li, H., Zhu, G., Lv, T., Liu, X., et al., 2011. Microwave-assisted synthesis of graphene−ZnO nanocomposite for electrochemical supercapacitors. J. Alloy. Compds 509 (18), 5488−5492.

Luo, J., Wei, H., Li, F., Huang, Q., Li, D., Luo, Y., et al., 2014. Microwave assisted aqueous synthesis of core-shell $CdSe_xTe_{1-x}$-CdS quantum dots for high performance sensitized solar cells. Chem. Commun. 50, 3464–3466.

Ma, R., Zhou, P.-J., Zhan, H.-J., Chen, C., He, Y.-N., 2013. Optimization of microwave-assisted synthesis of high-quality ZnSe/ZnS core/shell quantum dots using response surface methodology. Opt. Commun. 291, 476–481.

Malankowska, A., Kulesza, D., Sowik, J., Cavdar, O., Klimczuk, T., Trykowski, G., et al., 2020. The effect of $AgInS_2$, SnS, CuS_2, Bi_2S_3 quantum dots on the surface properties and photocatalytic activity of QDs-sensitized TiO_2 composite. Catalysts 10 (4), 403.

Mao, L.-H., Zhang, Q.-H., Zhang, Y., Wang, C.-F., Chen, S., 2014. Construction of highly luminescent CdTe/CdS@ZnS−SiO_2 quantum dots as conversion materials toward excellent color-rendering white-light-emitting diodes. Ind. Eng. Chem. Res. 53 (43), 16763–16770.

Mathew, M.E., Mohan, J.C., Manzoor, K., Nair, S.V., Tamura, H., et al., 2010. Folate conjugated carboxymethyl chitosan–manganese doped zinc sulphide nanoparticles for targeted drug delivery and imaging of cancer cells. Carbohydr.Polym. 80 (2), 442–448.

Mehrjoo, M., Molaei, M., Karimipour, M., 2017. A novel process for synthesis of CdSe/ZnS core-shell QDs and their application for the methyl orange (MO) degradation. Mater. Chem. Phys. 201, 165–169.

Mir, I.A., Radhakrishanan, V.S., Rawat, K., Prasad, T., Bohidar, H.B., 2018a. Bandgap tunable AgInS based quantum dots for high contrast cell imaging with enhanced photodynamic and antifungal applications. Sci. Rep. 8 (1). Available from: https://doi.org/10.1038/s41598-018-27246-y.

Mir, I.A., Das, K., Akhter, T., Ranjan, R., Patel, R., Bohidar, H.B., 2018b. Eco-friendly synthesis of $CuInS_2$ and $CuInS_2$@ZnS quantum dots and their effect on enzyme activity of lysozyme. RSC Adv. 8 (53), 30589–30599.

Mirahmadi, F.S., Marandi, M., Karimipour, M., Molaei, M., 2020. Microwave activated synthesis of Ag_2S and Ag_2S@ ZnS nanocrystals and their application in well-performing quantum dot sensitized solar cells. Sol. Energy 202, 155–163.

Moghaddam, M.M., Baghbanzadeh, M., Keilbach, A., Kappe, C.O., 2012. Microwave assisted synthesis of CdSe quantum dots: can the electromagnetic field influence the formation and quality of the resulting nanocrystals? Nanoscale. 4, 7435–7442.

Mohanta, D., Ahmaruzzaman, M., 2020. Biogenic synthesis of SnO_2 quantum dots encapsulated carbon nanoflakes: an efficient integrated photocatalytic adsorbent for the removal of bisphenol A from aqueous solution. J. Alloy. Compd. 828. Available from: https://doi.org/10.1016/j.jallcom.2020.154093.

Molaei, M., Hasheminejad, H., Karimipour, M., 2015. Synthesizing and investigating photoluminescence properties of CdTe and CdTe@CdS core-shell quantum dots (QDs): a new and simple microwave activated approach for growth of CdS shell around CdTe core. Electron. Mater. Lett. 11 (1), 7–12.

Molaei, M., Bardsiri, F.S., Bahador, A.R., Karimipour, M., 2016. One-pot microwave assisted approach for synthesis of CdSe/CdS core-shell quantum dots (QDs) and investigating optical properties. Mod. Phys. Lett. B. 30. Available from: https://doi.org/10.1142/S0217984916500743.

Molaei, M., Karimipour, M., Abbasi, S., Khanzadeh, M., Dehghanipour, M., 2020. PbS and PbS/CdS quantum dots: synthesized by photochemical approach, structural, linear and nonlinear response properties, and optical limiting. J. Mater. Res. 35, 401–409.

Mubiayi, K.P., Neto, D.M.G., Morais, A., Nogueira, H.P., de Almeida Santos, T.E., Mazon, T., et al., 2020. Microwave assisted synthesis of $CuInGaSe_2$ quantum dots and spray deposition

of their composites with graphene oxide derivatives. Mater. Chem. Phys. 242. Available from: https://doi.org/10.1016/j.matchemphys.2019.122449.

Nakagomi, F., Cerruti, S.E., de Freitas, M.R., Neto, E.S.F., de Andrade, F.V., Siqueira, G.O., 2019. Niobium pentoxide produced by a novel method microwave assisted combustion synthesis. Chem. Phys. Lett. 729, 37–41.

Nazzal, A.Y., Qu, L., Peng, X., Xiao, M., 2003. Photoactivated CdSe nanocrystals as nanosensors for gases. Nano Lett. 3, 819–822.

Nethravathi, C., Rajamathi, J.T., Rajamathi, M., 2019. Microwave-assisted synthesis of porous aggregates of CuS nanoparticles for sunlight photocatalysis. ACS Omega 4 (3), 4825–4831.

Pang, G., Chen, S., Koltypin, Y., Zaban, A., Feng, S., Gedanken, A., 2001. Controlling the particle size of calcined SnO_2 nanocrystals. Nano Lett. 1 (12), 723–726.

Parthibavarman, M., Sathishkumar, S., Jayashree, M., BoopathiRaja, R., 2019. Microwave assisted synthesis of pure and Ag doped SnO_2 quantum dots as novel platform for high photocatalytic activity performance. J. Clust. Sci. 30 (2), 351–363.

Peng, X., 2002. Green chemical approaches toward high-quality semiconductor nanocrystals. Chem. Eur. J. 8 (2), 334–339.

Peng, Z.A., Peng, X., 2001. Formation of high-quality CdTe, CdSe, and CdS nanocrystals using CdO as precursor. J. Am. Chem. Soc. 123, 183–184.

Pradhan, N., Peng, X., 2007. Efficient and color-tunable Mn-doped ZnSe nanocrystal emitters: control of optical performance via greener synthetic chemistry. J. Am. Chem. Soc. 129 (11), 3339–3347.

Qian, H., Li, L., Ren, J., 2005. One-step and rapid synthesis of high quality alloyed quantum dots (CdSe–CdS) in aqueous phase by microwave irradiation with controllable temperature. Mater. Res. Bull 40 (10), 1726–1736.

Radzi, N.M., Latif, A.A., Ismail, M.F., Liew, J.Y.C., Wang, E., Lee, H.K., et al., 2020. Q-switched fiber laser based on CdS quantum dots as a saturable absorber. Results Phys. 16. Available from: https://doi.org/10.1016/j.rinp.2020.103123.

Rangel-Mendez, J.R., Matos, J., Cházaro-Ruiz, L.F., González-Castillo, A.C., Barrios-Yáñez, G., 2018. Microwave-assisted synthesis of C-doped TiO_2 and ZnO hybrid nanostructured materials as quantum-dots sensitized solar cells. Appl. Surf. Sci. 434, 744–755.

Ren, F., Zhao, H., Vetrone, F., Ma, D., 2013. Microwave-assisted cation exchange toward synthesis of near-infrared emitting PbS/CdS core/shell quantum dots with significantly improved quantum yields through a uniform growth path. Nanoscale 05 (17), 7800–7804.

Ribeiro, D.S., de Souza, G.C., Melo, A., Soares, J.X., Rodrigues, S.S.M., Araújo, A.N., et al., 2017. Synthesis of distinctly thiol-capped CdTe quantum dots under microwave heating: multivariate optimization and characterization. J. Mater. Sci. 52 (6), 3208–3224.

Rodrigues, S.S.M., Ribeiro, D.S.M., Soares, J.X., Passos, M.L.C., Saraiva, M.L.M.F.S., Santos, J.L.M., 2017. Application of nanocrystalline CdTe quantum dots in chemical analysis: implementation of chemo-sensing schemes based on analytetriggered photoluminescence modulation. Coord. Chem. Rev. 330, 127–143.

Sai, L.-M., Kong, X.Y., 2011. Microwave-assisted synthesis of water-dispersed CdTe/CdSe core/shell type II quantum dots. Nanoscale Res. Lett. 6. Available from: https://doi.org/10.1186/1556-276X-6-399.

Saravanan, R.S.S., Pukazhselvan, D., Mahadevan, C.K., 2012. Studies on the synthesis of cubic ZnS quantum dots, capping and optical–electrical characteristics. J. Alloy. Comp. 517, 139–148.

Shaheen, A., Arif, R., Sharma, D., Singh, T., 2020. Microwave-mediated synthesis of surface-active ionic liquid-capped ZnS quantum dots: morphological studies and their applicability

for fluorometric sensing of ascorbic acid. Appl. Phys. A. 126 (10). Available from: https://doi.org/10.1007/s00339-020-03968-7.

Shahid, R., Toprak, M.S., Muhammed, M., 2012. Microwave-assisted low temperature synthesis of wurtzite ZnS quantum dots. J. Solid. State Chem. 187, 130–133.

Shen, Y., Li, L., Lu, Q., Ji, J., Fei, R., Zhang, J., et al., 2012. Microwave-assisted synthesis of highly luminescent CdSeTe@ZnS-SiO_2 quantum dots and their application in the detection of Cu(II). Chem. Commun. 48, 2222–2224.

Shi, L., Lin, H., 2010. Facile fabrication and optical property of hollow SnO_2 spheres and their application in water treatment. Langmuir 26 (24). Available from: https://doi.org/10.1021/la103769d.

Shin, Y., Lee, J., Yang, J., Park, J., Lee, K., Kim, S., et al., 2014. Mass production of graphene quantum dots by one-pot synthesis directly from graphite in high yield. Small 10, 866–870.

Shorie, M., Kaur, H., Chadha, G., Singh, K., Sabherwal, P., 2019. Graphitic carbon nitride QDs impregnated biocompatible agarose cartridge for removal of heavy metals from contaminated water samples. J. Hazard. Mater. 367, 629–638.

Singh, M.K., Mathpal, M.C., Agarwal, A., 2012. Optical properties of SnO_2 quantum dots synthesized by laser ablation in liquid. Chem. Phys. Lett. 536, 87–91.

Singh, S., Sabri, Y.M., Jampaiah, D., Selvakannan, P.R., Nafady, A., Kandjani, A.E., et al., 2017. Easy, one-step synthesis of CdTe quantum dots via microwave irradiation for fingerprinting application. Mater. Res. Bullet. 90, 260–265.

Song, H., Lee, K.-H., Jeong, H., Um, S.H., Han, G.-S., Jung, H.S., et al., 2013. A simple self-assembly route to single crystalline SnO_2 nanorod growth by oriented attachment for dye sensitized solar cells. Nanoscale. 5, 1188–1194.

Soren, S., Jena, S.R., Samanta, L., Parhi, P., 2015. Antioxidant potential and toxicity study of the cerium oxide nanoparticles synthesized by microwave-mediated synthesis. App. Biochem. Biotechnol. 177 (1), 148–161.

Soumya, S., Sheemol, V.N., Amba, P., Mohamed, A.P., Ananthakumar, S., 2018. Sn and Ag doped ZnO quantum dots with PMMA by in situ polymerization for UV/IR protective, photochromic multifunctional hybrid coatings. Sol. Energy Mater. Sol. Cell 174, 554–565.

Van Tam, T., Altahtamouni, T.M., Le Minh, V., Ha, H.K.P., Chung, N.T.K., Van Thuan, D., 2019. One-pot microwave-assisted green synthesis of amine-functionalized graphene quantum dots for high visible light photocatalytic application. C R Chim. 22 (11–12), 822–828.

Wang, Y., Tang, Z., Correa-Duarte, M.A., Pastoriza-Santos, I., Giersig, M., Kotov, N.A., et al., 2004. Mechanism of strong luminescence photoactivation of citrate-stabilized water-soluble nanoparticles with CdSe cores. J. Phys. Chem. B. 108, 15461–15469.

Wang, C., Ma, Q., Su, X., 2008. Synthesis of CdTe nanocrystals with mercaptosuccinic acid as stabilizer. J. Nanosci. Nanotechnol. 8 (9), 4408–4414.

Wang, H., Liang, Q., Wang, W., An, Y., Li, J., Guo, L., 2011a. Preparation of flower-like SnO_2 nanostructures and their applications in gas-sensing and lithium storage. Cryst. Growth Des. 11 (7), 2942–2947.

Wang, Q., Zheng, H., Long, Y., Zhang, L., Gao, M., Bai, W., 2011b. Microwavehydrothermal synthesis of fluorescent carbon dots from graphite oxide. Carbon. 49, 3134–3140.

Wang, H.E., Xi, L.J., Ma, R.G., Lu, Z.G., Chung, C.Y., Bello, I., et al., 2012. Microwave-assisted hydrothermal synthesis of porous SnO_2 nanotubes and their lithiumion storage properties. J. Solid. State Chem. 190, 104–110.

Wang, J., Lu, Y., Peng, F., Zhong, Y., Zhou, Y., Jiang, X., et al., 2013. Photostable water-dispersible NIR-emitting CdTe/CdS/ZnS core–shell–shell quantum dots for high-resolution tumor targeting. Biomaterials 34 (37), 9509–9518.

Wang, S., Kershaw, S.V., Li, G., Leung, M.K., 2015a. The self-assembly synthesis of tungsten oxide quantum dots with enhanced optical properties. J. Mater. Chem. C. 3 (14), 3280−3285.

Wang, H., Yuan, X., Zeng, G., Wu, Y., Liu, Y., Jiang, Q., et al., 2015b. Three dimensional graphene-based materials: synthesis and applications from energy storage and conversion to electrochemical sensor and environmental remediation. Adv. Colloid Interface Sci. 221, 41−59.

Xiao, L., Shen, H., von Hagen, R., Pan, J., Belkoura, L., Mathur, S., 2010. Microwave assisted fast and facile synthesis of SnO_2 quantum dots and their printing applications. Chem. Commun. 46, 6509−6511.

Xu, Z., Jiang, Y., Li, Z., Chen, C., Kong, X., Chen, Y., et al., 2021. Rapid microwave-assisted synthesis of SnO_2 quantum dots for efficient planar perovskite solar cells. ACS Appl. Energy Mater. 4 (2), 1887−1893.

Xuan, T., Wang, X., Zhu, G., Li, H., Pan, L., Sun, Z., 2013. One-step microwave-assisted synthesis of water soluble CdSe quantum dots for white light-emitting diodes with excellent color rendering. J. Alloy. Comp. 558, 105−108.

Yang, Y., Liang, S., Yu, X., Wang, Q., 2012. Microwave synthesis of Cu-doped ternary ZnCdS quantum dots with composition-controllable photoluminescence. Wuhan. Univ. J. Nat. Sci. 17 (3), 217−222.

Yang, F., Xu, Z., Wang, J., Zan, F., Dong, C., Ren, J., 2013. Microwave-assisted aqueous synthesis of new quaternary-alloyed CdSeTeS quantum dots; and their bioapplications in targeted imaging of cancer cells. Luminescence. 28, 392−400.

Yang, P., Zhu, Z., Chen, M., Chen, W., Zhou, X., 2018. Microwave-assisted synthesis of xylan-derived carbon quantum dots for tetracycline sensing. Opt. Mater. 85, 329−336.

Zhan, H., Zhou, P., Pan, K., He, T., He, X., Zhou, C., et al., 2013. One-pot aqueous-phase synthesis of ultra-small CdSe/CdS/CdZnS core−shell−shell quantum dots with high-luminescent efficiency and good stability. J. Nanopart. Res. 15 (6). Available from: https://doi.org/10.1007/s11051-013-1680-8.

Zhang, X., Liu, Z., 2012. Recent advances in microwave initiated synthesis of nanocarbon materials. Nanoscale. 4, 707−714.

Zhang, T., Jin, J., Yang, C., Peng, H., Lai, L., Han, J., et al., 2012a. Microwave synthesis CdSe quantum dot clusters via ribonuclease A protein. Micro Nano Lett. 7 (12), 1289−1291.

Zhang, P., Hu, G.X., Bao, S.J., Guo, J., Lei, C., Cai, C.J., et al., 2012b. One step microwave synthesis and magnetic properties of Co_3O_4 octahedrons. Mater. Lett. 83, 195−197.

Zhang, H., Wang, H., Wang, Y., Xin, B., 2020. Controlled synthesis and photocatalytic performance of biocompatible uniform carbon quantum dots with microwave absorption capacity. Appl. Surf. Sci. 512. Available from: https://doi.org/10.1016/j.apsusc.2020.145751.

Zheng, X., Weng, J., Hu, B., 2010. Microwave-assisted synthesis of mesoporous CdS quantum dots modified by oleic acid. Mater. Sci.Semicond. Process. 13 (3), 217−220. Available from: https://doi.org/10.1016/j.mssp.2010.10.012.

Zhou, X., Shi, J., Liu, Y., Su, Q., Zhang, J., Du, G., 2014. Microwave irradiation synthesis of Co_3O_4 quantum dots/graphene composite as anode materials for Li-ion battery. Electrochim. Acta 143, 175−179.

Zhu, M.-Q., Gu, Z., Fan, J.-B., Xu, X.-B., Cui, J., Liu, J.-H., et al., 2009. Microwave-mediated nonaqueous synthesis of quantum dots at moderate temperature. Langmuir 25 (17), 10189−10194.

Zhu, D., Li, W., Wen, H.-M., Chen, Q., Ma, L., Hu, Y., 2014. Microwave-assisted aqueous synthesis of Mn-doped ZnS quantum dots and their room-temperature phosphorescence detection of indapamide. Anal. Methods 6 (18), 7489−7495.

Zhu, L., Wang, M., Kwan Lam, T., Zhang, C., Du, H., Li, B., et al., 2016. Fast microwave-assisted synthesis of gas-sensing SnO_2 quantum dots with high sensitivity. Sensor. Actuator. B Chem. 236, 646–653.

Ziegler, J., Merkulov, A., Grabolle, M., Resch-Genger, U., Nann, T., 2007. High-quality ZnS shells for CdSe nanoparticles: rapid microwave synthesis. Langmuir 23, 7751–7759.

This page intentionally left blank

Chapter 8

Sonochemical synthesis of quantum dots

Garima Ameta[1] **and Seema Kothari**[2]
[1]*Department of Chemistry, M. L. S. University, Udaipur, Rajasthan, India,* [2]*Department of Chemistry, PAHER University, Udaipur, Rajasthan, India*

8.1 Introduction

Sound frequencies beyond the upper audible limit of human hearing are normally categorized as ultrasound. The frequency range of ultrasound that has been used sonochemistry is 16−3000 kHz. Ultrasonic irradiation has been widely used in chemical synthesis and it has become an interesting field of research. When an ultrasonic wave passes through a liquid medium, than a large number of microbubbles are formed, they grow, and finally collapse in a very short time, which is of the order of a few microseconds. This is called ultrasonic cavitation (Fig. 8.1).

Extremely high pressures and temperatures are generated during the process of acoustic cavitation, which initiates a number of chemical and physical effects, such as microjetting, shock waves, shear forces, microstreaming, and generation of different radicals. Sonochemistry finds a variety of applications such as drug encapsulation and delivery, food science, electrochemistry, material engineering, synthesis of nanoparticles, etc.

Bang and Suslick (2010) have reviewed the application of ultrasound in the synthesis of nanostructured materials. Sonochemical approach can provide control morphology over size. Cavitation-induced sonochemistry with the temperature and pressures provides hot spots inside the bubbles of the order of ∼5000 K, and ∼1000 bar, respectively. These extraordinary conditions permit the synthesis of a wide range of nanostructured materials, particularly quantum dots.

The field of sonochemistry has been excellently delivered by various workers over time (Einhorn et al., 1989; Pestman et al., 1994; Mason, 1999; Suslick and Flannigan, 2008; Ameta et al., 2018).

The high energy and pressure for chemical reaction is generated by collapsing bubbles. This can be divided into three regions (Fig. 8.2):

Quantum Dots. DOI: https://doi.org/10.1016/B978-0-12-824153-0.00008-2

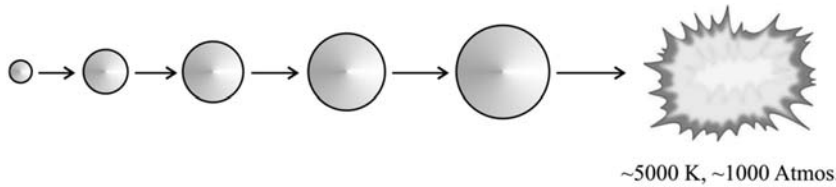

FIGURE 8.1 Growth and implosion of a bubble. *Adapted from Ameta et al., Sonochemistry: An Emerging Green Technology, Apple Academic Press, New Jersey, 2018, with permission.*

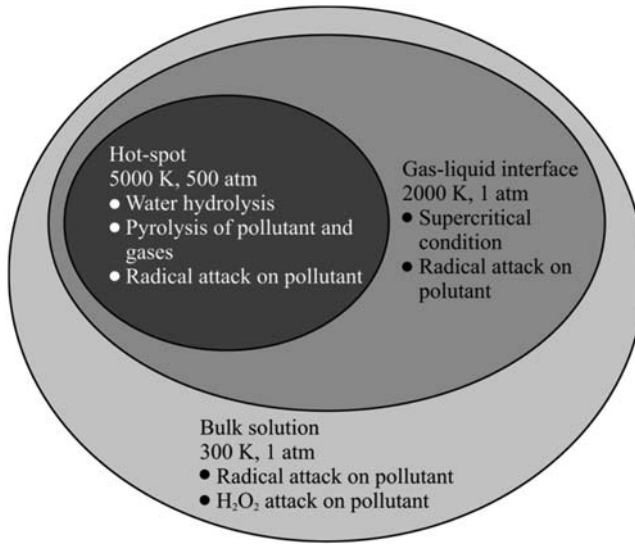

FIGURE 8.2 Reaction zone in cavitation process (Chowdhury and Viraraghavan, 2009). *Adapted from Chowdhury, P.; Viraraghavan, T. Sonochemical degradation of chlorinated organic compounds, phenolic compounds and organic dyes—a review. Sci. Total. Environ., 2009, 407 (8), 2474—2492. With permission.*

1. First region is a hot spot region or thermolytic center, which has a quite high temperature of 5000 K and a high pressure of 500 atm during the collapse of a bubble or cavitation.
2. Second region is a interfacial region between the bulk liquid cavitation bubble.
3. Third region is a bulk region. Here, temperature is almost equal to room temperature due to process of adiabatic cavitation.

8.1.1 Advantages

There are some advantages of using the sonochemical route for the synthesis of quantum dots. These include:

1. It improves the reaction rate.
2. It involves high energies and pressures in a short time.
3. No additives are required.
4. It reduces the number of reaction steps.
5. It provides uniform size distribution, higher surface area, with improved phase purity.
6. It is a solvent-free synthesis producing less waste.

8.1.2 Disadvantage

The sonochemical method has a disadvantage as:

1. It affords relatively low yield of the product.

8.2 Instrumentation

Various sources are used for generating ultrasound.

1. The first ultrasound transducer was developed by Galton (1883), now known as Galton's whistle (Fig. 8.3A). It is a brass tube and a jet of gas is passed through an orifice into a resonating cavity.
2. Liquid whistle is also used for this purpose (Fig. 8.3B). Cavitation is generated in this transducer through motion of a liquid in place of gas.
3. Piezoelectric transducers are also used for generation of ultrasound (Fig. 8.3C). A transducer is based on electrical and mechanical vibrations via piezoelectric effect. There are many materials that have a range of piezoelectric effects. Some examples of natural materials are quartz, topaz. tourmaline, belemnite, etc., while synthetic materials are bismuth ferrite, lithium tantalite, $Ba_2Na\ Nb_5\ O_5$, $Pb_2KNb_5O_{15}$, etc.
4. Cup horn (Fig. 8.3D). It is a high intensity ultrasonic bath. In this transducer, indirect sonication technology is involved. This cup horn sonication is effective, where the liquid sample is higher in volume.

8.3 Synthesis of quantum dots

8.3.1 Metals

Liu et al. (2011) prepared highly fluorescent and water-soluble gold nanoclusters (AuNCs) and Au@AgNCs emitting near-infrared via a sonochemical approach. It was reported that yellow emission was observed from Au@AgNCs. It was revealed that as-prepared Au NCs could be successfully applied in the determination of copper ions in a wider of range of concentration with a lower of limit NCs. A facile and fast sonochemical route was proposed by Wang et al. (2017) to synthesize fluorescent AgNCs. They used glutathione (GSH) and hydrazine hydrate, respectively, as capping and reducing agent. It was revealed that

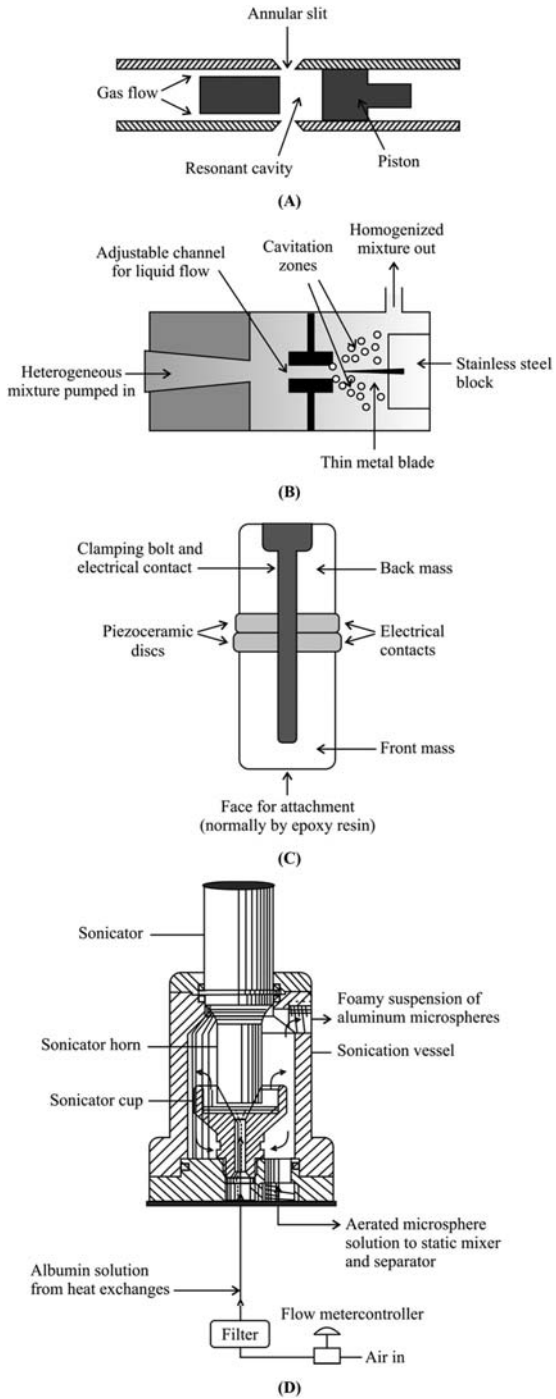

FIGURE 8.3 Various sources for ultrasound generation: (A) Galton whistle; (B) liquid whistle; (C) piezoelectric transducer; and (D) cup horn. *Adapted from Ameta et al., Sonochemistry: An Emerging Green Technology, Apple Academic Press, New Jersey, 2018, With Permission.*

AgNCs waweres formed quickly within 15 min in the presence of ultrasonic waves. As-prepared QDs show red fluorescence and good dispersion in aqueous solution. The size of AgNCs was found to be small enough ($\sim$2 nm). Use of GSH as protecting agent on the surface of these AgNCs provides high, photo-, and pH-stability. They designed a stable Ag nanoclusters-based nanosensor for detection of Pb^{2+} ions with high sensitivity and selectivity. The as-fabricated nanosensor can also be used as a probe for monitoring Pb^{2+} ions in living cells. It was proposed that these stable and fluorescent AgNCs can find potential applications for sensing and biolabeling.

Mallikarjuna et al. (2021) fabricated g-C_3N_4 and Ag-g-C_3N_4 composite structures by the ultrasonication method. It was reported that the silver quantum dots anchored to g-C_3N_4 structures may show better photocatalytic activities for dye degradation, H_2 production, and antimicrobial activity in the presence of visible-light. As-prepared Ag/g-C_3N_4 composite (Ag loading of 0.02 mole) exhibited optimum photoactivity for production of H_2 (335.40 $\mu molg^{-1}h^{-1}$), which is much better than other Ag loaded g-C_3N_4 composites. These synthesized Ag/g-C_3N_4 nanoparticles also show potential antimicrobial activity and inhibition zones were found comparable to that of an antibiotic chloramphenicol. Calderón-Jiménez et al. (2022) reported a sonochemical synthesis of silver nanoparticles in aqueous suspension. These Ag NPs were found to be quasi-spherical in shape and highly stable. The particle size of as-prepared sample was found to be 8.1 $\pm$ 2.4 nm with narrow dispersion of the size distribution. The bandgap of these Ag NPs was 2.795 $\pm$ 0.002 eV. A high stability of the optical properties of these Ag NPs were found at 10 h (short term) and 24 weeks.

8.3.2 Metal oxides

Sedghi et al. (2010) prepared SnO_2 QDs by sonication-assisted precipitation. It was reported that they can be used as a low temperature sensor for detecting CO as well as methane. There was a good of selectivity to CO in the presence of methane below 375°C using this sensor. The average particle size of SnO_2 QDs was found to be 3−4 nm and their sensing properties were compared with the nanoparticles prepared by conventional sol−gel method. It was observed that bandgap measurements of as-prepared sample indicated a 2.1 eV blueshift. Majumdar and Devi (2010) synthesized SnO_2 nanoparticles at room temperature by a sonication-assisted precipitation method. It was reported that 3 h sonication was found to produce nanoparticles with size below 10 nm. It was found that a gradual increase of the sonication time gradually decreases the particle size with interesting morphology and increased surface area. It was also observed that as-synthesized powders exhibited a direct influence by the sonication time on the sensing properties of butane. A maximum response of 98.88% was reported toward butane (5000 ppm) at 450°C along with a fast recovery time.

A sonochemical approach was developed by Islam et al. (2011) for large-scale synthesis of iron oxide magnetic nanoparticles (Fe_3O_4 NPs) using inexpensive and nontoxic metal salts as reactants. It was revealed that as-prepared nanoparticles had average particle size around 11 nm and these were almost spherical in shape. It was also proved that these particles were super paramagnetic with magnetization values of 80 emu g^{-1}. Chlorine-doped titanium dioxide (anatase) nanocrystallites were prepared by Wang et al. (2012) through sonicating sodium chloride solution of tetraisopropyl titanate in water/ethanol at 70°C. The presence of dopant (chloride) was confirmed and it was found that Cl is incorporated into TiO_2. It was reported that as-prepared samples were used in the photodegradation of butyl benzyl phthalate (BBP) in aqueous condition in the presence of visible light irradiation. It was reported that photodegradation of BBP could reach to 92% in 4 h.

N-doped TiO_2 nanocrystals were synthesized by Jia et al. (2014) via a sonochemical route. The urea, titanium tetrachloride, and aqueous ammonia were used as starting materials. It was revealed that as-synthesized nanocrystals had size of 10 nm. It was reported that the adsorption band edge of N-doped TiO_2 samples exhibited redshift to the visible region compared to TiO_2. The photocatalytic activity of as-prepared photocatalyst was observed for degradation of rhodamine B under visible light. It was revealed that the use of an optimal amount of urea enhanced the photocatalytic activity of TiO_2 due to its mesoporous structure and incorporation of nitrogen as a dopant.

Yang et al. (2016a) synthesized ZnO quantum dots using an ultrasonic microreactor. It was observed that flow rate, ultrasonic power, and temperature affected type and quantity of defects in ZnO quantum dots, and size of ZnO quantum dots can also be controlled by variation of these conditions. It was reported that the size of ZnO quantum dots decreased on increasing flow rate but quantum yields first increased and then decreased. The size of ZnO quantum dots was found to decrease first, and then increased on increasing ultrasonic power while the quantum yields kept on increasing. Moreover, the quantum yields of ZnO QDs synthesized by ultrasonic microreactor could reach 64.7%, which is higher than those synthesized only under ultrasonic radiation or only by microreactor.

The ZnO quantum dots were synthesized by Yang et al. (2016b) using an ultrasonic-assisted sol−gel method. It was reported that ultrasonic exposure time and temperature both affected type and amount of defects in as-prepared ZnO quantum dots. Total defects of ZnO quantum dots were found to decrease with the increasing ultrasonic time and temperature. The optical defects changed from oxygen interstitial defects to oxygen vacancy and then zinc interstitial defects. These were again transformed back to oxygen interstitial defects. It was observed that the sizes of ZnO quantum dots first decreased on increasing ultrasonic temperature and time and then increased.

Moghaddam et al. (2017) prepared two samples of ZnO quantum dots by sonochemical as well as conventional methods. It was indicated that the quantum dots prepared under ultrasonic waves had smaller size and also a narrow size distribution. It was observed that phase purity of nanocrystals could be obtained on using ultrasonic waves as there is complete conversion of precursors into ZnO, and as a result as-prepared ZnO can find application in optoelectronics.

8.3.3 Metal sulfides

The histidine functionalized CdS quantum dots were synthesized by Yadav et al. (2010) via a sonochemical method. It was revealed that as-prepared CdS QDs are well-defined with almost spherical shape. The X-ray diffraction pattern indicates the formation of cubic phase QDs. The confinement of histidine functionalized CdS QDs was confirmed. The photoluminescence property of CdS/histidine QDs was found to be better than that of CdS QDs. These as-functionalized QDs can find potential applications in the biological fields. Estandarte et al. (2011) synthesized ionic liquid-capped cadmium sulfide QDs in PET fibers as photocatatyst. Its photocatalytic activity was evaluated in the photodegradation of methylene blue. These CdS QDs and PET-CdS QDs nanocomposites were synthesized via a sonochemical route using an ionic liquid, 1-octyi-3-methylimidazolium lauryl sulfate ([OMIM]LS). They used PET fibers prepared from waste bottles and used these as matrix for preparation of the PET-CdS QDs nanocomposite. It was revealed that PET-CdS QDs nanocomposite has the highest bandgap energy (2.79 eV), which is suitable for absorption in the visible range. The CdS QDs and PET-CdS QDs nanocomposites were used as photocatalyst for photodegradation of methylene blue under visible light and degradation efficiency was 53.64 and 77.96%, respectively, which was much better than uncatalyzed degradation (19.57%).

Semiconductor nanoparticles of CdS have been prepared by Entezari and Ghows (2011) in microemulsion (O/W) under ultrasound irradiation. The effect of some operational parameters was observed, such as intensity of ultrasound, sonication time, temperature, and oil fraction. It was observed that as-prepared QDs had about 2 nm size with a hexagonal phase and this size can also be tuned. It was postulated that the collapse of bubbles generates high temperature and a number of nucleation sites, thus leading to uniform spherical particles with small size. It was revealed that the bandgap of as-prepared CdS NPs decreases with increasing sonication time. Goharshadi et al. (2012) developed a sonochemical method to prepare zinc sulfide nanoparticles with extremely small size (about 1 nm in diameter). They used a set of ionic liquids, which are based on the bis(trifluoromethylsulfonyl)imide anion and different 1-alkyl-3-methyl-imidazolium cations. This method provides wide bandgap ZnS nanocrystals, which can find application in different photonic devices.

A template-free chemical and sonochemical method was developed by Pejova and Bineva (2013) to prepare 3D assemblies of indium(III) sulfide quantum dots. This method allowed the deposition of cubic α-In2S3 nanocrystals (close packed) in thin film because of heterogeneous sonochemical effects. The average crystal radius of QD was reduced from 2.5 to 2.0 nm on sonication by continuous high-intensity ultrasound. It was observed that these values increased to 4.1 nm by postdeposition annealing treatment. It was reported that bandgap energy value (2.85 eV) was blueshifted (2.00 eV). It was revealed that Bohr's excitonic radius lies in the range of 2.5−4.1 nm.

Zhao et al. (2013) synthesized gamma-cyclodextrin-folate (gamma-CD/FA) inclusion-coated CdSe/ZnS quantum dots by a sonochemical method. It was observed that these gamma-CD/FA-coated CdSe/ZnS QDs were monodispersed and have smaller size, but with longer fluorescence lifetime and higher quantum yield. The cytotoxicity of gamma-CD/FA-coated CdSe/ZnS QDs was found to be lower and they could more effectively enter cancer cells. It is the smaller size of QDs (4−5 nm diameters) that allowed them to easily enter the cell and be removed through kidneys. These QDs are more suitable for some biomedical applications like bioprobes and bioimaging.

Das and Wai (2014) synthesized lead sulfide quantum dots. They used 1,2-benzenedimethanethiol, sodium sulfide, and lead nitrate solutions in ethanol under ultrasound irradiation. As-prepared PbS quantum dots had sizes of 2.7 and 3.6 nm in diameter. A simple one-pot method for synthesis of SWNT−PbS nanoparticle composite was also developed just by addition of single-walled carbon nanotubes (SWCNT) to the system under ultrasonic irradiation. This allowed the attachment of PbS nanoparticles to the SWCNTs' surface via π−π stacking. Kim et al. (2015) synthesized CdS quantum dots (QDs)/mesoporous TiO_2 (mp-TiO_2) by a sonochemical successive ionic layer adsorption and reaction (SC-SILAR) process. It was found that there is less growth time and larger absorbance of CdS QDs along with a uniform penetration into mp-TiO_2 films in the case of the SC-SILAR process as compared to the SILAR process. As-prepared CdS QDs/mp-TiO_2 was used to fabricate photoanode. This was used in quantum dot-sensitized solar cells (QDSCs) and these cells exhibited high efficiency.

Palanisamy et al. (2015) developed a continuous flow sonochemical reactor, which can produce metastable cadmium sulfide nanoplatelets. It was observed that continuous sonochemical synthesis was found to give high aspect ratio for hexagonal platelets of CdS with cubic crystal structures with thicknesses below 10 nm. It was revealed that uniformity in particle size was much better, when the continuous sonochemical process was used as compared to conventional synthesis processes and batch sonochemical process.

Xu et al. (2015) synthesized uniform molybdenum disulfide/tungsten disulfide quantum dots by the combination of solvothermal and sonication treatment. They used bulk MoS_2/WS_2 reactants at a mild temperature. It was observed that monolayer thickness had an average size of 3 nm. It was

reported that a highly exfoliated and defect-rich structure provides these quantum dots with enough active sites for catalyzing the hydrogen evolution reaction (HER) with long-term durability. These as-prepared particles had good cell permeability, strong fluorescence, and low cytotoxicity, which make them quite promising and biocompatible probes for imaging.

Sonochemical method for the synthesis of zinc sulfide quantum dots has been developed by Panda et al. (2016). They used a single precursor Zn ion and sulfur containing complex. It was indicated that the prepared complexes decomposed to form zinc sulfide quantum dots under high intensity ultrasound irradiation. It was revealed that as-obtained ZnS quantum dots had an 8.2 nm diameter with a cubic structure. The bandgap of these ZnS QDs was also calculated and was found to be 3.73 eV. The Cu and Mn-doped glutathione (GSH)−ZnS polypeptide quantum dots were prepared by Shi et al. (2016) via microwave-assisted sonochemical approach. The glutathione acted as a source of sulfide as well as a dispersant and reducing agent to form polypeptide QDs. It was indicated that the size of the polypeptides QDs was 2−3 nm. It was also reported that the doping of Cu and Mn could decrease the bandgap of GSH−ZnS from 3.67 to 2.86 eV. It was observed that photoelectrochemical (PEC) properties of GSH−ZnS were also enhanced due to the doping of Mn and Cu with excellent chemical stability.

ZnS quantum dots and ZnS:graphene QDs were synthesized by Jindal and Giripunje (2016) via a sonochemical method. It was reported that the average size of ZnS and ZnS:graphene QDs was 3.7 and 8.4 nm, respectively. The bandgap of ZnS:graphene QDs was calculated as 4.9 eV. An increase in current density from 2.44 to 98.4 $\mu A\ cm^{-1}$ was observed with lower turn on voltage from 0.40 to 0.12 V in the active layer as compared to pristine ZnS QDs. Such an enhancement in current density in these ZnS:graphene QDs indicated a great potential for such an active layer in photovoltaic devices. Kapatel et al. (2017) reported the synthesis of tungsten disulfide quantum dots, which were highly stable. They used sodium chloride, sodium hydroxide, lithium hydroxide, and ammonium hydroxide-assisted sonochemical exfoliation of bulk WS_2 powder in N-methyl-2-pyrrolidone for 2 h. It was observed that as-prepared WS_2 quantum dots (few-to-monolayer) have a size of 3 ± 0.5 nm. It was also revealed that better yield of WS_2 quantum dots was obtained in N-methyl-2-pyrrolidone. The as-obtained WS_2 quantum dots exhibited a blueshift with a bandgap of 2.7 eV.

Tin sulfide quantum dots were synthesized by Cheraghizade et al. (2017) via a sonochemical method. They kept sonication time as 10, 15, and 20 min. It was reported that SnS and Sn_2S_3 (orthorhombic phase) and Sn_2S_3 (hexagonal phase) was there in as-prepared QDs. The particle size of tin sulfide QDs was smaller than other QDs, when sonication time was kept at 20 min. It was revealed that smaller spherical shaped particles were obtained on increasing sonication time. The solar cell devices manufactured using tin sulfide QDs exhibited a better performance with the samples prepared with

more sonication time. It was concluded that sonication time is the key factor affecting the synthesis of Sn_2S_3 QDs. Not only this, it will also affect photocatalytic, optical, electrical, and photovoltaic conversion.

Kadeer et al. (2018) synthesized CdS quantum dots/Bi_2WO_6 three-dimensional (3D) heterojunction photocatalyst by ultrasonic method. These composites were found to be active for the degradation of rhodamine B and tetracycline hydrochloride under visible light irradiation and also for the reduction of Cr(VI) in aqueous solution. As-prepared CdS QDs/Bi_2WO_6 heterojunctions exhibited a significantly enhanced photocatalytic activity in all these cases as-compared with samples of CdS and Bi_2WO_6. The highest photocatalytic efficiency for degradation of rhodamine B was 94.5% with 3% CdS QDs/Bi_2WO_6 heterojunction in 30 min, which was about 6 and 1.5 times higher than that with those of pure Bi_2WO_6 and CdS QDs respectively. This enhancement was attributed to the synergetic effect between CdS QDs and Bi_2WO_6, including fast transfer of charge carriers between CdS QDs and Bi_2WO_6 and an efficient electron−hole separation.

Rajabi et al. (2018) developed a sono-assisted chemical precipitation method for synthesizing zinc sulfide quantum dots at room temperature. Then ZnS QDs doped with some transition metal ions (Ag, Mn and Cu) were also prepared using l-cysteine as the capping agent. It was revealed that the time required for a complete synthesis in the presence of ultrasonic irradiations was less than other conventional chemical methods. It takes hardly 15 min at a temperature of 40°C. The bandgap of colloidal ZnS QDs was found to be larger than 3.68 eV. The average particle size of these QDs was less than 5 nm. These were then used for driving the photocatalytic process for degradation of Victoria blue R. It was reported that the maximum removal of this dye (>95%) could be achieved under optimum conditions: pH 10.5, amount of QDs 3 mg, and time 30 min under UV irradiation. It was also revealed that these QDs can be reused six further times, without any significant loss in their photocatalytic properties.

A chemical precipitation method was used by Karimi et al. (2019) for thesynthesis of zinc sulfide quantum dots under the ultrasonic radiation, which was water based and fast also. They used two capping agents, l-cysteine and 2-mercaptoethanol, for this purpose. It was indicated that as-synthesized QDs were cubic in structure with a size less than 10 nm. These ZnS QDs were then used as photocatalysts for the degradation of crystalline violet under UV light. It was revealed that as-synthesized QDs can be reused five times without any significant decrease in their photocatalytic activities.

The cadmium sulfide QDs-sensitized mesoporous-TiO_2 (mp-TiO_2) photoanodes were fabricated by Kim et al. (2019) using the sonochemical successive ionic layer adsorption and reaction (SC-SILAR) methods to achieve highly efficient quantum dots (QDs)-sensitized solar cells. It was reported that the SC-SILAR method took a shorter time for synthesis of CdS QDs as

compared to the conventional SILAR method. It was suggested that the cavitation energy of microbubbles formed in the SC-SILAR method provided an additional energy for the synthesis of CdS QDs. Kandasamy et al. (2022) synthesized cadmium sulfide quantum dots through a green sonochemical method. They used *Delonix elata* leaves water extract as a capping as well as stabilizing agent. It was reported that the corrosion inhibition performance of as-prepared CdS QDs was studied in 3.5% NaCl, 1 M HCl, and 6 M KOH. It was observed that corrosion of zinc plate was reduced when the plates were coated with CdS QDs and these aqueous electrolytes, particularly with 3.5% NaCl.

Goharshadi et al. (2013) synthesized zinc sulfide nanoparticles under ultrasonic irradiation. They did not use any surfactant in this method under high temperature treatment. It was reported that the average particle size of as-prepared ZnS QDs was found to be 2 nm. The photocatalytic activity of ZnS quantum dots was evaluated for the degradation of reactive black 5 under UV light irradiation. It was revealed that about 95% of dye was removed within 10 min when using 0.2 g ZnS at a neutral pH.

8.3.4 Selenides

Three-dimensional (3D) assemblies of CdSe quantum dots (zinc blende structure) were synthesized by Pejova (2013) by two routes: (1) colloidal chemical and (2) sonochemical. A decreasing trend was observed on postdeposition thermal annealing treatment, with increasing average crystal size. Mousavi-Kamazani et al. (2016) synthesized $NiSe_2$ quantum dots from the reaction of selenium tetrachloride with pomegranate marc peels (PMP) dyes and Ni as a nickel precursor in the presence of potassium borohydride through a sonochemical-assisted method. They used PMP because it has several dyes (proanthocyanidins) and flavonoids and ions that can easily extract these from PMP.

Tavakolian and Tashkhourian (2018) prepared cadmium selenide quantum dots capped with reduced graphene oxide and then modified with thioglycolic acid in only 5 min under sonication. They used a solution of cadmium(II) nitrate, graphene oxide, thioglycolic acid, and selenium powder with $NaBH_4$ for this purpose. The glassy carbon electrode (GCE) was modified with as-prepared nanocomposite and used for the determination of ascorbic acid (AA), dopamine (DA), and uric acid (UA) simultaneously. The detection limit was found to be 0.11, 66 and 0.12 μM for DA, AA and UA, respectively. This electrode was also successfully applied for determination of these compounds in spiked urine samples. Kastilani et al. (2019) reported the sonochemical synthesis of CdSe quantum dots in single-liquid bulk phase as well as emulsion-based system. They used cadmium oleate and trioctylphosphine selenide as precursors. It was observed that synthesis of QDs was found to be slow in the case of a single-phase liquid system (1-octadecene)

but it was quite enhanced in a dispersed system (emulsions of 1-octadecene in ethylene glycol). It was also observed that the single-phase solvent system produced ultrasmall QDs exhibiting white-light emission (broad band), while the emulsion system produced well-defined magic-size clusters (MSCs) with high photoluminescence quantum yield (34%).

An ultrasound-assisted method was used by Zare and Tashkhourian (2020) for synthesis of L- and D-cysteine-capped CdSe quantum dots at room temperature. It was observed that as-prepared QDs were in the range of 5−7 nm diameters. These capped QDs exhibited green fluorescence, which was quenched differently by D- and L-tryptophen in a high selective manner, so that they can be used for their recognition with negligible interference by other species. It was reported that detection limits for the recognition of L- and D-tryptophen are 4.2 and 4.7 nm, respectively. However, it was 4.4 and 4.8 nm in the presence of other enantiomers. Tb-doped CdSe nanoparticles were synthesized by Hanifehpour et al. (2021) with variable Tb^{3+} content via a sonochemical route. The sonophotocatalytic activities of the as-prepared sample were evaluated for the photodegradation of reactive black 5. It was reported that the sonophotocatalytic process could degrade 85.25% of the dye, which was much more compared to individual sono- (22%) and photocatalytic degradation (8%) processes. It was observed that photodegradation was inhibited in the presence of benzoquinone and ammonium oxalate. Superoxide radicals and photogenerated holes were detected as the main oxidative species.

8.3.5 Tellurides

Luminescent CdTe quantum dots were produced in an aqueous medium by Menezes et al. (2011) within a few minutes using ultrasound irradiation. It was reported that as-produced QDs exhibited a strong quantum confinement effect and only one fluorescence band was present. These nanoparticles were monodispersed. It was revealed that the morphology of QDs can be better controlled and surface defects are also reduced by the use of ultrasound. The colloidal cadmium telluride quantum dots have been synthesized by Hwang et al. (2011) via one-pot sonochemical reaction. They used multibubble sonoluminescence (MBSL) conditions for this work. The tellurium powder and cadmium chloride with hexadecylamine and trioctylphosphine/trioctylphosphineoxide (TOP/TOPO) (dispersants) were sonicated in toluene (solvent) using ultrasound (20 kHz) at 60°C for 5−40 min. It was reported that a very wide size range of CdTe particles (2−30 μm), could be obtained by just controlling sonicating and thermal heating conditions. It was observed that as-prepared CdTe QDs exhibited different colors, ranging from pale yellow to dark brown, and they showed photoluminescence properties mainly due to the quantum confinement effect. The bandgap of these CdTe particles was found to be 1.53 eV.

Chen et al. (2012) prepared highly fluorescent and water-soluble CdTe quantum dots. They used β-cyclodextrin (β-CD) as surface-coating agents. This

involved a substitution reaction at the C-6 position of mono-6-deoxy-6-(p-tolylsulfonyl)-cyclodextrin (6-tso-β-CD) by the $-NH_2$ of (3-aminopropyl)triethoxysilane-coated CdTe QDs to afford APTES/ CdTe QDs under mild conditions. It was proved that the CdTe QDs were effectively modified by β-CD. The quantum yields of CdTe QDs, APTES/CdTe QDs, and β-CD/APTES/CdTe QDs in water were about 17%, 12%, and 9%, respectively. It was reported that β-CD/APTES/CdTe QDs could recognize molecules of p,p′-DDT and o,p′-DDT.

Shi et al. (2014) developed a fast one-pot method for synthesis of CdTe quantum dots in aqueous solution using a sonoelectrochemical route without the protection of N. It was indicated that the water-soluble CdTe QDs with high photoluminescence qualities can be synthesized without the preparation of precursor and N protection. The PL emission wavelength and quantum yield can be controlled by variation of some operational parameters. It was suggested that QDs prepared by this method have a great potential for application in the fields of sensors, photocatalysis, and solar cells. The cadmium telluride quantum dots were synthesized by Yoo et al. (2017) under ultrasonic irradiation. It was observed that bandgap reduces with the growth of CdTe quantum dots on increasing time of synthesis. There was a redshift in wavelength range (510 ~ 610 nm) on increasing the ratio of Te and cubic zinc blende structure was observed. The size of CdTe quantum dots was found to be about 2.5 nm and these were uniformly dispersed, when the time of synthesis was 210 min.

8.3.6 Carbon-based quantum dots

Li et al. (2011) synthesized monodispersed water-soluble fluorescent carbon nanoparticles. They used glucose as the source of carbon by a one-step alkali or acid-assisted ultrasonic treatment. It was reported that particle surfaces were quite rich in hydroxyl groups so as to provide a high hydrophilic nature. These could emit bright and colorful photoluminescence covering a broad range starting from visible to near infrared (NIR). It was also revealed that these particles had an excellent upconversion fluorescent properties also.

Bavireddi and Kikkeri (2012) synthesized highly fluorescent water-soluble glycoquantum dots through a sonochemical method. It was based on specific host−guest interactions between trioctylphosphine oxide (TOPO) surfactant and β-cyclodextrin (β-CD) on quantum dots. It was indicated that these QDs (β-CD modified) provided good cell viability of human hepatocellular carcinoma cell line (HepG2) cells. It was also revealed that β-CDgal-capped QDs can have a preferential binding with HepG2 cells and therefore could be a promising candidate for some biomedical applications.

Composite architectures consisting of graphitic carbon nitride quantum dots/bismuth phosphate were synthesized by Li et al. (2014). Then as-synthesized composite was used as a visible light-induced photocatalyst for photodegradation of methyl orange with appreciable efficiency.

A one-step sonochemical preparation of carbon dots (C-dots) doped with Ga atom (Ga@C-dots) have been reported by Kumar et al. (2015). This synthesis was carried out with molten Ga, and polyethylene glycol (PEG-400) as the reaction medium for 30−120 min under sonication. It was revealed that as-produced Ga@C-dots in PEG supernatant had an average diameter of 5 ± 2 nm. The fluorescence emission of Ga@C-dots was used as a probe and compared with pristine C-dots.

Kumar et al. (2016a,b) also used a sonochemical approach for the formation of C-dots using ultrasonic irradiation. They sonicated a two-phase mixture to yield Sn@C-dots and achieved Sn nanoparticles decorated by Sn@C-dots (Sn@C-dots@Sn). They directly deposited as-synthesized Sn@C-dots@Sn nanoparticles on the copper foil (current collector) and used them as a promising anode for Li-ion batteries. It was revealed that high lithiation and delithiation properties were present in Sn@C-dots@Sn nanoparticles with enhanced rate capabilities and high coulombic efficiency due to the conducting carbon dot network on the tin nanoparticles minimizing pulverization effects. They also reported a one-step synthesis of carbon dots (Kumar et al., 2016a,b) via sonication of polyethylene glycol (PEG-400) for 0.5−3 h. They also observed the effect of the different operational parameters on the size and the fluorescence of the C-dots such as temperature, amplitude, and sonication. The average diameter of the C-dots was found to be in between 2 and 9 nm; of course, it depends on the conditions of preparation. The highest quantum yield of emissions was found to be $\sim$16%. High fluorescence properties of C-dots can find applications in bioimaging and solar cells.

Sajjadi et al. (2017) prepared cadmium selenide/graphene quantum dots (CdSe/g-QDs) nanocatalyst via a three-step sonochemical−hydrothermal process. It was observed that they have a small bandgap and large specific surface area. It was also observed that the sonocatalytic activity of as-synthesized CdSe/g-QDs was enhanced in the degradation of methylene blue as compared to pure CdSe nanoparticles. It was reported that the degradation efficiency of methylene blue could reach 99% in 90 min under ultrasonic irradiation in the presence of CdSe/g QDs. It was revealed that degradation efficiency increased on the addition of $K_2S_2O_8$ and H_2O_2 as enhancers, while the presence of carbonate, sulfate, and chloride had an adverse effect. It was also indicated that the CdSe/g-QDs sonocatalyst can be reused for up to five successive runs.

The graphene/Ag_3PO_4 quantum dot (rGO/Ag_3PO_4 QD) composite was synthesized by Reheman et al. (2018) via photoultrasonic-assisted reduction method. It was confirmed that as-obtained Ag_3PO_4 QDs were of the size of 1−4 nm and these were dispersed uniformly on rGO nanosheets. The photocatalytic activity of as-synthesized rGO/Ag_3PO_4 QD composites was evaluated for the decomposition of methylene blue. It was found that the best results were obtained when the ratio W_{rGO}:$W_{composite}$ was kept at 2.3%. This composite could degrade 97.5% of methylene blue within 5 min. It was

indicated that enhanced photocatalytic activities and stabilities were due to a synergistic effect between rGO and Ag_3PO_4 QDs with a high specific surface area. It was suggested that these rGO/Ag_3PO_4 QDs photocatalysts can find a great potential in water splitting and sewage treatment. Kumar et al. (2019) used sonochemistry to develop a one-pot synthesis of carbon dots, and metal-doped CDs M@CDs (where M = Zn, Ag, Ga, and Au). The size of these CDs was found to range between 2 and 10 nm. The highest quantum yield of fluorescence emission was measured as ~16%. It was revealed that M@CDs can be used for imaging and neuronal interactions. They also have potential selective affinity, photostability, and biocompatibility. As-prepared M@CD nanocomposites were biocompatible, as well as photostable, so that these can be used for different multifunctional biomedical applications.

Lu and Zhou (2019) prepared fluorescent carbon quantum dots via a sonochemical approach. As-prepared QDs were low cost with high efficiency. They prepared nitrogen-doped CQDs (NCQDs) by ultrasonic treatment of dopamine in dimethylformamide for 8 h. It was reported that as-obtained NCQDs had high water dispersibility as well as stability, within a range of pH and ionic strength, and exhibited bright and stable fluorescence, high photostability, and low cytotoxicity. The fluorescence of CQDs can be quenched by Fe ions in the range of 0−50 μm in both water as well as in the interior of cancer cells. The limit of detection was found to be 38 nm. It was also proposed that the QDs can serve as a nanothermometer to sense temperature both in water as well as in cells.

A template-free sonochemical synthesis of α-Bi_2O_3/C-dots was reported by Sharma et al. (2019). It was confirmed that α-Bi_2O_3 in the nanocomposite was present in monoclinic phase and crystallite size with 28.75 nm. The bandgap of as-prepared nanocomposite was determined to be 2.49 eV. This photocatalyst was used for photocatalytic degradation of 86% of indigo carmine dye under visible light. It was reported that dye was degraded in 2 h as compared to pure α-Bi_2O_3, which only degraded 57%. The Bi_2O_3/C-dots could also achieve about 79% degradation of levofloxacin within 2 h. It was revealed that hydroxyl radicals and electrons played major roles in the photocatalytic degradation of indigo carmine, as evident from scavenger studies.

Yuan et al. (2019) reported a sonochemistry-assisted synthesis of hybrid black/red phosphorus quantum dots (BP/RPQDs). As-prepared quantum dots have small sizes, tunable bandgaps, and high absorption coefficients. They can find application in dye-sensitized solar cells (DSSCs). It was observed that as-prepared hybrid BP/RPQDs exhibited high light-response over a wide range of wavelength (ultra-violet to visible and even near-infrared region) along with longer recombination lifetime of photo generated carriers. It was revealed that DSSCs with BP/RPQDs and BP/RPQDs-N719 cosensitizer could achieve efficiencies of 0.12% and 8.02%, respectively as compared to 7.60% for N719-only solar cell.

Kaimal et al. (2022a) synthesized graphene quantum dots (GQDs) via ultrasonication and fabricated a glassy carbon electrode embedded on

amine-functionalized silica nanoparticles (Si NPs). It was reported that as-developed electrode exhibited a good response to glutathione (most abundant antioxidant in the majority of cells and tissues) with a wide linear range (0.5−7 μm) and a low detection limit of 0.5 μm with high sensitivity. It was revealed that reproducibility, outstanding selectivity, and long-term stability of these as-prepared QDs can find application in real sample analysis even in the presence of interferences.

Kaimal et al. (2022b) prepared gold-loaded boron-doped graphene quantum dots (Au@B-GQDs) interface using the ultrasound-aided reduction method. A sensor was constructed by depositing these as-prepared Au@B-GQDs (thin layer) on a glassy carbon (GC) electrode and they were used for electrochemical studies. These as-obtained QDs have good reproducibility, long-lasting stability, prominent selectivity, and repeatability. It was reported that as-fabricated Au@B-GQDs/GC electrodes can be used as simple and effective sensing platforms for the detection of guanine and adenine in neutral media.

8.3.7 Others

Pejova et al. (2011) studied transport properties of sonochemically synthesized three-dimensional (3D) assemblies of $AgBiS_2$ quantum dots (thin films). The bandgap energy was determined as ∼1.18 eV, which was found to be higher than the optical bandgap of a bulk semiconductor. It may be attributed to 3D confinement effects on the charge carrier motions within individual QDs. Panda et al. (2017) prepared $AgInS_2$ (silver indium sulfide) quantum dots with size ∼1.4 nm by a sonochemical method in 5 min. They used dodecylamine as a capping agent. The bandgap of as-prepared $AgInS_2$ QDs was found to be about 2.15 eV.

Pejova et al. (2020) synthesized quantum nanocrystals of $CuInS_2$ (cubic modification) by a sonochemical route. It was reported that average particle size, size distribution and degree of structural disorder of these $CuInS_2$ can be controlled by adjusting reactor content and exposure to ultrasonic irradiation. It was revealed that bandgap of as-prepared material can also be tuned. As-prepared material can find application in materials in optoelectronics and solar cells based on inorganic semiconductor systems. Zhang et al. (2020) fabricated AgCl quantum dots via ultrasonic method. The average size of AgCl QDs was found to be 2.5 nm. It was reported that as-prepared AgCl QDs exhibited an excellent photocatalytic activity for degradation of rhodamine B and tetracycline under visible light irradiation. It was also revealed that degradation rate of rhodamine B and tetracycline could reach up to 96.6 and 72.2%, respectively in 20 min, which was much higher with AgCl nanoparticles (23 nm) and AgCl nanospheres (114 nm).

Ramalingam et al. (2021) deposited silver quantum dots particles and nanoparticles of magnetite on nanotubes of bismuth in situ doped manganese oxide (Bi-MnOx). It was reported that Ag QDs particles with very fine size

and Fe_3O_4 nanoparticles were incorporated into the Bi-MnOx polymer composite through high power ultrasonication deposition method. It was reported that nanoparticles of silver were spherical in shape with size ranging between 5−15 nm and these were deposited on the Bi-MnOx surfaces (porous). On the other hand, Fe_3O_4 particles (nanorods) were deposited on Bi-MnOx nanotube composite. As-prepared nanoparticle-modified Bi-MnOx composite electrode can be used as electrochemical sensor for hydrogen peroxide detector. It was also revealed that as-prepared Fe_3O_4 and Ag QDs particle-modified Bi-MnoOx nanotubes could remove more than 90% Cr (VI) within 60 min.

8.4 Conclusion

There is a wide range of available methods for synthesizing quantum dots including top-down and bottom-up approaches. Sonochemical synthesis of quantum dots has certain advantages over other conventional methods such as high purity, higher surface area, uniform size distribution, no requirement of additives, and a faster rate. However, it is associated with a disadvantage in that a relatively low yield is obtained, which can be overcome by certain modifications. Quantum dots of various metals, their chalcogenides, and some nonmetals-based QDs have been discussed with their applications. This approach can occupy a prominent position amongst other methods of synthesizing quantum dots in the coming few decades.

References

Ameta, S.C., Ameta, R., Ameta, G. (Eds.), 2018. Sonochemistry: An Emerging Green Technology. CRC Press, New Jersey.

Bang, J.H., Suslick, K.S., 2010. Applications of ultrasound to the synthesis of nanostructured materials. Adv. Mater. 22 (10), 1039−1059.

Bavireddi, H., Kikkeri, R., 2012. Glyco-β-cyclodextrin capped quantum dots: synthesis, cytotoxicity and optical detection of carbohydrate−protein interactions. Analyst 137 (21), 5123−5127.

Calderón-Jiménez, B., Montoro Bustos, A.R., Pereira Reyes, R., Paniagua, S.A., Vega-Baudrit, J.R., 2022. Novel pathway for the sonochemical synthesis of silver nanoparticles with near-spherical shape and high stability in aqueous media. Sci. Rep. 12 (1). Available from: https://doi.org/10.1038/s41598-022-04921-9.

Chen, X.F., Zhou, M., Chang, Y.P., Ren, C.L., Chen, H.L., Chen, X.G., 2012. Novel synthesis of β-cyclodextrin functionalized CdTe quantum dots as luminescent probes. Appl. Surf. Sci. 263, 491−496.

Cheraghizade, M., Jamali-Sheini, F., Yousefi, R., Niknia, F., Mahmoudian, M.R., Sookhakian, M., 2017. The effect of tin sulfide quantum dots size on photocatalytic and photovoltaic performance. Mater. Chem. Phys. 195, 187−194.

Chowdhury, P., Viraraghavan, T., 2009. Sonochemical degradation of chlorinated organic compounds, phenolic compounds and organic dyes−a review. Sci. Total Environ. 407 (8), 2474−2492.

Das, A., Wai, C.M., 2014. Ultrasound-assisted synthesis of PbS quantum dots stabilized by 1, 2-benzenedimethanethiol and attachment to single-walled carbon nanotubes. Ultrason. Sonochem. 21 (2), 892–900.

Einhorn, C., Einhorn, J., Luche, J.L., 1989. Sonochemistry-The use of ultrasonic waves in synthetic organic chemistry. Synthesis 1989 (11), 787–813.

Entezari, M.H., Ghows, N., 2011. Micro-emulsion under ultrasound facilitates the fast synthesis of quantum dots of CdS at low temperature. Ultrason. Sonochem. 18 (1), 127–134.

Estandarte, A.K., Paredes, F., Bartolome, A., Arco, S., Arellano, I.H., 2011. Synthesis, characterization and application of imidazolium ionic liquid-capped CdS quantum dots in PET fibers as a photocatalyst for the photodegradation of methylene blue. Quezon City (Philippines) .

Galton, F., 1883. Inquiries into Human Faculty and Development. McMillan, London.

Goharshadi, E.K., Sajjadi, S.H., Mehrkhah, R., Nancarrow, P., 2012. Sonochemical synthesis and measurement of optical properties of zinc sulfide quantum dots. Chem. Eng. J. 209, 113–117.

Goharshadi, E.K., Hadadian, M., Karimi, M., Azizi-Toupkanloo, H., 2013. Photocatalytic degradation of reactive black 5 azo dye by zinc sulfide quantum dots prepared by a sonochemical method. Mater. Sci. Semicond. Process. 16 (4), 1109–1116.

Hanifehpour, Y., Nozad Ashan, N., Amani-Ghadim, A.R., Joo, S.W., 2021. Sonochemical synthesis, characterization and optical properties of Tb-doped CdSe nanoparticles: Synergistic effect between photocatalysis and sonocatalysis. Nanomaterials. 11 (2), 378.

Hwang, C.H., Park, J.P., Song, M.Y., Lee, J.H., Shim, I.W., 2011. Syntheses of CdTe quantum dots and nanoparticles through simple sonochemical method under multibubble sonoluminescence conditions. Bull. Korean Chem. Soc. B 32 (7), 2207–2211.

Islam, M.N., Phong, L.V., Jeong, J.R., Kim, C., 2011. A facile route to sonochemical synthesis of magnetic iron oxide (Fe_3O_4) nanoparticles. Thin Solid. Films 519 (23), 8277–8279.

Jia, T., Fu, F., Zhao, J., Chen, J., Wang, X., Fan, Z., et al., 2014. Sonochemical synthesis, characterization, and photocatalytic activity of N-Doped TiO_2 nanocrystals with mesoporous structure. Int. J. Photoenergy 2014. Available from: https://doi.org/10.1155/2014/516806.

Jindal, S., Giripunje, S.M., 2016. Enhanced photovoltaic performance of bulk heterojunction based on ZnS quantum dots-grafted graphene. Superlattices Microstruct. 100, 683–693.

Kadeer, K., Tursun, Y., Dilinuer, T., Okitsu, K., Abulizi, A., 2018. Sonochemical preparation and photocatalytic properties of CdS QDs/Bi_2WO_6 3D heterojunction. Ceram. Int. 44 (12), 13797–13805.

Kaimal, R., Vinoth, V., Salunke, A.S., Valdés, H., Mangalaraja, R.V., Aljafari, B., et al., 2022a. Highly sensitive and selecstive detection of glutathione using ultrasonic aided synthesis of graphene quantum dots embedded over amine-functionalized silica nanoparticles. Ultrason. Sonochem. 82. Available from: https://doi.org/10.1016/j.ultsonch.2021.105868.

Kaimal, R., Mansukhlal, P.N., Aljafari, B., Anandan, S., Ashok kumar, M., 2022b. Ultrasound-aided synthesis of gold-loaded boron-doped graphene quantum dots interface towards simultaneous electrochemical determination of guanine and adenine biomolecules. Ultrason. Sonochem. 83. Available from: https://doi.org/10.1016/j.ultsonch.2022.105921.

Kandasamy, K.; Surendhiran, S.; Devi, R. C.; Khadar, Y. S.; Rajasingh, P.; Balamurugan, A. Facile and eco-friendly synthesis of CdS quantum dots for enhancing corrosion inhibition of Zn metal plate in various environments. In AIP Conference Proceedings. AIP Publishing LLC. 2022, 2385 (1), doi: 10.1063/5.0070727.

Kapatel, S., Mania, C., Sumesh, C.K., 2017. Salt assisted sonochemical exfoliation and synthesis of highly stable few-to-monolayer WS_2 quantum dots with tunable optical properties. J. Mater. Sci.: Mater. Electron. 28 (10), 7184–7189.

Karimi, F., Rajabi, H.R., Kavoshi, L., 2019. Rapid sonochemical water-based synthesis of functionalized zinc sulfide quantum dots: Study of capping agent effect on photocatalytic activity. Ultrason. Sonochem. 57, 139–146.

Kastilani, R., Bishop, B.P., Holmberg, V.C., Pozzo, L.D., 2019. On-Demand sonochemical synthesis of ultrasmall and magic-size CdSe quantum dots in single-phase and emulsion systems. Langmuir 35 (50), 16583–16592.

Kim, J.H., Kim, G.Y., Sohn, S.H., 2015. Sono-chemical successive ionic layer adsorption and reaction for the synthesis of CdS quantum dots onto mesoporous TiO_2 photoanodes. Japn. J. Appl. Phys. 54 (7). Available from: https://doi.org/10.7567/JJAP.54.070304.

Kim, J.H., Jang, T., Seo, S.R., Sohn, S.H., 2019. Properties of CdS quantum dots synthesized using sonochemical successive ionic layer adsorption and reaction method for quantum dot-sensitized solar cells. J. Phys. Chem. Solids 127, 101–106.

Kumar, V.B., Perelshtein, I., Lipovsky, A., Porat, Z.E., Gedanken, A., 2015. The sonochemical synthesis of Ga@ C-dots particles. Rsc Adv. 5 (32), 25533–25540.

Kumar, V.B., Tang, J., Lee, K.J., Pol, V.G., Gedanken, A., 2016a. In situ sonochemical synthesis of luminescent Sn@C-dots and a hybrid Sn@C-dots@Sn anode for lithium-ion batteries. RSC Adv. 6 (70), 66256–66265.

Kumar, V.B., Porat, Z.E., Gedanken, A., 2016b. Facile one-step sonochemical synthesis of ultrafine and stable fluorescent C-dots. Ultrason. Sonochem. 28, 367–375.

Kumar, V.B., Kumar, R., Gedanken, A., Shefi, O., 2019. Fluorescent metal-doped carbon dots for neuronal manipulations. Ultrason. Sonochem. 52, 205–213.

Li, H., He, X., Liu, Y., Huang, H., Lian, S., Lee, S.T., et al., 2011. One-step ultrasonic synthesis of water-soluble carbon nanoparticles with excellent photo luminescent properties. Carbon 49 (2), 605–609.

Li, Z., Li, B., Peng, S., Li, D., Yang, S., Fang, Y., 2014. Novel visible light-induced g C_3N_4 quantum dot/$BiPO_4$ nanocrystal composite photocatalysts for efficient degradation of methyl orange. RSC Adv. 4 (66), 35144–35148.

Liu, H., Zhang, X., Wu, X., Jiang, L., Burda, C., Zhu, J.J., 2011. Rapid sonochemical synthesis of highly luminescent non-toxic AuNCs and Au@AgNCs and Cu (II) sensing. Chem. Commun. 47 (14), 4237–4239.

Lu, M., Zhou, L., 2019. One-step sonochemical synthesis of versatile nitrogen-doped carbon quantum dots for sensitive detection of Fe^{2+} ions and temperature in vitro. Mater. Sci. Eng. C 101, 352–359.

Majumdar, S.; Devi, P. S. Synthesis of SnO_2 nanoparticles using ultrasonication. In AIP Conference Proceedings, American Institute of Physics. 2010, 1276 (1), doi: 10.1063/1.3504298.

Mallikarjuna, K., Vattikuti, S.V.P., Manne, R., Manjula, G., Munirathnam, K., Mallapur, S., et al., 2021. Sono-chemical synthesis of silver quantum dots immobilized on exfoliated graphitic carbon nitride nanostructures using ginseng extract for photocatalytic hydrogen evolution, dye degradation, and antimicrobial studies. Nanomaterials 11 (11). Available from: https://doi.org/10.3390/nano11112918.

Mason, T.J., 1999. Sonochemistry. Oxford University Press, New York.

Menezes, F.D., Galembeck, A., Junior, S.A., 2011. New methodology for obtaining CdTe quantum dots by using ultrasound. Ultrason. Sonochem. 18 (5), 1008–1011.

Moghaddam, E., Youzbashi, A.A., Kazemzadeh, A., 2017. Investigation of ultrasonic effect on morphology, optical and growth properties of ZnO quantum dots. J. Nano Res. 49, 10–17.

Mousavi-Kamazani, M., Salavati-Niasari, M., Goudarzi, M., Gharehbaii, A., 2016. A facile novel sonochemical-assistance synthesis of $NiSe_2$ quantum dots to improve the efficiency of dye-sensitized solar cells. J. Inorg. Organomet. Polym. Mater. 26 (1), 259–263.

Palanisamy, B., Paul, B., Chang, C.H., 2015. The synthesis of cadmium sulfide nanoplatelets using a novel continuous flow sonochemical reactor. Ultrason. Sonochem. 26, 452–460.

Panda, B.B., Sharma, B., Rana, R.K., 2016. Sonochemical synthesis and characterization of ZnS quantum dots. Adv. Sci. Eng. Med. 8 (4), 333–337.

Panda, B.B., Rana, R.K., Sharma, B., 2017. Sonochemical synthesis of $AgInS_2$ quantum dots and characterisation. J. Nano-Electron. Phys. 9. Available from: https://doi.org/10.21272/jnep.9(2)0.02002.

Pejova, B., 2013. Phonon confinement and related effects in three-dimensional assemblies of cubic cadmium selenide quantum dots synthesized by conventional chemical and sonochemical routes. J. Phys. Chem. C 117 (38), 19689–19700.

Pejova, B., Bineva, I., 2013. Sonochemically synthesized 3D assemblies of close-packed In_2S_3 quantum dots: Structure, size dependent optical and electrical properties. J. Phys. Chem. C 117 (14), 7303–7314.

Pejova, B., Nesheva, D., Aneva, Z., Petrova, A., 2011. Photoconductivity and relaxation dynamics in sonochemically synthesized assemblies of $AgBiS_2$ quantum dots. J. Phys. Chem. C 115 (1), 37–46.

Pejova, B., Sherif, E., Minde, M.W., 2020. Sonochemically synthesized quantum nanocrystals of cubic $CuInS_2$: Evidence for multifractal surface morphology, size-dependent structure, and particle size distribution. J. Phys. Chem., C 124 (37), 20240–20255.

Pestman, J.M., Engberts, J.B., de Jong, F., 1994. Sonochemistry: theory and applications. Recl. des Trav. Chimiques des Pays-Bas 113 (12), 533–542.

Rajabi, H.R., Karimi, F., Kazemdehdashti, H., Kavoshi, L., 2018. Fast sonochemically-assisted synthesis of pure and doped zinc sulfide quantum dots and their applicability in organic dye removal from aqueous media. J. Photochem. Photobiol. B: Biol. 181, 98–105.

Ramalingam, R.J., Arunachalam, P., Appaturai, J.N., Thiruchelvi, P., Al-othman, Z.A., Alanazi, A.G., et al., 2021. Facile sonochemical synthesis of nanoparticle modified Bi-MnOx and Fe_3O_4 deposited Bi-MnOx nanocomposites for sensor and pollutant degradation application. J. Alloy. Compd. 859. Available from: https://doi.org/10.1016/j.jallcom.2020.158263.

Reheman, A., Tursun, Y., Dilinuer, T., Halidan, M., Kadeer, K., Abulizi, A., 2018. Facile one-step sonochemical synthesis and photocatalytic properties of graphene/Ag_3PO_4 quantum dots composites. Nanoscale Res. Lett. 13 (1). Available from: https://doi.org/10.1186/s11671-018-2466-9.

Sajjadi, S., Khataee, A., Kamali, M., 2017. Sonocatalytic degradation of methylene blue by a novel graphene quantum dots anchored CdSe nanocatalyst. Ultrason. Sonochem. 39, 676–685.

Sedghi, S.M., Mortazavi, Y., Khodadadi, A., 2010. Low temperature CO and CH_4 dual selective gas sensor using SnO_2 quantum dots prepared by sonochemical method. Sens. Actuators B Chem. 145 (1), 7–12.

Sharma, S., Mehta, S.K., Ibhadon, A.O., Kansal, S.K., 2019. Fabrication of novel carbon quantum dots modified bismuth oxide (α-Bi_2O_3/C-dots): Material properties and catalytic applications. J. Colloid Interface Sci. 533, 227–237.

Shi, J.J., Wang, S., He, T.T., Abdel-Halim, E.S., Zhu, J.J., 2014. Sono electrochemical synthesis of water-soluble CdTe quantum dots. Ultrason. Sonochem. 21 (2), 493–498.

Shi, J.J., Gong, L., Zhang, Y.H., Yang, P., He, J., 2016. Microwave-assisted sonochemical synthesis of Cu and Mn doped GSH–ZnS polypeptide quantum dots and their enhanced photoelectrochemical properties. RSC Adv. 6 (111), 109386–109393.

Suslick, K.S., Flannigan, D.J., 2008. Inside a collapsing bubble: Sonoluminescence and the conditions during cavitation. Annu. Rev. Phys. Chem. 59 (1), 659–683.

Tavakolian, E., Tashkhourian, J., 2018. Sonication-assisted preparation of a nanocomposite consisting of reduced graphene oxide and CdSe quantum dots, and its application to simultaneous voltammetric determination of ascorbic acid, dopamine and uric acid. Microchim. Acta 185 (10). Available from: https://doi.org/10.1007/s00604-018-2988-y.

Wang, X.K., Wang, C., Jiang, W.Q., Guo, W.L., Wang, J.G., 2012. Sonochemical synthesis and characterization of Cl-doped TiO_2 and its application in the photodegradation of phthalate ester under visible light irradiation. Chem. Eng. J. 189, 288−294.

Wang, C., Wu, J., Jiang, K., Humphrey, M.G., Zhang, C., 2017. Stable Ag nanoclusters-based nano-sensors: Rapid sonochemical synthesis and detecting Pb^{2+} in living cells. Sens. Actuators B Chem. 238, 1136−1143.

Xu, S., Li, D., Wu, P., 2015. One-pot, facile, and versatile synthesis of monolayer MoS_2/WS_2 quantum dots as bioimaging probes and efficient electrocatalysts for hydrogen evolution reaction. Adv. Funct. Mater. 25 (7), 1127−1136.

Yadav, R.S., Mishra, P., Mishra, R., Kumar, M., Pandey, A.C., 2010. Histidine functionalised biocompatible CdS quantum dots synthesized by sonochemical method. J. Exp. Nanosci. 5 (4), 348−356.

Yang, W., Yang, H., Ding, W., Zhang, B., Zhang, L., Wang, L., et al., 2016a. High quantum yield ZnO quantum dots synthesizing via an ultrasonication micro reactor method. Ultrason. Sonochem. 33, 106−117.

Yang, W., Zhang, B., Ding, N., Ding, W., Wang, L., Yu, M., et al., 2016b. Fast synthesize ZnO quantum dots via ultrasonic method. Ultrason. Sonochem. 30, 103−112.

Yoo, J.Y., Kim, W.S., Park, S.A., Kim, J.G., 2017. Study on Sonochemical Synthesis and Characterization of CdTe Quatum Dot. Appl. Chem. Eng. 28 (5), 571−575.

Yuan, H., Zhao, Y., Wang, Y., Duan, J., He, B., Tang, Q., 2019. Sonochemistry-assisted black/red phosphorus hybrid quantum dots for dye-sensitized solar cells. J. Power Sources 410, 53−58.

Zare, S., Tashkhourian, J., 2020. Ultrasound-assisted synthesis of chiral cysteine-capped CdSe quantum dots for fluorometric differentiation and quantitation of tryptophan enantiomers. Microchim. Acta 187 (1). Available from: https://doi.org/10.1007/s00604-019-4046-9.

Zhang, J., Maimaitizi, H., Zhang, T., Tursun, Y., Talifu, D., Abulizi, A., 2020. Facile one-step sonochemical synthesis of AgCl quantum dots with enhanced photocatalytic activity and its size effects. Funct. Mate. Lett. 13 (06). Available from: https://doi.org/10.1142/S1793604720510364.

Zhao, M.X., Li, Y., Wang, C.J., 2013. Synthesis and bioactivity of the folate receptor targeted gamma-cyclodextrin-folate inclusion-coated CdSe/ZnS quantum dots. Yao xue xue bao = Acta Pharmaceutica Sin. 48 (4), 566−572.

This page intentionally left blank

Chapter 9

Application of quantum dots in photocatalysis

Shubang Vyas[1], **Rameshwar Ameta**[1] **and Rakshit Ameta**[2]
[1]*Department of Chemistry, PAHER University, Udaipur, Rajasthan, India,* [2]*Department of Chemistry, J. R. N. Rajasthan Vidhyapeeth (Deemed to be University), Udaipur, Rajasthan, India*

9.1 Introduction

Photocatalysis is a branch of chemistry that deals with chemical reactions taking place in the presence of light and a photocatalyst. A photocatalyst is a semiconductor that enhances the rate of reaction by its presence. Thus photocatalysis is a phenomenon, where an electron−hole pair (exciton) is generated on exposing semiconducting materials to light of suitable energy. Thus the chemical reactions that occur in the presence of a semiconductor and light are collectively termed as photocatalytic reactions. Photocatalytic reactions are mainly classified into two categories: (1) homogeneous photocatalysis, where substrate and photocatalyst both exist in the same phase; and (2) heterogeneous photocatalysis, in which substrate and photocatalyst exist in different phases.

Different dyes and some soluble coordination compounds are used as homogeneous photocatalysts, whereas different semiconducting powders are good examples of heterogeneous photocatalysts. The importance of photocatalysis lies in the fact that a photocatalyst provides both an oxidation and reduction environment simultaneously. This field has been extensively reviewed by various researchers (e.g., Fox and Dulay, 1993; Ameta et al., 1999; Chong et al., 2010; Pelaez et al., 2012; Ameta et al., 2013; Ibhadon and Fitzpatrick, 2013; Schneider et al., 2014; Ameta and Ameta, 2016; Zhang et al., 2019; Djurišić et al., 2020; Ren et al., 2021).

Photocatalysis is a main tool in dealing with some major problems of the world such as environmental pollution, wastewater treatment, water splitting for combating energy crises, self-cleaning, antifogging, biomedicals, solar cells, etc.

Thus heterogeneous photocatalysis involves a chain of oxidative and reductive reactions on the surface of the photocatalyst. The energy difference between

Quantum Dots. DOI: https://doi.org/10.1016/B978-0-12-824153-0.00009-4

the valence band and the conduction band is called the bandgap (Eg). When a photocatalyst is exposed to light of the desired wavelength (sufficient energy, i.e., equal to or more than bandgap), the energy of photons is absorbed by an electron (e^-) of the valence band and it is excited to the conduction band. In this process, a hole (h^+) is created in the valence band. This process leads to the formation of photoexcitation state e^- and h^+ pair. This excited electron is used for reducing an acceptor, while a hole is used for oxidation of donor molecules.

There are some advantages of photocatalysts and these are:

- The catalyst is low cost, nontoxic, and reusable.
- The only requirement for such a reaction is the presence a semiconductor and light.
- The process takes place at ambient conditions.
- The pollutants may be degraded finally to CO_2, H_2O, and other inorganic substances, that is, complete mineralization.

Water is a universal solvent and it is required for the survival of life on this planet. Water is polluted due to an increased utilization in domestic and industrial activities, which poses a special threat of contaminating surface and groundwater. In recent years, advanced oxidation processes (AOPs), particularly photocatalysis, have been applied to treat wastewater problems. This is a green method to oxidize organic contaminants with strong reactive oxidizing radical species like $^{\bullet}OH$, $HOO^{\bullet}$, $O_2^{-\bullet}$, etc. It fulfills the goals of being environmentally friendly and showing sustainable development due to the unique electronic, optical, and structural properties. The important aspect of these nanoscale materials is their large surface area-to-volume ratio and quantum confinement effects, which are necessary for catalysis.

After the discovery of quantum dots (QDs), their potential applications for chemical sensing, bioimaging, drug delivery, and photocatalysis have been tremendously developed. It is due to their excellent aqueous solubility, magnificent electron transfer, and ability to harness light to make full utilization of solar insolation. Green QDs, particularly carbon QDs (CQDs), have received considerable interest in this blooming field due to their nontoxic behavior, greater sustainability, outstanding photostability, and their natural photoluminescence properties. These CQDs also have tunable optical properties and high biocompatibility; as a result, they have a number of applications. The importance of such studies lies in designing efficient photocatalysts, surface modification, charge transfer, and development of ternary photocatalysis. These techniques will significantly increase the photocatalytic activity of semiconductors with wide bandgaps, which can be utilized for solar energy conversion.

9.2 Quantum dots

QDs are semiconductor nanoparticles that exhibit size and composition-dependent optical and electronic (optoelectronic) properties. These are ultrasmall

in terms of size, ranging between 2.0 and 10.0 nm. These can be used in wastewater treatment (removal or degradation of pollutants), hydrogen generation from water (as the fuel of future), reduction of carbon dioxide (putting a check on ever increasing amount of CO_2 in atmosphere, that is, controlling global warming), and converting solar energy into electrical energy (solar cell, drug delivering), etc.

9.3 Wastewater treatment

Industries are regularly increasing the level of manufacture of materials due to the demands of society. These materials include different drugs, dyes, pesticides, etc. These industries release their effluents into the water resources with no or negligible treatment. As a result, water is polluted. Most of the chemicals are quite toxic and some of them are even carcinogenic, and therefore there is a necessity to treat wastewater by any alternate but eco-friendly and effective method. Photocatalysis can degrade most of these pollutants through oxidation because it is one of the techniques involving AOPs (green chemical pathways).

Wahab et al. (2013) compared the photocatalytic properties of TiO_2 and ZnO QDs for oxidation and degradation of acetaldehyde in gaseous phase. It was observed that rate constant for as-prepared ZnO QDs and Degussa P-25 was 8.3×10^{-3} and 1.9×10^{-2} min., respectively about, which was about two times. Their efficiencies were 70% and 92% for Degussa P-25 and ZnO-QDs, respectively in 2 h. It was observed that as-prepared QDs were of 6−7 nm size with wurzite phase.

Quan et al. (2016) prepared quasinoble-metal graphene QDs (GQDs) deposited stannic oxide by just sintering citric acid and SnO_2 together. A redox process between GQDs and SnO_2 generated oxygen vacancy (OV) states somewhere below the conduction band of stannic oxide. These VOs will shift the optical absorption band of SnO_2 towards the visible light region. The GQDs can also effectively increase the charge separation efficiency through noble metal promoting visible light response to some extent. The best performance was exhibited by samples calcinated at 450 °C due to relatively high concentrations of VOs. This study revealed that a combination of defect modulation and noble metal deposition together increased the photocatalytic activity.

Zeng et al. (2016) reported that when graphene oxide QDs (GOQDs) are covalently bonded onto amino modified polyvinylidene fluoride (PVDF) membrane, it resulted into a new type of nanocarbon functionalized membrane with remarkable enhanced antibacterial and antibiofouling properties. An *Escherichia coli* containing water exhibited a decrease in relative flux over GOQDs modified PVDF, which was 23%, and it is significantly lower than with GO-sheet modified PVDF (62%) and pristine PVDF (86%) after 10 h of filtration. The GOQD coating layer effectively inactivated *Staphylococcus aureus* and *E. coli* cells

such that the biofilm could not form a membrane surface. As a result, antimicrobial activity and antibiofouling capability was improved as compared to GO and CNTs modified membranes. This better performance may be due to uniform dispersion and unique structure of GOQDs. A long-term stability and durability was observed in GOQDs modified membrane due to strong covalent interaction between GOQDs and PVDF.

Cheraghizade et al. (2017) synthesized tin sulfide QDs by sonication. It was indicated that SnS and Sn_2S_3 (orthorhombic phase) and SnS_2 (hexagonal phase) wer present and the particle size of these QDs was smaller than other QDs. It was observed that smaller spherical shaped particles were obtained on increasing sonication time. A greater photocatalytic activity was observed for tin sulfide QDs, which were synthesized with longer sonication time. It was reported that solar cell devices constructed using as-prepared tin sulfide QDs exhibited a better performance. This shows that the duration of sonication is an important factor that affects the synthesis process as well as the optical, electrical, photocatalytic, and photovoltaic conversion properties of these QDs.

Xu et al. (2019) fabricated CQDs-N-TiO_{2-x} nanocomposites by decorating CQDs on the Ti^{3+} and nitrogen codoped TiO_2 nanoparticles via a combination of the hydrothermal−calcination method. The formation of N/Ti^{3+} codoping levels and introduction of CQDs in the nanocomposite was also confirmed. It was observed that as-prepared CDs-N-TiO_{2-x} nanocomposite showed increased visible light absorption as well as better charge separation compared to pristine CQDs-TiO_2, TiO_2, N-doped TiO_2 (N-TiO_2), N and Ti^{3+} codoped TiO_2 (N-TiO_{2-x}). As-prepared CQDs-N-TiO_{2-x} nanocomposite exhibited an excellent performance for Cr(VI) reduction in the presence of visible light (Fig. 9.1). It was reported that there was significant increase in the reduction of Cr(VI) on addition of citric acid (hole scavenger). As-prepared CQDs-N-TiO_{2-x} nanocomposite was found to exhibit efficient photocatalytic reduction of Cr(VI) in real samples of wastewater.

There are three important factors that control recovery: draw solution (DS), forward osmosis, and membrane. Doshi and Mungray (2020) reported the synthesis of a novel DS based on CQDs via two different hydrothermal methods (autoclave, A-1; reflux, R-1). They used tulsi (*Ocimum tenuiflorum*) for this purpose. It was found that 5% CQDs prepared by R-1 with 50% glycerol DS (TCQD-G) was found to be effective in inhibiting microbial growth. It was observed that the highest water flux (5.34 LMH) could be achieved with synthetic wastewater (feed solution) using TCQD-G as a DS.

Zhang et al. (2020) studied the use of dual QDs cocatalyst for remediation of organic pollutants. H_2O_2 is considered a green oxidant. They reported that FeOOH QDs/CQDs/g-C_3N_4 composite (FCCN) showed excellent photoactivity for the degradation of oxytetracycline (OTC) under visible light irradiation. The enhanced photoactivity was due to photoexcited electron transfer, where electrons can be quickly utilized by molecular oxygen to form H_2O_2. This results in facilitating the activation of oxygen molecules.

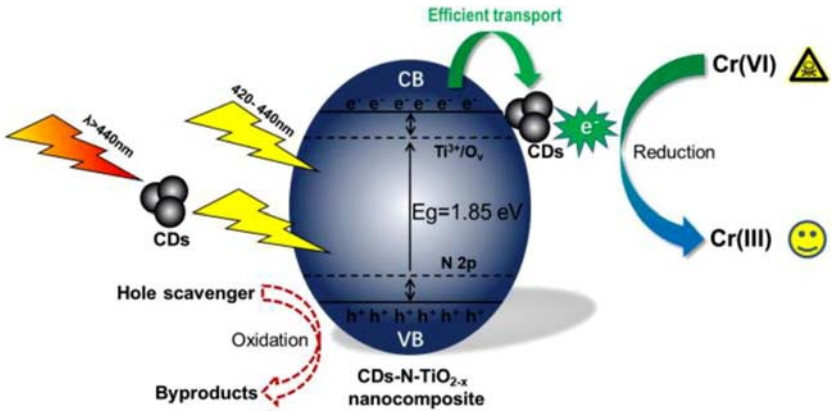

FIGURE 9.1 Photocatalytic reduction of Cr (VI). *Adapted from Xu et al., 2019. Chem. Eng. J., 357, 473–486. With Permission.*

The Fe^{3+} in FeOOH QDs was also reduced to Fe^{2+} by these photoexcited electrons, which react with H_2O_2 to produce the $^{\bullet}OH$ radicals responsible for photodegradation. As a result, surface carrier transfer efficiency (41.01%) was enhanced as compared to only g-C_3N_4 and CQDs/g-C_3N_4 photocatalyst.

9.3.1 Dyes

Different dyes are synthesized and manufactured to fulfill the demand of different color shades by the society, but these are very harmful. If these dyes are accumulated in nearby water resources, this can harm aquatic life, animal life, and human beings on consumption of this polluted water. Thus effluents containing different dyes are to be given photocatalytic treatment, before release to water bodies.

Colloidal oil-soluble Bi_2O_3 QDs were synthesized by Zhang et al. (2010). Water-soluble Bi_2O_3 QDs were produced from oil-soluble QDs through phase transfer by modifying the surface with mercaptopropionic acid. It was reported that water-soluble Bi_2O_3 QDs exhibited outstanding photocatalytic activity for the degradation of methyl orange over a wide range of pH. As-prepared Bi_2O_3 QDs maintained high degradation efficiency even after several cycles. Kusic et al. (2011) reported the use of QDs nanoparticles for treatment of colored wastewater. They used chemical processes for water treatment and disinfection (direct ozonation and direct UV photolysis) for the degradation of colored organic pollutant (reactive azo dye), in the presence of CdSe/ZnS core–shells QDs.

Chen et al. (2013) reported hybrid metal oxide QDs, where Cu_xO and Fe_xO, were anchored on TiO_2 blocks (Cu_xO/TiO_2 and Fe_xO/TiO_2). Their photocatalytic activities were examined by photocatalytic decoloration of methylene blue in the presence of visible light as well as simulated sunlight.

It was observed that these hybrid metal oxide QDs were dispersed uniformly on TiO_2 blocks and both copper and iron were present in mixed valence states (Fe^{2+} and Fe^{3+}; Cu^{+} and Cu^{2+}).

Mansur et al. (2014) reported the fabrication of nanophotocatalysts based on ZnS QDs, which were functionalized with chitosan (CHI) using a green method at room temperature. It was observed that in as-prepared ZnS/CHI nanophotocatalysts (ZnS−CHI) CHI was acting as an effective capping ligand to produce water-soluble ZnS QDs with an average size of 3.8 nm. They selected two model organic pollutants (methylene blue and methyl orange), and these were effectively degraded by ZnS/CHI under UV irradiation. It was also observed that ZnS−CHI nanoconjugates displayed blue photoluminescent behavior, when excited by UV radiation.

Muthulingam et al. (2015) prepared composites containing CQDs/nitrogen-doped ZnO (CQD/N-ZnO) via a one-step method. Three dyes were selected as model pollutants: fluorescein, methylene blue, and malachite green. It was reported that as-prepared CQD/N-ZnO photocatalyst exhibited an increased cohesiveness to degrade all these three dyes within 30−45 min in the presence of daylight. Also, it was found that the composite can be reused because of its antiphotocorrosion behavior furnished by CQDs.

Saud et al. (2015) prepared CQDs/titanium dioxide (CQDs/TiO_2) composite nanofibers through hydrothermal route. It was revealed that the photocatalytic efficiency of as-prepared composite nanofibers was found to be higher than pristine TiO_2 nanofibers for the degradation of methylene blue under visible light irradiation as well as antibacterial properties against *E. coli*. The anchored CQDs can increase light absorption as well as suppressed recombination of photogenerated electron−hole pair resulting in an increase in photocatalytic and antibacterial properties.

Vidhya et al. (2015) reported a modified green synthesis route to prepare pure and starch-capped ZnO (ZnO/starch) QDs. It was observed that a hexagonal crystal structure was present in both pure and ZnO/starch QDs, as evident from XRD data. It was reported that the particles were spherical in shape with a size of 5−10 nm. It was revealed that ZnO/starch QDs showed an increased emission behavior as compared to ZnO QDs. The photocatalytic activity of ZnO QDs was evaluated using the degradation of rhodamine B. Here, it was found that ZnO/starch QDs showed a higher decomposition of dye as compared to pure ZnO QDs.

Fan et al. (2016) synthesized GQDs and polymer-modified GQDs using a hydrothermal method. They used citric acid as a precursor of carbon. The GQDs were modified with polyethylene glycol and polyethylenimine. It was revealed that GQDs were uniform in size (2−5 nm). The photocatalytic activity of these samples was evaluated for the degradation of methylene blue. It was observed that the rate of photocatalytic degradation was found to be in the order:

$$\text{GQDs} > \text{GQDs-PEIs} > \text{GQDs-PEGs}$$

Miao et al. (2016) prepared CQDs embedded in mesoporous TiO_2 materials via a sol−gel method. It was observed that the nanoparticles were randomly packed in inverse surfactant micelles and mesopores are formed by interconnected intraparticles. The photocatalytic activity of as-prepared CQDs/meso-Ti-450 was observed in the degradation of methylene blue. It was observed that photocatalytic activity of the composite material was greatly increased due to the upconversion property and electron withdrawing property of CQDs. The highest photocatalytic activity was obtained by the sample (5% CQDs/meso-Ti-450). It was observed that almost 98% dye was removed while only 10% methylene blue can be degraded by commercial P 25.

Rajabi and Farsi (2016) studied the effect of capping agent on the photocatalytic properties of zinc sulfide QDs. They synthesized ZnS QDs by an aqueous chemical precipitation method using different capping agents (thiourea, 2-mercaptoethanol, and l-cysteine). It was observed that the optical absorption band of ZnS nanostructures also changed with capping agents. As-prepared ZnS QDs were used for photodegradation of crystal violet as a model dye in an alkaline medium with a low concentration of QDs.

Zhang et al. (2016) prepared nitrogen-doped CQDs/TiO_2 (NCQDs/TiO_2) hybrid composites. It was reported that the NCQDs were introduced onto the TiO_2 surface. The photocatalytic activity of as-prepared NCQDs/TiO_2 hybrid composites was evaluated by selecting methylene blue as the target pollutant. It was found that the photodegradation efficiency of dye over 1NCQDs/TiO_2 was about 86.9%, which was much more than pristine TiO_2 (53.8%) The increased photocatalytic activities of NCQDS/TiO_2 hybrid may be due to interfacial transfer of photogenerated charges to NCQDs from the conductive band of TiO_2; leading to effective charge separation in TiO_2.

Anh et al. (2017) fabricated N, S-codoped GQDs (N, S-GQDs) by a hydrothermal route. It can be used for selective and sensitive detection of mercury ions (Hg^{2+}) in water as well as wastewater. It was reported that as-prepared N, S-GQDs were uniform in size with an average particle size of 3.5 ± 0.5 nm. It was reported that doping of nitrogen atoms increased the quantum yield up to 41.9%, whereas sulfur atoms were responsible for better selectivity of Hg^{2+} through strong coordination interaction. It was found that the fluorescence intensity of N, S-GQDs was proportional to Hg^{2+} quenching with a limit of detection of 0.14 nM. As-prepared N, S-GQDs were used for detecting mercuric ions samples of sewage and dye wastewater.

Kumar et al. (2018) synthesized GQDs decorated ZnO nanorods heterojunctions. They evaluated photocatalytic performance of these heterojunctions for the degradation of methylene blue and also carbendazim, a fungicide in the presence of sunlight. It was observed that this heterojunction with 2 wt.% of GQD (ZGQD2) exhibited best photocatalytic degradation (about 95%) of methylene blue and carbendazim as compared to ZnO and GQD in 70 min. Higher photocatalytic activity of these ZnO-GQD heterojunctions may be due to an efficient charge carrier separation, increased light

absorption from UV to visible region, as well as high specific surface area of the ZGQD2 heterojunction.

Qu et al. (2018) prepared CQDs/$KNbO_3$ photocatalyst, via hydrothermal and mixed-calcination methods, and it was a visible light driven composite. They also evaluated the photocatalytic activity of CQDs/$KNbO_3$ composites for the degradation of crystal violet dye along with hydrogen production under visible light (Fig. 9.2). It was reported that CQDs/$KNbO_3$ composites exhibited much higher photocatalytic activity than the $KNbO_3$. This is all due to the presence of CQDs as cocatalyst on $KNbO_3$ particles surface. This formed much more active sites, which can trap electrons; thus inhibiting recombination of photogenerated electron−hole pairs. It was also observed that as-prepared CQDs/$KNbO_3$ can be used again even after four repetitive cycles.

Gao et al. (2019) synthesized CQDs via a hydrothermal method. They used waste larch wood as the raw material. The 3D Bi_2MoO_6 hollow microspheres can be prepared by a mixed solvothermal method without using any surfactants. The Bi_2MoO_6 was used as a matrix and it was doped with CQDs to get a new composite material (CQDs/Bi_2MoO_6). It was observed that methylene blue was degraded by Bi_2MoO_6 hollow microspheres in the presence of visible light. This photocatalytic performance was found to increase when these hollow microspheres were modified with CQDs.

Jat et al. (2019) investigated the photocatalytic degradation of fast green in the presence of visible light using SnO_2-TiO_2. They prepared SnO_2 QDs by a hydrothermal method using stannic chloride (hydrate) as the source of tin. This composite exhibited more photocatalytic activity than titania nanopowder for the degradation of fast green. Karimi et al. (2019) synthesized zinc sulfide QDs by chemical precipitation method under ultrasonic radiation. They used two capping agents, l-cysteine and 2-mercaptoethanol. It was

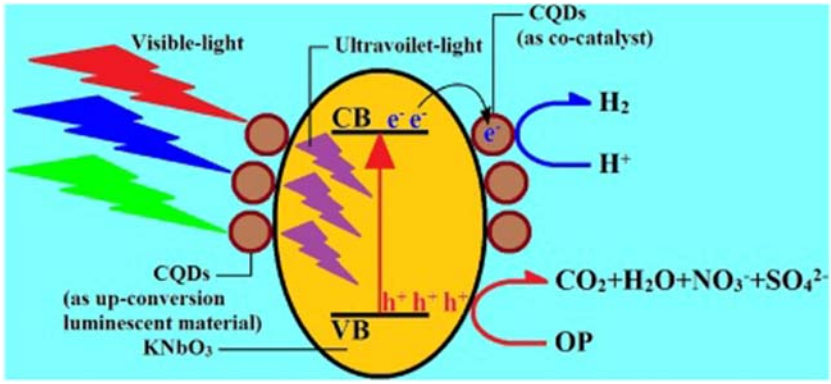

FIGURE 9.2 Photocatalytic hydrogen generation by CQDs/KN composite. *Adapted from Qu et al., 2018. Mol. Catal., 445, doi: 10.1016/j.mcat.2017.11.002. With Permission.*

observed that the as-synthesized QDs were cubic in structure with a particle size less than 10 nm. These QDs were then used for the degradation of crystal violet. It was also revealed that QDs can be reused five times without any significant loss in photocatalytic activity.

Lin et al. (2019) synthesized ternary heterostructure photocatalyst by coanchoring the NCQDs and graphitic carbon nitride QDs (CNQDs) on the surface of $BiVO_4$ microspheres. The as-synthesized $BiVO_4$/CNQDs/NCDs ternary heterostructure was found to exhibit an excellent photocatalytic activity for the degradation of rhodamine B and tetracycline in the presence of visible light as compared to pure $BiVO_4$, $BiVO_4$/NCDs, and $BiVO_4$/CNQDs. The higher photocatalytic activity in this composite may be attributed to an efficient separation and transport of photogenerated charge carriers.

Sharma et al. (2019) reported a template-free sonochemical synthesis of α-Bi_2O_3/C-dots. They used this composite for the degradation of indigo carmine and levofloxacin under visible light (Fig. 9.3). It was reported that α-Bi_2O_3 in the nanocomposite has a monoclinic phase. Its bandgap was found to be 2.49 eV. The as-prepared photocatalyst exhibited higher visible light driven photocatalytic activity for the degradation of indigo carmine (86%) than α-Bi_2O_3 (57%) and levofloxacin (79%) within 2 h. It was confirmed that hydroxyl radicals played a dominant role in the photocatalytic degradation of indigo carmine.

The plasmonic Au nanoparticle (NP)/SnO_2 quantum dot (SQD) (Au/SQD) nanocomposites were prepared by Babu et al. (2019) via a solvothermal method. The photocatalytic activity of as-prepared plasmonic Au/SQD nanocomposites was evaluated for the degradation of rhodamine B. The Au/SQD photocatalyst prepared by using tin chloride (1.0 g), exhibited better dye degradation as compared to pristine SQDs. This increased catalytic performance may be attributed to a shift of the bandgap from the UV to visible region. It was also revealed that synergistic coupling of the semiconductor and metal QDs as well as surface

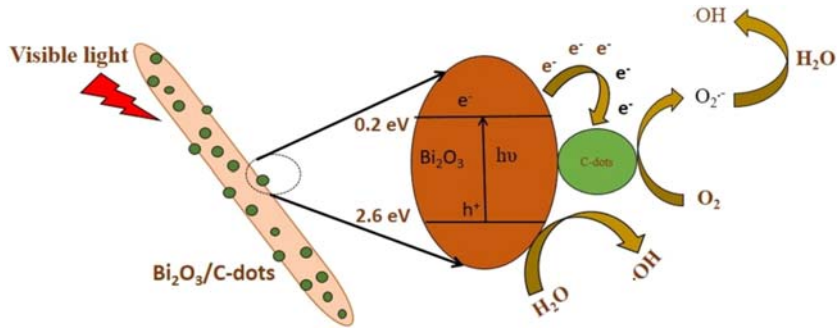

FIGURE 9.3 Photocatalytic degradation of indigo carmine and levofloxacin in the presence of α-Bi_2O_3/C-dot. *Adapted from Sharma et al., 2019. J. Colloid Interf. Sci., 533, 227–237. With Permission.*

plasmon resonance effect of Au NPs played an important role in increasing the catalytic performance.

Xu et al. (2022a) synthesized TiO_2 thin flakes modified with g-C_3N_4 QDs. It was revealed that g-C_3N_4 QDs were in the size of $\sim$10 nm. It was observed that TiO_2 nanoflakes/g-C_3N_4 QDs hybrid exhibited an excellent activity for hydrogen evolution from methanol degradation of rhodamine B (Fig. 9.4).

Jacob et al. (2020) reported the coupling of sulfate reduction with the precipitation of zinc as ZnS QDs at ambient conditions. It was observed that biogenic ZnS QDs had average sizes of 5−7 nm and their formation took 2−4 days of incubation. There was an absorption peak (<325 nm), which may be due to surface plasmon resonance of ZnS QDs and the bandgap of these biogenic ZnS QDs was found to be 3.84 eV. These QDs were successfully used as effective photocatalysts for photoassisted decolorization of Congo red.

Jamila et al. (2020a) fabricated an effective CuO/NCQDs solar photocatalyst using p-type copper oxide, which was modified with NCQDs. A leaf-like morphology for CuO was confirmed for CuO/NCQDs composites by SEM images. It was confirmed that NCQDs are well incorporated on nanoleaves of CuO. As-prepared photocatalyst was used for the degradation of methyl orange (Fig. 9.5). It was observed that this composite catalyst showed higher degradation efficiency as compared to pure CuO nanoleaves, which was attributed to an increased charge separation ability and visible light absorption.

Jamila et al. (2020b) also prepared NCQDs by modifying the surface of graphene oxide (GO) incorporated WO_3 nanosheets. It was observed that the surface of WO_3 nanosheets was modified with morphological defects so that more active sites were available there. As-synthesized ternary composites were used to degrade methyl orange photocatalytically. These ternary

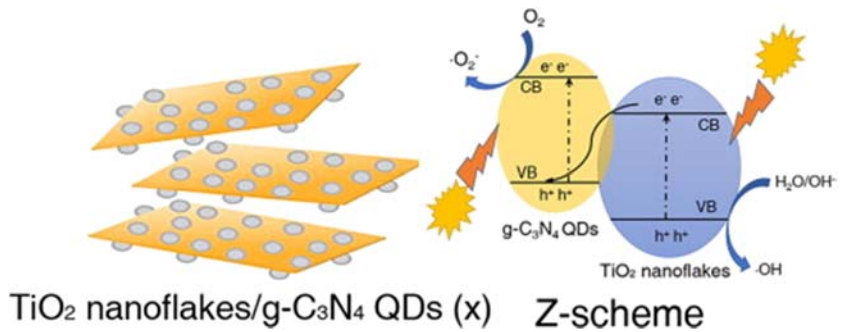

FIGURE 9.4 Use of TiO_2 nanoflakes/g-C_3N_4 for hydrogen generation along with degradation of rhodamine B. *Adapted from Xu et al., 2022a. Chem. Eng. J. 430, doi: 10.1016/j.cej.2021.132861. With Permission.*

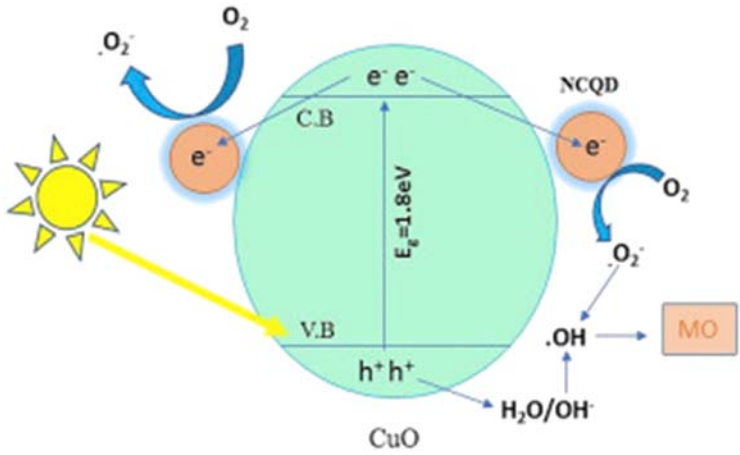

FIGURE 9.5 Photocatalytic degradation of methyl orange on CuO/NCQDs. *Adapted from Jamila et al., 2020. J. Phys. Chem. Solids 138, doi: 10.1016/j.jpcs.2019.109233. With Permission.*

composites exhibited an excellent photocatalytic activity as compared to binary and WO_3 photocatalysts.

The NCQDs were modified with defect-rich g-C_3N_4 (DCN) (NCDs/DCN) by Liu et al. (2020) using an impregnation method. As-prepared NCDs/DCN with narrow bandgap showed excellent visible light absorption and electron transfer ability, which were found useful for photocatalysis of rhodamine B degradation and simultaneous production of H_2. These NCDs/DCN expressed better efficiency in removal of different combination pollutants such as bisphenol A (BPA)/Cr(VI), ofloxacin (OFL)/Cr(VI), and ciprofloxacin (CIP)/Cr (VI) than in a single system. This is due to the synergistic effect between oxidation of organic pollutants and reduction of Cr(VI). An excellent photocatalytic H_2 generation activity and degradation of rhodamine B was there simultaneously with the evolution of H_2 (3.68 μmol h^{-1} g^{-1}) and 100% removal of dye, respectively.

Vatanpour et al. (2020) used GQDs for preparing polyvinyl chloride (PVC) blended matrix. It was then used for the removal of reactive blue 19 dye from wastewater. An improved antifouling performance was also reported by the filtration of bovine serum albumin (BSA) solution. When GQDs were added to the PVC matrix (1 wt.%), it was found that water flux reached 19.1 Lm^{-2} h^{-1}, which was around 56% higher than the unfilled membrane. It was observed that as-prepared PVC membranes have rejection of reactive blue 19 (>96%) and BSA (>98%).

Hui et al. (2021) synthesized heteroatoms-doped CQDs using rice husk as a biowaste precursor. They studied the effects of nitrogen and bismuth doping. They used ethylenediamine and bismuth nitrate pentahydrate as the source of nitrogen and bismuth, respectively. It was observed that these CQDs were spherical in shape with a size of less than 10 nm. The addition

of bismuth nitrate pentahydrate and ethylenediamine tuned the fluorescence intensity and shifted the emission to higher wavelength from the blue to green region. The activity of rice husk derived CQDs (RHCQDs) was examined by photodegradation of methylene blue as well as removal of copper (II). It was revealed that Bi-RHCQDs (5 wt.%) and N-RHCQDs (10 vol.%) exhibited the highest methylene blue degradation performance, 68.91% and 72.16%, respectively. These doped RHCQDs were also tested for removal of copper(II) with 56.23% and 33.13%, efficiency.

Sahu et al. (2021) decorated GO with SnO_2 QDs and used them for the degradation of methylene blue under visible light. It was revealed that about ~94% methylene blue was degraded using only 0.5 mg of GO-SnO_2 catalyst in 30 min. The preparation of GQDs from pyrocatechol has been reported by Mandal et al. (2021) at different pH. The photocatalytic behavior of as-synthesized GQDs was evaluated in the degradation of two dyes, methyl orange and methylene blue, in the presence of visible light irradiation.

Empty fruit bunches by-products of palm oil mill industry containing lignin were used as raw material in the fabrication of sulfur-doped CQDs (SCQDs) by Abd Rani et al. (2021) through a hydrothermal treatment. The SCQDs remained unchanged even after several hours of UV light exposure and also after storage for 8 months, which indicates the excellent stability. The average particle size of as-prepared SCQDs was found to be 2.9 nm. The photocatalytic activity of SCQDs was evaluated for the degradation of crystal violet dye under UV light, which could reach 99.7% degradation in 200 min.

The TiO_2/GQDs nanocomposite was synthesized by Niazi et al. (2021) and used for the degradation of textile dye, reactive black 5 (RB5). It was reported that almost complete (100%) degradation of 50 ppm RB5 could be achieved by TiO_2/GQDs within 30 min under sunlight irradiation. The main active species for the degradation of RB5 was confirmed as surface hydroxyl radicals based on scavenger studies.

Ahlawat et al. (2021) synthesized CQDs via a microwave-assisted method. It was reported that CQDs were small in size (about 2 nm) with spherical shapes. The photocatalytic degradation of rhodamine B was studied in the presence of CQDs and the highest degradation of 99.7% could be achieved under UV light irradiation.

Hatefi et al. (2021a,b) reported that photocatalytic activity was enhanced in electron-rich GQDs with Fe_3O_4/TiO_2 nanocomposites. They could achieve 86.08% removal efficiency of methylene blue, which was more than with TiO_2. The as-synthesized material improved photocatalytic efficiency for the degrading MB under UVA light irradiation compared with merely pure anatase TiO_2.

Two samples of zinc oxide QDs (ZQs) (S_1 and S_2) were synthesized by Mohamed et al. (2021) via a solvothermal method. The crystallite size of these samples, S_1 and S_2, was found to be 8.4 and 9.6 nm, respectively. It

was revealed that the sample S_1 exhibited the best degradation of dianix blue dye. Sharma et al. (2021) synthesized CQDs via a hydrothermal method. They used m-phenylenediamine and l-glutamic acid for this purpose. Then these were combined with nano-TiO_2 to obtain CQDs/TiO_2 composites. It was observed that CQDs/TiO_2 (CT-1) composite with 1:1 molar ratio of l-glutamic acid to TiO_2 exhibited the best degradation efficiency for methyl orange. It was revealed that sample CT-1 can degrade 70.56% of methyl orange, which was almost is 12.7 times higher than that of TiO_2.

The ZQs was synthesized by Mohamed et al. (2022) using a modified precipitation process. The crystallite size of ZQs was found to be 4.4 and 5.3 nm for the ZQ1 and ZQ2 samples, respectively. The photodegradation process of indigo carmine dye ZQ1 reached the highest synthetic levels equal to $1.718 \times 10^{-2}\ s^{-1}$. They tried it on 16 factory effluents samples, and it was observed that it can be used for 10 replication cycles after recovery in the presence of ZQs by sunlight for 2 months.

Smrithi et al. (2022) reported the green synthesis of NCQDs via a hydrothermal technique using extract of *Cucurbita pepo*. The photocatalytic activities of NCQDs were evaluated for the degradation of crystal violet under visible light. They could achieve 99.9% degradation of crystal violet in 3 h in the presence of 1 mL H_2O_2. It was revealed that a prominent role was played by $^{\bullet}OH$ radicals in this degradation.

The black phosphorus QDs (BPQDs) were prepared by Fan et al. (2022) and photocatalytic activity of BPQDs was investigated by selecting indigo carmine as a model dye. It was observed that decolorization efficiency of this dye could reach 98.22% in the presence of sunlight.

Sun et al. (2022) synthesized cerium dioxide QDs modified graphitic carbon nitride. It was reported that CeO_2QDs was dispersed homogeneously on the surface of g-C_3N_4. It was observed that as-prepared CeO_2QDs/g-C_3N_4 exhibited a higher rate for the photodegradation ($0.00985\ min^{-1}$) for rhodamine B, which was found to be that seven times higher than that with single g-C_3N_4 (Fig. 9.6).

9.3.2 Drugs

Pharmaceuticals and personal care products are required by the society and their use is increasing day by day. These are emerging as water contaminants as they can affect the quality of water adversely. This results into a potential harm to water supplies, ecosystem and human health. Photocatalysis can degrade these water pollutants into almost harmless products.

Shi et al. (2015) used CdS QDs modified nitrogen-doped TiO_2 plates (NTP) for decomposition of diclofenac (DCF). They used thiolactic acid as a linker to bind CdS QDs on NTP in situ. This composite NTP/CdS exhibited much higher photocatalytic activity for the degradation of DCF under visible light. It was observed that degradation rate was significantly increased as

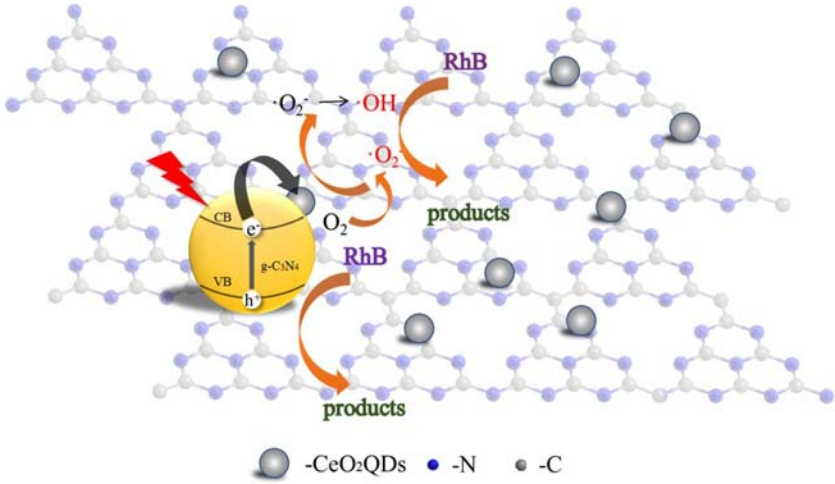

FIGURE 9.6 Photocatalytic degradation of rhodamine B on CeO_2QDs/g-C_3N_4. *Adapted from Sun et al., 2022. Appl. Surf. Sci., 576, doi: 10.1016/j.apsusc.2021.151901. With Permission.*

compared to NTP and CdS, which was about 1.95 and 2.88 times, respectively. The TiO_2 QDs were synthesized by Kaur et al. (2015) via ultrasonic-assisted hydrothermal process. They used as-prepared QDs for photocatalytic degradation of ketorolac tromethamine in the presence of sunlight. It was revealed that ~99% ketorolac tromethamine drug was photodegraded.

Ionic liquid induced strategy was used by Xia et al. (2016) for controlled synthesis of CQDs (CQDs)/BiOX (X = Br, Cl) hybrid nanosheets. They selected three different types of pollutants, such as CIP rhodamine B (RhB), and bisphenol A (BPA) to evaluate the photocatalytic activity of CQDs/BiOX composite nanosheets. The highest photocatalytic activity was observed with sample 3 wt.% CQDs/BiOBr nanosheets for the degradation of CIP, RhB, and BPA under visible light irradiation. It was revealed that are three factors are responsible for enhanced photocatalysis: Lower resistance, high visible light absorbance and high separation efficiency of photoinduced holes and electrons.

Di et al. (2017) prepared NCQDs/$BiPO_4$ composite using ionic liquid assisted solvothermal method. This N-CQDs/$BiPO_4$ exhibited an enhanced photocatalytic activity for the degradation of three antibiotics (CIP, tetracycline and enrofloxacin) under UV irradiation The main active species was found to be superoxide radicals and not hydroxyl radicals. Kaur et al. (2017) synthesized Ag_2O/TiO_2 QDs using pH-mediated precipitation method. It was revealed that as-obtained Ag_2O/TiO_2 QDs were spherical in shape with size ranging between 2−9 nm. As-synthesized composite exhibited significant photocatalytic activity for the degradation of levofloxacin under visible light than TiO_2.

A metal-free composite photocatalyst (GQDs) decorated graphitic carbon nitride nanorods (g-CNNR), was obtained by Yuan et al. (2019) via

hydrothermal technique. The GQDs/g-CNNR exhibited higher photocatalytic activity for removal of antibiotics. It was observed that photocatalytic reaction rate was 2.03 and 3.46 times higher as compared with g-CNNR and pristine graphitic carbon nitride (g-C_3N_4), respectively. It was revealed that this composite show excellent stability and reusability. It was confirmed that photoinduced holes as well as superoxide radicals are main active species in the photocatalytic degradation.

Chen et al. (2019) synthesized CQDs modified potassium titanate nanotubes (CQDs/$K_2Ti_6O_{13}$) via hydrothermal treatment. The successful deposition of CQDs on $K_2Ti_6O_{13}$ photocatalyst was evident from TEM images. The performance of CQDs/$K_2Ti_6O_{13}$ composite was evaluated by degradation of amoxicillin (AMX) under visible light (Fig. 9.7). The photocatalytic activity of CQDs/$K_2Ti_6O_{13}$ hybrid material was found to be higher as compared to neat $K_2Ti_6O_{13}$. It was confirmed that hole (h^+) and hydroxyl radical ($^{\bullet}OH$) played important roles in photocatalytic degradation of AMX.

Jiang et al. (2019) synthesized Fe_3O_4 QDs modified BiOCl/$BiVO_4$ p-n heterojunction. It was observed that 20% Fe_3O_4QDs@BiOCl/$BiVO_4$ p-n heterojunction exhibited an excellent photocatalytic activity for removal of four different broad-spectrum antibiotics in the presence of visible light. The improved photocatalytic performance for the degradation of broad-spectrum antibiotics was mainly attributed to the strong visible light absorption, effective charge carrier mobility, and large specific surface areas. As-fabricated photocatalyst was found stable even after four cycles and it can also be easily separated using an external magnetic field.

Mou et al. (2019) fabricated ultrathin two dimensional (2D) BiOCl/nitrogen-doped GQDs (BiOCl/NGQDs) composites using a hydrothermal process.

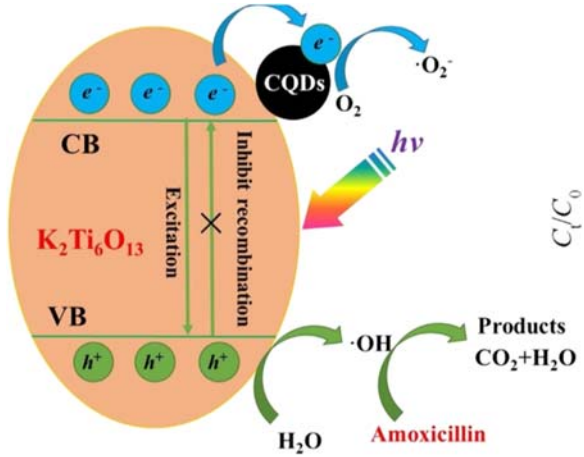

FIGURE 9.7 Photocatalytic degradation of amoxicillin by CQDs/$K_2Ti_6O_{13}$. *Adapted from Chen et al., 2019. Chin. Chem. Lett., 30(6), 1214–1218. With Permission.*

It was observed that BiOCl/NGQDs composites exhibited an increase in both adsorption and photodegradation of CIP as compared to BiOCl. The optimum degradation efficiency of CIP was 82.5% within an hour under visible light, when NGQDs was kept 6.9%, which was much better as compared to BiOCl (34.9%). It was also revealed that this removal efficiency could reach to 95.5% within 5 h.

SCQDs/hollow tubular g-C_3N_4 photocatalyst (HTCN-C) was prepared by Wang et al. (2019) via ultrasonic-assisted method. It was used as catalyst for the degradation of tetracycline (TC) as well as destruction of *E. coli*. It was reported that HTCN-C(2) exhibited an excellent performance for the degrading tetracycline degradation (rate = 0.0293 min^{-1}) and could distract 99.99% *E. coli* under visible destructed light.

Zhao et al. (2019) decorated Co_3O_4 QDs onto phosphorus-doped g-C_3N_4 nanosheets via thermal polymerization method. They used vitamin B_{12} (VB_{12}) as precursor of cobalt and phosphorus mixed with melamine. It was observed that as-prepared sample exhibited the maximum photodegradation efficiency for metronidazole (MTZ), when the sample was prepared with weight ratio of VB12 in precursors at 1%. The efficiency was almost two times better than the removal rate with pure g-C_3N_4. An inhibition was also observed by NO_3^-, Ca^{2+} and HCO_3^-, but Fe^{3+} was found to promote this photodegradation.

The synthesis of self-assembled CQDs and reduced graphene oxide layers modified S@g-C_3N_4/B@g-C_3N_4 (CRSB) (all metal free) was reported by Kumar et al. (2020a). Later, it was used as photocatalyst for the degradation of chloramphenicol (CMP) under visible light and sunlight. It was reported that 99.1% CMP was photodegraded by CRSB in the presence to visible light within 90 min. It was revealed that rate of degradation over CRSB was ten times higher than with g-C_3N_4.

Huang et al. (2020) fabricated up-converted CQDs incorporated goethite (α-FeOOH) nanohybrids (CQDs/α-FeOOH) via hydrolysis method. As-fabricated CQDs/α-FeOOH exhibited excellent degradation of tetracycline (TC), which was almost 3.7 times as compared to α-FeOOH under visible light.

Koe et al. (2020) fabricated a novel photocatalytic membrane by incorporating N,S-CQDs/TiO_2 nanocomposite on polysulfone (PSF) membrane. They used it for photodegradation of DCF in water. The N,S-CQDs/TiO_2 nanocomposites were synthesized with different loadings of N,S-CQDs on TiO_2 nanoparticles. It was observed that N,S-CQDs/TiO_2 (1.5 g) membrane exhibited the best photodegradation performance for DCF removal (62.3%) in the presence of visible light, while TiO_2 membrane showed 3.33% removal only.

Patel et al. (2020) prepared Mn-doped ZnS (Mn:ZnS) QDs through chemical precipitation method. It was observed that as-obtained Mn:ZnS QDs exhibited excellent properties for photodegradation of norfloxacin (NOFX)

in the presence of both UV light and sunlight. These QDs showed excellent stability and reusability up to four consecutive cycles. It was also concluded that these Mn:ZnS QDs could also prove to be useful as efficient as photocatalytic materials in ecological remediation and energy conversion.

Wang et al. (2021) constructed CdS−TiO_2 heterostructure using potato extract as a modifier and a stabilizer. It was revealed that as-prepared CdS−TiO_2 composite exhibited high photocatalytic degradation efficiency with the degradation rate of penicillin (88%). Liu et al. (2021) prepared CQD oxygen-rich titanium dioxide nanosheets (CQD-OTNs) via two-step hydrothermal method. As-prepared composite was used in photodegradation of tetracycline. It was reported that CQD-OTNs could increase the degradation rate of drug to 94.1% within 2 h under visible light irradiation; which was about 2.3 times higher than that with titanium dioxide nanosheets.

Singh et al. (2021) synthesized CdS and CdSe QDs. It was reported that size of the QDs can be controlled by using different mole ratio of water and surfactant. They used thioglycolic acid as capping agent prevent ratio aggregation of QDs The photocatalytic activity of as-synthesized CdSe and CdS QDs was evaluated by selecting 3-aminopyridine as a pollutant.

Wang et al. (2021) used olive leaves as the carbon source to prepare CQDs through hydrothermal treatment. These CQDs were then loaded on the surface of TiO_2 (CQDs/TiO_2 composite). The photocatalytic performance of CQDs/TiO_2 composites was evaluated in the degradation of tetracycline under visible light for 10 min. It was observed that degradation rate of 5% CQDs/TiO_2 could achieve about 81% tetracycline removal.

The silicon-doped CQD were decorated on bismuth molybdate to prepare (1.0SiCQDs/Bi_2MoO_6) nanocomposite by Kumar et al. (2022) via hydrothermal method. It was reported that about 97 and 95% of tetracycline (TC) and of CIP were degraded in 90 min on sunlight exposure.

Xu et al. (2022b) synthesized a series of 0D boron carbon nitride QDs (BCNQDs) modified 2D $Bi_4O_5I_2$ (0D/2D $Bi_4O_5I_2$/BCNQDs) composites. They used these composite for photodegradation of tetracycline (TC) and OTC. It was observed that as-prepared $Bi_4O_5I_2$/BCNQDs composite exhibited highest photocatalytic performance for the degradation of TC and OTC and it was about 4.95 and 2.17 times as compared with $Bi_4O_5I_2$, respectively.

9.3.3 Pesticides

Demand for pesticides, insecticides, weedicides, herbicides, etc. is regularly increasing due to their widespread use in agricultural practices. These are required to safeguard the food grains, foods, vegetables, etc. against any infection or wastage by pest, rodents, etc. and also harm by weeds. These pesticides will reach animals and humans through the food chain causing a number of health problems. It is therefore necessary to treat or degrade these harmful materials. Photocatalysts can play an important role in achieving this object.

Shahnazi et al. (2020) synthesized poly N-isopropylacrylamide (NIPAM) coated MWCNTs/TiO_2 nanocomposite (MWCNTs/TiO_2/TMIP). They selected pendimethalin (PM) herbicide as the target pollutant. This photocatalyst exhibited a higher activity in the degradation of PM (rate constant of 0.0438 min^{-1}) under visible light as compared to other photocatalysts.

The GQDs-ZnO nanocomposites were synthesized by Phophayu et al. (2020). They added GQDs solution into starting precursors during the precipitation. Photocatalytic activity was evaluated for the degradation of glyphosate herbicide over GQDs-ZnO nanocomposites. It was observed that as-prepared GQDs−ZnO nanocomposites exhibited an increased (23% increase) photocatalytic degradation as compared to ZnO.

Xu et al. (2021) fabricated ultrathin CoO/Bi QDs Bi_2MoO_6. It was observed that as-prepared composites exhibited an excellent photocatalytic activity for the removal of diazinon (DZN) (94.2%). They attributed this enhanced photocatalytic activity to the synergistic effect of SPR, ultrathin hollows, oxygen valencies (OVs), and the Z-scheme heterostructure, which will increase visible light absorption and also prevent the recombination of change carriers.

9.3.4 Phenol

Phenols in one or other form are essential at some stages. These also have certain adverse effects on the health of human beings, animals, and aquatic organisms. These phenols can be degraded using an eco-friendly photocatalyst route.

Vertically aligned CdTe−ZnO composite nanorods were fabricated by Liu et al. (2013) from indium tin oxide substrates (ITO). They used a layer-by-layer deposition method formation (CdTe QDs on ZnO nanorod arrays). It was observed that 75% phenol was removed from wastewater in the presence of visible light and composite and 53.2% total organic carbon removal could be achieved within 150 min.

SnO_2 QDs were synthesized by Bhattacharjee and Ahmaruzzaman (2015) via a green biological method using sugar cane juice. The biomolecules of the juice were used as complexing and capping agents and no external agents were required for this purpose. It was observed that as-prepared SnO_2 QDs were spherical in shape with a particle size of ∼3−4.5 nm. They observed a blueshift in the bandgap energy with decreasing particle size, which may be due to quantum confinement effects. The SnO_2 QDs were used for the conversion of *p*-nitrophenol to *p*-aminophenol in the presence of $NaBH_4$ in an aqueous medium. It was reported that 99.5% of *p*-nitrophenol could be reduced in the presence of SnO_2 QDs within an hour.

Kandi et al. (2017) synthesized CdS QDs sensitized self-doped Bi_2MoO_6 via a hydrothermal method. They used glucose as a reducing agent. As-synthesized catalyst was then used to degrade phenol and reduce toxic

Cr(VI) from the aqueous solution. It was reported that 47.5% and 97% degradation of phenol and reduction of Cr(VI), respectively, was obtained using 3% CdS QDs-sensitized self-doped Bi_2MoO_6 in the presence of solar light. Their photostability and reusability was also evaluated and it was observed that this catalyst can be reused for up to five cycles without any significant loss in its activity.

Bajorowicz et al. (2018) comodified CdS quantum dot-decorated $KNbO_3$ composite with Bi_2S_3 QDs by a combination of hydrothermal method with a linker-assisted adsorption route. They used starch and thioglycolic acid as capping agents. It was observed that as-prepared $KNbO_3$-based composites exhibited enhanced photocatalytic performance for the degradation of phenol in an aqueous solution under visible light. It was also reported that the highest photocatalytic performance with better stability were obtained in ternary 30% CdS−5%Bi_2S_3 quantum dot-decorated $KNbO_3$ composite. They also observed catechol, benzoquinone, hydroquinone, and 1,2,4-benzenetriol as the oxidation intermediates of phenol.

Bhatt et al. (2019a) synthesized SnO_2 QDs decorated on TiO_2 nanospheres. Later, they used these composites as photocatalyst for the degradation of 2-nitrophenol. It was found that photocatalytic activity of as-synthesized samples exhibited an efficient degradation of 2-nitrophenol as compared to pure TiO_2 nanospheres.

They also used SnO_2 QDs/TiO_2 nanospheres composite for photocatalytic degradation of picric acid (2,4,6-trinitrophenol) Bhatt et al. (2019b). It is all due to high tunability, high specific surface area, and visible light absorbing ability. It was reported that photocatalytic behavior of as-synthesized samples exhibited better activity compared to only TiO_2 nanospheres.

Hasija et al. (2019) employed a green synthesis approach using bamboo leaves (precursors) for CQDs production via a hydrothermal method. As-fabricated CQDs were then used for the construction of Z-scheme P-doped g-C_3N_4/AgI/ZnO/CQDs (PGCN) heterojunction via immobilization of AgI/ZnO/CQD on graphitic carbon nitride (g-C_3N_4). This composite was then used for the degradation of 2,4-dinitrophenol. The photocatalytic activity of this composite was attributed to electron sink behavior of CQDs. It was reported that this photocatalyst exhibited good stability and recyclability for almost ten cycles.

A solvothermal route was selected by Kumar et al. (2020b) to construct O and S codoped graphitic carbon nitride QDs (OSCNQDs), which were hybridized with Bi_2MoO_6 (BMO). They used these composites for the degradation of aqueous phenol under visible light. As-prepared OSCNQDs/BMO hybrid photocatalyst exhibited almost complete degradation of phenol (98%).

Liang et al. (2020) prepared ZnO composites, which were sensitized by CQDs. They used these composites for the photocatalytic degradation of phenol in the presence of visible light. It was reported that photocatalytic performance of as-prepared ZnO composites (sensitized by CQDs) was

almost 60% higher than that with ZnO. It was also observed that there is good stability and reusability of these composites, as there was no significant change in their activity even after 10 cycles.

9.4 Reduction of carbon dioxide

Scarcity of fossil fuel resources is increasing regularly along with more and more demand for energy in any form. Photocatalytic reduction of carbon dioxide into useful fuels (value-added chemicals) may provide a solution to both these worldwide problems, that is, the problem of the energy crisis and the ever deteriorating environmental quality. Here, photocatalysts have many added advantages. However, some photocatalytic conversion approaches for efficient, economical, and industrialized scalable are to be developed, which can utilize visible and near infrared irradiation.

Wang et al. (2011) sensitized TiO_2 catalysts with PbS QDs. It was observed that PbS QDs enhanced photoreduction rates of CO_2 with TiO_2 almost fivefold as compared to unsensitized TiO_2.

Shao et al. (2017) synthesized ZnO QDs and KNb_3O_8 nanosheets by a hydrothermal technique. They used it for the photocatalytic reduction of CO_2 to methanol. It was observed that the formation rate of pure methanol was only 1257.21 $\mu mol\ g^{-1}\ h^{-1}$, and was found to increase to 1539.77 $\mu mol\ g^{-1}\ h^{-1}$ on deposition of 2 wt.% ZnO QDs on the surface of KNb_3O_8 nanosheets.

The CQDs decorated ultrathin Bi_2WO_6 nanosheets (UBW) were used by Kong et al. (2017) for photoreduction of CO_2 under Vis−NIR irradiation. It was reported that 1CQDs/UBW (1 wt.% CQD content) exhibited higher rate of reduction under visible light irradiation, which has almost 3.1 and 9.5 times enhancement in CH_4 production over UBW and pristine Bi_2WO_6 nanoplatelets (PBW).

ZnO QDs/KNb_3O_8 nanosheets were synthesized by Shao et al. (2017) via a hydrothermal method. The photocatalytic activity of as-prepared materials was evaluated for the photoreduction of CO_2 into formaldehyde under UV light irradiation. The rate with KNb_3O_8 nanosheets was found to be 1257.21 $\mu mol\ g^{-1}\ h^{-1}$, which was increased to 1539.77 $\mu mol\ g^{-1}\ h^{-1}$ on using 2 wt.% ZnO QDs on the surface of KNb_3O_8 nanosheets.

Zubair et al. (2018) reported a photocatalyst composed of graphene-TNT (G-TNT) films and TiO_2 nanotube arrays (TNTs) sensitized with electrodeposited GQDs. It was observed that optimal G-TNT samples could promote the reduction of CO_2 to CH_4 with a rate of 1.98 ppm $cm^{-2}\ h^{-1}$.

Kumar et al. (2019) prepared a hybrid photocatalyst that consisted of a cobalt phthalocyanine tetracarboxylic acid (CoPc-COOH) complex immobilized on organic graphitic carbon nitride. They used triethylamine as a sacrificial electron donor. It was observed that 88.5 μmol (1770 $\mu mol\ g^{-1}$cat) and 59.2 μmol (1184 $\mu mol\ g^{-1}$cat) yield of methanol was obtained (6.5 μmol Co, equivalent to g-C_3N_4/CoPc-COOH) and g-C_3N_4 (50 mg).

A simple complexation−oxidation method was used by Li et al. (2020) to encapsulate CuO QDs in the pores of a metal−organic framework (MOF) of MIL-125(Ti). Then they combined it with g-C_3N_4 to develop a composite photocatalyst, g-C_3N_4/CuO@MIL-125(Ti). It was reported that the photogenerated electrons in MIL-125(Ti) and g-C_3N_4 could be easily transferred to the confined CuO QDs, resulting in enhancement of photocatalytic activity of g-C_3N_4/CuO@MIL-125(Ti) for reducing CO_2 in the presence of water. Use of this photocatalyst could afford CO, methanol, ethanol, and acetaldehyde with yields up to 180.1, 997.2, 1505.7, and 531.5 $\mu mol\ g^{-1}$, respectively.

Indium phosphide (InP) QDs and CdS nanorods were integrated by Do et al. (2020). They used CdS-InP composites for the photoreduction of CO_2 in aqueous solution, where triethanolamine was used as a sacrificial donor. It was observed that photocatalytic activity of the as-synthesized composites was better compared to that of pure CdS alone. The evolution rate of CO over composite was 216 $\mu mol\ h^{-1}\ g^{-1}$ in 3 h.

Qin et al. (2020) synthesized g-C_3N_4 photocatalyst modified by NiS_2 QDs (cocatalyst) via a hydrothermal method. It was observed that this composite exhibited higher activity and stability in the photocatalytic reduction of CO_2. They could achieve the highest evolution rate of CO (10.68 $\mu mol\ h^{-1}\ g^{-1}$) on NSQD/CN-25 catalyst, which was almost 3.88-fold higher compared to g-C_3N_4.

Wang et al. (2020) fabricated 0D/2D heterojunction of $CsPbBr_3$ QDs/Bi_2WO_6 nanosheet (CPB/BWO). Pristine $CsPbBr_3$ has a low catalytic performance due to severe charge recombination. As-prepared CPB/BWO photocatalyst could achieve excellent photocatalytic performance in photocatalytic CO_2 reduction. The total yield of CH_4/CO was 503 $\mu mol\ g^{-1}$, which was nearly 9.5 times higher than that achieved with pristine $CsPbBr_3$.

Que et al. (2021) anchored $FAPbBr_3$ QDs on Ti_3C_2 nanosheets to fabricate $FAPbBr_3$/Ti_3C_2 composite. It was observed that $FAPbBr_3$/Ti_3C_2 composite photocatalyst exhibited an excellent photocatalytic reduction of CO_2. The Ti_3C_2 nanosheet acted as an electron acceptor to promote the rapid separation of excitons and supply specific catalytic sites. It was reported that a consumption rate of 717.18 $\mu mol\ g^{-1}\ h^{-1}$ could be obtained by $FAPbBr_3$/0.2-Ti_3C_2 composite and it was almost 2.08 times the rate of the pristine $FAPbBr_3$ QDs (343.90 $\mu mol\ g^{-1}\ h^{-1}$). This photocatalyst also exhibited good stability during photocatalytic reaction.

A direct Z-scheme 0D/2D heterojunction of CuO QDs/ultrathin CoAl-LDH (CuO/CoAl-u) was prepared by Jiang et al. (2022). It was revealed that 4.5%CuO/CoAl-u heterojunction could achieve yield of CH_3OH as 283.26 $\mu mol\ g^{-1}\ h^{-1}$ by photocatalytic reduction of CO_2.

9.5 Hydrogen production

It has become almost certain that future energy demands cannot be fulfilled by fossil fuel resources because they are reaching a level of

complete exhaustion. Therefore, it is necessary to find an alternate renewable energy source. Nature is playing an indirect role in converting carbon dioxide to carbohydrate (biomass). Here, water is utilized as a reducing agent. Hydrogen can be produced by photosplitting of water in the presence of a photocatalyst and light. It has also been advocated as a fuel of the future creating no pollution, as the final product of combustion is water.

Ge et al. (2012) synthesized CdS quantum dot-coupled graphitic carbon nitride photocatalysts. It was observed that the H_2 evolution rate was 17.27 μmol h^{-1} with CdS QD content (30 wt.%) under visible light irradiation, which was about nine times higher than that with pure g-C_3N_4.

Yu et al. (2014) prepared cobalt sulfide QDs (CoS_x QDs) modified TiO_2 nanoparticles using a precipitation−deposition method. They used cobalt acetate, TiO_2, and sodium sulfide as the precursors of Co, Ti, and S, respectively. The CoS_x QDs act as an effective cocatalyst in photocatalytic H_2 production by TiO_2. It was reported that the amount of CoS_x exhibited an optimum value at about 5% (mole ratio to TiO_2), where the production rate of H_2 could reach 838 μmol h^{-1} g^{-1}, which was 35 times more than with pure TiO_2. Here, ethanol was used as a sacrificial reagent.

Kuang et al. (2016) embedded Au QDs rimous cadmium sulfide nanospheres to synthesize hybrid photocatalysts via a hydrothermal process followed by photoreduction. The rimous cadmium sulfide nanospheres had irregular fissures and a rough surface, which will greatly strengthen their adhesion and interaction with (Au) QDs. It was revealed that the highest photocatalytic activity for hydrogen generation was 601.2 μmol h^{-1} g^{-1} and it was achieved by adjusting the Au mass loading.

Lee et al. (2018) synthesized molybdenum disulfide QDs decorated bismuth sulfide photocatalyst and used them for the generation of hydrogen by photosplitting water. They could achieve the highest hydrogen yield (17.7 mmol g^{-1} h^{-1}) with 0.14MoS_2QD/Bi_2S_3, and this yield was 4.5-fold higher than undoped Bi_2S_3 in the presence of stimulated solar light. As-prepared photocatalyst could achieve a yield of hydrogen (53.6 μmol g^{-1}) in 6 h under NIR irradiation.

Pan et al. (2018) prepared thermally stable and highly dispersed TiO_2 QDs (TiO_2-QDs) in pore channels of SiO_2 foams with large pore size (14−20 nm) using in situ hydrolysis of Ti-alkoxide. It was observed that there was an anchoring effect between the pore-wall of SiO_2 foam and TiO_2-QDs, which resulted in the efficient prohibition of the change in both the TiO_2 phases (anatase to rutile) as well as aggregation of TiO_2-QDs. The crystal size was found to be less than 7 nm. These hybrid photocatalysts show higher efficiency in hydrogen evaluation with a quantum efficiency 17.8% using UV irradiation. It was reported that TiO_2-QDs/SiO_2

photocatalysts exhibited a significant H_2 evolution rate. The outstanding activity of these photocatalysts in hydrogen evolution was due to high anatase crystallinity, short electron-transfer distance, excellent stability of TiO_2-QDs, and uniform dispersity in silica foam.

Sun et al. (2018) adopted two facile synthetic routes for the synthesis of MoS_2 QDs: (1) hydrothermal process and (2) liquid exfoliation strategy. They were used as cocatalyst in photocatalytic hydrogen production under visible light. It was reported that MoS_2 QDs-L (L = liquid exfoliation method) can increase the photocatalytic hydrogen activity of CdS under visible light irradiation. The composite MoS_2 QDs-L/CdS could achieve maximum hydrogen production activity with a rate of 1032.1 $\mu mol\ h^{-1}$ using lactic acid as a sacrificial agent, which was almost 2.7 and 15.4 times more than MoS_2/CdS (383.5 $\mu mol\ h^{-1}$) and CdS (66.9 $\mu mol\ h^{-1}$), respectively.

Luo et al. (2018) fabricated CNQDs on $SnNb_2O_6$ ultrathin nanosheets via a hydrothermal method. It was reported that upconversion behavior of CNQDs in CNQDs/$SnNb_2O_6$ nanocomposites provided the ability of photocatalytic production of H_2 utilizing wavelengths >600 nm.

Yang et al. (2019) reported the development of noble-metal-free catalysts having enhanced photocatalytic activity. The cobalt sulfide QDs g-C_3N_4 nanosheets (Co_3S_4/CNNS) nanocomposites were synthesized by a two-step method, using in situ deposition. It was observed that the particle size of highly dispersed Co_3S_4 QDs was 2−4 nm. These were uniformly fixed on carbon nitride nanosheets (CNNS), which can be a good alternative to noble metals for the improvement of photocatalytic activity of CNNS. It was revealed that Co_3S_4/CNNS-900 had apparent quantum efficiency of the order of 7.85% at 400 nm. It was also observed that the H_2 evolution rate of Co_3S_4/CNNS-900 was found to be 20,536.4 $\mu mol\ g^{-1}\ h^{-1}$, which was about 555 times greater than that with CNNS. The Co_3S_4 QDs were highly dispersed on 2D CNNS, facilitating the formation of more active sites. It also shortened the migration distance of as-generated photogenerated carriers, which finally resulted in an increased photocatalytic performance.

The functionalized carbon nanotubes−titania QDs (FCNT-TQDs) were prepared by Reddy et al. (2020). The CNTs may play a dual role as cocatalyst and photosensitizer to increase light harvesting and reduce the recombination rate of charge carriers. It was observed that the maximum production rate of hydrogen could be obtained up to 54.4 $mmol\ h^{-1}g^{-1}$ by the addition of copper. This rate was 5.4 and 2.5 times higher compared to pristine TiO_2 QDs and FCNT-TQDs composite, respectively.

The nickel (atomically dispersed) in cadmium−zinc sulfide QDs (ZCS QDs) exhibited excellent and stable photocatalytic performance for splitting of water

under sunlight (Su et al., 2020). It was observed that finely tuned Ni atoms dispersed in ZCS QDs exhibited hydrogen production of 18.87 mmol g^{-1}.

Li et al. (2021) anchored small-sized TiO_2 photocatalysts onto large-sized Ti_3C_2-Mxene cocatalysts. A higher hydrogen production rate was observed to be 62.5 μmol with as-prepared photocatalyst, which was about 15.2 times higher than that with TiO_2 (4.1 μmol).

You et al. (2022) prepared (0D/2D) heterojunction nanocomposite [Ag_2S QDs (g-C_3N_4)]. The average particle size of Ag_2S QDs was around 5.8 nm. It was observed that composite (0.5 wt.% Ag_2S QDs) loading could give the highest hydrogen evolution rate of 471.1 μmol g^{-1} h^{-1}.

9.6 Other applications

Cadmium sulfide QDs sensitized mesoporous TiO_2 (photocatalysts) were prepared by Li et al. (2009). First, cadmium oxide was preplanted as crystal seeds in ordered mesoporous titanium dioxide and then CdO was converted to CdS QDs via ion-exchange. As-prepared photocatalyst exhibited an excellent photocatalytic efficiency for oxidation of NO gas in air as well as the degradation of organic compounds in an aqueous medium under visible light.

Bismuth monoxide QDs (average size of 2−5 nm) were prepared by Sun et al. (2017) and then used for the synthesis of ammonia under simulated solar light using photocatalytic reduction of nitrogen. The highest rate (1226 μmol g^{-1} h^{-1}) was achieved for ammonia synthesis without using any cocatalyst or a sacrificial agent. It is about 10^3 times higher than with the Fe-TiO_2 photocatalyst. Zhang et al. (2017) synthesized Pt QDs (2−4 nm) and deposited them on N-doped $(BiO)_2CO_3$ hierarchical superstructures via a hydrothermal method. They used H_2PtCl_6 and ammonium bismuth citrate as precursors. It was reported that as-prepared Pt/N-doped $(BiO)_2CO_3$ catalysts exhibited an enhanced visible light photocatalytic removal of NO removal.

Xie et al. (2018) prepared tin oxide GQDs (SnO_2/GQDs) composite. They used it for the photocatalytic removal of nitric oxide (NO). It was observed that this composite exhibited an enhanced activity compared to SnO_2 only. Visible light response and charge separation efficiency of this composite was increased due to the presence of GQDs in the composite. A series of SnO_2/g-C_3N_4 composites was prepared by Zou et al. (2019). They decorated SnO_2 QDs onto g-C_3N_4 sheets. It was reported that SnO_2/g-C_3N_4 had an excellent response toward visible light and higher ability to inhibit the NO_2 generation.

9.7 Recent developments

Some recent advances are shown in Table 9.1

TABLE 9.1 Some recent applications of quantum dots in photocatalysis.

Quantum dots	Method of synthesis	Application	References
g-C_3N_4 and Ag-g-C_3N_4	Ultrasonication	H_2 production, dye degradation, antimicrobial activity	Mallikarjuna et al. (2021)
SnO_2/$AgVO_3$/g-C_3N_4	Hydrothermal	H_2 production	Koyyada et al. (2021)
Ag/cellulose nanocrystal (CNC)-doped CeO_2	Coprecipitation	Degradation of methylene blue and ciprofloxacin	Ikram et al. (2021)
Covalent organic frameworks (COFs) quantum dots	Solvothermal	Degradation of methyl red, methyl orange and methyl blue	Bahadori et al. (2021)
Carbon dots	Ultrasonication	Degradation of Congo red and methylene blue.	Zaib et al. (2021)
Boron-doped CQD (BCQD)-hybridized g-C_3N_4 homojunction (CN) nanocomposite	Hydrothermal	Degradation of rhodamine B	Phang et al. (2022)
Metal-free boron nitride quantum dots (BNQDs) $BiFeO_3$	Impregnation	Degradation of tetracycline hydrochloride	Balta and Simsek (2021)
Cu-doped carbon quantum dots(CD(Cu)) modified Ni-MOL (CD (Cu)-Ni-MOL)	Hydrothermal	Degradation of Tetracycline	Li et al. (2021)
Silver vanadate quantum dots ($AgVO_3$ QDs)-doped reduced graphene oxide and graphitic carbon nitride nanocomposites modified polyvinylidene fluoride (PVDF) membrane (AgVO3/RGO/C3N4-PVDF)	Fabricated	Degradation of tetracycline, excellent antifouling activity rejection of 97.4% of *Escherichia coli*, self-cleaning capacity	Cui et al. (2022)
Zero-dimensional WO_3 quantum dots on two-dimensional ultrathin $CdIn_2S_2$		Photocatalytic reduction of CO_2	Zhang et al. (2022)

(*Continued*)

TABLE 9.1 (Continued)

Quantum dots	Method of synthesis	Application	References
Graphitic carbon nitride quantum dots coupled Zr(IV)		Photoreduction of CO_2	Sonowal et al. (2022)
Zero-dimensional (0D) Bi_3TaO_7 (BTO) quantum dots/three-dimensional (3D) onion-ring-like g-C_3N_4 (OR-CN) S-scheme heterojunction	Solvothermal	Photocatalytic evolution of H_2	Shi et al. (2022)
N-doped carbon quantum dots (NCQDs) modified CdS nanocomposite	Hydrothermal	Photocatalytic evolution of H_2	Xu et al. (2022c)

9.8 Conclusion

Photocatalysis makes use of hydroxyl radicals as oxidants; they are considered the strongest oxidants after fluorine. They can degrade the majority of organic pollutants to harmless products such as CO_2, H_2O, and inorganic ions. In other words, it leads to complete mineralization. The ever increasing amount of carbon dioxide is creating havoc in the form of melting glaciers, raising sea level, global warming, etc. which can be controlled by photocatalytic reduction of carbon dioxide to provide some value-added chemicals (synthetic fuels). Use of these fuels will return the same amount of CO_2 to the atmosphere. Thus it can be considered as a short-term loan of CO_2. Another problem of green fuel can be solved by generating hydrogen through photosplitting of water. Hydrogen has a high storage capacity and this fuel will not add any kind of pollution to the atmosphere as water is produced on burning this fuel, which is harmless. Photocatalysis will find a prominent position in solving all these problems in the years to come.

References

Abd Rani, U., Ng, L.Y., Ng, C.Y., Mahmoudi, E., Ng, Y.S., Mohammad, A.W., 2021. Sustainable production of nitrogen-doped carbon quantum dots for photocatalytic degradation of methylene blue and malachite green. J. Water Proc. Eng. 40. Available from: https://doi.org/10.1016/j.jwpe.2020.101816.

Ahlawat, A., Rana, P.S., Solanki, P.R., 2021. Studies of photocatalytic and optoelectronic properties of microwave synthesized and polyethyleneimine stabilized carbon quantum dots. Mater. Lett. 305. Available from: https://doi.org/10.1016/j.matlet.2021.130830.

Ameta, R., Ameta, S.C. (Eds.), 2016. Photocatalysis: Principles and Applications. CRC Press, Florida.

Ameta, S.C., Ameta, R., Vardia, J., Ameta, R., Ali, Z., 1999. Photocatalysis: a frontier of photochemistry. J. Indian. Chem. Soc. 76 (6), 281–287.

Ameta, R., Benjamin, S., Ameta, A., Ameta, S.C., 2013. Photocatalytic degradation of organic pollutants: a review. Mater. Sci. Forum 734, 247–272.

Anh, N.T.N., Chowdhury, A.D., Doong, R.A., 2017. Highly sensitive and selective detection of mercury ions using N, S-codoped graphene quantum dots and its paper strip based sensing application in wastewater. Sens. Actuators B: Chem. 252, 1169–1178.

Babu, B., Koutavarapu, R., Harish, V.V.N., Shim, J., Yoo, K., 2019. Novel in-situ synthesis of Au/SnO_2 quantum dots for enhanced visible-light-driven photocatalytic applications. Ceram. Int. 45 (5), 5743–5750.

Bahadori, A., Ranjbar, M., Asadipour, A., Kalantari-Khandani, S., 2021. Covalent organic frameworks (COFs) quantum dots as supramolecular cages modified with biochar as nanobio photocatalyst for degradation of organic dyes. J. Mater. Sci.: Mater. Electron. 32 (18), 23018–23029.

Bajorowicz, B., Kowalska, E., Nadolna, J., Wei, Z., Endo, M., Ohtani, B., et al., 2018. Preparation of CdS and Bi_2S_3 quantum dots co-decorated perovskite-type $KNbO_3$ ternary heterostructure with improved visible light photocatalytic activity and stability for phenol degradation. Dalton Trans. 47 (42), 15232–15245.

Balta, Z., Simsek, E.B., 2021. Uncovering the systematical charge separation effect of boron nitride quantum dots on photocatalytic performance of $BiFeO_3$ perovskite towards degradation of tetracycline antibiotic. J. Environ. Chem. Eng. 9 (6), 106567.

Bhatt, J., Jat, K.K., Rai, A.K., Ameta, R., Ameta, S.C., 2019a. Photodegradation of 2-nitrophenol, an endocrine disruptor, using TiO_2 nanospheres/SnO_2 quantum dots 2. Green Chemistry and Biodiversity. Apple Academic Press, Cambridge, pp. 1–8.

Bhatt, J., Benjamin, S., Ameta, R., Ameta, S.C., 2019b. Enhancement of photodegradation of picric acid (2, 4, 6-trinitrophenol) by fabrication of visible-light-active SnO_2 quantum dots/TiO_2 nanospheres composite. J. Appl. Chem. 8 (4), 1805–1812.

Bhattacharjee, A., Ahmaruzzaman, M., 2015. Photocatalytic-degradation and reduction of organic compounds using SnO_2 quantum dots (via a green route) under direct sunlight. RSC Adv. 5 (81), 66122–66133.

Chen, J.W., Shi, J.W., Wang, X., Ai, H.Y., Cui, H.J., Fu, M.L., 2013. Hybrid metal oxides quantum dots/TiO_2 block composites: facile synthesis and photocatalysis application. Powder Technol. 246, 108–116.

Chen, Q., Chen, L., Qi, J., Tong, Y., Lv, Y., Xu, C., 2019. Photocatalytic degradation of amoxicillin by carbon quantum dots modified $K_2Ti_6O_{13}$ nanotubes: effect of light wavelength. Chin. Chem. Lett. 30 (6), 1214–1218.

Cheraghizade, M., Jamali-Sheini, F., Yousefi, R., Niknia, F., Mahmoudian, M.R., Sookhakian, M., 2017. The effect of tin sulfide quantum dots size on photocatalytic and photovoltaic performance. Mater. Chem. Phys. 195, 187–194.

Chong, M.N., Jin, B., Chow, C.W., Saint, C., 2010. Recent developments in photocatalytic water treatment technology: a review. Water Res. 44 (10), 2997–3027.

Cui, Y., Wang, Z., Zheng, J., Li, B., Yan, Y., Meng, M., 2022. Fabrication of silver vanadate quantum dots/reduced graphene oxide/graphitic carbon nitride Z-scheme heterostructure modified polyvinylidene fluoride self-cleaning membrane for enhancing photocatalysis and mechanism insight. J. Coll. Interf. Sci. . Available from: https://doi.org/10.1016/j.jcis.2022.01.008.

Di, J., Xia, J., Chen, X., Ji, M., Yin, S., Zhang, Q., et al., 2017. Tunable oxygen activation induced by oxygen defects in nitrogen doped carbon quantum dots for sustainable boosting photocatalysis. Carbon 114, 601–607.

Djurišić, A.B., He, Y., Ng, A.M., 2020. Visible-light photocatalysts: prospects and challenges. APL. Mater. 8 (3). Available from: https://doi.org/10.1063/1.5140497.

Do, K.H., Kumar, D.P., Rangappa, A.P., Hong, Y., Reddy, D.A., Kim, T.K., 2020. Indium phosphide quantum dots integrated with cadmium sulfide nanorods for photocatalytic carbon dioxide reduction. ChemCatChem 12 (18), 4550–4557.

Doshi, K., Mungray, A.A., 2020. Bio-route synthesis of carbon quantum dots from tulsi leaves and its application as a draw solution in forward osmosis. J. Environ. Chem. Eng. 8 (5). Available from: https://doi.org/10.1016/j.jece.2020.104174.

Fan, J., Li, D., Wang, X., 2016. Effect of modified graphene quantum dots on photocatalytic degradation property. Diam. Relat. Mater. 69, 81–85.

Fan, X., Zhang, S., Guan, R., Shao, X., Jiang, S., Hu, Y., et al., 2022. Black phosphorus quantum dots as photocatalyst for dye degradation with a high efficiency and rate constant. J. Mol. Struct. 1252. Available from: https://doi.org/10.1016/j.molstruc.2021.132163.

Fox, M.A., Dulay, M.T., 1993. Heterogeneous photocatalysis. Chem. Rev. 93 (1), 341–357.

Gao, X., Ji, X., Nguyen, T.T., Gong, X., Chai, R., Guo, M., 2019. A novel composite material with wood-based carbon quantum dots modified Bi_2MoO_6 hollow microspheres. Vacuum 164, 256–264.

Ge, L., Zuo, F., Liu, J., Ma, Q., Wang, C., Sun, D., et al., 2012. Synthesis and efficient visible light photocatalytic hydrogen evolution of polymeric g-C_3N_4 coupled with CdS quantum dots. J. Phys. Chem. C. 116 (25), 13708–13714.

Hasija, V., Sudhaik, A., Raizada, P., Hosseini-Bandegharaei, A., Singh, P., 2019. Carbon quantum dots supported AgI/ZnO/phosphorus doped graphitic carbon nitride as Z-scheme photocatalyst for efficient photodegradation of 2, 4-dinitrophenol. J. Environ. Chem. Eng. 7 (4). Available from: https://doi.org/10.1016/j.jece.2019.103272.

Hatefi, R., Younesi, H., Mashinchian-Moradi, A., Nojavan, S., 2021a. A facile decoration of anatase Fe_3O_4/TiO_2 nanocomposite with graphene quantum dots: synthesis, characterization, and photocatalytic activity. Adv. Powder Technol. 32 (7), 2410–2422.

Hatefi, R., Younesi, H., Mashinchian-Moradi, A., Nojavan, S., 2021b. The efficiency of magnetic TiO2 anatase loaded by graphen quantum dots for photocatalytic degradation of imipramine from aquatic media. Environ. Sci. 20. Available from: https://doi.org/10.52547/envs.2021.1021.

Huang, S., Zhang, Q., Liu, P., Ma, S., Xie, B., Yang, K., et al., 2020. Novel up-conversion carbon quantum dots/α-FeOOH nanohybrids eliminate tetracycline and its related drug resistance in visible-light responsive fenton system. Appl. Catal. B: Environ. 263. Available from: https://doi.org/10.1016/j.apcatb.2019.118336.

Hui, K.C., Ang, W.L., Sambudi, N.S., 2021. Nitrogen and bismuth-doped rice husk-derived carbon quantum dots for dye degradation and heavy metal removal. J. Photochem. Photobiol. A: Chem. 418. Available from: https://doi.org/10.1016/j.jphotochem.2021.113411.

Ibhadon, A.O., Fitzpatrick, P., 2013. Heterogeneous photocatalysis: recent advances and applications. Catalysts 3 (1), 189–218.

Ikram, M., Hayat, S., Imran, M., Haider, A., Naz, S., Ul-Hamid, A., et al., 2021. Novel Ag/cellulose-doped CeO_2 quantum dots for efficient dye degradation and bactericidal activity with molecular docking study. Carbohydr. Polym. 269. Available from: https://doi.org/10.1016/j.carbpol.2021.118346.

Jacob, J.M., Sinharoy, A., Lens, P.N., 2020. Photocatalytic degradation of congo red by zinc sulfide quantum dots produced by anaerobic granular sludge. Environ. Technol. . Available from: https://doi.org/10.1080/09593330.2020.1856940.

Jamila, G.S., Sajjad, S., Leghari, S.A.K., Mahmood, T., 2020a. Role of nitrogen doped carbon quantum dots on CuO nano-leaves as solar induced photo catalyst. J. Phys. Chem. Solids. 138. Available from: https://doi.org/10.1016/j.jpcs.2019.109233.

Jamila, G.S., Sajjad, S., Leghari, S.A.K., Long, M., 2020b. Nitrogen doped carbon quantum dots and GO modified WO_3 nanosheets combination as an effective visible photo catalyst. J. Hazard. Mater. 82. Available from: https://doi.org/10.1016/j.jhazmat.2019.121087.

Jat, K.K., Bhatt, J., Ameta, S.C., 2019. Photodegradation of fast green by using SnO_2 quantum dots/TiO_2 nanoparticles composite. J. Appl. Chem. 8 (1), 139–145.

Jiang, R., Wu, D., Lu, G., Yan, Z., Liu, J., Zhou, R., et al., 2019. Fabrication of Fe_3O_4 quantum dots modified BiOCl/$BiVO_4$ pn heterojunction to enhance photocatalytic activity for removing broad-spectrum antibiotics under visible light. J. Taiwan. Inst. Chem. Eng. 96, 681–690.

Jiang, Y., Guo, J., Li, X., Wu, G., Mu, M., Yin, X., 2022. Direct Z-scheme 0D/2D heterojunction of CuO quantum Dots/ultrathin CoAl-LDH for boosting charge separation and photocatalytic CO_2 reduction. Sol. Energy 231, 705–715.

Kandi, D., Martha, S., Thirumurugan, A., Parida, K.M., 2017. CdS QDs-decorated self-doped γ-Bi_2MoO_6: a sustainable and versatile photocatalyst toward photoreduction of Cr (VI) and degradation of phenol. ACS Omega 2 (12), 9040–9056.

Karimi, F., Rajabi, H.R., Kavoshi, L., 2019. Rapid sonochemical water-based synthesis of functionalized zinc sulfide quantum dots: study of capping agent effect on photocatalytic activity. Ultrason. Sonochem. 57, 139–146.

Kaur, A., Umar, A., Kansal, S.K., 2015. Sunlight-driven photocatalytic degradation of non-steroidal anti-inflammatory drug based on TiO_2 quantum dots. J. Colloid Interface Sci. 459, 257–263.

Kaur, A., Salunke, D.B., Umar, A., Mehta, S.K., Sinha, A.S.K., Kansal, S.K., 2017. Visible light driven photocatalytic degradation of fluoroquinolone levofloxacin drug using Ag_2 O/TiO_2 quantum dots: a mechanistic study and degradation pathway. N. J. Chem. 41 (20), 12079–12090.

Koe, W.S., Chong, W.C., Pang, Y.L., Koo, C.H., Ebrahim, M., Mohammad, A.W., 2020. Novel nitrogen and sulphur co-doped carbon quantum dots/titanium oxide photocatalytic membrane for in-situ degradation and removal of pharmaceutical compound. J. Water Process. Eng. 33. Available from: https://doi.org/10.1016/j.jwpe.2019.101068.

Kong, X.Y., Tan, W.L., Ng, B.J., Chai, S.P., Mohamed, A.R., 2017. Harnessing Vis–NIR broad spectrum for photocatalytic CO_2 reduction over carbon quantum dots-decorated ultrathin Bi_2WO_6 nanosheets. Nano Res. 10 (5), 1720–1731.

Koyyada, G., Siva Kumar, N., Al-Ghurabi, E.H., Asif, M., Mallikarjuna, K., 2021. Enhanced solar-driven photocatalytic performance of a ternary composite of SnO_2 quantum dots// $AgVO_3$ nanoribbons//g-C_3N_4 nanosheets (0D/1D/2D) structures for hydrogen production and dye degradation. Environ. Sci. Pollut. Res. 28 (24), 31585–31595.

Kuang, P.Y., Zheng, P.X., Liu, Z.Q., Lei, J.L., Wu, H., Li, N., et al., 2016. Embedding Au quantum dots in rimous cadmium sulfide nanospheres for enhanced photocatalytic hydrogen evolution. Small. 12 (48), 6735–6744.

Kumar, G., Cilamkoti, V., Dutta, R.K., 2022. Sunlight mediated enhanced photocatalytic degradation of antibiotics in aqueous medium using silicon doped carbon quantum dots decorated Bi_2MoO_6 nanoflakes. Colloids Surf. A: Physicochem. Eng. Asp. 639. Available from: https://doi.org/10.1016/j.colsurfa.2022.128368.

Kumar, S., Dhiman, A., Sudhagar, P., Krishnan, V., 2018. ZnO-graphene quantum dots heterojunctions for natural sunlight-driven photocatalytic environmental remediation. Appl. Surf. Sci. 447, 802–815.

Kumar, A., Prajapati, P.K., Aathira, M.S., Bansiwal, A., Boukherroub, R., Jain, S.L., 2019. Highly improved photoreduction of carbon dioxide to methanol using cobalt phthalocyanine grafted to graphitic carbon nitride as photocatalyst under visible light irradiation. J. Colloid Interf. Sci. 543, 201–213.

Kumar, A., Kumari, A., Sharma, G., Du, B., Naushad, M., Stadler, F.J., 2020a. Carbon quantum dots and reduced graphene oxide modified self-assembled S@ C_3N_4/B@ C_3N_4 metal-free nano-photocatalyst for high performance degradation of chloramphenicol. J. Mol. Liq. 300. Available from: https://doi.org/10.1016/j.molliq.2019.112356.

Kumar, A., Raizada, P., Singh, P., Hosseini-Bandegharaei, A., Thakur, V.K., 2020b. Facile synthesis and extended visible light activity of oxygen and sulphur co-doped carbon nitride quantum dots modified Bi_2MoO_6 for phenol degradation. J. Photochem. Photobiol. A: Chem. 397. Available from: https://doi.org/10.1016/j.jphotochem.2020.112588.

Kusic, H., Leszczynska, D., Koprivanac, N., Peternel, I., 2011. Role of quantum dots nanoparticles in the chemical treatment of colored wastewater: catalysts or additional pollutants. J. Environ. Sci. 23 (9), 1479–1485.

Lee, W.C., Kong, X.Y., Tan, L.L., Gui, M.M., Sumathi, S., Chai, S.P., 2018. Molybdenum disulfide quantum dots decorated bismuth sulfide as a superior noble-metal-free photocatalyst for hydrogen evolution through harnessing a broad solar spectrum. Appl. Catal. B: Environ. 232, 117–123.

Li, G.S., Zhang, D.Q., Yu, J.C., 2009. A new visible-light photocatalyst: CdS quantum dots embedded mesoporous TiO_2. Environ. Sci. Technol. 43 (18), 7079–7085.

Li, N., Liu, X., Zhou, J., Chen, W., Liu, M., 2020. Encapsulating CuO quantum dots in MIL-125 (Ti) coupled with g-C_3N_4 for efficient photocatalytic CO_2 reduction. Chem. Eng. J. 399. Available from: https://doi.org/10.1016/j.cej.2020.125782.

Li, W., Zhuang, C., Li, Y., Gao, C., Jiang, W., Sun, Z., et al., 2021. Anchoring ultra-small TiO_2 quantum dots onto ultra-thin and large-sized Mxene nanosheets for highly efficient photocatalytic water splitting. Ceram. Int. 47 (15), 21769–21776.

Liang, H., Tai, X., Du, Z., Yin, Y., 2020. Enhanced photocatalytic activity of ZnO sensitized by carbon quantum dots and application in phenol wastewater. Opt. Mater. 100. Available from: https://doi.org/10.1016/j.optmat.2020.109674.

Lin, X., Liu, C., Wang, J., Yang, S., Shi, J., Hong, Y., 2019. Graphitic carbon nitride quantum dots and nitrogen-doped carbon quantum dots co-decorated with $BiVO_4$ microspheres: a ternary heterostructure photocatalyst for water purification. Sep. Purif. Technol. 226, 117–127.

Liu, D., Zheng, Z., Wang, C., Yin, Y., Liu, S., Yang, B., 2013. CdTe quantum dots encapsulated ZnO nanorods for highly efficient photoelectrochemical degradation of phenols. J. Phys. Chem. C. 117 (50), 26529–26537.

Liu, H., Liang, J., Fu, S., Li, L., Cui, J., Gao, P., 2020. N doped carbon quantum dots modified defect-rich g-C_3N_4 for enhanced photocatalytic combined pollutions degradation and hydrogen evolution. Colloids Surf. A: Physicochem. Eng. Asp. 591. Available from: https://doi.org/10.1016/j.colsurfa.2020.124552.

Liu, X., Yang, Y., Li, H., Yang, Z., Fang, Y., 2021. Visible light degradation of tetracycline using oxygen-rich titanium dioxide nanosheets decorated by carbon quantum dots. Chem. Eng. J. 408. Available from: https://doi.org/10.1016/j.cej.2020.127259.

Luo, B., Hong, Y., Li, D., Fang, Z., Jian, Y., Shi, W., 2018. Fabrication of 0D/2D carbon nitride quantum dots/$SnNb_2O_6$ ultrathin nanosheets with enhanced photocatalytic hydrogen production. ACS Sustain. Chem. Eng. 6 (11), 14332–14339.

Mallikarjuna, K., Vattikuti, S.V.P., Manne, R., Manjula, G., Munirathnam, K., Mallapur, S., et al., 2021. Sono-chemical synthesis of silver quantum dots immobilized on exfoliated

graphitic carbon nitride nanostructures using ginseng extract for photocatalytic hydrogen evolution, dye degradation, and antimicrobial studies. Nanomaterials 11 (11). Available from: https://doi.org/10.3390/nano11112918.

Mandal, P., Nath, K.K., Saha, M., 2021. Efficient blue luminescent graphene quantum dots and their photocatalytic ability under visible light. Biointerface Res. Appl. Chem. 11 (1), 8171–8178.

Mansur, A.A., Mansur, H.S., Ramanery, F.P., Oliveira, L.C., Souza, P.P., 2014. "Green" colloidal ZnS quantum dots/chitosan nano-photocatalysts for advanced oxidation processes: study of the photodegradation of organic dye pollutants. Appl. Catal. B: Environ. 158, 269–279.

Miao, R., Luo, Z., Zhong, W., Chen, S.Y., Jiang, T., Dutta, B., et al., 2016. Mesoporous TiO_2 modified with carbon quantum dots as a high-performance visible light photocatalyst. Appl. Catal. B: Environ. 189, 26–38.

Mohamed, W.A., Handal, H.T., Ibrahem, I.A., Galal, H.R., Mousa, H.A., Labib, A.A., 2021. Recycling for solar photocatalytic activity of Dianix blue dye and real industrial wastewater treatment process by zinc oxide quantum dots synthesized by solvothermal method. J. Hazard. Mater. 404. Available from: https://doi.org/10.1016/j.jhazmat.2020.123962.

Mohamed, W.A., Abd El-Gawad, H.H., Mekkey, S.D., Galal, H.R., Labib, A.A., 2022. Facile synthesis of quantum dots metal oxide for photocatalytic degradation of organic hazardous materials and factory effluents. Arab. J. Chem. 15 (2). Available from: https://doi.org/10.1016/j.arabjc.2021.103593.

Mou, Z., Zhang, H., Liu, Z., Sun, J., Zhu, M., 2019. Ultrathin BiOCl/nitrogen-doped graphene quantum dots composites with strong adsorption and effective photocatalytic activity for the degradation of antibiotic ciprofloxacin. Appl. Surf. Sci. 496. Available from: https://doi.org/10.1016/j.apsusc.2019.143655.

Muthulingam, S., Lee, I.H., Uthirakumar, P., 2015. Highly efficient degradation of dyes by carbon quantum dots/N-doped zinc oxide (CQD/N-ZnO) photocatalyst and its compatibility on three different commercial dyes under daylight. J. Colloid Interf. Sci. 455, 101–109.

Niazi, Z., Goharshadi, E.K., Mashreghi, M., Jorabchi, M.N., 2021. Highly efficient solar photocatalytic degradation of a textile dye by TiO_2/graphene quantum dots nanocomposite. Photochem. Photobiol. Sci. 20 (1), 87–99.

Pan, D., Han, Z., Miao, Y., Zhang, D., Li, G., 2018. Thermally stable TiO_2 quantum dots embedded in SiO_2 foams: characterization and photocatalytic H_2 evolution activity. Appl. Catal. B: Environ. 229, 130–138.

Patel, J., Singh, A.K., Carabineiro, S., 2020. Assessing the photocatalytic degradation of fluoroquinolone norfloxacin by Mn: ZnS quantum dots: kinetic study, degradation pathway and influencing factors. Nanomaterials. 10 (5). Available from: https://doi.org/10.3390/nano10050964.

Pelaez, M., Nolan, N.T., Pillai, S.C., Seery, M.K., Falaras, P., Kontos, A.G., et al., 2012. A review on the visible light active titanium dioxide photocatalysts for environmental applications. Appl. Catal. B: Environ. 125, 331–349.

Phang, S.J., Lee, J., Wong, V.L., Tan, L.L., Chai, S.P., 2022. Synergistic effects of the hybridization between boron-doped carbon quantum dots and n/n-type g-C_3N_4 homojunction for boosted visible-light photocatalytic activity. Environ. Sci. Pollut. Res. Available from: https://doi.org/10.1007/s11356-021-18253-0.

Phophayu, S., Pimpang, P., Wongrerkdee, S., Sujinnapram, S., Wongrerkdee, S., 2020. Modified graphene quantum dots-zinc oxide nanocomposites for photocatalytic degradation of organic dyes and commercial herbicide. J. Reinf. Plast. Compos. 39 (3–4), 81–94.

Qin, H., Guo, R.T., Liu, X.Y., Shi, X., Wang, Z.Y., Tang, J.Y., et al., 2020. 0D NiS_2 quantum dots modified 2D g-C_3N_4 for efficient photocatalytic CO_2 reduction. Colloids Surf. A: Physicochem. Eng. Asp. 600. Available from: https://doi.org/10.1016/j.colsurfa.2020.124912.

Qu, Z., Wang, J., Tang, J., Shu, X., Liu, X., Zhang, Z., et al., 2018. Carbon quantum dots/$KNbO_3$ hybrid composites with enhanced visible-light driven photocatalytic activity toward dye waste-water degradation and hydrogen production. Mol. Catal. 445. Available from: https://doi.org/10.1016/j.mcat.2017.11.002.

Quan, B., Liu, W., Liu, Y., Zheng, Y., Yang, G., Ji, G., 2016. Quasi-noble-metal graphene quantum dots deposited stannic oxide with oxygen vacancies: synthesis and enhanced photocatalytic properties. J. Colloid Interf. Sci. 481, 13–19.

Que, M., Zhao, Y., Yang, Y., Pan, L., Lei, W., Cai, W., 2021. Anchoring of formamidinium lead bromide quantum dots on Ti_3C_2 nanosheets for efficient photocatalytic reduction of CO_2. ACS Appl. Mater. Interf. 13 (5), 6180–6187.

Rajabi, H.R., Farsi, M., 2016. Study of capping agent effect on the structural, optical and photocatalytic properties of zinc sulfide quantum dots. Mater. Sci. Semicond. Proc. 48, 14–22.

Reddy, N.R., Bharagav, U., Kumari, M.M., Cheralathan, K.K., Shankar, M.V., Reddy, K.R., 2020. Highly efficient solar light-driven photocatalytic hydrogen production over Cu/FCNTs-titania quantum dots-based heterostructures. J. Environ. Manag. 254. Available from: https://doi.org/10.1016/j.jenvman.2019.109747.

Ren, G., Han, H., Wang, Y., Liu, S., Zhao, J., Meng, X., et al., 2021. Recent advances of photocatalytic application in water treatment: a review. Nanomaterials 11 (7). Available from: https://doi.org/10.3390/nano11071804.

Sahu, B.K., Juine, R.N., Sahoo, M., Kumar, R., Das, A., 2021. Interface of GO with SnO_2 quantum dots as an efficient visible-light photocatalyst. Chemosphere 276. Available from: https://doi.org/10.1016/j.chemosphere.2021.130142.

Saud, P.S., Pant, B., Alam, A.M., Ghouri, Z.K., Park, M., Kim, H.Y., 2015. Carbon quantum dots anchored TiO_2 nanofibers: effective photocatalyst for wastewater treatment. Ceram. Int. 41 (9), 11953–11959.

Schneider, J., Matsuoka, M., Takeuchi, M., Zhang, J., Horiuchi, Y., Anpo, M., et al., 2014. Understanding TiO_2 photocatalysis: mechanisms and materials. Chem. Revs. 114 (19), 9919–9986.

Shahnazi, A., Nabid, M.R., Sedghi, R., Heidari, B., 2020. A thermosensitive molecularly imprinted poly-NIPAM coated MWCNTs/TiO_2 photocatalyst for the preferential removal of pendimethalin pesticide from wastewater. J. Photochem. Photobiol. A: Chem. 402. Available from: https://doi.org/10.1016/j.jphotochem.2020.112802.

Shao, X., Xin, W., Yin, X., 2017. Hydrothermal synthesis of ZnO quantum dot/KNb_3O_8 nanosheet photocatalysts for reducing carbon dioxide to methanol. Beilstein J. Nanotech 8 (1), 2264–2270.

Sharma, S., Mehta, S.K., Ibhadon, A.O., Kansal, S.K., 2019. Fabrication of novel carbon quantum dots modified bismuth oxide (α-Bi_2O_2/C-dots): material properties and catalytic applications. J. Colloid Interf. Sci. 533, 227–237.

Sharma, K., Raizada, P., Hasija, V., Singh, P., Bajpai, A., Nguyen, V.H., et al., 2021. ZnS-based quantum dots as photocatalysts for water purification. J. Water Process. Eng. 43. Available from: https://doi.org/10.1016/j.jwpe.2021.102217.

Shi, J.W., Wang, Z., He, C., Wang, H., Chen, J.W., Fu, M.L., et al., 2015. CdS quantum dots modified N-doped titania plates for the photocatalytic mineralization of diclofenac in water under visible light irradiation. J. Mol. Catal. A: Chem. 399, 79–85.

Shi, W., Sun, W., Liu, Y., Li, X., Lin, X., Guo, F., et al., 2022. Onion-ring-like g-C_3N_4 modified with Bi_3TaO_7 quantum dots: a novel 0D/3D S-scheme heterojunction for enhanced photocatalytic hydrogen production under visible light irradiation. Renew. Energy 182, 958–968.

Singh, S., Garg, S., Saran, A.D., 2021. Photocatalytic activity of CdS and CdSe quantum dots for degradation of 3-aminopyridine. Nanotechnol. Environ. Eng. 6 (3). Available from: https://doi.org/10.1007/s41204-021-00159-4.

Smrithi, S.P., Kottam, N., Vergis, B.R., 2022. Heteroatom modified hybrid carbon quantum dots derived from cucurbita pepo for the visible light driven photocatalytic dye degradation. Top. Catal. . Available from: https://doi.org/10.1007/s11244-022-01581-x.

Sonowal, K., Nandal, N., Basyach, P., Kalita, L., Jain, S.L., Saikia, L., 2022. Photocatalytic reduction of CO_2 to methanol using Zr (IV)-based MOF composite with g-C_3N_4 quantum dots under visible light irradiation. J. CO_2 Util. 57. Available from: https://doi.org/10.1016/j.jcou.2022.101905.

Su, D.W., Ran, J., Zhuang, Z.W., Chen, C., Qiao, S.Z., Li, Y.D., 2020. Atomically dispersed Ni in cadmium-zinc sulfide quantum dots for high-performance visible-light photocatalytic hydrogen production. Sci. Adv. 6 (33). Available from: https://doi.org/10.1126/sciadv.aaz8447.

Sun, S., An, Q., Wang, W., Zhang, L., Liu, J., Goddard III, W.A., 2017. Efficient photocatalytic reduction of dinitrogen to ammonia on bismuth monoxide quantum dots. J. Mater. Chem. A 5 (1), 201–209.

Sun, J., Duan, L., Wu, Q., Yao, W., 2018. Synthesis of MoS_2 quantum dots cocatalysts and their efficient photocatalytic performance for hydrogen evolution. Chem. Eng. J. 332, 449–455.

Sun, Y., Yuan, X., Wang, Y., Zhang, W., Li, Y., Zhang, Z., et al., 2022. CeO_2 quantum dots anchored g-C_3N_4: synthesis, characterization and photocatalytic performance. Appl. Surf. Sci. 576. Available from: https://doi.org/10.1016/j.apsusc.2021.151901.

Vatanpour, V., Khadem, S.S.M., Masteri-Farahani, M., Mosleh, N., Ganjali, M.R., Badiei, A., et al., 2020. Anti-fouling and permeable polyvinyl chloride nanofiltration membranes embedded by hydrophilic graphene quantum dots for dye wastewater treatment. J. Water Process. Eng. 38. Available from: https://doi.org/10.1016/j.jwpe.2020.101652.

Vidhya, K., Saravanan, M., Bhoopathi, G., Devarajan, V.P., Subanya, S., 2015. Structural and optical characterization of pure and starch-capped ZnO quantum dots and their photocatalytic activity. Appl. Nanosci. 5 (2), 235–243.

Wahab, R., Tripathy, S.K., Shin, H.S., Mohapatra, M., Musarrat, J., Al-Khedhairy, A.A., 2013. Photocatalytic oxidation of acetaldehyde with ZnO-quantum dots. Chem. Eng. J. 226, 154–160.

Wang, C., Thompson, R.L., Ohodnicki, P., Baltrus, J., Matranga, C., 2011. Size-dependent photocatalytic reduction of CO_2 with PbS quantum dot sensitized TiO_2 heterostructured photocatalysts. J. Mater. Chem. 21 (35), 13452–13457.

Wang, J., Wang, J., Li, N., Du, X., Ma, J., He, C., et al., 2020. Direct Z-scheme 0D/2D heterojunction of $CsPbBr_3$ quantum dots/Bi2WO6 nanosheets for efficient photocatalytic CO_2 reduction. ACS Appl. Mater. Interf. 12 (28), 31477–31485.

Wang, W., Zeng, Z., Zeng, G., Zhang, C., Xiao, R., Zhou, C., et al., 2019. Sulfur doped carbon quantum dots loaded hollow tubular g-C_3N_4 as novel photocatalyst for destruction of *Escherichia coli* and tetracycline degradation under visible light. Chem. Eng. J. 378. Available from: https://doi.org/10.1016/j.cej.2019.122132.

Wang, S., Liu, D., Yu, J., Zhang, X., Zhao, P., Ren, Z., et al., 2021. Photocatalytic penicillin degradation performance and the mechanism of the fragmented TiO_2 modified by CdS quantum dots. ACS Omega 6 (28), 18178–18189.

Xia, J., Di, J., Li, H., Xu, H., Li, H., Guo, S., 2016. Ionic liquid-induced strategy for carbon quantum dots/BiOX (X = Br, Cl) hybrid nanosheets with superior visible light-driven photocatalysis. Appl. Catal. B: Environ. 181, 260–269.

Xie, Y., Yu, S., Zhong, Y., Zhang, Q., Zhou, Y., 2018. SnO_2/graphene quantum dots composited photocatalyst for efficient nitric oxide oxidation under visible light. Appl. Surf. Sci. 448, 655–661.

Xu, L., Bai, X., Guo, L., Yang, S., Jin, P., Yang, L., 2019. Facial fabrication of carbon quantum dots (CDs)-modified N-TiO_{2-x} nanocomposite for the efficient photoreduction of Cr (VI) under visible light. Chem. Eng. J. 357, 473–486.

Xu, X., Meng, L., Luo, J., Zhang, M., Wang, Y., Dai, Y., et al., 2021. Self-assembled ultrathin CoO/Bi quantum dots/defective Bi_2MoO_6 hollow Z-scheme heterojunction for visible light-driven degradation of diazinon in water matrix: intermediate toxicity and photocatalytic mechanism. Appl. Catal. B: Environ. 293. Available from: https://doi.org/10.1016/j.apcatb.2021.120231.

Xu, C., Li, D., Liu, X., Ma, R., Sakai, N., Yang, Y., et al., 2022a. Direct Z-scheme construction of g-C_3N_4 quantum dots/TiO_2 nanoflakes for efficient photocatalysis. Chem. Eng. J. 430. Available from: https://doi.org/10.1016/j.cej.2021.132861.

Xu, Z., Wang, Y., Zhuang, J., Li, Y., Jia, L., 2022b. High temperature hydrothermal etching of g-C_3N_4 for synthesis of N doped carbon quantum dots-supported CdS photocatalyst to enhance visible light driven hydrogen generation. Mol. Catal. 517. Available from: https://doi.org/10.1016/j.mcat.2021.111900.

Xu, K., Zhang, Q., Wang, C., Xu, J., Bu, Y., Liang, B., et al., 2022c. 0D boron carbon nitride quantum dots decorated 2D $Bi_4O_5I_2$ as 0D/2D efficient visible-light-driven photocatalysts for tetracyclines photodegradation. Chemosphere 289. Available from: https://doi.org/10.1016/j.chemosphere.2021.133230.

Yang, H., Yin, J., Cao, R., Sun, P., Zhang, S., Xu, X., 2019. Constructing highly dispersed 0D Co_3S_4 quantum dots/2D g-C_3N_4 nanosheets nanocomposites for excellent photocatalytic performance. Sci. Bull. 64 (20), 1510–1517.

You, Z., Yue, X., Zhang, D., Fan, J., Xiang, Q., 2022. Construction 0D/2D heterojunction by highly dispersed Ag_2S quantum dots (QDs) loaded on the g-C_3N_4 nanosheets for photocatalytic hydrogen evolution. J. Colloid Interf. Sci. 607, 662–675.

Yu, Z., Meng, J., Xiao, J., Li, Y., Li, Y., 2014. Cobalt sulfide quantum dots modified TiO_2 nanoparticles for efficient photocatalytic hydrogen evolution. Int. J. Hydrog. Energy 39 (28), 15387–15393.

Yuan, A., Lei, H., Xi, F., Liu, J., Qin, L., Chen, Z., et al., 2019. Graphene quantum dots decorated graphitic carbon nitride nanorods for photocatalytic removal of antibiotics. J. Colloid Interf. Sci. 548, 56–65.

Zaib, M., Akhtar, A., Maqsood, F., Shahzadi, T., 2021. Green synthesis of carbon dots and their application as photocatalyst in dye degradation studies. Arab. J. Sci. Eng. 46 (1), 437–446.

Zeng, Z., Yu, D., He, Z., Liu, J., Xiao, F.X., Zhang, Y., et al., 2016. Graphene oxide quantum dots covalently functionalized PVDF membrane with significantly-enhanced bactericidal and antibiofouling performances. Sci. Rep. 6 (1). Available from: https://doi.org/10.1038/srep20142.

Zhang, H., Wu, P., Li, Y., Liao, L., Fang, Z., Zhong, X., 2010. Preparation of bismuth oxide quantum dots and their photocatalytic activity in a homogeneous system. ChemCatChem 2 (9), 1115–1121.

Zhang, J., Zhang, X., Dong, S., Zhou, X., Dong, S., 2016. N-doped carbon quantum dots/TiO_2 hybrid composites with enhanced visible light driven photocatalytic activity toward dye wastewater degradation and mechanism insight. J. Photochem. Photobiol. A: Chem. 325, 104–110.

Zhang, W., Cui, W., Sun, Y., Huang, H., Wu, Z., Dong, F., 2017. Pt quantum dots deposited on N-doped $(BiO)_2$ CO_3: enhanced visible light photocatalytic NO removal and reaction pathway. Catal. Sci. Technol. 7 (6), 1324–1332.

Zhang, F., Wang, X., Liu, H., Liu, C., Wan, Y., Long, Y., et al., 2019. Recent advances and applications of semiconductor photocatalytic technology. Appl. Sci. 9 (12). Available from: https://doi.org/10.3390/app9122489.

Zhang, M., Lai, C., Li, B., Xu, F., Huang, D., Liu, S., 2020. Unravelling the role of dual quantum dots cocatalyst in 0D/2D heterojunction photocatalyst for promoting photocatalytic organic pollutant degradation. Chem. Eng. J. 396. Available from: https://doi.org/10.1016/j.cej.2020.125343.

Zhang, Z., Cao, Y., Zhang, F., Li, W., Li, Y., Yu, H., et al., 2022. Tungsten oxide quantum dots deposited onto ultrathin $CdIn_2S_4$ nanosheets for efficient S-scheme photocatalytic CO_2 reduction via cascade charge transfer. Chem. Eng. J. 428. Available from: https://doi.org/10.1016/j.cej.2021.131218.

Zhao, Z., Fan, J., Deng, X., Liu, J., 2019. One-step synthesis of phosphorus-doped g-C_3N_4/Co_3O_4 quantum dots from vitamin B_{12} with enhanced visible-light photocatalytic activity for metronidazole degradation. Chem. Eng. J. 360, 1517–1529.

Zou, Y., Xie, Y., Yu, S., Chen, L., Cui, W., Dong, F., et al., 2019. SnO_2 quantum dots anchored on g-C_3N_4 for enhanced visible-light photocatalytic removal of NO and toxic NO_2 inhibition. Appl. Surf. Sci. 496. Available from: https://doi.org/10.1016/j.apsusc.2019.143630.

Zubair, M., Kim, H., Razzaq, A., Grimes, C.A., In, S.I., 2018. Solar spectrum photocatalytic conversion of CO_2 to CH_4 utilizing TiO_2 nanotube arrays embedded with graphene quantum dots. J. CO2 Util. 26, 70–79.

This page intentionally left blank

Chapter 10

Application of quantum dots in light-emitting diodes

Anca Armăşelu[1] and Monika Jangid[2]
[1]Department of Electrical Engineering and Applied Physics, Faculty of Electrical Engineering and Computer Science, Transilvania University of Brasov, Brasov, Romania, [2]Department of Chemistry, PAHER University, Udaipur, Rajasthan, India

10.1 Introduction

Quantum dots (QDs) have been extensively investigated in the past few decades owing to their unique properties. QDs are called artificial nanocrystals possessing confinement in all three dimensions with nanometer size that can carry electrons; optical and electrical attributes of QDs can be effectively adjusted by modifying their dimensions, resulting in the emission of specific wavelengths of light (Chen et al., 2020a; Motomura et al., 2020; Singh et al., 2021a).

QDs exhibit numerous unique optical properties such as high photoluminescence (PL) quantum yield (QY), pure and saturated colors, narrow bandwidth, tunable band gap, narrow and symmetric emission, broad and strong absorption (Shirasaki et al., 2013; Pietryga et al., 2016; Bang et al., 2020; Jia et al., 2020; Huang et al., 2020a). Due to their remarkable properties, QDs have found uses in a variety of unusual categories of electronics and optoelectronic tools with potential for application in information displays, solid-state lighting (SSL), biology (Armăşelu et al., 2011a,b), and other structures (Colvin et al., 1994; Ugarte et al., 2012; Nguyen et al., 2019).

Light-emitting diodes (LEDs) reshaped the lighting and display industry and have accomplished considerable developments compared to traditional lighting sources (Zhang et al., 2021a). Exceptional luminescence and charge transport characteristics of QDs show that they are promising alternative emitting materials for the LEDs industry (Colvin et al., 1994; Mattousi et al., 1998; Coe et al., 2002; Kagan et al., 2016; Yang et al., 2019a; Huang et al., 2020b; Bang et al., 2021).

Given the requirements for high resolution and high color saturation, technologies comprising organic LEDs (OLEDs), mini-LEDs (mLEDs), micro-LEDs (μLEDs or μ-LEDs), QD LEDs (QD-LEDs, QD LEDs, or

Quantum Dots. DOI: https://doi.org/10.1016/B978-0-12-824153-0.00010-0

QLEDs) (Armăşelu, 2017), and laser displays have been produced to substitute liquid crystal displays (LCDs) (Ameta et al., 2019; Ye et al., 2021), μLEDs (Wu et al., 2018; Huang et al., 2019; Wong et al., 2019; Huang et al., 2020b; Bai et al., 2020; Wu et al., 2020; Biwa et al., 2021; Zhuang et al., 2021) and mLEDs (Tan et al., 2018; Huang et al., 2019, 2020b; Sun et al., 2020) and have emerged as next-generation displays providing ultrahigh luminance and long lifetimes.

Ghamsari (2017) reminded that the display industry is interested to mix QD with OLED, noting that an improvement in operation time of OLED device can be realized with the help of QDs. Luo et al. (2018) presented that electroemissive QD displays possess the capability to revolutionize the display industry in the coming years, offering not only the thinness and flexibility of OLED displays, but with the advantages of price, color, and brightness of QDs. High color purity and wide color gamut (WCG) that can be realized using QDs have drawn much attention in display applications (Jiang et al., 2018). The QD-based consumer displays such as LED TVs, tablets, and smartphones offer a reasonable power efficiency and an accessible cost, exhibiting improved competitive edge to OLED technics (Jang, 2018).

A QD display represents a device, which utilizes QDs as a component of panel construction to produce monochromatic red, green, and blue light (Sellers, 2018). They explained that photoemissive QD particles are utilized in LED-backlit LCDs, where a QD layer converts the backlight to give out pure basic colors and electroemissive QD displays constitute a model of novel display based on QD-LEDs (QLED or QD-LED). Liu et al. (2020a) reviewed the newest advances in the implementation of μ-LEDs and QDs in display technology, together with the μ-LED design and QD full-color procedure and provided some insights on the progress of favorable QD film deposition mechanisms, showing the modern uses of QD-based μ-LED displays.

LED-based communication links can be used in both open space and optical interconnect applications. The LEDs based on evolving semiconductor materials are of special importance in the progress of the next-generation data communications (Ren et al., 2021). They are examining the advancement of some LED materials, including the case of colloidal QDs for application in optical communications systems.

This chapter reviews the latest developments on applications of QDs for LEDs, focusing on some key areas such as display, lighting, data communications, agriculture, horticulture, and antimicrobial technology.

10.2 Display and lighting

QDs have a great potential in different optoelectronic applications. They have also found application in LEDs for lighting of different colors due to their tunable fluorescence emission, characteristic broad emission, and high thermal stability. These LEDs are also useful in both SSL and flat-panel

displays. Flexible information displays hold a great promise for future optoelectronic applications, but most of these are fabricated on glass substrates and only a little work has been done LEDs based on flexible substrates.

10.2.1 White light-emitting diodes

Among the optoelectronics applications, the white LED (WLED) exhibits a considerable capability in flat panel displays and SSL (Kim et al., 2016a).

Amorphous silicon QDs (*a-Si* QDs) were grown by Park et al. (2001) in a silicon nitride film via plasma-enhanced chemical vapor deposition. Four types of PL (Red, blue, green, and white) were observed from these *a-Si* QD structures just by control of size of QDs. They fabricated orange LEDs using *a-Si* QDs with average size of 2.0 nm. An external quantum efficiency of 2×10^{-3}% was obtained. It was indicated that LED using *a-Si* QDs embedded in the silicon nitride film was found to be much better than Si-based LEDs in terms of optical and electrical properties.

Park et al. (2004) obtained white light emission from a LEDs. They prepared this diode from polymer/QD nanocomposites using poly(9,9′-dihexylfluorene-2,7-divinylene-*m*-phenylenevinylene-*stat*-*p*-phenylenevinylene) (PDHFPPV) and two kinds of CdSe nanoparticles (NPs) with different particle sizes. It was observed that blue, green, and red emission from the polymer, ~3 nm, and emission from the ~7 nm CdSe, contribute jointly to white emission of the organic−inorganic hybrid device.

Song and Lee (2007a) synthesized (CdSe)ZnS QD−polymethylmethacrylate (PMMA) polymer composite. Then they fabricated QD−polymer composite films. It was observed that 28% (wt./wt.) of PMMA in MMA was desired concentration to produce a film white good quality and the solubility of QDs was also maximized. They fabricated red or green light-emitting (CdSe)ZnS QD−PMMA polymer composite film by combining the red or green light-emitting (CdSe)ZnS dots with PMMA. It was revealed that a white light-emitting device can be prepared by a combination of these green/red light-emitting QD−polymer composites with a blue light-emitting LED (excitation source). It was proposed that as-fabricated QD−polymer composites can be used in full color displays, large-area colored wall-papers, and flexible colored filters.

Jang et al. (2010) used highly luminescent multiply passivated red− and green−light−emitting QDs as color converters in InGaN blue LEDs. They could achieve external quantum efficiencies of 34% and 72%, respectively for these LEDs. As-obtained white QD-LEDs exhibited efficacy of 41 lm W^{-1} and color reproducibility of 100%. Kim et al. (2011) studied $CuInS_2$ QDs as an excellent red emitting source for WLED due to its nontoxic deep red emission. It was revealed that $CuInS_2$ QDs can be synthesized by a one-pot method. Then ZnS shells were formed on QD surfaces so as to

reduce nonradiative recombination on its surface defects. It was observed that core/shell QDs exhibited maximum PL wavelength blue shifts by about 80 nm on increasing intensity more than six times and the QY of as-prepared $CuInS_2$/ZnS QDs was 67%. The transparent and hydrophobic dispersion of QDs in polystyrene was also observed using toluene as codispersing agent. The polystyrene/QD composite was applied on blue LEDs, which exhibited luminous efficacy (LE) of 10.7 lm W^{-1}.

A large-scale synthesis of InP/ZnS core/shell nanocrystal QDs was reported by Kim et al. (2012) using a customized hybrid flow reactor. They synthesized InP cores and InP/ZnS core/shell QDs successively in the hybrid reactor in one-step process only. The flow rate of the solutions was kept typically 1 mL min^{-1} in the reactor, which is about hundred times larger than as kept in conventional microfluidic reactors. The flow rate as well as crystal growth temperature were controlled to synthesize high-quality InP/ZnS QDs. It was revealed that high-quality InP/ZnS QDs (bluish green to red) were obtained and these core/shell QDs could be incorporated into WLEDs devices to improve performance of color rendering.

Song et al. (2012) reported the synthesis of Cu−In−Ga−S (CIGS) QDs. They applied these QDs for WLED with variation of In:Ga ratios. It was found that band gap and emission energies of as-prepared CIGS QDs were higher an increasing Ga contents. It was observed that ZnS shell-capped QDs of the CIGS/ZnS core−shell emitted tunable wavelengths (520−578 nm) with an excellent PL QY of 72%−83%. They reported high LEs of 69.1−75.0 lm W^{-1}, when highly fluorescent CIGS/ZnS QDs as color converters with a blue-emitting LED were combined with efficient white QD-based LEDs. A white QD-LED was also fabricated by blending of two kinds of CIGS/ZnS QDs, which exhibited enhanced color rendering property.

A simple solution method was used by Son et al. (2012) to prepare emissive hybrid QDs, which consists of a ZnO core wrapped in a shell of single-layer graphene. Then these QDs were used to make a WLEDs with a brightness of 798 cd m^{-2}. White emission could also be achieved by combining these QDs with some other emissive materials in a multilayer LEDs.

The color rendering index (CRI) of YAG:Ce-based WLEDs is poor. The core/shell/shell CdSe/CdS/ZnS QDs were synthesized by Shen et al. (2012) and blended into nano-YAG:Ce^{3+} phosphors to improve this index. They obtained a WLED with a combination of blue LED (with the blends of nano-YAG phosphors) and orange- and red-emission QDs in the weight ratio (1:1:1). It was revealed that as-fabricated WLEDs exhibited excellent white light with luminescent efficiency of 82.5 lm W^{-1}.

Song et al. (2013) reported the synthesis of two bright noncadmium QDs of orange (583 nm)-emitting $CuInS_2$ (CIS)/ZnS and green (512 nm)-emitting InP/ZnS core/shell. These were applied for fabrication of SSL devices. It was obtained that spectral overlap between absorptions from both emissions from InGaN-based blue LED chip and QDs was excellent. There was an

efficient downconversion of blue-to-QD emission for the generation of white light by dispensing sequentially InP/ZnS QDs on top of CIS/ZnS within epoxy resin. It was revealed that white QD-LED generated a white light with high quality having a high CRI of 90 and a warm color temperature of 3803K.

Erdem and Volkan (2013) presented that on using QDs in color-conversion LEDs, it is possible to simultaneously achieve remarkable color rendition of the illuminated objects together with an excellent spectral overlap between the emission spectrum of the tool and the sensitivity of the human eye, in addition to a warm white color, unlike other standard sources such as phosphor-based LEDs. They reviewed some modern evolutions in quantum-dot-integrated WLEDs (QD-WLEDs) based on color conversion.

Kubendhiran et al. (2019) reported in a review that WLEDs are an excellent alternative to fluorescent tubes and classical light bulbs in most lighting uses because WLEDs have greater operating lifetimes and important energy savings compared to traditional incandescent light bulbs. They noticed that at the moment there are different types of QD-WLEDs that show these kinds of benefits.

Roy et al. (2014) prepared graphene QDs (GQDs) using plant leaf extracts of Fenugreek (*Trigonella foenum-graecum*) and Neem (*Azadirachta indica*) via a hydrothermal method. They did not use any passivizing, reducing agents or organic solvents. It was reported that the average sizes of the GQDs from Fenugreek (F-GQDs) and Neem (N-GQDs) were 7 and 5 nm, respectively. F-GQDs and N-GQDs exhibited high QYs of 38.9% and 41.2%, respectively. It was revealed that as-prepared GQDs can be utilized to prepare a white light converting cap based on the red-green-blue color mixing method.

The green red Zn−Cu−In−S (ZCIS) and Zn−Ag−In−S (ZAIS)core/shell-like alloyed QDs were synthesized by Yoon et al. (2015) via a hot-injection method. They obtained tunability of red ZCIS and green ZAIS QDs by choosing a high temperature multiple alloyed reaction and low temperature core growth. It was observed that the alloyed red ZCIS and green ZAIS QDs could reach PL QYs of 0.53 and 0.61, respectively was also carried out by them. Practical realization of white downconverted LEDs (DC-LEDs). They also characterized based on CRI, LE, vision & color performance and color quality scale (CQS) of white DC-LEDs incorporated with red ZCIS and green ZAIS QDs. It was reported that tricolor white DC-LED using red-emitting ZCIS core/shell-like alloyed QDs exhibited a moderate LE 31.2 lm W^{-1} with ultrahigh color qualities CRI and CQS as 97and 94, respectively.

Kang et al. (2015) synthesized cadmium-free and water soluble $AgInS_2$/ZnS core/shell QDs. These QD powders exhibited bright orange, yellow, and orange-red luminescence in presence of UV light depending upon Ag/In ratio and PL QYs could reach as high as 57, 50.5, and 52%, respectively. They

obtained warm-WLEDs by a combination of orange-emitting QDs with blue InGaN chip having LE of 39.85 lm W^{-1} and CRI of 71.

Zhang et al. (2018a) synthesized all-inorganic halide perovskite nanocrystals. They used hot-injection method and anion exchange reaction to obtain NPs in the range of 15−40 nm and whole visible light region (410−700 nm). They also constructed a WLED by stacking $CsPbBr_3$ QDs-ethyl acetate composite film and $CaSrAlN_3:Eu^{2+}$-poly (methyl methacrylate) composite film on the blue LED chip. This displayed the ideal white light. It was reported that although WLED is not stable at higher operation current, but it can smoothly work under a lower operation current. Shen et al. (2018) fabricated an efficient flexible white QLED with mixed green, red, and blue QDs as emitters. It was reported that as-prepared flexible white QLED exhibited pure white light emission with brightness of up to 3554 cd m^{-2} and current efficiency of 10.5 cd A^{-1}.

Chen et al. (2018) fabricated silica-wrapped Mn-doped $CsPbCl_3$ QDs with improved operational stability (Fig. 10.1). They hydrolyzed (3-aminopropyl) triethoxysilane for this purpose. They could achieve high PL QY (55.4%) for the $CsPbMnCl_3@SiO_2$ composite. It was reported that wrapping by silica can protect these perovskite QDs from any damage by humidity and temperature. They prepared WLED devices by mixing of green $CsPbBr_3$ QDs and orange-red $CsPbMnCl_3@SiO_2$ composites, which exhibited high LE (77.59 lm W^{-1}) and CRI (82). It was also revealed that electroluminescence spectrum showed almost no variation even after 24 h operation.

Cesium-lead-halide perovskite QDs (PQDs) have excellent superior optical and electronic properties and therefore, these are considered potential materials for various optoelectronic devices. Yang et al. (2019c) developed to hydrolysis encapsulation method by embed PQDs into mesoporous polystyrene microspheres (MPMs), which was followed by silica shell covering process. It generated luminescent PQDs/MPMs@SiO_2 hybrid microspheres with excellent stability. It was reported that as-obtained $CsPbBr_3$-PQDs/MPMs@SiO_2 hybrid microspheres show a high PL QY (84%). As-prepared hybrid microspheres exhibited good chemical/physical stability seven under harsh conditions of environments, particularly acid/alkali solution, deionized water, anion-exchange reactions, isopropanol, and heating. It was also revealed that about 48% proportion of the initial fluorescence intensity is there, even after a quite long storage period of 30 days with water. It was also observed that WLED are achieved by mixing green $CsPbBr_3$-PQDs/MPMs@SiO_2 microspheres with red commercial phosphors on a blue chip with a high power efficiency (81 lm W^{-1}) and good electroluminescence stability.

Sadeghi et al. (2019) optimized the QY of magic-sized CdSe QDs up to 22% through controlling parameters of synthesis without shelling or posttreatment. They integrated them in liquid-state on blue LED so as to prevent the efficiency drop due to host-material effect. It was revealed that

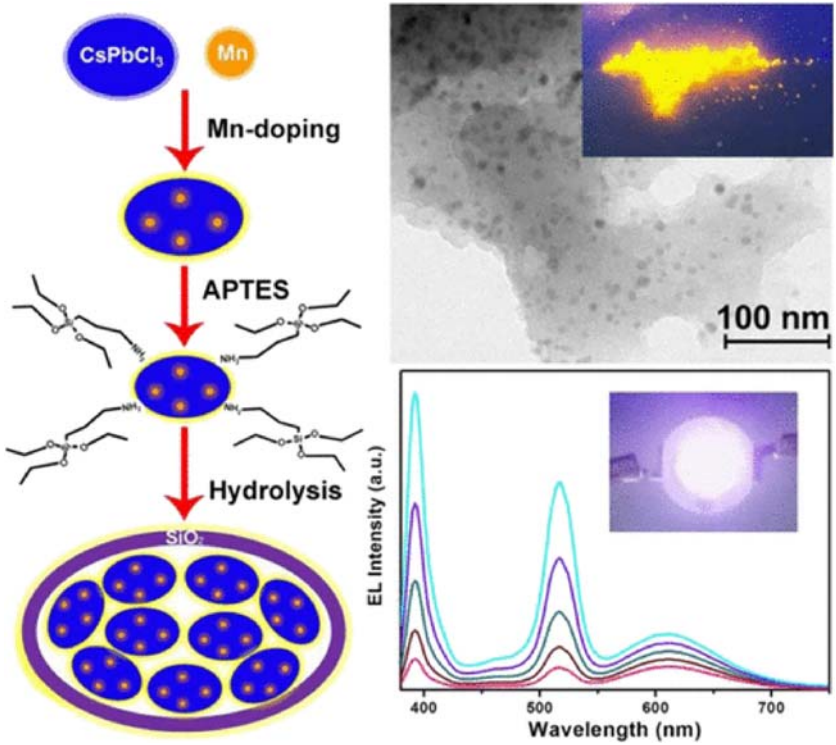

FIGURE 10.1 Fabrication of silica-wrapped Mn-doped $CsPbCl_3$ QDs for LED application. *Adapted from Chen et al., 2018. ACS Appl. Mater. Interfaces,10(50), 43978–43986. With Permission.*

as-prepared WLEDs showed color-rendering index of 89 and LE of 11.7 lmW^{-1}.

Yin et al. (2019) fabricated yellow-green emitting GQDs using low-cost as well as eco-friendly method. As-obtained GQDs were cast in UV-curable siloxane and a polymer film to obtain excellent monodispersity properties and better optical transparency through just adjusting thickness and the concentration of the color convert matrix, so as to achieve tunable color temperatures (3196K−10 870K) of the GQD-based WLEDs. Using the fluorescent polymeric matrix in WLEDs, good quality emission and gratifying stability could be obtained. It was also indicated that this technology has a great potential for applications in high-end lighting.

The synthesis of $CH_3NH_3Pb_{1-x}Mn_xI_3$ PQDs (where manganese is substituted at sites of lead) was reported by Singh et al. (2019). It was observed that these QDs exhibited strong color tunability ranging from red to orange,

when concentration of Mn^{2+} was varied from 0 to 60%. A high external PL QY (98%) was observed for unsubstituted $CH_3NH_3PbI_3$. They developed a WLED using $CH_3NH_3Pb_{1-x}Mn_xI_3$ QDs with green QDs on a blue LED chip.

Yang et al. (2019b) developed a novel package structure to prepare QD-WLEDs using dip-coating red and green QDs/polyurethane composites into TV lens and combine them with a blue LED to form white light. They demonstrated that the in-lens technique has high stability and that a 32-inch prototype LCD TV possesses a WCG of 108% under the National Television Systems Committee standard with this in-lens encapsulation construction.

Perikala and Bhardwaj (2021) reported that QD-WLEDs use diverse colors (red, blue, and green), emitting QDs to achieve white light. They communicated an open air atmosphere synthesis of highly luminescent single system white light-emitting carbon dots (CDs). It was revealed that CDs have been embedded in polydimethylsiloxane (PDSM) polymer and as-produced CD-PDMS phosphor indicated exceptional CRI $\sim$96; the maximal communicated so far with Commission Internationale de l'Eclairage coordinates (0.31, 0.33), which are very similar to pure white light. This research establishes a scaffold for the uses of CD-phosphor-based WLEDs in lighting systems.

The influence of the pore structure of SBA-15 particle was observed by Li et al. (2020) on light emission from inner adsorbed QDs and outer LEDs chips. It is was found that the particle features of a high refractive index, comparable feature size of pore structure, and lower amount of QD adsorption help with QD light extraction, demonstrating a mechanism to suppress QD light propagating through pores and thus reducing the reabsorption loss. Then they developed highly efficient QD WLEDs by wet-mixing QD/SBA-15 NPs. It was observed that as-fabricated LEDs exhibited a record LE of 206.8 lm W^{-1} for WLEDs by integration of green−red QD and green QDs color convertors with improved stability.

Chen et al. (2020b) could obtain uniform blue-green emissive GQDs and modified efficient orange-emitting GQDs (D-GQDs). These QDs were derived from fullerene under acid-free conditions. As-prepared D-GQDs exhibited excellent conversion efficiency with QY of 52.4% at an emission peak of 617 nm. These GQDs and D-GQDs were blended with a polymer; poly(vinyl alcohol) to prepare photoluminescent films (transparent) with excellent flexibility and white emission property. Hu et al. (2020) developed composite orange-red QDs (composite-QDs) by mixing red QDs (R-QDs) and CdSe/ZnS-based orange QDs (O-QDs). It was reported that optimized composite-QDs can improve the CRI of the WLED as compared to monochromatic QDs.

A simple method was developed by Rad et al. (2021) to prepare white light emissive diodes. These are based on colloidal solutions of carbon QDs (CQDs) and $CsPbI_3$ perovskite (PQDs). It was reported that a right combination generates emission across the complete visible spectrum on excitation

by UV light. It was observed that white light emission of the final films provided high and stable CRI (92%). It was also revealed that a mixture can be obtained emitting the cold, neutral, and warm white lights by changing concentration of $CsPbI_3$ QDs for indoor lighting applications. The syntheses of these materials are also low cost and scalable. The colloidal mixture of CQDs and $CsPbI_3$ PQDs shows a facile deposition for LED application, which exhibited white electroluminescence, indicating that both these QDs are stable during LED operation. It was revealed that the PL QY of as-prepared colloidal mixtures was higher (up to 75%) than single white emitters, which indicates a great potential for white emission with tunable properties.

Chen et al. (2021) used Zn doped CdS QD with ZnS shell together with green light emission phosphor. It was observed that degradation of LEDs on degradation of QDs can limit its practical applications, if used for a longer time. There was a reduction in intensity as well as a blue shift of the emitted wavelength from the white light was also observed during degradation. There were three stages of degradation and there are:

1. An enhancement state, where light intensity was increased.
2. It was followed by a rapid degradation stage, where light intensity rapidly decreases, and
3. Slower degradation stage, where the degradation rate of light intensity slows down and goes on decreasing.

The degradation of LEDs was attributed to degradation of CdS core structure, which started with oxidation of sulfur vacancy of CdS QDs by the closely available oxygen atoms. This was all due to imperfection caused in ZnS protective coating around the QDs on explosive to blue light. It was indicated that oxidation transformed CdS into CdO in the initial stage where as $CdSO_4$ is formed via some intermediate processes in final stage.

Zhang et al. (2021b) synthesized green, blue, orange-red, and yellow−green carbon QDs doped with some heteroatoms (Fig. 10.2). They showed emission peaks at 495, 435, 595, and 525 nm with high PL QY (88.9%). A WLED was fabricated with high CRI of 90.8.

10.2.2 Blue light-emitting diodes

In recent years, significant advances have been achieved in the red and green PQDs-based LEDs. However, the performances of the blue perovskite LEDs are still seriously lagging behind that of the green and red counterparts. The visualization of accurate color information using QDs has been explored for decades, and commercial products employing environment friendly materials are currently available. However, next-generation electroluminescent displays based on QDs require the development of an efficient and stable cadmium-free blue light-emitting device, which has remained a

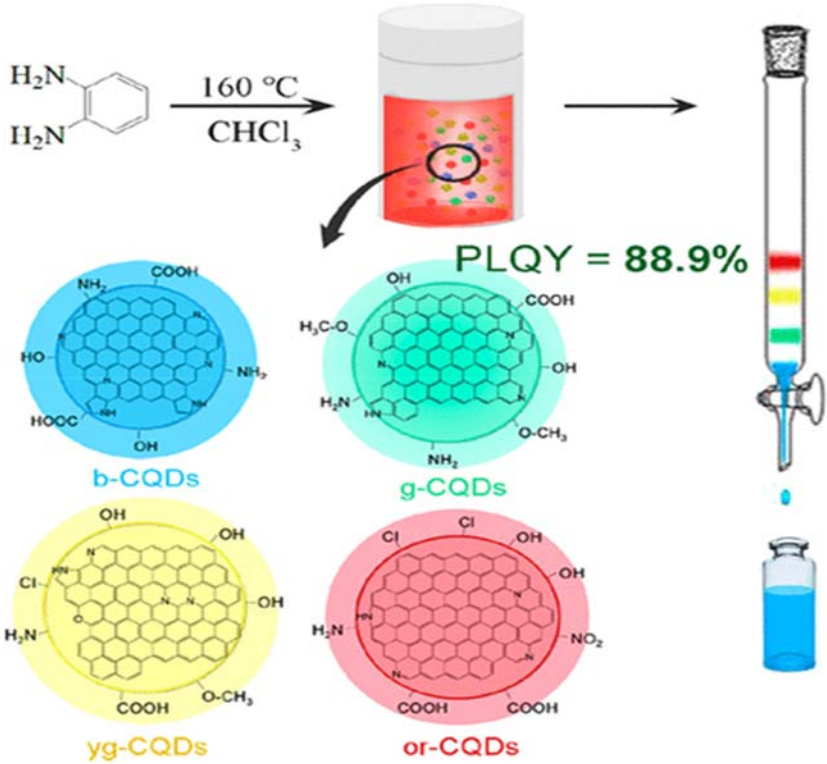

FIGURE 10.2 Synthesis of different colored carbon quantum dots doped with heteroatoms. *Adapted from Zhang et al. J. Phys. Chem. Lett.;12 (37), 8939−8946, 2021. With Permission.*

challenge because of the inferior photophysical properties of blue light-emitting materials.

Realizing of full-color quantum-dot LEDs display remains a challenge because of the poor stability of the blue quantum-dot and the immature inkjet-printing color patterning technology. For colloidal QD QD-LEDs, blue emissive device has always been inferior to green and red counterparts with respect to device efficiency, primarily because blue QDs possess inherently unfavorable energy levels relative to green and red ones, rendering hole injection to blue QDs from neighboring hole transport layer (HTL) inefficient.

Arakawa et al. (2000) have grown InGaN self-assembled QDs on a GaN epitaxial layer via atmospheric-pressure metalorganic chemical vapor deposition. The average diameter of QDs was found to be 8.4 nm. It was also observed that InGaN QDs could be formed even after 10 QD layers were stacked and as a result, the total QD density increased. Luk et al. (2012) fabricated a GQD−agar composite. As-prepared composite exhibited an

excellent optical stability, but no luminescence quenching. This composite was applied successfully as a color converting material to achieve white light emission in blue LEDs. It was reported that light conversion efficiency and LE of the WLED were 61.1% and 42.2 lm W^{-1}, respectively.

It was reported that deep-blue, high color purity electroluminescence was observed in an inverted light-emitting device using nontoxic ZnSe/ZnS core/shell QDs as the emitter (Ji et al., 2013). As-prepared device exhibited a peak at 441 nm. It was observed that current efficiency and maximum luminance could reach 0.51 cdA^{-1} and 1170 cd m^{-2}, respectively. A high performances could be achieved using a ZnO nanoparticle based electron-transporting layer, which can assist in efficient electron injection into ZnSe/ZnS QDs. It was calculated that these efficient deep-blue QD-LEDs can find application in full-color panel displays and QD-based lighting sources.

Lee et al. (2013) synthesized blue CdZnS/ZnS core/shell QDs. It was reported that as-prepared QDs exhibited high PL QY (98%), and high stability. All these solution−processed blue QD-LEDs (multilayered), consisted of HTL of poly(9-vinlycarbazole), electron transport layer of ZnO NPs, and an emissive layer of CdZnS/ZnS QDs. This as-fabricated device exhibited a maximum luminance (2624 cdm^{-2}), external quantum efficiency (7.1%), and LE of 2.2 cdA^{-1}.

Biswas et al. (2016) embedded GQDs into synthesized Amoc (*N*-anthracenemethyloxycarbonyl) capped aromatic amino acid based units. These QDs exhibited blue emission under UV irradiation at a wavelength of 365 nm. It was reported that quenching in emission spectra revealed that there are strong $\pi-\pi$ stacking interactions within Amoc-amino acids and aromatic GQDs. It was also revealed that self-healing properties and thixotropic nature of as-prepared hydrogels can be tuned by introduction of GQDs.

Bharathi et al. (2017) reported the preparation of micron-sized sheets by interconnecting GQDs (GQDs solid sheets) with intrinsic absorption and emission properties. It was observed that metal atoms interconnecting GQDs in hydrothermal growth process, induced some semiconducting behavior in these GQD solid sheets. As-prepared GQDs exhibit a 36% PL QY in the blue region (440 nm). Wang et al. (2017) synthesized highly−efficient blue CdSe/ZnS QDs with emission peak ($>$ 460 nm) with the object to protect human eyes from the harmful effect of short-wavelength light. They fabricated QLEDs based on as-prepared blue QDs and optimized ZnO NPs. It was revealed that using small-size of ZnO NPs, a maximum external quantum efficiency (19.8%) and current efficiency (14.1 cd A^{-1}) for QLEDs were observed. It was proposed that color saturation blue QLEDs have a great potential for use in next-generation full-color displays.

Yuan et al. (2017) synthesized multicolor band gap fluorescent carbon QDs (MCBF-CQDs) via a solvothermal method. The as-prepared QDs have blue to red color with high QY (75%). It was observed that maximum

luminance of as-prepared blue LEDs could reach 136 cd m^{-2}. Lin et al. (2018) synthesized blue nonblinking (> 98% "on" time) ZnCdSe/ZnS//ZnS QDs (Fig. 10.3). The absolute fluorescence QY was found to be 92% ($\lambda_{peak} = 472$ nm). It was reported that these bright nonblinking ZnCdSe/ZnS//ZnS core/shell QDs exhibited not only good tunability in the blue-cyan range (450−495 nm) but also high absolute PL quality yield, but excellent chemical and photochemical stability also.

Wang et al. (2019) synthesized four surface-modified (positively charged metal NPs) with different localized surface plasmon resonance wavelengths and then linked with red-emitting colloidal CdZnSeS/ZnS QDs (negatively charged) on the top surface of a blue-emitting InGaN/GaN quantum well (QW) LEDs. There is strong surface plasmon coupling due to short distance of NP and QD in NP-QD linkage; thus enhancing absorption and emission. A stronger QD excitation was also observed. All the factors together resulted in an increase of color conversion efficiency of the QDs.

Kim et al. (2020) reported the synthesis of ZnSe-based blue light-emitting QDs with a QY of unity. They observed that zinc chloride and hydrofluoric acid additives were found effective in increasing luminescence efficiency. It was anticipated that these efficient and stable blue QD light-emitting devices can find potential application in development of electroluminescent full-color displays.

Pan et al. (2020) developed Ni^{2+} ion-doped $CsPbCl_xBr_{3-x}$ PQDs via supersaturated recrystallization synthesis. It was simultaneously realized that the doping of various concentrations of Ni^{2+} cations modulating the Cl/Br element ratios by introducing different amounts of $NiCl_2$ solution in the reaction medium. It was reported that emission wavelength of Ni^{2+} ion-doped $CsPbCl_xBr_{3-x}$ QDs shifted from 508 to 432 nm. It was observed that blue

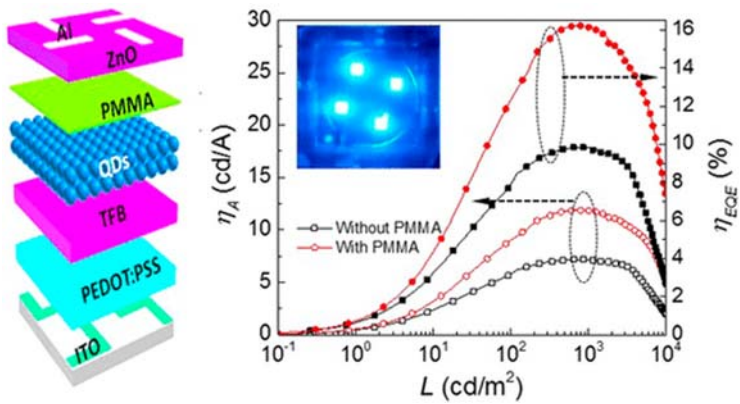

FIGURE 10.3 Luminescence efficiency of blue LEDs based on high quality nonblinking QDs. *Adapted from Lin et al., 2018. ACS Photonics, 5 (3), 939−946. With Permission.*

emission (470 nm) with PL QY 89% was achieved in 2.5% Ni^{2+} ion-doped $CsPbCl_{0.99}Br_{2.01}$ QDs, which was almost three times more than that of undoped $CsPbClBr_2$ QDs. It was revealed that external quantum efficiency of 2.4% could be achieved along with maximum luminance of 612 cd m^{-2}, which is highest amongst other blue-emitting PQD-based LED reported earlier.

Zhang et al. (2020) developed a yellow quantum-dot LED of stacking with a blue organic multifunctional tandem LED using an indium−zinc oxide intermediate connecting electrode. It was reported that as-fabricated tandem LED was full-color-tunable and it can emit green, red, and blue colors (primary color) as well as other arbitrary colors. It was revealed that this tandem LED can emit efficient white light with brightness (107000 cd m^{-2}) and maximum external quantum efficiency (26.02%). It was suggested that white light-emission and multi-functionality of full-color-tunability could find a great potential application in both solid-state lighting and full-color-display.

10.2.3 Red light-emitting diodes

Taylor et al. (2007) used a hybrid layer of poly(2-methoxy,5(2-ethylhexyloxy)-*p*-phenylene vinylene) (MEH-PPV) and CdSe QDs to convert the light emitted by electroluminescent ZnS phosphor into red light. It was revealed that emission wavelength of the display was related directly to the emission of CdSe QDs. It was observed that thin film electroluminescent displays have a potential to increase its color spectrum on integrating QDs.

Song and Lee (2007b) prepared core−shell (CdSe)ZnSe QDs by colloidal chemical synthesis and surface-passivation. They coated a core CdSe with a larger-band gap material ZnSe. As-prepared (CdSe)ZnSe QDs played a role of color conversion center (QDs nanophosphors). The red light-emitting hybrid devices were fabricated consisting of (CdSe)ZnSe QDs and a near-UV GaN LED. They also tested the possibility of using (CdSe)ZnSe QDs as red nanophosphors for UV excitation. It was indicated that (CdSe)ZnSe QDs are quite promising red nanophosphors for NUV excitation. The red LED based on these QDs and a NUV excitation source has proved to be an efficient hybrid device with good luminance.

Stouwdam and Janssen (2008) studied ZnO nanocrystals as an electron injection layer for red, green, and blue LEDs based on core−shell CdSe/ZnS QDs. The deposition of ZnO nanocrystals from isopropanol permits fabrication of multilayer QD-LEDs that include both hole and electron transport layers by simple solution processing. The ZnO nanocrystals improved electron injection in the light-emitting QD layer as evident from a decreased turn-on voltage and a reduction of emission originating from other layers than the QD layer of the LEDs.

Huang et al. (2008) fabricated a hybrid CdSe-ZnS QD (QD)-InGaN-GaN QW red LEDs. It was reported that the blue light from the InGaN QWs can be easily down converted to the red light using different blend ratios. The luminous flux and LE from the hybrid LED of 0.65 lm and 9.3 lmW^{-1} could be obtained keeping QD concentration as 40 $mg\,mL^{-1}$ of resin. It was revealed that from electroluminescence spectrum that the contribution of red light emission to the total light intensity was found to be 98%.

Cho et al. (2009) crosslinked colloidal quantum-dot layer. It can reduce charge injection barrier in a red light-emitting quantum-dot, LEDs by using a sol−gel TiO_2 layer for electron transport. It exhibited a high luminance (12,380 cd m^{-2}) and high power efficiency (2.41 lm W^{-1}). This technique may be incorporated in display device with a great promise for possible use in easy-to-fabricate, high-performance, illumination sources and large-area displays. A gold nanorod-enhanced light emission was reported by Yang et al. (2014a) in quantum-dot-doped polymer nanofibers. It was observed that there was a 67% increment in 600 nm red light emission efficiency on incorporating gold nanorods into quantum-dot-doped polymer nanofiber. The photostability was found to be increased by 100 min.

A highly efficient, ultrabright, low roll-off, inverted QD-based red light-emitting device (QLED) was reported by Dong et al. (2015). They used cesium carbonate films and solution-processed zinc oxide NPs as the hole blocking layers and electron injection, respectively. It was revealed that luminance of 165,000 Cdm^{-2} was obtained at a current density of 1000 $mAcm^{-2}$ for deep red device.

Fine tuning of emission color of Ce-doped yttrium aluminum garnet ($Y_3Al_5O_{12}:Ce^{3+}$, YAG:Ce) nanophosphor-based WLED was reported by Kim et al. (2016b). They coated CdSe/CdS/ZnS QDs onto the surface of the YAG:Ce NPs. It was observed that the luminescence spectra of the QD@YAG:Ce can be tuned by variation of QD to YAG:Ce weight ratios. Lin et al. (2016) reported highly efficient deep-red LEDs, which is based on type-II CdTe/CdSe core/shell QDs. CdTe/CdSe core/shell QDs synthesized through a green process have different PL emissions peaks at 642, 664 and 689 nm and it was observed these using three devices QDs with different PL peaks exhibited maximum external quantum efficiency of 5.24%, 5.74% and 6.19%, respectively.

Indium phosphide (InP) QDs have shown great potential as a replacement for CdSe QDs in display applications. However, the performance of InP-based QLEDs is still far behind that of the CdSe-based devices. The effects of different methods for improving the performance of InP-based QLED devices was investigated by Li et al. (2019a). They evaluated effect of magnesium doping in ZnO NPs used as an n-type electron transport layer, so as to balance charge transfer in InP-based QLED devices. It was found that ZnO band gap is broadened and its energy levels are shifted along with increase in resistivity by doping on increasing Mg content. It was revealed

that electron current density was reduced and device efficiency was improved. It was indicated that QD structures and devices in optimum conditions could prove be as current efficiencies of 11.6 cdA^{-1} to red InP QLEDs.

A highly efficient and stable red QLED was reported by Liu et al. (2020b). They used codoped lithium and magnesium along with magnesium oxide shell-coated zinc oxide nanoparticle layer (electron transport layer). It was observed that optimized QLED show a high peak EQE of (20.6%), long lifetime T_{95} of >11000 h, and low efficiency roll-off at high current.

10.2.4 Green light-emitting diodes

Steckel et al. (2006) synthesized $Cd_xZn_{1-x}Se$ alloy core nanocrystals. Then these were overcoated with $Cd_yZn_{1-y}S$ to create core−shell nanocrystals for use in QD-LED displays. It was found that these $Cd_xZn_{1-x}SeCd_yZn_{1-y}S$ core−shell nanocrystals can be used to fabricate color-saturated green−emitting QD-LEDs, which can be a potential for display applications.

Sun et al. (2007) reported green, orange, red, and yellow LEDs using CdSe core and ZnS or CdS/ZnS shell as emissive layers in the devices and it was observed that the maximum luminance was 3700, 3200, 9064, and 4470 cd m^{-2}, respectively. It was indicated that improved electroluminescent efficiency (1.1−2.8 cd A^{-1}), low turn-on voltages (3−4 V) and longer operation lifetimes of quantum-dot-based LEDs can be obtained by optimizing the thicknesses of the constituent layers of the devices. It was suggested that these QDs LEDs may be promising flat-panel displays applications.

The growth of InN, GaN, and InGaN QDs by molecular beam epitaxy (MBE) on either GaN or AlN templates was reported by Moustakas et al. (2008). InN QDs on GaN templates were found to occur without an InN wetting layer. The self-assembled GaN QDs were grown on AlN templates. It was observed that the self-assembly of InGaN QDs on GaN templates can find the applications in blue-green LEDs. It was indicated that InGaN/GaN multiple QDs (MQDs) were highly strained and at low injection, their emission is red shifted as compared to a single layer of QDs.

Park and Park (2011) fabricated LEDs with emission in the green range (540−610 nm). They grow self-assembled In-rich InGaN QDs on n-GaN via metal-organic chemical-vapor deposition. It was observed that emission wavelength of LED was red shifted from green (540 nm) to red (610 nm). This shift was attributed to an increase in the depth of potential wells of the InGaN QDs with increased roughness of the surface n-GaN layer.

Park et al. (2015) reported bright yellow−green-emitting $CuInS_2$ (CIS)-based QDs and two−band WLEDs using these QDs. They used metal−oleate precursors and 1-dodecanethiol for synthesis of yellow-green-emitting CIS QDs with CIS cores (QE = 31.7%). These CIS/ZnS/ZnS QDs exhibited a high QE (80.0%) and a peak at 559 nm, which is dominant wavelength of

blue LEDs. It was revealed that white light LEDs can be fabricated with coating of CIS/ZnS/ZnS on blue LEDs, which exhibited LE (80.3 $\mathrm{lm \cdot W^{-1}}$), CRI (73) and a high light conversion efficiency of 72.6%.

The InP/ZnS QDs were synthesized by Yang et al. (2015) via hot injection method. They used nontoxic $P(N(CH_3)_2)_3$ as precursor. It was found that triple-shell-coated InP/ZnS core−shell QDs of green, orange-red, and yellow colors could reach PL QYs as high as 0.50, 0.63, and 0.55; and FWHMs as narrow as 55, 71, and 76 nm, respectively.

Li et al. (2016) synthesized perovskite $CsPbBr_3$ QDs via hot-injection method as green phosphor for LEDs. It was reported that green light with an emission peak at 534 nm could be achieved using $CsPbBr_3$ QDs and GaN LEDs. The current-voltage characteristic of the green LED did not show any degradation as compared to GaN LEDs. It was also revealed that as-fabricated green LEDs exhibited a LE of 31.92 $\mathrm{lm\ W^{-1}}$.

Ko et al. (2017) synthesized highly efficient bright green-emitting Zn−Ag−In−S (ZAIS)/Zn−In−S (ZIS)/ZnS alloy core/inner-shell/shell QDs. They used a multistep hot injection method and zinc acetate dihydrate as precursor. It was reported that as-synthesized ZAIS/ZIS/ZnS QDs displayed a high PLQY (87%) with peak wavelength (501 nm). The green, red, and blue tripackage white DC−LEDs exhibited high LE of 72 $\mathrm{lm\ W^{-1}}$ and CRI of 95.

The heavy-metal-free InP/ZnS core/shell QDs with different fluorescence were prepared by Kuo et al. (2017) via green route. These InP/ZnS core/shell QDs exhibited maximum fluorescence at $\sim$ 530 nm and high fluorescence QY (60.1%). As-prepared multilayered InP/ZnS core/shell QD-LEDs showed highest luminance of 160 $\mathrm{cd\ m^{-2}}$ and external quantum efficiency (0.223%). It was predicted that these multilayered InP/ZnS core/shell QD-LEDs have a great potential in heavy-metal-free QD-LEDs for display applications in next generation.

The green QDs were prepared by Li et al. (2017). They used tris(mercaptomethyl)nonane (TMMN) as the capping ligand. It was observed that these TMMN-capped QDs exhibited QYs of $\sim$90% after ligand exchange with external quantum efficiency of 16.5%. The current efficiency and power efficiency of these were found to be 70.1 $\mathrm{cd\ A^{-1}}$ and 57.6 $\mathrm{l\,m\ W^{-1}}$, respectively. It was revealed that as-prepared devices exhibited high environmental stability.

It was reported by Kumar et al. (2018) that the structural and optical control of InP-based QDs can lead to high-performance LEDs. It was observed that zinc sulfide shells passivate the InP QD core and as a result, increase the QY in red and green-emitting QDs was observed by eight- and thirteen-fold, respectively. They fabricated WLEDs with LE up to 14.7 $\mathrm{lm\ W^{-1}}$ as well as color-rendering index up to 80.

QDs have high potential to fulfill the ever increasing demands for high-quality displays due to their outstanding size-tunable optical properties, high QY and reduced costs. The synthesis of efficient materials and their

integration in uniform and thin polymeric films are necessary for displays. Sadeghi et al. (2018) synthesized green− and red−emitting Cd-based QDs with QYs of 74% and 52%, respectively. These QDs were incorporated into the PDMS polymer matrix, which provide polymeric films with 123 × 68 mm for smart phone displays. It was suggested that these QD polymeric films show promising applications in smart phones.

In recent, the QY and stability of green QDs have been significantly improved. However, most of the progresses were achieved by using alloyed QDs, and the control of green emission QDs still remains challenging. Hao et al. (2019) reported synthesized thick-shell structure QDs (TSQDs) with saturated green-emission. They used tri-n-octylphosphine as both ligand as well as solvent to extract the redundant ions from the QDs surface. It was observed that as-prepared TSQDs exhibited high QY reaching up to 75% and tunable precise emission properties (532 nm).

The CdSe/ZnS core−shell QDs were synthesized by Ramalingam et al. (2019) via a chemical route. They used bioconjugated organic amino acid (L-Cysteine). The diameter of as-prepared QDs was found to be 3 nm with uniform size distribution. The optical properties QDs exhibited an absorption and emission peak at 515 and 525 nm respectively, at room temperature. It was indicated that these QDs exhibited emission in the spectral range at 516−535 nm, which is particularly find application in green LEDs.

The synthesis of heavy metal (or Cd) free QD-LEDs have been reported by Ippen et al. (2019) for all three colors. They developed heavy metal free QDs with high QY (> 95% for red and green and >80% for blue). A high efficiency was observed for these heavy metal free QD-LEDs with EQE = 16.9, 13, and 9% for red, green, and blue, respectively. The impact of shell thickness on efficiency performance of device was also evaluated.

Yang et al. (2020) reported QD films based on a poly(zinc methacrylate) coating. These alloyed CdZnSeS/ZnS QDs (QDs@PZnMA) are green−emitting with high refractive-index $BaTiO_3$ NPs. A 7.5−, 11.3−, 8.5−, and 8.6− fold increase in the absorption coefficient, scattering coefficient, optical density and green light emission QD films was observed as compared to films having identical mass percentage of pristine QDs. It was proposed that it has a potential for developing QD optical films with enhanced light emission and high scattering for flexible displays.

Zheng et al. (2020) prepared green carbon QDs (g-CQDs) with high fluorescent QY and high product yield via solvothermal method using 2,7-dihydroxynaphthalene and ethylenediamine as the carbon source and nitrogen dopant, respectively. It was revealed that the maximum product yield (70.90%) and QY (62.98%) values of g-CQDs could be achieved. They prepared WLEDs by combining these g-CQDs and blue chip.

μLEDss are considered as ideal source of light for next generation and high-speed visible light communication InGaN QDs have been proposed as the active region of (Wang et al., 2021a, b). Green InGaN QDs have an

external quantum efficiency of 18.2%, which is almost two−folds than present green μLEDss. It was indicated that InGaN QDs can provide a solution to μLEDss for display and visible light communication applications, as these are fully compatible with current LEDs industrial technology.

10.2.5 Orange light-emitting diodes

Kim et al. (2008) synthesized Mn-doped $Zn_{1-x}Cd_xS$ QDs via reverse micelle approach. It was found that band gap energy of $Zn_{1-x}Cd_xS$:Mn QDs can be tuned to a higher energy by increasing the Zn content. The average size of these QDs was calculated as 3.6 nm. A high QYs (14%−30%) was exhibited depending on the composition of the core QDs. Orange and WLEDs were fabricated using these CdS:Mn/ZnS QDs.

Nizamoglu and Demir (2009) reported Förster resonance energy transfer-enhanced color-conversion. They used colloidal semiconductor QD nanocrystals to make reddish-orange LEDs, which can find applications in ultraefficient SSL. Energy gradient hybrid structure from cyan- and orange-emitting CdSe/ZnS NCs (492 and 588 nm, respectively) can be obtained. A relative increase in quantum efficiency of 15.1% in reddish-orange full color-conversion was observed for the integrated hybrid cyan-orange NC layer.

Song and Yang (2012) reported core/shell structured QDs (CIS/ZnS) exhibited tunable emissions of yellow-orange with excellent QYs (55%−91%). A white QD-LED was fabricated using by CIS (2 h)/ZnS QD as a blue-to-yellow color converter. They also fabricated white QD-LED by blending of yellow and O-QDs so as to improve a color rendering property.

Shen et al. (2013) used solution-processed ZnO NPs as the electron injection/transport layer, bilayer structure of poly[9,9-dioctylfluorene-*co*-*N*-[4-(3-methylpropyl)]-diphenylamine] (TFB)/poly(ethylenedioxythiophene): polystyrene sulfonate (PEDOT:PSS) as the hole transport/injection layer and CdSe/CdS/ZnS core−shell QDs as the emitting layer. It was observed that highly bright orange-red and green QD-LEDs could be obtained with peak luminances and power efficiencies as $\sim 30\,000$ & $\sim 52\,000$ cd m^{-2}, and 16 & 19.7 lm W^{-1}, respectively. It was proposed that these can be commercialized for use in QD-based displays and SSLs.

Aniline GQDs (Chemically derived) were used as lumophores and LEDs exhibiting orange, green, and red electroluminescence with high color purity were fabricated by Kwon et al. (2016). They evaluated external quantum efficiency and maximum current efficiency of 1.28% and 3.47 cd A^{-1}, respectively.

The synthesis of Mn-doped cesium lead halide ($CsPbX_3$) PQDs has been reported by Zhu et al. (2017). It was observed that optical properties of as-prepared nanocrystals remained same even after several months. They fabricated red-orange LEDs by coating the composite onto ultraviolet LED chips.

This present approach may open new avenue for doping other ions in $CsPbX_3$ QDs at room temperature and developed capability in as − prepared essential material for applications in memristors and other devices.

Ren et al. (2020) proposed a facile posttreatment doping method enabling preparation of highly luminescent low-toxic $CsPbX_3$:Mn^{2+} PQDs from nonluminescent Cs_4PbX_6 PeQDs. It was reported that monodispersed $CsPbX_3$:Mn^{2+} PeQDs exhibited excellent photophysical properties such as PL QY (87%). It was revealed that variation of halide composition in Cs_4PbX_6 PeQDs or Mn doping concentration, they were able to prepare a series of $CsPbX_3$:Mn^{2+} PeQDs, which can have tunable emission. They fabricated $CsPbX_3$:Mn^{2+} Q-LED, which exhibited excellent orange light with LE of 24 lm W^{-1}.

10.2.6 Yellow light-emitting diodes

Lv et al. (2012) used InGaN/GaN multilayer QD in active regions for yellow-green LEDs. It was observed that on increasing growth temperature and switching the carrier gas (from N_2 to H_2), using improved growth parameters, a 10-layer InGaN/GaN QD LED was obtained. It was revealed that electroluminescence peak wavelength also shifted from 574 to 537 nm.

Denault et al. (2013) fabricated devices using CdSe/ZnS core/shell QDs (red-emitting) with $Y_3Al_5O_{12}$:Ce^{3+} (yellow-emitting) or $Lu_3Al_5O_{12}$:Ce^{3+} (green-emitting) and InGaN LED (blue-emitting). It was reported that devices with $Y_3Al_5O_{12}$:Ce^{3+} with QDs (590 nm) could achieve LE (57 lm W^{-1}) and CRI (81), while devices with $Lu_3Al_5O_{12}$:Ce^{3+} with QDs could achieve CRI (90) and LE (22 lm W^{-1}).

He et al. (2018) studied inorganic perovskite $CsPb(Br_xI_{1-x})_3$ QDs with QY of 50% as yellow light convertor for LEDs. It was reported that highly pure yellow LEDs were obtained, when x was kept 0.55. It gave LE (13.51 l m W^{-1}) with an emission peak at ∼570 nm. It was concluded that $CsPb(Br_xI_1 - _x)_3$ QDs are potential candidate for yellow LEDs with high purity.

Gu et al. (2021) used hydrothermal method for the preparation of nitrogen doped GQDs (N-GQDs). They used citric acid and o-phenylenediamine as precursors. It was reported that as-produced N-GQDs exhibited blue color with a QY (58%) in presence of 365 nm UV light illumination. As the concentration of N-GQDs increases, the PL exhibits an obvious red-shift from blue to yellow. A high PL QY of 28% could be with yellow luminescence is achieved under 405 nm excitation, using N-GQDs in solid state. A WLEDs device was constructed by adjusting thickness and concentration of N-GQDs in blue emitting InGaN chips.

10.2.7 Other light-emitting diodes

Qian et al. (2011) developed devices consisting of a quantum-dot emissive layer, which was sandwiched between an electron transport layer of ZnO

NPs and an organic HTL. It was reported that as-fabricated devices exhibited maximum luminance and power efficiency values of 4,200 cd m^{-2} & 0.17 lm W^{-1}, 68,000 cd m^{-2} & 8.2 lm $W^{-1}$and 31,000 cd m^{-2} and 3.8 lm W^{-1} for blue, green, and orange−red emission, respectively. It was also revealed that with the incorporation of the ZnO NPs, these devices have high environmental stability with operating lifetimes more than 250 h in low vacuum.

Jun et al. (2013) prepared a highly luminescent and photostable QD−silica monolith substance via base-catalyzed sol−gel condensation of silica. They heavily doped SM with 6-mercaptohexanol exchanged QDs up to 26 wt.% (12 vol.%) without any particle aggregation. These green and red light-emitting QD−SMs were then applied as color-converting layers on blue LEDs. It was observed that external quantum efficiency could reach up to 89% and 63% for the red and green QD−SM, respectively. A WLED made with a mixture of these green and R-QDs in the SM exhibited an efficacy of 47 lmW^{-1}.

Highly efficient tandem quantum-dot LEDs were proposed by Zhang et al. (2018b). They used an interconnecting layer (ICL) with the structure of ZnMgO/Al/HATCN/MoO_3. It was reported that as-prepared ICL exhibited efficient charge generation/injection capability, high transparency, and high robustness. The tandem QLEDs [full color (red (R)/green (G)/blue (B)] show high current efficiency and external quantum efficiency: 41.5 cdA^{-1} and 23.1%, 17.9 cdA^{-1} and 21.4%, 121.5 cdA^{-1} and 27.6% for R-QLEDs, B-QLEDs, and G-QLEDs, respectively. The EQEs of R-, G-, and B-QLEDs were more than 21%. The R-, G-, and B-QLEDs can still sustain their external quantum efficiency at 96%, 99%, and 78%, respectively. It was suggested that these full-color tandem QLEDs have long operational lifetime, high efficiency, high color purity, and low roll-off efficiency, and hence can prove to be ideal candidate for the SSL and full-color displays.

10.3 Night vision

Taking into account the requirements of different practical usages at night, LEDs are applied for infrared lighting in night vision operations comprising security cameras. It has been shown that a ring of LEDs around a video camera is a low-cost and successful kit for chroma keying in video production applications (Cabrera, 2019). Night Vision Imaging Systems (NVIS) are used in military domains such as electronic combat reconnaissance aircraft (Sabatini et al., 2016; Chen et al., 2017a).

Wu et al. (2012) examined the feasibility of using QD phosphor-based LEDs in aviation uses that solicit NVIS conformity, recommending that white QD phosphor-based LEDs can be tailored to show greater suitability with NVIS than commercial LEDs. It was expected that the QD

phosphor-based LEDs reach important goals in cockpit illumination and LED indicator lights of aviation panels.

Chen et al. (2017a) stated that LED night vision imaging detection has been applied in numerous areas. The usage of LED array as a light source possesses the advantages of reduced price and small dimension. It was revealed that utilizing the degradation model, the target image was recovered with the help of the model-based image processing algorithms and that the experimental results confirmed the efficacy of this method.

An interesting review by Zheng and Zhu (2020) emphasizes three classes of emerging near-infrared (NIR) emitting materials used in LEDs. They reported the advantages and disadvantages of these three types of materials (organic materials, inorganic QD materials, and organic−inorganic hybrid perovskite materials) used to fabricate the appropriate devices (OLEDss, QD LEDs, and perovskite LEDs), showing that NIR QLEDs possess the potential for military uses, such as night vision-readable display and iris identification systems.

Vasilopoulou et al. (2021) reported NIR LEDs based on solution-processed semiconductors, such as halide perovskites and colloidal QDs, which are suitable technological stages for night vision, surveillance, and optical communications. This research listed new developments on emissive materials synthetic methods and essential qualities that increase the performance of manufactured light-emitting devices.

10.4 Data communication

In the data communication structure, there is a requirement for higher data rates with great reliability and secure means of accessibility (Kate and Husain, 2017). The use of LEDs increases efficiency in terms of data fidelity, data rate and cost; thus permitting the progress of light fidelity (Li-Fi) technology and the Visible Light Communication (VLC) system (Kate and Husain, 2017; Yu et al., 2021). The unique properties of QDs determine their notable application in optical technologies, such as QD-LEDs that can be used as an optical transmitter in VLC (Xiao et al., 2016; Yulin et al., 2017; Choi et al., 2018; Pradhan et al., 2019; Vahabzad et al., 2019).

A new procedure has been described by Ruan et al. (2016) for the manufacture of a type of QD-WLEDs from green- and red-emitting $AgInS_2$/ZnS core/shell QDs coated on GaN LEDs. It has been mentioned that the modulation bandwidth of QD-WLEDs was much enhanced in comparison to that of YAG:Ce phosphor-based WLEDs, showing that $AgInS_2$/ZnS core/shell QDs have the potential to improve the bandwidth in VLC. The use of colloidal semiconductor QDs for light conversion of InGaN sources in VLC applications was analyzed by Leitao et al. (2017). They presented a colloidal QD/polymer composite format of color converters and reported some samples of such color converting composite that were hybridized with a μLED to create

hybrid sources for a demonstration of free-space VLC over 10 cm with data rates up to 1 Gb s^{-1}.

A microwave-assisted heating technique to manufacture multicolor QD-based phosphors in 30 s was investigated by Zhou et al. (2018) using a combination of QDs and sodium silicate aqueous solution. They indicated an application of the QD-based phosphors in VLC, noting that the bandwidth modulation reaches 42 MHz. Cao et al. (2019) developed a high bandwidth GaN-based WLED that was obtained using blue LED chip (GHz bandwidth) with a combination of CdSe/ZnS QDs. It provides an advantageous solution for the creation of high bandwidth WLEDs for VLC uses in free space. Li et al. (2019b) exhibited an interesting portable VLC system, which is suitable for indoor short-distance communication technology using CdSe/ZnS QDs as a light converter, creating a portable transmitter and receiver based on digital signal processors and observing that under a direct bias voltage of 2.70 V, the highest transmission rate is 267 Kbs^{-1}.

Recently, Singh et al. (2020) reviewed the latest advances for VLC applications based on LEDs but principally on semipolar μ-LEDs and μ-LED-based arrays with high bandwidths. It has been highlighted that a significant application of great interest for marine exploration and underwater connectivity is the use of VLC for underwater optical wireless communication, recalling the reported case of a data rate of 2 Gbps over a 3 m air-underwater channel using a single layer QD blue μ-LED (Singh et al., 2020. Wei et al., 2020a).

Li-Fi, which represents a wireless technology that is not only environment-friendly, but also low cost for the future of communication (Meshram and Meshram, 2020), demands wearable and full duplex configuration because of its important role in applications such as smart wearables and "Internet of Things" (Shan et al., 2020). They described a perovskite QD-based light-emitting/detecting bifunctional fiber built with the help of a hybrid strategy and showed that the creation of this type of fiber is promising for the manufacture of future smart wearables.

Wan et al. (2021) proposed a new plasmonic WLED using the combination of a nanohole LED (H-LED) with QDs and silver NPs (Ag NPs) together (M-LED), explaining that the improved M-LED exhibited a maximum CRI of 91.2 and a data rate of 2.21 Gbs^{-1} at a low current density of 96 Acm^{-2} (60 mA). Here, a promising scope for WLEDs in lighting and VLC applications has been discussed.

10.5 Agriculture and horticulture

In recent years, a lot of research has been carried out in the fields of horticulture and agriculture, due to the diverse successful characteristics; LED lighting systems are considered a new profitable technology for plant growth and a promising tool to improve crop production (Mitchell et al., 2012; D'Souza

et al., 2015; Hasan et al., 2017; Viršilė et al., 2017). Many studies have revealed that the monochromatic character of LEDs can help diminish the incidence of pest and diseases pressure in growing plants and that some valuable features such as energy efficiency, long lifetime, and flexibility have indicated that LEDs are more adequate for future agricultural lighting methods than conventional lighting methods (Darko et al., 2014; Gomez and Izzo, 2018; Al Murad et al., 2021; Koushik et al., 2021).

The feature, related to the fact that QD can emit specific wavelengths of light, when supplied with energy, has been exploited to shift incoming light into a certain part of spectrum that plants can most effortlessly utilize for photosynthesis (Mission, 2021). QDs technology has demonstrated some excellent benefits for the lighting sector, including the application area related to horticulture.

A new procedure has been developed by Song (2016) for the manufacture of a LED utilizing QDs as phosphor. He constructed the multiwavelength LED device to show the possibility of its application for the plant factory. It was indicated that the good use of QD can be made with the multifunction LED light source.

Zhang et al. (2019) have fabricated some exceptional WLEDs and LEDs for plant growth with the help of red-emitting $CsPb_{1-x}Ti_xI_3$QDs@glasses, showing that a series of Ti-doped $CsPbI_3$ QDs were prepared in borosilicate glass ($SiO_2-B_2O_3$-ZnO) and that the WLED was built with the help of red-emitting $CsPb_{1-x}Ti_xI_3$QDs@glasses and yellow-emitting Ce^{3+}:YAG phosphor under excitation of InGaN blue chip.

Chung et al. (2020) reported that four kinds of QD lamps (QDLs) that emit different wavelengths of light were positioned in the perilla greenhouse in Milayang (Korea) revealing that QDLs considerably increased in the perilla leaf growth in comparison with control LED lamps and that perilla leaves exposed by Q2R lamps considerably improved the contents of biologically functional constituents (chlorophyll, total flavonoid, and phenolic-acid compounds).

Choi et al. (2019) have studied the consequences of LED and QD-LED irradiation on seed germination and microbial growth, in the time of the red radish (*Raphanus sativus* L.) sprouts cultivation. It was reported that the red hypocotyl was exceptional in blue light and QD-LED light. It was revealed that when red radish seeds were germinated in the dark and cultivated for a period of 7 days as sprouts and then irradiated with QD-LED light for 24 h, the seeds furnished some superior quality red radish sprout showing a diminished level of *E. coli* contamination.

Liu et al. (2021a) investigated the luminescent spectrum of LEDs based on QD materials, which was projected depending on the photosynthetic action spectrum (PAS) of plants. For the case of the three-band QD-based LEDs (QLEDs), it was found that photosynthetic action factor (PAF) has the maximal value of 8.088 and the induced photosynthetic index (IPI) has the

maximal value of 4.012. In the case of the four-band QLEDs, the maximal value of 7.689 was calculated for PAF and the maximal value of 3.818 was determined for IPI. They showed that in the issue related to the vision features, the four-band device exhibited a maximal value of 93 for CRI and a maximal value of 2053K for the correlated color temperature (CCT). They observed that the obtained results had consistence with the simulation ones, certifying the feasibility of manufacturing growing lamps with QD materials.

Jung et al. (2021) demonstrated that the quantity of Rg1 and Rg3, the most abundant ginsenosides, which are found in ginseng sprout, increased remarkably in the root of ginseng sprouts under the QD-LED method in comparison with the LED method, indicating that the cultivation of ginseng seeds using QD-LED method can determine the progress of high-productivity products.

10.6 Antimicrobial technology

LEDs have been used to obtain air disinfection, water disinfection and purification, surface decontamination, and food preservation (Koutchma and Orlowska, 2012; Kim and Kang, 2018; Ogonowska et al., 2019; Prasad et al., 2020; Singh et al., 2021b; Kim and Kang, 2021). Ultraviolet (particularly UVC) irradiation has especially attracted tremendous attention as one of the most successful antiviral procedures (Bhardwaj et al., 2021; Memarzadeh, 2021). The UV-LEDs have shown the potential for an extensive domain of applications in sterilization, sensing, and detection (Muramoto et al., 2014; Chen et al., 2017b; Won et al., 2018; Memarzadeh, 2021).

Yang et al. (2014b) showed that high internal efficiency and high temperature stability of UV LEDs at 308 nm were obtained utilizing high density GaN/AlN QDs grown with the help of metal organic vapor phase epitaxy (MOVPE). It was observed that the value of the internal quantum efficiency was 62%.

Chen et al. (2016) communicated the enhanced excitation and directional fluorescence emission (DFE) of QD by Ag NPs using theoretical calculations, emphasizing that enhanced DFE is important for biological and medical detection processes. It has been established that a monolayer Ag NPs showed a dominant enhancement in DFE for monolayer or low concentration QDs in LED, highlighting the significance for the design and progress of high-efficiency QD LEDs.

A new solid-state-based broadband UV light source was developed by Cho et al. (2020), which could substitute arc-lamp-based uses. Taking into account that group III-nitride UV LEDs did not exhibit a broad UV spectrum region, which limits their use in areas such as medical therapy and UV spectrophotometry, they obtained different emission wavelengths in the UV

region from the GaN QDs grown on the truncated pyramid structures, which furnish a high-efficiency broadband UV spectrum.

Elgammal (2020) reported that silicon QD-based LEDs produced with the help of cyclohexasilane can affect a number of industries but in response to the COVID-19 crisis, their efficiency recommends them for public areas, where infected droplets constitute important risks for public health.

Deep ultraviolet (DUV) LEDs furnish some important benefits such as compact size, low consumption, and long lifetimes. Brault et al. (2021) presented that $Al_xGa_{1-x}N$ LEDs emitting in the UVB (230−320 nm) and UVC (below 280 nm) regions are of significant technological interest for the medical and environmental applications as alternatives to mercury-based lamps. Noticing that some improvements of their characteristics are needed, they examined the potential of $Al_yGa_{1-y}N$ QDs as DUV emitters.

10.7 Recent developments

QDs are useful in LEDs for displays, memristors, smartphones, etc. These fabricated LEDs can exhibit a variety of colors, apart from WLEDs such as blue, red, green, orange, etc. These LEDs can also find applications in data communication, night vision, agriculture, horticulture, etc. Some recent developments of QDs-based LEDs are summarized in Table 10.1.

TABLE 10.1 Recent advancement on LED application of quantum dots.

Material used	Application	References
	Display and lighting	
$CsPbBr_{3-x}Cl_x/PbBr_y$ (or $PbCl_y$) (core/shell) quantum dot	Blue light-emitting diodes, emission peak at 492−435 nm	Park et al. (2021)
Polyethylene glycol (PEG)-coated CQD clusters	Optical properties used in high-performance sensors as well as next−generation energy/biological devices; fluorescent green (540 nm) and red (620 nm)	Juang et al. (2020)
InGaN quantum dots	Green light-emitting diode (550 nm)	Wang et al. (2018)
	Night vision	
Lead-free perovskite-type material	Photoelectric effect producing a voltage that affects the silicon/IR material interface, controlling the depletion layer	Aleksandrova (2021)

(*Continued*)

TABLE 10.1 (Continued)

Material used	Application	References
Bi^{3+}-doped $Sr_3Y_2Ge_3O_{12}$ (SYGO) phosphor	Night vision signage and optical information storage	Zhou et al. (2021)
Cr^{3+}-doped $LiScGeO_4$	Night vision surveillance and short-wave infrared (SWIR) spectroscopy technology	Miao et al. (2021)
White light GaN-μLEDs employing green/red perovskite quantum dots	Color converters for visible light communication	Liu et al. (2022)
$CsPbBr_3$ quantum dots	White light-emitting diodes and visible light communication	Li et al. (2021)
	Data communication	
Micro LED based on InGaN	Displays, data communication tools, photodetectors, and sensors	Liu et al. (2021b)
WSe_2 crystals	Photonics, imaging, spectroscopy, and data communications	Ghods et al. (2022)
Single layer quantum dot	Blue μLEDs with 4-Gbps QAM-OFDM (Quadrature Amplitude Modulation Orthogonal Frequency-Division Multiplexing)	Wei et al. (2020b)
	Agriculture and horticulture	
Carbon dots@ $Mg(OH)_2$	Blue, and red LED for horticulture	Xie et al. (2021)
CRISPR/Cas9-mediated	Horticulture food crops	Wang et al. (2021a, b)
Indoor LED light	Horticulture	Appolloni et al. (2022)
Lactuca sativa L. (Cos Lettuce)	Cultivation	Jishi et al. (2022)
Mesoporous silica nanoparticle	Light harvesting	Huang et al. (2021a, b)
Luminescent nanoparticles of $Sr_{0.46}Ba_{0.50}Yb_{0.02}Er_{0.02}F_{2.04}$	Photosynthetic activity and plant growth	Yanykin et al. (2022)
	Antimicrobial technology	
Polyimine substituted zinc phthalocyanine	Antimicrobial activity	Sen and Nyokong (2021)

(*Continued*)

TABLE 10.1 (Continued)

Material used	Application	References
Graphene quantum dots	Visible light-activated antibacterial activity	Huang et al. (2021a, b)
Carbon dots	Antimicrobial photodynamic	Romero et al. (2021)
ZnO QDs	Antimicrobial	Gangadoo et al. (2021)
Carbon QDs	Antimicrobial	Ayad et al. (2021)
Nitrogen–doped graphene QDs	Antimicrobial therapy	Kuo et al. (2021)

10.8 Conclusion

LEDs are presented as an attractive option to standard light sources, being considered today's perfect lighting technology due to their high energy efficiency, low cost, and longer lifetime. QDs have produced considerable interest due to their unique properties, and are being presented as one of the promising candidates for application in LEDs. The recent trends in QDs applications for LEDs have been reviewed, including those related to the following areas of utilization: displays, lighting, data communication, agriculture, horticulture, and antimicrobial technology. There is great potential for QDs as a unique material solution that can allow the successful achievement of a broad range of applications in the field of LEDs.

References

Al Murad, M., Razi, K., Jeong, B.R., Samy, P.M.A., Muneer, S., 2021. Light emitting diodes (LEDs) as agricultural lighting: impact and its potential on improving physiology, flowering, and secondary metabolites of crops. Sustainability 13 (4). Available from: https://doi.org/10.3390/su13041985.

Aleksandrova, M., 2021. Study of lead-free perovskite and quantum dots core-shell infrared photodetector integrated with the silicon technology. Devices for Integrated Circuit (DevIC). IEEE, pp. 494–497.

Ameta, R., Jat, K.K., Bhatt, J., Ameta, S.C., 2019. Quantum dots and their applications. In: Vakhrushev, A.V., Ameta, S.C., Susanto, H., Haghi, A.K. (Eds.), Advances in Nanotechnology and the Environmental Sciences: Applications; Innovations and Visions for the Future (1sted.); Series: AAP Research Notes on Nanoscience &Nanotechnology. CRC Press/Taylor&Francis Group; Apple Academic Press, Boca Raton, p. 32. Available from: https://doi.org/10.1201/9780429425837.

Appolloni, E., Pennisi, G., Zauli, I., Carotti, L., Paucek, I., Quaini, S., et al., 2022. Beyond vegetables: effects of indoor LED light on specialized metabolite biosynthesis in medicinal and aromatic plants; edible flowers; and microgreens. J. Sci. Food Agric. 102 (2), 472–487.

Arakawa, Y., Someya, T., Tachibana, K., 2000. Progress in GaN-based nanostructures for blue light emitting quantum dot lasers and vertical cavity surface emitting lasers. IEICE Trans. Electron. 83 (4), 564–572.

Armăşelu, A., 2017. Recent developments in applications of quantum-dot based light-emitting diodes. In: Ghamsari;, M.S. (Ed.), Quantum-Dot Based Light Emitting Diodes. IntechOpen, pp. 7–23. Available from: http://doi.org/10.5772/intechopen.69177.

Armăşelu, A., Popescu, A., Apostol, I., Ardelean, I., Damian, V., Iordache, I., et al., 2011a. Passive nonspecific labeling of cyanobacteria in natural samples using quantum dots. Optoelectron. Adv. Mater. Rapid Commun. 5 (10), 1084–1090.

Armăşelu, A., Popescu, A., Damian, V., Ardeleanu, I., Apostol, D., 2011b. Fluorescence properties of quantum dots used in the study of microorganisms. J. Optoelectron. Adv. Mater. 13 (4), 439–444.

Ayad, M.F., Trabik, Y.A., Abdelrahman, M.H., Fares, N.V., Magdy, N., 2021. Potentiometric carbon quantum dots-based screen-printed arrays for nano-tracing gemifloxacin as a model fluoroquinolone implicated in antimicrobial resistance. Chemosensors 9 (1). Available from: https://doi.org/10.3390/chemosensors9010008.

Bai, J., Cai, Y., Feng, P., Fletcher, P., Zhu, C., Tian, Y., et al., 2020. Ultrasmall, ultracompact and ultrahigh efficient InGaN micro light emitting diodes (μLEDs) with narrow spectral line width. ACS Nano 14 (6), 6906–6911.

Bang, S.Y., Fan, X.B., Jung, S.M., Yang, J., Shin, D.W., Suh, Y.H., et al., 2020. Highly stable and scalable blue QD-LED via an evaporated TiO_2 thin film as an electron transport layer. Adv. Opt. Mater. 8 (21). Available from: https://doi.org/10.1002/adom.202001172.

Bang, S.Y., Suh, Y.H., Fan, X.B., Shin, D.W., Lee, S., Choi, H.W., et al., 2021. Technology progress on quantum dot light-emitting diodes for next-generation displays. Nanoscale Horiz. 6 (2), 68–77.

Bharathi, G., Nataraj, D., Premkumar, S., Sowmiya, M., Senthilkumar, K., Thangadurai, T.D., et al., 2017. Graphene quantum dot solid sheets: strong blue-light-emitting & photocurrent-producing band-gap-opened nanostructures. Sci. Rep. 7 (1). Available from: https://doi.org/10.1038/s41598-017-10534-4.

Bhardwaj, S.K., Singh, H., Deep, A., Khatri, M., Bhaumik, J., Kim, K.H., et al., 2021. UVC–based photoinactivation as an efficient tool to control the transmission of coronaviruses. Sci. Total Environ. 792. Available from: https://doi.org/10.1016/j.scitotenv.2021.148548.

Biswas, S., Rasale, D.B., Das, A.K., 2016. Blue light emitting self-healable graphene quantum dot embedded hydrogels. RSC Adv. 6 (60), 54793–54800.

Biwa, G., Aoyagi, A., Doi, M., Tomoda, K., Yasuda, A., Kadota, H., 2021. Technologies for the Crystal LED display system. J. Soc. Info. Display 29 (6), 435–445.

Brault, J., Khalfioui, M.A., Leroux, M., Matta, S., Ngo, T.-H., Zaiter, A., et al., 2021. DUV LEDs based on AlGaN quantum dots. Proc. SPIE 11686, Gallium Nitride Materials and Devices XVI, 11686OT, 11685, Available from: https://doi.org/10.1117/12.2576135.

Cabrera, R., 2019. Chapter 1: Diodes. Electronic Devices and Circuits. ED-Tech Press, London, pp. 1–102.

Cao, H., Lin, S., Ma, Z., Li, X., Li, J., Zhao, L., 2019. Color converted white light-emitting diodes with 637.6 MHz modulation bandwidth. IEEE Electron Device Lett. 40 (2), 267–270.

Chen, Z.H., He, L., Wang, Y., Gan, Z., 2016. Effects of size and distribution of silver nanoparticles on directional fluorescence emission enhancement. IEEE Photonics J. 9 (1). Available from: https://doi.org/10.1109/JPHOT.2016.2636741.

Chen, Y., Yang, L., Zeng, Z., Ren, Q., Xu, X., Zhang, Q., et al., 2017a. Degradation in LED night vision imaging and recovery algorithms. Optik. 144, 240–245.

Chen, J., Loeb, S., Kim, J.H., 2017b. LED revolution: fundamentals and prospects for UV disinfection applications. Environ. Sci.: Water Res. Technol. 3 (2), 188–202.

Chen, W., Shi, T., Du, J., Zang, Z., Yao, Z., Li, M., et al., 2018. Highly stable silica-wrapped Mn-doped $CsPbCl_3$quantum dots for bright white light-emitting devices. ACS Appl. Mater. Interfaces 10 (50), 43978–43986.

Chen, F., Lin, Q., Shen, H., Tang, A., 2020a. Blue quantum dot-based electroluminescent light emitting diodes. Mater. Chem. Front. 4, 1340–1365.

Chen, Y.X., Lu, D., Wang, G.G., Huangfu, J., Wu, Q.B., Wang, X.F., et al., 2020b. Highly efficient orange emissive graphene quantum dots prepared by acid-free method for white LEDs. ACS Sustain. Chem. Eng. 8 (17), 6657–6666.

Chen, H.C., Shabir, A., Tan, C.M., Singh, P., Lin, J.H., 2021. Degradation dynamics of quantum dots in white LED applications. Sci. Rep. 11 (1). Available from: https://doi.org/10.1038/s41598-021-02714-0.

Cho, K.S., Lee, E.K., Joo, W.J., Jang, E., Kim, T.H., Lee, S.J., et al., 2009. High-performance crosslinked colloidal quantum-dot light-emitting diodes. Nat. Photonics 3 (6), 341–345.

Cho, J.-H., Lim, S.-H., Jang, M.-H., Lee, C., Yeo, H.-S., Sim, Y.C., et al., 2020. A broadband ultraviolet light source using GaN quantum dots formed on hexagonal truncated pyramid structures. Nanoscale Adv. 2, 1449–1455.

Choi, M.K., Yamg, J., Hyeon, T., Kim, D.-H., 2018. Flexible quantum dot light-emitting diodes for next-generation displays. NPJ Flex Electron 2 (10). Available from: https://doi.org/10.1038/s41528-018-0023-3.

Choi, I.-L., Wang, L., Lee, J.H., Han, S.J., Ko, Y.-W., Kim, Y., et al., 2019. Effect of LED and QD-LED (quantum dot) treatments on production and quality of red radish (Raphanus sativus L.) sprout. Protected Horticulture and Plant Factory 28 (3), 265–272. Society for Bio-Environment Control.

Chung, S.I., Kang, M.Y., Lee, S.C., 2020. The growth and enhancement of functional ingredients for health improvement of perilla leaves using LED light source with QD application. J. Crop Sci. Biotechnol. 23, 163–169.

Coe, S., Woo, W.-K., Bawendi, M., Bulović, V., 2002. Electroluminescence from single monolayers of nanocrystals in molecular organic deveices. Nature 420 (6917), 800–803.

Colvin, V.L., Schlamp, M.C., Alivisatos, A.P., 1994. Light emitting diodes made from cadmium selenide nanocrystals and semiconducting polymer. Nature 370 (6488), 354–357.

D'Souza, C., Yuk, H.-G., Khoo, G.H., Zhou, W., 2015. Application of light-emitting diodes in food production, postharvest preservation and microbiological food safety. Compr. Rev. Food Sci. Food Saf. 14 (6), 719–740.

Darko, E., Heydarizadeh, P., Schoefs, B., Sabzalian, M.R., 2014. Photosynthesis under artificial light: the shift in primary and secondary metabolism. Phil. Trans. R. Soc. Lond. B. Biol. Sci. 369 (1640). Available from: https://doi.org/10.1098/rstb.2013.0243.

Denault, K.A., Mikhailovsky, A.A., Brinkley, S., DenBaars, S.P., Seshadri, R., 2013. Improving color rendition in solid state white lighting through the use of quantum dots. J. Mater. Chem. C 1 (7), 1461–1466.

Dong, Y., Caruge, J.M., Zhou, Z., Hamilton, C., Popovic, Z., Ho, J., et al., 2015. 20.2: ultra-bright, highly efficient, low roll-off inverted quantum-dot light emitting devices (QLEDs). SID Symp. Dig. Tech. Pap. 46 (1), 270–273.

Elgammal, R., 2020. Material advances for LED quantum dot efficiency. NASA Tech. Briefs. 44 (11), 14A–16A.

Erdem, T., Volkan, D.H., 2013. Color science of nanocrystal quantum dots for lighting and displays. Nanophotonics 2 (1), 57−81.

Gangadoo, S., Xu, C., Cozzolino, D., Latham, K., Della Gaspera, E., Chapman, J., et al., 2021. Probing nanoscale interactions of antimicrobial zinc oxide quantum dots on bacterial and fungal cell surfaces. Adv. Mater. Interfaces . Available from: https://doi.org/10.1002/admi.202101484.

Ghamsari, M.S., 2017. Quantum-dots based organic light-emitting diodes-thestate-of-the-art. In: Ghamsari, M.S. (Ed.), Quantum-Dot Based Light-Emitting Diodes. IntechOpen. Available from: http://doi.org/10.5772/intechopen.69744.

Ghods, S., Esfandiar, A., Irajizad, A., Vardast, S., 2022. Enhanced photoresponse and wavelength selectivity by SILAR-coated quantum dots on two-dimensional WSe_2crystals. ACS Omega 7 (2), 2091−2098.

Gomez, C., Izzo, L.G., 2018. Increasing efficiency of crop production with LEDs. AIMS Agric. Food 3 (2), 135−153.

Gu, B., Liu, Z., Chen, D., Gao, B., Yang, Y., Guo, Q., et al., 2021. Solid-state fluorescent nitrogen doped graphene quantum dots with yellow emission for white light-emitting diodes. Synth. Met. 277. Available from: https://doi.org/10.1016/j.synthmet.2021.116787.

Hao, J., Liu, H., Miao, J., Lu, R., Zhou, Z., Zhao, B., et al., 2019. A facile route to synthesize CdSe/ZnS thick-shell quantum dots with precisely controlled green emission properties: towards QDs based LED applications. Sci. Rep. 9 (1). Available from: https://doi.org/10.1038/s41598-019-48469-7.

Hasan, M.M., Bashir, T., Ghosh, R., Lee, S.K., Bae, H., 2017. An overview of LED's effects on the production of bioactive compounds and crop quality. Molecules (Basel, Switzerland) 22 (9). Available from: https://doi.org/10.3390/molecules22091420.

He, Y., Gong, J., Zhu, Y., Feng, X., Peng, H., Wang, W., et al., 2018. Highly pure yellow light emission of perovskite CsPb $(BrxI_{1-x})_3$quantum dots and their application for yellow light-emitting diodes. Opt. Mater. 80. Available from: https://doi.org/10.1016/j.optmat.2018.04.009.

Hu, X., Xie, Y., Geng, C., Xu, S., Bi, W., 2020. Study on the color compensation effect of composite orange-red quantum dots in WLED application. Nanoscale Res. Lett. 15 (1). Available from: https://doi.org/10.1186/s11671-020-03350-9.

Huang, C.Y., Su, Y.K., Chen, Y.C., Tsai, P.C., Wan, C.T., Li, W.L., 2008. Hybrid CdSe-ZnS quantum dot-InGaN-GaN quantum well red light-emitting diodes. IEEE Electron Device Lett. 29 (7), 711−713.

Huang, Y., Tan, G., Gou, F., Li, M.-C., Lee, S.-L., Wu, S.-T., 2019. Prospects and challenges of mini-LED and micro-LED displays. J. Soc. Inf. Disp. 27, 387−401.

Huang, Y.-M., Singh, K.J., Liu, A.-C., Lin, C.-C., Chen, Z., Wang, K., et al., 2020a. Advances in quantum-dot-based displays. Nanomaterial 10 (7). Available from: https://doi.org/10.3390/nano10071327.

Huang, Y., Hsiang, E.-L., Deng, M.Y., Wu, S.-T., 2020b. Mini-LED, micro-LED and OLED displays: present status and future perspectives. Light Sci. Appl. 9 (105). Available from: https://doi.org/10.1038/s41377-020-0341-9.

Huang, H.H., Anand, A., Lin, C.J., Lin, H.J., Lin, Y.W., Harroun, S.G., et al., 2021a. LED irradiation of halogen/nitrogen-doped polymeric graphene quantum dots triggers the photodynamic inactivation of bacteria in infected wounds. Carbon N. Y. 174, 710−722.

Huang, W.T., Su, T.Y., Chan, M.H., Tsai, J.Y., Do, Y.Y., Huang, P.L., et al., 2021b. Near-infrared nanophosphor embedded in mesoporous silica nanoparticle with high light-harvesting efficiency for dual photosystem enhancement. Angew. Chem. Int. Edi. 60 (13), 6955−6959.

Ippen, C., Guo, W., Zehnder, D., Kim, D., Manders, J., Barrera, D., et al., 2019. High efficiency heavy metal free QD-LEDs for next generation displays. J. Soci. Info. Display 27 (6), 338–346.

Jang, E., 2018. Environmentally friendly quantum dots for display applications. IEEE International Electron Devices Meeting (IEDM) . Available from: https://doi.org/10.1109/IEDM.2018.8614647.

Jang, E., Jun, S., Jang, H., Lim, J., Kim, B., Kim, Y., 2010. White-light-emitting diodes with quantum dot color converters for display backlights. Adv. Mater. 22 (28), 3076–3080.

Ji, W., Jing, P., Xu, W., Yuan, X., Wang, Y., Zhao, J., et al., 2013. High color purity ZnSe/ZnS core/shell quantum dot based blue light emitting diodes with an inverted device structure. Appl. Phy. Lett. 103 (5), 053106. Available from: https://doi.org/10.1063/1.4817086.

Jia, H., Wang, F., Tan, Z., 2020. Material and device for engineering high-performance blue quantum dot light-emitting diodes. Nanoscale 12 (25), 13186–13224.

Jiang, Y., Cho, S.-Y., Shim, M., 2018. Light-emitting diodes of colloidal quantum dots and nanorod heterostructures for future emissive displays. J. Mater. Chem. C 6, 2618–2634.

Jishi, T., Ishii, T., Shoji, K., 2022. Cultivation of cos lettuce using blue LED and quantum dot wavelength conversion sheets. Sci. Hortic. (Amsterdam) 295. Available from: https://doi.org/10.1016/j.scienta.2021.110772.

Juang, R.S., Fu, C.C., Hsieh, C.T., Gu, S., Gandomi, Y.A., Liu, S.H., 2020. Highly luminescent aggregate-induced emission from polyethylene glycol-coated carbon quantum dot clusters under blue light illumination. J. Mater. Chem. C 8 (46), 16569–16576.

Jun, S., Lee, J., Jang, E., 2013. Highly luminescent and photostable quantum dot–silica monolith and its application to light-emitting diodes. ACS Nano 7 (2), 1472–1477.

Jung, S.-M., Eom, H.-J., Lee, S.-Y., Seo, E.-H., Kim, Y.-D., Yoo, Y.-H., et al., 2021. Evaluating the contents of ginsenoside based on the growth of ginseng sprouts using QD-LED (quantum dot) plant lighting. J. Agric. Life Environ. Sci. 33 (3), 225–235.

Kagan, C.R., Lifshitz, E., Sargent, E.H., Talapin, D.V., 2016. Building devices from colloidal quantum dot. Science 353 (6302). Available from: https://doi.org/10.1126/science.aac5523.

Kang, X., Yang, Y., Wang, L., Wei, S., Pan, D., 2015. Warm white light emitting diodes with gelatin-coated $AgInS_2$/ZnS core/shell quantum dots. ACS Appl. Mater. Interfaces 7 (50), 27713–27719.

Kate, D.M., Husain, K.M.R., 2017. A real time data transmission with LED bulb using Li-Fi technology. Int. J. Sci. Technol. Eng. 3 (09), 553–556.

Kim, D.-K., Kang, D.-H., 2018. UVC LED irradiation effectively inactivates aerosolized viruses bacteria, and fungi in a chamber-type air disinfection system. Appl. Environ. Microbiol. 84 (17). Available from: https://doi.org/10.1128/AEM.00944-18.

Kim, D.-K., Kang, D.-H., 2021. Investigation of a new UVC LEDs array continuous type water disinfection system for inactivating Escherichia coli O157:H7 according to flow rate and electrical energy efficiency analysis. Food Control 119. Available from: https://doi.org/10.1016/j.foodcont.2020.107470.

Kim, J.U., Lee, M.H., Yang, H., 2008. Synthesis of $Zn_{1-x}Cd_xS$:Mn/ZnS quantum dots and their application to light-emitting diodes. Nanotechnology 19 (46). Available from: https://doi.org/10.1088/0957-4484/19/46/465605.

Kim, H., Han, J.Y., Kang, D.S., Kim, S.W., Jang, D.S., Suh, M., et al., 2011. Characteristics of $CuInS_2$/ZnS quantum dots and its application on LED. J. Crystal Growth 326 (1), 90–93.

Kim, K., Jeong, S., Woo, J.Y., Han, C.S., 2012. Successive and large-scale synthesis of InP/ZnS quantum dots in a hybrid reactor and their application to white LEDs. Nanotechnology 23 (6). Available from: https://doi.org/10.1088/0957-4484/23/6/065602.

Kim, H.H., Park, J.-S., Han, I.K., Won, S.O., Park, C., Hwang, D.K., et al., 2016a. Emissive CdTe/ZnO/GO quasi-core-shell-shell hybrid quantum dots for white light emitting diodes. Nanoscale 8 (47), 19737–19743.

Kim, M.J., Song, H.J., Cho, I.S., Jeong, S., Shin, H., Lee, S., et al., 2016b. Fine tuning of emission property of white light-emitting diodes by quantum-dot-coating on YAG: Ce nanophosphors. Appl. Surface Sci. 379, 467–473.

Kim, T., Kim, K.H., Kim, S., Choi, S.M., Jang, H., Seo, H.K., et al., 2020. Efficient and stable blue quantum dot light-emitting diode. Nature 586 (7829), 385–389.

Ko, M., Yoon, H.C., Yoo, H., Oh, J.H., Yang, H., Do, Y.R., 2017. Highly efficient green Zn–Ag–In–S/Zn–In–S/ZnS QDs by a strong exothermic reaction for down-converted green and tripackage white LEDs. Adv. Funct. Mater. 27 (4). Available from: https://doi.org/10.1002/adfm.201602638.

Koushik, P., Karthikeyan, P., Keerthi, M., Manikandan, M., 2021. Organic LED farming for self sustainability during post-COVID 19. J. Phys. Conf. Ser. 1969 (1). Available from: https://doi.org/10.1088/1742-6596/1969/1/012053.

Koutchma, T., Orlowska, M., 2012. Ultraviolet light for processing fruits and fruit products. In: Rodrigues, S., Fernandez, F.A.N. (Eds.), Advances in Fruit Processing Technologies, first ed. CRC Press/Taylor & Francis Group, Boca Raton. Available from: http://doi.org/10.1201/b12088.

Kubendhiran, S., Bao, Z., Dave, K., Liu, R.-S., 2019. Microfluidic synthesis of semiconducting colloidal quantum dots and their applications. ACS Appl. Nano Mater. 2 (4), 1773–1790.

Kumar, B.G., Sadeghi, S., Melikov, R., Aria, M.M., Jalali, H.B., Ow-Yang, C.W., et al., 2018. Structural control of InP/ZnS core/shell quantum dots enables high-quality white LEDs. Nanotechnology 29 (34). Available from: https://doi.org/10.1088/1361-6528/aac8c9.

Kuo, T.R., Hung, S.T., Lin, Y.T., Chou, T.L., Kuo, M.C., Kuo, Y.P., et al., 2017. Green synthesis of InP/ZnS core/shell quantum dots for application in heavy-metal-free light-emitting diodes. Nanoscale Res. Lett. 12 (1). Available from: https://doi.org/10.1186/s11671-017-2307-2.

Kuo, W.S., Wu, P.C., Hung, C.Y., Chang, C.Y., Wang, J.Y., Chen, P.C., et al., 2021. Nitrogen functionalities of amino-functionalized nitrogen-doped graphene quantum dots for highly efficient enhancement of antimicrobial therapy to eliminate methicillin-resistant *Staphylococcus aureus* and utilization as a contrast agent. Int. J. Mol. Sci. 22 (18). Available from: https://doi.org/10.3390/ijms22189695.

Kwon, W., Kim, Y.H., Kim, J.H., Lee, T., Do, S., Park, Y., et al., 2016. High color-purity green, orange, and red light-emitting diodes based on chemically functionalized graphene quantum dots. Sci. Rep. 6 (1). Available from: https://doi.org/10.1038/srep24205.

Lee, K.H., Lee, J.H., Song, W.S., Ko, H., Lee, C., Lee, J.H., et al., 2013. Highly efficient, color-pure, color-stable blue quantum dot light-emitting devices. ACS Nano 7 (8), 7295–7302.

Leitao, M.F., Santos, J.M.M., Guihabert, B., Watson, S., Kelly, A.E., Islim, M.S., et al., 2017. Gb/s visible light communications with colloidal quantum dot color converters. IEEE J. Sel. Topics. Quantum Electron. 23 (5). Available from: https://doi.org/10.1109/JSTQE.2017.2690833.

Li, C., Zang, Z., Chen, W., Hu, Z., Tang, X., Hu, W., et al., 2016. Highly pure green light emission of perovskite $CsPbBr_3$ quantum dots and their application for green light-emitting diodes. Opt. Express 24 (13), 15071–15078.

Li, D., Kristal, B., Wang, Y., Feng, J., Lu, Z., Yu, G., et al., 2019a. Enhanced efficiency of InP-based red quantum dot light-emitting diodes. ACS Appl. Mater. Interfaces 11 (37), 34067–34075.

Li, Z., Xue, D., Liu, D., Liu, Y., Ye, W., Zhang, Y., et al., 2019b. Portable visible light communication transmitter and receiver using core-shell CdSe/ZnS quantum dots white light-emitting diode. IET Comun. 13 (7), 873–878.

Li, Z., Hu, Y., Shen, H., Lin, Q., Wang, L., Wang, H., et al., 2017. Efficient and long-life green light-emitting diodes comprising tridentate thiol capped quantum dots. Laser Photonics Rev. 11 (1). Available from: https://doi.org/10.1002/lpor.201600227.

Li, J.S., Tang, Y., Li, Z.T., Li, J.X., Ding, X.R., Yu, B.H., et al., 2020. Toward 200 lumens per watt of quantum-dot white-light-emitting diodes by reducing reabsorption loss. ACS Nano 15 (1), 550–562.

Li, X., Cai, W., Guan, H., Zhao, S., Cao, S., Chen, C., et al., 2021. Highly stable $CsPbBr_3$ quantum dots by silica-coating and ligand modification for white light-emitting diodes and visible light communication. Chem. Eng. J. 419. Available from: https://doi.org/10.1016/j.cej.2021.129551.

Lin, Q., Song, B., Wang, H., Zhang, F., Chen, F., Wang, L., et al., 2016. High-efficiency deep-red quantum-dot light-emitting diodes with type-II CdSe/CdTe core/shell quantum dots as emissive layers. J. Mater. Chem. C 4 (30), 7223–7229.

Lin, Q., Wang, L., Li, Z., Shen, H., Guo, L., Kuang, Y., et al., 2018. Nonblinking quantum-dot-based blue light-emitting diodes with high efficiency and a balanced charge-injection process. ACS Photonics 5 (3), 939–946.

Liu, Z., Lin, C.-H., Hyun, B.-R., Sher, C.-W., Lv, Z., Luo, B., et al., 2020a. Micro-light-emitting diodes with quantum dots in display technology. Light Sci. Appl. 9 (23). Available from: https://doi.org/10.1038/s41377-020-0268-1.

Liu, D., Cao, S., Wang, S., Wang, H., Dai, W., Zou, B., et al., 2020b. Highly stable red quantum dot light-emitting diodes with long T 95 operation lifetimes. J. Phy. Chem. Lett. 11 (8), 3111–3115.

Liu, Z., Li, F., Huang, G., Wei, J., Jiang, G., Huang, Y., et al., 2021a. Spectral design of light-emitting diodes for plant photosynthesis based on quantum dots. IEEE Access 9, 156229–156238.

Liu, Z., Hyun, B.R., Sheng, Y., Lin, C.J., Changhu, M., Lin, Y., et al., 2021b. Micro-light-emitting diodes based on InGaN materials with quantum dots. Adv. Mater. Technol. . Available from: https://doi.org/10.1002/admt.2021011892101189.

Liu, X., Tao, L., Mei, S., Cui, Z., Shen, D., Sheng, Z., et al., 2022. White light GaN-μLEDs employing green/red perovskite quantum dots as color converters for visible light communication. Nanomaterial 12 (4). Available from: https://doi.org/10.3390/nano12040627.

Luk, C.M., Tang, L.B., Zhang, W.F., Yu, S.F., Teng, K.S., Lau, S.P., 2012. An efficient and stable fluorescent graphene quantum dot–agar composite as a converting material in white light emitting diodes. J. Mater. Chem. 22 (42), 22378–22381.

Luo, Z., Manders, J., Yurek, J., 2018. Your quide to television's quantum-dot future, IEEE Spectrum <https://spectrum.ieee.org/your-quide-to-televisions-quantumdot-future>.

Lv, W., Wang, L., Wang, J., Hao, Z., Luo, Y., 2012. InGaN/GaN multilayer quantum dots yellow-green light-emitting diode with optimized GaN barriers. Nanoscale Res. Lett. 7 (1). Available from: https://doi.org/10.1186/1556-276X-7-617.

Mattousi, H., Radzilowski, L.H., Dabboussi, B.O., Thomas, E.L., Bawendi, M.G., Rubner, M.F., 1998. Electroluminescence from heterostructures of poly(phenylene vinylene) and inorganic CdSe nanocrystals. J. Appl. Phys. 83 (12), 7965–7974.

Memarzadeh, F., 2021. A review of recent evidence for utilizing ultraviolet irradiation technology to disinfect both indoor air and surfaces. Appl. Biosafety 26 (1), 52–56.

Meshram, S.S., Meshram, S., 2020. Light fidelity (Li-Fi): a wireless technology. J. Biomater. Nanotechnol. 9, 7–13.

Miao, S., Liang, Y., Zhang, Y., Chen, D., Wang, X.J., 2021. Broadband Short-Wave Infrared Light-Emitting Diodes Based on Cr^{3+}–Doped $LiScGeO_4$ Phosphor. ACS Appl. Mater. Interfaces 13 (30), 36011–36019.

Mission, E.G., 2021. Recent development in agriculture based on nanomaterials. In: Singh, R.P., Singh, K.R. (Eds.), Nanomaterials in Bionanotechnology: Fundamentals and Applications, first ed. CRC Press, Boca Raton. Available from: http://doi.org/10.1201/9781003139744.

Mitchell, C.A., Both, A.-J., Bourget, C.M., Burr, J.F., Kubola, C., Lopez, R.G., et al., 2012. LEDs: the future of greenhouse lighting!. Chron. Horticult. 52, 5–13.

Motomura, G., Ogura, K., Iwasaki, Y., Nagakubo, J., Hirakawa, M., Nishihashi, T., et al., 2020. Improvement of electroluminescent characteristics in quantum dot light emitting diodes using ZnInP/ZnSe/ZnS quantum dots by mixing an electron transport material into the light-emitting layer. AIP Adv. 10. Available from: https://doi.org/10.1063/5.0010203.

Moustakas, T.D., Xu, T., Thomidis, C., Nikiforov, A.Y., Zhou, L., Smith, D.J., 2008. Growth of III-nitride quantum dots and their applications to blue-green LEDs. Phys. Status Solidi (A) 205 (11), 2560–2565.

Muramoto, Y., Kimura, M., Nouda, S., 2014. Development and future of ultraviolet light-emitting diodes: UV-LED will replace the UV lamp. Semicond. Sci. Technol. 29 (8). Available from: https://doi.org/10.1088/0268-1242/29/8/084004.

Nguyen, T.C., Can, T.T.T., Choi, W.-S., 2019. Optimization of quantum dot thin films using electrohydrodynamic jet spraying for solution-processed quantum dot light—emitting diodes. Sci. Rep. 9. Available from: https://doi.org/10.1038/s41598-019-50181-5.

Nizamoglu, S., Demir, H.V., 2009. Förster resonance energy transfer enhanced color-conversion using colloidal semiconductor quantum dots for solid state lighting. Appl. Phy. Lett. 95 (15). Available from: https://doi.org/10.1063/1.3222902.

Ogonowska, P., Woźniak, A., Pierański, M.K., Wasylew, T., Kwiek, P., Brasel, M., et al., 2019. Application and characterization of light-emitting diodes for photodynamic inactivation of bacteria. Light. Res. Technol. 51 (4), 612–624.

Pan, G., Bai, X., Xu, W., Chen, X., Zhai, Y., Zhu, J., et al., 2020. Bright blue light emission of Ni^{2+}ion-dopedCsPbCl$_x$Br$_{3-x}$perovskite quantum dots enabling efficient light-emitting devices. ACS Appl. Mater. Interfaces 12 (12), 14195–14202.

Park, I.K., Park, S.J., 2011. Green gap spectral range light-emitting diodes with self-assembled InGaN quantum dots formed by enhanced phase separation. Appl. Phys. Express 4 (4). Available from: https://doi.org/10.1143/APEX.4.042102.

Park, N.M., Kim, T.S., Park, S.J., 2001. Band gap engineering of amorphous silicon quantum dots for light-emitting diodes. Appl. Phys. Lett. 78 (17), 2575–2577.

Park, J.H., Kim, J.Y., Chin, B.D., Kim, Y.C., Kim, J.K., Park, O.O., 2004. White emission from polymer/quantum dot ternary nanocomposites by incomplete energy transfer. Nanotechnology 15 (9). Available from: https://doi.org/10.1088/0957-4484/15/9/018.

Park, S.H., Hong, A., Kim, J.H., Yang, H., Lee, K., Jang, H.S., 2015. Highly bright yellow-green-emitting $CuInS_2$ colloidal quantum dots with core/shell/shell architecture for white light-emitting diodes. ACS Appl. Mater. Interfaces 7 (12), 6764–6771.

Park, Y.R., Kim, H.H., Eom, S., Choi, W.K., Choi, H., Lee, B.R., et al., 2021. Luminance efficiency roll-off mechanism in CsPbBr$_{3-x}$Cl$_x$ mixed-halide perovskite quantum dot blue light-emitting diodes. J. Mater. Chem. C 9 (10), 3608–3619.

Perikala, M., Bhardwaj, A., 2021. Excellent color rendering index single system white light emitting carbon dots for next generation, lighting devices. Sci. Rep. 11. Available from: https://doi.org/10.1038/s41598-021-91074-w.

Pietryga, J.M., Park, Y.-S., Lim, J., Fidler, A.F., Bae, W.K., Brovelli, S., et al., 2016. Spectroscopic and device aspects of nanocrystal quantum dots. Chem. Rev. 116 (18), 10513–10622.

Pradhan, S., Di Stasio, F., Bi, Y., Gupta, S., Christodoulou, S., Stavrinadis, A., et al., 2019. High-efficiency colloidal quantum dot infrared light-emitting diodes via engineering at the supra-nanocrystalline level. Nat. Nanotechnol. 14 (1), 72–79.

Prasad, A., Du, L., Zubair, M., Subedi, S., Ullah, A., Roopesh, M.S., 2020. Applications of light-emitting diodes (LEDs) in food processing and water treatment. Food Eng. Rev. 12, 268–289.

Qian, L., Zheng, Y., Xue, J., Holloway, P.H., 2011. Stable and efficient quantum-dot light-emitting diodes based on solution-processed multilayer structures. Nat. Photonics 5 (9), 543–548.

Rad, R.R., Gualdrón-Reyes, A.F., Masi, S., Ganji, B.A., Taghavinia, N., Gené-Marimon, S., et al., 2021. Tunable carbon–$CsPbI_3$ quantum dots for white LEDs. Adv. Optical Mater. 9 (4). Available from: https://doi.org/10.1002/adom.202001508.

Ramalingam, G., Ragupathi, C., Kaviyarasu, K., Letsholathebe, D., Mohamed, S.B., Magdalane, C.M., et al., 2019. Up-scalable synthesis of size-controlled white-green emitting behavior of core/shell (CdSe/ZnS) quantum dots for LED applications. J. Nanosci. Nanotechnol. 19 (7), 4026–4032.

Ren, J., Zhou, X., Wang, Y., 2020. Water triggered interfacial synthesis of highly luminescent $CsPbX_3$: Mn^{2+} quantum dots from nonluminescent quantum dots. Nano Res. 13 (12), 3387–3395.

Ren, A., Wang, H., Zhang, W., Wu, J., Wang, Z., Penty, R.V., et al., 2021. Emerging light-emitting diodes for next-generation data communications. Nat. Electron. 4 (8), 559–572.

Romero, M.P., Alves, F., Stringasci, M.D., Buzzá, H.H., Ciol, H., Inada, N.M., et al., 2021. One-pot microwave-assisted synthesis of carbon dots and in vivo and in vitro antimicrobial photodynamic applications. Front. Microbiol. 12. Available from: https://doi.org/10.3389/fmicb.2021.662149.

Roy, P., Periasamy, A.P., Chuang, C., Liou, Y.R., Chen, Y.F., Joly, J., et al., 2014. Plant leaf-derived graphene quantum dots and applications for white LEDs. New J. Chem. 38 (10), 4946–4951.

Ruan, C., Zhang, Y., Lu, M., Ji, C., Sun, C., Chen, X., et al., 2016. White light-emitting diodes based on $AgInS_2$/ZnS quantum dots with improved bandwidth in visible light communication. Nanomater. 6 (1). Available from: https://doi.org/10.3390/nano6010013.

Sabatini, R., Richardson, M.A., Cantiello, M., Toscano, M., Fiorini, P., 2016. A novel approach to night vision imaging system development, integration and verification in military aircraft. Aerospace Sci. Technol. 31 (1), 10–23.

Sadeghi, S., Mutcu, S.E., Srivastava, S.B., Aydindogan, G., Caynak, S., Karslı, K., et al., 2018. High quality quantum dots polymeric films as color converters for smart phone display technology. Mater. Res. Exp. 6 (3). Available from: https://doi.org/10.1088/2053-1591/aaf3ef.

Sadeghi, S., KhabbazAbkenar, S., Ow-Yang, C.W., Nizamoglu, S., 2019. Efficient white LEDs using liquid-state magic-sized CdSe quantum dots. Sci. Rep. 9 (1). Available from: https://doi.org/10.1038/s41598-019-46581-2.

Sellers, N., 2018. Chapter 3: Terahertz and infrared quantum photodetectors. Handbook of Terahertz Technology. ED-Tech Press, London, pp. 100–136.

Sen, P., Nyokong, T., 2021. Promising photodynamic antimicrobial activity of polyimine substituted zinc phthalocyanine and its polycationic derivative when conjugated to nitrogen, sulfur, co-doped graphene quantum dots against *Staphylococcus aureus*. Photodiagnosis Photodyn. Ther. 34. Available from: https://doi.org/10.1016/j.pdpdt.2021.102300.

Shan, Q., Wei, C., Jiang, Y., Song, J., Zou, Y., Xu, L., et al., 2020. Perovskite light-emitting/detecting bifunctional fibres for wearable LiFi communication. Light Sci Appl. 9. Available from: https://doi.org/10.1038/s41377-020-00402-8.

Shen, C., Chu, J., Qian, F., Zou, X., Zhong, C., Li, K., et al., 2012. High color rendering index white LED based on nano-YAG: Ce^{3+} phosphor hybrid with CdSe/CdS/ZnS core/shell/shell quantum dots. J. Modern Opt. 59 (14), 1199–1203.

Shen, H., Lin, Q., Wang, H., Qian, L., Yang, Y., Titov, A., et al., 2013. Efficient and bright colloidal quantum dot light-emitting diodes via controlling the shell thickness of quantum dots. ACS Appl. Mater. Interfaces 5 (22), 12011–12016.

Shen, P., Li, X., Cao, F., Ding, X., Yang, X., 2018. Highly efficient, all-solution-processed, flexible white quantum dot light-emitting diodes. J. Mater. Chem. C 6 (36), 9642–9648.

Shirasaki, Y., Supran, G.J., Bawendi, M.G., Bulović, V., 2013. Emergence of colloidal quantum-dot light-emitting technologies. Nat. Photon. 7, 13–23.

Singh, R.K., Som, S., Dutta, S., Jain, N., Kuo, M.T., Singh, J., et al., 2019. Rapid synthesis of hybrid methylammonium lead iodide perovskite quantum dots and rich MnI_2 substitution favouring Pb-free warm white LED applications. Nanoscale Adv. 1 (8), 2999–3008.

Singh, K.J., Huang, Y.-M., Ahmed, T., Liu, A.-C., Chen, S.-W.H., Liou, F.-J., et al., 2020. Micro-LED as a promising candidate for high-speed visible light communication. Appl. Sci. 10 (20). Available from: https://doi.org/10.3390/app10207384.

Singh, K.J., Ahmed, T., Gautam, P., Sadhu, A.S., Lien, D.-H., Chen, S.C., et al., 2021a. Recent advances in two-dimensional quantum dots and their applications. Nanomaterial 11 (6). Available from: https://doi.org/10.3390/nano11061549.

Singh, H., Bhardwaj, S.K., Khatri, M., Kim, K.-H., Bhardwaj, N., 2021b. UVC radiation for food safety: an emerging technology for the microbial disinfection of food products. Chem. Eng. J. 417. Available from: https://doi.org/10.1016/j.cel.2020.128084.

Son, D.I., Kwon, B.W., Park, D.H., Seo, W.S., Yi, Y., Angadi, B., et al., 2012. Emissive ZnO–graphene quantum dots for white-light-emitting diodes. Nat. Nanotechnol. 7 (7), 465–471.

Song, J.-W., 2016. Grow light for plant factory using quantum dot LED. J. Int. Counc. Electr. Eng. 6 (1), 13–16.

Song, H., Lee, S., 2007a. Photoluminescent (CdSe) ZnS quantum dot–polymethylmethacrylate polymer composite thin films in the visible spectral range. Nanotechnology 18 (5). Available from: https://doi.org/10.1088/0957-4484/18/5/055402.

Song, H., Lee, S., 2007b. Red light emitting solid state hybrid quantum dot–near-UV GaN LED devices. Nanotechnology 18 (25). Available from: https://doi.org/10.1088/0957-4484/18/25/255202.

Song, W.S., Yang, H., 2012. Fabrication of white light-emitting diodes based on solvothermally synthesized copper indium sulfide quantum dots as color converters. Appl. Phys. Lett. 100 (18), 183104. Available from: https://doi.org/10.1063/1.4711019.

Song, W.S., Kim, J.H., Lee, J.H., Lee, H.S., Do, Y.R., Yang, H., 2012. Synthesis of color-tunable Cu–In–Ga–S solid solution quantum dots with high quantum yields for application to white light-emitting diodes. J. Mater. Chem. 22 (41), 21901–21908.

Song, W.S., Lee, S.H., Yang, H., 2013. Fabrication of warm, high CRI white LED using non-cadmium quantum dots. Opt. Mater. Express 3 (9), 1468–1473.

Steckel, J.S., Snee, P., Coe-Sullivan, S., Zimmer, J.P., Halpert, J.E., Anikeeva, P., et al., 2006. Color-saturated green-emitting QD-LEDs. Angew. Chem. Int. (Ed.) 45 (35), 5796–5799.

Stouwdam, J.W., Janssen, R.A., 2008. Red, green, and blue quantum dot LEDs with solution processable ZnO nanocrystal electron injection layers. J. Mater. Chem. 18 (16), 1889–1894.

Sun, Q., Wang, Y.A., Li, L.S., Wang, D., Zhu, T., Xu, J., et al., 2007. Bright, multicoloured light-emitting diodes based on quantum dots. Nat. Photon. 1 (12), 717–722.

Sun, Y., Fan, J., Liu, M., Zhang, L., Jiang, B., Zhang, M., et al., 2020. Highly transparent ultra-thin flexible, full-color mini-LED display with indium-gallium-zinc oxide thin-film transistor substrate. J. Soc. Inf. Disp. 28, 926–935.

Tan, G., Huang, Y., Li, M.-C., Lee, S.-L., Wu, S.-T., 2018. High dynamic range liquid crystal displays with a mini-LED backlight. Opt. Express 26 (13), 16572–16584.

Taylor, R.M., Church, K.H., Sluch, M.I., 2007. Red light emission from hybrid organic/inorganic quantum dot AC light emitting displays. Displays 28 (2), 92–96.

Ugarte, I., Castello, I., Palomares, E., Pacios, R., 2012. Quantum dots as a light indicator for emitting diodes and biological coding. In: Al-Ahmadi, A. (Ed.), Quantum Dots—A Variety of New Applications. IntechOpen. Available from: https://www.intechopen.com/chapters/34816.

Vahabzad, F., Rostami, A., Dolatyari, M., Rostami, G., Amiri, I.S., 2019. Solution-processed QD-LEDs in visible range: modulation bandwith enhancement. Phys. B 574. Available from: https://doi.org/10.1016/j.physb.2019.411667.

Vasilopoulou, M., Fakharuddin, A., Garcia de Arquer, F.P., Georgiadou, D.G., Kim, H., Gao, F., et al., 2021. Advances in solution-processed near-infrared light-emitting diodes. Nat. Photon. 15, 656–669.

Viršilė, A., Olle, M., Duchovskis, P., 2017. LED lighting in horticulture. In: Gupta, S.D. (Ed.), Light Emitting Diodes for Agriculture: Smart Lighting. Springer Nature Singapore, pp. 113–147. Available from: http://doi.org/10.1007/978-981-10-5807-3_7.

Wan, R., Li, G., Gao, X., Liu, Z., Li, J., Xiaoyan, Y., et al., 2021. Nanohole array structured GaN-based white LEDs with improved modulation bandwidth via plasmon resonance and non-radiative energy transfer. Photon. Res. 9 (7), 1213–1217.

Wang, L., Lin, J., Hu, Y., Guo, X., Lv, Y., Tang, Z., et al., 2017. Blue quantum dot light-emitting diodes with high electroluminescent efficiency. ACS Appl. Mater. Interfaces 9 (44), 38755–38760.

Wang, L., Wang, L., Yu, J., Hao, Z., Luo, Y., Sun, C., et al., 2018. Abnormal Stranski–Krastanov mode growth of green InGaN quantum dots: morphology, optical properties, and applications in light-emitting devices. ACS Appl. Mater. Interfaces 11 (1), 1228–1238.

Wang, Y.T., Liu, C.W., Chen, P.Y., Wu, R.N., Ni, C.C., Cai, C.J., et al., 2019. Color conversion efficiency enhancement of colloidal quantum dot through its linkage with synthesized metal nanoparticle on a blue light-emitting diode. Opt. Lett. 44 (23), 5691–5694.

Wang, L., Wang, L., Chen, C.J., Chen, K.C., Hao, Z., Luo, Y., et al., 2021a. Green InGaN quantum dots breaking through efficiency and bandwidth bottlenecks of micro–LEDs. Laser Photonics Rev. 15 (5). Available from: https://doi.org/10.1002/lpor.202000406.

Wang, T., Zhang, C., Zhang, H., Zhu, H., 2021b. CRISPR/Cas9-mediated gene editing revolutionizes the improvement of horticulture food crops. J. Agric. Food Chem. 69 (45), 13260–13269.

Wei, Z., Zhang, L., Wang, L., Chen, C.-J., Pepe, A., Liu, X., et al., 2020a. 2 Gbps/3 m air-underwater optical wireless communication based on a single-layer quantum dot blue micro-LED. Opt. Lett. 45 (9), 2616–2619.

Wei, Z., Zhang, L., Wang, L., Chen, C. J., Pepe, A., Liu, X., et al., 2020b. High-speed visible light communication system based on a packaged single layer quantum dot blue micro-LED with 4-Gbps QAM-OFDM. Optical Fiber Communications Conference and Exhibition, 1–3, doi: 10.1364/OFC.2020.M3I.7.

Won, W.S., Tran, L.G., Park, W.T., Kim, K.K., Shin, C.S., Kim, N., et al., 2018. UV-LEDs for disinfection and bio-sensing applications. Int. J. Precis. Eng. Manuf. 19, 1901–1915.

Wong, M.S., Nakamura, S., Den Baars, S.P., 2019. Review-progress in high performances III – nitride micro-light-emitting diodes. ECS J. Solid State Sci. Technol. 9 (1). Available from: https://doi.org/10.1149/2.0302001jss.

Wu, F., Zhang, D., Shang, S., Zhu, Y., Zhuang, S., Xu, J., 2012. Developing quantum dot phosphor-based light-emitting diodes for aviation lighting applications. J. Nanomater. 2012. Available from: https://doi.org/10.1155/2012/629157.

Wu, T., Sher, C.-W., Lin, Y., Lee, C.-F., Liang, S., Lu, Y., et al., 2018. Mini-LED and micro-LED: promising candidates for the next generation display technology. Appl. Sci. 8 (9). Available from: https://doi.org/10.3390/app8091557.

Wu, Y., Ma, J., Su, P., Zhang, L., Xia, B., 2020. Full-color realization of micro-led displays. Nanomaterials 10 (12). Available from: https://doi.org/10.3390/nano10122482.

Xiao, X., Tang, H., Zhang, T., Chen, W., Chen, W., Wu, D., et al., 2016. Improving the modulation bandwidth of LED by CdSe/ZnS quantum dots for visible light communication. Opt. Express 24 (19), 21577–21586.

Xie, Y., Geng, X., Gao, J., Shi, W., Zhou, Z., Wang, H., et al., 2021. Synthesis of carbon dots@ $Mg(OH)_2$ solid-state composites with blue, red emitting for horticultural application. J. Alloys Comp. 873. Available from: https://doi.org/10.1016/j.jallcom.2021.159663.

Yang, X., Xu, R., Bao, D., Li, B., 2014a. Gold nanorod-enhanced light emission in quantum-dot-doped polymer nanofibers. ACS Appl. Mater. Interfaces 6 (15), 11846–11850.

Yang, W., Li, J., Zhang, Y., Huang, P.K., Lu, T.-C., Kuo, H.-C., et al., 2014b. High density GaN/AlN quantum dots for deep UV LED with high quantum efficiency and temperature stability. Sci. Rep. 4. Available from: https://doi.org/10.1038/srep05166.

Yang, S.J., Oh, J.H., Kim, S., Yang, H., Do, Y.R., 2015. Realization of InP/ZnS quantum dots for green, amber and red down-converted LEDs and their color-tunable, four-package white LEDs. J. Mater. Chem. C 3 (15), 3582–3591.

Yang, Z., Gao, M., Wu, W., Yang, X., Sun, X.W., Zhang, J., et al., 2019a. Recent advances in quantum dot-based light-emitting devices: challenges and possible solutions. Mater. Today 24, 69–93.

Yang, X., Lan, X.-Y., Liu, Y.-S., Yang, H.-Y., Li, Y., Zheng, S.-W., et al., 2019b. Highly stable white light-emitting diodes based on quantum dots dispersed into the backlight lens for display backlight. IEEE Photon. J. 11 (3). Available from: https://doi.org/10.1109/JPHOT.2019.2916084.

Yang, W., Gao, F., Qiu, Y., Liu, W., Xu, H., Yang, L., et al., 2019c. $CsPbBr_3$-Quantum–dots/Polystyrene@ silica hybrid microsphere structures with significantly improved stability for white LEDs. Adv. Optical Mater. 7 (13). Available from: https://doi.org/10.1002/adom.201900546.

Yang, H., Zhou, M., Tang, H., Sun, M., Liu, P., Liu, Y., et al., 2020. Enhanced light emission of quantum dot films by scattering of poly (zinc methacrylate) coating CdZnSeS/ZnS quantum dots and high refractive index $BaTiO_3$ nanoparticles. RSC Adv. 10 (53), 31705–31710.

Yanykin, D.V., Burmistrov, D.E., Simakin, A.V., Ermakova, J.A., Gudkov, S.V., 2022. Effect of up-converting luminescent nanoparticles with increased quantum yield incorporated into the

fluoropolymer matrix on solanum lycopersicum growth. Agronomy 12 (1). Available from: https://doi.org/10.3390/agronomy12010108.

Ye, Z.T., Cheng, Y.H., Liu, K.H., Yang, K.S., 2021. Mini-LEDs with diffuse reflection cavity arrays and quantum dot film for thin, large-area, high-luminance flat light source. Nanomaterial 11 (9). Available from: https://doi.org/10.3390/nano11092395.

Yin, L., Zhou, J., Li, W., Zhang, J., Wang, L., 2019. Yellow fluorescent graphene quantum dots as a phosphor for white tunable light-emitting diodes. RSC Adv. 9 (16), 9301–9307.

Yoon, H.C., Oh, J.H., Ko, M., Yoo, H., Do, Y.R., 2015. Synthesis and characterization of green Zn–Ag–In–S and red Zn–Cu–In–S quantum dots for ultrahigh color quality of down-converted white LEDs. ACS Appl. Mater. Interfaces 7 (13), 7342–7350.

Yu, T.-C., Huang, W.-T., Lee, W.-B., Chow, C.-W., Chang, S.-W., Kuo, H.-C., 2021. Visible light communications system technology review: devices architectures and applications. Crystals 11 (9). Available from: https://doi.org/10.3390/cryst11091098.

Yuan, F., Wang, Z., Li, X., Li, Y., Tan, Z.A., Fan, L., et al., 2017. Bright multicolor bandgap fluorescent carbon quantum dots for electroluminescent light-Emitting diodes. Adv. Mater. 29 (3). Available from: https://doi.org/10.1002/adma.201604436.

Yulin, H., Weisher, C., Hsieh, D.H., Chen, X.Y., Chen, H.M.P., Chen, T.M., et al., 2017. Optical cross-talk reduction in a quantum dot-based full-color micro-light-emitting diode display by a lithographic-fabricated photoresist mold. Photon. Res. 5 (5), 411–416.

Zhang, M., Wang, M., Yang, Z., Li, J., Qiu, H., 2018a. Preparation of all-inorganic perovskite quantum dots-polymer composite for white LEDs application. J. Alloys Compd. 748, 537–545.

Zhang, H., Chen, S., Sun, X.W., 2018b. Efficient red/green/blue tandem quantum-dot light-emitting diodes with external quantum efficiency exceeding 21%. ACS Nano 12 (1), 697–704.

Zhang, Z., Shen, L., Zhang, H., Ding, L., Shao, G., Liang, X., et al., 2019. Novel red-emitting $CsPb_{1-x}Ti_xI_3$perovskite QDs@glasses with ambient stability for high efficiency white LEDs and plant growth LEDs. Chem. Eng. J. 378. Available from: https://doi.org/10.1016/j.cej.2019.122125.

Zhang, H., Su, Q., Chen, S., 2020. Quantum-dot and organic hybrid tandem light-emitting diodes with multi-functionality of full-color-tunability and white-light-emission. Nature Commun. 11 (1). Available from: https://doi.org/10.1038/s41467-020-16659-x.

Zhang, L., Sun, C., He, T., Jiang, Y., Wei, J., Huang, Y., et al., 2021a. High-performance quasi − 2D perovskite light − emitting diodes: from materials to devices. Light Sci. Appl. 10. Available from: https://doi.org/10.1038/s41377-021-00501-0.

Zhang, D., Chao, D., Yu, C., Zhu, Q., Zhou, S., Tian, L., et al., 2021b. One-step green solvothermal synthesis of full-color carbon quantum dots based on a doping strategy. J. Phys. Chem. Lett. 12 (37), 8939–8946.

Zheng, Y., Zhu, X., 2020. Recent progress in emerging near-infrared emitting materials for light-emitting diode applications. Org. Mater. 02 (04), 253–281.

Zheng, J., Xie, Y., Wei, Y., Yang, Y., Liu, X., Chen, Y., et al., 2020. An efficient synthesis and photoelectric properties of green carbon quantum dots with high fluorescent quantum yield. Nanomaterial 10 (1). Available from: https://doi.org/10.3390/nano10010082.

Zhou, D., Wang, Y., Tian, P., Jing, P., Sun, M., Chen, X., et al., 2018. Microwave-assisted heating method toward multicolor quantum dot-based phosphors with much improved luminescence. ACS Appl. Mater. Interfaces 10 (32), 27160–27170.

Zhou, Z., Wang, X., Yi, X., Ming, H., Ma, Z., Peng, M., 2021. Rechargeable and sunlight-activated $Sr_3Y_2Ge_3O_{12}$: Bi^{3+} UV–Visible-NIR persistent luminescence material for night-vision signage and optical information storage. Chem. Eng. J. 421. Available from: https://doi.org/10.1016/j.cej.2020.127820.

Zhu, J., Yang, X., Zhu, Y., Wang, Y., Cai, J., Shen, J., et al., 2017. Room-temperature synthesis of Mn-doped cesium lead halide quantum dots with high Mn substitution ratio. J. Phys. Chem. Lett. 8 (17), 4167−4171.

Zhuang, Z., Iida, D., Velazquez-Rizo, M., Ohkawa, K., 2021. 630-nm red InGaN micro-light-emitting diodes ($< 20\ \mu m \times 20\ \mu m$) exceeding 1 mW/mm2 for full-color micro-displays. Photon. Res. 9 (9), 1796−1802.

Chapter 11

Application of quantum dots in biomedical and biotechnological fields

Anca Armăşelu[1] **and Priyanka Jhalora**[2]

[1]*Department of Electrical Engineering and Applied Physics, Faculty of Electrical Engineering and Computer Science, Transilvania University of Brasov, Brasov, Romania,* [2]*Department of Chemistry, PAHER University, Udaipur, Rajasthan, India*

11.1 Introduction

Owing to their unique size-dependent features, fluorescent nanoparticles (NPs) or quantum dots (QDs) have attracted the attention of scientists all over the globe in the last few decades. There is an increasing concern in developing environment-friendly procedures to synthesize these NPs because they enhance biocompatibility and avoid the production of toxic by-products (Plaza et al., 2016).

Due to the advent of nanobiotechnology, some modern biological synthesis works of nanomaterials (NMs) have succeeded in implementing "Green chemistry" strategies, which are globally sustainable and economically viable (Abdel-Salam et al., 2020). The green revolution and scientific developments in the realm of biological sciences, agricultural biotechnology, food technology, and nanotechnology follow the route of a novel scientific perceptiveness (Palit, 2020).

Some substantial studies have explained the conception or synthesis of materials with nanoscale accuracy (Ameta and Ameta, 2016a,b) using material science, which is nanotechnology (Pandey et al., 2015; Ameta and Ameta, 2016c). These studies have described the diverse aspects of synthesis of NPs, characterization, and their crucial applications, focusing on the biogenic synthesis of NPs and their use (Ingale and Chaudhari, 2013; Bhatt et al., 2020a).

QDs have been presented as the central notion of nanoscience and nanotechnology since their inception and remain an active and intense domain of exploration in applied nanomaterial research (Damian et al., 2011; Ameta et al., 2014;

Quantum Dots. DOI: https://doi.org/10.1016/B978-0-12-824153-0.00011-2

Benjamin et al., 2014; Solanki et al., 2018; Ameta et al., 2019a,b; Armăşelu, 2019; Liu et al., 2020a; Ameta et al., 2020). QDs possess numerous distinctive constitutional, physicochemical, and photochemical characteristics that make them encouraging candidates in the areas of solar cells, laser, memory, light-emitting diodes (LEDs) (Armăşelu, 2017), photovoltaics, photodetectors, photocatalysts (Ameta et al., 2019c; Bhatt et al., 2019a), quantum computers (Ameta et al., 2019c), wastewater treatment (Bhatt et al., 2019b,c; Jat et al., 2019), and bioimaging applications (Ardelean et al., 2011; Armăşelu et al., 2011a,b; Damian et al., 2010).

The QDs show unique optical properties, which depend on their size, shape, and surface chemistry, and in spite of the fact that research on QDs is at a relatively early phase, their high biocompatibility and reduced cytotoxicity have already been established in vitro and in vivo, increasing the interest in this type of NM as compared to others (Perini et al., 2020).

QDs and their composites are modern and notable structures, which present unique and significant properties. Here, the basic properties of QDs, some key aspects related to the synthesis techniques of QDs, and the latest advances in the field of QDs applications in sensing, bioimaging, biolabeling, and targeted drug delivery have been presented. This work also provides some toxicological characteristics of QDs and their composites.

11.2 Biolabeling and bioimaging

Biolabeling is nothing but tracking individual cells using any material. QDs have been used for labeling of cells. It is all due to the florescence of QDs. This can pass to daughter cells upon cell division with florescence labels in such cases. These have also being used before surgery by labeling lymph nodes with florescence. Bioimaging refers to any imaging technique in the field of biomedical and biotechnology. Here, bioluminescence is used in the diagnosis of some diseases. One can visualize different infections, localizing cancer growth by creating bioimages of different internal organs and their functions.

Wolcott et al. (2006) reported a simple aqueous synthesis of silica-capped, highly fluorescent CdTe QDs. These CdTe QDs are quite useful as the emission can be tuned to the near-infrared, where tissue absorption is at the minimum. Leakage of toxic Cd^{2+} can be prevented by a silica shell. These silica shells help in increasing photostability in tris-borate-ethylenediaminetetraacetate and phosphate-buffered saline buffers. They used poly(ethylene glycol) and thiol-terminated biolinkers to functionalize silica-capped QDs to improve their biocompatibility. Conjugation specificity and bioactivity of as-synthesized thiolated QDs was confirmed by streptavidin − maleimide and biotinylated polystyrene microbeads. It was reported that these functionalized, silica-capped QDs are ideal labels, safe, robust, easily synthesized, and readily conjugated to biomolecules. They find a number of applications in biolabeling and imaging.

Li et al. (2007) synthesized aqueous CdS QDs in a direct and environment-friendly manner at room temperature. They reported the feasibility of aqueous CdS QDs as an imaging tool with *Salmonella typhimurium* cells, when 3-mercaptopropionic acid (MPA) was used as the capping molecule. The QDs exhibited stronger emission at higher pH and MPA/Cd ratio of 2. It was claimed that aqueous CdS QDs displayed a lifetime of 12 h under UV light with an excellent stability. An ease of processing and good PL properties of these aqueous CdS QDs provided a low-cost and practical approach for single-target imaging application.

Erogbogbo et al. (2008) prepared highly stable aqueous suspensions of Si QDs. It was found that the optical properties of Si nanocrystals are retained. These micelle-encapsulated Si QDs can be used for detecting pancreatic cancer cells. These silicon QDs may prove to be a significant optical probe in biomedical diagnostics.

Biologically compatible and water-soluble CdSe QDs were synthesized in aqueous medium by Liu et al. (2009) using L-cysteine as the capping agent. It was revealed that molar ratio of Se/Cd and the reaction time are deciding factors for the size distribution of CdSe/L-cysteine QDs. The fluorescence intensity of bovine serum albumin (BSA) was largely quenched with the addition of QDs, but it slightly enhanced initially and then quenched on addition of BSA to solution of QDs. They suggested that CdSe/L-cysteine QDs can be used as a probe for labeling bacterial cells and biological molecules.

Allen et al. (2010) reported the synthesis of InAs QDs with a ZnCdS shell. These can be used for biological imaging as they show stable and bright emission in the near-infrared (NIR, 700−900 nm) region. They opined that these NIR QDs can image tumor vasculature in vivo at deeper penetration depths with higher contrast than visible emitting CdSe(CdS) QDs. Tan et al. (2013) prepared nanoscaled light-triggered nitric oxide (NO) delivery consisting of chitosan (CS)-based *S*-nitrosothiols (SNO) and encapsulated silver sulfide QDs (Ag_2S QDs) and used for vehicles NIR fluorescence imaging. They used ethylenediaminetetraacetic acid (EDTA) to conjugate water-soluble Ag_2S QDs with the CS-SNO. They performed cell imaging. It was demonstrated that Ag_2S-CS-SNO nanospheres could emit observable NIR fluorescence and also release NO in living cells.

Uniform molybdenum disulfide (MoS_2)/tungsten disulfide (WS_2) QDs were prepared by Xu et al. (2015) via a combination of sonication and solvothermal treatment at a mild temperature. It was reported that as-prepared QDs have monolayer thickness (average size of about 3 nm). A good cell permeability, strong fluorescence, and low cytotoxicity make these QDs quite promising and biocompatible probes for in vitro imaging.

Justin et al. (2016) synthesized reduced graphene oxide (GO)−iron oxide QDs with photoluminescent and superparamagnetic properties. They used a green, hydrothermal method that reduced and shattered graphene nanosheets simultaneously to form QDs. A drug could be loaded onto the surface of

these QDs, with a loading ratio of drug to QD as 0.31:1. These have a potential to be used in cancer photothermal therapy. A suspension of QDs ($100\ \mu g\ mL^{-1}$) can be used for photothermal ablation of HeLa cells in vitro in presence of near infrared irradiation.

Nitrogen and phosphorus functionalized Ti_3C_2 MXene-based QDs (N,P-MQDs) were prepared via a top−bottom hydrothermal method by Guan et al. (2019). It exhibited pH resistance capacities and excellent photostability. These N,P-MQDs are highly sensitive toward Cu^{2+} ions and may be used for label-free fluorescence platform for Cu^{2+} detection. This is a low cost, sensitive, and environment-friendly method.

Xue et al. (2019) synthesized lignin hybridized CQDs (L-CQDs) via hydrothermal route. They used different molar ratios of ethanediamine and citric acid. As-obtained L-CQDs with almost spherical morphology were found to be <10 nm (diameter). It was reported that L-CQDs exhibited excitation-dependent photoluminescence (PL) behavior and maximum emission of L-CQDs exhibited a red-shift (longer wavelength) with a decrease in intensity on increasing excitation wavelengths. As-prepared L-CQDs have low good cellular biocompatibility and cytotoxicity indicating that there is a potential of these L-CQDs for bioimaging applications.

Qu et al. (2020) reported synthesis of bifunctional ibuprofen-based carbon QDs (ICQDs) via a simple one-step microwave-assisted method. As-prepared ICQDs exhibited low toxicity, high stability, good biocompatibility, and negligible cytotoxicity in water. It was reported that as-produced ICQDs had a decent imaging ability and excellent antiinflammatory effects in vivo, simultaneously. Shahid et al. (2020) reported hydrothermal synthesis of biocompatible, polyethyleneimine (PEI) surface passivated carbon dots (CDP) using mint leaves as a green source. The biolabeling potentials of nonpassivated C-dots and CDP was evaluated in the breast cancer (MCF-7) cells, when cytotoxicity was found to be concentration dependent. It was reported that C-dots synthesized from a herbal source (mint) can be used for different biolabeling applications as well as antioxidant activity.

11.3 Targeted drug delivery

Nanotechnology has the potential to develop quantitative and sensitive methods to diagnose and detect cancer. Semiconductor QDs are NPs that have intense and stable fluorescence, and these could help in the detection of various cancer biomarkers in blood assays, cancer tissue biopsies, and also as contrast agents for medical imaging. QDs are promising materials to expand to in vitro analysis, which can be extended to cellular, tissue, and whole-body multiplexed cancer biomarker imaging.

Detecting cancer at an early stage is a current challenge in the treatment of cancer. This will be supported by targeted drug delivery in and around tumors at concentrations, which decreases the growth rate of the tumors and

continues to be the primary challenge in the treatment of cancer. In most of the cases, the malignancy of tumors is only detected when it has reached an advanced stage and then chemotherapeutic drugs will be increasingly toxic to healthy cells. A targeting drug delivery system has a moiety that can recognize a tumor with a drug-loaded vesicle. Detection systems of malignant tumors involve tissue biopsy and magnetic resonance imaging (MRI), where a single system is needed that is capable of targeting drug delivery as well as imaging the delivery process, simultaneously. Here, the integration of biomaterials and semiconductor QDs can be useful for addressing these problems of cancer therapy.

Misra (2008) used biodegradable chitosan (*N*-acetyglucosamine) for targeted drug delivery to tumors and QDs noninvasive imaging. It was reported that drug-loaded chitosan-encapsulated ZnO:Mn^{2+} QDs provided a potential platform for drug delivery to targeted tumors and this delivery process was documented, simultaneously. Core−shell structured multifunctional nanocarriers (NCs) of ZnO QDs-conjugated gold NPs (Au NPs) were synthesized by Chen et al. (2013). It was indicated that camptothecin (CPT) release from these NCs was much higher at pH 7.4 than 5.3. It was reported that both NCs; and CPT-loaded NCs provided high anticancer activity against Hela cells.

Wang et al. (2013a) prepared GQDs with strongly green-PL, which were surface-passivated by polyethylene glycol (GQDs-PEG). It was observed that the PL quantum yield of as-prepared GQDs-PEG was around 18.8% with 400 nm excitation. They reported that surface-passivated PEG on GQDs can load the drug by hydrogen bonding apart from enhancing PL intensity. The GQDs-PEG have high specific surface area, which provide these higher loading capabilities (2.5 mg mg^{-1}) to carry the drug. As-fabricated GQDs-PEG were suitable for cell imaging and as drug carrier.

A novel QDs-based multifunctional nanovehicle (DOX-QD-PEG-FA) was designed for targeted drug delivery, fluorescent imaging, tracking, and cancer therapy, in which the GSH−CdTe QDs play a key role in imaging and drug delivery. The antineoplastic drug doxorubicin hydrochloride (DOX) was loaded on the GSH−CdTe QDs by Chen et al. (2014) via a condensation reaction. A PEG shell was introduced to wrap these DOX-QDs. The NPs were then decorated with folic acid (FA) to actively target particularly cancer cells and prevent the nanovehicles from being used up by normal cells allowing them to target HeLa cells that express the FA receptor. In vitro studies revealed that this multifunctional nanovehicle can deliver DOX specifically to the targeted cancer cells, and on reaching the tumor cells the FA on the DOX-QD-PEG surface increased the drug concentration so as to achieve higher curative effect. It was reported that this multifunctional DOX-QD-PEG-FA system exhibited great promise for tumor imaging, targeting, and therapy.

Wu et al. (2014) prepared dual-functional NMs consisting of QDs and an anticancer drug methotrexate (MTX). Hydrophilic $AgInS_2$/ZnS QDs were

obtained by ultrasonication by introducing the amphiphilic polymer, poly (maleic anhydride-alt-1-octadecene) (PMAO). Then MTX was covalently coupled to the surface of the $AgInS_2$/ZnS QDs by carbodiimide chemistry. It was indicated that these hydrophilic PMAO-coated $AgInS_2$/ZnS QDs exhibited negligible cytotoxicity, but $AgInS_2$/ZnS QDs conjugated with MTX were taken up effectively by human cervical (HeLa) cancer cells. It was suggested that $AgInS_2$/ZnS QDs conjugated with MTX may be a promising candidate for cancer therapeutics and diagnosis in future.

Samantara et al. (2016) developed a method to synthesize carbon QDs from Good's buffer. As-synthesized CQDs emitted a bright greenish blue colored fluorescence on exposure to UV irradiation (365 nm). This bright fluorescence of CQDs makes them useful probes for cellular imaging. More than 95% survival rate was found when H357 (human oral squamous carcinoma) and HEK293 (human embryonic kidney) cells were treated with these CQDs. The low cytotoxicity of Good's buffer-derived CQDs opens the door to biomedical applications. They easily loaded an anticancer drug DOX on as-prepared CQDs. They also explored delivery efficiency to the target cells via in vitro treatment of cancerous cells. CQDs-supported DOX exhibited a higher killing rate as compared to only DOX, which may be due to easy internalization and effective pH-triggered release inside the cells.

Rai et al. (2017) used lignosulfonate lignin as a carbon source for the synthesis of water-soluble reduced fluorescent carbon dots (r-FCDs). Then these r-FCDs were employed for bioimaging applications and as a curcumin nanocarrier. As-prepared r-FCDs were obtained under microwave irradiation after reduction with $NaBH_4$. The average diameter of r-FCDs was found to be 4.9 nm. These were water dispersible with strong photostability. It was reported that r-FCDs were efficiently taken up by cancerous cells (SW480 and A549) and illuminated the whole cell with a clear distinction between cytoplasm and nucleus. It was revealed that as-prepared r-FCDs can be used as a promising probe for diagnosis and treatment of cancer.

A novel drug delivery system was synthesized by Dong et al. (2018), which was based on arginine−glycine−aspartic acid (RGD)-conjugated GQDs. Later, it was used to load the antitumor drug, DOX for monitoring drug delivery even in the absence of external dyes. It was reported that the release of DOX was strongly pH dependent, which involves hydrogen-bonding interaction between GQDs and DOX as compared to free DOX. It was observed that DOX-GQDs-RGD conjugates exhibited substantial cytotoxicity to U251 glioma cells within a wide range of DOX concentrations. This enhancement combined with efficient nuclear delivery improved the cytotoxicity of the drug DOX on application of GQDs.

A pH responsive nanodrug delivery system was reported by Wang et al. (2018). It was based on ZnO QDs for controlled release of drugs. They introduced poly(2-(dimethylamino) ethyl methacrylate) (PDMAEMA) and zwitterionic poly(carboxybetaine methacrylate) (PCBMA) for modification of

ZnO QDs. These helped in increasing blood circulation time, water stability, and also promoted endocytosis. The DOX (anticancer drug) was successfully loaded on ZnO@P(CBMA-*co*-DMAEMA) with a 24.6% drug loading. As-prepared ZnO@P(CBMA-*co*-DMAEMA) loaded with DOX could achieve lysosomal acid degradation and release DOX after endocytosis by tumor cells, which resulted in a synergistic treatment of cancer by an anticancer effect of Zn^{2+} and DOX, both.

Flak et al. (2018) have studied the preparation of GQDs−mesoporous silica NPs (MSNs) (GQDs-MSNs) nanocomposite as an efficacious intracellular drug delivery system and as a fluorescent factor for optical imaging. GQDs-MSNs nanocomposite NPs composed of GQDs and MSNs were presented as a proficient DOX delivery agent and nontoxic nanocomposite. It has been reported that the effectiveness of prepared GQDs-MSMs nanocomposite NPs for the drug delivery and release next to the bioimaging was analyzed for the case of HeLa cancer cells using a confocal laser scanning microscope and the transmission electron microscopy imaging technique.

Qian et al. (2018) synthesized GQDs hydrothermally and then encapsulated them with supramolecular β-cyclodextrin (β-CD) as a drug delivery system. Two drugs were selected, ranibizumab (Ran) and bevacizumab (Bev), which displayed an initial burst delivery percentage of 52.2% ± 2.6% and 55.7% ± 1.6%, respectively, within the first 15 min. This release from the β-CD encapsulated GQDs reached in a sustained manner 94.2% (Ran) and 93.1% (Bev) of loaded drug molecules after an hour. The biocompatibility of these carriers was evaluated qualitatively as well as quantitatively with the mouse Fibroblast L929 cell line. It was revealed that samples are nontoxic and highly compatible to the cells with >90% cell viability after 5 days of cell culture. The observed results indicate that developed NCs were suitable for the drug delivery system in the AMD.

The fact that graphene (G) is very hydrophobic, whereas GO is decorated by oxygen−containing hydrophilic group, permits both physical and chemical binding of drugs to the surface of G/GO for drug delivery uses (Zhang et al., 2017; Tadyszak et al., 2018; Wychowaniec et al., 2018). The GQDs, which are the most proficient carbon-based nanostructures, have a notable function in biological works (Khosravanian et al., 2021). It has been observed that owing to their small dimension, GQDs present a better perspective in biomedical applications than G or GO and when compared with graphene sheets, GQDs show improved biocompatibility and low toxicity, as promising materials used for the delivery of biologically active loads into living systems (Sangam et al., 2018; Mondal et al., 2019; Fasbender et al., 2019). In recent years, many researchers have shown that GQDs are very encouraging substrates for drug delivery systems. (Li et al., 2019a; Liang et al., 2019; Wang et al., 2019b; Zhao et al., 2020; Jahdaly et al., 2021).

Thovhogi et al. (2018) investigated the use of peptide-functionalized QDs for the imaging of prohibiting (PHB)-expressing cells in vitro and in diet-induced obese rats, which could potentially be used as NCs of antiobesity

drugs, dual targeted drug delivery, and molecular imaging of adipose tissues in obese patients in real time. Abdelhamid et al. (2019) loaded a natural cytotoxic agent (sesamol) onto cadmium sulfide QDs modified chitosan (CTS) to improve its activity. It was found that sesamol-CdS@CTS was more effective against cancer cells as compared to sesamol alone. It was revealed that half maximal inhibitory concentration values (IC_{50}) of CdS@CTS, sesamol, and sesamol-CdS@CTS were 1730 ± 54, 495 ± 16.4, and 117 ± 3.2 $\mu g\ mL^{-1}$, respectively, which indicated that CdS@CTS exhibited high loading efficiency, and can be used for drug delivery.

Triple negative breast cancer (TNBC) is the most fatal type of breast cancer. No targeted chemotherapy is available for the treatment of TNBC because of the absence of progesterone receptor, estrogen receptor, and human epidermal growth factor receptor-2. Ghosh et al. (2019) developed a targeted nonviral vector, which can diagnose TNBC and deliver the gene of interest efficiently. They synthesized carbon QDs from sweet lemon peel and then conjugated it with various generation of polyamidoamine (PAMAM) dendrimers to obtain CD-PAMAM conjugates (CDPs). The RGDS peptide was then further conjugated to CDP to target $\alpha v\beta 3$ integrin. Cellular cytotoxicity, DNA complexation assay, DNase I assay, hemolysis assay, cellular uptake, and in vitro transfection supported the fact that CDP3 is a promising gene carrier system for TNBC gene therapy. The CDP3 also exhibited selective quenching of fluorescence in the presence of Cu(II) with high efficiency (93%). The Cu(II) ion concentration remains upregulated in TNBC. It was predicted that CDP3 could be a promising theranostic tool for the treatment of TNBC.

A multifunctional $(Fe_3O_4/nGO)@mSiO_2/GQDs$ drug transporter, which consists of magnetic core Fe_3O_4, microwave−absorbing nanographene oxide, fluorescent GQDs, and intermediate barrier layer (mesoporous silica), used for loading and microwave-controlled release of an etoposide (VP16) as the anticancer drug, was developed by Wang et al. (2020). The loading rate of VP16 was found to be as high as 68%, and the release rate was observed to be 87% within 280 min.

Alarfaj et al. (2020) synthesized carbon QDs conjugated zinc oxide nanocomposite and used it as highly sensitive fluorescence immunosensing solution for fast determination of CYFRA 21−1 antigen in human serum. They used a hydrothermal method to prepare these QDs using *Citrus limon* pericarp. As-prepared carbon QDs were used to synthesize carbon QDs−zinc oxide nanocomposite by the reduction and stabilization of zinc acetate. As-fabricated immunosensing system based on this nanocomposite (CQDs-ZnO) provided its potential application in rapid diagnoses of lung cancer by detecting CYFRA 21−1 in human serum.

Large doses of anticancer drugs entering cancer cell nuclei are found to be effective for killing cancer cells and increasing chemotherapeutic effectiveness. Red-emitting carbon QDs were reported by Su et al. (2020) that can not only enter into nuclei of cancer cells but also stem cells of cancer.

The DOX was loaded (30 μg mL^{-1}) on the surfaces of carbon QDs. It was observed that average cell viability of HeLa cells was decreased to only 21%, whereas it was decreased to 50% for free DOX. Thus DOX-loaded carbon QDs shows a good therapeutic effect in elimination of cancer stem cells. This has great potential for carbon quantum-dot-based anticancer drug carriers to effectively eradicate cancers.

Nasrollahi et al. (2020) encapsulated GQDs in ferritin protein nanocages to design multifunctional nanoplatforms for cancer therapy and multimodal imaging. Encapsulation of ultrasmall GQDs is expected to reduce their quick excretion from the body and increase their bioimaging efficiency. They encapsulated GQDs and iron inside the core of AfFtn-AA (it is an engineered ferritin nanocage derived from the archaeon *Archaeoglobus fulgidus*). It was achieved through an iron-mediated, self-assembly of ferritin dimers, which afforded GQD−iron complex in the ferritin nanocages, (GQDs/Fe)AA. This (GQDs/Fe)AA showed strong fluorescence at low pH values and high relaxivities in MRI. These were used as a drug nanocarrier and imaging agent. These exhibited negligible cytotoxicity on the MDA-MB-231 cells and a high loading capacity (35%) of DOX. The (GQDs/Fe)AA can find potential applications as MRI agent, drug nanocarrier, and cancer diagnosis and therapy.

Traceable and pH-responsive DDS (MoS_2-PEG-DOX) based on MoS_2 QDs (MoS_2 QDs) was fabricated by Liu et al. (2020a) by covalently grafting MoS_2 QDs with diamine-terminated oligomeric PEG. Then a fluorescent antineoplastic anthracycline drug, DOX was loaded onto it. It was found that MoS_2-PEG-DOX nanoassembly can be effectively taken up by U251 cells, and as a result, enhanced DOX release is then triggered by intracellular acid condition. It reduces or diminishes the undesired side effects derived by the incorporation of DOX into healthy cells. It was concluded that MoS_2-PEG-DOX has a potential for high treatment efficacy in future therapy with minimal side effects.

Felix et al. (2021) decorated the GQDs through carbodiimide crosslinking reaction, where the imatinib molecule, projected to obstruct tyronise kinase, was used to cure leukemia. It has been shown that the integration of the imatinib on the surface of the GQDs did not modify the morphology and the properties of the NPs and that this type of the drug nanoplatform could destroy cancer cells inducing apoptosis. Han et al. (2021) constructed CQDs-based drug delivery system (Arg-Ag@Cu). They used l-arginine as precursor with duplex metal codoping (Cu and Ag) for DOX-loading/releasing and tumor theranostics. It was observed that Ag-doping increased PL intensity while Cu^{2+} could act as an anchor resulting in adjustable size of CQD for increasing the drug loading capacity. It was revealed that the structure of Arg-Ag@Cu was disrupted due to Cu^{2+} depletion, which supported in situ DOX-releasing. It was also revealed that there were synergistic effects, which suppressed tumor progression and migration with relatively no or minimal side effects.

Liu et al. (2021) presented some GQDs functionalized with polyethyleneimime (PEI) as a new messager RNA (mRNA) delivery system demonstrating that these modified GQDs can be utilized to provide intact and functional mRNA to Huh−7 hepatocarcinoma cells at low quantities and that these functionalized GQDs can be considered as ideal delivery system. Ruzycka-Ayoush et al. (2021) used Ag−In−Zn−S QDs modified with L-cysteine, 11-mercaptoundecanoic acid, and lipoic acid decorated with FA. It was then used as a novel target drug delivery system for targeting DOX to folate receptors on adenocarcinomic human alveolar basal epithelial cells (A549).

It has been shown that GQDs are materials capable of responding to physical stimuli, such as magnetic fields, ultrasound, and light, and this fact permitted the precise control of drug release (Dai et al., 2017; Gu et al., 2019; Liu et al., 2021). Some researchers have reported that small molecule-modified GQDs could be used for simultaneous cellular drug delivery imaging, modifying GQDs with arginine−glycine−aspartic acid (RGD) (Qiu et al., 2015) and FA (Wang et al., 2014), explaining that the antitumor drug DOX-loaded RGD- or FA-modified GQDs could not only transport drugs to target cells, but supervise the cellular operation uptake of the drug in real time without using external dyes (Wang et al., 2017).

11.4 Sensing

It has been established that biotechnology, in combination with nanotechnology, provides the enhanced evolutionary biological components needed to create novel smart sensors and advanced characterization and manufacturing mechanisms to solve environmental and biological problems (Ray et al., 2009; Choi and Montemagno, 2016).

A selective chemiresistive gas sensor for detection of carbon dioxide at room temperature (~25°C) was prepared by Rathi and Pal (2020). It contains ruthenium-decorated tungsten disulfide (Ru@WS_2) QDs as the sensing material. They used a mixed solvent of lithium hydroxide and N-methyl-2-pyrrolidone (NMP) to prepare Ru-decorated WS_2 QDs from the exfoliated WS_2 nanoflakes. The gas sensors were fabricated by spraying the QDs (WS_2 QDs and Ru@WS_2 QDs) on gold interdigitated electrodes, which were then exposed to different concentrations of CO_2 gas in dry air conditions. It was reported that Ru@WS_2 QD-based sensor exhibit superior sensitivity and good selectivity to CO_2 gas as compared to WS_2 QD to isopropanol, acetone, ethanol, methanol and benzene at room temperature. This sensor showed an increase in resistance when it was exposed to CO_2 gas ranging from 500 to 5000 ppm.

Bhatt et al. (2020b) performed some excellent approaches, which present all significant aspects of QDs properties. Such unique properties have been created for successful applications, which comprise photodetectors, photovoltaic devices, photocatalysis, biosensors, chemical sensors, displays, photodynamic therapy,

laser diodes, and so on. Due to their special PL and electrochemical features, GQDs are among the most interesting carbon-based NMs used to fabricate biosensors (Xie et al., 2016).

In accordance with the technique that is applied, GQDs-based sensors can be classified into the following broad groups: PL sensors, chemiluminescence (CL) sensors, and electrochemical (ECL) sensors; these QDs-based sensors and biosensors provide a plethora of opportunities to diagnose an extensive range of diseases and improve therapeutic actions (Henna and Pramod, 2020).

Bhakat et al. (2021) developed a facile method to prepare ZnO QDs into three-dimensional superstructures through surface complexation between zinc ions and phosphate. It was reported that the addition of phosphate to ZnO QD dispersion led to growth of such parahopeite structures along with crystalline assembly of QDs in the colloidal medium. It was revealed that the as-prepared ZnO QD−phosphate crystalline assembly can be successfully applied to fabricate a gas (CO_2) sensor, which exhibited great selectivity and sensitivity toward carbon dioxide gas at room temperature.

11.4.1 Photoluminescence sensors

A new, simple and highly sensitive PL evaluation method for the activity of a protein kinase depending on the selective aggregation of the phosphorylated peptide-GQD conjugates triggered by Zr^{4+} ion coordination was proposed by Wang et al. (2013b). The developed technique has revealed some feasible uses in kinase inhibitor screening. The inhibition of CK2 phosphorylation activity by four various inhibitors was examined in human serum by analyzing the signals from samples incubated with and without any inhibitors. It was revealed that PL intensity was enhanced by improving the efficiency of the inhibitor.

Sun et al. (2013) presented various methods and some future prospects for the progress of the smart sensing platform based on GQDs, showing that GQDs, which are produced using diverse procedures, can emit PL with different colors and in these GQDs, PL is controlled by numerous parameters, such as size, shape, excitation wavelength, pH, concentration, surface oxidation degree and surface functionalization.

A precise technique for the preconcentration and the determination of GO in natural river water samples utilizing fluorescent GQDs was studied by Benitez-Martinez et al. (2014). The functioning of the presented GQDs sensor is related to the interaction between GO and GQDs via hydrophobic $\pi-\pi$ stacking of the GO with aromatic network at the GQDs surface; this fact causes a quenching effect of the fluorescence of GQDs, that was used as an investigative indicator for their quantification. The LOD was calculated to be $35\,\mu g \cdot L^{-1}$. It was reported that the precision for a $200\,\mu g \cdot L^{-1}$ concentration of GO was found to be 5.16%.

Benitez-Martinez and Valcárcel (2015) reviewed the principal analytical uses of GQDs, highlighting more details on the progress of various categories of sensors, which are used to detect metal ions, small organic molecules and biomaterials with enhanced sensitivity. They have shown that GQDs are recent materials for designing and tuning sensors (and biosensors) and they focused mostly on the presentation of some important analytical applications in the field of PL-based sensors.

Zor et al. (2015) studied the synthesis and characterization of a new multifunctional composite material, magnetic silica beads/GQDs/molecularly imprinted polypyrrole (mSGP), where mSGP is designed to capture and signal small molecules; thanks to the synergy among chemical, magnetic, and optical attributes that are connected with the molecular printing of tributyltin. It was observed that the studied multifunctional material allowed a fast and highly sensitive scaffold for small molecules detection even in complex media such as seawater without any sample treatment.

All-inorganic cesium lead halide ($CsPbBr_3$) perovskite QDs, as one kind of promising material, have attracted considerable attention in optoelectronic applications. Colloidal $CsPbBr_3$ QDs were synthesized by Chen et al. (2017a) by adjusting the reaction temperatures with tunable PL (493−531 nm). It revealed narrow emission bandwidths of 25 nm. Average diameters of the QDs were calculated and it was found that this could be adjusted from 7.1 to 12.3 nm on increasing temperature from 100°C to 180°C. They also fabricated green LEDs using $CsPbBr_3$ QDs cast on blue LED chips, which have a great potential for applications in the field of lighting technology and display.

Quaternary $Zn_xAgInSe$ QDs were synthesized by Ding et al. (2017) with different Zn/Ag ratios. These were then evaluated as temperature sensors. A correlation between different temperatures and emission intensity, luminescence energy, and full-width at half-maximum of the emission band was observed; where only a small deviation was observed from the actual temperature, indicating that $Zn_xAgInSe$ QDs can be used as temperature sensors with high sensitivity.

Duran et al. (2017) presented a modern, rapid, inexpensive, and acid treatment procedure for the synthesis of copper-modified GQDs. Then this was used for the quantification of penicillamine (PA) in pharmaceutical samples using interaction of the drug with Cu-modified GQDs (Cu−GQDs). It was reported that under the best conditions for interaction, a linear response was remarked (in the concentration range 0.10−7.50 pmol L^{-1} PA) and the viability of the recommended fluorescent sensor has been demonstrated.

The $CsPbBr_3$@Ag hybrid nanocrystals were synthesized by Ye et al. (2017). They treated $CsPbBr_3$ nanocrystals with silver halides (Cl, Br, or I) powders in hexane for this purpose. It was indicated that particle size of Ag NPs varied between 2 and 5 nm and these were nucleated randomly outside these hybrid $CsPbBr_3$ nanocrystals. An enhanced PL intensity of $CsPbBr_3$@Ag hybrid nanocrystals was observed as compared to $CsPbBr_3$ nanocrystals under the light of

400 nm, to achieve an enhanced PL. They optimized $CsPbCl_xBr_{3-x}$@Ag hybrid nanocrystals so that the effect of plasmonic resonance enhancement occupied a significantly advantageous position. It was suggested that as-constructed $CsPbBr_3$@Ag hybrid nanocrystals can find new opportunities for application in optoelectronic devices and LEDs.

Sahub et al. (2018) developed a novel real-time biosensor of GQDs-based enzymatic reaction (GQDs AChE/CHOx) for monitoring the organophosphate (PO) pesticides. It was observed that H_2O_2 created from the active enzymatic reaction of acetylcholinesterase (AChE) and choline oxidase (CHOx) allowed to react with GQDs inducing a "turn-off" PL of GQDs. The limit of detection of this biosensor was calculated to be 0.172 ppm (0.778 μM). The suggested biosensor was successfully applied for the determination of dichlorvos, utilizing a reduced price procedure via a connection with green chemistry approach.

Xu et al. (2018) produced a high PL quantum yield for transition metal carbide (2D) MXene (nitrogen-doped, N-doped Ti_3C_2) QDs. They used Ti_3C_2 and ethylenediamine as a precursor and nitrogen source, respectively. The average size of hydrothermally treated N-doped Ti_3C_2 QDs was 3.4 nm and PLQY of up to 18.7% was observed. As-prepared N-doped Ti_3C_2 QDs were then used as an ultrasensitive detector probe for iron ion (Fe^{3+}) with a limit of detection up to 100 μM. It was also reported that as-developed MXene QDs can find application in biological sensing for detection of H_2O_2 with high sensitivity. These QDs have a lot of applications such as solar cells, electronics, biomedical, optical, photocatalysis, biosensors, white light emission devices, and environmental fields.

Li et al. (2019b) introduced a stoichiometry control over both; core and shell regions of InP/ZnSe/ZnS QDs. As-obtained QDs exhibited PL quantum yield (almost approaching 1), narrow line width, monoexponential decay dynamics and nonblinking at a single-dot level. These quantum-dot LEDs (QLEDs) based on InP/ZnSe/ZnS core/shell/shell QDs are good emitters exhibiting a peak external quantum efficiency (12.2%) and a maximum brightness ($>10\ 000\ cd\ m^{-2}$), which is more than Cd/Pb-free QLEDs. It was revealed that these Cd/Pb-free QDs can prove to be outstanding optical and optoelectronic materials.

11.4.2 Chemiluminescence sensors

The L-cysteine capped CdS QDs were prepared by Hassanzadeh et al. (2017) via a hydrothermal route. It was found that as-prepared CdS QDs show a significant effect on the CL reaction of the rhodamine B (RhB)-cetyltrimethylammonium bromide (CTAB)-$KMnO_4$ system. It was also found that CL emission intensities of these QDs exhibited a change in the presence of methamphetamine (MA) (even in low quantities). It was observed that MA can remarkably increase the intensity of CL system and this improved CL intensity was found to be proportional to MA concentration in the range of

0.25−125 ng mL^{-1} with a limit of detection of 0.086 ng mL^{-1}, which was more than 20 times higher than the FL method. The as-developed CL method was used for accurate determination of MA in real samples (human urine).

The *N*-(Aminobutyl)-*N*-(ethylisoluminol)/(ABEI) functionalized GQDs (ABEI-GQDs) with outstanding CL and FL attributes were synthesized by Gao et al. (2017). They observed that as-synthesized ABEI-GQDs exhibited exceptional CL features, when reacted with H_2O_2 and wavelength−tunable FL emission with increasing excitation wavelength. They built a pesticide−sensing array for pesticide differentiation using their CL and FL properties. It was reported that new CL and FL dual-signal GQDs (ABEI−GQDs) have been developed, which could find more interesting future uses in bioassays and bioimaging.

Khataee et al. (2018) developed a modern and high CL system using the promoting effect of GQDs/bisulfite on rhodamine B(RB)−H_2O_2 CL reaction. It was reported that the existence of sodium dodecyl sulfonate (SDS) and sodium bisulfite resulted in a much improved action of GQDs. It was recalled that the International Agency for Research on Cancer and the Environmental Protection Agency estimated the cancer risk of formaldehyde (HCHO) on human and classified this compound as carcinogenic (Lobo et al., 2015; Khataee et al., 2018). This CL system, which is dependent on the oxidation of rhodamine B, has been shown to be a successful chemosensor for HCHO, noting that HCHO can decrease the developed CL system. It was found that a linear change of the CL response was achieved in HCHO concentration ranges of 0.02−5 and 5−11 μg L^{-1} with a limit of detection and quantification of 6 and 20 ng L^{-1}, respectively.

The captivating contribution of GQDs in introducing sensors is due to the fact that they can be used as a luminescent donor, energy acceptor, or amplification (catalyst) pathway for the system of CL resonance energy transfer (CRET), enhancing the sensitivity of detection (Pang et al., 2018; Chen et al., 2020). Pang et al. (2018) showed that GQDs could notably improve the CL reaction of Ce(IV) with $NaHSO_3$ using energy and electron transfer. It was observed that the CL intensity of the GQDs-Ce(IV)-$NaHSO_3$ model was inhibited by tyrosine (Tyr), which has a significant function in the metabolism and growth of human and animals. The recommended (CRET) method can be successfully used for Tyr evaluation in milk samples with a high precision.

Irani-Nezhad et al. (2019) synthesized WS_2 QDs through solvothermal method. As-obtained WS_2 QDs had a size of 1−1.5 nm with fluorescence emission depending on excitation wavelength. These WS_2 QDs show a catalytic effect in the decomposition of H_2O_2. As-prepared WS_2 QDs exhibit a mimetic effect in the H_2O_2−rhodamine B CL system. The H_2O_2 is one of the products in the enzymatic reaction of glucose, which can be easily determined using WS_2 QDs. It was reported that H_2O_2 can be detected in the concentration range (0−1000 nmol L^{-1}) with a limit of detection as 2.4 nmol L^{-1}.

Vahid et al. (2019) developed a method for the sensitive determination of cyanide ions (CN^-) in biological as well as environmental samples. They used a CRET-induced CL system for this purpose. Hydrogen peroxide−bicarbonate system was selected for CL reaction. It was reported that glutathione-stabilized CdSe QDs (CdSe QDs) increase CL intensity significantly. On the contrary, it was observed the CRET system could be prohibited and CL emission turned off by gold nanoclusters (Au NCs). On efficient dissolution of Au NCs, the CRET to CdSe QDs was restored and CL emission was turned on. It can be used as a highly sensitive and reliable measurement of cyanide ions in the concentration range of 2−225 nM, with a limit of detection of 0.46 nM.

Hallaj et al. (2020) prepared S,N-doped carbon QDs (S,N-CQDs) via a hydrothermal method. They observed effect of as-prepared CQDs on the luminol−Mn(IV) CL reaction and it was found that S,N-CQDs increased the CL intensity of this reaction about 13-fold. It was also revealed that the CL intensity of this system was drastically reduced in the presence of uric acid. They designed a probe for the detection of uric acid using the amplified CL system and it was observed that it was proportional to the logarithm of uric acid concentration in the range 0.05−1.5 μM with a detection limit of 17 nM. Thus they developed a sensitive CL method for the detection of uric acid in biological fluids.

Rasoulzadeh and Amjadi (2021) prepared highly luminescent water-soluble $AgInS_2$ QDs (AIS QDs) via a green and hydrothermal method. It was reported that $NaIO_4$ in alkaline solution elicits a remarkable CL from as-prepared QDs. It was also revealed that the addition of glutathione to this $NaIO_4$-AIS QDs system enhanced CL intensity effectively, and therefore it was used as a sensing platform for the assay of GSH. It was reported that there is a relation between GSH concentration and CL intensity, which was linear in the range (1.0×10^{-9} mol L^{-1} to 5.0×10^{-6} mol L^{-1}) with a limit of detection of 2.8×10^{-10} mol L^{-1}. They also confirmed its usefulness in the analysis of human plasma.

Yahyai et al. (2021) developed a paper-based analytical device integrated with a potent CL system to find out deltamethrin (DM), using the enhancing effect of polyphosphate (PP) on GQDs-$KMnO_4$ CL reaction. They showed that the realized multiemission CL structure was investigated for analytical applications. It was revealed that under the optimized conditions, the generated signal is reduced by increasing the DM concentration in the range of 0.3−10 μg mL^{-1} with LOD as 0.15 μg mL^{-1}. This can be presented as an advanced analytical detection technique determination for DM in food samples, for on-site screening scopes.

11.4.3 Electroluminescence sensors

A high sensitivity label-free ECL immunosensor has been constructed by Wu et al. (2016) for the detection of prostate−specific antigen (PSA) based on GQDs. They used Au/Ag-rGO as electrode material to load the amounts

of aminated GQDs and carboxyl GQDs to amplify the ECL signal. The developed methodology shows that the ECL intensity decreased linearly with the logarithm of PSA concentration and the LOD is 0.29 pg mL^{-1}. The immunosensor can be successfully utilized in disease and drug analysis.

Shan et al. (2016) proposed CdS QDs as electrochemical sensing materials for determination of ciprofloxacin (CIP). It was reported that CdS QDs-modified glassy carbon electrode (GCE) exhibited a good anodic stripping response in acidic medium, which was attributed to the release of Cd(II) ions from CdS QDs. It was observed that anodic stripping current of Cd(II) on CdS QDs/GCE was found to decrease in solution, when CIP was added, which may be due to the complexation of CIP with in situ generated Cd(II) ions. A linear relationship was obtained between the anodic stripping voltammetric response of CdS QDs/GCE and concentration of CIP in the range (1.0×10^{-7}–1.0×10^{-5} mol L^{-1}) with a limit of detection as 2.2×10^{-8} mol L^{-1}. The use of CdS QDs-modified electrode for determination of CIP was observed in biological fluids.

The black phosphorus QDs (BPQDs) were synthesized by Ding et al. (2018) and then added into the solution of ZnO nanorods to obtain BPQDs-doped ZnO NPs (BPQDs@ZnO). They used a hydrothermal route for this purpose. The doping of BPQDs resulted in the formation of cubic BPQDs@ZnO NPs. The ECL of BPQDs@ZnO was investigated under neutral conditions. They obtained a cathodic ECL signal in the presence of $K_2S_2O_8$ that is relatively stronger than for ZnO nanorods. It was observed that cytochrome c exhibited an inhibiting effect on BPQDs@ZnO ECL, which can be sensitively detected in the range of 1.0×10^{-9}–5.0×10^{-7} mol L^{-1} with a limit of detection as 9.6×10^{-10} mol L^{-1}. It was revealed that such ECL characteristic of BPQDs-based nanocomposite has a potential in biosensing application.

Jie et al. (2019) developed an innovative procedure for amplified ECL detection of DNA utilizing the magnificent ECL activity of GQDs combined with a multiple cycling amplification mechanism. They used a novel poly (diallyldimethylammonium chloride) (PDDA)-GO complex to immobilize GQDs on the electrode to improve the ECL signal. This method is based on ECL quenching of Au NPs to GQDs combined with endonuclease aided cyclic amplification scheme, which has good application perspective in biosensing research, mainly in clinical diagnoses.

Wang et al. (2019a) reported a novel highly sensitive cloth-based closed bipolar ECL (C–BP–ECL) sensor with nanostructured electrode surface. The proposed method is based on the combination of chitosan (CS), poly (diallyldimethylammonium chloride)-functioned multiwalled carbon nanotubes (PDDA-MWCNTs), and GQDs–gold NPs (GQDs–AuNPs/PDDA) on the wax/carbon ink-screen-printed cloth-based device. The combination of GQDs–AuNPs-MWCNTs/CS, C-BP-ECL, and cloth-based microfluids for the detection of highly sensitive glucose has been established for the first

time, showing that glucose concentrations in complex human serum samples can be determined with this technique.

A novel ultrasensitive ECL sensor was studied by Niu et al. (2020) that can be used to detect a common food additive (sunset yellow). They used GQDs as the luminescent factor and potassium persulfate as the coreactant, showing that the ECL signal of the GQDs changed with the inclusion of sunset yellow. It has been observed that this method provides fast screening of possibly harmful food additives and, under optimized conditions, the GQD sensor exhibits a good linearity in the detection of sunset yellow in the concentration range of 0.0025−25 μM with a LOD as 7.6 nM.

de França et al. (2021) modified graphite working electrode (5 mm diameter) with CdSe/CdS magic-sized QDs (MSQDs) to increase its sensitivity. This modified electrode was fully characterized and optimized. It was reported that the best results were obtained when MSQDs (10 μg) were deposited on the electrode surface. It was revealed that a QDs-based sensor exhibited good stability, reproducibility, and repeatability. Such an electrochemical sensor was used for detecting dopamine. The signal showed dependence in the concentration range 0.5−15 $\mu mol\ L^{-1}$ with a limit of detection of 96 $nmol\ L^{-1}$. This was also successfully used for sensing of dopamine in real samples (human blood serum) with recovery rates ranging between 95.2% and 102.6%.

11.5 Others

Shao et al. (2012) linked most the promising suicide genes (herpes simplex virus thymidine kinase, HSV-TK gene) with CdTe/CdS core/shell QDs using the EDC/NHS coupling method. It was reported that plasmid TK intracellular trafficking can be distinctly and effectively traced via monitoring QDs' luminescence for up to 4 days after transfection of QDs-TK conjugates into Hela cells. It was observed that QDs-TK conjugates have more efficient cytotoxicity on addition of GCV into Hela cells, and these QDs do not show any detectable adverse effects on the cellular processes. It was revealed that photonic NMs (QDs) can be used as a tool for monitoring TK gene delivery and anticancer activity.

Ng et al. (2013) investigated cell-based cytotoxicity of N-acetyl-cysteine (NAC) QDs and also the effect of QDs on the beta (1−40) amyloid ($A\beta_{1-40}$)-induced cytotoxicity on human neuroblastoma SH-SY5Y cells by MTT (3-(4,5-dimethylthiazol-2-yl)-2,5-diphenyltetrazolium bromide) and reactive oxidative species (ROS) assays, respectively. It was reported that the inhibition of $A\beta_{1-40}$ peptides from fibrillation using NAC−QDs had a neuroprotection effect on the neural SH-SY5Y (neuron) cells.

Shao et al. (2014) also reported a QD-based technique that revealed a method of herpes simplex virus thymidine kinase (HSV-TK) suicide gene therapy by forming a covalent linkage between the TK gene and NIR fluorescent QDs. It was interesting to note that stable QD labeling did not affect

either the biological activity of the TK gene or QDs fluorescence. They traced the intracellular behavior antitumor effect of the TK gene in vivo and in vitro. It was revealed that the TK gene was shuttled to the nucleus after 24 h treatment. A single dose of GCV administration at that time exerted a gradually increasing lethal effect for 72 h. It was proposed that this technique may be useful for cancer therapy in the future.

Weng et al. (2015) synthesized mannose-modified fluorescent carbon QDs (Man-CQDs) via a simple one-step dry heating method from solid ammonium citrate and mannose. It was reported that highly soluble Man-CQDs had average particle diameter of 3.1 ± 1.2 nm. It can be successfully applied for labeling *Escherichia coli*. The labeling efficiency of Man-CQDs can be optimized by controlling the ratio of ammonium citrate/mannose. They demonstrated that quantitative detection of the bacteria *E. coli* (450 CFU) is possible because of specific binding of the mannose units to *E. coli* in lab samples, and it can be also applied to real samples (tap water, human urine, and apple juice).

Magnesium and nitrogen codoped carbon QDs (Mg-N-CQDs) were prepared by Liu et al. (2016) via a hydrothermal method. It can be used as a fluorescent switch for selective and sensitive sensing of Hg(II) and cysteine (Cys). The fluorescence of Mg-N-CQDs aqueous solution was quenched on addition of Hg(II) and it has been attributed to the formation of a nonfluorescent complex between Mg-N-CQDs and Hg(II). But the fluorescence of these QDs aqueous solution containing Hg(II) could be recovered back in the presence of Cys in a gradual manner, as Hg(II) has stronger binding affinity toward Cys than toward Mg-N-CQDs. They designed a fluorescent probe and applied it to detect Hg(II) ions in real water samples with satisfactory results.

A green hydrothermal strategy has been devised by Bao et al. (2018) to produce water-soluble nitrogen/phosphorus (N/P) codoped CQDs using edible *Eleocharis dulcis*. As-prepared CQDs exhibited high quantum yield, remarkable excitation-dependent emission, long lifetime, and superior fluorescence stability. The N/P codoped CQDs had a wide-range capability to determine inorganic cations as fluorescence sensor. They showed remarkable selectivity and sensitivity for Fe^{3+} ions.

Kumari et al. (2018) used the residue obtained from the pyrolysis of waste polyolefins, for preparing highly green-visual fluorescent carbon QDs via a simple one-step hydrothermal approach, which consists of ultrasonic-assisted chemical oxidation. The use of as-synthesized CQDs as a fluorescent sensor for Cu^{2+} ions detection was investigated, where excellent sensitivity and selectivity were exhibited for detecting Cu^{2+} ions with a limit of detection of 6.33 nM in the detection range of $1-8.0\,\mu M$. It was also revealed that these CQDs show their use in the analysis of real water samples. Apart from this, CQDs have the potential for TNBC cells (MDA-MB 468 cells) imaging.

Xiang et al. (2018) conjugated FA onto the surface of ZnO QDs (QDs)-NH_2 via an amidation reaction. As-prepared titania nanotubes (TNTs) loaded with vancomycin (Van) are capped by these FA-functionalized ZnO (ZnO-FA) QDs. This arrangement keeps them stable in normal physiological environments, but dissolves as Zn^{2+} in the mildly acidic environment after bacterial infections. The antibacterial ratio of TNTs-Van@ZnO-FA QDs against *Staphylococcus aureus* was increased from 60.8% to 98.8%, while it only increased from 85.2% to 95.1% for TNTs-Van, when the pH of the environment was decreased from 7.4 to 5.5. It was suggested that this surface system has a promising bioplatform on Ti-based metallic implants as it prevents bacterial infection with a long-lasting effect. It is suitable for various applications like antifungal, antibacterial, antiinflammatory, antioxidant, and wound healing.

Murugan et al. (2019) developed facile, rapid and frugal approach for the synthesis of highly fluorescent carbon QDs by pyrolysis of finger millet ragi (*Eleusine coracana*) (carbon source). It was found that the size distribution was in the range of 3−8 nm. It was indicated that Cu^{2+} strongly quenched the fluorescent intensity of these CQDs as compared to other metal ions such as Mg^{2+}, Pb^{2+}, Ni^{2+}, Mn^{2+}, Hg^{2+} Al^{3+}, Ca^{2+}, and Cr^{3+}. A linear correlation was observed between quenching efficiency concentration of Cu^{2+} ions in the range from 0 to 100 μM. These CQDs were also applied in sensing of Cu^{2+} in real water samples and the limit of detection was 10 nM. It was found that Ni^{2+} and Cu^{2+} formed a very strong bonding with CQDs compared to other divalent ions. It was revealed that Cu^{2+} get adsorbed on aromatic C═C (π-bond) of CQDs preferentially while other divalent metals form σ-bond(s) with the CQDs.

An easy and economical synthesis of highly fluorescent nitrogen-rich carbon QDs (N-CQDs) was reported by Bao et al. (2019). It was observed that as-prepared N-CQDs can act as a sensor for the "turn-off" detection of Co^{2+} in the range of 0.5−3 μM with a detection limit of 0.12 μM. The fluorescence of the quenched N-CQDs was formed to reappear and get "turn-on," when GSH, AA, EDTA, and cyst were used. It was claimed that N-CQDs were also successful in detecting the trace level of Co^{2+} in vitamin B_{12} sample.

Fluorescent QDs with optical properties (such as tunable broad excitation, robust photostability high quantum output, and restricted emission spectra) are utilized as a new class of optical probe in biological and biomedical fields (Jahangir et al., 2019). Lei et al. (2019) proposed an eco-friendly synthetic procedure to prepare emission-tunable carbon QDs. The particle size of as-synthesized CQDs was found to be 2.4 nm. Significant properties of controllable emission make these QDs a potential candidate for sensor applications.

Chandra et al. (2020) developed a fast and eco-friendly one-pot hydrothermal technique for synthesizing nitrogen/sulfur-codoped fluorescent carbon QDs (NS-CQDs). They used simple precursors such as citric acid and thiosemicarbazide. The as-prepared NS-CQDs were used successfully as a

nanoprobe for detecting picric acid (PA) in different derivatives. It was also reported that this system exhibited low cytotoxicity and excellent biocompatibility in HeLa cervical cancer cells. It was reported that it can be used for the detection of PA in environmental, analytical, and pathological applications.

GQDs have low cytotoxicity and higher biocompatibility as compared to other QDs, The optical properties of QD and have the ability to cross the blood−brain barrier, and therefore GQDs can be useful in neuroscience diagnostics and therapeutics. Their smaller size, surface chemistry and ease of loading of different drugs make them potential drug delivery systems as they could travel through the bloodstream up to the brain. Perini et al. (2020) discussed the applications of GQDs in drug delivery to the central nervous system, bioimaging, and photophysical therapies.

Kateshiya et al. (2020) proposed a synthetic route for the preparation of highly blue fluorescent tyrosine coated molybdenum oxide QDs (Tyr-MoO_3 QDs). Here, tyrosine (Tyr) was used as a surface ligand to functionalize MoO_3 QDs. They obtained color changes in the solution of MoO_3 NPs, MoO_3-OH NPs and Tyr-MoO_3 QDs in presence of UV and day light. It was reported that as-prepared Tyr-MoO_3 QDs could act as a sensor for rapid and sensitive identification of imidacloprid. It was revealed that emission peak of Tyr-MoO_3 QDs at 416 nm exhibited a linear quenching on increasing concentration of imidacloprid in the range (0.045−1.00 μM). The proposed method was successfully applied for the detection of imidacloprid in real samples also.

The activities of ions are closely associated with the physiology of brain such as neural activity, intracranial cell membrane potential, and neuropathology. Therefore, monitoring the levels of ion in the brain is of utmost importance in neuroscience. A powerful tool has emerged as nanosensors for monitoring brain ion levels, cell function, neural activity, and it can also be used in the diagnosis of diseases. The advances in the design and application of these ion level nanosensors at different physiological levels have been reviewed by Wei et al. (2020).

Jlassi et al. (2021) prepared GQDs from graphitic waste. These GQDs were evaluated as resistive humidity sensors. Such resistive humidity sensors were fabricated on the prepatterned interdigital indium tin oxide electrodes with three different concentrations (2.5, 5.0, and 10 mg) of GQDs in N, N-dimethylformamide (DMF). It was observed that GQDs (10 mg mL^{-1})-based impedance sensors exhibited good sensitivity as compared to the other ratios (2.5 and 5 mg). They reported that the maximum calculated hysteresis of the GQDs-based humidity sensor was found to be around 2.2% at 30%RH while the minimum was 0.79% at 60%RH. It was revealed that response and recovery time were 15 s and 55 s, respectively.

11.6 Toxicity of quantum dots

Yan et al. (2011) investigated the potential vascular endothelial toxicity of QDs, particularly of mercaptosuccinic acid-capped CdTe QDs in vitro. They

synthesized pH stable and water-soluble CdTe QDs and their cell viability were tested. The presence of CdTe QDs ($0.1-100\ \mu g\ mL^{-1}$) decreased the cell viability of human umbilical vein endothelial cells (HUVECs), which indicated that these QDs induced significant endothelial toxicity. It was also revealed that CdTe QDs ($10\ \mu g\ mL^{-1}$) exhibited mitochondrial network fragmentation, significant oxidative stress, and disruption of mitochondrial membrane potential. It was suggested that these QDs not only impaired mitochondria but also induced endothelial apoptosis and exerted endothelial toxicity, providing strong evidence of the direct toxic effects of QDs on human vascular ECs, and indicating that exposure to QDs is a significant risk for the development of cardiovascular diseases.

Smith et al. (2012) selected primary human liver (PHL) cells and HepG2 cells as in vitro tissue culture models to observe the possible adverse effects of copolymer-coated CdSe/ZnS QDs poly(maleic anhydride-*alt*-1-tetradecene) (TOPO-PMAT copolymer CdSe/ZnS QDs) (when TOPO = tri-*n*-octylphosphine oxide) and PMAT. However, PHL cells did not take up TOPO-PMAT CdSe/ZnS QDs, but some nonparenchymal cells did, particularly Kupffer cells. No acute toxicity or morphological change was noted in these systems up to 40 nM. It was observed that cellular stress markers and proinflammatory cytokines/chemokines were increased in PHL cell cultures, which suggests that these QDs are not likely to cause acute cytotoxicity in the liver but may elicit inflammation or hepatitis.

Liu et al. (2015) evaluated cytotoxicity of four types of QD formulations (PEGylated phospholipid encapsulated CdSe/CdS/ZnS QDs (CdSe-Phos), MPA modified CdSe/CdS/ZnS QDs (CdSe-MPA), Pluronic F127 encapsulated CdTe/ZnS QDs (CdTe-F127), and PEGylated phospholipid encapsulated InP/ZnS QDs (InP-Phos)) in two different human cancer cell models (neuroblastoma (SH-SY5Y), gastric adenocarcinoma (BGC-823) cell lines).

Wang et al. (2016) reviewed the toxicity of GQDs, including raw GQDs, chemically doped GQDs, and chemically functionalized GQDs and also presented some important details related to the uptake process by cells and parameters managing the toxicity of GQDs (concentration, synthesis methods, particle size, and surface chemistry). Various issues related to the toxicity regulation of GQDs through chemical modification were discussed, exposing some important aspects about the toxicity mechanism through generation of ROS by some GQDs.

Xiao et al. (2016) studied the cytotoxicity of two types of QDs on *Chlorella pyrenoidosa* at different concentrations:

- carbon QDs (CQDs): Undoped CQDs, N-doped CQDs, N,S-doped-CQDs; and
- metal QDs (MQDs): CdS QDs, CdTe QDs, $CuInS_2$/ZnS QDs.

The Chla contents were found to be consistent to the number of algae cells, when *C. Pyrenoidosa* was treated by different concentrations of QDs.

It indicates a good dose-response relationship. The EC_{50} of undoped CQDs, N-doped CQDs, N,S-doped CQDs, CdS QDs, CdTe QDs, and $CuInS_2$/ZnS QDs was observed as 232.47, 185.83,38.56, 4.88, 0.015, and 459.5 mgL^{-1}, respectively at 96 h. They observed toxicity order as follows:

$CuInS_2$/ZnS QDs <Undoped CQDs <N-doped CQDs <N,S-doped CQDs <CdS QDs <CdTe QDs.

It was concluded that the toxicity of CQDs was relatively less as compared to MQDs, but $CuInS_2$/ZnS QDs exhibited the lowest toxicity.

The toxicity of NMs is one of the crucial challenges facing their use in biotechnology (Chen et al., 2017b). The growing biomedical domain of G-based material applications, including GQDs, raises some queries about their short- and long-term cytotoxicity (Tadyszak et al., 2018).

A comparison of the toxic effects was made by Pramanik et al. (2018) between CdSeQDs, silicon QDs, and CdSe/ZnS QDs. They selected two model bacteria: Gram-negative bacterium (*Shewanella oneidensis* Mr-1) and a Gram-positive bacterium (*Bacillus subtilis* SB 491). It was indicated that the silicon QDs not associated with the cell membranes are benign to these bacteria. On the other hand, CdSe cores exhibited significant toxicity to these bacteria while CdSe/ZnS QDs are relatively less toxic.

Deng et al. (2018) have utilized the Illumina high-throughput RNA sequencing to examine the whole-transcriptome profiling of zebrafish larvae after exposure to GQDs, identifying 2116 differentially expressed genes between GQDs exposed groups and control. Zebrafish is a preferred type of an organism for toxicity testing due to its small dimension, reduced maintenance price, and optical transparency (Grunwald and Eisen, 2002; Hill et al., 2005; Dai et al., 2014; Sonthanasamy et al., 2016; Chen et al., 2016; Tang et al., 2017; Deng et al., 2018; Liu et al., 2020b).

Little is known about the developmental disturbance in animals after GQDs exposure at some concentration values that are higher than the tolerable level (Deng et al., 2018). It has been reported that the acute inflammatory responses and detoxifying complex represent the principal GQDs-activated pathways and that GQDs can perturb the blood homeostasis via upregulating the renin−angiotensin system structure. Some results related to the molecular processes of possible bleeding risks and detoxifying operations have been reported as an effect to GQDs exposure.

Nikazar et al. (2020) pointed out that even if the latest classes of new manufactured QDs exhibit ever-better physical properties, some details related to their cytotoxicity are some major drawbacks, and in order to address the challenges of QD research it is vital to examine the type of the characteristics that make these QDs toxic. They also reviewed changes in toxicity of GQDs, when they are in association with other metal ions.

Gu et al. (2021) developed highly fluorescent Ti_3C_2 and Nb_2C MXene QDs for labeling of in vitro models cytotoxicity of the QDs to human umbilical vein endothelial cells HUVECs. It was observed that a significant

cytotoxicity was induced on exposure by 100 μg ML^{-1} Ti_3C_2 but Nb_2C QDs could not exhibit it even after 24 h. It was also revealed that Nb_2C QDs were found to be more biocompatible to HUVECs as compared to Ti_3C_2 QDs at the same mass concentrations.

The in vitro toxicity of $CuInS_2$/ZnS QDs was investigated by Xue et al. (2022) on U87 human glioma cell line. It was observed that these QDs enter the cells and are located mainly in the cytoplasm. It was reported that 1515 genes were downregulated and 220 genes were upregulated, which significantly changed gene functions, including chromosome-DNA binding, nucleosome, and chromosome assembly.

11.7 Conclusion

This chapter furnishes a complete overview of the most recent emerging advances in the research domain of QDs and QD−based composites, focusing on their applications in sensing, targeted drug delivery, cancer therapy, etc. Some size-dependent aspects, as well as the structural, morphological composition and outstanding properties of QDs are summarized. Considering that the risk and health hazard of the QDs must be eliminated prior to human exposure, some new toxicity issues of QDs are also presented. Due to their unique properties including good biocompatibility and low cytotoxicity, QDs are of great value in diverse fields and perform a major role in the progress of research in bioimaging, cancer therapy, tissue engineering, sensors, drug delivery, etc.

References

Abdelhamid, H.N., El-Bery, H.M., Metwally, A.A., Elshazly, M., Hathout, R.M., 2019. Synthesis of CdS-modified chitosan quantum dots for the drug delivery of sesamol. Carbohydr. Polym. 214, 90−99.

Abdel-Salam, M., Omran, B., Whitehead, K., Baek, K.-H., 2020. Superior properties and biomedical applications of microorganism−derived fluorescent quantum dots. Molecules 25 (19). Available from: https://doi.org/10.3390/molecules25194486.

Alarfaj, N.A., El-Tohamy, M.F., Oraby, H.F., 2020. New immunosensing-fluorescence detection of tumor marker cytokeratin-19 fragment (CYFRA 21-1) via carbon quantum dots/zinc oxide nanocomposite. Nanoscale Res. Lett. 15 (1). Available from: https://doi.org/10.1186/s11671-020-3247-9.

Allen, P.M., Liu, W., Chauhan, V.P., Lee, J., Ting, A.Y., Fukumura, D., et al., 2010. In As (ZnCdS) quantum dots optimized for biological imaging in the near-infrared. J. Am. Chem. Soc. 132 (2), 470−471.

Ameta, R., Ameta, S.C., 2016a. Binary semiconductors. In: Ameta, R., Ameta, S.C. (Eds.), Photocatalysis: Principles and Applications. CRC Press/Taylor & Francis Group; Apple Academic Press, Boca Raton.

Ameta, R., Ameta, S.C., 2016b. Metallization. In: Ameta, R., Ameta, S.C. (Eds.), Photocatalysis: Principles and Applications. CRC Press/Taylor & Francis Group; Apple Academic Press, Boca Raton.

Ameta, R., Ameta, S.C., 2016c. Ternary semiconductors. In: Ameta, R., Ameta, S.C. (Eds.), Photocatalysis: Principles and Applications. CRC Press/Taylor & Francis Group; Apple Academic Press, Boca Raton.

Ameta, K.L., Papnai, N., Ameta, R., 2014. Photocatalytic degradation of malachite green using nano-sized cerium-iron oxide. Orbital: Electron. J. Chem. 6 (1), 14−19.

Ameta, K., Trivedi, M., Bhatt, J., Soni, D., Benjamin, S., Ameta, S.C., 2019a. Antimicrobial activity of nanosized photocatalytic materials. In: Balköse, D., Ribeiro, A.C.F., Haghi, A.K., Ameta, S.C., Chakaborty, T. (Eds.), Chemical Science and Engineering Technology: Perspectives on Interdiciplinary Research. CRC Press/Taylor & Francis Group; Apple Academic Press, Boca Raton, p. 24.

Ameta, R., Kapoor, N., Pathak, B., Bhatt, J., Ameta, S.C., 2019b. Carbon nanotube composites as photocatalytic materials. In: Vakhrushev, A.V., Kodolov, V.I., Haghi, A.K., Ameta, S.C. (Eds.), Carbon Nanotubes and Nanoparticles: Current and Potential Applications Series: AAP Research Notes on Nanoscience and Nanotechnology. CRC Press/Taylor & Francis Group; Apple Academic Press, Boca Raton.

Ameta, R., Jat, K.K., Bhatt, J., Ameta, S.C., 2019c. Quantum dots and their applications. In: Vakhrushev, A.V., Ameta, S.C., Susanto, H., Haghi, A.K. (Eds.), Advances in Nanotechnology and the Environmental Sciences: Applications, Innovations and Visions for the Future Series: AAP Research Notes on Nanoscience & Nanotechnology. CRC Press/Taylor & Francis Group; Apple Academic Press, Boca Raton.

Ameta, S.K., Rai, A.K., Hiran, D., Ameta, R., Ameta, S.C., 2020. Use of nanomaterials in food science. In: Ghorbanpour, M., Bhargava, P., Varma, A., Choudhary, D. (Eds.), Biogenic Nano - Particles and their Use in Agro-ecosystems. Springer Singapore, pp. 457−488.

Ardelean, I.I., Sarchizian, I., Manea, M., Damian, V., Apostol, I., Cîrnu, M., et al., 2011. CdSe/ZnS quantum dots cytotoxicity against phototrophic and heterotrophic bacteria. Proc. NANOCON 9, 21−23.

Armăşelu, A., 2017. Chapter 2: Recent developments in applications of quantum-dot based light-emitting diodes. In: Ghamsari, M.S. (Ed.), Quantum-Dot Based Light Emitting Diodes. IntechOpen, Rijeka, Croatia, pp. 7−24.

Armăşelu, A., 2019. Chapter 3: Recent advancement on the excitonic and biexcitonic properties of low-dimensional semiconductors. In: Thirumalai, J., Pokutnyi, S.I. (Eds.), Advances in Condensed-Matter and Materials Physics Rudimentary Research to Topical Technology. IntechOpen, Rijeka, Croatia, pp. 41−54.

Armăşelu, A., Popescu, A., Damian, V., Ardelean, I., Apostol, D., 2011a. Fluorescence properties of quantum dots used in the study of microorganism. J. Optoelectron. Adv. Mater. 13 (4), 439−443.

Armăşelu, A., Popescu, A., Apostol, I., Ardelean, I., Damian, V., Iordache, I., et al., 2011b. Passive nonspecific labeling of cyanobacteria in natural samples using quantum dots. Optoelectron. Adv. Mater. Rapid Commun. 5 (10), 1084−1090.

Bao, R., Chen, Z., Zhao, Z., Sun, X., Zhang, J., Hou, L., et al., 2018. Green and facile synthesis of nitrogen and phosphorus co-doped carbon quantum dots towards fluorescent ink and sensing applications. Nanomater 8 (6). Available from: https://doi.org/10.3390/nano8060386.

Bao, D., Kumar, V., Chandra, S., Singh, V.K., Mohan, S., Singh, D.K., et al., 2019. Synthesis of highly fluorescent nitrogen-rich carbon quantum dots and their application for the turn-off detection of cobalt (II). Opt. Mater. 92, 311−318.

Benitez-Martinez, S., Valcárcel, M., 2015. Graphene quantum dots in analytical science. Trends Analyt. Chem. 72, 93−113.

Benitez-Martinez, S., Lopez-Lorente, A.I., Valcárcel, M., 2014. Graphene quantum dots sensor for the determination of graphene oxide in environmental water samples. Anal. Chem. 86 (24), 12279–12284.

Benjamin, S., Sharma, S., Ameta, R., 2014. Nanomaterials. In: Ameta, S.C., Punjabi, P.B., Ameta, R., Ameta, C. (Eds.), Microwave—Assisted Organic Synthesis: A Green Chemical Approach, first ed. CRC Press/Taylor & Francis Group; Apple Academic Press, New York, p. 24.

Bhakat, A., Pal, A., Siddaramaiah, R., Chattopadhyay, A., 2021. Complexation-based super crystalline assembly of zinc oxide quantum dots for sensitive carbon dioxide gas sensing. J. Phys. Chem. C. 125, 12316–12323.

Bhatt, J., Benjamin, S., Ameta, R., Ameta, S.C., 2019a. Enhancement of photodegradation of picric acid (2, 4, 6-trintrophenol) by fabrication of visible-light-active SnO_2 quantum dots/TiO_2 nanospheres composite. J. Appl. Chem. 8 (4), 1805–1812.

Bhatt, J., Jat, K.K., Rai, A.V., Ameta, R., Ameta, S.C., 2019b. Photodegradation of 2-nitrophenol an endocrine disruptor, using TiO_2 nanosphere/SnO_2 quantum dots. In: Aquilar, C.N., Ameta, S.C., Haghi, A.K. (Eds.), Green Chemistry and Biodiversity: Principles, Technique and Correlations. CRC Press/Taylor & Francis Group; Apple Academic Press, New York, pp. 1–8.

Bhatt, J., Benjamin, S., Ameta, R., Ameta, S.C., 2019c. Enhanced visible light photocatalytic activity of TiO_2 nanospheres/SnO_2 quantum dots composite for degradation of 4—Nitrophenol. J. Nanosci. Technol. 5 (4), 748–750.

Bhatt, J., Jangid, M., Kapoor, N., Ameta, R., Ameta, S.C., 2020a. Detection and degradation of pesticides using nanomaterials. In: Ghorbanpour, M., Bhargava, P., Varma, A., Choudhary, D. (Eds.), Biogenic Nano-Particles and their Use in Agro-ecosystems. Springer, Singapore, pp. 431–455.

Bhatt, J., Jat, K.K., Rai, A.K., Ameta, R., Ameta, S.C., 2020b. Quantum dots and their sensing applications. In: Pogliani, L., Ameta, S.C., Haghi, A.K. (Eds.), Chemistry and Industrial Techniques for Chemical Engineers Innovations in Physical Chemistry: Monograph Series. CRC Press/Taylor & Francis Group; Apple Academic Press, New York, p. 18.

Chandra, S., Bano, D., Pradhan, P., Singh, V.K., Yadav, P.K., Sinha, D., et al., 2020. Nitrogen/sulfur-co-doped carbon quantum dots: a biocompatible material for the selective detection of picric acid in aqueous solution and living cells. Anal. Bioanal. Chem. 412 (15), 3753–3763.

Chen, T., Zhao, T., Wei, D., Wei, Y., Li, Y., Zhang, H., 2013. Core–shell nanocarriers with ZnO quantum dots-conjugated Au nanoparticle for tumor-targeted drug delivery. Carbohydr. Polym. 92 (2), 1124–1132.

Chen, X., Tang, Y., Cai, B., Fan, H., 2014. 'One-pot'synthesis of multifunctional GSH–CdTe quantum dots for targeted drug delivery. Nanotechnol 25 (23). Available from: https://doi.org/10.1088/0957-4484/25/23/235101.

Chen, Y., Hu, X., Sun, J., Zhou, Q., 2016. Specific nanotoxicity of graphene oxide during zebrafish embryogenesis. Nanotoxicology 10 (1), 42–52.

Chen, W., Xin, X., Zang, Z., Tang, X., Li, C., Hu, W., et al., 2017a. Tunable photoluminescence of $CsPbBr_3$ perovskite quantum dots for light emitting diodes application. J. Solid. State Chem. 255, 115–120.

Chen, F., Gao, W., Qiu, X., Zhang, H., Liu, L., Liao, P., et al., 2017b. Graphene quantum dots in biomedical applications: recent advances and future challenges. Front. Lab. Med. 1 (4), 192–199.

Chen, J., Qiu, H., Zhao, S., 2020. Fabrication of chemiluminescence resonance energy transfer platform based on nanomaterial and its application in optical sensing, biological imaging and photodynamic therapy. Trend. Anal. Chem. 122. Available from: https://doi.org/10.1016/j.trac.2019.115747.

Choi, H.-J., Montemagno, C.D., 2016. Convergence of nanotechnology and biotechnology. In: Bainbridge, W., Roco, M. (Eds.), Handbook of Science and Technology Convergence. Springer, Cham, pp. 253–277.

Dai, Y.-B., Jia, Y.-F., Chen, N., Bian, W.-P., Li, Q.-K., Ma, Y.-B., et al., 2014. Zebrafish as a model system to study toxicology. Environ. Toxicol. Chem. 33 (1), 11–17.

Dai, C., Zhang, S., Liu, Z., Wu, R., Chen, Y., 2017. Two-dimensional graphene augments nanosonosensitized sonocatalytic tumor eradication. ACS Nano 11, 9467–9480.

Damian, V., Ardelean, I., Armăşelu, A., Popescu, A., Apostol, I., Fourier transform spectra of quantumdots. In: Proc. SPIE 7469, ROMOPTO 2009: NinthConference on Optics: MicrotoNanophotonics II, 74690E, 17 May 2010. Available from: https://doi.org/10.1117/12.862053.

Damian, V., Udrea, C., Bojan, M., Luculescu, C., Armăşelu, A., Apostol, I., Aluminum nanoparticles production by laser ablation in liquids. In: Proc. SPIE 8001, International Conference on Applications of Optics and Photonics, 80012G, 26 July 2011. Available from: https://doi.org/10.1117/12.894525.

de França, C.C.L., Meneses, D., Silva, A.C.A., Dantas, N.O., de Abreu, F.C., Petroni, J.M., et al., 2021. Development of novel paper-based electrochemical device modified with CdSe/CdS magic-sized quantum dots and application for the sensing of dopamine. Electrochim. Acta 367. Available from: https://doi.org/10.1016/j.electacta.2020.137486.

Deng, S., Jia, P.P., Zhang, J.H., Junaid, M., Niu, A., Ma, Y.-B., et al., 2018. Transcriptomic response and perturbation of toxicity pathways in zebrafish larvae after exposure to graphene quantum dots (GQDs). J. Hazard. Mater. 357, 146–158.

Ding, Q., Zhang, X., Li, L., Lou, X., Xu, J., Zhou, P., et al., 2017. Temperature dependent photoluminescence of composition tunable $Zn_xAgInSe$ quantum dots and temperature sensor application. Opt. Express 25 (16), 19065–19076.

Ding, H., Tang, Z., Dong, Y., 2018. Synthesis of black phosphorus quantum dots doped ZnO nanoparticles and its electrogenerated chemiluminescent sensing application. ECS J. Solid. State Sci. Technol. 7 (9). Available from: https://doi.org/10.1149/2.0151809jss.

Dong, J., Wang, K., Sun, L., Sun, B., Yang, M., Chen, H., et al., 2018. Application of graphene quantum dots for simultaneous fluorescence imaging and tumor-targeted drug delivery. Sens. Actuators B. Chem. 256, 616–623.

Duran, G.M., Benavidez, T.E., Contento, A.M., Rios, A., Garcia, C.D., 2017. Analysis of penicillamine using Cu-modified graphene quantum dots, synthesized from uric acid as single precursor. J. Pharm. Anal. 7 (5), 324–331.

Erogbogbo, F., Yong, K.T., Roy, I., Xu, G., Prasad, P.N., Swihart, M.T., 2008. Biocompatible luminescent silicon quantum dots for imaging of cancer cells. ACS Nano 2 (5), 873–878.

Fasbender, S., Zimmermann, L., Cadeddu, R.P., Luysberg, M., Moll, B., Janiak, C., et al., 2019. The low toxicity of graphene quantum dots is reflected by marginal gene expression changes of primary human hematopoietic stem cells. Sci. Rep. 9. Available from: https://doi.org/10.1038/s41598-019-48567-6.

Felix, D.M., Alencar, L.M.R., de Menezes, F.D., Midlej, V.V.P., Aguilar, L., Piperni, S.G., et al., 2021. Graphene quantum dots decorated with imatinib for leukemia treatment. J. Drug. Deliv. Sci. Technol. 61. Available from: https://doi.org/10.1016/j.jddst.2020.102117.

Flak, D., Przysiecka, Ł., Nowaczyk, G., Scheibe, B., Kościński, M., Jesionowski, T., et al., 2018. GQDs-MSMs nanocomposite nanoparticles for simultaneous intracellular drug delivery and fluorescent imaging. J. Nanopart. Res. 20. Available from: https://doi.org/10.1007/s11051-018-4416-y.

Gao, L., Ju, L., Cui, H., 2017. Chemiluminescent and fluorescent dual-signal graphene quantum dots and their application in pesticide sensing arrays. J. Mater. Chem. C. 31, 7753–7758.

Ghosh, S., Ghosal, K., Mohammad, S.A., Sarkar, K., 2019. Dendrimer functionalized carbon quantum dot for selective detection of breast cancer and gene therapy. Chem. Eng. J. 373, 468–484.

Grunwald, D.J., Eisen, J.S., 2002. Headwaters of the zebrafish [mdash] emergence of a new model vertebrate. Nat. Rev. Genet. 3 (9), 717–724.

Gu, Z., Zhu, S., Yan, L., Zhao, F., 2019. Graphene-based smart platforms for combined cancer therapy. Adv. Mater. 31 (9). Available from: https://doi.org/10.1002/adma.201800662.

Gu, M., Dai, Z., Yan, X., Ma, J., Niu, Y., Lan, W., et al., 2021. Comparison of toxicity of Ti_3C_2 and Nb_2C Mxene quantum dots (QDs) to human umbilical vein endothelial cells. J. Appl. Toxicol. 41 (5), 745–754.

Guan, Q., Ma, J., Yang, W., Zhang, R., Zhang, X., Dong, X., et al., 2019. Highly fluorescent Ti_3C_2MXene quantum dots for macrophage labeling and Cu^{2+} ion sensing. Nanoscale 11 (30), 14123–14133.

Hallaj, T., Amjadi, M., Mirbirang, F., 2020. S, N-doped carbon quantum dots enhanced Luminol-Mn (IV) chemiluminescence reaction for detection of uric acid in biological fluids. Microchem. J. 156. Available from: https://doi.org/10.1016/j.microc.2020.104841.

Han, C., Zhang, X., Wang, F., Yu, Q., Chen, F., Shen, D., et al., 2021. Duplex metal co-doped carbon quantum dots-based drug delivery system with intelligent adjustable size as adjuvant for synergistic cancer therapy. Carbon 183, 789–808.

Hassanzadeh, J., Khataee, A., Lotfi, R., 2017. Sensitive fluorescence and chemiluminescence procedures for methamphetamine detection based on CdS quantum dots. Microchem. J. 132, 371–377.

Henna, T.K., Pramod, K., 2020. Graphene quantum dots redefine nanobiomedicine. Mater. Sci. Eng. C. 110. Available from: https://doi.org/10.1016/j.msec.2020.110651.

Hill, A.J., Teraoka, H., Heideman, W., Peterson, R.E., 2005. Zebrafish as a model vertebrate for investigating chemical toxicity. Toxicol. Sci. 86 (1), 6–19.

Ingale, A.G., Chaudhari, A.N., 2013. Biogenic synthesis of nanoparticles and potential applications: an eco-friendly approach. J. Nanomed. Nanotechol. 4 (1). Available from: https://doi.org/10.4172/2157-7439.1000165.

Irani-Nezhad, M.H., Khataee, A., Hassanzadeh, J., Orooji, Y., 2019. A chemiluminescent method for the detection of H_2O_2 and glucose based on intrinsic peroxidase-like activity of WS_2 quantum dots. Molecules 24 (4). Available from: https://doi.org/10.3390/molecules24040689.

Jahangir, M.A., Gilani, S.J., Muheem, A., Jafar, M., Aslam, M., Ansari, M.T., 2019. Quantum dots: next generation of smart nano-systems. Pharm. Nanotechnol. 7 (3), 234–245.

Jahdaly, B.A.A., Elsadek, M.F., Ahmed, B.M., Farahat, M.F., Taher, M.M., Khalil, A.M., 2021. Outstanding graphene quantum dots from carbon source for biomedical and corrosion inhibition applications: a review. Sustainability 13 (4). Available from: https://doi.org/10.3390/su13042127.

Jat, K.K., Bhatt, J., Ameta, S.C., 2019. Photodegradation of fast green by using SnO_2 quantum dots / TiO_2 nanoparticles composite. J. Appl. Chem. 8 (1), 139–145.

Jie, G., Zhou, Q., Jie, G., 2019. Graphene quantum dots-based electrochemiluminescence detection of DNA using multiple cycling amplification strategy. Talanta 194, 658–663.

Jlassi, K., Mallick, S., Eribi, A., Chehimi, M.M., Ahmad, Z., Touati, F., et al., 2021. Facile preparation of NS co-doped graphene quantum dots (GQDs) from graphite waste for efficient humidity sensing. Sens. Actuators B. Chem. 328. Available from: https://doi.org/10.1016/j.snb.2020.129058.

Justin, R., Tao, K., Román, S., Chen, D., Xu, Y., Geng, X., et al., 2016. Photoluminescent and superparamagnetic reduced graphene oxide–iron oxide quantum dots for dual-modality imaging, drug delivery and photothermal therapy. Carbon 97, 54–70.

Kateshiya, M.R., Malek, N.I., Kailasa, S.K., 2020. Facile synthesis of highly blue fluorescent tyrosine coated molybdenum oxide quantum dots for the detection of imidacloprid pesticide. J. Mol. Liq. 319. Available from: https://doi.org/10.1016/j.molliq.2020.114329.

Khataee, A., Hassanzadeh, J., Lotfi, R., Joo, S.W., 2018. Graphene quantum dots/bisulfite assisted chemiluminescence of rhodamine B-H_2O_2 system for sensitive recognition of HCHO. Sens. Actuators B: Chem. 254, 402–410.

Khosravanian, A., Moslehipour, A., Ashrafian, H., 2021. A review on bioimaging, biosensing and drug delivery systems based on graphene quantum dots. Prog. Chem. Biomed. Res. 4 (1), 44–56.

Kumari, A., Kumar, A., Sahu, S.K., Kumar, S., 2018. Synthesis of green fluorescent carbon quantum dots using waste polyolefins residue for Cu^{2+} ion sensing and live cell imaging. Sens. Actuators B. Chem. 254, 197–205.

Lei, C.W., Hsieh, M.L., Liu, W.R., 2019. A facile approach to synthesize carbon quantum dots with pH-dependent properties. Dye. Pigm 169, 73–80.

Li, H., Shih, W.Y., Shih, W.H., 2007. Synthesis and characterization of aqueous carboxyl-capped CdS quantum dots for bioapplications. Ind. Eng. Chem. Res. 46 (7), 2013–2019.

Li, Z., Fan, J., Tong, C., Zhou, H., Wang, W., Li, B., et al., 2019a. A smart drug-delivery nano-system based on carboxylated graphene quantum dots for tumor–targeted chemotherapy. Nanomedicine 14. Available from: https://doi.org/10.2217/nnm-2018-0378.

Li, Y., Hou, X., Dai, X., Yao, Z., Lv, L., Jin, Y., et al., 2019b. Stoichiometry-controlled InP-based quantum dots: synthesis, photoluminescence, and electroluminescence. J. Am. Chem. Soc. 141 (16), 6448–6452.

Liang, J., Huang, Q., Hua, C., Hu, J., Chen, B., Wan, J., et al., 2019. pH—responsive nanoparticles loaded with graphene quantum dots and doxorubicin for intracellular imaging, drug delivery and efficient cancer therapy. ChemistrySelect 4 (20), 6004–6012.

Liu, P., Wang, Q., Li, X., 2009. Studies on CdSe/L-cysteine quantum dots synthesized in aqueous solution for biological labeling. J. Phys. Chem. C. 113 (18), 7670–7676.

Liu, J., Hu, R., Liu, J., Zhang, B., Wang, Y., Liu, X., et al., 2015. Cytotoxicity assessment of functionalized CdSe, CdTe and InP quantum dots in two human cancer cell models. Mater. Sci. Eng. C. 57, 222–231.

Liu, T., Li, N., Dong, J.X., Luo, H.Q., Li, N.B., 2016. Fluorescence detection of mercury ions and cysteine based on magnesium and nitrogen co-doped carbon quantum dots and implication logic gate operation. Sens. Actuators B. Chem. 231, 147–153.

Liu, L., Jiang, H., Dong, J., Zhang, W., Dang, G., Yang, M., 2020a. PEGylated MoS_2 quantum dots for traceable and pH-responsive chemotherapeutic drug delivery. Colloids Surf. B: Biointerfaces 185. Available from: https://doi.org/10.1016/j.colsurfb.2019.110590.

Liu, W., Huang, G., Su, X., Li, S., Wang, Q., Zhao, Y., et al., 2020b. Zebrafish: a promising model for evaluating the toxicity of carbon dot—based nanomaterials. ACS Appl. Mater. Interfaces 12 (43), 49012–49020.

Liu, Y., Zhao, C.H., Sabirsh, A., Ye, L.L., Wu, X.Q., Lu, H.B., et al., 2021. A novel graphene quantum dot-based mRNA delivery platform. Chem. Open. Available from: https://doi.org/10.1002/open.202000200.

Lobo, F.A., Santos, T., Vieira, K.M., Osorio, V.M., Taylor, J.G., 2015. Determination of formaldehyde in hair creams by gas chromatography-mass spectrometry. Drug. Test. Anal. 7, 848–852.

Misra, R.D., 2008. Quantum dots for tumor-targeted drug delivery and cell imaging. Nanomedicine 3 (3). Available from: https://doi.org/10.2217/17435889.3.3.271.

Mondal, M.K., Mukherjee, S., Joardar, N., Roy, D., Chowdhury, P., Sinha Babu, S.P., 2019. Synthesis of smart graphene quantum dots: a benign biomaterial for prominent intracellular imaging and improvement of drug efficacy. Appl. Surf. Sci. 495. Available from: https://doi.org/10.1016/j.apsusc.2019.143562.

Murugan, N., Prakash, M., Jayakumar, M., Sundaramurthy, A., Sundramoorthy, A.K., 2019. Green synthesis of fluorescent carbon quantum dots from eleusine coracana and their application as a fluorescence 'turn-off' sensor probe for selective detection of Cu^{2+}. Appl. Surf. Sci. 476, 468–480.

Nasrollahi, F., Sana, B., Paramelle, D., Ahadian, S., Khademhosseini, A., Lim, S., 2020. Incorporation of graphene quantum dots, iron, and doxorubicin in/on ferritin nanocages for bimodal imaging and drug delivery. Adv. Ther. 3 (3). Available from: https://doi.org/10.1002/adtp.201900183.

Ng, O.T., Wong, Y., Chan, H.M., Cheng, J., Qi, X., Chan, W.H., et al., 2013. N-Acetyl-l-cysteine capped quantum dots offer neuronal cell protection by inhibiting beta (1–40) amyloid fibrillation. Biomater. Sci. 1 (6), 577–580.

Nikazar, S., Sivasankarapillai, V.S., Rahdar, A., Gasmi, S., Anumol, P.S., Shanavas, M.S., 2020. Revisiting the cytotoxicity of quantum dots: an in- depth overview. Biophys. Rev. 12 (3), 703–718.

Niu, H., Yang, X., Wang, Y., Li, M., Zhang, G., Pan, P., et al., 2020. Electroluminescence detection of sunset yellow by graphene quantum dots. Front. Chem. 8. Available from: https://doi.org/10.3389/fchem.2020.00505.

Palit, S., 2020. Frontiers of applications of nanotechnology in biological sciences and green chemistry. In: Dake, S.A., Shinde, R.S., Ameta, S.C., Haghi, A.K. (Eds.), Green Chemistry and Sustainable Technology: Biological, Pharmaceutical and Macromolecular Systems, first ed. CRC Press/Taylor & Francis Group; Apple Academic Press, New York, p. 25.

Pandey, A., Kalal, S., Ameta, C., Ameta, R., Kumar, S., Punjabi, P.K., 2015. Synthesis, characterization and application of naïve and nano-sized titanium dioxide as photocatalyst for degradation of methylene blue. J. Saudi Chem. Soc. 19 (5), 528–536.

Pang, C., Han, S., Li, Y., Zhang, J., 2018. Graphene quantum dot-enhanced chemiluminescence through energy and electron transfer for the sensitive detection of tyrosine. J. Chin. Chem. Soc. 65 (12), 1504–1509.

Perini, G., Palmieri, V., Ciasca, G., De Spirito, M., Papi, M., 2020. Unravelling the potential of graphene quantum dots in biomedicine and neuroscience. Int. J. Mol. Sci. 21 (10). Available from: https://doi.org/10.3390/ijms21103712.

Plaza, D.O., Gallardo, C., Straub, Y.D., Bravo, D., Perez-Donaso, J.M., 2016. Biological synthesis of fluorescent nanoparticles by cadmium and tellurite resistant Antarctic bacteria: exploring novel natural nanofactories. Microb. Cell Fact. 15 (76). Available from: https://doi.org/10.1186/s12934-016-0477-8.

Pramanik, S., Hill, S.K., Zhi, B., Hudson-Smith, N.V., Wu, J.J., White, J.N., et al., 2018. Comparative toxicity assessment of novel Si quantum dots and their traditional Cd-based counterparts using bacteria models *Shewanellaoneidensis* and *Bacillus subtilis*. Environ. Sci. Nano 5 (8), 1890–1901.

Qian, C., Yan, P., Wan, G., Liang, S., Dong, Y., Wang, J., 2018. Facile synthetic photoluminescent graphene quantum dots encapsulated β-cyclodextrin drug carrier system for the management of macular degeneration: detailed analytical and biological investigations. J. Photochem. Photobiol. B: Biol. 189, 244–249.

Qiu, J., Zhang, R., Li, J., Sang, Y., Tang, W., Gil, P.R., et al., 2015. Fluorescent graphene quantum dots as traceable, ph-sensitive drug delivery systems. Int. J. Nanomed. 10, 6709–6724.

Qu, Z., Liu, L., Sun, T., Hou, J., Sun, Y., Yu, M., et al., 2020. Synthesis of bifunctional carbon quantum dots for bioimaging and anti-inflammation. Nanotechnology 31 (17). Available from: https://doi.org/10.1088/1361-6528/ab6b9d.

Rai, S., Singh, B.K., Bhartiya, P., Singh, A., Kumar, H., Dutta, P.K., et al., 2017. Lignin derived reduced fluorescence carbon dots with theranostic approaches: nano-drug-carrier and bioimaging. J. Lumin. 190, 492–503.

Rasoulzadeh, F., Amjadi, M., 2021. The chemiluminescence of $AgInS_2$ quantum dots and its application as a sensing platform for glutathione assay. J. Photochem. Photobiol. A: Chem. 420. Available from: https://doi.org/10.1016/j.jphotochem.2021.113493.

Rathi, K., Pal, K., 2020. Ruthenium-decorated tungsten disulfide quantum dots for a CO_2 gas sensor. Nanotechnology 31 (13). Available from: https://doi.org/10.1088/1361-6528/ab5cd3.

Ray, P.C., Yu, H., Fu, P.P., 2009. Toxicity and environmental risks of nanomaterials: challenges and future needs. J. Environ. Sci. Health C. Envirom. Ecotoxicol. Rev. 27 (1). Available from: https://doi.org/10.1080/10590500802708267.

Ruzycka-Ayoush, M., Kowalik, P., Kowalczyk, A., Bujak, P., Nowicka, A.M., Wojewodzka, M., et al., 2021. Quantum dots as targeted doxorubicin drug delivery nanosystems. Cancer Nanotechnol. 12 (1). Available from: https://doi.org/10.1186/s12645-021-00077-9.

Sahub, C., Tuntulani, T., Nhujak, T., Tomapatanaget, B., 2018. Effective biosensor based on graphene quantum dots via enzymatic reaction for directly photoluminescence detection of organophosphate pesticide. Sens. Actuat. B: Chem. 258, 88–97.

Samantara, A.K., Maji, S., Ghosh, A., Bag, B., Dash, R., Jena, B.K., 2016. Good's buffer derived highly emissive carbon quantum dots: excellent biocompatible anticancer drug carrier. J. Mater. Chem. B. 4 (14), 2412–2420.

Sangam, S., Gupta, A., Shakeel, A., Bhattacharya, R., Sharma, A.K., Suhag, D., 2018. Sustainable synthesis of single crystalline sulphur-doped graphene quantum dots for bioimaging and beyond. Green. Chem. 20, 4245–4259.

Shahid, S., Mohiyuddin, S., Packirisamy, G., 2020. Synthesis of multi-color fluorescent carbon dots from mint leaves: a robust bioimaging agent with potential antioxidant activity. J. Nanosci. Nanotechnol. 20 (10), 6305–6316.

Shan, J., Li, R., Yan, K., Zhu, Y., Zhang, J., 2016. In situ anodic stripping of Cd (II) from CdS quantum dots for electrochemical sensing of ciprofloxacin. Sens. Actuators B: Chem. 237, 75–80.

Shao, D., Zeng, Q., Fan, Z., Li, J., Zhang, M., Zhang, Y., et al., 2012. Monitoring HSV-TK/ganciclovir cancer suicide gene therapy using CdTe/CdS core/shell quantum dots. Biomaterials 33 (17), 4336–4344.

Shao, D., Li, J., Xiao, X., Zhang, M., Pan, Y., Li, S., et al., 2014. Real-time visualizing and tracing of HSV-TK/GCV suicide gene therapy by near-infrared fluorescent quantum dots. ACS Appl. Mater. Interf. 6 (14), 11082–11090.

Smith, W.E., Brownell, J., White, C.C., Afsharinejad, Z., Tsai, J., Hu, X., et al., 2012. In vitro toxicity assessment of amphiphillic polymer-coated CdSe/ZnS quantum dots in two human liver cell models. ACS Nano 6 (11), 9475–9484.

Solanki, M.N., Benjamin, S., Ameta, S.C., 2018. Nanomaterials. In: Ameta, S.C., Ameta, R., Ameta, G. (Eds.), Sonochemistry: An Emerging Green Technology. CRC Press/Taylor & Francis Group; Apple Academic Press, Boca Raton, p. 37.

Sonthanasamy, R.S.A., Ahmad, W.Y.W., Fazry, S., Hassan, N.I., Lazim, A.M., 2016. Transformation of crystalline starch nanoparticles into highly luminescent carbon nanodots: toxicity studies and their applications. Carbohydr. Polym. 137, 488–496.

Su, W., Guo, R., Yuan, F., Li, Y., Li, X., Zhang, Y., et al., 2020. Red-emissive carbon quantum dots for nuclear drug delivery in cancer stem cells. J. Phys. Chem. Lett. 11 (4), 1357–1363.

Sun, H., Wu, L., Wei, W., Qu, X., 2013. Recent advances in graphene quantum dots for sensing. Mater. Today 16 (11), 433–442.

Tadyszak, K., Wychowaniec, J.K., Litowczenko, J., 2018. Biomedical applications of graphene-based structures. Nanomaterials 8 (11). Available from: https://doi.org/10.3390/nano8110944.

Tan, L., Wan, A., Li, H., 2013. Ag_2S quantum dots conjugated chitosan nanospheres toward light-triggered nitric oxide release and near-infrared fluorescence imaging. Langmuir 29 (48), 15032−15042.

Tang, Y.-M., Junaid, M., Niu, A., Deng, S., Pei, D.-S., 2017. Diverse toxicological risks of PAHs in surface water with an impounding level of 175m in the three Gorges Reservoir Area. Chin. Sci. Total. Environ. 580, 1085−1096.

Thovhogi, N., Sibuyi, N.R.S., Onani, M.O., Meyer, M., Madiehe, A.M., 2018. Peptide-functionalized quantum dots for potential applications in the imaging and treatment of obesity. Int. J. Nanomed. 13, 2551−2559.

Vahid, B., Hassanzadeh, J., Khodakarami, B., 2019. CdSe quantum dots-sensitized chemiluminescence system and quenching effect of gold nanoclusters for cyanide detection. Spectrochim. Acta Part. A: Mol. Biomol. Spectrosc. 212, 322−329.

Wang, Z., Xia, J., Zhou, C., Via, B., Xia, Y., Zhang, F., 2013a. Synthesis of strongly green-photoluminescent graphene quantum dots for drug carrier. Colloid. Surf. B 112, 192−196.

Wang, Y., Zhang, L., Liang, R.-P., Bai, J.-M., Qiu, J.-D., 2013b. Using graphene quantum dots as photoluminescent probes for protein kinase sensing. Anal. Chem. 85 (19), 9148−9155.

Wang, X.J., Sun, X., Lao, J., He, H., Cheng, T.T., Wang, M.Q., et al., 2014. Multifunctional graphene quantum dots for simultaneous targeted cellular imaging and drug delivery. Colloid Surf. B 122, 638−644.

Wang, S., Cole, I.S., Li, Q., 2016. The toxicity of graphene quantum dots. RSC Adv. 6 (92), 89867−89878.

Wang, Z., Ciacchi, L.C., Wei, G., 2017. Recent advances in the synthesis of graphene-based nanomaterials for controlled drug delivery. Appl. Sci. 7 (11). Available from: https://doi.org/10.3390/app7111175.

Wang, Y., He, L., Yu, B., Chen, Y., Shen, Y., Cong, H., 2018. ZnO quantum dots modified by pH-activated charge-reversal polymer for tumor targeted drug delivery. Polymers 10 (11). Available from: https://doi.org/10.3390/polym10111272.

Wang, D., Liang, Y., Su, Y., Shang, Q., Zhang, C., 2019a. Sensitivity enhancement of cloth-based closed bipolar electroluminescence glucose sensor via electrode decoration with chitosan/multi-walled carbon nanotubes/graphene quantum dots-gold nanoparticles. Biosens. Bioelectron. 130, 55−64.

Wang, Y., Xu, N., He, Y., Wang, J., Wang, D., Gao, Q., et al., 2019b. Loading graphene quantum dots into optical-magneto nanoparticles for real-time tracking in vivo. Mater. (Basel) 12 (13). Available from: https://doi.org/10.3390/ma12132191.

Wang, L.H., Bu, Y.M., Liu, Y., Yao, Y.P., Yang, Z.F., Chen, P., 2020. A strategy for microwave-controlled release of anticancer drugs: $(Fe_3O_4/nGO)@mSiO_2/GQDs$ nanocomposite carrier jointly enhanced by nGO and GQDs. Nano 15 (6). Available from: https://doi.org/10.1142/S179329202050071X.

Wei, M., Lin, P., Chen, Y., Lee, J.Y., Zhang, L., Li, F., et al., 2020. Applications of ion level nanosensors for neuroscience research. Nanomedicine 15 (29), 2871−2881.

Weng, C.I., Chang, H.T., Lin, C.H., Shen, Y.W., Unnikrishnan, B., Li, Y.J., et al., 2015. One-step synthesis of biofunctional carbon quantum dots for bacterial labeling. Biosens. Bioelectron. 68. Available from: https://doi.org/10.1016/j.bios.2014.12.028.

Wolcott, A., Gerion, D., Visconte, M., Sun, J., Schwartzberg, A., Chen, S., et al., 2006. Silica-coated CdTe quantum dots functionalized with thiols for bioconjugation to IgG proteins. J. Phys. Chem. B. 110 (11), 5779−5789.

Wu, P.J., Ou, K.L., Chen, J.K., Fang, H.P., Tzing, S.H., Lin, W.X., et al., 2014. Methotrexate-conjugated $AgInS_2$/ZnS quantum dots for optical imaging and drug delivery. Mater. Lett. 128, 412–416.

Wu, D., Liu, Y., Wang, Y., Hu, L., Ma, H., Wang, G., et al., 2016. Label-free electroluminescent immunosensor for detection of prostate specific antigen based on aminated graphene quantum dots and carboxyl graphene quantum dots. Sci. Rep. 6. Available from: https://doi.org/10.1038/srep20511.

Wychowaniec, J.K., Iliut, M., Zhou, M., Moffat, J., Elsawy, M.A., Pinheiro, W.A., et al., 2018. Designing peptide/graphene hybrid hydrogels through fine-tuning of molecular interactions. Biomacromolecules 19 (7), 2731–2741.

Xiang, Y., Liu, X., Mao, C., Liu, X., Cui, Z., Yang, X., et al., 2018. Infection-prevention on Ti implants by controlled drug release from folic acid/ZnO quantum dots sealed titania nanotubes. Mater. Sc. Eng. C. 85, 214–224.

Xiao, A., Wang, C., Chen, J., Guo, R., Yan, Z., Chen, J., 2016. Carbon and Metal Quantum Dots toxicity on the microalgae Chlorella pyrenoidosa. Ecotoxicol. Environ. Safe 133, 211–217.

Xie, R., Wang, Z., Zhou, W., Liu, Y., Fan, L., Li, Y., et al., 2016. Graphene quantum dots as smart probes for biosensing. Anal. Methods 8 (20), 4001–4016.

Xu, S., Li, D., Wu, P., 2015. One-pot, facile, and versatile synthesis of monolayer MoS_2/WS_2 quantum dots as bioimaging probes and efficient electrocatalysts for hydrogen evolution reaction. Adv. Funct. Mater. 25 (7), 1127–1136.

Xu, Q., Ding, L., Wen, Y., Yang, W., Zhou, H., Chen, X., et al., 2018. High photoluminescence quantum yield of 18.7% by using nitrogen-doped Ti_3C_2MXene quantum dots. J. Mater. Chem. C. 6 (24), 6360–6369.

Xue, B., Yang, Y., Sun, Y., Fan, J., Li, X., Zhang, Z., 2019. Photoluminescent lignin hybridized carbon quantum dots composites for bioimaging applications. Int. J. Biol. Macromol. 122, 954–961.

Xue, D., Zou, W., Liu, D., Li, L., Chen, T., Yang, Z., et al., 2022. Cytotoxicity and transcriptome changes triggered by $CuInS_2$/ZnS quantum dots in human glial cells. Neurotoxicology 88, 134–143.

Yahyai, I.A., Hassanzadeh, J., Al-Lawati, H.A.J., 2021. A novel and selective multi-emission chemiluminescence system for the quatification of delthamethrin in food samples. Sens. Actuat. B: Chem. 327. Available from: https://doi.org/10.1016/j.snb.2020.128927.

Yan, M., Zhang, Y., Xu, K., Fu, T., Qin, H., Zheng, X., 2011. An in vitro study of vascular endothelial toxicity of CdTe quantum dots. Toxicology 282 (3), 94–103.

Ye, S., Yu, M., Yan, W., Song, J., Qu, J., 2017. Enhanced photoluminescence of $CsPbBr_3$@ Ag hybrid perovskite quantum dots. J. Mater. Chem. C. 5 (32), 8187–8193.

Zhang, Q., Wu, Z., Li, N., Pu, Y., Wang, B., Zhang, T., et al., 2017. Advanced review of graphene-based nanomaterials in drug delivery systems: synthesis, modification, toxicity and application. Mater. Sci. Eng. C. 77, 1363–1375.

Zhao, C., Song, X., Liu, Y., Fu, Y., Ye, L., Wang, N., et al., 2020. Synthesis of graphene quantum dots and their applications in drug delivery. J. Nanobiotechnol. 18 (142). Available from: https://doi.org/10.1186/s12951-020-00698-z.

Zor, E., Morales-Narváez, E., Zamora-Gálvez, A., Bingol, H., Ersoz, M., Merkoçi, A., 2015. Graphene quantum dots—based photoluminescent sensor: a multifunctional composite for pesticide detection. ACS Apple. Mater. Interf. 7, 20272–20279.

Chapter 12

Application of quantum dots in solar cells

Shwetharani R[1], Chandan Hunsur Ravikumar[1,2], M.S. Jyothi[3] and R. Geetha Balakrishna[1]

[1]Centre for Nano and Material Sciences, Jain University, Bengaluru, Karnataka, India, [2]Pilot Plant Development and Training Institute, King Mongkut's University of Technology Thonburi, Thakam, Bangkok, Thailand, [3]Department of Chemistry, AMC Engineering College, Bengaluru, Karnataka, India

12.1 Introduction

The limited availability of fossil fuels and global warming are demanding the use of renewable energy. The potential of solar energy as an alternative for fossil fuels has been investigated over the past half century and its reliability along with marketability is understood thoroughly. The 4.3×10^{20} J h^{-1} of energy known to reach Earth from the Sun is sufficient to accomplish the annual energy consumption of Earth, 4.1×10^{20} J (Lewis and Crabtree, 2005). Highly efficient and low-cost solar cells were introduced to collect solar energy. Here, the photovoltaic cells (PVs) convert the solar energy into electrical and chemical energies (Kazacos et al., 1980). The first kind of solar cells were of p-n junction technology and Schottky barrier, which adopt the PV characteristics of appropriate semiconductor (Badawy et al., 1990). The best example is Si (Badawy and El-Dessouki, 1985; Decker et al., 1983).

Launching with Si-single crystals, and proceeding to bulk polycrystalline silica wafers, these cells are considered as first-generation cells. A 12%–16% conversion efficiency has been achieved for these cells and these are marketed widely, where the principle of energy storage is lead-acid batteries (Sharma et al., 2015). The second-generation solar cells evolved with the science of thin films. Si-wafers, CdTe, a-Si, $CuInSe_2$, and CdS are the key candidates for thin-film solar cells. In comparison with the first-generation solar cells, these thin-film solar cells presented a cost-efficient engineering process in association with integrated lower temperature progressions for the insulation of cells. Besides the use of flexible substrates helped to spread their

Quantum Dots. DOI: https://doi.org/10.1016/B978-0-12-824153-0.00012-4

accessibility for a wide spectra of applications. A conversion efficiency of nearly 20% was achieved for combination PVs such as CIGS (Cu/In/Ga/Se) (Schock and Noufi, 2000; Wada et al., 2001; Kaelin et al., 2004). However, due to the lesser stability, the thin-film solar cells shared a lower market and the efforts of researchers into improved versions of PVs were anticipated. A combination of polymers and semiconductors came into existence, where polymers were doped to form Schottky barriers (Amani-Ghadim et al., 2022; Gamboa et al., 1998). Nonetheless, the lower conversion efficiency restricted their practice.

An association of nanoscience, nanotechnology, and surface science resulted in sustainable energy conversions and consideration for third generation solar cells. Nanocrystals and nanoporous materials are employed to increase the efficiency as well as stability of solar cells. Attention to catalysts and light harvesting materials such as TiO_2, quantum dots, and many other nanocomposites has been increased to work on the nanostructured solar cells to bring out the breakthrough potentials. This chapter deals with the exercise on fabrication and advancements in one of such nanostructured materials, QDs involved solar cells.

QDs are the semiconductor clusters of nanoscale and are known for their extraordinary optoelectronic properties. The size-dependent quantum physical features of QDs present tunable optoelectronic properties attributed to the production of electron−hole pairs, which extend their use in solar cells. The cells also offer a tunable bandgap to match with the wavelength of illuminating light to generate more electricity (Badawy, 1993). QDs pose a simple method of synthesis and are economically feasible. The remarkable excitation coefficients and wide adsorption spectra depending on their size are attractive features for PV applications. The carrier multiplication phenomenon in QDs demonstrating the generation of more than one electron for an adsorption of one electron at broader wavelength spectra results in higher quantum efficiencies of QDs sensitized solar cells (QDSSCs) (Nozik, 2002; Sambur et al., 2010). This phenomenon is known as multiple exciton generation (MEG).

12.1.1 Basic structure of quantum dot sensitized solar cells

An elementary structure of QDSSCs is given in Fig. 12.1.

The key structure involves four major portions:

- photoanode;
- sensitizer, which is QD;
- electrolyte; and
- counter electrode (CE).

A photoanode is generally a semiconducting material deposited on transparent substrate and is usually a fluorine-doped tin oxide (FTO) and or

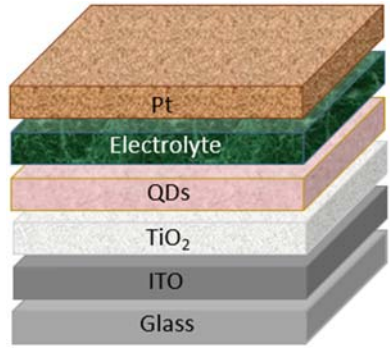

FIGURE 12.1 Primary structure of QDSSCs. *QDSSCs*, QD-sensitized solar cells.

indium tin oxide (ITO). FTO usually maintains the semiconducting layer and employs current collection. An ideal FTO should have higher transparency and lower electrical resistance, which allows the maximum transmittance of sunlight to facilitate an efficient charge transfer phenomena (Shin et al., 2019). The importance of a photoanode in QDSSCs is attributed to the contribution of a matrix for adsorption of QDs and it also acts as a charge transport medium, which could transport electrons from the sensitizer to the conducting oxide substrate. Photoanodes must have higher electron mobility and surface area and must not react with redox electrolytes. These ideal characteristics allow the maximum loading of QDs and reduce unwanted photon adsorption. TiO2 is considered as the best material as a photoanode due to its wider and tunable bandgap, low cost, stability, and nontoxicity, as well as its mesoporous features, higher surface area, conduction band edge, and greater electron affinity (Ahmad et al., 2017).

The second portion is a sensitizer. In QDSSCs it is QDs. QDs such as InP (Crisp et al., 2018), CdS (Vázquez et al., 2016), CdSe (Lee and Lo, 2009), Si (Hao et al., 2009), PbS (Park et al., 2019), PbSe (Zhang et al., 2014), CdTe (Badawi et al., 2013), graphene (Guo et al., 2010), $CuInS_2$ (Li et al., 2012), Bi_2S_3 (Zumeta-Dube et al., 2014), and many others have been used in QDSSCs. The QDs, which are stable upon visible light irradiation, with high adsorption efficiency and suitable bandgap energy, are the most preferred ones. These QDs are fabricated to act as sensitizers by two different methods. The first one is a successive ionic layer adsorption reaction (SILAR) method, and it is an example for in situ fabrication (Yang et al., 2015a,b). The other is a linker-assisted assembly method and it is an example for ex situ fabrication (Li and Zhong, 2015). However, in situ methods have shown improved performance (Bhambhani, 2018).

The third major part is a redox electrolyte, which transfers the charges between photoanodes and CEs and aids the restoration of oxidized QDs (Wu et al., 2015). These are also called hole conductors. As Cd chalcogenides

QDs are not stable in an iodide/triiodide electrolyte system, this system is most commonly practiced with an addition of suitable organic solvents (Yella et al., 2011). Several efforts have been tried out to stabilize the polysulfide electrolyte systems to avoid the leaching of QDs and the protective films have been coated (Shalom et al., 2009). Yet, the overall performance of the cell remained insignificant with just 3% of power conversion efficiency. However, polysulfide redox system (S_2/Sn^{2-}) is used instead with greater challenges like high redox potential (Hod and Zaban, 2014). To overcome this challenge, scientist have tried to control the concentration of polysulfide (Liao et al., 2015), varied solvent systems (Li et al., 2011), coupling with additives such as poly(vinyl pyrrolidone) (PVP) (Jiang et al., 2016), SiO_2 (Wei et al., 2016a), guanidine thiocyanate (Chou et al., 2011), etc. The research has been also concentrated on using a material that possesses lower redox potential like Mn poly(pyrazolyl) borate (Haring et al., 2014). Besides, the toxicity of liquid electrolytes vapor is another challenge, which arises due to leakage of solvents due to their lower boiling points. This aids to degradation of solvents and reduces the durability of the solar system. Hence solid-state electrolytes and/or quasisolid-state electrolytes are used as a substitute for liquid ones (Yu et al., 2010; Huo et al., 2015; Feng et al., 2016). Poly(ethylene oxide)/poly(vinylidene fluoride) (Yang and Wang, 2015), PVP (Jiang et al., 2016), and P3HT (poly-3-hexylthiophene) (Shaw et al., 2008) are the accomplished solid electrolytes. Some hydrogels (Zhang et al., 2017), ionic liquids (Jovanovski et al., 2011), and gels (Kim et al., 2014) are used as quasisolid-state electrolytes.

The last major portion is the CE, which allows the movement of electrons from therexternal circuit to electrolytes and also acts as a catalyst in reducing the oxidized electrolyte. The reduction reaction takes place at the interface of electrolyte and CE. For an ideal CE, the material must be highly electrical conductive with great electrocatalytic activity and also stability. Platinum is the widely used CE for QDSSCs with an electrolyte system of iodide/triiodide. But for a polysulfide system, the conversion efficiency decreased as the sulfur atoms are likely to adsorb on Pt. To overcome this, metal chalcogenides (Meng et al., 2015), many composite materials (Yang et al., 2012; Gopi et al., 2018), and also carbon-based materials (Zhang et al., 2010; Du et al., 2016) are emerging as new CEs for QDSSCs.

12.1.2 Working principle of quantum dot sensitized solar cells

QDSSCs work in a similar fashion to DSSCs. The schematic representation of the working principle of QDSSC is provided in Fig. 12.2. The photoexcitation of the sensitizer takes place with an irradiation of light. The excited electrons from QDs are transferred to the TiO_2 conduction band. These injected electrons breach through the TiO_2 nanocrystal film and reach the conducting substrate. These electrons then flow through the external circuit

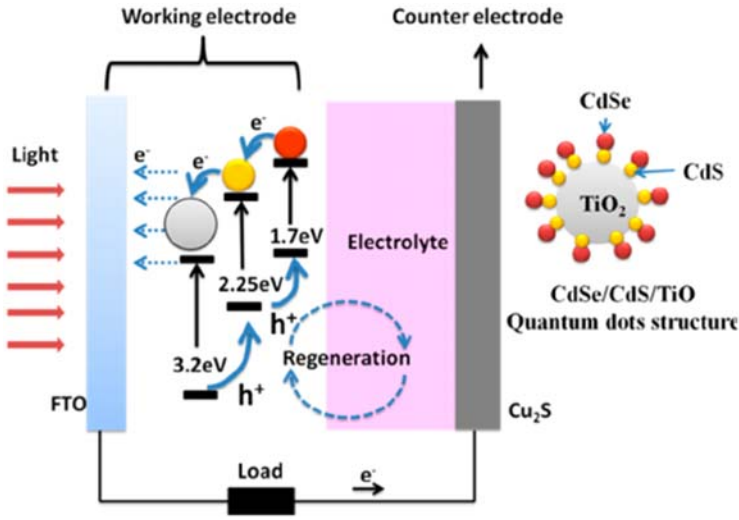

FIGURE 12.2 Working principle of QDSSCs. *QDSSCs*, QD-sensitized solar cells (Tian et al., 2012). *Adapted from Tian, J., Gao, R., Zhang, Q., Zhang, S., Li, Y., Lan, J., et al., 2012. Enhanced performance of CdS/CdSe quantum dot cosensitized solar cells via homogeneous distribution of quantum dots in TiO_2 film. J. Phys. Chem. C. 116 (35), 18655–18662. With permission.*

and reach the CE. Proceeding further, the reduction of oxidized compound of the electrolyte takes place at CE and hence the regeneration of sensitizer, that is, QDs are there for the continuing process.

12.2 Properties of quantum dots

12.2.1 Energy gap tuning

The bandgap of QDs plays a major role in QDSSCs, because an appropriate bandgap can enhance/control the photon absorption in the solar spectrum. QDs possess tunable bandgap energy, which can be tuned by varying the size of QDs because of the quantum confinement effect, which occurs in the particles having a smaller size than the exciton. QDs solution displays a different color that corresponds to the change in the particle size, which exhibits a different absorption band of light. This effect increases the bandgap along with a blueshift in photoluminescence (PL). Therefore, the selection of an appropriate absorber for designing an efficient solar cell is very important. Anttu (2015) have found that the balance limit for photon conversion efficiency in a single junction solar cell depends strongly on the bandgap of absorbing material. Literature reports that the driving force of 0.25 eV is sufficient for the electron injection into photoanode (Weller, 1991). Therefore for better electron transport, the conduction band (CB) of QDs absorber

should be 0.25 eV above the CB of the photoanode for efficient exciton dissociation and the valence band level of QDs should be lower than the redox level of the hole transporting material.

A decrease in size of CdSe QDs increases the bandgap (Fig. 12.3) and hence the emission of PL shifts from red to blue. A decrease in particle size of CdSe increases the photocurrent, attributed to the shift of the CB towards a more negative potential, which enhances the driving force for charge injection. However, the higher particle size materials shows better absorption in the visible region but the disadvantage of these materials is lower electron injection into TiO_2, unlike with small-sized QDs. Vogel et al. (1994) reported that the charge separation can be optimized through tuning the size of QDs and Kongkanand et al. (2008) demonstrated that the photoelectrochemical response and photoconversion efficiency (PCE) can be enhanced by varying the size of QDs.

The sufficiently small QD particles represent wider bandgap energy; consequently, the optical absorption and emission with regard to excitation across the bandgap shift to higher energy. Gorer and Hodes (1994) have investigated the quantum size effect in CdSe films and observed blueshift of the absorption spectra with the decrease in crystal size. This phenomenon is also reported in CdS QDs by Thambidurai et al. (2011). Jun et al. (2013) have suggested that the use of a combination of different sizes of QDs having a range of bandgaps in a solar cell may show better efficiency due to a

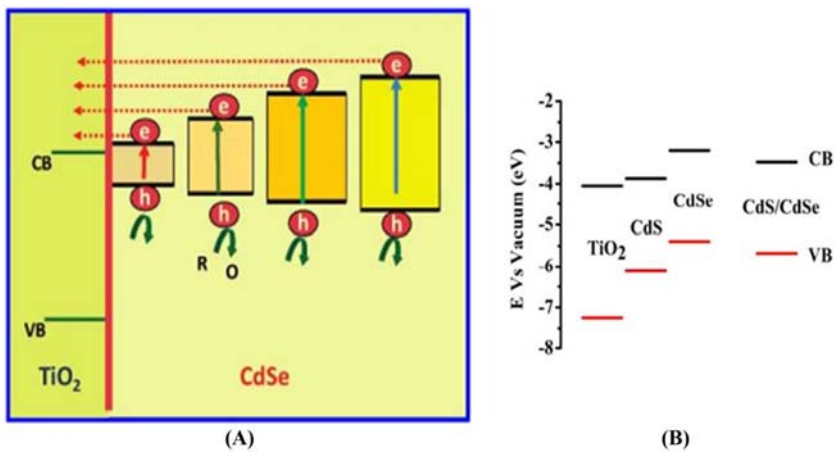

FIGURE 12.3 (A) Schematic illustration of energy band structure of different sized CdSe QDs and TiO_2. (B) Band energy of TiO_2, CdS, CdSe and co**sensitized** CdS/CdSe. *Adapted from Kongkanand, A., Tvrdy, K., Takechi, K., Kuno, M., Kamat, P. V., 2008. Quantum dot solar cells. Tuning photoresponse through size and shape control of CdSe − TiO_2 architecture. J. Am. Chem. Soc. 130 (12), 4007–4015; (B) Esparza, D., Zarazúa, I., López-Luke, T., Cerdán-Pasarán, A., Sánchez-Solís, A., Torres-Castro, A., et al., 2015. Effect of different sensitization technique on the photoconversion efficiency of CdS quantum dot and CdSe quantum rod sensitized TiO_2 solar cells. J. Phys. Chem. C. 119 (24), 13394–13403. With permission.*

wider absorption of light. Esparza et al. (2015) have sensitized two different QDs with a varied range of light absorption on TiO_2 and demonstrated that the PCE for CdS/CdSe (PCE = 4.7%) is higher than CdS alone (PCE = 2.5%), which are prepared by SILAR (CdS), electrophoretic deposition (CdSe), and pipetting (CdSe) methods, respectively. The use of different kinds of QDs sensitizers is a promising technique to enhance the light absorption wavelength region, increase electron injection, and also enhance the charge transport, which improves the photon conversion efficiency.

12.2.2 Multiple exciton generation

The effectual formation of more than one photoinduced electron−hole (e^-−h^+) pair upon absorption of a single photon is potentially important for the development of optoelectronic devices (photovoltaic and photoelectrochemical cells), which convert solar radiation (energy) into electricity. In some cases, stored chemical potential is there in solar-derived fuels like hydrogen, alcohols, and hydrocarbons. Several workers explain the dynamics of such a conversion process (Hanna and Nozik, 2006; Klimov, 2006). The conversion process increases because of the excess kinetic energy of the electrons and holes that are produced by the absorption of photons in a cell, with the energies above the bandgap energy for absorption, and can create additional e^- /h^+ pairs with at least the twice the bandgap energy (Nozik, 2008). The additional e^- /h^+ pair is created by the bandgap in a semiconductor and HOMO−LUMO energy difference in molecular systems. These extra e^- /h^+ pair can be separated, transported, and collected to yield higher photocurrent in the cells. In such a process, the excess kinetic energy is converted to heat and can become unavailable for conversion into electrical free energy, thus limiting the cell to achieve the maximum thermodynamic conversion efficiency. The hot carrier and relaxation of electrons in semiconductor is shown in Fig. 12.4. The creation of the (e^- - h^+) pair, which absorbs the proton, has been studied for over 50 years in bulk semiconductors. It has also been observed in photocurrent of bulk p-n junctions in Si, PbS, PbSe, PbTe, and InSb, and in these systems, they are termed as impact ionization (Tauc, 1959; Vavilov, 1959; Beattie, 1962; Christensen, 1976; Kolodinski et al., 1993). Nevertheless, the impact of ionization is not an effective process in bulk semiconductors and may require more multiples of photoenergy for threshold absorption of energy. For an Si-based semiconductor PV, which is dominant in the present-day photovoltaic market, impact ionization does not become significant until the incident photons energy exceeds 3.5 eV. This energy is an ultraviolet energy threshold, which is beyond the photon energies present in the solar spectrum. Even with absorption of 5 eV photons, impact ionization only generates a quantum yield (QY) of 1.3. Hence it is not a meaningful approach to increase the efficiency of conventional bulk Si PV with impact ionization.

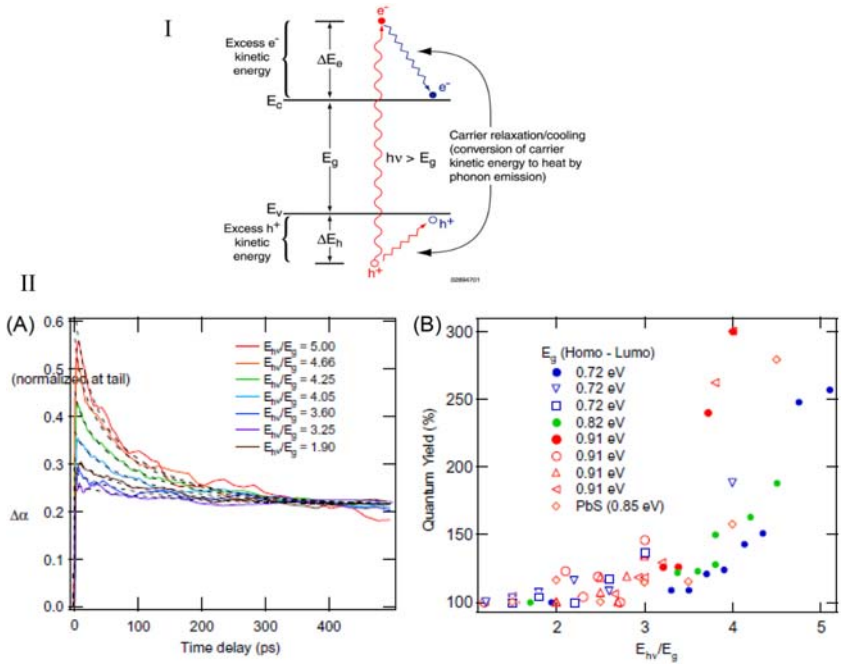

FIGURE 12.4 (I) Hot carrier relaxation/cooling in semiconductors. (II) (A) Exciton population decay dynamics obtained by probing intraband (intraexciton) transitions in the mid-IR at 5.0 μm for a sample of 5.7 nm diameter PbSe QDs, and (B) QY for exciton formation from a single photon versus photon energy expressed as the ratio of the photon energy to the QD bandgap (HOMO−LUMO energy) for three PbSe QD sizes and one PbS (dia. = 3.9, 4.7, 5.4, and 5.5 nm, respectively, and Eg = 0.91, 0.82, 0.73, and 0.85 eV, respectively). Solid symbols indicate data acquired using mid-infrared probe; open symbols indicate band edge probe energy. Quantum yield results were independent of the probe energy utilized (Beard et al., 2015). *Adapted (I) from Beard, M. C., Johnson, J. C., Luther, J. M., Nozik, A. J., 2015. Multiple exciton generation in quantum dots vs singlet fission in molecular chromophores for solar photon conversion. Phil. Trans. R. Soc. A: Maths, Phys. Eng. Sci. 373 (2044), doi: 10.1098/rsta.2014.0412.; (II) Ellingson, R. J., Beard, M. C., Johnson, J. C., Yu, P., Micic, O. I., Nozik, A. J., et al., 2005. Highly efficient multiple exciton generation in colloidal PbSe and PbS quantum dots. Nano Lett. 5 (5), 865−871. With permission.*

On the other side, the semiconductor nanocrystals (QDs) generating the multiple (e^- /h^+) pairs from a single photon are more efficient. The threshold photons required to generate become more efficient and such photon energy for the same process generates two (e^- /h^+) pairs per photon absorbed, which can approach values as low as twice the threshold energy for the absorption. In QDs, the rate of Auger recombination including the inverse Auger process of MEG can be increased. The enhancement is due to the carrier confinement and this correspondingly increases the (e^- /h^+) coulomb interaction with a time scale reported to be more than 100 fs (Ellingson

et al., 2005; Shabaev et al., 2006). The rate of velocity of generation of MEG is much faster than the hot exciton cooling rate produced during the process of recombination and thus MEG can be become more efficient. However, Nozik (2001) noted that crystal momentum is not a good quantum number and momentum need not to be conserved. This allows the threshold photon energy to generate two (e^- /h^+) pairs per photon absorbed. Lowering the threshold to absorb more photons would lower the kinetic energy lost due to heat and reflection. This allows the solar spectrum to contribute more photons with a particular ideal or particular bandgap of the material, which could possibly enhance the MEG.

MEG has been detected by several spectroscopic techniques and is consistent (Schaller and Klimov, 2004; Ellingson et al., 2005; Schaller et al., 2005). The first method is by using transient absorption spectroscopy, which measures with respect to time (can measure from femto to microsecond transition). It can measure the data from delays as low as 5 ps, by which in some material, the carrier multiplication and cooling are complete and probe pulse is catechizing the exciton population at their lowest possible state (band edges) (Schaller et al., 2006). It also monitors the interband bleach dynamics with excitation across the QD bandgap. In the other set of experiments, probe pulse is in mid-IR and monitors the interband transitions of the new excitons that are created. The peak magnitude of the initial time induced photon absorption change is created by the pump pulse and the Auger decay dynamics of the generated excitons and it is equal to the number of excitons generated. The dynamics of the mid IR interband absorptions are monitored after the pump pulse. Fig. 12.4B gives the excitation decay probing interband transition of PbSe QDs.

The exciton multiplication was first reported and presented by Schaller and Klimov (2004) for PbSe QDs. They showed that an excitation energy threshold for the efficient formation of two excitons per photon at 3 Eg, where Eg is the absorption energy gap of the QDs (HOMO-LUMO transition energy) commonly called bandgap in QDs. They also reported that the QY of 218% (118% Impact Ionization (I.I.) efficiency) at 3.8 Eg, and value of QYs above 200% indicates the formation of more than two excitons per photon absorbed. The research group from NREL (Ellingson et al., 2005) reported QY of 300% for 3.9 nm QDs at a photon energy of 4 Eg. This indicated that there is formation of three excitons per photon absorbed for every photoexcited QDs in the sample. They have also shown that the threshold Eg of MEG by optical excitation is 2 Eg. It was also revealed that efficient MEG occurs in PbS (Ellingson et al., 2005) and PbTe QDs (Murphy et al., 2006). MEG is also seen in other types QDs such as CdS, CdSe, CdTe, ZnS, ZnSe, CdSe/CdS, CdSe/CdTe, and CdTe/ZnS but it is not limited to these only. These core−shell type of QDs mentioned not only gives the stability to the core but also stabilizes the generation of MEG.

12.3 Synthesis of quantum dots

12.3.1 Chalcogenide quantum dots

The synthesis of QDs took a rapid phase of development from its discovery by Alexy Emikov (Ekimov and Onushchenko, 1981) in a glass matrix. It took almost a decade to synthesize these in a stable colloidal form by Murray et al. (1993). There are mainly two ways to synthesize the QDs and these are: (1) solution phase synthesis (colloidal route) and (2) vapor phase synthesis. The solution phase synthesis involves the hot injection method, where the precursor is injected into the hot solution of another precursor. This development in technique led to improved QD photophysical properties such as quantum confinement, reproducibility, and size-tunable PL. The main advantage of the colloidal method is that it uses injection and growth temperature to control the QD particle size. It is well known that nucleation and growth of the QDs depends on the time and temperature of the colloidal precursor solution, which can be controlled (Chandan and Geetha, 2013; Chandan et al., 2014). This led to the development of QDs such as CdSe, CdS, CdTe, ZnSe, and ZnS. This enhancement of photophysical properties with stability of QDs marked their presence and importance in photovoltaics, energy, biosensors, and bioimaging (D'Souza et al., 2015; Venkataramana et al., 2016; Kusuma et al., 2019; Ravikumar et al., 2019, 2020). Apart from these QDs, near infrared emitting QDs are InP, InAs, and other lead and copper chalcogenides (Micic et al., 1994, 1995; Allen and Bawendi, 2008; Tan et al., 2017).

The stable CdSe colloidal QDs were first synthesized and reported by Murray et al. (1993). They were the first to report the use of TOPO/TOP (Trioctyl phosphine oxide/Trioctyl phosphine) as a coordinating and stabilizing agent. They were successfully able to synthesize group II−VI QDs with PL. But this technique was plagued by Ostwald's ripening. To overcome this, Katari et al. (1994) replaced TOP with tributylphosphine, which allowed spontaneous nucleation with a relatively slow rate of growth; incidentally increasing the stability of the QDs with TOPO as capping agent. $CdMe_2$ was used previously as the precursor for the synthesis of QDs and needed to be replaced due to their pyrophoric and toxic nature. Peng and Peng (2001) solved this problem with use of less toxic CdO (cadmium oxide) along with a long-chain fatty acid, oleic acid. This reduced the use of the toxic phosphine derivative, paving the way for much greener solvents for the synthesis. Chandan et al. (2014) reported the use of more environment-friendly ligands such as oleic acid and octadecyl amine as growth and nucleating ligands for CdSe synthesis. They investigated the effect of these ligands on the nucleation and growth of CdSe QDs and found these were stable over months. Such QDs with increased stability are better suited for photovoltaic application, keeping in the mind that it has to be exposed to an outdoor

environment. QDs were also synthesized in an aqueous solution of respective salts. Even though, there are several research reports on such synthesis, they lack stability and better confinement is not possible due to an elongated reaction time. Some reactions can be as long as 6 days, which can lead to polydispersed QDs.

Electron−hole pair recombination and leaching is the main concern in QDs, which affects the performance and stability of the device. This can be mitigated by forming the shell structure or inserting the dopant on the surface of the core QDs structure. Such an introduction can reduce recombination and increase the stability. Thus plain core QDs (CdSe, CdS, ZnS and CdTe) have countered comparatively less attention than core−shell structures such as CdSe/CdS, CdSe/ZnS, CdTe/CdS, etc. but it is not limited to these only. The thickness of the shell can be monitored and controlled by varying the same ligand used by monitoring the injection time, concentration of the shell precursor, and capping material used (Zhu et al., 2010a,b). CdSe/CdZnS QDs were reported by Schrier et al. (2012) and the maximum QY was 100%, which is the highest reported QY for the chalcogenide series of QDs. If the shell coating on the core is smaller, then it can lead to complete transmittance of electromagnetic radiation (light) through the shell to reach the core. Such a process can increase the QY of the material and reduce the electron−hole pair recombination. Another strategy to increase the PL QY is to incorporate the dopant into the energy level of the QDs. Dopants such as Mn, Cu and Ag can significantly increase PL QY over 50% (Chen et al., 2009). Doped QDs can emit significantly in the visible region with large Stokes shifts and decay time ranging from micro- to milliseconds timescales (Wood et al., 2009). Fig. 12.5 shows the schematic representation of surface passivation and related surface chemistry.

Vapor phase synthesis of QDs is a rather less known technique than the hot injection method due to its complexity. It can be formed via deposition from vapor onto the appropriate substrates in molecular beam epitaxy (MBE) or metal organic chemical vapor deposition. There are two approaches to form the QDs. The first is Stranski−Krastinov (SK) growth, where nanosized islands are formed with several monolayers deposited upon one another. This leads to the large lattice mismatch between the two semiconductor materials. This was observed in Ge/Si, InP/AlGaAs, and InP/GaInP. For such highly strained system, growth initiates with the addition of layer by layer and thus minimizes the strain energy. Such islands then grow articulately on the substrate without any misfit until a critical strain density with corresponding to its critical size is exceeded. Incidentally, coherent SK islands can be overgrown with a suitable passivating and carrier confining epitaxial layer to produce QDs with better PL efficiency—typically colloidal QDs—which depend on the capping layer. The second method is to produce the near surface quantum well (QW) and then deposit coherent SK islands on to those wells. Such deposition has a large lattice mismatch with the barrier to

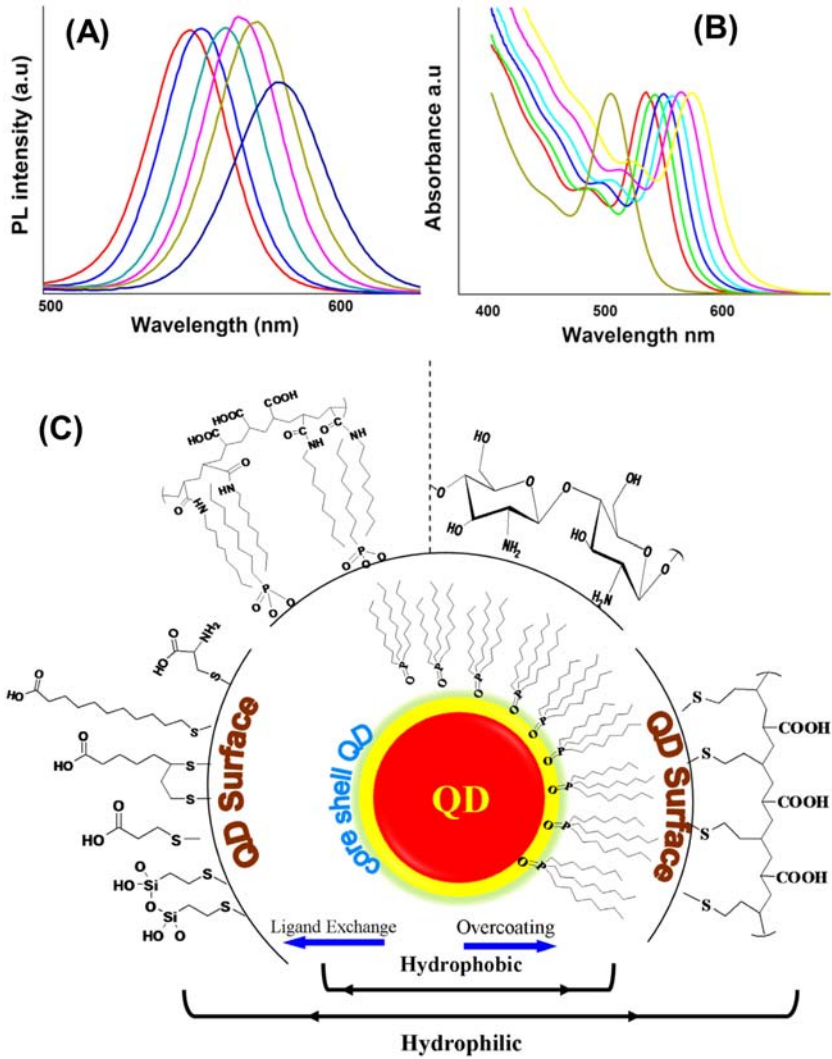

FIGURE 12.5 (A) PL; (B) UV−visible spectra of CdTe QDs; and (C) possible schemes for surface modification of QDs using ligand exchange and polymer coatings (Chandan et al., 2018). *Adapted from Chandan, H. R., Schiffman, J. D., Balakrishna, R. G., 2018. Quantum dots as fluorescent probes: synthesis, surface chemistry, energy transfer mechanisms, and applications. Sens. Actuator, B 258, 1191−1214. With permission.*

produce strain in the island formed. The strain created by the island can be extended to the QW and thus it can penetrate through its outer barrier and well region. Such a strain field can expand the lattice of the QW and lowers the bandgap below the SK island formed and thus produces the quantum

dots by confining its electrons three dimensionally. Such SK islands are referred to as stress islands. Stress-induced InGaAs and GaAs have been reported for InP stress islands on GaAs/InGaAs/GaAs QW and for InP stressor islands on an AlGaAs/GaAs/AlGaAs QW (Petroff and DenBaars, 1994; Willardson et al., 1999).

12.3.2 Perovskite quantum dots

Hybrid organic−inorganic perovskite quantum dots is the new entry to the QDs family with enhanced fluorescence intensity and QY. The metal halide perovskite has the simple ABX_3 structure. "A" is occupied by organic or inorganic materials such CH_3NH_3 (MA), $CH(NH_2)$ (FA), or Cs^+. "B" by a divalent metal cation such as lead, strontium, and germanium. "X" usually is halide ions. The octahedral BX_6 structure is the basis of the perovskite and "A" is occupied by the cation, which fills the voids between these structures. Synthesis of such a structure can be also achieved through the hot injection method. During the initial stage of the development, organic−inorganic halide perovskite, such as methyl ammonium lead halide ($MAPbI_3$) and formammonium lead halide ($FAPbI_3$), gained more attention (Choi et al., 2017; Lee et al., 2019). However, these PQDs are less stable due to the organic content and soon the focus was shifted toward inorganic halide perovskites (Xiang and Tress, 2019). But the toxicity of the lead limited their use in practical applications. Until recently, most of the studies shifted their focus from $CsPbX_3$ to lead-free structures (Han et al., 2019). Hot injection method is the most common method used for the synthesis of the PQDs, with OA and ODE being the predominant ligand system for the synthesis of the PQDs (Zhang et al., 2015; Sun et al., 2018). The temperature was adjusted ranging from 150 to 200°C depending on the type of the material. Typically, the Cs oleate precursor was injected into the degassed PX_3 (X = Cl, Br, I) solution. This hot injection leads to nucleation and growth of the particle. The reaction is arrested by reducing the reaction temperature using ice cold water (immersing the round bottom flask). The synthesis of lead-free perovskite gained more interest.

Zhou et al. (2018) demonstrated the synthesis of $Cs_2AgBiBr_6$ perovskite QDs. Typically, the Cs-oleate was injected into the mixture of $BiBr_3$, $AgNO_3$, ODE, OA, and HBr at 200°C under inert condition or N_2 atmosphere. This led to the formation of $Cs_2AgBiBr_6$ PQDs with a time span of 5 s. In fact, the morphology of the PQDs synthesized by hot injection method is monitored by three factors influencing it (Wang et al., 2016; Dolzhnikov et al., 2017; Zhou et al., 2018; Xu et al., 2019). This includes the reaction time of the two precursors, the temperature and the ratio of the ligands. Wang et al. (2015) reported the synthesis of Cs_2SnI_6 PQDs. They demonstrated that reaction time is very important in the hot injection method. Usually the reaction is short with less than a minute, and it results in cubic

structured PQDs. However, when the reaction time is progressed, a different morphology of the PQDs was formed. The formation of nanorods, nanowires, nanobelts, and nanoplatelets was reported with a time scan of 5, 10, 30, and 60 min, respectively (Zhou et al., 2018). Similarly, the effect on the morphology of PQDs by variation of temperature and ligand ration was also reported by Dolzhnikov et al. (2017) and Xu et al. (2019), respectively. Fig. 12.6 gives schematic presentation for hot injection method and effect of reaction time over morphology.

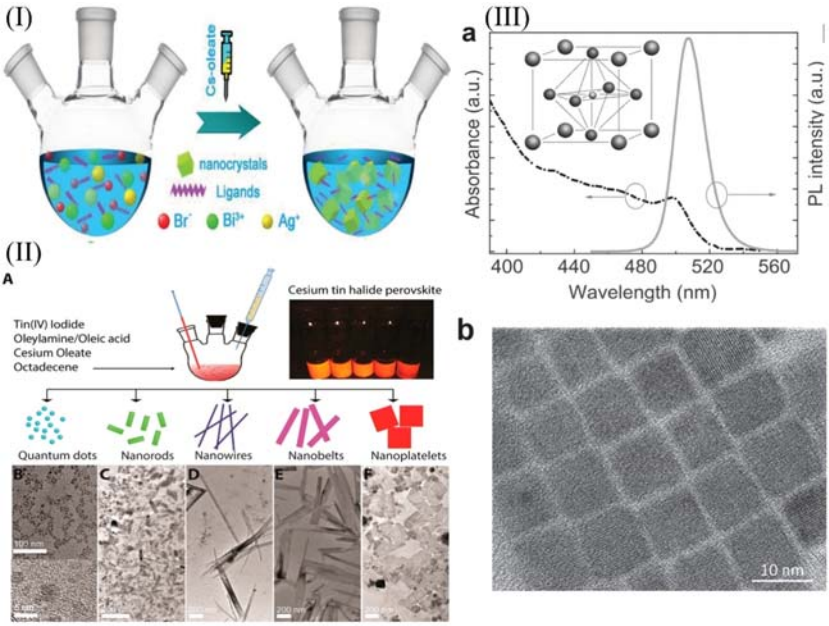

FIGURE 12.6 (I) Schematic illustration of the hot-injection method for the synthesis of $Cs_2AgBiBr_6$ QDs. (II) (a) Absorption and emission spectra of $CsPbBr_3$ IPQDs in solution. Inset: Cubic perovskite structure of $CsPbBr_3$ IPQDs: medium spheres in the centers of the cubic faces: Br; small sphere in the center of the cubic: Pb; large spheres in the cubic corners: Cs. (b) TEM image of $CsPbBr_3$ IPQDs. (III) Synthesis of Cs_2SnI_6 nanocrystals: (A) Schematic of procedures for the controlled synthesis of perovskite Cs_2SnI_6 nanocrystals (*left panel*) and photograph of the as-prepared Cs_2SnI_6 samples under UV light (*right panel*); (B−F) TEM images of Cs_2SnI_6 nanocrystals with different shapes (the inset of B gives an HRTEM image of Cs_2SnI_6 spherical quantum dots). *Adapted (I) from Zhou, L., Xu, Y. F., Chen, B. X., Kuang, D. B., Su, C. Y. 2018. Synthesis and photocatalytic application of stable lead-free Cs2AgBiBr6 perovskite nanocrystals. Small 14 (11) doi: 10.1002/smll.201703762. (II) from Wang, Y., Li, X., Song, J., Xiao, L., Zeng, H., Sun, H., 2015. All-inorganic colloidal perovskite quantum dots: a new class of lasing materials with favorable characteristics. Adv. Mater. 27 (44), 7101−7108. (III) from Wang, A., Yan, X., Zhang, M., Sun, S., Yang, M., Shen, W., et al., 2016. Controlled synthesis of lead-free and stable perovskite derivative Cs2SnI6 nanocrystals via a facile hot-injection process. Chem. Mater. 28 (22), 8132−8140. With permission.*

Another method of synthesizing PQDs is ligand-assisted synthesis. To solve some of the challenges associated with the hot injection method (high reaction temperature and low reproducibility for large-scale synthesis), this method came to existence. It is a simple synthetic process, which involves the principle of supersaturation in the presence of ligands. PQDs were synthesized by dropwise addition of precursor solution in polar solvent into a solvent containing ligands. The difference in the polarity of the solvent system influences the miscibility of solvents. Thus it resulted in two solvent systems, which cannot mix, and the precursor present encounters a nonequilibrium state. Due to this supersaturation, nucleation and growth occurs immediately even at room temperature and the product can be produced at gram scale with reproducibility.

Gram-scale synthesis of lead-based PQDs was reported using this method (Liang et al., 2016; Wei et al., 2016b). Yang et al. (2017) reported the synthesis of $Cs_3Bi_2Br_9$ PQDs by a one-step reaction without ligands. CsBr and $BiBr_3$ were dissolved in dimethylsulfoxide (DMSO) to form a precursor solution. As DMSO is a polar solvent, therefore when such a precursor solution was added to the less polar solvent such as isopropanol (which can act as antisolvent), a yellow-green colloidal solution was formed. This indicates the nucleation and growth of $Cs_3Bi_2Br_9$ PQDs formation even without the presence of ligands. Nevertheless, the low QY of 0.2% indicates the requirement of ligands.

Leng et al. (2018), synthesized $Cs_3Bi_2Br_9$ by this method using OA and oleylamine (OLA) as ligands. This protocol for the synthesis is similar to Yang et al. (2017) except for two reaction conditions. The first one is that actone was used as the antisolvent and second is that precursor solution was prepared using OLA and antisolvent OA. It resulted in PQDs $Cs_3Bi_2Br_9$ having an average diameter of 3.88 nm and QY of 19.4%. Even though the ligand-assisted method is advantageous in terms of reaction temperature, there are some issues that need to be addressed. Typical to chalcogenide QDs synthesis using hot injection method, the nucleation occurs at early stage of the reaction, which is followed by the growth. This allows one to arrest the reaction depending on time or temperature. But in ligand-assisted synthesis, the nucleation and growth stages cannot be separated, indicating the difficulties in controlling the size and morphology of the PQDs (Lignos et al., 2016). Another problem associated with halide PQDs is that the polar solvents are used in ligand-assisted reaction. The halide PQDs are vulnerable to the polar solvents with the possibility that PQDs may undergo degradation or aggregation losing their properties. Other than this method, one-step synthesis using an ultrasonication method has also been reported, where all the precursors have been dissolved in appropriate solvent and sonicated. The PQDs can be synthesized with the use of the same ligand system (Tong et al., 2016; Jang et al., 2016). Nevertheless, there is always scope to improve the synthetic route for better quality products.

12.4 Quantum dot sensitized solar cells

Several QDs are used in QDSSCs as sensitizers, which include $CsPbX_3$, CdS, CdSe, CdTe, ZnS, Ag_2Se, PbSeS, $AgInSe_2$, PbS, $CuInS_2$, and $MAPbX_3$ (Lin et al., 2020). Among all these QDs sensitizers, CdS and CdSe QDs are considered significant choice as stable materials in QDSSCs. The enhancement in PCE observed in QDSSCs are mainly contributed by the increase in size of QD, enhanced light harvesting, reduced defects, improved charge carrier migration and higher surface area covered by the QDs on the photoelectrode. Lee and Lo (2009) have used CdS/CdSe cosensitized photoelectrode for QDSSC application and reported that CdS and CdSe QDs exhibits complementary effect in light harvesting due to stepwise arrangement of band edge levels, which is beneficial for the injection of electron and recovery of hole between CdS and CdSe (Fig. 12.7) resulting in a PCE of 4.22% using a TiO_2/CdS/CdSe/ZnS electrode. Introduction of ZnS layer acted as a passivation layer to protect QD materials from photocorrosion and improves the photovoltaic effect of QDSSCs.

Archana et al. (2020) have studied the cosensitization effect of CdS and InSb QDs and reported an improved PCE for TiO_2/CdS/InSb QDSSC that is 0.8% (InSb) and 3.52% (CdS QDs) to 4.94% (InSb QDs and CdS QDs). The cosensitization of InSb improves the light absorption range along with reduced spectral overlap leading to better light harvesting and decreased defects causing suppressed recombination of charge carriers. Liu et al. (2019) have used zinc titanium mixed metal oxides as photoanodes with CdS/CdSe QDs for QDSSCs and reported PCE of 3.95%. Yu et al. (2012) have prepared CdSe/CdS core/shell nanocrystals and showed an improved Jsc, Voc, and η compared to single CdSe QDSSCs, due to higher light

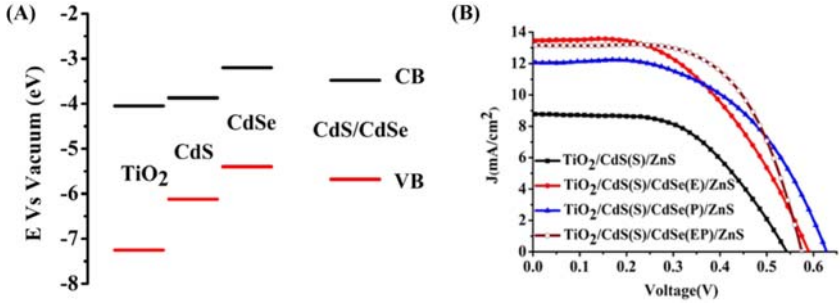

FIGURE 12.7 (A–B) Band edge structure for TiO_2, CdS and CdSe electrodes and (C) I–V curves for QDs sensitized solar cells. *Adapted from Esparza, D., Zarazúa, I., López-Luke, T., Cerdán-Pasarán, A., Sánchez-Solís, A., Torres-Castro, A., et al., 2015. Effect of different sensitization technique on the photoconversion efficiency of CdS quantum dot and CdSe quantum rod sensitized TiO_2 solar cells. J. Phys. Chem. C. 119 (24), 13394–13403. With permission.*

harvesting ability. In addition, CdSe/CdS prevents recombination of charges inside QDs by decreasing surface states and by accelerating charge separation, suggesting that cosensitized QDs are better than single QDs. Another approach to improve QDSSCs performance is by incorporating passivation layer like ZnS between TiO_2 (photoanode) and electrolyte in CdS QDs solar cell. The decreased recombination of charge carriers from TiO_2 to electrolyte was observed in the presence of passivation layer, leading to enhanced charge collection efficiency (Jung et al., 2012).

Li et al. (2020) have introduced TiO_2 as a passivation layer between ZnO hollow microspheres photoanode and CdS/CdSe/ZnS, which showed an improved PCE of 3.16% as compared to bare ZnO of 1.54%. This enhancement was attributed to improved light absorption and electron transport resulting from TiO_2 incorporation. Yu et al. (2012) studied effect of different annealing temperatures (100°C, 150°C, 200°C and 250°C). QDSSC performance in CdSe/CdS QDs, exhibited an increased IPCE from 0.46% to 2.83%. A significant enhancement in efficiency of 4.21% was observed with 300°C annealing temperature as compared to the photoanode, which was not treated with heat, which exhibited only 3.2%. In addition, CE and electrolyte can also be modified to enhance the properties of QDSSC. CoS (Yang et al., 2010) and Cu_2S are used as CE in ZnS/CdSe/CdS multilayer QDSSCs and they showed an increased efficiency of 2.7% and 1.9%, respectively in comparison to Pt CE with an efficiency of 1.6%. Furthermore, recently Cu_2S and rGO composites have open up new path for CE material choice for QDSSCs (Kusuma et al., 2018).

Huang et al. (2011) reported a flexible photoelectrode for CdS/CdSe quantum dot-QDSSCs with a PCE of 3.47% under AM 1.5G illumination using Cu_2S CE and polysulfide electrolyte between the electrodes. The conventional flexible transparent conductive oxides substrates like ITOs−polyethylene terephthalate (ITO-PET) cannot tolerate high temperature and hence they have also investigated a new technique of depositing the TiO_2 and FTO layer first, followed by PET substrate at lower temperature in order to avoid temperature issues for CdS/CdSe QDSSCs photoelectrodes. Yu et al. (2011) have used electrodeposition method to fabricate CdS/CdSe QDs with TiO_2 as a photoanode and reported an improved electron transport and electron collection efficiency with a PCE of 4.81%.

Li et al. (2011) have used modified polysulfide $[(CH_3)_4N]_2S/[(CH_3)_4N]_2S_n$, in organic solvent (3-methoxypropionitrile) to improve the QDSSCs performance. They observed an increased PCE of 3.2% under AM 1.5G irradiation by employing CdS QDSSCs. The modified polysulfide contributes in linking QDs with nanoporous TiO_2 through covalent bonds using thioglycolic acid resulting in high wettability and superior penetration capability of TiO_2 with an improved fill factor of 0.89. Pan et al. (2012) prepared CdS/CdSe inverted type-I core/shell structure deposited on TiO_2 photoanode with a bifunctional linker mercaptopropionic acid (MPA), which showed an

improved PCE of 5.32%. It was attributed to modified deposition technique using linker MPA.

Zhu et al. (2010a,b) have used Zn-doped TiO_2 screen printed on FTO as a photoanode for CdS QDSSCs and reported an improved PCE by 24% and it was attributed to reduced electron recombination and enhanced electron transport by Zn doping. Santra and Kamat (2012) have reported that QDSSCs exhibited a significant enhancement in PCE (5.4%) on doping Mn^{2+} to CdS. Mn-doped ZnS, ZnSe and CdS depicted emission at 585 nm resulting from d-d transition, but these transitions are both; spin and orbitally forbidden, leading to a very long lifetime in the range of several hundreds of micro seconds (Fig. 12.8). Hence it is advantageous to utilize long lived charge carriers to enhance the PCE in QDSSCs using Mn-doped QDs (Santra and Kamat, 2012). Some parameters of CdQDs-based solar cells are tabulated in Table 12.1.

12.4.1 Perovskite quantum dots-based quantum dot sensitized solar cells

Organometallic halide perovskites having the formula ABX_3 (where A is an organic cation, B is commonly Pb^{2+}, and X is a halide) have inspired photovoltaics field due to their unique photophysical properties like high emission efficiencies, long carrier diffusion lengths and low production cost. It makes them as potential candidate for photovoltaics and optoelectronics applications. The research in this field is highly focused on organic−inorganic hybrid perovskites, for example, $CH_3CH_3PbI_3$, $CH_3NH_3PbI_3$, etc. and later the volatile organic part is substituted by inorganic materials such as $CsPbX_3$, X = Cl, Br, and I with cubic perovskite structure. The organic−inorganic $CH_3CH_3PbI_3$ perovskites will dissociate into PbI_2 and CH_3NH_3I under environmental stress; the latter is volatile, and therefore,

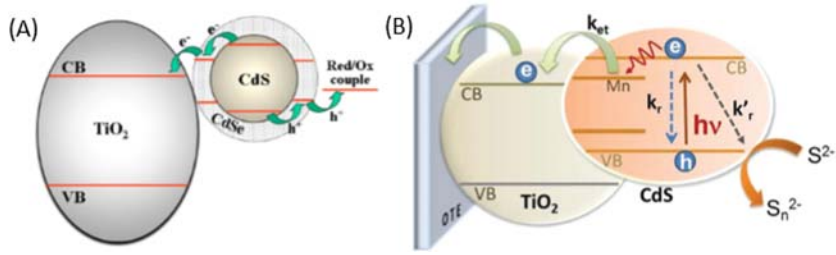

FIGURE 12.8 Band alignment for (A) Inverted type-I CdS/CdSe core/shell structure and (B) Mn-doped CdS QDSSC solar cells. *Adapted (A) from Pan, Z., Zhang, H., Cheng, K., Hou, Y., Hua, J., Zhong, X., 2012. Highly efficient inverted type-I CdS/CdSe core/shell structure QD-sensitized solar cells. ACS Nano 6(5), 3982−3991.; (B) Santra, P. K., Kamat, P. V., 2012. Mn-doped quantum dot sensitized solar cells: a strategy to boost efficiency over 5%. J. Am. Chem. Soc. 134 (5), 2508−2511. With permission.*

TABLE 12.1 Cd QDs-based solar cell parameter.

QDs material	Voc (V)	Jsc (mA cm^{-2})	Fill factor (%)	η (%)	References
$TiO_2/CdS_3/CdSe_4/ZnS$, Au	0.513	16.8	0.49	4.22	Lee et al. (2012)
TiO_2/CdS/InSb/CuS	0.533	18.58	49.88	4.94	Archana et al. (2020)
Zn−Ti/CdS/CdSe/ZnS	0.57	13.36	0.52	3.95	Liu et al. (2019)
$TiO_2/CdS_8/ZnS$	0.49	7.813	44.83	1.72	Jung et al. (2012)
ZnS/CdSe/CdS/TiO_2@ZnO	0.45	14.57	0.46	2.99	Li et al. (2020)
TiO_2/TGA/CdS-3	1.2	3	0.89	3.2	Li et al. (2011)
TiO_2/CdS/CdSe core shell structure-inverted Type-I	0.527	18.02	0.56	5.32	Pan et al. (2012)
Mn-doped-CdS/CdSe	0.558	20.7	0.47	5.42	Santra and Kamat (2012)
TiO_2/ZnSe/QDs/ZnSe (CdS/CdSe)	0.61	21.49	0.55	7.24	Huang et al. (2016)

replaced with inorganic material. The first perovskite-based solar cells was reported by Kojima et al. (2009) with PCE of 3.8% using $MAPbI_3$ and $MAPbBr_3$ as a liquid sensitizer in DSSC-based structure. Im et al. (2011) have used quantum dots of nanocrystalline material and enhanced the PCE to 6.54%. The incorporation of solid hole transporting layer (HTL) spiro-OMeTAD instead of liquid HTL has boosted the PCE in recent years. Presently, perovskites cells have reached an efficiency of 25.5% to convert sunlight into electricity and perovskite silicon tandem solar cells reached PCE of 29.5% as depicted in NREL chart (Fig. 12.9), which is at par with the best thin-film chalcogenide and silicon devices.

Swarnkar et al. (2016) have prepared phase stabilized $CsPbI_3$ QDs at lower temperature for photovoltaic applications. $CsPbI_3$ undergoes immediate transformation to orthorhombic phase, when exposed to ambient conditions. The phase stabilized $CsPbI_3$ QDs stable for months at ambient conditions are developed by modifying the purification process, which includes washing with methyl acetate, an antisolvent, which eliminates

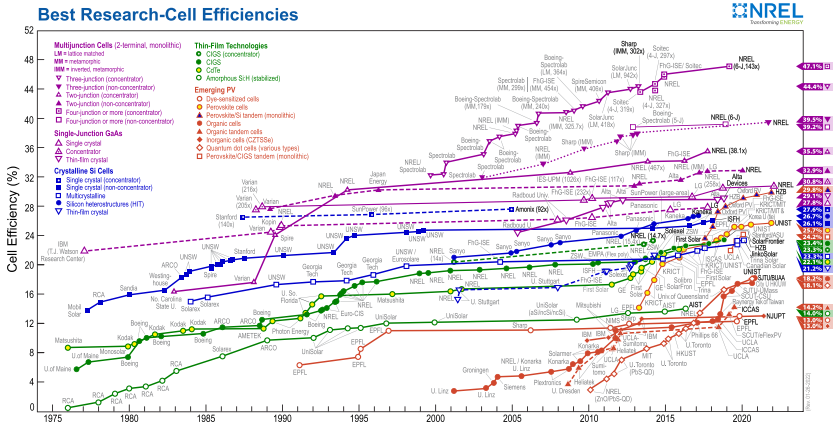

FIGURE 12.9 NREL cell efficiency chart.

unreacted precursor material without inducing agglomeration. Lee et al. (2012) have modified structure of device by replacing m- (mesoporous)-TiO_2 with insulating m-Al_2O_3, which is fabricated above the thin compact layer of TiO_2. It resulted in ten times faster charge collection with an enhanced photocurrent. Here, they concluded that mesoporous structure acts as a scaffold for perovskite structure.

Chen et al. (2017) reported that efficient vacuum deposited $CsPbI_3$ and $CsPbI_2Br$ enhances the PCE in solar cells to 11.8%. Sanehira et al. (2017) have reported that A-site cation halide salt treatment (formamidinium FA^+) enhances charge carriers mobility, resulting in increased photocurrent contributing to higher PCE of 13.43%. Here, the interaction of QDs and FA^+ might be a surface reaction or partial cation exchange resulting $Cs_xFA_{1-x}PbI_3$ QD core or a core shell structure formed by $FAPbI_3$ matrix around $CsPbI_3$ QDs, suggesting that individual QDs are no longer present. Frolova et al. (2017) have used coevaporation by thermal annealing of CsI and PbI_2 to fabricate $CsPbI_3$ perovskite solar cells, which delivered an enhanced power conversion efficiency of 10.5%. Thermal annealing contributes to phase changes in crystal structure and morphology in order to enhance the device performance by producing a well crystalline, uniform and highly pure perovskite film compared to solution-based process, where the film is affected by solvent, wetting, evaporation and deposition process (Fig. 12.10).

Lv et al. (2015) have used colloidal surface modified $CuInS_2$ QDs with improved carrier transport ability as hole transporting agent in TiO_2/$CH_3NH_3PbI_3$/HTM/Au solar cell, which showed an enhanced PCE of 8.38% along with ZnS as shell layer. The improved PCE is contributed by decreased charge recombination between TiO_2 and hole transporting material HTM. Stolterfoht et al. (2018) have visualized nonradiative recombination pathways in

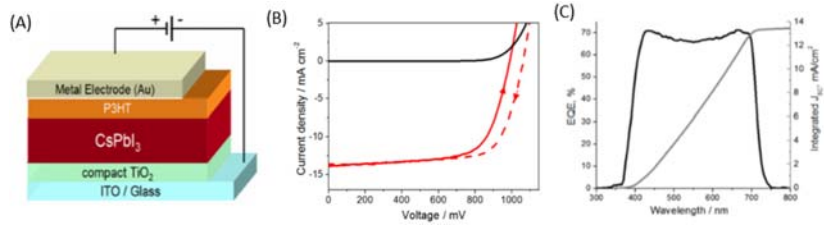

FIGURE 12.10 (A) Schematic of the PQDs solar cell, (B) current-voltage curve of device and (C) EQE spectrum. *Adapted from Frolova, L. A., Anokhin, D. V., Piryazev, A. A., Luchkin, S. Y., Dremova, N. N., Stevenson, K. J., et al., 2017. Highly efficient all-inorganic planar heterojunction perovskite solar cells produced by thermal coevaporation of CsI and PbI_2. J. Phys. Chem. Lett. 8 (1), 67−72. With permission.*

perovskite solar cells $(CsPbI_3)_{0.05}[(FAPbI_3)_{0.89}(MAPbBr_3)_{0.11}]_{0.95}$ using transient and absolute PL. They found quasi-Fermi-level splitting losses and interfacial recombination resulting in 135 and 80 meV, free energy loss. Incorporation of thin interlayers of PFN-P2—a conjugated polyelectrolyte and LiF between perovskite and transport layer contributes to a considerable decrease of these interfacial losses at both p and n contacts, by 65 and 35 meV respectively. The PCE has improved to 19.83% with a record fill factor of 81%. Zheng et al. (2020) have reported that introduction of long-chain surface anchoring alkylamine ligands into precursor solution suppressing the nonradiative recombination, which improves the optoelectronic properties of mixed-cation mixed-halide perovskite films. The resulting modified film shows (100) orientation, low trap state density in addition to improved charge carrier mobility and diffusion lengths leading to a highly enhanced efficiency of 22.3%. Some perovskite-based solar cell parameter are summarized in Table 12.2.

12.4.2 Other quantum dots-based quantum dot sensitized solar cells

QDSSCs are potential photovoltaic device systems, attributed to their low material requirements and simplicity. However, in order to achieve high efficiencies, complicated and expensive processes or toxic materials are used, which limit their large-scale application. By overcoming these limits, the QDSSCs can be used for commercial applications. Pan et al. (2014) have prepared green QDs that are free of Cd or Pb. They have applied surface passivation to the ternary $CuInS_2$ (CIS) QDs using ZnS and reported a high efficiency of 7.04% as compared to other green QDs-based QDSSCs, suggesting the possibility of better or comparable performance with green CIS QDs (Fig. 12.11). This enhanced efficiency was attributed to a high absorption range, more QDs loading, and reduced recombination with type-I core/shell structure.

TABLE 12.2 Perovskite-based solar cells characteristics.

QDs material	Voc (V)	Jsc (mA cm^{-2})	Fill factor (%)	η (%)	References
Phase stable $CsPbI_3$	1.23	13.47	0.65	10.77	Swarnkar et al. (2016)
$CH_3NH_3PbI_2Cl$	0.98	17.8	0.63	10.9	Singh and Nagarjuna (2014)
$CsPbI_2Br$	1.15	15.2	0.67	11.8	Chen et al. (2017)
$CsPbI_3$	1.06	13.8	71.6	10.5	Frolova et al. (2017)
$TiO_2/CH_3NH_3PbI_3/CuInS_2/ZnS/Au$	0.924	18.6	48.7	8.38	Lv et al. (2015)
$(CsPbI_3)_{0.05}[(FAPbI_3)_{0.89}(MAPbBr_3)_{0.11}]_{0.95}$	1.05	25.1	0.75	19.83	Stolterfoht et al. (2018)
$Cs_{0.05}(FA_{0.92}MA_{0.08})_{0.95}Pb(I_{0.92}Br_{0.08})_3$	1.14	23.9	0.82	22.34	Zheng et al. (2020)

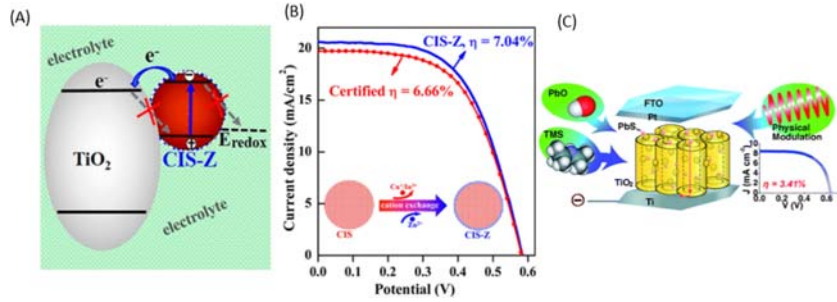

FIGURE 12.11 (A) Schematic of band structure of TiO_2 and $CuInS_2$ (CIS) QDs passivated by ZnS (B) I−V curves of CIS QDs solar cells and (C) Schematic of PbS QDs solar cell along with I−V curves. *Adapted from Tao, L., Xiong, Y., Liu, H., Shen, W. 2014. High performance PbS quantum dot sensitized solar cells via electric field assisted in situ chemical deposition on modulated TiO_2 nanotube arrays. Nanoscale. 6 (2), 931−938. With permission. Adapted from Pan, Z., Mora-Seró, I., Shen, Q., Zhang, H., Li, Y., Zhao, K., et al., 2014. High-efficiency "green" quantum dot solar cells. J. Am. Chem. Soc. 136 (25), 9203−9210. With permission.*

Tao et al. (2014) have prepared PbS QDs-based TiO_2 nanotube arrays (NTAs) through an in situ chemical bath deposition method controlled by low electric field. They could achieve an efficiency of 3.41%. These methods enhance QDs loading on the NTAs with high Voc and fill factor (FF) contributed by shorter electron path, less structural and electronic defects, optimal film thickness ($\sim 4\ \mu m$), and reduced recombination in the ordered TiO_2 NTAs produced by oscillating anodic voltage. Bi et al. (2018) could harvest the short-wave infrared range of the solar spectrum using PbS colloidal quantum dots for solar cells using hybrid inorganic−organic ligand treatment by combining ZnI_2 with 3-mercaptapropionic acid for surface passivation of PbS QDs. The modified PbS solar cell has delivered an efficiency of 7.9% and an additional 3.3% enhancement by placing this cell at the back of the $MAPbI_3$ perovskite film due to enhanced light absorption up to 750 nm. It suggests that the modification of a passivation layer can boost the PCE.

Inorganic nanostructured materials and hybrid carbon materials have attracted a potential interest and open an exciting field in the design and fabrication of efficient catalysts. Guo et al. (2014) have prepared a novel CE consisting of Co_9S_8 nanotube arrays grown on carbon fiber (CF) (Co_9S_8/CF) for fiber-shaped flexible QDSSCs and achieved high PCE of 3.79% as compared to CE and Pt. The redox mediator plays an important role in determining photovoltage and photocurrent in QDSSCs. As per kinetics, reduction of oxidized QDs by the redox mediator should happen faster than the back transfer of electron between TiO_2 and oxidized QDs to sustain the photocurrent. Thermodynamically, the redox mediator should possess effectively

positive reduction potential to provide high photovoltage. Haring et al. (2014) have investigated Mn(II/III) complexes as potential redox mediator for CdS/CdSe/ZnS QDSSCs. Mn poly(pyrazolyl)borates showed high photovoltages ~ 1 V with reduction potential of ~ 0.51 V versus Ag/AgCl. Reduction rates were slower compared to $Co(bpy)_3$, where bpy = 2,2′-bipyridine, which was confirmed by enhanced electron lifetimes up to four orders of magnitude longer as the low solubility prevents the sustaining of high current. The Mn(II/III) complexes redox mediator exhibited higher fill factor (~ 0.6) and photovoltage than $Co(bpy)_3$ and it can be ascribed to more positive reduction potential and reduced recombination.

Interface engineering is an important path to enhance the photovoltaic performance in QDSSCs. Zhang et al. (2019) have studied the interface modification between TiO_2 and QDs using ZnS and ZnSSe semiconductors. Here, the main limitations are the passivation effect and the matching of lattice with TiO_2 and QDs. Though, ZnS has a large energy bandgap due to higher CB edge, its lattice mismatch with TiO_2 and QDs largely leads to the formation of defect states. In contrast, ZnSe alloy exhibited a small lattice mismatch with TiO_2 and QDs with a lower CB edge. They have prepared ZnS_xSe_{1-x} alloy material as a passivation layer on the Zn−Cu−In−Se (ZCISe) QD-sensitized TiO_2 photoanode and reported that alloy material is more constructive for the inhibition of charge recombination between photoanode/electrolyte interfaces, and it also improves extraction of photogenerated electron leading to the photon efficiency improvement from 12.17% to 13.08%.

12.5 Recent developments

Solar cell parameters of some quantum dots-based solar cells are summarized in Table 12.3.

12.6 Conclusion

QDSSCs are a promising alternative for dye-sensitized solar cells due to unique properties of QDs. Numerous factors limit the PCE of QDSSCs, which include narrow absorption of solar spectrum, recombination at interfaces, lower QD deposition on semiconductor film, poor charge carrier transportation, photocorrosion of electrode, and low fill factor, because of the low performance of CE. The research work in QDSSCs has mainly focused on the improvement of PCE in recent years. Among all QDs sensitizers, Cd chalcogenide-based sensitizers, especially CdS and CdSe, are the preferred choice for solar cell devices. The researchers have investigated various modifications to improve the PCE of Cd-based QDSSCs and reported on the cosensitization of CdS/CdSe, introduction of passivation layer (ZnS), annealing temperature, CE modification (Cu_2S, CoS, and composites of Cu_2S/

TABLE 12.3 Some quantum dots-based solar cell parameters.

QDs material	V_{oc} (V)	J_{sc} (mA cm^{-2})	Fill factor (%)	η (%)	References
$CuInS_2$	0.586	20.65	58.1	7.04	Pan et al. (2014)
PbS	0.63	8.48	64	3.41	Tao et al. (2014)
CdS/CdSe	0.37	17.95	57	3.79	Guo et al. (2014)
CdS/CdSe	0.9	0.12	55	0.33	Haring et al. (2014)
Zn−Cu−In−Se (ZCISe) QD	0.733	26.49	68.52	13.08	Zhang et al. (2019)
Ag_2S (scattering layer)	0.33	7.3	40.8	0.98	Tubtimtae et al. (2010)
CdSe/ZnS	0.44	2.29	27	0.27	Ning et al. (2011)
$CuInSe_xS_{2-x}$	0.55	10.5	60.4	3.54	McDaniel et al. (2013a)
$CsPbBr_3$/CdS	0.77	9.88	40	3.59	Hunsur Ravikumar et al. (2022)
Mn/CdS	0.6	10.27	49	3.29	Shen et al. (2016)
$CuInSe_xS_{2-x}$	0.54	17.565	54.1	5.13	McDaniel et al. (2013b)
CdTe/CdSe core/shell QD	0.6	19.59	56.9	6.76	Wang et al. (2013)
ZnTe/CdSe	0.64	19.65	57	7.17	Jiao et al. (2015)
$AgInSe_2$/CdS/ZnS	0.654	18.27	52.5	6.27	Abate and Chang (2018)
$CuInS_2$−Mn-doped CdS	0.581	19.29	48	5.38	Luo et al. (2013)
$Cd_{1-X}Zn_XTe$/CdS core/shell	0.6	10.05	54	3.27	Lu et al. (2020)
PbSe	0.61	25.39	67	10.38	Liu et al. (2020)
N and S codoped carbon QDs	0.43	0.61	52	1.36	Riaz and Park (2022)
Gd-doped CdS@CdSe	0.71	16.34	65.2	7.57	Amani-Ghadim et al. (2022)
Mn-doped CdS@CdSe	0.558	20.7	47	5.42	Santra and Kamat (2012)

(*Continued*)

TABLE 12.3 (Continued)

QDs material	V_{oc} (V)	J_{sc} (mA cm^{-2})	Fill factor (%)	η (%)	References
Ni-doped CdS	0.643	8.91	54.3	3.11	Gopi et al. (2016)
Sn:InP	0.59	10.58	56.7	3.54	Yang et al. (2015a,b)

rGO), polysulfide electrolyte modification and doping of QDs (e.g., Mn), and wide bandgap semiconductor (TiO_2/ZnO). Apart from Cd chalcogenide QDs, other QDs also have promising properties as sensitizers, such as $CuInS_2$, PbS, and Zn-Cu-In-Se. Recently, PQDs and tandem silicon solar cells (PQDs and silicon) have gained significant importance due to the low production cost and high PCE (reported up to 29.5%). To further enhance PCE and to achieve breakthroughs in QDs solar cell device, the focus of investigation should be channeled to research on materials such as doping/composite/different tandem structure of wide bandgap material, QDs, surface treatment of electron transport layer, electrolytes, and CE modification.

References

Abate, M.A., Chang, J.-Y., 2018. Boosting the efficiency of $AgInSe_2$ quantum dot sensitized solar cells via core/shell/shell architecture. Sol. Energy Mater. Sol. Cell 182, 37–44.

Ahmad, M.S., Pandey, A.K., Abd Rahim, N., 2017. Advancements in the development of TiO_2 photoanodes and its fabrication methods for dye sensitized solar cell (DSSC) applications. A review. Renew. Sustain. Energy Rev. 77, 89–108.

Allen, P.M., Bawendi, M.G., 2008. Ternary I − III − VI quantum dots luminescent in the red to near-infrared. J. Am. Chem. Soc. 130 (29), 9240–9241.

Amani-Ghadim, A.R., Mohammad-Gholipour-Rezaei, E., Bayat, F., Agbolaghi, S., Khodam, F., 2022. Enhancement in photovoltaic properties of exciplex quantum dot sensitized solar cells via gadolinium doping and formation of type II Core/Shell (Gd-doped CdS@CdSe) structure. Sol. Energy 231, 402–413.

Anttu, N., 2015. Shockley–Queisser detailed balance efficiency limit for nanowire solar cells. ACS Photonics 2 (3), 446–453.

Archana, T., Vijayakumar, K., Subashini, G., Nirmala Grace, A., Arivanandhan, M., Jayavel, R., 2020. Effect of co-sensitization of InSb quantum dots on enhancing the photoconversion efficiency of CdS based quantum dot sensitized solar cells. RSC Adv. 10 (25), 14837–14845.

Badawi, A., Al-Hosiny, N., Abdallah, S., Negm, S., Talaat, H., 2013. Tuning photocurrent response through size control of CdTe quantum dots sensitized solar cells. Sol. Energy 88, 137–143.

Badawy, W.A., 1990. Improvement of n-Si/SnO_2/electrolyte photoelectrochemical cells by Ru deposits. J. Electroanal. Chem. Interfacial Electrochem. 281 (1), 85–95.

Badawy, W.A., 1993. Preparation and characterization of TiO_2/Sb thin films for solar energy applications. Sol. Energy Mater. Sol. Cell 28 (4), 293–303.

Badawy, W.A., El-Dessouki, M.S., 1985. A study of the stability of n-Si/SnO_2 solar cells under normal working conditions. Phys. Status Solidi 92 (2). Available from: https://doi.org/10.1002/pssa.2210920258.

Beattie, A.R., 1962. Quantum efficiency in InSb. J. Phys. Chem. Solids 23 (8), 1049–1056.

Beard, M.C., Johnson, J.C., Luther, J.M., Nozik, A.J., 2015. Multiple exciton generation in quantum dots vs singlet fission in molecular chromophores for solar photon conversion. Phil. Trans. R. Soc. A: Maths, Phys. Eng. Sci. 373 (2044). Available from: https://doi.org/10.1098/rsta.2014.0412.

Bhambhani, P., 2018. Quantum dot-sensitized solar cells: a review. Bull. Electr. Eng. Inform. 7 (1), 42–54.

Bi, Y., Pradhan, S., Gupta, S., Akgul, M.Z., Stavrinadis, A., Konstantatos, G., 2018. Infrared solution-processed quantum dot solar cells reaching external quantum efficiency of 80% at 1.35 μm and Jsc in Excess of 34 mA cm^{-2}. Adv. Mater. 30 (7). Available from: https://doi.org/10.1002/adma.201704928.

Chandan, H., Geetha, B.R., 2013. Study on precipitation efficiency of solvents in postpreparative treatment of nanocrystals. J. Mater. Res. 28 (21), 3003–3009.

Chandan, H., Saravanan, V., Pai, R.K., Balakrishna, R.G., 2014. Synergistic effect of binary ligands on nucleation and growth/size effect of nanocrystals: studies on reusability of the solvent. J. Mater. Res. 29 (14), 1556–1564.

Chandan, H.R., Schiffman, J.D., Balakrishna, R.G., 2018. Quantum dots as fluorescent probes: synthesis, surface chemistry, energy transfer mechanisms, and applications. Sens. Actuator, B 258, 1191–1214.

Chen, D., Viswanatha, R., Ong, G.L., Xie, R., Balasubramaninan, M., Peng, X., 2009. Temperature dependence of "elementary processes" in doping semiconductor nanocrystals. J. Am. Chem. Soc. 131 (26), 9333–9339.

Chen, C.Y., Lin, H.Y., Chiang, K.M., Tsai, W.L., Huang, Y.C., Tsao, C.S., et al., 2017. All-vacuum-deposited stoichiometrically balanced inorganic cesium lead halide perovskite solar cells with stabilized efficiency exceeding 11. Adv. Mater. 29 (12). Available from: https://doi.org/10.1002/adma.201605290.

Choi, J., Le, Q.V., Hong, K., Moon, C.W., Han, J.S., Kwon, K.C., et al., 2017. Enhanced endurance organolead halide perovskite resistive switching memories operable under an extremely low bending radius. ACS Appl. Mater. Interfaces 9 (36), 30764–30771.

Chou, C.-Y., Lee, C.-P., Vittal, R., Ho, K.-C., 2011. Efficient quantum dot-sensitized solar cell with polystyrene-modified TiO_2 photoanode and with guanidine thiocyanate in its polysulfide electrolyte. J. Power Sources 196 (15), 6595–6602.

Christensen, O., 1976. Quantum efficiency of the internal photoelectric effect in silicon and germanium. J. Appl. Phys. 47 (2), 689–695.

Crisp, R.W., Kirkwood, N., Grimaldi, G., Kinge, S., Siebbeles, L.D., Houtepen, A.J., 2018. Highly photoconductive InP quantum dots films and solar cells. ACS Appl. Energy Mater. 1 (11), 6569–6576.

D'Souza, L.P., Amoli, V., Chandan, H.R., Sinha, A.K., Krishna Pai, R., Balakrishna, G.R., 2015. Atomic force microscopic study of nanoscale interaction between N719 dye and CdSe quantum dot in hybrid solar cells and their enhanced open circuit potential. Sol. Energy 116, 25–36.

Decker, F., Fracastoro-Decker, M., Badawy, W., Doblhofer, K., Gerischer, H., 1983. The Photocurrent-voltage characteristics of the heterojunction combination n - Si/SnO_2 /redox - electrolyte. J. Electrochem. Soc. 130 (11), 2173–2179.

Dolzhnikov, D.S., Wang, C., Xu, Y., Kanatzidis, M.G., Weiss, E.A., 2017. Ligand-free, quantum-confined $CsSnI_6$ perovskite nanocrystals. Chem. Mater. 29 (18), 7901–7907.

Du, Z., Pan, Z., Fabregat-Santiago, F., Zhao, K., Long, D., Zhang, H., et al., 2016. Carbon counter-electrode-based quantum-dot-sensitized solar cells with certified efficiency exceeding 11%. J. Phys. Chem. Lett. 7 (16), 3103–3111.

Ekimov, A.I., Onushchenko, A.A., 1981. Quantum size effect in three-dimensional microscopic semiconductor crystals. Jetp Lett. 34 (6), 345–349.

Ellingson, R.J., Beard, M.C., Johnson, J.C., Yu, P., Micic, O.I., Nozik, A.J., et al., 2005. Highly efficient multiple exciton generation in colloidal PbSe and PbS quantum dots. Nano Lett. 5 (5), 865–871.

Esparza, D., Zarazúa, I., López-Luke, T., Cerdán-Pasarán, A., Sánchez-Solís, A., Torres-Castro, A., et al., 2015. Effect of different sensitization technique on the photoconversion efficiency of CdS quantum dot and CdSe quantum rod sensitized TiO_2 solar cells. J. Phys. Chem. C. 119 (24), 13394–13403.

Feng, W., Zhao, L., Du, J., Li, Y., Zhong, X., 2016. Quasi-solid-state quantum dot sensitized solar cells with power conversion efficiency over 9% and high stability. J. Mater. Chem. A. 4 (38), 14849–14856.

Frolova, L.A., Anokhin, D.V., Piryazev, A.A., Luchkin, S.Y., Dremova, N.N., Stevenson, K.J., et al., 2017. Highly efficient all-inorganic planar heterojunction perovskite solar cells produced by thermal coevaporation of CsI and PbI_2. J. Phys. Chem. Lett. 8 (1), 67–72.

Gamboa, S., Nguyen-Cong, H., Chartier, P., Sebastian, P., Calixto, M., Rivera, M., 1998. Photovoltaic structures based on polymer/semiconductor junctions. Sol. Energy Mater., Sol. Cell 55 (1–2), 95–104.

Gopi, C.V.V.M., Venkata-Haritha, M., Seo, H., Singh, S., Kim, S.-K., Shiratani, M., et al., 2016. Improving the performance of quantum dot sensitized solar cells through CdNiS quantum dots with reduced recombination and enhanced electron lifetime. Dalton Trans. 45 (20), 8447–8457.

Gopi, C.V.M., Singh, S., Eswar Reddy, A., Kim, H.-J., 2018. CNT@ rGO@ MoCuSe composite as an efficient counter electrode for quantum dot-sensitized solar cells. ACS Appl. Mater. Interface 10 (12), 10036–10042.

Gorer, S., Hodes, G., 1994. Quantum size effects in the study of chemical solution deposition mechanisms of semiconductor films. J. Phys. Chem. 98 (20), 5338–5346.

Guo, C.X., Yang, H.B., Sheng, Z.M., Lu, Z.S., Song, Q.L., Li, C.M., 2010. Layered graphene/quantum dots for photovoltaic devices. Angew. Chem. Int. (Ed.) 49 (17), 3014–3017.

Guo, W., Chen, C., Ye, M., Lv, M., Lin, C., 2014. Carbon fiber/Co_9S_8 nanotube arrays hybrid structures for flexible quantum dot-sensitized solar cells. Nanoscale 6 (7), 3656–3663.

Han, J.S., Le, Q.V., Choi, J., Kim, H., Kim, S.G., Hong, K., et al., 2019. Lead-free all-inorganic cesium tin iodide perovskite for filamentary and interface-type resistive switching toward environment-friendly and temperature-tolerant nonvolatile memories. ACS Appl. Mater. Interface. 11 (8), 8155–8163.

Hanna, M., Nozik, A., 2006. Solar conversion efficiency of photovoltaic and photoelectrolysis cells with carrier multiplication absorbers. J. Appl. Phys. 100 (7). Available from: https://doi.org/10.1063/1.2356795.

Hao, X., Cho, E.-C., Flynn, C., Shen, Y., Park, S.-C., Conibeer, G., et al., 2009. Synthesis and characterization of boron-doped Si quantum dots for all-Si quantum dot tandem solar cells. Sol. Energy Mater. Sol. Cell 93 (2), 273–279.

Haring, A.J., Pomatto, M.E., Thornton, M.R., Morris, A.J., 2014. MnII/III complexes as promising redox mediators in quantum-dot-sensitized solar cells. ACS Appl. Mater. Interface 6 (17), 15061–15067.

Hod, I., Zaban, A., 2014. Materials and interfaces in quantum dot sensitized solar cells: challenges, advances and prospects. Langmuir 30 (25), 7264–7273.

Huang, X., Huang, S., Zhang, Q., Guo, X., Li, D., Luo, Y., et al., 2011. A flexible photoelectrode for CdS/CdSe quantum dot-sensitized solar cells (QDSSCs). Chem. Commun. (Camb.) 47 (9). Available from: https://doi.org/10.1039/c0cc04419a.

Huang, F., Zhang, L., Zhang, Q., Hou, J., Wang, H., Wang, H., et al., 2016. High efficiency CdS/CdSe quantum dot sensitized solar cells with two ZnSe layers. ACS Appl. Mater. Interface. 8 (50), 34482–34489.

Hunsur Ravikumar, C., Maroli, N., Kulkarni, B., Kolandaivel, P., Balakrishna, R.G., 2022. Heterostructure of $CsPbBr_3$-CdS perovskite quantum dots for enhanced stability and charge transfer. Mater. Sci. Eng.: B 275. Available from: https://doi.org/10.1016/j.mseb.2021.115513.

Huo, Z., Tao, L., Wang, S., Wei, J., Zhu, J., Dong, W., et al., 2015. A novel polysulfide hydrogel electrolyte based on low molecular mass organogelator for quasi-solid-state quantum dot-sensitized solar cells. J. Power Sources 284, 582–587.

Im, J.-H., Lee, C.-R., Lee, J.-W., Park, S.-W., Park, N.-G., 2011. 6.5% efficient perovskite quantum-dot-sensitized solar cell. Nanoscale 3 (10), 4088–4093.

Jang, D.M., Kim, D.H., Park, K., Park, J., Lee, J.W., Song, J.K., 2016. Ultrasound synthesis of lead halide perovskite nanocrystals. J. Mater. Chem., C. 4 (45), 10625–10629.

Jiang, G., Pan, Z., Ren, Z., Du, J., Yang, C., Wang, W., et al., 2016. Poly (vinyl pyrrolidone): a superior and general additive in polysulfide electrolytes for high efficiency quantum dot sensitized solar cells. J. Mater. Chem. A 4 (29), 11416–11421.

Jiao, S., Shen, Q., Mora-Seró, I., Wang, J., Pan, Z., Zhao, K., et al., 2015. Band engineering in core/shell ZnTe/CdSe for photovoltage and efficiency enhancement in exciplex quantum dot sensitized solar cells. ACS Nano 9 (1), 908–915.

Jovanovski, V., González-Pedro, V., Giménez, S., Azaceta, E., Cabañero, G.N., Grande, H., et al., 2011. A sulfide/polysulfide-based ionic liquid electrolyte for quantum dot-sensitized solar cells. J. Am. Chem. Soc. 133 (50), 20156–20159.

Jun, H.K., Careem, M.A., Arof, A.K., 2013. Quantum dot-sensitized solar cells—perspective and recent developments: a review of Cd chalcogenide quantum dots as sensitizers. Renew. Sustain. Energy Rev. 22, 148–167.

Jung, S.W., Kim, J.-H., Kim, H., Choi, C.-J., Ahn, K.-S., 2012. ZnS overlayer on in situ chemical bath deposited CdS quantum dot-assembled TiO_2 films for quantum dot-sensitized solar cells. Curr. Appl. Phys. 12 (6), 1459–1464.

Kaelin, M., Rudmann, D., Tiwari, A., 2004. Low cost processing of CIGS thin film solar cells. Sol. Energy 77 (6), 749–756.

Katari, J.B., Colvin, V.L., Alivisatos, A.P., 1994. X-ray photoelectron spectroscopy of CdSe nanocrystals with applications to studies of the nanocrystal surface. J. Phys. Chem. 98 (15), 4109–4117.

Kazacos, M.S., McHenry, E., Heller, A., Miller, B., 1980. Fluorescent window for liquid junction solar cells. Sol. Energy Mater. 2 (3), 333–342.

Kim, H., Hwang, I., Yong, K., 2014. Highly durable and efficient quantum dot-sensitized solar cells based on oligomer gel electrolytes. ACS Appl. Mater. Interface 6 (14), 11245–11253.

Klimov, V.I., 2006. Detailed-balance power conversion limits of nanocrystal-quantum-dot solar cells in the presence of carrier multiplication. Appl. Phys. Lett. 89 (12). Available from: https://doi.org/10.1063/1.2356314.

Kojima, A., Teshima, K., Shirai, Y., Miyasaka, T., 2009. Organometal halide perovskites as visible-light sensitizers for photovoltaic cells. J. Am. Chem. Soc. 131 (17), 6050–6051.

Kolodinski, S., Werner, J.H., Wittchen, T., Queisser, H.J., 1993. Quantum efficiencies exceeding unity due to impact ionization in silicon solar cells. Appl. Phys. Lett. 63 (17), 2405–2407.

Kongkanand, A., Tvrdy, K., Takechi, K., Kuno, M., Kamat, P.V., 2008. Quantum dot solar cells. Tuning photoresponse through size and shape control of CdSe − TiO_2 architecture. J. Am. Chem. Soc. 130 (12), 4007–4015.

Kusuma, J., Balakrishna, R.G., Patil, S., Jyothi, M.S., Chandan, H.R., Shwetharani, R., 2018. Exploration of graphene oxide nanoribbons as excellent electron conducting network for third generation solar cells. Sol. Energy Mater. Sol. Cell 183, 211–219.

Kusuma, J., Chandan, H.R., Balakrishna, R.G., 2019. Conjugated molecular bridges: a new direction to escalate linker assisted QDSSC performance. Sol. Energy 194, 74–78.

Lee, Y.L., Lo, Y.S., 2009. Highly efficient quantum-dot-sensitized solar cell based on co-sensitization of CdS/CdSe. Adv. Funct. Mater. 19 (4), 604–609.

Lee, M.M., Teuscher, J., Miyasaka, T., Murakami, T.N., Snaith, H.J., 2012. Efficient hybrid solar cells based on meso-superstructured organometal halide perovskites. Science 338 (6107), 643–647.

Lee, S., Choi, J., Jeon, J.B., Kim, B.J., Han, J.S., Kim, T.L., et al., 2019. Conducting bridge resistive switching behaviors in cubic $MAPbI_3$, orthorhombic $RbPbI_3$, and their mixtures. Adv. Elect. Mater 5 (2). Available from: https://doi.org/10.1002/aelm.201800586.

Leng, M., Yang, Y., Zeng, K., Chen, Z., Tan, Z., Li, S., et al., 2018. All-inorganic bismuth-based perovskite quantum dots with bright blue photoluminescence and excellent stability. Adv. Funct. Mater. 28 (1). Available from: https://doi.org/10.1002/adfm.201704446.

Lewis, N. S., Crabtree, G., 2005. Basic research needs for solar energy utilization: report of the basic energy sciences workshop on solar energy utilization, April 18–21, 2005. US Department of Energy, Office of Basic Energy Science.

Li, W., Zhong, X., 2015. Capping ligand-induced self-assembly for quantum dot sensitized solar cells. J. Phys. Chem. Lett. 6 (5), 796–806.

Li, L., Yang, X., Gao, J., Tian, H., Zhao, J., Hagfeldt, A., et al., 2011. Highly efficient CdS quantum dot-sensitized solar cells based on a modified polysulfide electrolyte. J. Am. Chem. Soc. 133 (22), 8458–8460.

Li, T.-L., Lee, Y.-L., Teng, H., 2012. High-performance quantum dot-sensitized solar cells based on sensitization with $CuInS_2$ quantum dots/CdS heterostructure. Energy Environ. Sci. 5 (1), 5315–5324.

Li, Z., Yu, L., Wang, H., Yang, H., Ma, H., 2020. TiO_2 passivation layer on ZnO hollow microspheres for quantum dots sensitized solar cells with improved light harvesting and electron collection. Nanomater 10 (4), 631. Available from: https://doi.org/10.3390/nano10040631.

Liang, D., Peng, Y., Fu, Y., Shearer, M.J., Zhang, J., Zhai, J., et al., 2016. Color-pure violet-light-emitting diodes based on layered lead halide perovskite nanoplates. ACS Nano 10 (7), 6897–6904.

Liao, Y., Zhang, J., Liu, W., Que, W., Yin, X., Zhang, D., et al., 2015. Enhancing the efficiency of CdS quantum dot-sensitized solar cells via electrolyte engineering. Nano Energy 11, 88–95.

Lignos, I., Stavrakis, S., Nedelcu, G., Protesescu, L., deMello, A.J., Kovalenko, M.V., 2016. Synthesis of cesium lead halide perovskite nanocrystals in a droplet-based microfluidic platform: fast parametric space mapping. Nano Lett. 16 (3), 1869–1877.

Lin, X., Cui, D., Luo, X., Zhang, C., Han, Q., Wang, Y., et al., 2020. Efficiency progress of inverted perovskite solar cells. Energy Environ. Sci. 13 (11), 3823–3847.

Liu, D., Liu, J., Liu, J., Liu, S., Wang, C., Ge, Z., et al., 2019. The effect of CuS counter electrodes for the CdS/CdSe quantum dot co-sensitized solar cells based on zinc titanium mixed metal oxides. J. Mater. Sci. 54 (6), 4884–4892.

Liu, Y., Li, F., Shi, G., Liu, Z., Lin, X., Shi, Y., et al., 2020. PbSe quantum dot solar cells based on directly synthesized semiconductive inks. ACS Energy Lett. 5 (12), 3797–3803.

Lu, W., Song, B., Li, H., Zhou, J., Dong, W., Zhao, G., et al., 2020. Strategy for performance enhancement of $Cd_{1-X}Zn_XTe$/CdS core/shell quantum dot sensitized solar cells through band adjustment. J. Alloy. Comp. 826. Available from: https://doi.org/10.1016/j.jallcom.2020.154050.

Luo, J., Wei, H., Huang, Q., Hu, X., Zhao, H., Yu, R., et al., 2013. Highly efficient core–shell $CuInS_2$–Mn doped CdS quantum dot sensitized solar cells. Chem. Commun. 49 (37), 3881–3883.

Lv, M., Zhu, J., Huang, Y., Li, Y., Shao, Z., Xu, Y., et al., 2015. Colloidal $CuInS_2$ quantum dots as inorganic hole-transporting material in perovskite solar cells. ACS Appl. Mater. Interface 7 (31), 17482–17488.

McDaniel, H., Fuke, N., Pietryga, J.M., Klimov, V.I., 2013a. Engineered $CuInSe_xS_{2-x}$ quantum dots for sensitized solar cells. J. Phys. Chem. Lett. 4 (3), 355–361.

McDaniel, H., Fuke, N., Makarov, N.S., Pietryga, J.M., Klimov, V.I., 2013b. An integrated approach to realizing high-performance liquid-junction quantum dot sensitized solar cells. Nat. Commun. 4 (1). Available from: https://doi.org/10.1038/ncomms3887.

Meng, K., Chen, G., Thampi, K.R., 2015. Metal chalcogenides as counter electrode materials in quantum dot sensitized solar cells: a perspective. J. Mater. Chem. A 3 (46), 23074–23089.

Micic, O.I., Curtis, C.J., Jones, K.M., Sprague, J.R., Nozik, A.J., 1994. Synthesis and characterization of InP quantum dots. J. Phys. Chem. 98 (19), 4966–4969.

Micic, O., Sprague, J., Curtis, C., Jones, K., Machol, J., Nozik, A., et al., 1995. Synthesis and characterization of InP, GaP, and $GaInP_2$ quantum dots. J. Phys. Chem. 99 (19), 7754–7759.

Murphy, J.E., Beard, M.C., Norman, A.G., Ahrenkiel, S.P., Johnson, J.C., Yu, P., et al., 2006. PbTe colloidal nanocrystals: synthesis, characterization, and multiple exciton generation. J. Am. Chem. Soc. 128 (10), 3241–3247.

Murray, C., Norris, D.J., Bawendi, M.G., 1993. Synthesis and characterization of nearly monodisperse CdE (E = sulfur, selenium, tellurium) semiconductor nanocrystallites. J. Am. Chem. Soc. 115 (19), 8706–8715.

Ning, Z., Tian, H., Yuan, C., Fu, Y., Qin, H., Sun, L., et al., 2011. Solar cells sensitized with type-II ZnSe–CdS core/shell colloidal quantum dots. Chem. Commun. 47 (5), 1536–1538.

Nozik, A.J., 2001. Spectroscopy and hot electron relaxation dynamics in semiconductor quantum wells and quantum dots. Annu. Rev. Phys. Chem. 52 (1), 193–231.

Nozik, A.J., 2002. Quantum dot solar cells. Phys. E 14 (1–2), 115–120.

Nozik, A.J., 2008. Multiple exciton generation in semiconductor quantum dots. Chem. Phys. Lett. 457 (1–3), 3–11.

Pan, Z., Zhang, H., Cheng, K., Hou, Y., Hua, J., Zhong, X., 2012. Highly efficient inverted type-I CdS/CdSe core/shell structure QD-sensitized solar cells. ACS Nano 6 (5), 3982–3991.

Pan, Z., Mora-Seró, I., Shen, Q., Zhang, H., Li, Y., Zhao, K., et al., 2014. High-efficiency "green" quantum dot solar cells. J. Am. Chem. Soc. 136 (25), 9203–9210.

Park, D., Azmi, R., Cho, Y., Kim, H.M., Jang, S.-Y., Yim, S., 2019. Improved passivation of PbS quantum dots for solar cells using triethylamine hydroiodide. ACS Sustain. Chem. Eng. 7 (12), 10784–10791.

Peng, Z.A., Peng, X., 2001. Formation of high-quality CdTe, CdSe, and CdS nanocrystals using CdO as precursor. J. Am. Chem. Soc. 123 (1), 183–184.

Petroff, P., DenBaars, S., 1994. MBE and MOCVD growth and properties of self-assembling quantum dot arrays in III–V semiconductor structures. Superlattices Microstruct 15 (1). Available from: https://doi.org/10.1006/spmi.1994.1004.

Ravikumar, C.H., Gowda, M.I., Balakrishna, R.G., 2019. An "OFF–ON" quantum dot–graphene oxide bioprobe for sensitive detection of micrococcal nuclease of *Staphylococcus aureus*. Analyst 144 (13), 3999–4005.

Ravikumar, C.H., Shwetharani, R., Balakrishna, R.G., 2020. Surface modified glass substrate for sensing *E. coli* using highly stable and luminescent CdSe/CdS core shell quantum dots. J. Photochem. Photobiol. B: Biol. 204. Available from: https://doi.org/10.1016/j.jphotobiol.2020.111799.

Riaz, S., Park, S.-J., 2022. Thioacetamide-derived nitrogen and sulfur co-doped carbon quantum dots for "green" quantum dot solar cells. J. Ind. Eng. Chem. 105, 111–120.

Sambur, J.B., Novet, T., Parkinson, B., 2010. Multiple exciton collection in a sensitized photovoltaic system. Sci 330 (6000), 63–66.

Sanehira, E.M., Marshall, A.R., Christians, J.A., Harvey, S.P., Ciesielski, P.N., Wheeler, L., et al., 2017. Enhanced mobility $CsPbI_3$ quantum dot arrays for record-efficiency, high-voltage photovoltaic cells. Sci. Adv. 3 (10). Available from: https://doi.org/10.1126/sciadv.aao4204.

Santra, P.K., Kamat, P.V., 2012. Mn-doped quantum dot sensitized solar cells: a strategy to boost efficiency over 5%. J. Am. Chem. Soc. 134 (5), 2508–2511.

Schaller, R.D., Klimov, V.I., 2004. High efficiency carrier multiplication in PbSe nanocrystals: implications for solar energy conversion. Phys. Rev. Lett. 92 (18). Available from: https://doi.org/10.1103/PhysRevLett.92.186601.

Schaller, R.D., Petruska, M.A., Klimov, V.I., 2005. Effect of electronic structure on carrier multiplication efficiency: comparative study of PbSe and CdSe nanocrystals. Appl. Phys. Lett. 87 (25). Available from: https://doi.org/10.1063/1.2142092.

Schaller, R.D., Sykora, M., Pietryga, J.M., Klimov, V.I., 2006. Seven excitons at a cost of one: redefining the limits for conversion efficiency of photons into charge carriers. Nano Lett. 6 (3), 424–429.

Schock, H.W., Noufi, R., 2000. CIGS-based solar cells for the next millennium. Prog. Photovolt.: Res. 8 (1), 151–160.

Schrier, M., Zehnder, D., Treadway, J., Bartel, J., 2012. Preparation of stable, bright luminescent nanoparticles having compositionally engineered properties. Google Patents.

Shabaev, A., Efros, A.L., Nozik, A.J., 2006. Multiexciton generation by a single photon in nanocrystals. Nano Lett. 6 (12), 2856–2863.

Shalom, M., Dor, S., Ruhle, S., Grinis, L., Zaban, A., 2009. Core/CdS quantum dot/shell mesoporous solar cells with improved stability and efficiency using an amorphous TiO_2 coating. J. Phys. Chem. C. 113 (9), 3895–3898.

Sharma, S., Jain, K.K., Sharma, A., 2015. Solar cells: in research and applications—a review. Mater. Sci. Appl. 6 (12). Available from: https://doi.org/10.4236/msa.2015.612113.

Shaw, P.E., Ruseckas, A., Samuel, I.D., 2008. Exciton diffusion measurements in poly (3-hexylthiophene). Adv. Mater. 20 (18), 3516–3520.

Shen, T., Tian, J., Lv, L., Fei, C., Wang, Y., Pullerits, T., et al., 2016. Investigation of the role of Mn dopant in CdS quantum dot sensitized solar cell. Electrochim. Acta 191, 62–69.

Shin, S.S., Lee, S.J., Seok, S.I., 2019. Metal oxide charge transport layers for efficient and stable perovskite solar cells. Adv. Funct. Mater. 29 (47). Available from: https://doi.org/10.1002/adfm.201900455.

Singh, S.P., Nagarjuna, P., 2014. Organometal halide perovskites as useful materials in sensitized solar cells. Dalton Trans. 43 (14), 5247–5251.

Stolterfoht, M., Wolff, C.M., Márquez, J.A., Zhang, S., Hages, C.J., Rothhardt, D., et al., 2018. Visualization and suppression of interfacial recombination for high-efficiency large-area pin perovskite solar cells. Nat. Energy 3 (10), 847–854.

Sun, C., Xu, G., Jiang, X.-M., Wang, G.-E., Guo, P.-Y., Wang, M.-S., et al., 2018. Design strategy for improving optical and electrical properties and stability of lead-halide semiconductors. J. Am. Chem. Soc. 140 (8), 2805–2811.

Swarnkar, A., Marshall, A.R., Sanehira, E.M., Chernomordik, B.D., Moore, D.T., Christians, J. A., et al., 2016. Quantum dot–induced phase stabilization of α-$CsPbI_3$ perovskite for high-efficiency photovoltaics. Sci 354 (6308), 92–95.

Tan, L., Zhou, Y., Ren, F., Benetti, D., Yang, F., Zhao, H., et al., 2017. Ultrasmall PbS quantum dots: a facile and greener synthetic route and their high performance in luminescent solar concentrators. J. Mater. Chem. A 5 (21), 10250–10260.

Tao, L., Xiong, Y., Liu, H., Shen, W., 2014. High performance PbS quantum dot sensitized solar cells via electric field assisted in situ chemical deposition on modulated TiO_2 nanotube arrays. Nanoscale 6 (2), 931–938.

Tauc, J., 1959. Electron impact ionization in semiconductors. J. Phys. Chem. Solids 8, 219–223.

Thambidurai, M., Muthukumarasamy, N., Sabari Arul, N., Agilan, S., Balasundaraprabhu, R., 2011. CdS quantum dot-sensitized ZnO nanorod-based photoelectrochemical solar cells. J. Nanopart. Res. 13 (8), 3267–3273.

Tian, J., Gao, R., Zhang, Q., Zhang, S., Li, Y., Lan, J., et al., 2012. Enhanced performance of CdS/CdSe quantum dot cosensitized solar cells via homogeneous distribution of quantum dots in TiO_2 film. J. Phys. Chem. C. 116 (35), 18655–18662.

Tong, Y., Bladt, E., Aygüler, M.F., Manzi, A., Milowska, K.Z., Hintermayr, V.A., et al., 2016. Highly luminescent cesium lead halide perovskite nanocrystals with tunable composition and thickness by ultrasonication. Angew. Chem. Int. (Ed.) 55 (44), 13887–13892.

Tubtimtae, A., Wu, K.-L., Tung, H.-Y., Lee, M.-W., Wang, G.J., 2010. Ag_2S quantum dot-sensitized solar cells. Electrochem. Commun. 12 (9), 1158–1160.

Vavilov, V.S., 1959. On photo-ionization by fast electrons in germanium and silicon. J. Phys. Chem. Solids 8, 223–226.

Vázquez, C.I., Baruzzi, A.M., Iglesias, R.A., 2016. Charge extraction from TiO_2 nanotubes sensitized with CdS quantum dots by SILAR method. IEEE J. Photovolt. 6 (6), 1515–1521.

Venkataramana, M., Chandan, H.R., Kurkuri, M.D., Balakrishna, R., 2016. G. Simple quantum dot bioprobe/label for sensitive detection of *Staphylococcus aureus* TNase. Sens. Actuators, B Chem. 222, 1201–1208.

Vogel, R., Hoyer, P., Weller, H., 1994. Quantum-Sized PbS, CdS, Ag_2S, Sb_2S_3, and Bi_2S_3 particles as sensitizers for various nanoporous wide-bandgap semiconductors. J. Phys. Chem. 98 (12), 3183–3188.

Wada, T., Kohara, N., Nishiwaki, S., Negami, T., 2001. Characterization of the Cu (In, Ga) Se2/Mo interface in CIGS solar cells. Thin Solid. Films 387 (1–2), 118–122.

Wang, J., Mora-Seró, I., Pan, Z., Zhao, K., Zhang, H., Feng, Y., et al., 2013. Core/Shell Colloidal quantum dot exciplex states for the development of highly efficient quantum-dot-sensitized solar cells. J. Am. Chem. Soc. 135 (42), 15913–15922.

Wang, Y., Li, X., Song, J., Xiao, L., Zeng, H., Sun, H., 2015. All-inorganic colloidal perovskite quantum dots: a new class of lasing materials with favorable characteristics. Adv. Mater. 27 (44), 7101–7108.

Wang, A., Yan, X., Zhang, M., Sun, S., Yang, M., Shen, W., et al., 2016. Controlled synthesis of lead-free and stable perovskite derivative Cs_2SnI_6 nanocrystals via a facile hot-injection process. Chem. Mater. 28 (22), 8132–8140.

Wei, H., Wang, G., Shi, J., Wu, H., Luo, Y., Li, D., et al., 2016a. Fumed SiO_2 modified electrolytes for quantum dot sensitized solar cells with efficiency exceeding 11% and better stability. J. Mater. Chem. A 4 (37), 14194–14203.

Wei, S., Yang, Y., Kang, X., Wang, L., Huang, L., Pan, D., 2016b. Room-temperature and gram-scale synthesis of $CsPbX_3$ (X = Cl, Br, I) perovskite nanocrystals with 50–85% photoluminescence quantum yields. Chem. Commun. 52 (45), 7265–7268.

Weller, H., 1991. Quantum sized semiconductor particles in solution and in modified layers. Ber. Bunsen. Phys. Chem. 95 (11), 1361–1365.

Willardson, R.K., Weber, E.R., Sugawara, M., 1999. Self-Assembled InGaAs/GaAs Quantum Dots. Academic Press.

Wood, V., Halpert, J.E., Panzer, M.J., Bawendi, M.G., Bulovic, V., 2009. Alternating current driven electroluminescence from ZnSe/ZnS: Mn/ZnS nanocrystals. Nano Lett. 9 (6), 2367–2371.

Wu, M., Lin, X., Wang, Y., Ma, T., 2015. Counter electrode materials combined with redox couples in dye-and quantum dot-sensitized solar cells. J. Mater. Chem. A 3 (39), 19638–19656.

Xiang, W., Tress, W., 2019. Review on recent progress of all-inorganic metal halide perovskites and solar cells. Adv. Mater 31 (44). Available from: https://doi.org/10.1002/adma.201902851.

Xu, Y., Li, S., Zhang, Z., Hu, Y., Yuan, L., Chen, W., et al., 2019. Ligand-mediated synthesis of colloidal Cs_2SnI_6 three-dimensional nanocrystals and two-dimensional nanoplatelets. Nanotechnol 30 (29). Available from: https://doi.org/10.1088/1361-6528/ab13f6.

Yang, Y., Wang, W., 2015. A new polymer electrolyte for solid-state quantum dot sensitized solar cells. J. Power Sources 285, 70–75.

Yang, Z., Chen, C.Y., Liu, C.W., Chang, H.T., 2010. Electrocatalytic sulfur electrodes for CdS/CdSe quantum dot-sensitized solar cells. Chem. Commun. 46 (30). Available from: https://doi.org/10.1039/c0cc00642d.

Yang, Y., Zhu, L., Sun, H., Huang, X., Luo, Y., Li, D., et al., 2012. Composite counter electrode based on nanoparticulate PbS and carbon black: towards quantum dot-sensitized solar cells with both high efficiency and stability. ACS Appl. Mater. Interface. 4 (11), 6162–6168.

Yang, P., Tang, Q., Ji, C., Wang, H., 2015a. A strategy of combining SILAR with solvothermal process for In2S3 sensitized quantum dot-sensitized solar cells. Appl. Surf. Sci. 357, 666–671.

Yang, S., Zhao, P., Zhao, X., Qu, L., Lai, X., 2015b. InP and Sn:InP based quantum dot sensitized solar cells. J. Mater. Chem. A. 3 (43), 21922–21929.

Yang, B., Chen, J., Hong, F., Mao, X., Zheng, K., Yang, S., et al., 2017. Lead-free, air-stable all-inorganic cesium bismuth halide perovskite nanocrystals. Angew. Chem. 129 (41), 12645–12649.

Yella, A., Lee, H.-W., Tsao, H.N., Yi, C., Chandiran, A.K., Nazeeruddin, M.K., et al., 2011. Porphyrin-sensitized solar cells with cobalt (II/III)–based redox electrolyte exceed 12 percent efficiency. Sci 334 (6056), 629–634.

Yu, Z., Zhang, Q., Qin, D., Luo, Y., Li, D., Shen, Q., et al., 2010. Highly efficient quasi-solid-state quantum-dot-sensitized solar cell based on hydrogel electrolytes. Electrochem. Commun. 12 (12), 1776–1779.

Yu, X.Y., Liao, J.Y., Qiu, K.Q., Kuang, D.B., Su, C.Y., 2011. Dynamic study of highly efficient CdS/CdSe quantum dot-sensitized solar cells fabricated by electrodeposition. ACS Nano 5 (12), 9494–9500.

Yu, X.-Y., Lei, B.-X., Kuang, D.-B., Su, C.-Y., 2012. High performance and reduced charge recombination of CdSe/CdS quantum dot-sensitized solar cells. J. Mater. Chem. 22 (24), 12058–12063.

Zhang, Q., Zhang, Y., Huang, S., Huang, X., Luo, Y., Meng, Q., et al., 2010. Application of carbon counterelectrode on CdS quantum dot-sensitized solar cells (QDSSCs). Electrochem. Commun. 12 (2), 327–330.

Zhang, J., Gao, J., Miller, E.M., Luther, J.M., Beard, M.C., 2014. Diffusion-controlled synthesis of PbS and PbSe quantum dots with in situ halide passivation for quantum dot solar cells. ACS Nano 8 (1), 614–622.

Zhang, F., Zhong, H., Chen, C., Wu, X.-g, Hu, X., Huang, H., et al., 2015. Brightly luminescent and color-tunable colloidal $CH_3NH_3PbX_3$ (X = Br, I, Cl) quantum dots: potential alternatives for display technology. ACS Nano 9 (4), 4533–4542.

Zhang, H., Yang, C., Du, Z., Pan, D., Zhong, X., 2017. Graphene hydrogel-based counter electrode for high efficiency quantum dot-sensitized solar cells. J. Mater. Chem. A 5 (4), 1614–1622.

Zhang, L., Rao, H., Pan, Z., Zhong, X., 2019. ZnSxSe1−x alloy passivation layer for high-efficiency quantum-dot-sensitized solar cells. ACS Appl. Mater. Interface. 11 (44), 41415–41423.

Zheng, X., Hou, Y., Bao, C., Yin, J., Yuan, F., Huang, Z., et al., 2020. Managing grains and interfaces via ligand anchoring enables 22.3%-efficiency inverted perovskite solar cells. Nat. Energy 5 (2), 131–140.

Zhou, L., Xu, Y.F., Chen, B.X., Kuang, D.B., Su, C.Y., 2018. Synthesis and photocatalytic application of stable lead-free $Cs_2AgBiBr_6$ perovskite nanocrystals. Small 14 (11). Available from: https://doi.org/10.1002/smll.201703762.

Zhu, H., Song, N., Lian, T., 2010a. Controlling charge separation and recombination rates in CdSe/ZnS type I core − shell quantum dots by shell thicknesses. J. Am. Chem. Soc. 132 (42), 15038–15045.

Zhu, G., Cheng, Z., Lv, T., Pan, L., Zhao, Q., Sun, Z., 2010b. Zn-doped nanocrystalline TiO_2 films for CdS quantum dot sensitized solar cells. Nanoscale 2 (7), 1229–1232.

Zumeta-Dube, I., Ruiz-Ruiz, V.-F., Diaz, D., Rodil-Posadas, S., Zeinert, A., 2014. TiO_2 sensitization with Bi_2S_3 quantum dots: the inconvenience of sodium ions in the deposition procedure. J. Phys. Chem. C. 118 (22), 11495–11504.

This page intentionally left blank

Chapter 13

Application of quantum dots in sensors

Neelam Kunwar[1], Hetal Zala[2] and Kushnuma Parveen[3]
[1]*Department of Chemistry, PAHER University, Udaipur, Rajasthan, India,* [2]*1197-1, Uchigashimacho, A-101, Gunma, Ota-Shi, Japan,* [3]*Khamis Mushayt, Ahad Rafaidah, Kingdom of Saudi Arabia*

13.1 Introduction

Any change in biological or chemical environment is likely to affect the life of human beings, plants, animals, and aquatic plants and organisms. Similarly, humidity and temperature may also affect some physical or chemical phenomena. Therefore sometimes it becomes very much necessary to know the changes in these parameters. The slight variation in chemical environment can affect the health of living beings as some chemicals available in the atmosphere are toxic in nature if present even in very low concentrations. Sometimes, the presence of these chemicals can be fatal also and thus these should be detected in time otherwise any reaction may be totally undesirable. There are some limits on their concentrations, above which these are harmful and they may create disease or harm. Development of any disease or deformation in the body can be detected in advance if a proper sensing system is available. Then, such diseases can be diagnosed in a timely manner and treatment can be started at an early stage. Therefore, such chemical or biological changes should be monitored so as the protect the society from their adverse effects.

The variation of temperature and/or the presence of high humidity also affect some physical or chemical entities adversely, that is, corrosion of metals, stability of hygroscopic compounds, etc., depending on the circumstances. Hence, the correct measurement of humidity and temperature becomes necessary to safeguard certain materials or reactions from high humidity or temperature. Although various sensing systems are commercially available for sensing the presence of some chemical changes such as liquefied petroleum gas, ammonia, alcohol, carbon monoxide, etc., these have some other limits or demerits. Quantum dots (QDs) have some interesting properties like smaller size, large surface area-to-volume ratio, and

Quantum Dots. DOI: https://doi.org/10.1016/B978-0-12-824153-0.00013-6

fluorescence/photoluminescence, and as a result these QDs can find potential applications in fabricating effective, sensitive, and selective sensors. In this chapter, the development of chemical, biological, temperature, and humidity sensors has been discussed.

13.2 Sensors

QDs can find numerous applications in fabricating sensors such as temperature, humidity, alcohol, hydrogen sulfide, ammonia, carbon dioxide, nitrogen dioxide, pesticides, biosensors, etc.

13.2.1 Chemical sensors

Various chemicals are hazardous in nature and their presence in the atmosphere can affect the lives of human beings, animals, plants, aquatic organisms, etc. They can create a number of dreadful diseases including cancer. Therefore, it is very important to know their presence, even if they are present in very low concentrations. Here, QDs can help us in sensing their presence as their florescence or photoluminescence can be quenched by their presence. Very good and effective sensors are now available involving mainly QDs.

13.2.1.1 Alcohol sensors

A high-performance ethanol sensor based on iron (Fe)-doped titanium dioxide (TiO_2)/molybdenum disulfide (MoS_2) nanocomposite was demonstrated. Wu et al. (2018) synthesized flower-like MoS_2 and Fe-TiO_2 QDs by a facile hydrothermal route. Then they prepared Fe-TiO_2/MoS_2 composite via a layer-by-layer (LbL) self-assembly technique. As-fabricated Fe-TiO_2/MoS_2 film sensor was used to determine different concentrations of ethanol (gas) at room temperature. It was indicated that this sensor has a short response/recovery time, high response, excellent selectivity, stable repeatability, long-term stability, along with detection low limit (ppb level).

Abbasi and Alizadeh (2020) prepared a hybrid of ZnS:Mn^{2+} QDs and soluble N-methylpolypyrrole (NMPPy). It was reported that the determination of methanol can be carried out using as-prepared ZnS:Mn^{2+} QDs/NMPPy hybrid with high selectivity, sensitivity, and a limit of detection of 1 mM in the concentration range of 25−230 mM. As-fabricated hybrid was successfully used to determine the amount of methanol in real samples of alcoholic beverages.

Masemola et al. (2021) synthesized NGQDs via a microwave-assisted hydrothermal method. They used urea and citric acid as nitrogen and carbon sources, respectively. It was reported that uniformly distributed NGQDs (spherical) were obtained in 4 min. Then these dots were further loaded onto PANI/PAN to fabricate NGQDs/PANI/PAN composite. It was observed that

optimized electrospun composite fibers can be used for sensing of alcohol vapors.

13.2.1.2 Liquid petroleum gas sensor

Liquid petroleum gas-sensing behavior of graphene/SrO QDs composites was also investigated by Nemade and Waghuley (2013a). They evaluated gas-sensing properties of composites by the change in resistance as a function of gas concentration of LPG.

They also synthesized graphene/Bi_2O_3 QDs composites (Nemade and Waghuley 2013b). It was reported that as-prepared composites exhibited better performance toward the sensing of LPG. The graphene/CeO_2 QDs composite was synthesized by Nemade and Waghuley (2013c). They used this composite for sensing of liquid petroleum gas at room temperature. This composite of graphene/CeO_2 QDs was prepared on mixing 20 wt.% of graphene in CeO_2 (1 g). This composite shows excellent stability and sensing response.

Mishra et al. (2015) synthesized rGO/SnO_2 QDs and investigated its LPG gas sensing behavior. It was reported that this sensor exhibited a high response of ~92.4% to LPG (500 ppm) at 250°C. As-fabricated rGO/SnO_2 QDs-based sensor also has a good selectivity for LPG even in the presence of other chemicals such as chloroform, ammonia, benzene, toluene, acetone, formic acid, acetic acid, and *n*-butylacetate. It was observed that the gas response to LPG was about 17.8 times higher compared to formic acid. An excellent reproducibility was also observed in this sensor. Zhang et al. (2018b) prepared zinc oxide/polypyrrole/lead sulfide QDs (ZnO/PPy/PbS QDs) nanocomposite film and used it as a liquefied petroleum gas sensor. It was reported that it can detect LPG and the response at 1000 ppm LPG could reach 45.47%. It was also revealed that it showed excellent repeatability and good selectivity.

13.2.1.3 Ammonia (NH_3) sensors

Liu et al. (2016) prepared PbS QDs/TiO_2 nanotubes arrays (PbS QDs/TiO_2 NTARs) via ionic-layer adsorption. Then they fabricated a gas sensor for ammonia based on these. It was observed that PbS QDs/TiO_2 NTARs had a good response toward ammonia gas and could detect 17.49−100 ppm ammonia with a limit of detection of 2 ppm. It was also revealed that as-fabricated PbS QDs/TiO_2 NTARs show good selectivity toward ammonia as compared with methanol, ethanol, acetone, and toluene.

Hollow indium trioxide nanofibers were fabricated by Hong et al. (2021) via a combination of electrospinning and high-temperature calcinations. Then these were coated with nitrogen-doped graphene QDs (N-GQDs). As-prepared N-GQD-coated hollow In_2O_3 nanofibers served as a core for synthesizing polyaniline (PANI)/N-GQD/hollow In_2O_3 nanofiber ternary

composites using in situ chemical oxidative polymerization. It was observed that the response value of the PANI/20%N-GQD/hollow In_2O_3 nanofiber sensor was 15.2 on exposure to 1 ppm ammonia. This was almost 4.4 times more than the PANI sensor. It was revealed that this composite sensor proved to be very sensitive in the detection of NH_3 in the concentration range of 0.6−2.0 ppm at room temperature. This sensor also exhibited higher selectivity and repeatability in the range of 1.0−2.0 ppm NH_3. Hence, it was suggested that it will prove to be a good gas-sensing material in the case of human breath for detecting hepatic or kidney disease.

Kumar et al. (2018) fabricated poly(3, 3-dialkylquaterthiophene) (PQT-12) and CdSe QDs composite. It was based on back-gated organic thin-film transistors (OTFTs) SiO_2-coated heavily doped p-Si substrates. It was reported that an estimated gas response of ∼51% was obtained for sensing ammonia gas using a PQT-12/CdSe QDs composite, which was higher than an OTFT pristine PQT-12 OTFT-based sensor (41%). Liu et al. (2018) self-assembled 3-D cocoon-like architectures of PbS QDs−reduced graphene oxide composites. It was observed that 3-D PbS QDs/rGO nanococoons exhibited a good detection limit of 750 ppb toward sensing ammonia gas at room temperature, which was higher than rGO and pure PbS QDs. It was also revealed that these 3-D PbS QDs/rGO nanococoons show a good selectivity toward ammonia gas compared to ethanol, acetone, etc. with excellent sensing stability in the long term.

Ouyang et al. (2018) prepared monolayer WS_2 NSs modified with Pt QDs. It was reported that the response of nanocomposite to NH_3 (250 ppm) was almost ten times that of WS_2 NSs. Liu et al. (2019) self-assembled $CuSbS_2$ QDs/reduced graphene oxide composites via a hot-injection method. It was reported that a gas sensor based on $CuSbS_2$ QDs/rGO composites exhibited a good response toward ammonia with a limit of detection of 500 ppb with an average response time of 50 s at room temperature. It was revealed that the sensing performance of the composites was improved in the presence of visible light.

Wongrat et al. (2021) prepared ZnO nanostructures combined with GQDs. It was reported that GQDs have an average size distribution of 2.6 nm. It was revealed that as-prepared ZnO:GQD heterojunctions exhibited a selective response (high) to the vapor of ammonia. As-fabricated ZnO: GQDs sensors have the optimum sensor response at an ammonia concentration of 1000 ppm. This sensor was found to be highly responsive and gave a selective performance for sensing ammonia at room temperature. Bai et al. (2022) prepared flower-like MoS_2 decorated with SnO_2 QDs via a solvothermal method. It was reported that SnO_2 QDs have a uniform particle size of 2−4 nm and these were uniformly distributed on the ultrathin nanosheets of MoS_2 hierarchical architectures. It was found that as-prepared SnO_2 QDs@MoS_2 composites-based gas sensor exhibited a good response of 8.6 with short response and recovery times of 6 s/121 s, respectively to 100 ppm

ammonia with good selectivity, excellent repeatability, and outstanding long-term stability.

13.2.1.4 Hydrogen sulfide (H_2S) sensors

Keshtkar et al. (2018) synthesized SnO_2 QDs−fullerene (SnO_2 QDs-C_{60}) nanohybrid via a hydrothermal method. It was observed that the as-prepared hybrid could detect H_2S (70 ppm). This sensor exhibited a good selectivity toward H_2S gas in the range 5.4−70 ppm. Dun et al. (2019) prepared CdS QDs supported by ultrathin porous nanosheets and further assembled into hollowed-out Co_3O_4 microspheres (CdS QD/Co_3O_4 HMSs). It was observed that CdS QDs of ∼4.5 nm size were well dispersed on Co_3O_4 HMSs (ultrathin porous nanosheet). It was reported that this sensor exhibited a high response (12.7) for 100 ppm H_2S as well as fast response and recovery rates of 0.6−1.0 s, respectively.

Yang et al. (2019) prepared In_2O_3 colloidal QDs and then they deposited In_2O_3 QDs followed by surface ligand exchange treatment via Cu inorganic salts to fabricate H_2S sensor devices. It was reported that the as-prepared sensor exhibited a high response up to 90 for H_2S (5 ppm) with response and recovery time of 72 and 200 s, respectively. Xu et al. (2021) prepared carbon dots passivated with polyethylene glycol. These were then used for detection of H_2S. This proposed sensor can detect Na_2S with a concentration limit of detection approximately 7.0 nM. It was proposed that this probe can also be used successfully for the detection of H_2S in live cells.

13.2.1.5 Carbon dioxide (CO_2) sensors

Chu and Hsieh (2019) designed an optical fiber carbon dioxide sensor, which was based on the emission wavelength shift of $CuInS_2$/ZnS QDs. It was all due to changes in the absorption of α-naphtholphthalein (a pH indicator). With a change in concentration of CO_2. It allowed the detection of CO_2 concentration over the range of 0%−100%. Bhakat et al. (2021) assembled ZnO QDs. It was reported that as-prepared ZnO QD−phosphate was successfully used for designing a gas sensor that showed great sensitivity and selectivity toward CO_2 gas at room temperature. Hajikhanloo et al. (2021) created a valley in the core of the ring and then PbSe QDs were deposited in this valley. This sensor was used to detect CO_2 gas. It was reported that the refractive index of PbSe QDs was found to increase with the increase in the concentration of gas flow. It was revealed that the as-prepared sensor operated in a wide range of concentrations for CO_2 gas with a detection limit of 0.001%.

13.2.1.6 Nitrogen dioxide (NO_2) sensors

Wang et al. (2013) functionalized silica aerogels branched polyethyleniminecapped QDs. The fluorescence quantum yield of CQD-aerogel hybrid material yield was more than 40%. Its fluorescence was sensitively and

selectively quenched by NO_2 gas. Dong et al. (2018) synthesized germanium QDs (GeQDs)/graphene hybrids. They fabricated a NO_2 gas sensor by introducing GeQDs on graphene and the gas sensor sensitivity to NO_2 was improved substantially. With the optimization of the growth time of GeQDs (600 s), the response sensitivity to 10 ppm NO_2 can be as high as 3.88, which is 20 times higher than that of the graphene sensor without GeQDs decoration. The 600 s GeQDs/graphene hybrid sensor exhibited fast response and recovery rates as well as excellent stability.

Lv et al. (2021) prepared SnO_2 hierarchical hollow cubes (ultrathin mesoporous nanosheets) and then N-GQDs were decorated on the surface of SnO_2. It was reported that as-prepared N-GQDs modified SnO_2 (NG/Sn_x) exhibited an improved response toward 1 ppm NO_2, which was almost 2.2 times that of pure SnO_2. Thus sensing material exhibited long-term stability, fast response, recovery repeatability, and good selectivity. This NG/$Sn_{1.5}$ sensor can even detect lower concentrations of NO_2 at the level of 100 ppb.

Zhang et al. (2021) modified ZnO composite with N-GQDs. The sample G-Z-2 (N-GQD_S doping amount of 2 mL) exhibited excellent sensing performance for NO_2 compared with pure ZnO. It was found to be sensitive to 5 ppm NO_2, which was 11.6 times more than others. The detection limit of NO_2 was found to be 0.1 ppm. It was also revealed that there is selectivity, excellent reproducibility, and stability in this sensor for the detection of NO_2. Luo et al. (2022) modified MoS_2 with SnO_2. The MoS_2 nanoflowers were prepared via a hydrothermal method with a high surface/volume ratio and SnO_2 was fabricated using a solvothermal method. It was revealed that its response was increased by 1.5 times on modification, supported by fast response and recovery time for sensing of NO_2 gas.

13.2.1.7 Pesticide sensors

Liang et al. (2021) developed a fluorescence/colorimetric sensor, which was based on a nanocomposite of carbon QDs and gold nanoparticles (CQDs-GNPs). It was observed that fluorescence intensity increased, but absorption decreased with the addition of malathion, a pesticide. Finally, the approximate concentrations of malathion in cabbage samples were estimated by the standard arrays and the naked eye. It was revealed that malathion can be accurately detected in cabbage samples with two methods with recoveries of 89.9%−103.4% (fluorescence) and 88.7%−107.6% (colorimetric).

Nair et al. (2020) prepared a fluorescent sulfur-doped GQDs (S-GQDs)-based sensor. It was reported that the particle size distribution was uniform in the order of $\sim$5 nm with high crystallinity. It was revealed that green fluorescent S-GQDs exhibited a detection limit of 0.45 and 1.6 ppb for carbofuran and thiram, respectively. A sensor was developed by Liang et al. (2021) that was based on CQDs-GNPs. It was observed that fluorescence intensity was increased on the addition of malathion in the range of 1×10^{-9}

to 1×10^{-2} M. It was reported that concentrations of malathion in cabbage samples can also be determined. Alvandi et al. (2021) prepared multicolor fluorescent carbon dots via a hydrothermal method using greengage plums. These carbon dots were used to detect pesticides (duplosan, confidor, and dialen super). It was also revealed that the as-prepared nanosensor did not detect other pesticides such as diazinon, bromoxynil, malathion, glyphosate, and deltamethrin, confirming that it is sensitive and specific toward the three intended pesticides.

Ghiasi et al. (2021) fabricated a selective and sensitive electrochemical sensor based on the modification of activated glassy carbon electrode with nickel molybdate GQDs, and chitosan nanocomposites. It was reported that the as-fabricated sensor can be used in a concentration range between 0.1 and 330 μM with a limit of detection of 30 nM. The function of the sensor was also evaluated for the recovery analysis of diazinon in real samples of tomato and cucumber.

Yellowish-green emitting CQDs were prepared by Huo et al. (2021) via hydrothermal treatment. They used p-phenylenediamine and citric acid as precursors. It was observed that phoxim can quench the fluorescence emission of CQDs by an inner filter effect. As-prepared CQDs showed a good selectivity and sensitivity for detection of phoxim in the concentration ranges of 1−10 and 10−98 μM with a detection limit of 0.09 μM. It was revealed that phoxim can also be detected in real samples with satisfactory recoveries ranging between 93% and 105.9%. The low cytotoxicity and excellent biocompatibility of these CQDs was suitable for cell imaging also.

Yang et al. (2021b) synthesized cadmium telluride QDs. As-prepared CdTeQDs exhibited good water dispersion bright emission, and long emission wavelength as well as a unique response inhibition of organophosphorus pesticides (OPs) on acetylcholinesterase (AChE) activity. It was reported that the detection of OPs can be done with sensitivity, with the limit of detection of 0.027 ng mL^{-1}. It was observed that a CdTe-QD-based sensor can monitor methidathion in cultivated soil as well as Chinese cabbage.

Yi et al. (2021) first modified molybdenum disulfide QDs (MoS_2 QDs) with 3-aminophenyl boronic acid, and then it was functionalized with hydropropyl-β-cyclodextrin (β-CD), (β-CD functionalized MoS_2 QDs β-CD-MoS_2 QDs). It was used for fluorescent detection of parathion-methyl (MP), hydrolyzed to p-nitrophenol which can enter into the β-CD cavity; thus resulting in fluorescence quenching. It was reported that as-prepared β-CD-MoS_2 QDs nanoprobe exhibited a wide detection range of 0.01−18.0 ppm and a low detection limit of 3.3 ppb for the detection of parathion-methyl. An excellent selectivity was also reported for detection of MP, and it can be applied in real samples. Fluorescent CQDs (J-CQDs) were prepared by Chandra et al. (2022) using jatropha fruit via a hydrothermal route. The catalytic activity of AChE was inhibited in the presence of OPs, and a fluorescence signal was recovered. A sensitive and selective nanoprobe was designed as a sensor,

which can detect chlorpyrifos with a limit of detection (2.7 ng mL^{-1}). It was also revealed that this can be applied for pesticide detection in environmental and agricultural samples successfully with acceptable recovery.

13.2.1.8 Others

Lu et al. (2019) prepared a carbon dot-decorated hybrid nanocomposite (CD@RCC3) (chiral porous organic cage) and used it to fabricate a fluorescent sensor. It was reported that the as-fabricated sensor was used for the determination of isomers of nitrophenol. It could also differentiate phenylethanol and phenylalaninol enantiomers.

Yang et al. (2021c) prepared CdTeS QDs-coated silica shell (CdTeS QDs@SiO_2). Then ZnCdS QDs were encapsulated in a 3D network imprinted polymer (ZnCdS QDs@MIP) to give a response signal. It was observed that the fluorescence emission of ZnCdS QDs@MIP was quenched in the presence of ascorbic acid (1−500 μM) with a detection limit of 0.78 μM. It was reported that satisfactory results were obtained in the detection of ascorbic acid in vitamin C tablets.

Liu et al. (2021) designed an ECL sensor based on a dual-emission luminophore (NSGQDs-PEI-luminol-Pt). It was composed of nitrogen and sulfur codoped GQDs (NSGQDs) (main luminophore), luminol (auxiliary luminophore), platinum nanoparticles (coreaction accelerator), and polyetherimide linker of NSGQDs and luminal, respectively. This ECL senor can detect ascorbic acid in the concentration range of 10−360 nM with a limit of detection of 3.3 nM. It was also used for monitoring ascorbic acid in human serum.

Yanyan et al. (2021) fabricated a sensor based on N-GQDs. This sensor was used for the detection of H_2O_2 and glucose in the concentration range of 0.3−100.0 and 0.7−90.0 μM with a limit of detection of 63 nM. The sensitive detection of glucose is also realized in the concentration range (0.7−90.0 μM) with LOD of 96 nM, because the oxidation of glucose by glucose oxidase (GOx) produces H_2O_2.

A fluorescence sensor with dual-emission was developed by Gan et al. (2021) based on CQDs and Eu^{3+} complexes. It was observed that dual-emission fluorescence intensity was increased in the presence of Hg^{2+} ions. It was reported that the as-developed sensor exhibited an excellent sensitivity and selectivity in the concentration range of 1−20 nM with a detection limit of 0.2 nM. It was revealed that this sensor gave satisfactory recovery from 97.6% to 105.4% for the detection of Hg^{2+} ions in drinking water and milk samples.

A single-step synthesis of positively charged Pd NPs and green synthesis of GQDs from graphite was reported by Ahmed et al. (2021). An aptamer-induced fluorescence fluctuation of GQDs and palladium nanoparticles for the detection of tetracycline has been observed with a limit of detection of

45 ng mL^{-1}. CQDs were synthesized via a facile one-step hydrothermal treatment of purslane leaves by Amer et al. (2021). It was reported that a CQDs-based sensor could detect formaldehyde. It was revealed that the as-fabricated sensor exhibited a good reversibility and reproducibility.

Carneiro et al. (2021) synthesized CQDs via a hydrothermal route using the seed of *Caelsalpinia pulcherrima*. They could detect five food additives—lactic acid, citric acid, ascorbic acid, potassium sorbate, and sodium benzoate—with a detection limit of 252 ng mL^{-1}. They also successfully identified all these additives in a sample of a pickled olives with 100% of the combinations correctly identified.

Huangfu and Feng (2021) synthesized $CsPbBr_3$ QDs and used them to sense various solvents with different polarities. A good linear relationships was found between the fluorescence intensity of $CsPbBr_3$ QDs and the volume of different polar solvents, ethanol, methanol, and acetone. It is all due to the fast change of polarity, which makes perovskite QDs useful as polarity sensors. They used as-fabricated $CsPbBr_3$ QDs for total polar materials detection in edible oils. The quenching effect of fluorescence intensity was observed for soybean oil, olive oil, and sunflower oil, in the range of 17%−31.5%, 25%−31.5%, and 21.5%−33%, respectively.

Khose et al. (2021) synthesized novel red-fluorescent GQDs (G-GQD) using therapeutic guava (*Psidium guajava*) leaf. It was reported that the emission property of as-fabricated G-GQD can be used as a fluorescence turn-off probe for the determination of Hg^{2+} ions with a detection limit of 82 μM. It was also reported that other ions such as Co^{2+}, Cu^{2+}, Al^{3+}, and Fe^{2+}, are also known fluorescence quenchers, but they did not show any interference with the selectivity of Hg^{2+} ions. The G-GQD can be used as a sensor for Hg^{2+} ions even in polluted water sources.

Kongsanan et al. (2021) synthesized GQDs by pyrolyzing solid citric acid. The as-prepared sample can be used for the simultaneous detection of ferricyanide $[Fe(CN)_6]^{3-}$ and cyanide (CN^-) in wastewater samples (Fig. 13.1). It was reported that the fluorescence intensity of GQDs decorated with Hg^{2+} could be turned on in the presence of CN^- and back to turn-off mode by $[Fe(CN)_6]^{3-}$. These can be detected simultaneously in the range of 5.0−15.0 and 10.0−50.0 μM, with detection limits of 3.10 and 9.48 μM for CN^- ion and $[Fe(CN)_6]^{3-}$, respectively. This sensor was successfully used for CN^- and $[Fe(CN)_6]^{3-}$ detection (simultaneous and selective) in wastewater samples of municipal water reservoirs.

Lu et al. (2021) fabricated functionalized carbon nitride QDs (CNQDs) using a microwave-assisted solvothermal method. It was reported that these CNQDs were monodispersed with a narrow size distribution of particles with an average size of 3.5 nm. They exhibited excellent sensitivity and selectivity of fluorescence quenching for 2,4,6-trinitrophenol (TNP) in the range of 0.1−15 μM with a limit of detection of 87 nM. They also obtained satisfactory results with this probe for detecting TNP in spiked water samples.

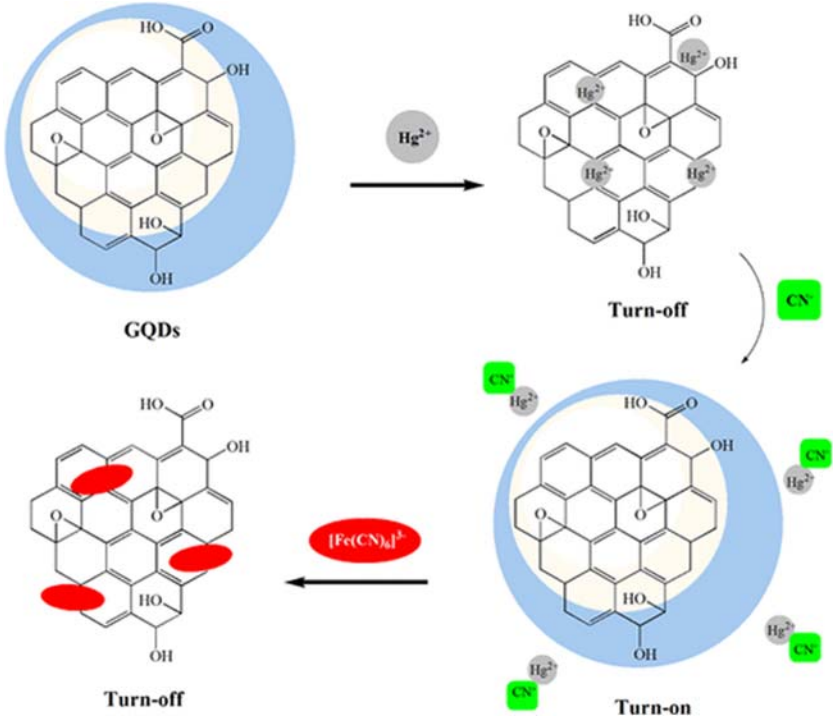

FIGURE 13.1 Use of GQDs for detection of ferricyanide and cyanide ions. *Adapted from Kongsanan, N., Pimsin, N., Keawprom, C., Sricharoen, P., Areerob, Y., Nuengmatcha, P., et al., 2021. A fluorescence switching sensor for sensitive and selective detections of cyanide and ferricyanide using mercuric cation-graphene quantum dots. ACS Omega 6(22), 14379–14393, with permission.*

Mehata and Biswas (2021) prepared GQDs–silver nanoparticles (GQDs@AgNPs) hybrid structure using GOD as a reducing and stabilizing agent. As-prepared composite exhibited strong surface plasmon resonance along with the absorption of GQDs. It was also reported in the sensing of hydrogen peroxide in an aqueous medium and therefore as-prepared GQDs@AgNPs nanohybrids can be used as a sensing probe.

The mannitol capped boron-doped CQDs (B-CQDs) were synthesized by Ali et al. (2021) and used for detection of sparfloxacin and orbifloxacin. As-prepared samples exhibited an increase of fluorescence intensity in the range of 1.5×10^{-9}–1.3×10^{-7} and 1.2×10^{-9}–1.1×10^{-7} M with limits of detection of 5.0×10^{-10} and 4.0×10^{-10} M for sparfloxacin and orbifloxacin, respectively. This probe gave satisfactory results determination for these antibiotics in milk and natural water samples. Zhang and Fan (2021) synthesized cerium–nitrogen codoped CQDs (Ce–N–CDs) via a hydrothermal method. They used cerium nitrate with citric acid, and ethylenediamine.

It was observed that as-prepared Ce−N−CDs exhibited excellent detection selectivity for tetracyclines (TCs). It was reported that this probe detected doxycycline (DC) in a concentration range of 0.4−35 μM with a limit of detection of 0.25 μM. This method was also used successfully for the determination of DC and total TCs in pork and milk. It was revealed that as-prepared Ce−N−CDs had low cytotoxicity and did not affect cell viability. It was proposed that as-prepared Ce−N−CDs can be used in cell imaging.

A dual-signal fluorescent sensor was developed for the detection of tetracycline in milk with excellent reproducibility and stability. Molybdenum disulfide QDs (blue fluorescence) and cadmium telluride QDs with yellow fluorescence were synthesized by (Liang et al., 2022). They prepared MoS_2/CdTe-based sensor with two fluorescence emission peaks at 433 and 573 nm. It was observed that the fluorescence of MoS_2/CdTe was quenched by photoinduced electron transfer. As-prepared CdTe QDs composite can be used for the determination of tetracyline in the concentration range of 0.1−1 μM. This sensor was also applied for the detection of tetracyline in milk samples with recovery of 95.53%−104.22%.

Şen et al. (2022) synthesized fluorescent polyethylenimine capped CQDs (PEI-C-dots) via microwave irradiation. They used polyethylenimine and citric acid as precursors for this purpose. It was observed that fluorescence quantum yield of as-synthesized PEI-C-dots was found to be 54% and the detection limit for 2,4,6-trinitrotoluene was 93 $\mu g\ L^{-1}$. It was interesting to note that that neither the HMX or RDX explosives interfered with this determination. Xu et al. (2022) prepared molecularly imprinted polymers based on Si QDs (Si QDs@SiO_2 @MIPs) via a sol−gel method. It was observed that as-prepared Si QDs@SiO_2 @MIPs exhibited a strong fluorescent emission at 447 nm, which was quenched in the presence of catechol. This sensor can be used to determine concentrations of catechol in the range of 0.018−100 μM with a limit of detection of 0.018 μM. This method was also applied by detecting catechol in real river water samples with satisfactory results.

Afshary et al. (2022) fabricated an electrochemiluminescence sensor based on nitrogen-doped CQDs (N-CQDs). It was reported that the as-prepared N-CQD-based sensor can be used for the determination of ceftazidime in the concentration range of 1×10^{-7} to 5×10^{-4} mol L^{-1} with a limit of detection of 2.3×10^{-8} mol L^{-1}. It was suggested that this ECL sensor is also applicable for the analysis of ceftazidime in some real samples (milk powder, bovine milk, and human serum).

Jiang et al. (2022) decorated 0D/2D heterostructure of ZnO QDs on nitrogen-doped Ti_3C_2 MXene (ZnO/N-Ti_3C_2). The size of ZnO QDs was found to be in the range of 2−5 nm. It was reported that the as-prepared sensor could be used for selective and sensitive detection of chloramphenicol in the concentration range of linear range (0.1−100 ng mL^{-1}) with a detection limit of 0.019 ng mL^{-1}. Praoboon et al. (2022) developed an

electrochemiluminescence sensor using tris(2,2′-bipyridyl)ruthenium(II) complex coupled with water-soluble thioglycolic acid-capped CdSe QDs. It was revealed that the trimethylamine can be determined using this sensor in the concentration range of 1×10^{-12} to 1×10^{-7} M with a limit of detection of 2.09×10^{-13} M. A rapid estimation of concentration of trimethylamine can be done in fish tissue using the as-prepared sensor.

13.2.2 Biosensors

Any disease has its origin in changes in biological environment and organs of the body, and therefore detecting such changes at an early stage can safeguard our health because one can plan the treatment of any disease in a timely manner. It is possible to sense these changes with the help of QDs, which are very sensitive to any variation in the biological environment.

Hwang et al. (2021) reported the synthesis of reduced graphene oxide QDs (rGOQDs) in perfluorotributylamine solution. It was observed that the as-prepared sample exhibited good photostability without any loss in intensity even after a month and it can be used for an optical device (Fig. 13.2). It was revealed that PL spectra from the rGOQDs-solution changed color from blue to green when mixed with GOx for glucose concentration of 0−2 mM. Thus rGOQDs can be used as colorimetric biosensors with the help of smartphone.

Mostafa et al. (2021) synthesized highly photoluminescent $Mn^{2+}{}_xZn_{2-x}S$ ($0 \leq x \leq 0.1$)-doped QDs. These QDs were capped with 3-mercaptopropionic acid. It was reported that ZnS and $Mn^{2+}{}_{0.04}Zn_{1.96}S$ QDs were of average particle size 13 and 16 nm, respectively. As-prepared Mn-doped ZnS QDs were used as an optical sensor for determination of bovine serum albumin with limit of detection of 1.56×10^{-7} M.

Pothipor et al. (2021) constructed an electrochemical biosensor based on gold nanoparticles/GQDs/graphene oxide (AuNPs/GQDs/GO) modified three-screen-printed carbon electrode to detect miRNA-21, miRNA-155, and

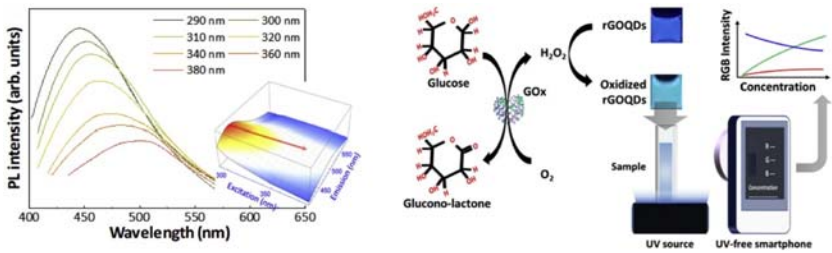

FIGURE 13.2 Use of reduced graphene oxide quantum dots in detection of glucose. *Adapted from Hwang, J., Le, A.D.D., Trinh, C.T., Le, Q.T., Lee, K.G., Kim, J., 2021. Green synthesis of reduced-graphene oxide quantum dots and application for colorimetric biosensor. Sens. Actuators A: Phys. 318. https://doi.org/10.1016/j.sna.2020.112495, with permission.*

miRNA-210 biomarkers. They used different redox species (polydopamine, anthraquinone, and methylene blue) as redox indicators for anchoring to capture miRNA probes, which are hybridized with the miRNA-21, miRNA-155, and miRNA-210. It was reported that the as-developed AuNPs/GQDs/GO-based biosensor exhibited an excellent performance for miRNA sensing simultaneously, in a wide concentration range (0.001−1000 pM) with a lower detection limit of 0.04, 0.33, and 0.28 fM for the detection of miRNA-21, miRNA-155, and miRNA-210, respectively. It was revealed that this method can be used with selectivity for the detection of miRNAs in human serum samples and such a multiplex label-free miRNA biosensor has a great potential for the diagnosis of breast cancer.

Van Tam et al. (2021) synthesized aniline functionalized GQDs (a-GQDs) via microwave-assisted pyrolysis of fructose. Then these GQDs were modulated with phenylboric acid (PBA). It was reported that the as-prepared fluorescent sensor using a-GQDs/PBA exhibited high selectivity and sensitivity toward glucose. Furthermore, a-GQD/PBA system exhibited excellent biocompatibility and can be satisfactorily applied to detect glucose in HeLa cells with a limit of detection of 2.1 μM. A highly compatible graphene nanofilm decorated with Prussian blue (PB) (electroactive) and photoelectric responsive QDs was prepared by Ma et al. (2022). An impressive biosensing performance could be obtained by as-prepared enzyme-modified PB-rGO-QDs film, which exhibited high sensitivity for H_2O_2. It was reported that wearable devices of PB-rGO-QDs films on textile showed flexible bending lifetime over several thousands of cycles, with photoelectronic properties and as a stable sensor.

A sensitive photoelectrochemical biosensor was fabricated by Tu et al. (2022) with ZnSe QDs (QDs)/Au nanoparticles. It was reported that ZnSe QDs were enhanced in the presence of light irradiation as a result of surface plasmon resonance of AuNPs. The photocurrent intensity of AuNPs/ZnSe QDs was also increased by six times that of ZnSe QDs only. This biosensor was able to detect target DNA in the range from 1 fM to 10 nM with a very low limit of detection of 0.33 fM. Acrylamide (AM) is a potential carcinogen produced during food thermal processing. Wei et al. (2021) developed a simple fluorescent biosensor that was based on single-stranded DNA (ssDNA). CQDs and ssDNA were preferentially bound to AM by hydrogen bonding. It was observed that the degree of reduction of fluorescence was smaller compared to in the absence of AM. This sensor could detect AM in the concentration range of 5×10^{-3} to 1×10^{-7} M with a detection limit of 2.41×10^{-8} M.

Deng et al. (2022) fabricated CQD functionalized solution-gated graphene transistors and used them for highly sensitive label-free detection of DNA. These CQDs were immobilized on the surface of the gate electrode using mercaptoacetic acid using its thiol group. The ssDNA probe can hybridize with the ssDNA target and form double-stranded DNA. It was

revealed that the detection limit was as low as 1 aM. The proposed sensor exhibited a good linear range (1 aM to 0.1 nM). It was interesting to note that it can effectively distinguish one-base mismatched target DNA and response time was only 326 s for 1 aM target DNA molecules. Mao et al. (2022) coated colloidal gold nanoparticles with polydopamines (PDA) to obtain Au@PDA nanoparticles. It was reported that Au@PDA nanoparticles mediated ZnCdSe/ZnS QDs fluorescence quenching and recovery, and it could assist in the detection, resulting in a reverse fluorescence enhancement detection format of carbendazim (CBD). It was observed that the sensitivity of lateral flow immunoassay (LFIA) of the fluorescence was 32 times higher compared to the colorimetry mode. A negligible cross reactivity was there for the determination of thiabendazole, benomyl, thiophanate-methyl, and thiophanate-ethyl on using LFIA. They could achieve satisfactory results in testing spiked strawberry and cucumber samples, which indicated that the as-prepared probe Au@PDAs-QDs-LFIA was more reliable.

The 3-mercaptopropionic acid capped CdSe QDs graphene nanocomposite (rGO-CdSe QDs/ITO) was fabricated by Khandelwal et al. (2022) and used as an electrochemical biosensor for the detection of low-density lipoprotein (LDL). It was reported that as-prepared immunoelectrodes could detect LDL in a wide concentration range ($2-125\ \text{mg dL}^{-1}$). Zhu et al. (2022) prepared CdTe QDs (CA-CdTe QDs) (cysteamine stabilized) and gold nanoparticles (sodium citrate stabilized). These CA-CdTe and Au NPs were self-assembled to from large clusters. The fluorescence of CA-CdTe was quenched as a result of fluorescence resonance energy transfer (FRET). It was reported that positive glutathione (GSH) could assemble with negative Au NPs through electrostatic interaction at pH 5.5 and it could destroy the FRET system of CA-CdTe and Au NPs. The recovered fluorescence efficiency of CA-CdTe shows a linear relationship with GSH concentrations in the range of 6.7 nM to 0.40 μM, with a limit of detection of 3.3 nM. It was revealed that this sensing system can be applied in the detection of GSH in real human blood plasma samples with good recovery (99.5%−102.3%).

13.2.3 Humidity sensors

Humidity of an area is a necessary parameter for knowing the moisture content, which can sometime adversely affect some materials. Therefore it is important to know about humidity. Various sensors are available for determining humidity in a particular area, but QDs can measure humidity more selectively as these are very sensitive toward any change in humidity.

Chaloeipote et al. (2021) synthesized GQDs and silver nanoparticles via a hydrothermal method and a green reducing agent route, respectively. They confirmed the successful formation of a core/shell-like AgNPs/GQDs structure. It was reported that a ratio of 1:1 of GQDs/AgNPs in nanocomposite exhibited the best humidity response of about 98.14%. Chaudhary et al. (2021)

synthesized CQDs of two types: (1) C-1 and (2) C-2, depending on carbonization temperatures. It was revealed that average particle size was 5.5 and 2 nm for samples C-1 and C-2, respectively. It was reported that C-2 gave an enhanced sensing performance with an average sensitivity of 254.861 pF/%RH with a fast response and recovery times of 7.3 and 4.7 s, respectively. Holemadlu et al. (2022) synthesized GQDs via carbonization of citric acid monohydrate. This process is low cost and has scalability. They fabricated a humidity sensor using GQD solution as the sensing material, which showed a rapid and high sensitivity to changes in humidity.

13.2.4 Temperature sensors

Temperature variation is a quite common feature but it is likely to affect some chemical and biochemical reactions, and therefore the correct measurement of temperature becomes necessary. Although various techniques are available for temperature measurement, QDs are very sensitive to such temperature changes and these are used in different devices for determining temperature at a particular site.

Zhang et al. (2018a) prepared lead sulfide QDs decorated zinc oxide nanorods. Then PbS QDs/ZnO film was fabricated by tuning deposition of PbS QDs on ZnO nanorods via a successive ionic-layer adsorption and reaction (SILAR) method. The sensor based on PbS QDs/ZnO nanorods can be used for sensing of room temperature.

Glass stabilized Mn-doped $CsPb(Cl/Br)_3$ QDs have been synthesized by Zhuang et al. (2019). They used a glass composition design and in situ glass crystallization for this purpose. It was reported that Mn-doped $CsPb(Cl/Br)_3$ QDs exhibited superior thermal stability and water resistance (about 100%). It is interesting to know that complete luminescence could be retained even after immersing this composite in water for a month or so. It was revealed that rapid thermal quenching for exciton recombination relative to Mn^{2+} d−d transition at lower temperatures (cryogenic) may provide it a promising position as a ratiometric temperature sensing medium.

Li et al. (2020) developed an optical thermometer with high sensitivity by using exciton recombination of $CsPbBr_3$ QDs for detecting a signal for temperature. It was reported that the fluorescence intensity ratio of exciton recombination and Eu^{3+} emission in nanocomposite exhibited a good temperature sensing property in as-prepared temperature ranging between 93K and 383K. It was observed that maximum absolute and relative temperature sensitivity could reach 0.0224% and $2.25\%K^{-1}$, respectively. It provides an effective pathway for developing a noncontact optical thermometric materials.

A simple one-pot strategy was reported by Lei et al. (2021) for preparing polyvinyl alcohol (PVA)-capped SQDs. They used low cost sulfur and PVA as a ligand. It was observed that as-prepared SQDs had sizes in the range of

1.5−5 nm. They also exhibited good water dispersibility and stability, good optical stability, bright fluorescence, and low cytotoxicity. As-prepared SQDs show selective and sensitive fluorescence quenching behavior toward Fe^{3+} ions with a detection limit of 9.2×10^{-9} M. SQDs also show temperature-dependent fluorescence. It was revealed that SQDs can be used for monitoring Fe^{3+} ions and also as a nanothermometer for temperature in the interior of cells.

Han et al. (2021) fabricated a highly sensitive ratiometric thermal sensor. This sensor was based on colloidal C-dots as these C-dots exhibited a temperature-dependent photoluminescence response. It was reported that C-dots@OH exhibited an absolute thermal sensitivity of $-0.082\ ^{\circ}C^{-1}$, which makes it a very promising candidate for high-sensitivity, and a self-calibrated nanoscale thermometer. These as-prepared C-dots@OH were used to monitor the intracellular temperature in the range of 32°C−42°C, with a clear trend for temperature variation in a single cell. It was reported that as-prepared thermal sensors can find potential application in nanoelectronic and optoelectronic devices.

Lee et al. (2021) developed nanothermometers based on luminescence of GQDs to probe temperature-sensitive processes at the nanoscale,. These QDs were synthesized via top-down (RGQDs) or bottom-up (N-GQDs) approaches using reduced graphene oxide and glucosamine as precursors, respectively. The average particle size of QDs was found to be 3−6 nm. It was reported that both GQDs exhibited temperature-sensitive fluorescence, which was photostable. A linear as well as reversible fluorescence quenching was observed up to 19.3% for the visible and near-infrared GQD emission in the temperature range 25°C−49°C. It was revealed that these GQD nanothermometers can give more than 40% quenching response in the range of 25°C−45°C, when internalized into the cytoplasm of HeLa cells. It was suggested that as-prepared sensors can be used for temperature sensing in microscopic subcellular biological environments.

Kumbhakar et al. (2021) synthesized Mn^{2+}-doped ZnS QDs (MZQDs) and used its reversible temperature-dependent PL emission quenching properties in the development of a smartphone-based optical thermometer. It was observed that temperature-dependent variations are present in PL intensity on using MZQDs in different forms, like powder form, aqueous dispersion, and polymer-encapsulated thin film. They have demonstrated a smartphone-based colorimetric imaging method for the measurement of temperature.

Yang et al. (2021a) synthesized N-GQDs with high blue fluorescence via a hydrothermal method using benzimidazoles as the precursor. It was reported that as-fabricated N-GQDs had a particle size of 3.8 nm with good water solubility, crystallinity, and photostability. It was observed that fluorescence of N-GQDs was quenched by tetracycline at elevated temperature and fluorescence intensity exhibited a linear reduction with temperature between 25°C and 100°C. They reported reversible and stable abilities of temperature sensing of as-prepared N-GQDs.

Sharma and Mehata (2022a) synthesized undoped as well as manganese-doped zinc selenide QDs in the temperature range of 77-300K. It was observed that intense blue and orange PL were exhibited by these as-prepared ZnSe and Mn@ZnSe QDs, respectively. It was found that PL intensity is dependent on temperature, decreasing with increasing temperature, and the maximum sensitivity values were 0.58% (225K) and 0.44%K^{-1} (250K) for ZnSe and Mn@ZnSe QDs, respectively.

13.3 Recent developments

Some recent developments in the use of QDs in fabricating different sensors have been summarized in Table 13.1.

TABLE 13.1 Recent advances in use of quantum dots in sensors.

Material	Application	Limit of detection	References
Carbon quantum dots	Detection of ammonia	10 nM	Ganesan et al. (2022)
Nitrogen-doped graphene quantum dots (N-GQDs) polyaniline (PANI)	Detection of ammonia	1500 ppm	Hakimi et al. (2018)
SnO_2 QDs	Detection of ammonia	–	Sahu et al. (2019)
Titanium dioxide quantum dots	Detection of hydrogen sulfide	500 ppb	Wu et al. (2022)
Graphene quantum dots	Detection of carbon dioxide	10–20 nm	Raeyani et al. (2020)
N-type nitrogen-doped carbon oxide quantum dots	Detection of humidity	20%–90%	Kondee et al. (2022)
Nitrogen-doped carbon quantum dots and red-emitting copper nanoclusters (CuNCs) complex	Detection of pesticide	7.49 and 3.03 nM	Chen et al. (2022)
Gold nanoparticles decorated quantum dots	Pesticide detection	Response range of 0.01–20 μM and limit of detection (LOD) of 7 nM	Jin et al. (2021)
MIP/$CsPbBr_3$ QDs	Detection of pesticide	0.10–500.0 μg L^{-1}	Zhang et al. (2022)
CdSe@CdS quantum dots	Detection of ochratoxin A	0.89 ng mL^{-1}	Jia et al. (2022)

(*Continued*)

TABLE 13.1 (Continued)

Material	Application	Limit of detection	References
ZnS/PbS core-shell quantum dots	Detection of hydrogen sulfide	300 ppm	Azimi and Rostami (2021)
Films of CdSe/ZnS core-shell type quantum dots	Detection of nitrogen dioxide	1–100 ppm	Ando et al. (2022)
PbS CQDs	Detection of nitrogen dioxide	–	Li et al. (2020)
Aptamer-modified quantum dots	Detection of *Staphylococcus aureus* in food and serum samples	2 CFU mL^{-1}	Tao et al. (2021)
CdSe/CdS/ZnS quantum dots	Detection of *Escherichia coli* and *P. Aeruginosa*	58 and 97 CFU mL^{-1}	Ye et al. (2022)
Tungsten trioxide quantum dots	Detection of *Listeria monocytogenes*	$1.3–1.3 \times 10^7$ CFU mL^{-1}	Zhu et al. (2021)
Carbon quantum dots	Detection of *E. coli* O157: H7 (*E. coli*)	487 CFU mL^{-1}	Hu et al. (2021) and Hong et al. (2021)
Fe_3O_4 nanoparticles and CdTe quantum dots	Detection of human serum albumin (HSA)	12 ng mL^{-1}	Liao et al. (2021)
S,N-CQDs	Detection of bendiocarb	0.02 μg mL^{-1}	Al Yahyai et al. (2021)
MoS_2 QDs and GQDs mixture (3:2)	Detection of cholesterol	35 nmol L^{-1}	Hassanzadeh and Khataee (2018)
3-Mercaptoproponic acid protected Mn@ZnSe QDs	Detection of Hg^{2+} and Pb^{2+} ions	Hg^{2+} and Pb^{2+} (0–100 μL)	Sharma and Mehata (2022b)
CdTe quantum dots	Thimerosal (TM), an organic mercury compound	26.6 μg L^{-1}	Tall et al. (2021)
CdZnTeS alloyed QDs	Detection of Pb^{2+} or Hg^{2+} ions	–	Hoang et al. (2022)

13.4 Conclusion

QDs are very sensitive toward any changes in chemical and biological environment, temperature, humidity, etc. Hence, these are successfully used for sensing the presence of certain chemicals. such as alcohol, liquefied petroleum gas, pesticides, drugs, hydrogen sulfide, ammonia. and many more, even if these are present in very low concentrations (ppm or even ppb level). The timely detection of any abnormality in body will help us in its immediate treatment. The leakage of toxic material can also be traced in time to have a safeguard. The list of sensors is not complete and it will continue increasing day by day.

References

Abbasi, F., Alizadeh, N., 2020. Highly selective detection of methanol in aqueous and ethanol medium based on hybrid ZnS: Mn^{2+} quantum dots/N-methylpolypyrrole as a fluorescence switchable sensor. Food Chem. 328. Available from: https://doi.org/10.1016/j.foodchem.2020.127091.

Afshary, H., Amiri, M., Bezaatpour, A., Wark, M., 2022. Electrochemiluminescence sensor based on N-doped carbon quantum dots for determination of ceftazidime in real samples. J. Electrochem. Soc. 169. Available from: https://doi.org/10.1149/1945-7111/ac53ce.

Ahmed, S.R., Kumar, S., Ortega, G.A., Srinivasan, S., Rajabzadeh, A.R., 2021. Target specific aptamer-induced self-assembly of fluorescent graphene quantum dots on palladium nanoparticles for sensitive detection of tetracycline in raw milk. Food Chem. 346. Available from: https://doi.org/10.1016/j.foodchem.2020.128893.

Al Yahyai, I., Al-Lawati, H.A., Hassanzadeh, J., 2021. A paper-based chemiluminescence detection device based on S, N-doped carbon quantum dots for the selective and highly sensitive recognition of bendiocarb. Anal. Methods. 13 (31), 3461–3470.

Ali, H.R.H., Hassan, A.I., Hassan, Y.F., El-Wekil, M.M., 2021. Mannitol capped magnetic dispersive micro-solid-phase extraction of polar drugs sparfloxacin and orbifloxacin from milk and water samples followed by selective fluorescence sensing using boron-doped carbon quantum dots. J. Environ. Chem. Eng. 9 (2). Available from: https://doi.org/10.1016/j.jece.2021.105078.

Alvandi, N., Assariha, S., Esfandiari, N., Jafari, R., 2021. Off–on sensor based on concentration-dependent multicolor fluorescent carbon dots for detecting pesticides. Nano-Struct. Nano-Objects 26. Available from: https://doi.org/10.1016/j.nanoso.2021.100706.

Amer, W.A., Rehab, A.F., Abdelghafar, M.E., Torad, N.L., Atlam, A.S., Ayad, M.M., 2021. Green synthesis of carbon quantum dots from purslane leaves for the detection of formaldehyde using quartz crystal microbalance. Carbon 179, 159–171.

Ando, M., Inagaki, K., Kawasaki, H., Shigeri, Y., 2022. Reversible sensing of nitrogen dioxide using photoluminescent CdSe/ZnS quantum dots and enhanced response by combination with noble metals. J. Ceram. Soc. Jpn. 130 (1), 180–186.

Azimi, M., Rostami, A.M. 2021. Room temperature chemiresistor H2S Gas sensor based on ZnS/PbS core-shell quantum dots. In: 2021 29th Iranian Conference on Electrical Engineering (ICEE). IEEE, pp. 65–68.

Bai, J., Shen, Y., Zhao, S., Chen, Y., Li, G., Han, C., 2022. Flower-like MoS2 hierarchical architectures assembled by 2D nanosheets sensitized with SnO_2 quantum dots for

high-performance NH3 sensing at room temperature. Sens. Actuators B: Chem. 353. Available from: https://doi.org/10.1016/j.snb.2021.131191.

Bhakat, A., Pal, A., Siddaramaiah, R., Chattopadhyay, A., 2021. Complexation-based super crystalline assembly of zinc oxide quantum dots for sensitive carbon dioxide gas sensing. J. Phys. Chem. C. 125 (22), 12316−12323.

Carneiro, S.V., Holanda, M.H.B., Cunha, H.O., Oliveira, J.J.P., Pontes, S.M.A., Cruz, A.A.C., 2021. Highly sensitive sensing of food additives based on fluorescent carbon quantum dots. J. Photochem. Photobiol. A: Chem. 411. Available from: https://doi.org/10.1016/j.jphotochem.2021.113198.

Chaloeipote, G., Samarnwong, J., Traiwatcharanon, P., Kerdcharoen, T., Wongchoosuk, C., 2021. High-performance resistive humidity sensor based on Ag nanoparticles decorated with graphene quantum dots. R. Soc. Open. Sci. 8 (7). Available from: https://doi.org/10.1098/rsos.210407.

Chandra, S., Bano, D., Sahoo, K., Kumar, D., Kumar, V., Yadav, P.K., 2022. Synthesis of fluorescent carbon quantum dots from Jatropha fruits and their application in fluorometric sensor for the detection of chlorpyrifos. Microchem. J. 172. Available from: https://doi.org/10.1016/j.microc.2021.106953.

Chaudhary, P., Maurya, D.K., Yadav, S., Pandey, A., Tripathi, R.K., Yadav, B.C., 2021. Ultrafast responsive humidity sensor based on roasted gram derived carbon quantum dots: experimental and theoretical study. Sens. Actuators B: Chem. 329. Available from: https://doi.org/10.1016/j.snb.2020.129116.

Chen, L., Lu, J., Luo, M., Yu, H., Chen, X., Deng, J., 2022. A ratiometric fluorescent sensing system for the selective and ultrasensitive detection of pesticide residues via the synergetic effects of copper nanoclusters and carbon quantum dots. Food Chem. 379. Available from: https://doi.org/10.1016/j.foodchem.2022.132139.

Chu, C.S., Hsieh, M.W., 2019. Optical fiber carbon dioxide sensor based on colorimetric change of α-naphtholphthalein and CIS/ZnS quantum dots incorporated with a polymer matrix. Opt. Mater. Express 9 (7), 2937−2945.

Deng, M., Li, J., Xiao, B., Ren, Z., Li, Z., Yu, H., 2022. Ultrasensitive label-free DNA detection based on solution-gated graphene transistors functionalized with carbon quantum dots. Anal. Chem. 94 (7), 3320−3327.

Dong, L., Zheng, P., Yang, Y., Zhang, M., Xue, Z., Wang, Z., 2018. NO_2 gas sensor based on graphene decorated with Ge quantum dots. Nanotechnology 30 (7). Available from: https://doi.org/10.1088/1361-6528/aaf3d7.

Dun, M., Tan, J., Tan, W., Tang, M., Huang, X., 2019. CdS quantum dots supported by ultrathin porous nanosheets assembled into hollowed-out Co_3O_4 microspheres: a room-temperature H2S gas sensor with ultra-fast response and recovery. Sens. Actuators B: Chem. 298. Available from: https://doi.org/10.1016/j.snb.2019.126839.

Ganesan, S., Kalimuthu, R., Kanagaraj, T., Kulandaivelu, R., Nagappan, R., Pragasan, L.A., 2022. Microwave-assisted green synthesis of multi-functional carbon quantum dots as efficient fluorescence sensor for ultra-trace level monitoring of ammonia in environmental water. Environ. Res. 206. Available from: https://doi.org/10.1016/j.envres.2021.112589.

Gan, Z., Hu, X., Huang, X., Li, Z., Zou, X., Shi, J., et al., 2021. A dual-emission fluorescence sensor for ultrasensitive sensing mercury in milk based on carbon quantum dots modified with europium (III) complexes. Sens. Actuators B: Chem. 328. Available from: https://doi.org/10.1016/j.snb.2020.128997.

Ghiasi, T., Ahmadi, S., Ahmadi, E., Olyai, M.R.T.B., Khodadadi, Z., 2021. Novel electrochemical sensor based on modified glassy carbon electrode with graphene quantum dots, chitosan

and nickel molybdate nanocomposites for diazinon and optimal design by the Taguchi method. Microchem. J. 160. Available from: https://doi.org/10.1016/j.microc.2020.105628.

Hajikhanloo, A.S., Sarraf, M.J., Rostami, A., Dolatyari, M., 2021. Micro ring resonator based CO_2 gas sensor using PbSe quantum dots. Opt. Quantum Electron. . Available from: https://doi.org/10.21203/rs.3.rs-638041/v1.

Hakimi, M., Salehi, A., Boroumand, F.A., Mosleh, N., 2018. Fabrication of a room temperature ammonia gas sensor based on polyaniline with N-doped graphene quantum dots. IEEE Sens. J. 18 (6), 2245–2252.

Han, Y., Liu, Y., Zhao, H., Vomiero, A., Li, R., 2021. Highly efficient ratiometric nanothermometers based on colloidal carbon quantum dots. J. Mater. Chem. B 9 (20), 4111–4119.

Hassanzadeh, J., Khataee, A., 2018. Ultrasensitive chemiluminescent biosensor for the detection of cholesterol based on synergetic peroxidase-like activity of MoS_2 and graphene quantum dots. Talanta 178, 992–1000.

Hoang, Q.B., Nguyen, T.N., Nguyen, T.P., Nguyen, A.D., Chu, N.H., Ta, V.T., 2022. Size-dependent reactivity of highly photoluminescent CdZnTeS alloyed quantum dots to mercury and lead ions. Chem. Phys. 552. Available from: https://doi.org/10.1016/j.chemphys.2021.111378.

Holemadlu, A., Keerthana, G., Purohit, K.B., Shaik, H., Nagaraja, V.S., 2022. Synthesis of graphene quantum dots and fabrication of humidity sensor. Emerging Research in Computing, Information, Communication and Applications. Springer, Singapore, pp. 407–415.

Hong, S.Z., Huang, Q.Y., Wu, T.M., 2021. The room temperature highly sensitive ammonia gas sensor based on polyaniline and nitrogen-doped graphene quantum dot-coated hollow indium oxide nanofiber composite. Polymers 13 (21). Available from: https://doi.org/10.3390/polym13213676.

Hu, X., Li, Y., Xu, Y., Gan, Z., Zou, X., Shi, J., et al., 2021. Green one-step synthesis of carbon quantum dots from orange peel for fluorescent detection of Escherichia coli in milk. Food Chem 339. Available from: https://doi.org/10.1016/j.foodchem.2020.127775.

Huangfu, C., Feng, L., 2021. High-performance fluorescent sensor based on CsPbBr3 quantum dots for rapid analysis of total polar materials in edible oils. Sens. Actuators B: Chem. 344. Available from: https://doi.org/10.1016/j.snb.2021.130193.

Huo, X., Liu, L., Bai, Y., Qin, J., Yuan, L., Feng, F., 2021. Facile synthesis of yellowish-green emitting carbon quantum dots and their applications for phoxim sensing and cellular imaging. Anal. Chim. Acta . Available from: https://doi.org/10.1016/j.aca.2021.338685.

Hwang, J., Le, A.D.D., Trinh, C.T., Le, Q.T., Lee, K.G., Kim, J., 2021. Green synthesis of reduced-graphene oxide quantum dots and application for colorimetric biosensor. Sens. Actuators A: Phys. 318. Available from: https://doi.org/10.1016/j.sna.2020.112495.

Jiang, D., Wei, M., Du, X., Qin, M., Shan, X., Chen, Z., 2022. One-pot synthesis of ZnO quantum dots/N-doped Ti_3C_2 MXene: tunable nitrogen-doping properties and efficient electrochemiluminescence sensing. Chem. Eng. J. 430. Available from: https://doi.org/10.1016/j.cej.2021.132771.

Jia, M., Jia, B., Liao, X., Shi, L., Zhang, Z., Liu, M., 2022. A CdSe@ CdS quantum dots based electrochemiluminescence aptasensor for sensitive detection of ochratoxin A. Chemosphere 287. Available from: https://doi.org/10.1016/j.chemosphere.2021.131994.

Jin, Y., Liu, K., Li, G., Li, C., Xiao, Z., Yuan, C., 2021. In situ reduction triggers the highly sensitive detection of pesticide by classic gold nanoparticle and quantum dots nanocomposite. Anal. Chim. Acta 1172. Available from: https://doi.org/10.1016/j.aca.2021.338679.

Keshtkar, S., Rashidi, A., Kooti, M., Askarieh, M., Pourhashem, S., Ghasemy, E., 2018. A novel highly sensitive and selective H_2S gas sensor at low temperatures based on SnO_2 quantum dots-C60 nanohybrid: experimental and theory study. Talanta 188, 531–539.

Khandelwal, D., Jain, D., Solanki, P.R., Ranjan, K.R., Mukherjee, M.D., 2022. A novel nanocomposite platform of mercaptopropionic acid stabilized CdSe quantum dots-graphene for impedimetric detection of low density lipoprotein. Mater. Lett. 308. Available from: https://doi.org/10.1016/j.matlet.2021.131236.

Khose, R.V., Chakraborty, G., Bondarde, M.P., Wadekar, P.H., Ray, A.K., Some, S., 2021. Red-fluorescent graphene quantum dots from guava leaf as a turn-off probe for sensing aqueous Hg (II). N. J. Chem. 45 (10), 4617–4625.

Kondee, S., Arayawut, O., Pon-On, W., Wongchoosuk, C., 2022. Nitrogen-doped carbon oxide quantum dots for flexible humidity sensor: experimental and SCC-DFTB study. Vacuum 195. Available from: https://doi.org/10.1016/j.vacuum.2021.110648.

Kongsanan, N., Pimsin, N., Keawprom, C., Sricharoen, P., Areerob, Y., Nuengmatcha, P., et al., 2021. A fluorescence switching sensor for sensitive and selective detections of cyanide and ferricyanide using mercuric cation-graphene quantum dots. ACS Omega 6 (22), 14379–14393.

Kumar, C., Rawat, G., Kumar, H., Kumar, Y., Kumar, A., Prakash, R., et al., 2018. Electrical and ammonia gas sensing properties of PQT-12/CdSe quantum dots composite-based organic thin film transistors. IEEE Sens. J. 18 (15), 6085–6091.

Kumbhakar, P., Karmakar, A.R., Das, G.P., Chakraborty, J., Tiwary, C.S., Kumbhakar, P., 2021. Reversible temperature-dependent photoluminescence in semiconductor quantum dots for the development of a smartphone-based optical thermometer. Nanoscale 13 (5), 2946–2954.

Lee, B.H., McKinney, R.L., Hasan, M., Naumov, A.V., 2021. Graphene quantum dots as intracellular imaging-based temperature sensors. Materials 14 (3). Available from: https://doi.org/10.3390/ma14030616.

Lei, J., Huang, Z., Gao, P., Sun, J., Zhou, L., 2021. Polyvinyl alcohol enhanced fluorescent sulfur quantum dots for highly sensitive detection of Fe^{3+} and temperature in cells. Part. Part. Syst. Charact. 38 (4). Available from: https://doi.org/10.1002/ppsc.202000332.

Liang, N., Hu, X., Li, W., Mwakosya, A.W., Guo, Z., Xu, Y., 2021. Fluorescence and colorimetric dual-mode sensor for visual detection of malathion in cabbage based on carbon quantum dots and gold nanoparticles. Food Chem. 343. Available from: https://doi.org/10.1016/j.foodchem.2020.128494.

Liang, N., Hu, X., Li, W., Wang, Y., Guo, Z., Huang, X., 2022. A dual-signal fluorescent sensor based on MoS_2 and CdTe quantum dots for tetracycline detection in milk. Food Chem. 378. Available from: https://doi.org/10.1016/j.foodchem.2022.132076.

Li, X., Yu, Y., Hong, J., Feng, Z., Guan, X., Chen, D., 2020. Optical temperature sensing of Eu3 + -doped oxyhalide glasses containing CsPbBr3 perovskite quantum dots. J. Lumin. 219. Available from: https://doi.org/10.1016/j.jlumin.2019.116897.

Liao, B.Y., Chang, C.J., Wang, C.F., Lu, C.H., Chen, J.K., 2021. Controlled antibody orientation on Fe_3O_4 nanoparticles and CdTe quantum dots enhanced sensitivity of a sandwich-structured electrogenerated chemiluminescence immunosensor for the determination of human serum albumin. Sens. Actuators B: Chem. 336. Available from: https://doi.org/10.1016/j.snb.2021.129710.

Liu, P., Meng, H., Han, Q., Zhang, G., Wang, C., Song, L., 2021. Determination of ascorbic acid using electrochemiluminescence sensor based on nitrogen and sulfur doping graphene quantum dots with luminol as internal standard. Microchim. Acta 188 (4). Available from: https://doi.org/10.1007/s00604-021-04761-w.

Liu, Y., Wang, H., Chen, K., Yang, T., Yang, S., Chen, W., 2019. Acidic site-assisted ammonia sensing of novel $CuSbS_2$ quantum dots/reduced graphene oxide composites with an ultralow detection limit at room temperature. ACS Appl. Mater. Interfaces 11 (9), 9573–9582.

Liu, Y., Wang, L., Wang, H., Xiong, M., Yang, T., Zakharova, G.S., 2016. Highly sensitive and selective ammonia gas sensors based on PbS quantum dots/TiO2 nanotube arrays at room temperature. Sens. Actuators B: Chem. 236, 529–536.

Liu, Y., Wang, H., Yang, S., Chen, K., Yang, T., Wei, J., et al., 2018. ppb Level ammonia detection of 3-D PbS quantum dots/reduced graphene oxide nanococoons at room temperature and Schottky barrier modulated behavior. Sens. Actuators B: Chem. 255, 2979–2987.

Luo, J., Li, C., Yang, Q., Yan, L., Zhang, B., Tao, R., et al., 2022. Facile fabrication of MoS2 nanoflowers/SnO2 colloidal quantum dots nanocomposite for enhanced NO_2 sensing at room temperature. IEEE Sens. J. . Available from: https://doi.org/10.1109/JSEN.2022.3151068.

Lu, Z., Lu, X., Zhong, Y., Hu, Y., Li, G., Zhang, R., 2019. Carbon dot-decorated porous organic cage as fluorescent sensor for rapid discrimination of nitrophenol isomers and chiral alcohols. Anal. Chim. Acta 1050, 146–153.

Lu, S., Xue, M., Tao, A., Weng, Y., Yao, B., Weng, W., 2021. Facile microwave-assisted synthesis of functionalized carbon nitride quantum dots as fluorescence probe for fast and highly selective detection of 2, 4, 6-trinitrophenol. J. Fluoresc. 31 (1), 1–9.

Lv, Y.K., Li, Y.Y., Yao, H.C., Li, Z.J., 2021. Nitrogen-doped graphene quantum dots-modified mesoporous SnO2 hierarchical hollow cubes for low temperature detection of nitrogen dioxide. Sens. Actuators B: Chem. 339. Available from: https://doi.org/10.1016/j.snb.2021.129882.

Mao, X., Wang, Y., Jiang, L., Zhang, H., Zhao, Y., Liu, P., et al., 2022. A Polydopamine-coated gold nanoparticles quenching quantum dots-based dual-readout lateral flow immunoassay for sensitive detection of carbendazim in agriproducts. Biosensors 12 (2). Available from: https://doi.org/10.1016/j.cej.2021.131824.

Masemola, C.M., Shumbula, N.P., Gqoba, S.S., Tetana, Z.N., Moloto, N., Linganiso, E.C. Electrospun NGQDs/PANI/PAN composite fibers for room temperature alcohol sensing. In: 2021 IEEE 3rd Eurasia Conference on IOT, Communication and Engineering (ECICE) IEEE, 2021, pp. 146–150.

Ma, J., Jiang, Y., Shen, L., Ma, H., Sun, T., Lv, F., et al., 2022. Oil-water self-assembly engineering of Prussian blue/quantum dots decorated graphene film for wearable textile biosensors and photoelectronic unit. Chem. Eng. J. 427. Available from: https://doi.org/10.1016/j.cej.2021.131824.

Mehata, M.S., Biswas, S., 2021. Synthesis of fluorescent graphene quantum dots from graphene oxide and their application in fabrication of GQDs@ AgNPs nanohybrids and sensing of H_2O_2. Ceram. Int. 47 (13), 19063–19072.

Mishra, R.K., Upadhyay, S.B., Kushwaha, A., Kim, T.H., Murali, G., Verma, R., et al., 2015. SnO_2 quantum dots decorated on RGO: a superior sensitive, selective and reproducible performance for a H_2 and LPG sensor. Nanoscale 7 (28), 11971–11979.

Mostafa, M., El Nady, J., Ebrahim, S.M., Elshaer, A.M., 2021. Synthesis, structural, and optical properties of Mn^{2+} doped ZnS quantum dots for biosensor application. Opt. Mater. 112. Available from: https://doi.org/10.1016/j.optmat.2020.110732.

Nair, R.V., Thomas, R.T., Mohamed, A.P., Pillai, S., 2020. Fluorescent turn-off sensor based on sulphur-doped graphene quantum dots in colloidal and film forms for the ultrasensitive detection of carbamate pesticides. Microchem. J. 157. Available from: https://doi.org/10.1016/j.microc.2020.104971.

Nemade, K.R., Waghuley, S.A., 2013a. LPG sensing application of graphene/CeO_2 quantum dots composite. AIP Conf. Proc. 1536 (1), 1258–1259.

Nemade, K.R., Waghuley, S.A., 2013b. LPG sensing application of graphene/Bi_2O_3 quantum dots composites. Solid. State Sci. 22, 27–32.

Nemade, K.R., Waghuley, S.A., 2013c. Strontium oxide quantum dot decorated graphene composites for liquid petroleum gas sensing. J. Chin. Adv. Mater. Soc. 1 (3), 219–228.

Ouyang, C., Chen, Y., Qin, Z., Zeng, D., Zhang, J., Wang, H., et al., 2018. Two-dimensional WS_2-based nanosheets modified by Pt quantum dots for enhanced room-temperature NH_3 sensing properties. App. Surf. Sci. 455, 45–52.

Pothipor, C., Jakmunee, J., Bamrungsap, S., Ounnunkad, K., 2021. An electrochemical biosensor for simultaneous detection of breast cancer clinically related microRNAs based on a gold nanoparticles/graphene quantum dots/graphene oxide film. Analyst 146 (12), 4000–4009.

Praoboon, N., Siriket, S., Taokaenchan, N., Kuimalee, S., Phaisansuthichol, S., Pookmanee, P., et al., 2022. Paper-based electrochemiluminescence device for the rapid estimation of trimethylamine in fish via the quenching effect of thioglycolic acid-capped cadmium selenide quantum dots. Food Chem. 366. Available from: https://doi.org/10.1016/j.foodchem.2021.130590.

Raeyani, D., Shojaei, S., Ahmadi-Kandjani, S., 2020. Optical graphene quantum dots gas sensors: experimental study. Mater. Res. Express 7 (1). Available from: https://doi.org/10.1088/2053-1591/ab637e.

Sahu, B.K., Juine, R., Das, A., 2019. Room temperature ammonia sensor using SnO2 quantum dots: an approach toward optical eye. AIP Conf. Proceed. 2115 (1). Available from: https://doi.org/10.1063/1.5112974.

Şen, F.B., Beğiç, N., Bener, M., Apak, R., 2022. Fluorescence turn-off sensing of TNT by polyethylenimine capped carbon quantum dots. Spectrochim. Acta—A: Mol. Biomol. 271. Available from: https://doi.org/10.1016/j.saa.2022.120884.

Sharma, V., Mehata, M.S., 2022a. A parallel investigation of un-doped and manganese ion-doped zinc selenide quantum dots at cryogenic temperature and application as an optical temperature sensor. Mater. Chem. Phys. 276. Available from: https://doi.org/10.1016/j.matchemphys.2021.125349.

Sharma, V., Mehata, M.S., 2022b. Photoluminescence turn-off based dual analytes (Hg^{2+} and Pb^{2+}) sensor in aqueous medium using 3-marcaptoproponic acid protected Mn2 + doped ZnSe quantum dots. Chem. Phys. Lett. 787. Available from: https://doi.org/10.1016/j.cplett.2021.139270.

Tall, A., da Costa, K.R., de Oliveira, M.J., Tapsoba, I., Rocha, U., Sales, T.O., 2021. Photoluminescent nanoprobes based on thiols capped CdTe quantum dots for direct determination of thimerosal in vaccines. Talanta 221. Available from: https://doi.org/10.1016/j.talanta.2020.121545.

Tao, X., Liao, Z., Zhang, Y., Fu, F., Hao, M., Song, Y., 2021. Aptamer-quantum dots and teicoplanin-gold nanoparticles constructed FRET sensor for sensitive detection of Staphylococcus aureus. Chin. Chem. Lett. 32 (2), 791–795.

Tu, Y.P., Wang, H.H., Long, D., Yuan, R., Chai, Y.Q., 2022. Highly sensitive photoelectrochemical biosensor based on Au nanoparticles sensitized zinc selenide quantum dots for DNA detection. Sens. Actuators B: Chem. 357. Available from: https://doi.org/10.1016/j.snb.2021.131255.

Van Tam, T., Hur, S.H., Chung, J.S., Choi, W.M., 2021. Novel paper-and fiber optic-based fluorescent sensor for glucose detection using aniline-functionalized graphene quantum dots. Sens. Actuators B: Chem. 329. Available from: https://doi.org/10.1016/j.snb.2020.129250.

Wang, R., Li, G., Dong, Y., Chi, Y., Chen, G., 2013. Carbon quantum dot-functionalized aerogels for NO_2 gas sensing. Anal. Chem. 85 (17), 8065–8069.

Wei, Q., Zhang, P., Liu, T., Pu, H., Sun, D.W., 2021. A fluorescence biosensor based on single-stranded DNA and carbon quantum dots for acrylamide detection. Food Chem. 356. Available from: https://doi.org/10.1016/j.foodchem.2021.129668.

Wongrat, E., Nuengnit, T., Panyathip, R., Chanlek, N., Hongsith, N., Choopun, S., 2021. Highly selective room temperature ammonia sensors based on ZnO nanostructures decorated with graphene quantum dots (GQDs). Sens. Actuators B: Chem. 326. Available from: https://doi.org/10.1016/j.snb.2020.128983.

Wu, J., Zhang, D., Cao, Y., 2018. Fabrication of iron-doped titanium dioxide quantum dots/molybdenum disulfide nanoflower for ethanol gas sensing. J. Colloid Interface Sci. 529, 556–567.

Wu, K., Zhang, W., Zheng, Z., Debliquy, M., Zhang, C., 2022. Room-temperature gas sensors based on titanium dioxide quantum dots for highly sensitive and selective H2S detection. Appl. Surf. Sci. 357. Available from: https://doi.org/10.1016/j.apsusc.2022.152744.

Xu, Y., Huang, T., Wang, S., Meng, M., Yan, Y., 2022. SiO_2-coated molecularly imprinted sensor based on Si quantum dots for selective detection of catechol in river water. J. Environ. Chem. Eng. 10 (1). Available from: https://doi.org/10.1016/j.jece.2021.106850.

Xu, Y., Yu, H., Chudal, L., Pandey, N.K., Amador, E.H., Bui, B., et al., 2021. Striking luminescence phenomena of carbon dots and their applications as a double ratiometric fluorescence probes for H2S detection. Mater. Today Phys. 17. Available from: https://doi.org/10.1016/j.mtphys.2020.100328.

Yang, Y., Liu, Z., Chen, D., Gu, B., Gao, B., Wang, Z., et al., 2021a. Multifunctional N-doped graphene quantum dots towards tetracycline detection, temperature sensing and high-performance WLEDs. J. Photochem. Photobiol. A: Chem. 405. Available from: https://doi.org/10.1016/j.jphotochem.2020.112977.

Yang, Q., Li, Q., Li, H., Li, F., 2021b. pH-response quantum dots with orange–red emission for monitoring the residue, distribution, and variation of an organophosphorus pesticide in an agricultural crop. J. Agri. Food Chem. 69 (9), 2689–2696.

Yang, S., Song, Z., Gao, N., Hu, Z., Zhou, L., Liu, J., et al., 2019. Near room temperature operable H2S sensors based on In2O3 colloidal quantum dots. Sens. Actuators B: Chem. 286, 22–31.

Yang, M., Wang, C., Liu, E., Hu, X., Hao, H., Fan, J., 2021c. A novel ascorbic acid ratiometric fluorescent sensor based on ZnCdS quantum dots embedded molecularly imprinted polymer and silica-coated CdTeS quantum dots. J. Mol. Liq. 337. Available from: https://doi.org/10.1016/j.molliq.2021.116438.

Yanyan, Z., Lin, J., Xie, L., Tang, H., Wang, K., Liu, J., 2021. One-step preparation of nitrogen-doped graphene quantum dots with anodic electrochemiluminescence for sensitive detection of hydrogen peroxide and glucose. Front. Chem. 9. Available from: https://doi.org/10.3389/fchem.2021.688358.

Ye, S., Han, T., Cheng, M., Dong, L., 2022. Wulff-type boronic acid-functionalized quantum dots for rapid and sensitive detection of Gram-negative bacteria. Sens. Actuators B: Chem. 356. Available from: https://doi.org/10.1016/j.snb.2021.131332.

Yi, Y., Zeng, W., Zhu, G., 2021. β-Cyclodextrin functionalized molybdenum disulfide quantum dots as nanoprobe for sensitive fluorescent detection of parathion-methyl. Talanta 222. Available from: https://doi.org/10.1016/j.talanta.2020.121703.

Zhang, D., Dong, G., Cao, Y., Zhang, Y., 2018a. Ethanol gas sensing properties of lead sulfide quantum dots-decorated zinc oxide nanorods prepared by hydrothermal process combining with successive ionic-layer adsorption and reaction method. J. Colloid Interface Sci. 528, 184–191.

Zhang, D., Dong, G., Wu, Z., Pan, W., Fan, X., et al., 2018b. Liquefied petroleum gas sensing properties of ZnO/PPy/PbS QDs nanocomposite prepared by self-assembly combining with SILAR method. IEEE Sens. J. 19 (8), 2855–2862.

Zhang, Z., Fan, Z., 2021. Application of cerium−nitrogen co-doped carbon quantum dots to the detection of tetracyclines residues and bioimaging. Microchem. J. 165. Available from: https://doi.org/10.1016/j.microc.2021.106139.

Zhang, R.R., Gan, X.T., Xu, J.J., Pan, Q.F., Liu, H., Sun, A.L., 2022. Ultrasensitive electrochemiluminescence sensor based on perovskite quantum dots coated with molecularly imprinted polymer for prometryn determination. Food Chem. 370. Available from: https://doi.org/10.1016/j.foodchem.2021.131353.

Zhang, Y.H., Wang, C.N., Yue, L.J., Chen, J.L., Gong, F.L., Fang, S.M., 2021. Nitrogen-doped graphene quantum dot decorated ultra-thin ZnO nanosheets for NO_2 sensing at low temperatures. Phys. E: Low-dimens. Syst. Nanostruct. 133. Available from: https://doi.org/10.1016/j.physe.2021.114807.

Zhuang, B., Liu, Y., Yuan, S., Huang, H., Chen, J., Chen, D., 2019. Glass stabilized ultra-stable dual-emitting Mn-doped cesium lead halide perovskite quantum dots for cryogenic temperature sensing. Nanoscale 11 (32), 15010−15016.

Zhu, Q., Du, J., Feng, S., Li, J., Yang, R., Qu, L., 2022. Highly selective and sensitive detection of glutathione over cysteine and homocysteine with a turn-on fluorescent biosensor based on cysteamine-stabilized CdTe quantum dots. Spectrochim. Acta A: Mol. Biomol. Spectrosc. 267. Available from: https://doi.org/10.1016/j.saa.2021.120492.

Zhu, L., Hao, H., Ding, C., Gan, H., Jiang, S., Zhang, G., et al., 2021. A novel photoelectrochemical aptamer sensor based on CdTe quantum dots enhancement and exonuclease I-assisted signal amplification for listeria monocytogenes detection. Foods 10 (12). Available from: https://doi.org/10.3390/foods10122896.

Chapter 14

Application of quantum dots in photosplitting of water

Luma M. Ahmed[1], Thaqeef M. Jawad[1], Hamad H. Kadium[1] and Jayesh P. Bhatt[2]
[1]*Department of Chemistry, College of Science, University of Kerbala, Karbala, Iraq,*
[2]*Department of Chemistry, PAHER University, Udaipur, Rajasthan, India*

14.1 Introduction

The whole world is facing scarcity of energy resources as presently available conventional fuels such as coal, kerosene, petrol, diesel, etc. will be reaching a point of complete exhaustion in the coming few decades. On the other hand, the demand for energy is increasing regularly, which cannot be fulfilled by the available resources, and therefore there is an urgent demand to find some alternate sources of energy, that are inexhaustible and/or renewable. Solar energy enters the scene here as it can fulfill the energy demands of society for many more centuries to come because it is abundantly available and free of cost. Hydrogen has a higher storage capacity than many other conventional fuels. There is a need for clean and eco-friendly energy sources as fossil fuel energy sources show adverse impacts on the environment also, whereas hydrogen is a clean energy source.

Hydrogen on combustion will produce water, which is a benign compound, and therefore it does not pollute our environment any more. Hydrogen has been very truly advocated as the fuel of the future and there is no doubt that it can fulfill the ever increasing requirement of energy and will replace the existing conventional fuels in the future. The use of hydrogen as a fuel for transportation and generation of electricity through fuel cells has been already established. Water covers almost three fourth of the Earth and if a method is developed to generate hydrogen gas from photosplitting of water, then it is welcome. Hydrogen produced from electrolysis of water is costly and does not help much because electricity is being used to decompose water. On the other hand, water is broken into hydrogen and oxygen by using solar energy as the source, which is freely and abundantly available.

Quantum Dots. DOI: https://doi.org/10.1016/B978-0-12-824153-0.00014-8

There are still some existing challenges in this direction, which should be overcome in order to improve efficiency, durability, and lower the cost. These are:

- Enhance absorption of sunlight and better catalysis on surface.
- Developing highly active and eco-friendly photocatalyst.
- Stability and durability for a longer time may be improved using protective surface coatings.
- Photocatalyst may be modified so that the higher recombination rate of photogeneration electron−hole pairs is lowered or completely checked.
- The costs of production of hydrogen should be lowered by using low-cost photocatalysts through lowering their processing costs.
- Quantum dots (QDs) have come to our rescue at this stage as these QDs have certain unique properties, such as larger surface area (high surface to volume ratio), quantum confinement effect, and shifting absorption wavelength in visible and near infrared regions.

14.2 Hydrogen production

Hydrogen has the potential to be a dependable renewable source of energy that can replace fossil fuels in the current energy crisis, because of its zero emissions and its enhanced energy content (Dahiya et al., 2020). In the few last years, the interest in producers of hydrogen gas production has increased with the growing human activity, because it is considered as a main fuel of the future, which is clean energy as it does not liberate any carbon dioxide during its combustion. It is also economic and very flexible in various applications compared to traditional energy sources such as fossil fuel or nuclear plant (Nemzer et al., 2003; Bičáková and Straka, 2010; Melo and Silva, 2011). Hydrogen gas is regarded as one of the common forms of renewable energy resources. It is produced in various ways with different sources like hydrocarbons, alcohol, or water, such as photodehydrogenation of methanol (Ahmed et al., 2016), electrochemical photolysis of water (Carey and Oliver, 1976), photolysis, sonolysis, and sonophotolysis of water (Penconi et al., 2015), and electrolysis of different materials that contain water, and it is used in photovoltaic solar energy (Slama, 2013).

The hydrogen gas was first liberated from the splitting of the water molecule by Fujishima and Honda (1972). They used an electrochemical cell and observed the hydrogen gas evaluation at the TiO_2 electrode, when the TiO_2 electrode surface was irradiated by light, generating an exciton, that is, a photoelectron (e^-)−photohole (h^+) pair. There is a key role played by this photoelectron (e^-)−photohole (h^+) pair in the redox reaction. This reaction occurs on the TiO_2 electrode surface and the photoelectron produces a proton

from water. This electron also reduced a proton at the Pt electrode surface to afford hydrogen gas (Eqs. 14.1–14.4):

$$TiO_2 + 2\,hv \rightarrow 2\,e^- + 2\,h^+ \tag{14.1}$$

$$2\,e^- + H_2O \rightarrow \frac{1}{2}O_2 + 2\,H^+ \tag{14.2}$$

$$2\,e^- + 2\,H^+ \rightarrow H_2 \tag{14.3}$$

Therefore, the overall reaction is:

$$2\,hv + H_2O \rightarrow \frac{1}{2}O_2 + H_2 \tag{14.4}$$

Wrighton et al. (1976) evolved hydrogen gas using an electrochemical cell that contains a Pt electrode and a Sb-SnO_2 single-crystal electrode, which was irradiated with ultraviolet light in an alkaline solution. Bockris et al. (1985) reported the possible routes of hydrogen production from the decomposition of water, such as electrolysis, plasmolysis, magnetolysis, biocatalysis, thermal method, use of light photolysis or photocatalyst, radiolysis, etc. However, the maximum purity for hydrogen produced was found to be 99.99% using the electrolysis method because it is one of the best methods and it is also regarded as a green method. The normal electrolysis of water uses direct current in two steps (Eqs. 14.5–14.6):

$$2\,H_2O \rightarrow \frac{1}{2}O_2 + 2\,H^+ + 2\,e^- \text{ at } E^o = 1.229\ (1.23)\ V \tag{14.5}$$

$$2\,e^- + 2\,H^+ \rightarrow H_2 \text{ at } E^o = 0.00\ V \tag{14.6}$$

14.2.1 Basic principle of overall water splitting

Over the years, there have been several proposals for water splitting. In the late 1970s, major attempts were made at photocatalytic water splitting (Fujishima and Honda, 1972; Bard, 1979; Van Damme and Hall, 1979; Domen et al., 1980; Kudo et al., 1988). The powdered semiconductor photocatalyst will be useful for the large-scale use of solar water splitting due to its simplicity (Jia et al., 2014). TiO_2 has been one of the most extensively researched photocatalysts for water splitting (Ma et al., 2014). Through water splitting, photon energy is transformed to chemical energy, with a largely positive change in Gibbs free energy $\left(\Delta G^o = 237\ kJ^{-1}\ mol\right)$ (Han et al., 2017). When a light is incident on a photocatalyst with energy larger than the bandgap, then electrons in the valance band (VB) are excited into the conductive band (CB) leaving holes in the valence band (Cao et al., 2017).

As the first step in the photocatalytic process, both excited electrons and holes are generated; which subsequently diffuse to the surface of the

semiconductor particles independently (Vaiano et al., 2018). Protons play a major role in hydrogen generation. Photogenerated electrons and holes promote redox processes that are comparable to electrolysis. Total water splitting into H_2 (reduced by the electrons) and O_2 (oxidized by the holes) on the photocatalyst surface can be achieved (Eqs. 14.7 and 14.8 and Fig. 14.1) (Liu et al., 2015; Qiao et al., 2020; Marschall, 2021).

$$H_2O + 2\,h^+ \rightarrow 2\,H^+ + \frac{1}{2}O_2 \tag{14.7}$$

$$2\,H^+ + 2\,e^- \rightarrow H_2 \tag{14.8}$$

Overall water splits into H_2 and O_2 (Eq. 14.9).

$$H_2O \rightarrow \frac{1}{2}O_2 + H_2 \tag{14.9}$$

The bandgap width and potentials of the conduction and valence bands of a semiconductor photocatalyst material are important. The bottom level of the CB must be located at a more negative potential than H^+/H_2 (0 V at pH 0), whereas the VB must be more positive than the O_2/H_2O energy level (1.23 V vs NHE). This indicates that the minimum photon energy thermodynamically necessary to cause photocatalytic water splitting is 1.23 eV (Strataki et al., 2007; Kudo and Miseki, 2009; Hisatomi et al., 2014; Peng et al., 2019; Niu et al., 2021).

A photocatalyst must fulfill these three requirements (Maeda et al., 2005; Hisatomi et al., 2014):

- it should have a bandgap smaller than 3 eV;
- it has stability during the photocatalytic process, and
- its band edge potentials are adequate for overall water splitting.

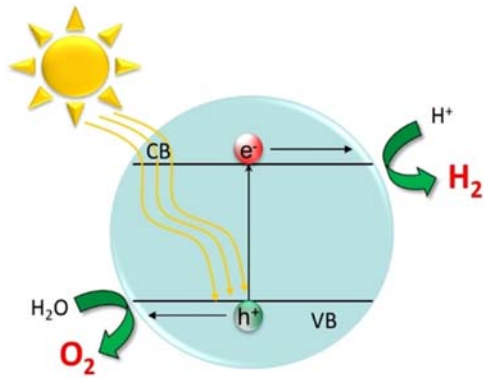

FIGURE 14.1 Schematic illustration of solar water splitting by using the photocatalyst. *Adapted from Marschall, R., 2021. 50 years of materials research for photocatalytic water splitting. Eur. J. Inorg. Chem. 2021(25), 2435–2441, with permission.*

The pure water splitting process exhibits a low efficiency because direct water splitting is still a difficult problem due to the inherent process drawbacks ($H_2 + O_2 = H_2O$) and it is a multistep process, in which four electrons are transferred. In addition, hydrogen is mostly created from fossil fuels such as natural gas, oil, and coal and only 2% is produced by water splitting (Miyoshi et al., 2018; Wang et al., 2018a; Fang et al., 2020; Dinda et al., 2020). Sacrificial reagents (as electron donors) are commonly used in water, such as alcohols (methanol, ethanol, and glycerol) to produce hydrogen efficiently by successfully scavenging photogenerated holes by suppressing back reaction, because O_2 is not evolved, and permitting a two-electron-transfer mechanism (Yang et al., 2013; Schneider and Bahnemann, 2013; Hisatomi et al., 2014).

Methanol is commonly employed as a sacrificial agent in photocatalysis for the evolution of H_2 from water under inert gas atmosphere, due to its strong reactivity, structural simplicity, and lack of C−C bonds (Cargnello et al., 2011). The water splitting reaction is a large uphill reaction with a ΔG° change. It is not an easy process compared to a reaction using a sacrificial agent (such as methanol), which is still an uphill reaction but less than that of water splitting. The energy change of sacrificial H_2 production is smaller than the energy change of water splitting. The use of sacrificial reagents leads to a significant decrease in ΔG° as it avoids the four-electron process of molecular oxygen formation. (Yasuda et al., 2018; Corredor et al., 2019) (Fig. 14.2).

Kawai and Sakata (1980) reported direct photocatalytic production of hydrogen from methanol and water over TiO_2-based catalysts, which produced H_2 and CO_2 from a mixture of H_2O/methanol (50:50 v/v %) after

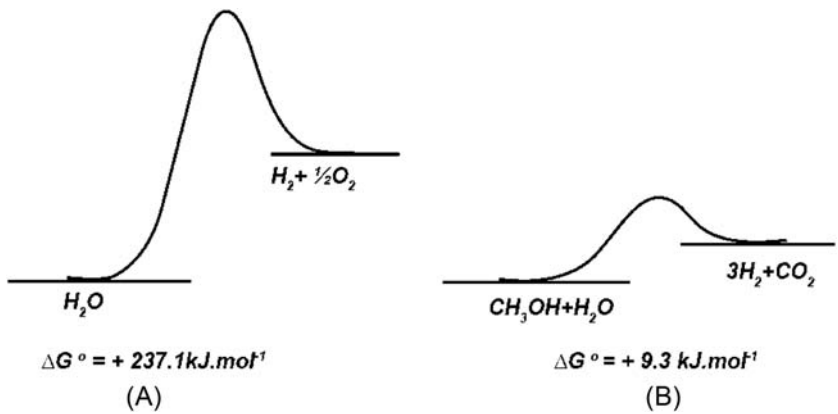

FIGURE 14.2 Comparison between H_2 production reaction: (A) from water splitting; and (B) from methanol. *Adapted from Yasuda, M., Matsumoto, T., Yamashita, T., 2018. Sacrificial hydrogen production over TiO_2-based photocatalysts: polyols, carboxylic acids, and saccharides. Renew. Sustain. Energy Rev. 81, 1627–1635, with permission.*

prolonged illumination. The absorption of photons from a light source with energy larger than the bandgap of the semiconductor photocatalyst promotes an electron from the VB of the semiconductor to the CB, generating an electron−hole pair. In this case, the photogenerated electrons are used to combine with protons in water to generate hydrogen (water reduction). The photogenerated holes are captured by sacrificial agents with a series of reactions (methanol oxidation) (Eqs. 14.10−14.14 and Fig. 14.3) (Wang et al., 2004; Puga, 2016; Huang et al., 2020; Zhao et al., 2020).

$$\text{Photocatalyst} \xrightarrow{hv} e^- + h^+ \tag{14.10}$$

$$CH_3OH + h^+ \rightarrow \cdot CH_2OH + H^+ \rightarrow HCHO + H \tag{14.11}$$

$$HCHO + H_2O + h^+ \rightarrow HCOOH + H_2 \tag{14.12}$$

$$HCOOH + h^+ \rightarrow CO_2 + H_2 \tag{14.13}$$

Overall process can be presented as Eq. (14.14).

$$CH_3OH + H_2O \xrightarrow{hv} CO_2 + 3H_2 \tag{14.14}$$

The reductive alkoxy radicals ($\bullet CH_2$-OH) are further oxidized to formaldehyde, formic acid, and carbon dioxide. The reductive alkoxy radicals $\bullet CH_2OH$ and $\bullet CO_2^-$ cannot react only with holes or hydroxyl radicals but also donate electrons to promote proton reduction to hydrogen, which is called the "doubling" effect. The same mechanisms are used for any other alcohol that carries a hydrogen atom on the carbon atom at the α-position of its OH group (Hainer et al., 2018). The by-products produced from methanol and other alcohols, such as formaldehyde, formic acid, and carbon dioxide, are also used as sacrificial agents for water splitting for hydrogen production

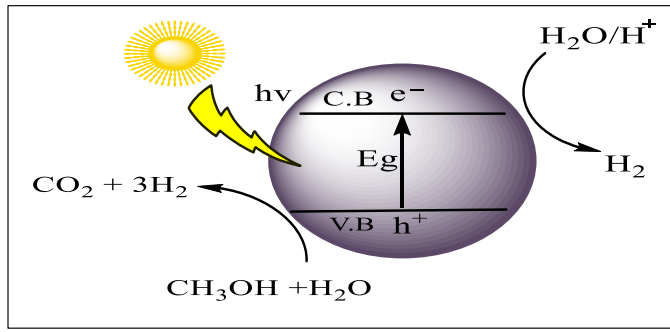

FIGURE 14.3 The photocatalytic hydrogen evolution process from aqueous methanol solution in the presence of inert gas (Kamat and Jin, 2018). *Adapted from Kamat, P.V., Jin, S., 2018. Semiconductor photocatalysis: tell us the complete story! ACS Energy Lett. 3, 622 − 623, with permission.*

(Bahruji et al., 2011; Coronado, 2013; Belhadj et al., 2017). The photocatalyst valence band potential has to be more positive than the sacrificial agent oxidation potential to oxidize such sacrificial agents (Luo et al., 2021).

Kumar et al. (2016) compared the activity for photocatalytic H_2 evolution under solar light irradiation in the presence of different scavengers. It was observed that hydrogen production was enhanced by using several organics such as ethylene glycol, because of the position of its oxidation potential with respect to the valence band potential of titania, and the generation of hydrogen was also found to be increased on increasing the polarity of alcohol. The photooxidation route of methanol depends on the molecular species adsorbed on the photocatalytic surface (Crampton et al., 2017). The carrier recombination rate was decreased after the traps of the hole by methanol on the catalytic surface; thus promoting the separation of electron−hole pairs (Chen et al., 2018).

Jitputti et al. (2008) have reported the photocatalytic evolution of H_2 from the water-splitting process using methanol as a sacrificial reagent in the presence of TiO_2 nanowires. The photogenerated holes or photogenerated oxygen are swiftly removed in an irreversible fashion, inhibiting mutual electron−hole recombination. Here, sacrificial reagents might compete with water in the reduction reaction. Fang et al. (2020) found that water was not the major source of hydrogen production in the photocatalytic process at Rh-loaded TiO_2 in the presence of sacrificial methanol at room temperature. It was found that the contribution of methanol decomposition ($\sim$60%) contributed even more than water splitting ($\sim$40%) because protons produced from both oxidation of methanol and ionization of water may be converted into hydrogen. In contrast, hydrogen generation was predominantly from water based on the combination of thermal and light energy over Rh-loading TiO_2.

Camacho et al. (2018) concluded that hydrogen production via water splitting is practically null compared to when methanol was added. It was revealed that the quantity of hydrogen produced increases with the increasing concentration of methanol. They could achieve the highest quantum efficiency under solar radiation of 7.7%. Gultom et al. (2017) reported that the highest activity could be achieved in 50% ethanol solution in the presence of ZnOS-10 with a hydrogen production rate of 14,800 $\mu mol\ g^{-1}\ h^{-1}$ and an apparent quantum yield (QY) of 31.5%. The QY and apparent quantum yield (AQY) are calculated by Eqs. (14.15 and 14.16), respectively, which define the stability and process efficiency of the photocatalytic system (Fukuzumi et al., 2018; Meng et al., 2020).

$$\text{QY}\ (\%) = \frac{\text{Number of reacted electrons}}{\text{Number of absorbed photons}} \times 100 \tag{14.15}$$

$$\text{AQY}\ (\%) = \frac{(\text{Number of photohydrogen molecules}) \times 2}{\text{Number of incident photons}} \times 100 \tag{14.16}$$

14.2.2 Photoelectrochemical cells

Photoelectrochemical (PEC) cells are one of the most efficient methods for converting solar energy into hydrogen (Landman et al., 2020). It was discovered that clean H_2 energy can be obtained by splitting water through a PEC cell using a TiO_2 photoanode. A typical PEC system consists of three electrodes:

- working electrode (photoanode);
- counter electrode (photocathode), for example, Pt or semiconductor, and
- reference electrode.

The typical PEC systems use photocatalysts [nanoparticles (NPs)] as photoelectrodes (such as TiO_2, ZnO, CdSe, CdS) (Gunasekaran et al., 2021). The electrodes are immersed in an aqueous electrolyte (Crespo-Quesada and Reisner, 2017). When a photoanode (semiconductor) comes in contact with an electrolyte, the Fermi energy level rises above the potential of electrocatalytic water splitting, which results in an upward band bending contact of a photocathode semiconductor with electrolyte. On the other hand, a downward band bending is present (Kibria et al., 2014; Guijarro et al., 2015). The difference in the electrochemical potential between the semiconductor electrode and the electrolyte causes a charge transfer process at the solid/liquid interface, resulting in an electric current flowing through the junction until an electronic equilibrium is reached (Jiang et al., 2017; Xiao and Liu, 2018).

The QDs having unique confined optical and electronic properties are applied to sensitize large bandgap photoanode materials (Zamiri and Bagheri, 2018). On irradiating the photoanode in the PEC cell, hydrogen is generated (Fig. 14.4) (Chen et al., 2016a).

They found that when photons are absorbed with an energy larger than their bandgap, the photoelectrons are excited and migrate into the unoccupied conduction band (CB) and holes are left in the valence band (VB) (exciton, i.e., electron−hole pairs generation). The exciton is separated by the built-in electric field, when photoexcited charge carriers have a longer lifetime and larger diffusion distance (Molaei, 2020), which leads to the higher process efficiencies due to easy separation and transport of the carriers (Xiao et al., 2019). Photoexcited electrons are swept toward the counter electrode through the back contact and an outside circuit, while the remaining holes participate in the oxidation reaction. In a PEC cell, electron−hole pairs produced by incident photons drive reduction−oxidation (redox) processes (Phang and Tan, 2019), in which holes oxidize the water/hole scavenger (HS) at the anode surface, while electrons travel to the counter electrode to reduce water and produce H_2 gas (Sahai et al., 2017).

The properties of the photoelectrode strongly influence the PEC efficiency of water splitting. An ideal photoelectrode should fulfill the following conditions:

- small bandgap for visible light absorption;

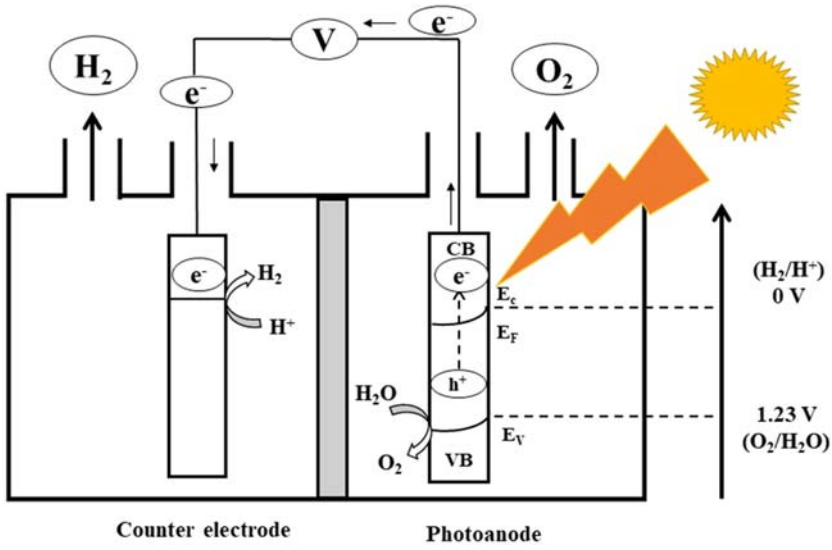

FIGURE 14.4 The basic principles of water splitting for a photoelectrochemical cell. E_F, Fermi level.

- photoelectrodes must be corrosion-resistant and chemically stable in aqueous solutions; under both conditions; dark and illumination;
- photogenerated charge separation ($e^- - h^+$) should be efficient; and
- the CB position of the semiconductor should be more negative than the (H^+/H_2) potential, and the VB should be more positive than the (O_2/H_2O) potential (1.23 V vs NHE) (Tamirat et al., 2016; Batubara and Zulys, 2019). It is shown in Fig. 14.5.

Semiconductor types, charge separation, transfer efficiency, crystal phases, and morphologies determine the efficiency for hydrogen production.

14.3 Metal-based quantum dots

14.3.1 Metals

Ye et al. (2012) prepared vertically oriented TiO_2 nanotube arrays (TNTAs) by a three-step electrochemical anodization technique. Then Pd QDs were prepared with uniform size and narrow size distribution on TiO_2 nanotubes by a modified hydrothermal method. It was reported that a high photocatalytic hydrogen production rate (592 $\mu mol\, h^{-1}\, cm^{-2}$) could be achieved with Pd@TNTAS. Chen et al. (2016b) prepared Ag QDs/g-C_3N_4 (Ag QDs/g-C_3N_4) photocatalysts via a novel one-step method using $AgNO_3$ and urea as precursors. As-composed Ag QDs with an average diameter of about 5 nm were found to be uniformly dispersed on the surface of g-C_3N_4 nanosheets.

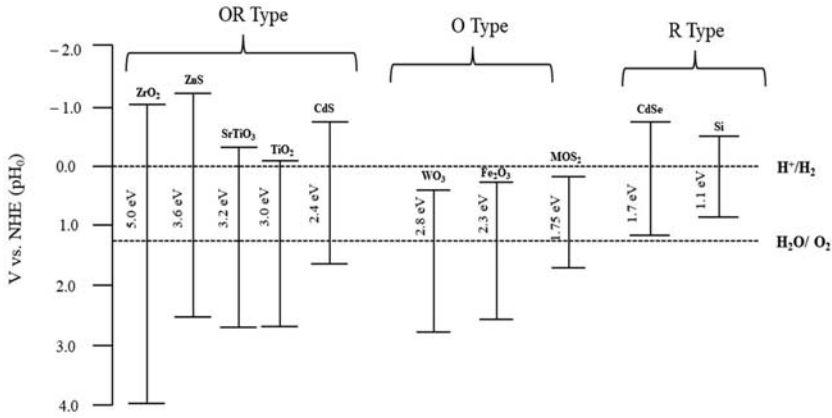

FIGURE 14.5 The band edge position and bandgaps for different semiconductors (OR, O, and R types). *OR*, oxidation and reduction; *O*, oxidation; *R*, reduction.

They used methanol as a sacrificial reagent. It was reported that as-prepared Ag QDs/g-C_3N_4 photocatalysts (0.5%) exhibited almost 4.6 times higher photoactivity for hydrogen production.

Kuang et al. (2016) embedded Au QDs in rimous cadmium sulfide nanospheres to synthesize hybrid photocatalyst via a simple hydrothermal process, which was followed by photoreduction. As rimous cadmium sulfide nanospheres had a rough surface and irregular fissures, these will strengthen their interaction and adhesion with Au QDs. It was revealed that the highest photocatalytic activity obtained for hydrogen generation was 601.2 $\mu mol\ h^{-1}\ g^{-1}$ by adjusting the Au loading. The synthesis of bimetallic (NiFe) quantum dot based electrocatalysts has been reported by Cirone et al. (2021). They optimized Ni:Fe ratio to tune QDs for increased electrochemical catalytic activity. The optimal compositions of these bimetallic QD based electrocatalysts was found to be 25.3% and 54.9% towards the hydrogen evolution reaction (HER) and oxygen evolution reaction (OER), respectively.

14.3.2 Oxides

Yang et al. (2009) have made use of N-doped ZnO concentrating on its PEC performance. The nitrogen has been commonly employed as a dopant to modify the electronic structures of metal oxide semiconductors as it resembles oxygen in size and low formation energy is required to replace oxygen (Zong et al., 2013). ZnO QDs dispersed in HS matrix were prepared by Xu et al. (2016). The HS contains S^{2-} and SO_3^{2-} groups. It was reported that as-synthesized ZnO QDs were hybridized with HS groups forming a stable ZnO QDs/HS hybrid hydrosol. This composite could produce H_2 with

a high rate of 260 μmol h^{-1} g^{-1}, which is almost 48-fold higher than for pure ZnO QDs.

Xie et al. (2017) decorated $BiVO_4$ QDs on the surface of screw-like SnO_2 nanostructures. They used the ionic layer absorption method for this purpose. It was revealed that the bandgap of $BiVO_4$ increases from 2.4 to 2.6 eV, when the particle size was decreased to about 5 nm. It was revealed that incident photon to current conversion efficiency was also increased up to 13.47%. It was reported that the rate of H_2 generation from splitting of water was 1.16 μmol h^{-1} cm^{-2} over $BiVO_4$ quantum dot/screw-like SnO_2 nanostructures in the presence of visible light. Liu et al. (2018) reported the synthesis of Co_3O_4 QDs TiO_2 nanobelts (NBs) hybrids via a facile hydrothermal method. They could obtain simultaneous production of H_2 and O_2 from pure water in the presence of light with high evolution rates of 22.0 and 41.8 μmol h^{-1} g^{-1}, respectively. It was observed that these production rates were higher compared to Co_3O_4 and TiO_2 NBs. The size of Co_3O_4 QDs was found to be ~3 nm, which not only improved the light sensitivity but also promoted the transfer of electrons from TiO_2 to Co_3O_4 QDs and as a result, H_2 generation was also enhanced.

Qian et al. (2018) reported the synthesis of p-type CuO/n-type CeO_2 heterojunction in situ grown on graphene. It was revealed that the H_2 evolution rate of the CeO_2−CuO QDs/graphene could reach 2481 μmol h^{-1} g^{-1} and remained unaffected for four consecutive hydrogen production cycles. The protonated graphitic carbon nitride (p-C_3N_4) loaded with IrO_2 QDs was fabricated by Wang and Li (2018) via a hydrothermal approach. It was found that IrO_2 QDs had an average diameter of approx 2 nm and these were highly dispersed and anchored on surfaces of p-C_3N_4. It was reported that as-prepared IrO_2/C_3N_4−0.6 wt.% photocatalyst could produce hydrogen and oxygen at a rate of 45 and 20 μmol h^{-1}, respectively.

Zhang et al. (2018a) constructed novel SnO_2 QDs modified TiO_2 nanorod arrays (NAs) by calcining $SnCl_2$-adsorbed on TiO_2 NAs. It was reported that photocurrent density of SnO_2 QDs/TiO_2 NAs was five times higher than that obtained with only TiO_2 NAs. It was also revealed that SnO_2 QDs/TiO_2 NAs exhibited a high photoelectrocatalytic activity for overall water splitting affording O_2 and H_2 at the rate of 11.87 and 27.85 μmol cm^{-2} h^{-1}, respectively. Such an excellent performance of water splitting may be due to its Z-scheme heterostructure. They also developed an effective strategy by distributing $BiVO_4$ QDs on nano tin oxide (Zhang et al., 2018a,b). They also used carbon QDs (CQDs) to enhance charge transfer and electrocatalytic properties at the $BiVO_4$-SnO_2 interface. It was observed that this composite afforded a hydrogen generation rate of 0.54 μmol h^{-1} without using any bias.

The dodecahedral nitrogen-doped carbon-coated CuO-In_2O_3 p−n heterojunction (DNCPH) was fabricated by Sun et al. (2019). As-prepared composite exhibited an excellent photocatalytic production efficiency of H_2. It was

revealed that improved separation efficiency of excitons (photogenerated electron/hole pairs) and coated N-doped C layer with CuO-In_2O_3 p−n heterojunction was responsible for enhanced photocatalytic hydrogen production efficiency of DNCPH. Reddy et al. (2020) prepared functionalized carbon nanotubes−titania QDs (FCNT-TQDs) and used them as photocatalysts in the presence of sunlight for hydrogen production. It was reported that the photocatalyst synthesized may be tuned by the addition of copper to achieve a highest hydrogen production rate up to 54.4 mmol $h^{-1}g^{-1}$, which was about 5.4 and 25 times higher than that obtained on using FCNT-TQDs composite and pristine TiO_2 QDs, respectively.

14.3.3 Metal sulfides

Although bulk CdSe produces H_2 from water under visible light irradiation, CdSe-nanoribbons were able to generate hydrogen from aqueous sodium sulfite/sulfide solution with a quantum efficiency (9.2%) at 440 nm (Frame and Osterloh, 2010). It was observed that ultrasonication and exfoliation of bulk MoS_2 can produce MoS_2 nanoplates. When the CdSe nanoribbons are chemically linked to these nanoplates, the activity was found to increase about four times. CdS quantum dot coupled graphitic carbon nitride photocatalysts were synthesized by Ge et al. (2012) through chemical impregnation. The effect of CdS content was observed on the rate of photocatalytic hydrogen evolution under visible light irradiation using platinum as a cocatalyst in aqueous solutions of methanol. It was revealed that the optimal CdS QD content was 30 wt.%, where H_2 evolution rate could reach 17.27 μmol h^{-1} in the presence of visible light, and it was about nine times more than that with pure g-C_3N_4.

The oil refineries are venting off almost 15%−20% H_2S and hardly 5% of it is utilized to produce sulfur and water. Apte et al. (2012) investigated a novel Q-CdS (highly monodispersed) germanate glass nanocomposite. The size of CdS QDs varied between 4−14 nm. A high rate of evolution of H_2 (3780 μmol h^{-1}) was obtained. It was also observed that as-prepared catalyst was stable and it can be also regenerated easily as compared to other catalysts. This glass nanocomposite also exhibited rapid methylene blue degradation in the presence of visible light. It was suggested that such orthorhombic QD−CdS−glass nanocomposites can find potential applications in LED, solar cells, and other optoelectronic devices.

Cao et al. (2013) grew well dispersed CdS QDs on g-C_3N_4 nanosheets via a solvothermal method. They used dimethyl sulfoxide. It was observed that as-prepared CdS−C_3N_4 nanocomposites exhibited an excellent efficiency for photocatalytic hydrogen evolution in the presence of visible light as compared to pure g-C_3N_4. It was revealed that composite with 2 wt.% CdS showed a higher hydrogen evolution rate (4.494 mmol h^{-1} g^{-1}), which is about 115 times more than that obtained with pure g-C_3N_4. Schweinberger et al. (2013)

synthesized Pt clusters of various sizes and embedded these on CdS quantum rods. They reported that the size of the Pt cluster had a significant impact on photocatalytic effectiveness. The highest efficiency could be achieved by a Pt cluster comprising Pt_{46}.

Li et al. (2014) decorated $ZnIn_2S_4$ microspheres (ZIS MSs) with CQDs as well as platinum NPs (dual cocatalysts). It was observed that ZIS MSs coloaded with Pt and CQDs exhibited a high photocatalytic production rate of H_2 of 1032.2 $\mu mol\ h^{-1}\ g^{-1}$ in triethanolamine aqueous solution in the presence of visible light, which was much higher compared to pure ZIS, CQDs-decorated ZIS, and Pt-loaded ZIS. The CdS QDs supported on two oxides (Ga_2O_3 and In_2O_3) were prepared by Pan et al. (2014) and used for the evolution of H_2 from aqueous solutions containing lactic acid under visible light. It was observed that H_2 evolution rates on CdS/Pt/In_2O_3 and CdS/Pt/Ga_2O_3 were 1032.2 and 995.8 $\mu mol\ h^{-1}$, respectively. These rates of H_2 evaluation were much higher compared to Pt/CdS (108.09 $\mu mol\ h^{-1}$), Pt/In_2O_3 (0.05 $\mu mol\ h^{-1}$), and Pt/Ga_2O_3 (0.12 $\mu mol\ h^{-1}$). It was suggested that the surface properties of the metal oxides played two important roles:

- anchoring of CdS QDs and Pt NPs; and
- efficient trapping of photogenerated electrons.

Wang et al. (2014) reported a photocatalyst, nickel-hybrid CdS QDs (Ni_h-CdS QDs), which was prepared in situ from nickel salts and CdS QDs. They used 3-mercaptopropionic acid as a stabilizer. It was found that 403.2 μmol of H_2 was obtained with a high evolution rate of 74.6 $\mu mol\ h^{-1}\ mg^{-1}$ under visible light irradiation for 20 h as compared to MPA-CdS QDs (mercaptopropionic-acid-stabilized CdS QDs). Cu_2S QDs coupled three-dimensional flower-like hierarchical BiOBr (Cu_2S QDs/BiOBr) were prepared by Wang et al. (2015) via a precipitation method. It was observed that Cu_2S QDs had an average diameter of 10 nm and these were uniformly attached on the surface of BiOBr. It was reported that as-prepared Cu_2SQDs/BiOBr composite exhibited higher water splitting and they could obtain 717 $\mu mol\ g^{-1}$ of H_2 with 3 wt.% Cu_2SQDs/BiOBr containing 1 wt.% Pt. This rate was about 3.1 times higher as compared to only Cu_2S NPs.

Yue et al. (2016) synthesized CdTe/CdS QDs using sulfur tolerant $[Mo_3S_{13}]^{2-}$ nanoclusters, which exhibited much better photocorrosion resistance than regular CdTe QDs for photocatalytic hydrogen generation. The sulfur compound covered CdTe/CdS QDs. It was observed that as-prepared composite exhibited higher visible light photocatalytic H_2 generation compared to CdTe QDs with cocatalyst Pt. A novel CdS/ZnO heterojunction was fabricated by Ma et al. (2017), which is composed of zero-dimensional CdS QDs and two-dimensional ZnO nanosheets (NSs). It was reported that as-obtained CdS/ZnO 0D/2D heterostructures exhibited excellent photocatalytic activity for the evolution of hydrogen from water splitting in comparison

with other CdS/ZnO heterostructures with different combinations (0D/3D, 2D/2D, and 3D/0D). It was observed that out of these, CdS/ZnO-12 (12 deposition cycles of CdS QDs) exhibited the highest evolution rate of hydrogen of 22.12 mmol g^{-1} h^{-1}, which was about 13 and 138 times higher than produced with single CdS (1.68 mmol g^{-1} h^{-1}) and ZnO (0.16 mmol g^{-1} h^{-1}), respectively. It was revealed that as-prepared CdS/ZnO-12 exhibited excellent stability without any significant loss for five cycles in 25 h.

A vertical self-assembly of ultrathin $CdIn_2S_4$ nanosheet arrays on the reduced graphene oxide (rGO) has been prepared by Xue et al. (2017) via a facile hydrothermal method. Here, ZnS QDs were in situ deposited on $CdIn_2S_4$ nanosheet arrays. It was reported that as-prepared 3D nanosheet arrays architecture with GO (13 wt.%) exhibited the optimum, highest hydrogen generation of 6.82 mmol g^{-1} h^{-1} corresponding to the photocurrent transient response (107.4 μA cm^{-2}). An inverse structure of $Cd_{0.5}Zn_{0.5}S$ QDs was reported by Zhou et al. (2017) loaded onto the onion-like carbon (OLC) matrix. It was observed that as-prepared $Cd_{0.5}Zn_{0.5}S$ QDs with average diameter of 6.9 nm were uniformly distributed on an OLC (30 nm) matrix. An optimum rate of H_2 generation, 58.6 and 2018 μmol h^{-1} g^{-1}, could be achieved on irradiation of visible light and 58.6 μmol h^{-1} g^{-1} under the irradiation of (550−900 nm), respectively using $Cd_{0.5}Zn_{0.5}S$/OLC composite samples. Such a reverse construction using hydrogen has a great potential for noble metal-free solar production of hydrogen.

Kitazono et al. (2017) photodeposited CdSe on a CdS-preloaded mesoporous TiO_2 nanocrystalline film. As a result, CdS(core)−CdSe(shell) QDs (CdS@CdSe/mp-TiO_2) were obtained with a heteroepitaxial nanojunction. They fabricated quantum-dot-sensitized PEC (QD-SPEC) cells with photoanode | 0.25 M Na_2S, 0.35 M Na_2SO_3 (in water)| cathode. It was observed that a CdS@CdSe QD-SPEC cell could achieve solar-to-current efficiency (STCE) of 0.03% under simulated sunlight (AM 1.5, one sol). An increase in STCE up to 0.048 was obtained on application of 0.1 V between the electrodes, far surpassing the CdSe/mp-TiO_2 and CdS/mp-TiO_2 photoanode cells. A WS_2/graphitic carbon nitride (CN) (2D/2D) nanosheet heterostructure was decorated with CdS QDs by Zou et al. (2018). It was observed that optimized CdS/WS_2/CN exhibited an excellent photocatalytic H_2 evolution rate of 1174.5 μmol h^{-1} g^{-1} without using any cocatalyst, which was about 67 times higher than for pure CN nanosheets. It was also revealed that CdS/WS_2/CN photocatalyst showed excellent stability as well as reusability without any significant loss role in photocatalytic H_2 evolution within four cycles in 20 h.

Hao et al. (2018) synthesized Bi_2WO_6 QDs decorated g-C_3N_4 nanoplates through a one-step hydrothermal method. The size of Bi_2WO_6 QDs was found to be about 3.5 nm. It was reported that a Bi_2WO_6 QDs/g-C_3N_4 Z-scheme not only increased the separation efficiency of charge, but it also enhanced the ability of PEC water splitting. Thick-shell CdSe/$CdSe_xS_{1-x}$/CdS QDs were synthesized by Zhao et al. (2018) with a pyramidal shape.

It was reported that these exhibited a QY of ~15%. As-prepared pyramidal QDs were then applied as light absorbers in a PEC system, leading to a saturated photocurrent density of ~12 mA cm^{-2}, which could provide an H_2 generation rate of 90 mL cm^{-2} day^{-1}.

Wang et al. (2018b) decorated TiO_2 nanotube arrays (TiO_2 NTAs) with MoS_2 QDs by an electrodeposition method. It was reported that as-prepared MoS_2 QDs/TiO_2 NTAs exhibited an increased photocatalytic activity compared to pristine TiO_2 NTAs for H_2 evolution in the presence of sunlight. They did not use any sacrificial agents or cocatalysts. The optimal H_2 evolution rates were observed to be 31.36, 5.29, and 1.67 μmol cm^{-2} h^{-1} in the presence of UV, visible, and near-infrared illumination, respectively. Such an enhanced photocatalytic activity may be due to decreased bandgap energy and surface plasmonic properties, which increased absorption capacity for visible and near-infrared light. Xue et al. (2018) fabricated high-density NiS_x QDs as a highly efficient cocatalyst on the surface of $Cd_{0.8}Zn_{0.2}S$/rGO nanosheet composites. It was reported that a two-dimensional (2D) $Cd_{0.8}Zn_{0.2}S$/rGO nanohybrid system with 2 wt.% NiSx loading could achieve H_2 evolution rate of 7.84 mmol g^{-1} h^{-1} under visible light irradiation, which is almost 1.4 times higher as compared to Pt/$Cd_{0.8}Zn_{0.2}S$/rGO.

The Se-doped CdS QDs with different Se doping levels were prepared via a solvothermal procedure (Shi et al., 2019). It was reported that photocatalytic performance of as-prepared $CdS_{0.9}Se_{0.1}$ QDs (without any cocatalysts) was enhanced to give a hydrogen evolution rate of 29.12 mmol h^{-1} g^{-1} under simulated solar irradiation, which was about 23.5 times higher as compared to CdS QDs. Yang et al. (2019) prepared a series of Zn−$AgIn_5S_8$/g-C_3N_4 (0D/2D) nanocomposites by growth (in situ) of the Zn−$AgIn_5S_8$ QDs (QDs) on g-C_3N_4 nanosheets. It was reported that the hydrogen production rate with Zn−$AgIn_5S_8$/g-C_3N_4 nanocomposites was found to be optimum, when the mass ratio of g-C_3N_4 was kept at 10%, which was 1.39, about 138.6 times higher than pure Zn−$AgIn_5S_8$ QDs and g-C_3N_4, respectively. It was also revealed that as-prepared Zn−$AgIn_5S_8$/g-C_3N_4 nanocomposites exhibited good cycle stability.

Yu et al. (2019) used Ag_2S QDs as both photocatalysts and electrocatalysts. It was observed that H_2 production rate could reach 858 μmol h^{-1} g_{catal}^{-1} under 100 mW cm^{-2}. Zheng et al. (2019) synthesized a p-n heterojunction photocatalyst for splitting of water. They incorporated p-type $CuInS_2$ QDs into n-type polymeric carbon nitride (CN) via a self-assembly and calcination method. It was reported that hydrogen evolution rate of $CuInS_2$/CN hybrid was two-fold more than that with pristine CN. A metal−organic framework (MOF)-derived synthesis was reported by Shi et al. (2020). They could obtain a controlled mixed-phase (rutile and anatase) of TiO_2 NPs, retaining MOF crystal morphology. It was observed that MOF-derived TiO_2 film, which was sensitized by core−shell CdSe@CdS QDs, exhibited an higher PEC device stability of +42.1% with PEC performance as +47.6%. It was suggested that

this protocol can improve the efficiency of the PEC system based on TiO_2-QDs heterojunction for hydrogen generation.

Chen et al. (2019) prepared ZnCdS QDs. It was reported that the photocatalytic H_2 production activity of as-prepared QDs can be optimized by adjusting their quantum sizes. It was revealed that maximum H_2 production rate of 3.70 mmol h^{-1} g^{-1} could be obtained with it, without using noble metal cocatalysts in the presence of visible light, which was much better than that of ZnCdS and ZnCdS-based catalysts. Miodyńska et al. (2020) increased the photoactivity of urchin-like rutile particles by decorating these with pristine as well as Er- or Yb-doped Bi_2S_3 QDs. They varied doping degrees (1−15 mol%), and QDs loadings (1−20 wt.%), and the best hydrogen evolution performance could be achieved with Er and Yb contents of 10 mol%. It was observed that hydrogen productivity of 1576.7 μmol g_{cat}^{-1} could be achieved for TiO_2 decorated by 10 mol% Yb-doped Bi_2S_3 QDs after 20 h irradiation. Su et al. (2020) reported that nickel in zinc blende cadmium−zinc sulfide QDs is an efficient and stable photocatalyst for splitting of water under sunlight. It was observed that finely tuned Ni atoms dispersed in these QDs exhibited H_2 production activity of 18.87 mmol h^{-1} g^{-1}.

14.3.4 Others

Chen et al. (2010) studied the utilization of CdTe quantum-dot-sensitized ZnO:nanowire arrays for water splitting. It was reported that photocurrent and stability was significantly improved. It was also revealed that the addition of nitrogen alters the electronic state, which improves the ability for water splitting. CoP QDs embedded in S,N-codoped graphite carbon (CoP@SNC) were reported by Meng et al. (2018). They used organophosphoric acid as a precursor of both phosphorus and carbon. Benefiting from the strong coupling and synergistic effect between CoP QDs and highly conductive S,N-codoped carbon, well-structured porosity and high specific surface area. It was observed that as-synthesized CoP@SNC exhibited excellent activities for HER, OER, and oxygen reduction reaction (ORR). It acts as a trifunctional electrocatalyst for overall splitting of water.

Zhu et al. (2018) loaded black phosphorus QDs (BP QDs) on MXene nanosheets. It was revealed that as-prepared BP QDs/MXene nanohybrids can serve as a bifunctional electrocatalyst in producing both hydrogen and oxygen. It was observed that a current density of 10 mA cm^{-2} was reached at a potential of only 1.78 V on using BP QDs/MXene nanohybrids cathode and anode in a full cell for overall water splitting. A composite consisting of CdSe QDs and indium-doped $BaTiO_3$ was synthesized by Zhong et al. (2019). The optimal load ratio of CdSe QDs with 2.5% indium (7.5 mol.%) was found to increase the production of hydrogen (0.437 mmol g^{-1} h^{-1}) as compared to undoped composite (0.258 mmol g^{-1} h^{-1}).

The $BiVO_4@ZnIn_2S_4/Ti_3C_2$ MXene QDs assembly (photocatalyst) was fabricated by Du et al. (2020). It was observed that $BiVO_4@ZnIn_2S_4/Ti_3C_2$ MXene QDs could achieve effective splitting of water into H_2 and O_2 in the presence of visible light with rates of 102.67 and 50.83 $\mu mol\ g^{-1}\ h^{-1}$, respectively. Yan and Jin (2021) derived NiP_2 QDs (n-type) in situ from the three-dimensional nanoflower NiAl-LDH. They also constructed n-type p-n heterojunction by coupling NiP_2 QDs and Cu_3P NPs (p-type) for hydrogen generation.

14.4 Carbon and graphene-based quantum dots

Yu et al. (2013) used an impregnation method to prepare graphene quantum dots (GQDs) anchored inside inversely structured TiO_2 nanotubes-array (TiO_2-NA) and CdS-modified TiO_2 nanotubes-array (CdS/TiO_2-NA). It was observed that the hydrogen evolution rate was greatly increased on loading GQDs into TiO_2-NA and CdS/TiO_2-NA. It was revealed that the light-filtering effect of graphene was inhibited as compared to graphene sheets, when graphene is broken into GQDs. However, the morphology of TiO_2 the nanotube array was still maintained even when anchoring GQDs inside, which favored mass transfer.

Nitrogen-doped graphene oxide QDs were prepared by Yeh et al. (2014). As-prepared catalyst samples exhibited both p- and n-type conductivities and overall water-splitting under visible light. It was reported that QDs contain p-n type photochemical diodes and active sites for O_2 and H_2 evolution were n- and p-domains, respectively. It was also revealed that this reaction mimics biological photosynthesis. Martindale et al. (2015) produced CQDs, as a homogeneous photocatalytic system with a Ni-bis(diphosphine) catalyst. It was observed that it could produce hydrogen at a rate of 398 $\mu mol\ (g_{CQD})^{-1}\ h^{-1}$. It was revealed that these CQDs exhibited activity in the visible region and maintained their photocatalytic activity for a day. Qu et al. (2015) prepared S,N-GQDs by doping GQDs with heteroatoms (S, N). It might be utilized as a sensitizer in photocatalytic processes. It was observed that loading of S,N-GQDs onto TiO_2 nanocrystals resulted in the generation of H_2 through splitting of water. They revealed that the H_2 generation rate was about 4.3 $mol\ h^{-1}$ under visible light.

CQDs were deposited by Li et al. (2016) onto graphite-like carbon nitride nanosheets (CNNS) to afford CNNS/CQDs composites. It was found that as-prepared CNNS/CQDs composites exhibited a much higher photocatalytic hydrogen production rate (116.1 $\mu mol\ h^{-1}$) under visible light irradiation, which was almost three times higher than with pure CNNS (37.8 $\mu mol\ h^{-1}$). The photoanodes were fabricated by Shi et al. (2016) consisting of WO_3 nanoflakes decorated with CQDs via seed-mediated solvothermal method and impregnation-assembling. It was revealed that the photocurrent density of 1.46 $mA\ cm^{-2}$ at 1.0 V versus Ag/AgCl could be achieved for CQDs/

WO_3 electrode, which was almost more than double as compared to only the WO_3 electrode. Such an enhancement was due to the increased light harvesting ability of CQDs and rapid charge transfer across the interface between the electrolyte and CQDs/WO_3 electrode.

Sulfur-doped graphene oxide QDs (S-GOQDs) were synthesized by Gliniak et al. (2017). They observed efficient photocatalytic hydrogen generation under direct sunlight irradiation. The doping of S atoms into the GOQDs was confirmed. They could achieve an initial rate of 18,166 and 30,519 $\mu mol\ h^{-1}\ g^{-1}$ in pure water and in 80% ethanol aqueous solution, respectively. Yan et al. (2017) prepared nitrogen-doped graphene QDs (NGQDs)-$ZnNb_2O_6$/g-C_3N_4 heterostructures and used them as hydrogen evolving catalysts. It was reported that as-prepared NGQDs-$ZnNb_2O_6$/g-C_3N_4 heterostructures could achieve a higher hydrogen evolution rate of 340.9 $\mu mol\ h^{-1}\ g^{-1}$, when the mole ratio Zn/gC_3N_4 and NGQDs were kept at 1:7 and 5%, respectively.

Pan et al. (2018) prepared CQDs modified porous g-C_3N_4/TiO_2 two-dimensional (2D) nanoheterojunctions. The TiO_2 NPs were introduced via a hydrothermal method while CQDs were successively introduced on the surface of the porous g-C_3N_4 and TiO_2 by coupling. It was observed that hydrogen production using these 2D nanoheterojunctions was almost double that obtained with unmodified samples. The cobalt carbide (Co_2C) was prepared by Guo et al. (2018). A combination of colloidal QDs/Co_2C can produce hydrogen at the rate of $\sim$18,000 $\mu mol\ g^{-1}\ h^{-1}$, which was about 10 times more than that of bare QDs under similar conditions.

Wang and Li (2018) and Wang et al. (2018a,b) reported that the coloading of graphene QDs and PdS on ZnCdS surface as cocatalysts can increase the efficiency of photocatalytic evolution of H_2 in the presence of visible light. This photocatalyst (GQDs/ZnCdS/PdS) was prepared by two steps: (1) hydrothermal coupling of GQDs on ZnCdS surface, and (2) an in situ chemical deposition of PdS. It was reported that as-prepared GQDs/ZnCdS/PdS exhibited an H_2 evolution rate of 517 $\mu mol\ h^{-1}$, which is about 15, 1.7, and 7 times higher as compared to ZnCdS, ZnCdS/PdS, and GQDs/ZnCdS respectively. This photocatalyst has a good stability. Enhancement of photocatalytic activity was attributed to coloading of the GQDs (reduction) and PdS (oxidation) as respective cocatalysts.

A facile method has been reported by Liu et al. (2019) to prepare efficient and robust Ru-M (M = Mn, Ni, Cu) bimetallic NPs and carbon quantum dot hybrid (RuM/CQDs). It was observed that RuNi/CQDs catalysts exhibited an excellent HER performance in all pH ranges. It was revealed that Ni doping resulted in a weakening of the hydrogen bonding energy of close surface Ru atoms, which played an important role in enhancing the HER activity. Zhang et al. (2019) reported that a dendrite-like plasmonic bimetal (CuNi) can be used as a photocatalyst, which is nonsemiconducting in nature. It produced electrons for photocatalytic splitting of water to

generate hydrogen, but when such a bimetal is supported by a catalyst like CQDs, then the photocatalytic water splitting rate was found to be highest at 55.19 μmol g^{-1} h^{-1}. The content of CQDs in the photocatalyst was kept at 3 wt.% for optimum conditions. It was reported that this photocatalyst was stable for four cycles over 20 h.

The B-doped g-C_3N_4 QDs (BCNQDs) were prepared by Wang et al. (2013) via a facile molten salt method. They used melamine and boron oxide as the precursors. The BCNQDs were introduced onto the surface of g-C_3N_4, via hydrothermal treatment and as a result a g-C_3N_4/BCNQDs heterojunction was constructed. As-prepared g-C_3N_4/BCNQDs heterojunction exhibited excellent hydrogen evolution performance for water splitting in the presence of visible light irradiation. *Bombyx mori* silk, a natural nitrogen-rich biopolymer protein, is earth-abundant and sustainable. Wang et al. (2020) derived nitrogen-doped CQDs (N-CQDs) from *Bombyx mori* silk fibroin and then immobilized them onto TiO_2 nanotube arrays (TiO_2 NTAs) using a hydrothermal approach. As-prepared N-CQDs decorated TiO_2 NTA heterostructures (N-CQDs@TiO_2 NTAs) could split water into H_2 and O_2 with production rates of 30.12 and 14.96 μmol cm^{-2} h^{-1}, respectively.

Liu et al. (2020) prepared N-doped CQDs (NCDs) modified defect-rich g-C_3N_4 (DCN) via an impregnation method. It was revealed that optimized NCDs/DCN exhibited excellent photocatalytic H_2 production with an evolution rate of 3.68 μmol h^{-1} g^{-1}. Nasir et al. (2020) prepared a 1D nanofiber of TiO_2 via electrospinning. Then they produced a needle-like structure on this fiber through an alkali hydrothermal method and chemical vapor deposition method. The g-C_3N_4 QDs and nanoflakes of $SnSe_2$ fiber (branched) were loaded on TiO_2 via a heterojunction. It was observed that the composite exhibited excellent photocatalytic performance for the production of hydrogen (2375 μmol g^{-1} h^{-1}) with quantum efficiency of HER (>16%).

Nitrogen-doped graphene QDs (N-GQDs) were synthesized by Tsai et al. (2020) via a hydrothermal cutting approach. The concentration of nitrogen was controlled with a change in concentration of nitrogen source urea. It was revealed that N-GQDs prepared by using 2 g of urea gave the highest photocurrent. They also observed that photocatalytic activity of 2N-GQDs (photocatalyst) for production of hydrogen was higher compared to pristine GQDs. Raza Naqvi et al. (2020) developed a nitrogen-doped carbon dots (NDCDs)-AgNi alloy. Then, it was used as an electrocatalyst for electrochemical water splitting. NDCDs-AgNi alloy NPs were synthesized by easy and scalable methods. NDCDs were prepared by the pyrolysis of ethanolamine. It acted as a good electrocatalyst for HER. It was also revealed that as-prepared NDCDs-AgNi alloy also exhibited superior OER activity.

Roy et al. (2020) demonstrated that chlorophyll(*a*)/CQDs (Chl/CQDs) bionanocomposite (b-NC)-decorated Si-nanowires (SiNWs) can surpass the efficiency for PEC generation of hydrogen. It was revealed that efficiency reaches ~7.86%, which is highest reported so far with hybrid Si-based

photocathodes. They measured the hydrogen evolution rate to be $\sim 113\ \mu mol\ h^{-1}$ at 0.8 V versus RHE under 1 sol illumination. Duan et al. (2021) developed a simple exfoliation−sonication approach to prepare nitrogen carbide QDs (CNQDs)-doped nitrogen carbide nanosheet (CNS) composite, which can be used as a photocatalyst to produce hydrogen in the presence of organic pollutants such as acridine orange, or aniline. In their presence, it was observed that hydrogen evolution efficiency was increased from 8.8 to 11.7 and 32.1 $mmol\ g^{-1}\ h^{-1}$ in the presence of aniline and acridine orange, respectively. It was revealed that heterojunction of CNQDs/CNS induced the separation of photogenerated electron−hole pairs, where electrons will migrate to CNQDs transforming protons into hydrogen molecules, and holes migrated to CNS, oxidizing organic pollutants, simultaneously.

Elsayed et al. (2021) have prepared N-doped carbon QDs (NCQDs) into polymer dots resulting in significant enhancement in their photocatalytic performance as well stability. The role of NCQDs was suggested to enhance the charge separation and the photocatalytic efficiency of the polymer dot. It was reported that NCQDs were easily introduced into the polymer dot, and as a result the hydrogen evolution rate was increased by about five times as compared to pure polymer dots.

Liang et al. (2021) prepared nitrogen doped graphene quantum dots as a photocatalyst dodecahedron nano-Au particles. It was revealed that as-obtained graphene@Au catalysts exhibited an efficient photocatalytic overall water splitting involving both; high valuable H_2O_2 and clean H_2 energy with generation rate as 49.7 and 65.6 $\mu mol\ g^{-1}\ h^{-1}$, respectively. The separation of hydrogen peroxide from hydrogen gas is easy as compared with most water splitting method that liberated hydrogen gas and oxygen gas, which further needs gas separation.

Nitrogen-doped graphene QDs (NGQDs) were prepared by Liu et al. (2021) and then used as a cocatalyst of $SrTiO_3(Al)/CoO_x$ for photocatalytic overall water splitting to generate hydrogen. It was found that as-prepared $NGQDs/SrTiO_3(Al)/CoO_x$ was highly active for splitting of water with an evolution rate of H_2 and O_2 as 18.8 and 9.0 $\mu mol\ h^{-1}$, respectively. Wu et al. (2021) synthesized an organic semiconductor (DAnTMS compound) using trimethylsilylacetylene (TMS) and 9,10-dibromoanthracene (DAn). Then, they designed a metal-free composite photocatalyst with carbon dots (DAnTMS/CD). It was reported that this DAnTMS/CD composite could achieve maximum production rates of H_2 and H_2O_2 of 265.0 and 396.7 $\mu mol\ g^{-1}\ h^{-1}$, respectively, with pure water.

14.5 Conclusion

QDs have many advantages compared to traditional materials as photocatalysts. These can create multiple excitons, which could lead to better control over the degree of charge. They can also be more efficient at producing hot

carriers with sufficient energy. Various surface atom ratios of QDs can modify the photoluminescence property. Dangling bonds or defects can reduce long-term photostability and reduce QY. As a result, passivating the surface is critical for enhancing stability and protecting its properties by the shelling of QDs and doping in the QDs.

The role of the quantum dot in photocatalysts developed for photocatalytic and PEC water splitting is a unique function. Water can be converted into hydrogen gas, when solar energy is applied to water in two technologies.

1. Indirectly through concentrated solar thermal and an electrolyzer, as well as solar-converted electricity, and electrolyzer, biological, and thermochemical processes. It has excessive costs, energy loss, and is unfeasible. Besides, the performance of electrolyzers, which have typical commercial efficiencies of around 73%, is always constrained when the energy conversion step is combined with electrolyzers.
2. Direct route including powdered photocatalysts and PEC cells, using photo-/photoelectrocatalysis of water.

The dispersion of powdered photocatalysts into water is ideal for major operations. The system needs to be motivated during the reaction and product separation after the reaction. PEC systems combined solar energy collection and water reduction in one device. Most hydrogen is generated from fossil fuels, including natural gas, oil, and coal. Electron donors like alcohols (methanol, ethanol, and glycerol) are commonly utilized as sacrificial reagents (SEDs) in water to efficiently generate hydrogen by successfully scavenging photogenerated holes to suppress the back reaction.

References

Ahmed, L.M., Alkaim, A.F., Halbus, A.F., Hussein, F.H., 2016. Photocatalytic hydrogen production from aqueous methanol solution over metallized TiO_2. Int. J. ChemTech Res. 9, 90−98.

Apte, S., Garaje, S., Valant, M., Kale, B., 2012. Eco-friendly solar light driven hydrogen production from copious waste H_2S and organic dye degradation by stable and efficient orthorhombic CdS quantum dots−GeO_2 glass photocatalyst. Green. Chem. 14 (5), 1455. Available from: https://doi.org/10.1039/c2gc16416g.

Bahruji, H., Bowker, M., Davies, P.R., Pedrono, F., 2011. New insights into the mechanism of photocatalytic reforming on Pd/TiO_2. Appl. Catal. B: Environ. 107 (1−2), 205−209.

Bard, A., 1979. Photoelectrochemistry and heterogeneous photocatalysis at semiconductors. J. Photochem. 10, 59−75.

Batubara, N.H., Zulys, A., 2019. Synthesis, Structural, spectroscopic, and morphology of metal-organic frameworks based on La (III) and ligand 2, 6-Napthalenedicarboxylic acid (La-MOFs) for hydrogen production. IOP Conf. Series: Mater. Sci. Eng. 546. Available from: https://doi.org/10.1088/1757-899X/546/4/042005.

Belhadj, H., Hamid, S., Robertson, P.K., Bahnemann, D.W., 2017. Mechanisms of simultaneous hydrogen production and formaldehyde oxidation in H_2O and D_2O over platinized TiO_2. Acs Catal. 7 (7), 4753−4758.

Bičáková, O., Straka, P., 2010. The resources and methods of hydrogen production. Acta Geodyn. Geomater. 7 (158), 175–188.

Bockris, J.O.M., Dandapani, B., Cocke, D., Ghoroghchian, J., 1985. On the splitting of water. Int. J. Hydrog. Energy 10 (3), 179–201.

Camacho, S.Y.T., Rey, A., Hernández-Alonso, M.D., Llorca, J., Medina, F., Contreras, S., 2018. Pd/TiO_2-WO_3 photocatalysts for hydrogen generation from water-methanol mixtures. Appl. Surf. Sci. 455, 570–580.

Cao, S., Yuan, Y., Fang, J., Shahjamali, M., Boey, F., Barber, J., et al., 2013. In-situ growth of CdS quantum dots on g-C_3N_4 nanosheets for highly efficient photocatalytic hydrogen generation under visible light irradiation. Int. J. Hydrog. Energy 38 (3), 1258–1266. Available from: https://doi.org/10.1016/j.ijhydene.2012.10.116.

Cao, S., Wang, C.J., Fu, W.F., Chen, Y., 2017. Metal phosphides as co-catalysts for photocatalytic and photoelectrocatalytic water splitting. ChemSusChem 10 (22), 4306–4323.

Carey, J.H., Oliver, B.G., 1976. Intensity effects in the electrochemical photolysis of water at the TiO_2 electrode. Nature 259 (5544), 554–556.

Cargnello, M., Gasparotto, A., Gombac, V., Montini, T., Barreca, D., Fornasiero, P., 2011. Photocatalytic H_2 and added-value by-products–the role of metal oxide systems in their synthesis from oxygenates. Eur. J. Inorg. Chem. 2011, 4309–4323.

Chen, H.M., Chen, C.K., Chang, Y.C., Tsai, C.W., Liu, R.S., Hu, S.F., et al., 2010. Quantum dot monolayer sensitized ZnO nanowire-array photoelectrodes: true efficiency for water splitting. Angew. Chem. 122 (34), 6102–6105.

Chen, X., Zhang, Z., Chi, L., Nair, A.K., Shangguan, W., Jiang, Z., 2016a. Recent advances in visible-light-driven photoelectrochemical water splitting: catalyst nanostructures and reaction systems. Nanomicro Lett. 8 (1). Available from: https://doi.org/10.1007/s40820-015-0063-3.

Chen, T., Quan, W., Yu, L., Hong, Y., Song, C., Fan, M., et al., 2016b. One-step synthesis and visible-light-driven H_2 production from water splitting of Ag quantum dots/g-C_3N_4 photocatalysts. J. Alloy. Comp. 686, 628–634. Available from: https://doi.org/10.1016/j.jallcom.2016.06.076.

Chen, Z., Zhang, Q., Luo, Y., 2018. Experimental identification of ultrafast reverse hole transfer at the interface of the photoexcited methanol/graphitic carbon nitride system. Angew. Chem. Int. (Ed.) 57 (19), 5320–5324.

Chen, J., Lv, S., Shen, Z., Tian, P., Chen, J., Li, Y., 2019. Novel ZnCdS Quantum dots engineering for enhanced visible-light-driven hydrogen evolution. ACS Sustain. Chem. Eng. 7 (16), 13805–13814.

Cirone, J., Dondapati, J., Chen, A., 2021. Design of bimetallic nickel-iron quantum dots with tunable compositions for enhanced electrochemical water splitting. Electrochim. Acta 392. Available from: https://doi.org/10.1016/j.electacta.2021.139016.

Coronado, J.M., 2013. Photons, electrons and holes: fundamentals of photocatalysis with semiconductors. Design of Advanced Photocatalytic Materials for Energy and Environmental Applications. Springer, London.

Corredor, J., Rivero, M.J., Rangel, C.M., Gloaguen, F., Ortiz, I., 2019. Comprehensive review and future perspectives on the photocatalytic hydrogen production. J. Chem. Technol. Biotechnol. 94 (10), 3049–3063.

Crampton, A.S., Cai, L., Janvelyan, N., Zheng, X., Friend, C.M., 2017. Methanol photooxidation on rutile TiO_2 nanowires: probing reaction pathways on complex materials. J. Phys. Chem. C. 121 (18), 9910–9919.

Crespo-Quesada, M., Reisner, E., 2017. Emerging approaches to stabilise photocorrodible electrodes and catalysts for solar fuel applications. Energy Environ. Sci. 10 (5), 1116–1127.

Dahiya, S., Chatterjee, S., Sarkar, O., Mohan, S.V., 2020. Renewable hydrogen production by dark-fermentation: current status, challenges and perspectives. Bioresour. Technol. Available from: https://doi.org/10.1016/j.biortech.2020.124354.

Dinda, D., Park, H., Lee, H.J., Oh, S., Park, S.Y., 2020. Graphene quantum dot with covalently linked Rhodamine dye: a high efficiency photocatalyst for hydrogen evolution. Carbon 167, 760–769.

Domen, K., Naito, S., Soma, M., Onishi, T., Tamaru, K., 1980. Photocatalytic decomposition of water vapour on an NiO–$SrTiO_3$ catalyst. J. Chem. Soc. Chem. Commun. 1980, 543–544.

Du, X., Zhao, T., Xiu, Z., Xing, Z., Li, Z., Pan, K., et al., 2020. $BiVO_4$@$ZnIn_2S_4$/Ti_3C_2 MXene quantum dots assembly all-solid-state direct Z-Scheme photocatalysts for efficient visible-light-driven overall water splitting. Appl. Mater. Today 20. Available from: https://doi.org/10.1016/j.apmt.2020.100719.

Duan, C., Xie, L., Wang, S., Dai, Y., Yin, L., 2021. Photocatalytic hydrogen evolution by degradation of organic pollutants over quantum dots doped nitrogen carbide. Chemosphere. Available from: https://doi.org/10.1016/j.chemosphere.2021.132873.

Elsayed, M.H., Jayakumar, J., Abdellah, M., Mansoure, T.H., Zheng, K., Elewa, A.M., et al., 2021. Visible-light-driven hydrogen evolution using nitrogen-doped carbon quantum dot-implanted polymer dots as metal-free photocatalysts. Appl. Catal. B: Environ. 283. Available from: https://doi.org/10.1016/j.apcatb.2020.119659.

Fang, S., Liu, Y., Sun, Z., Lang, J., Bao, C., Hu, Y.H., 2020. Photocatalytic hydrogen production over Rh-loaded TiO_2: what is the origin of hydrogen and how to achieve hydrogen production from water? Appl. Catal. B: Environ. 278. Available from: https://doi.org/10.1016/j.apcatb.2020.119316.

Frame, F.A., Osterloh, F.E., 2010. CdSe-MoS_2: a quantum size-confined photocatalyst for hydrogen evolution from water under visible light. J. Phys. Chem. C. 114 (23), 10628–10633.

Fujishima, A., Honda, K., 1972. Electrochemical photolysis of water at a semiconductor electrode. Nature. 238, 37–38.

Fukuzumi, S., Lee, Y.M., Nam, W., 2018. Thermal and photocatalytic production of hydrogen with earth-abundantmetal complexes. Coord. Chem. Rev. 355, 54–73.

Ge, L., Zuo, F., Liu, J., Ma, Q., Wang, C., Sun, D., 2012. Synthesis and efficient visible light photocatalytic hydrogen evolution of polymeric g-C_3N_4 coupled with CdS quantum dots. J. Phys. Chem. C. 116 (25), 13708–13714.

Gliniak, J., Lin, J., Chen, Y., Li, C., Jokar, E., Chang, C., et al., 2017. Sulfur-doped graphene oxide quantum dots as photocatalysts for hydrogen generation in the aqueous phase. Chemsuschem. 10 (16), 3260–3267.

Guijarro, N., Prévot, M.S., Sivula, K., 2015. Surface modification of semiconductor photoelectrodes. Phys. Chem. Chem. Phys. 17 (24), 15655–15674.

Gultom, N.S., Abdullah, H., Kuo, D.H., 2017. Enhanced photocatalytic hydrogen production of noble-metal free Ni-doped Zn (O, S) in ethanol solution. Int. J. Hydrog. Energy 42 (41), 25891–25902.

Gunasekaran, A., Anbarasan, N., Mukilan, N., 2021. CdS and CdSe nanoparticles activated 1D TiO_2 heterostructure nanoarray photoelectrodes for enhanced photoelectrocatalytic water splitting. Int. J. Hydrog. Energy. 46, 26381–26390.

Guo, Q., Liang, F., Gao, X.-Y., Gan, Q.-C., Li, X.-B., Li, J., et al., 2018. Metallic Co_2C: a promising co-catalyst to boost photocatalytic hydrogen evolution of colloidal quantum dots. ACS Catal. 8 (7), 5890–5895.

Hainer, A.S., Hodgins, J.S., Sandre, V., Vallieres, M., Lanterna, A.E., Scaiano, J.C., 2018. Photocatalytic hydrogen generation using metal-decorated TiO_2: sacrificial donors vs true water splitting. ACS Energy Lett. 3 (3), 542–545.

Han, B., Mo, J., Kang, Z., Yang, G., Barnhill, W., Zhang, F.Y., 2017. Modeling of two-phase transport in proton exchange membrane electrolyzer cells for hydrogen energy. Int. J. Hydrog. Energy 42 (7), 4478–4489.

Hao, H., Lu, D., Wang, Q., 2018. Photoelectrochemical study on charge separation mechanisms of Bi_2WO_6 quantum dots decorated g-C_3N_4. Int. J. Hydrog. Energy 43 (18), 8824–8834.

Hisatomi, T., Kubota, J., Domen, K., 2014. Recent advances in semiconductors for photocatalytic and photoelectrochemical water splitting. Chem. Soc. Rev. 43, 7520–7535.

Huang, C.W., Nguyen, B.S., Wu, J.C.S., Nguyen, V.H., 2020. A current perspective for photocatalysis towards the hydrogen production from biomass-derived organic substances and water. Int. J. Hydrog. Energy 45 (36), 18144–18159.

Jia, Q., Iwase, A., Kudo, A., 2014. $BiVO_4$–Ru/$SrTiO_3$: Rh composite Z-scheme photocatalyst for solar water splitting. Chem. Sci. 5 (4), 1513–1519.

Jiang, C., Moniz, S.J., Wang, A., Zhang, T., Tang, J., 2017. Photoelectrochemical devices for solar water splitting–materials and challenges. Chem. Soc. Rev. 46 (15), 4645–4660.

Jitputti, J., Suzuki, Y., Yoshikawa, S., 2008. Synthesis of TiO_2 nanowires and their photocatalytic activity for hydrogen evolution. Catal. Commun. 9 (6), 1265–1271.

Kamat, P.V., Jin, S., 2018. Semiconductor photocatalysis: tell us the complete story!. ACS Energy Lett. 3, 622–623.

Kawai, T., Sakata, T., 1980. Photocatalytic hydrogen production from liquid methanol and water. J. Chem. Soc. Chem. Commun. 1980 (15), 694–695.

Kibria, M.G., Zhao, S., Chowdhury, F.A., Wang, Q., Nguyen, H.P.T., Trudeau, M.L., et al., 2014. Tuning the surface fermi level on p-type gallium nitride nanowires for efficient overall water splitting. Nat. Commun. 5 (1), 1–6.

Kitazono, K., Akashi, R., Fujiwara, K., Akita, A., Naya, S., Fujishima, M., et al., 2017. Photocatalytic synthesis of CdS(core)-CdSe(shell) quantum dots with a heteroepitaxial junction on TiO_2: photoelectrochemical hydrogen generation from water. Chemphyschem 18 (20), 2840–2845.

Kuang, P., Zheng, P., Liu, Z., Lei, J., Wu, H., Li, N., et al., 2016. Embedding Au quantum dots in rimous cadmium sulfide nanospheres for enhanced photocatalytic hydrogen evolution. Small 12 (48), 6735–6744.

Kudo, A., Miseki, Y., 2009. Heterogeneous photocatalyst materials for water splitting. Chem. Soc. Rev. 38 (1), 253–278.

Kudo, A., Tanaka, A., Domen, K., Maruya, K.I., Aika, K.I., Onishi, T., 1988. Photocatalytic decomposition of water over NiO- $K_4Nb_6O_{17}$ catalyst. J. Catal. 111 (1), 67–76.

Kumar, D.P., Reddy, N.L., Srinivas, B., Durga kumari, V., Roddatis, V., Bondarchuk, O., 2016. Stable and active CuxO/TiO_2 nanostructured catalyst for proficient hydrogen production under solar light irradiation. Sol. Energy Mater. Sol. Cell 146, 63–71.

Landman, A., Halabi, R., Dias, P., Dotan, H., Mehlmann, A., Shter, G.E., 2020. Decoupled photoelectrochemical water splitting system for centralized hydrogen production. Joule 4 (2), 448–471.

Li, Q., Cui, C., Meng, H., Yu, J., 2014. Visible-Light photocatalytic hydrogen production activity of $ZnIn_2S_4$ microspheres using carbon quantum dots and platinum as dual co-catalysts. Chem. Asian J. 9 (7), 1766–1770.

Li, K., Su, F., Zhang, W., 2016. Modification of g-C_3N_4 nanosheets by carbon quantum dots for highly efficient photocatalytic generation of hydrogen. Appl. Surf. Sci. 375, 110–117. Available from: https://doi.org/10.1016/j.apsusc.2016.03.025.

Liang, J., Liu, Y., Si, Z., Wei, G., Weng, D., Kang, F., 2021. Graphene quantum dots piecing together into graphene on nano Au for overall water splitting. Carbon 178, 265–272.

Liu, J., Liu, Y., Liu, N., Han, Y., Zhang, X., Huang, H., et al., 2015. Metal-free efficient photocatalyst for stable visible water splitting via a two-electron pathway. Science 347, 970–974.

Liu, J., Ke, J., Li, Y., Liu, B., Wang, L., Xiao, H., et al., 2018. Co_3O_4 quantum dots/TiO_2 nanobelt hybrids for highly efficient photocatalytic overall water splitting. Appl. Catal. B: Env. 236, 396–403.

Liu, Y., Li, X., Zhang, Q., Li, W., Xie, Y., Liu, H., et al., 2019. A general route to prepare low-ruthenium-content bimetallic electrocatalysts for ph-universal hydrogen evolution reaction by using carbon quantum dots. Angew. Chem. Int. (Ed.) 59 (4), 1718–1726.

Liu, H., Liang, J., Fu, S., Li, L., Cui, J., Gao, P., et al., 2020. N doped carbon quantum dots modified defect-rich g-C3N4 for enhanced photocatalytic combined pollutions degradation and hydrogen evolution. Colloids Surf. A: Physicochem. Eng. Asp. 591. Available from: https://doi.org/10.1016/j.colsurfa.2020.124552.

Liu, Y., Xu, X., Lv, S., Li, H., Si, Z., Wu, X., et al., 2021. Nitrogen doped graphene quantum dots as a cocatalyst of $SrTiO_3$(Al)/CoOx for photocatalytic overall water splitting. Catal. Sci. Technol. 11 (9), 3039–3046.

Luo, H., Barrio, J., Sunny, N., Li, A., Steier, L., Shah, N., et al., 2021. Progress and perspectives in photo-and electrochemical-oxidation of biomass for sustainable chemicals and hydrogen production. Adv. Energy Mater. 11. Available from: https://doi.org/10.1002/aenm.202101180.

Ma, Y., Wang, X., Jia, Y., Chen, X., Han, H., Li, C., 2014. Titanium dioxide-based nanomaterials for photocatalytic fuel generations. Chem. Rev. 114 (19), 9987–10043.

Ma, D., Shi, J.W., Zou, Y., Fan, Z., Ji, X., Niu, C., 2017. Highly efficient photocatalyst based on a CdS quantum dots/ZnO nanosheets 0D/2D heterojunction for hydrogen evolution from water splitting. ACS Appl. Mater. Interf. 9 (30), 25377–25386.

Maeda, K., Teramura, K., Takata, T., Hara, M., Saito, N., Toda, K., et al., 2005. Overall water splitting on $(Ga_{1-x}\ Zn_x)(N_{1-x}\ O_x)$ solid solution photocatalyst: relationship between physical properties and photocatalytic activity. J. Phys. Chem. B 109 (43), 20504–20510.

Marschall, R., 2021. 50 years of materials research for photocatalytic water splitting. Eur. J. Inorg. Chem. 2021 (25), 2435–2441.

Martindale, B.C.M., Hutton, G.A.M., Caputo, C.A., Reisner, E., 2015. Solar Hydrogen production using carbon quantum dots and a molecular nickel catalyst. J. Am. Chem. Soc. 137 (18), 6018–6025. Available from: https://doi.org/10.1021/jacs.5b01650.

Melo, M., Silva, L., 2011. Review-photocatalytic production of hydrogen: an innovative use for biomass derivatives. J. Braz. Chem. Soc. 22. Available from: https://doi.org/10.1590/S0103-50532011000800002.

Meng, T., Hao, Y., Zheng, L., Cao, M., 2018. Organophosphoric acid-derived CoP quantum dots@S,N-codoped graphite carbon as a trifunctional electrocatalyst for overall water splitting and Zn–air batteries. Nanoscale 10 (30), 14613–14626.

Meng, X., Zhang, C., Dong, C., Sun, W., Ji, D., Ding, Y., 2020. Carbon quantum dots assisted strategy to synthesize Co@ NC for boosting photocatalytic hydrogen evolution performance of CdS. Chem. Eng. J. 389, 124432.

Miodyńska, M., Mikolajczyk, A., Bajorowicz, B., Zwara, J., Klimczuk, T., Lisowski, W., et al., 2020. Urchin-like TiO_2 structures decorated with lanthanide-doped Bi_2S_3 quantum dots to boost hydrogen photogeneration performance. Appl. Catal. B: Environ. 272. Available from: https://doi.org/10.1016/j.apcatb.2020.118962.

Miyoshi, A., Nishioka, S., Maeda, K., 2018. Water splitting on rutile TiO_2-based photocatalysts. Chem. A Eur. J. 24 (69), 18204–18219.

Molaei, M.J., 2020. The optical properties and solar energy conversion applications of carbon quantum dots: a review. Sol. Energy 196, 549–566.

Nasir, M., Yang, G., Ayub, I., Wang, S., Yan, W., 2020. Tin diselinide a stable co-catalyst coupled with branched TiO_2 fiber and g-C_3N_4 quantum dots for photocatalytic hydrogen evolution. Appl. Catal. B: Environ. 270. Available from: https://doi.org/10.1016/j.apcatb.2020.118900.

Nemzer, M., Page, D., Carter, A., 2003. CH 3 Energy for Keeps—Creating Clean Electricity from Renewable Resources, third ed. National Science Techers Association, Malaysia.

Niu, P., Dai, J., Zhi, X., Xia, Z., Wang, S., Li, L., 2021. Photocatalytic overall water splitting by graphitic carbon nitride. InfoMat 3 (9), 931−961.

Pan, Y., Zhuang, H., Hong, J., Fang, Z., Liu, H., Liu, B., et al., 2014. Cadmium sulfide quantum dots supported on gallium and indium oxide for visible-light-driven hydrogen evolution from water. Chemsuschem 7 (9), 2537−2544.

Pan, J., You, M., Chi, C., Dong, Z., Wang, B., Zhu, M., et al., 2018. The two dimension carbon quantum dots modified porous g-C_3 N_4/TiO_2 nano-heterojunctions for visible light hydrogen production enhancement. Int. J. Hydrog. Energy 43 (13), 6586−6593.

Penconi, M., Rossi, F., Ortica, F., Elisei, F., Gentili, P.L., 2015. Hydrogen production from water by photolysis, sonolysis and sonophotolysis with solid solutions of rare earth, gallium and indium oxides as heterogeneous catalysts. Sustainability 7 (7), 9310−9325.

Peng, R., Ma, Y., Huang, B., Dai, Y., 2019. Two-dimensional Janus PtSSe for photocatalytic water splitting under the visible or infrared light. J. Mater. Chem. A 7 (2), 603−610.

Phang, S.J., Tan, L.L., 2019. Recent advances in carbon quantum dots (CQDs)-based two dimensional materials for photocatalytic applications. Catal. Sci. Technol. 9, 5882−5905.

Puga, A.V., 2016. Photocatalytic production of hydrogen from biomass-derived feedstocks. Coord. Chem. Rev. 315. Available from: https://doi.org/10.1016/j.ccr.2015.12.009.

Qian, J., Chen, Z., Chen, F., Wang, Y., Wu, Z., Zhang, W., 2018. Exploration of CeO_2−CuO quantum dots in situ grown on graphene under hypha assistance for highly efficient solar-driven hydrogen production. Inorg. Chem. Available from: https://doi.org/10.1021/acs.inorgchem.8b0193.

Qiao, S., Feng, C., Guo, Y., Chen, T., Akram, N., Zhang, Y., et al., 2020. CdS nanoparticles modified Ni@ NiO spheres as photocatalyst for oxygen production in water oxidation system and hydrogen production in water reduction system. Chem. Eng. J. 395. Available from: https://doi.org/10.1016/j.cej.2020.125068.

Qu, D., Sun, Z., Zheng, M., Li, J., Zhang, Y., Zhang, G., et al., 2015. Three colors emission from S, N co-doped graphene quantum dots for visible light H_2 production and bioimaging. Adv. Opt. Mater. 3 (3), 360−367.

Raza Naqvi, S., Rasheed, T., Majeed, S., Hussain, D., Fatima, B., Najam ul Haq, M., et al., 2020. Nitrogen doped carbon quantum dots conjugated with AgNi alloy nanoparticles as potential electrocatalyst for efficient water splitting. J. Alloy. Comp. 847. Available from: https://doi.org/10.1016/j.jallcom.2020.156492.

Reddy, N., Bharagav, U., Kumari, M., Cheralathan, K., Shankar, M., Reddy, K., et al., 2020. Highly efficient solar light-driven photocatalytic hydrogen production over Cu/FCNTs-titania quantum dots-based heterostructures. J. Environ. Manag. 254, 109747. Available from: https://doi.org/10.1016/j.jenvman.2019.109747.

Roy, K., Ghosh, D., Sarkar, K., Devi, P., Kumar, P., 2020. Chlorophyll(a)/carbon quantum dot bio-nanocomposite activated nano-structured silicon as an efficient photocathode for photoelectrochemical water splitting. ACS Appl. Mater. Interf. Available from: https://doi.org/10.1021/acsami.0c10279.

Sahai, S., Ikram, A., Rai, S., Shrivastav, R., Dass, S., Satsangi, V.R., 2017. Quantum dots sensitization for photoelectrochemical generation of hydrogen: a review. Renew. Sust. Energy Rev. 68, 19−27.

Schneider, J., Bahnemann, D.W., 2013. Undesired role of sacrificial reagents in photocatalysis. J. Phys. Chem. Lett. 4, 3479–3483.

Schweinberger, F.F., Berr, M.J., Döblinger, M., Wolff, C., Sanwald, K.E., Crampton, A.S., et al., 2013. Cluster size effects in the photocatalytic hydrogen evolution reaction. J. Am. Chem. Soc. 135 (36), 13262–13265.

Shi, W., Zhang, X., Brillet, J., Huang, D., Li, M., Wang, M., et al., 2016. Significant enhancement of the photoelectrochemical activity of WO_3 nanoflakes by carbon quantum dots decoration. Carbon 105, 387–393. Available from: https://doi.org/10.1016/j.carbon.2016.04.051.

Shi, J., Sun, D., Zou, Y., Ma, D., He, C., Ji, X., et al., 2019. Trap-level-tunable Se doped CdS quantum dots with excellent hydrogen evolution performance without co-catalyst. Chem. Eng. J. 364, 11–19.

Shi, L., Benetti, D., Li, F., Wei, Q., Rosei, F., 2020. Phase-junction design of MOF-derived TiO_2 photoanodes sensitized with quantum dots for efficient hydrogen generation. Appl. Catal. B: Environ. 263. Available from: https://doi.org/10.1016/j.apcatb.2019.118317.

Slama, R.B., 2013. Production of hydrogen by electrolysis of water: effects of the electrolyte type on the electrolysis performances. Comput. Water, Energy, Environ. Eng. 2, 54–58.

Strataki, N., Bekiari, V., Kondarides, D.I., Lianos, P., 2007. Hydrogen production by photocatalytic alcohol reforming employing highly efficient nanocrystalline titania films. Appl. Catal. B: Env. 77 (1–2), 184–189.

Su, D.W., Ran, J., Zhuang, Z.W., Chen, C., Qiao, S.Z., Li, Y.D., et al., 2020. Atomically dispersed Ni in cadmium-zinc sulfide quantum dots for high-performance visible-light photocatalytic hydrogen production. Sci. Adv. 6 (33). Available from: https://doi.org/10.1126/sciadv.aaz8447.

Sun, L., Zhuang, Y., Yuan, Y., Zhan, W., Wang, X., Han, X., et al., 2019. Nitrogen-doped carbon-coated CuO-In_2O_3 p–n heterojunction for remarkable photocatalytic hydrogen evolution. Adv. Energy Mater. 9 (48). Available from: https://doi.org/10.1002/aenm.201902839.

Tamirat, A.G., Rick, J., Dubale, A.A., Su, W.N., Hwang, B.J., 2016. Using hematite for photoelectrochemical water splitting: a review of current progress and challenges. Nanoscale Horiz. 1 (4), 243–267.

Tsai, K.-A., Hsieh, P.-Y., Lai, T.-H., Tsao, C.-W., Pan, H., Lin, Y.-G., et al., 2020. Nitrogen-doped graphene quantum dots for remarkable solar hydrogen production. ACS Appl. Energy Mater. 3 (6), 5322–5332.

Vaiano, V., Lara, M.A., Iervolino, G., Matarangolo, M., Navío, J.A., Hidalgo, M.C., 2018. Photocatalytic H_2 production from glycerol aqueous solutions over fluorinated Pt-TiO_2 with high {001} facet exposure. J. Photochem. Photobiol. A: Chem. 365, 52–59.

Van Damme, H., Hall, W.K., 1979. Photoassisted decomposition of water at the gas-solid interface on titanium dioxide. J. Am. Chem. Soc. 101 (15), 4373–4374.

Wang, N., Li, X., 2018. Protonated carbon nitride nanosheet supported IrO_2 quantum dots for pure water splitting without sacrificial reagents. Inorg. Chem. Front. 5 (9), 2268–2275.

Wang, C.Y., Pagel, R., Bahnemann, D.W., Dohrmann, J.K., 2004. Quantum yield of formaldehyde formation in the presence of colloidal TiO_2-based photocatalysts: effect of intermittent illumination, platinization, and deoxygenation. J. Phys. Chem. B 108 (37), 14082–14092.

Wang, Y., Li, Y., Zhao, J., Wang, J., Li, Z., 2013. g-C_3N_4/B doped g-C_3N_4 quantum dots heterojunction photocatalysts for hydrogen evolution under visible light. Int. J. Hydrog. Energy 44 (2), 618–628.

Wang, J.J., Li, Z.J., Li, X.B., Fan, X.B., Meng, Q.Y., Yu, S., et al., 2014. Photocatalytic hydrogen evolution from glycerol and water over nickel-hybrid cadmium sulfide quantum dots under visible-light irradiation. ChemSusChem 7 (5), 1468–1475.

Wang, B., An, W., Liu, L., Chen, W., Liang, Y., Cui, W., 2015. Novel Cu_2S quantum dots coupled flower-like BiOBr for efficient photocatalytic hydrogen production under visible light. RSC Adv. 5 (5), 3224–3231.

Wang, F., Su, Y., Min, S., Li, Y., Lei, Y., Hou, J., 2018a. Synergistically enhanced photocatalytic hydrogen evolution performance of ZnCdS by co-loading graphene quantum dots and PdS dual cocatalysts under visible light. J. Solid. State Chem. 260, 23–30.

Wang, Q., Huang, J., Sun, H., Ng, Y., Zhang, K., Lai, Y., 2018b. MoS_2 quantum dots@TiO_2 nanotube arrays: an extended-spectrum-driven photocatalyst for solar hydrogen evolution. Chemsuschem 11 (10), 1708–1721.

Wang, Q., Cai, J., Biesold-McGee, G., Huang, J., Ng, Y., Sun, H., et al., 2020. Silk fibroin-derived nitrogen-doped carbon quantum dots anchored on TiO_2 nanotube arrays for heterogeneous photocatalytic degradation and water splitting. Nano Energy 78, 105313. Available from: https://doi.org/10.1016/j.nanoen.2020.105313.

Wrighton, M.S., Morse, D.L., Ellis, A.B., Ginley, D.S., Abrahamson, H.B., 1976. Photoassisted electrolysis of water by ultraviolet irradiation of an antimony doped stannic oxide electrode. J. Am. Chem. Soc. 98 (1), 44–48.

Wu, Z., Li, X., Zhao, Y., Li, Y., Wei, K., Shi, H., et al., 2021. Organic semiconductor/carbon dot composites for highly efficient hydrogen and hydrogen peroxide coproduction from water photosplitting. ACS Appl. Mater. Interf. 13 (50), 60561–60570.

Xiao, F.X., Liu, B., 2018. Plasmon-Dictated photo-electrochemical water splitting for solar-to-chemical energy conversion: current status and future perspectives. Adv. Mater. Inter. 5 (6). Available from: https://doi.org/10.1002/admi.201701098.

Xiao, M., Wang, Z., Lyu, M., Luo, B., Wang, S., Liu, G., et al., 2019. Hollow nanostructures for photocatalysis: advantages and challenges. Adv. Mater. 31 (38). Available from: https://doi.org/10.1002/adma.201801369.

Xie, M., Zhang, Z., Han, W., Cheng, X., Li, X., Xie, E., 2017. Efficient hydrogen evolution under visible light irradiation over $BiVO_4$ quantum dot decorated screw-like SnO_2 nanostructures. J. Mater. Chem. A. 5 (21), 10338–10346.

Xu, X., Zhou, G., Feng, B., Bao, Z., Hu, J., 2016. ZnO quantum dots arranged by hole scavenger groups for enhanced and stable photocatalyic hydrogen generation. Mater. Lett. 165, 196–199.

Xue, C., An, H., Yan, X., Li, J., Yang, B., Wei, J., et al., 2017. Spatial charge separation and transfer in ultrathin $CdIn_2S_4$/rGO nanosheet arrays decorated by ZnS quantum dots for efficient visible-light-driven hydrogen evolution. Nano Energy 39, 513–523.

Xue, C., Li, H., An, H., Yang, B., Wei, J., Yang, G., 2018. NiSx Quantum dots accelerate electron transfer in $Cd_{0.8}Zn_{0.2}S$ photocatalytic system viaan rgo nanosheet "bridge" toward visible-light-driven hydrogen evolution. ACS Catal. 8 (2), 1532–1545.

Yan, X., Jin, Z., 2021. Interface engineering: NiAl-LDH in-situ derived NiP_2 quantum dots and Cu_3P nanoparticles ingeniously constructed p-n heterojunction for photocatalytic hydrogen evolution. Chem. Eng. J. 420, 127682. Available from: https://doi.org/10.1016/j.cej.2020.127682.

Yan, M., Hua, Y., Zhu, F., Sun, L., Gu, W., Shi, W., 2017. Constructing nitrogen doped graphene quantum dots-$ZnNb_2O6$/g-C_3N_4 catalysts for hydrogen production under visible light. Appl. Catal. B: Environ. 206, 531–537.

Yang, X., Wolcott, A., Wang, G., Sobo, A., Fitzmorris, R.C., Qian, F., et al., 2009. Nitrogen-doped ZnO nanowire arrays for photoelectrochemical water splitting. Nano let. 9 (6), 2331–2336.

Yang, J., Wang, D., Han, H., Li, C., 2013. Roles of cocatalysts in photocatalysis and photoelectrocatalysis. Acc. Chem. Res. 46, 1900–1909 (2013).

Yang, Y., Mao, B., Gong, G., Li, D., Liu, Y., Cao, W., et al., 2019. In-situ growth of Zn–$AgIn_5S_8$ quantum dots on g-C_3N_4 towards 0D/2D heterostructured photocatalysts with enhanced hydrogen production. Int. J. Hydrog. Energy 44 (30), 15882–15891.

Yasuda, M., Matsumoto, T., Yamashita, T., 2018. Sacrificial hydrogen production over TiO_2-based photocatalysts: polyols, carboxylic acids, and saccharides. Renew. Sustain. Energy Rev. 81, 1627–1635.

Ye, M., Gong, J., Lai, Y., Lin, C., Lin, Z., 2012. High-efficiency photoelectrocatalytic hydrogen generation enabled by palladium quantum dots-sensitized TiO_2 nanotube arrays. J. Am. Chem. Soc. 134 (38), 15720–15723.

Yeh, T., Teng, C., Chen, S., Teng, H., 2014. Nitrogen-doped graphene oxide quantum dots as photocatalysts for overall water-splitting under visible light illumination. Adv. Mater. 26 (20), 3297–3303.

Yu, Y., Ren, J., Meng, M., 2013. Photocatalytic hydrogen evolution on graphene quantum dots anchored TiO_2 nanotubes-array. Int. J. Hydrog. Energy 38 (28), 12266–12272.

Yu, W., Yin, J., Li, Y., Lai, B., Jiang, T., Li, Y., et al., 2019. Ag_2S quantum dots as an infrared excited photocatalyst for hydrogen production. ACS Appl. Energy Mater. Available from: https://doi.org/10.1021/acsaem.9b00091.

Yue, D., Qian, X., Zhang, Z., Kan, M., Ren, M., Zhao, Y., 2016. CdTe/CdS core/shell quantum dots cocatalyzed by sulfur tolerant [Mo_3S13] 2–nanoclusters for efficient visible-light-driven hydrogen evolution. Acs Sustain. Chem. Eng. 4 (12), 6653–6658.

Zamiri, G., Bagheri, S., 2018. Fabrication of green dye-sensitized solar cell based on ZnO nanoparticles as a photoanode and graphene quantum dots as a photo-sensitizer. J. Colloid Inter. Sci. 511, 318–324.

Zhang, Z., Jiang, X., Mei, J., Li, Y., Han, W., Xie, M., et al., 2018a. Improved photoelectrocatalytic hydrogen generation through $BiVO_4$ quantum-dots loaded on nano-structured SnO_2 and modified with carbon quantum-dots. Chem. Eng. J. 331, 48–53.

Zhang, Y., Lin, Q., Tong, N., Zhang, Z., Zhuang, H., Zhang, X., et al., 2018b. Simple fabrication of SnO_2 quantum-dot-modified TiO_2 nanorod arrays with high photoelectrocatalytic activity for overall water splitting. Chemphyschem 19 (20), 2717–2723.

Zhang, P., Zeng, G., Song, T., Huang, S., Wang, T., Zeng, H., 2019. Synthesis of a plasmonic CuNi bimetal modified with carbon quantum dots as a non-semiconductor-driven photocatalyst for effective water splitting. J. Catal. 369, 267–275.

Zhao, H., Liu, G., Vidal, F., Wang, Y., Vomiero, A., 2018. Colloidal thick-shell pyramidal quantum dots for efficient hydrogen production. Nano Energy 53, 116–124.

Zhao, J., Shi, R., Li, Z., Zhou, C., Zhang, T., 2020. How to make use of methanol in green catalytic hydrogen production? Nano Sel. 1 (1), 12–29.

Zheng, Y., Chen, Y., Gao, B., Chen, J., Du, Z., Lin, B., 2019. Polymeric carbon nitride hybridized by $CuInS_2$ quantum dots for photocatalytic hydrogen evolution. Mater. Lett. 254, 81–84.

Zhong, D., Liu, W., Tan, P., Zhu, A., Qiao, L., Bian, Y., et al., 2019. Efficient hydrogen generation of indium doped $BaTiO_3$ decorated with CdSe quantum dots: novel understanding of the effect of doping strategy. Int. J. Hydrog. Energy 44 (3), 1627–1639.

Zhou, X., Wang, X., Feng, X., Zhang, K., Peng, X., Wang, H., et al., 2017. Loading $Cd_{0.5}Zn_{0.5}S$ quantum dots onto onion-like carbon nanoparticles to boost photocatalytic hydrogen generation. ACS Appl. Mater. Interf. 9 (27), 22560–22567.

Zhu, X., Xie, Y., Liu, Y., 2018. Exploring the synergy of 2D MXene-supported black phosphorus quantum dots in hydrogen and oxygen evolution reactions. J. Mater. Chem. A 6 (43), 21255–21260.

Zong, X., Sun, C., Yu, H., Chen, Z.G., Xing, Z., Ye, D., et al., 2013. Activation of photocatalytic water oxidation on N-doped ZnO bundle-like nanoparticles under visible light. J. Phys. Chem. C. 117 (10), 4937–4942.

Zou, Y., Shi, J., Ma, D., Fan, Z., Cheng, L., Sun, D., et al., 2018. WS_2/Graphitic carbon nitride heterojunction nanosheets decorated with CdS quantum dots for photocatalytic hydrogen production. Chemsuschem 11 (7), 1187–1197. Available from: https://doi.org/10.1002/cssc.201800053.

Index

Note: Page numbers followed by "*f*" and "*t*" refer to figures and tables, respectively.

T

U

W

Y

Quantum Dots

Fundamentals, Synthesis and Applications

With their adaptability and broad applicability, quantum dots have become an increasingly important tool for the development of new materials, approaches, and applications across a wide range of fields. Understanding the molecular fundamentals governing their structures, interactivity, and behaviors can provide a unique insight for researchers and help them design and apply quantum dots in novel ways. *Quantum Dots: Fundamentals, Synthesis and Applications* compiles such key information with practical guidance on quantum dot synthesis and applications.

Beginning with an introduction to quantum dots, Part 1 highlights foundational knowledge such as growth mechanisms, shape and composition, electrochemical properties, and production scale-up for quantum dots. Part 2 goes on to provide practical guides to key chemical, physical, and biological methods for the synthesis of quantum dots. Part 3 reviews a range of important applications of quantum dots, including photocatalysis, energy cells, and medical imaging.

Drawing on the knowledge of its expert authors, this book provides practical guidance for all those who already study, develop, or use quantum dots in their work and is a great introduction for anyone who would like to start doing so.

Key features

- Presents foundational information needed to effectively understand and manipulate quantum dot properties
- Consolidates key methods of quantum dot synthesis in a single volume
- Reviews both current and future practical applications of quantum dots across a range of important fields

About the editors

Dr. Rakshit Ameta has a thoroughly first-class career, securing first position in his MSc. and was awarded a Gold Medal. He was also given the Fateh Singh Award from Maharana Mewar Foundation, Udaipur for his meritorious performance. After completion of his Ph.D., he served in Hindustan Zinc Limited, Vedanta Group for 1 year. Under his supervision, 12 Ph.D. students have been completed their Ph.D. on various aspects of green chemistry. He has around 140 research publications to his credit in journals of national and international repute. Presently, he is the Director, Faculty of Science, J. R. N. Rajasthan Vidyapeeth (Deemed to be University), Udaipur.

Dr. Jayesh P. Bhatt received his MSc. from RSTM Nagpur University in 2011. He did his Ph.D. in the year 2019 from PAHER University, Udaipur and since 2019, he has been working as an Assistant Professor in the Department of Chemistry of the same university. Dr. Jayesh has published 11 research articles in various reputed national and international journals and contributed 12 chapters. Currently, four Ph.D. students are working under his supervision.

Prof. Suresh C. Ameta obtained his master's degree from the University of Udaipur and was awarded a gold medal in 1970. He obtained his Ph.D. degree from Vikram University in 1980. He has served as a Professor and Head of the Department of Chemistry, North Gujarat University, Patan (1994) and M. L. Sukhadia University, Udaipur (2002–05) and the Head of the Department of Polymer Science (2005–08). He has successfully guided 108 students through their course of Ph.D. Dr. Ameta has more than 400 research papers and 36 books to his credit.

ISBN 978-0-12-824153-0

9 780128 241530

ELSEVIER elsevier.com/books-and-journals